United States
Environmental Protection
Agency

Office of Air Quality
Planning and Standards
Research Triangle Park NC 27711

EPA-450/4-81-034
November 1981

Air

EPA

The Effects Of Chemistry And Meteorology On Ozone Control Calculations Using Simple Trajectory Models And The EKMA Procedure

EPA-450/4-81-034

The Effects Of Chemistry And Meteorology On Ozone Control Calculations Using Simple Trajectory Models And The EKMA Procedure

by

H.E. Jeffries, K.G. Sexton and
C.N. Salmi

U.S. Environmental Protection Agency
Region V, Library
230 South Dearborn Street
Chicago, Illinois 60604

Contract No. 68-02-3523

EPA Project Officer: Edwin L. Meyer, Jr.

Prepared for

U.S. Environmental Protection Agency
Office of Air, Noise and Radiation
Office of Air Quality Planning and Standards
Research Triangle Park, North Carolina 27711

November 1981

This report was furnished to the U.S. Environmental Protection Agency by the University of North Carolina, Chapel Hill, North Carolina in fulfillment of Contract No. 68-02-3523. The contents of this report are reproduced herein as received from the University of North Carolina. The opinions, findings, and conclusions expressed are those of the author and not necessarily those of the Environmental Protection Agency. Mention of company or product names is not to be considered as an endorsement by the Environmental Protection Agency.

U.S. Environmental Protection Agency

ACKNOWLEDGEMENTS

The authors gratefully acknowledge the time, efforts, and thoughtfulness of their friends and co-workers who contributed significantly to this project. At UNC: Douglas Case generated almost all the plots. Amy Gerhardt managed the business details of the project, produced plots, reviewed and proofed text, and dealt effectively with the myriad of details necessary for the project's success. Mario DeSousa generated some, and modified most, of the new computer code produced in this project. He effectively managed the computer libraries and disk files. Kenneth Crossen developed the histogram fitting algorithm, implemented the OZIPP plotting packages, and generated and supplied OAQPS with FORTRAN code to correct OZIPP; Richard Kamens and Michael Gery provided technical dialogue. Donna Simmons typed and corrected the report and tables; Phyllis Carlton assisted in typing many sections. We are especially grateful to Suzanne Spencer who applied the finishing touches to the figures and the text.

At EPA:
The project would not have been possible without the continual cooperation of Gerry Gipson at OAQPS who supplied large quantities of data; this required attention to meticulous detail and patience for which we are grateful. Robert Kelly and Edwin Meyer at OAQPS, and Joan Novak at the Meteorology Branch also assisted with data and discussion.

The most significant input to the project was that of the model developers. We gratefully acknowledge the willingness to cooperate, the significant time spent in discussion, and their patience with us while we sometimes mistreated their creative work. We thank Jim Killus and Gary Whitten of System Applications Inc., the source of the Carbon Bond mechanism. We thank Kenneth Demerjian of EPA not only for supplying his mechanism, but also for significant time spent discussing its use and the RAPS emission inventory. We thank Marcia Dodge for her cooperation and tolerance. We thank Gregory McRae and John Seinfeld of Cal Tech for their willingness to share their work before they had completed their efforts.

Portions of this work were partially supported by EPA Grant R807762-01, "Modeling Observed Hydrocarbon Mixture Reactivity Effects".

Table of Contents

	Page
List of Figures	vii
List of Tables	xiv
Glossary of Terms	xvii
1.0 SUMMARY, CONCLUSIONS, AND RECOMMENDATIONS	1
1.1 SUMMARY	1
1.1.1 Purpose	
1.1.2 Need	
1.1.3 Approach	
1.1.4 Results	
1.2 CONCLUSIONS	11
1.3 RECOMMENDATIONS	15
2.0 INTRODUCTION	17
2.1 THE REQUIREMENT FOR MODELLING	17
2.2 THE MODELS OF INTEREST TO THIS STUDY	18
2.2.1 Simple Trajectory Models	
2.2.2 Control Calculations	
2.2.2.1 Isopleth diagrams	
2.2.2.2 Application of EKMA	
2.3 PURPOSE	24
3.0 BACKGROUND AND APPROACH	29
3.1 PREVIOUS STUDIES	29
3.1.1 UNC mechanism modelling study	
3.1.2 EPA/OAQPS OZIPP/EKMA Study	
3.2 APPROACH	41
3.2.1 General Concept	
3.2.2 Tasks Undertaken	
4.0 CHEMICAL KINETICS MECHANISMS	44
4.1 SELECTION	44
4.2 MECHANISM REACTIONS	44
4.3 PHOTOLYTIC RATES	59
4.4 HYDROCARBON COMPOSITION INPUT CALCULATIONS	65
5.0 BUREAU OF MINES SMOG CHAMBER SIMULATIONS	70
5.1 THE BUREAU OF MINES DATABASE	70
5.2 ASSUMPTIONS	75
5.3 SIMULATION RESULTS	77
5.4 BOM ISOPLETHS AND CROSS SECTIONS	82
5.5 SUMMARY	88

6.0 REGIONAL AIR POLLUTION STUDIES DATABASE: EPA SUPPLIED INFORMATION 89
6.1 GENERAL DESCRIPTION 89
6.2 DAYS SELECTED 94
6.3 INFORMATION SUPPLIED BY EPA 97

7.0 INPUT DATA FOR SIMPLE TRAJECTORY MODELS FOR RAPS DAYS 98
7.1 TRAJECTORIES 98
7.2 AMBIENT DATA ALONG TRAJECTORIES 122
7.3 EMISSIONS DATA ALONG TRAJECTORIES 136
7.3.1 Procedure for Processing Emissions
7.3.2 Results
7.3.3 Method of Treating Hydrocarbon Composition
7.3.4 Sensitivity of Demerjian and Carbon Bond Mechanisms to RAPS Ambient Hydrocarbon Composition in Smog Chamber Simulations
7.4 MIXING HEIGHT PROFILES 167
7.5 OZONE ALOFT 178

8.0 RAPS SIMULATIONS WITH SIMPLE TRAJECTORY MODELS 180
8.1 METEOROLOGY ONLY SIMPLE TRAJECTORY MODEL SIMULATIONS OF RAPS DAYS 188
8.2 PHOTOCHEMICAL SIMPLE TRAJECTORY MODEL SIMULATIONS OF RAPS DAYS 199
8.3 RESPONSE OF SELECTED PHOTOCHEMICAL SIMULATIONS TO DIFFERENT INPUT ASSUMPTIONS 219
8.3.1 Carbon Bond Mechanisms' Response to Increased Aldehydes and Photolytic Rates
8.3.2 Demerjian and Carbon Bond Mechanisms' Response to Hydrocarbon Composition Changes
8.3.3 Effect of Trajectory Assumptions for Selected Days
8.3.4 Effect of Emission Pattern for Selected Days
8.3.5 Effect of Ozone Aloft Assumptions for Selected Days
8.4 SUMMARY 265

9.0 ISOPLETHS AND CONTROL CALCULATIONS 270
9.1 OZONE ISOPLETHS GENERATED FROM PHOTOCHEMICAL SIMPLE TRAJECTORY MODEL SIMULATIONS 270
9.2 OZONE PRECURSOR CONTROL CALCULATIONS FROM PKSTM ISOPLETHS AND THE EKMA PROCEDURE 285

10.0 RAPS SIMULATION WITH LEVEL III MODEL 297
10.1 INPUT DATA 297
10.2 SIMULATION RESULTS 304
10.3 OZONE-PRECURSOR CONTROL CALCULATIONS USING THE EKMA PROCEDURE 309

REFERENCES 327

APPENDIX A: THE HISFIT ALGORITHM: AN AREA TRUE HISTOGRAM 330
APPENDIX B: SPECIAL EKMA COMPARISONS 336
APPENDIX C: SIMULATIONS OF INDIVIDUAL BUREAU OF MINES EXPERIMENTS USING CARBON BOND, DEMERJIAN, DODGE, AND CIT MECHANISMS 342

List of Figures

Figure		Page
1	Components of a Simple Trajectory Model	20
2	The Standard OZIPP/DODGE Isopleth Diagram	23
3	An EKMA Example	25
4	Experimental Data from UNC Outdoor Smog Chamber, August 8, 1977	31
5	Models of August 8, 1977	32
6	Experimental Data from UNC Outdoor Smog Chamber, June 19, 1978	33
7	Models of June 19, 1978	34
8	Experimental Data from UNC Outdoor Smog Chamber September 18, 1976	35
9	Models of September 18, 1976	36
10	Experimental Data from UNC Outdoor Smog Chamber for Mix vs Mix and Toluene, November 19, 1973	37
11	Effects of Hydrocarbon Composition Change on Carbon Bond II Mechanism Predictions	38
12	Effects of Hydrocarbon Composition Change on Demerjian Mechanism Predictions	39
13	Scatter Diagram for OAQPS OZIPP/DODGE Simulation of RAPS Days	40
14	Comparison of Cal Tech Simulation Using the Cal Tech Mechanism with UNC Simulation Using the Cal Tech Mechanism	57
15	Simulation of University of California-Riverside Smog Chamber Experiment SUR-119J with the CIT Mechanism	58
16	Examples of Experimental Data from the Bureau of Mines Smog Chamber Auto Exhaust Data Set	71
17	Bureau of Mines Run Locations and Ozone Maxima	72

Figure		Page
18	Bureau of Mines Replicate Run Comparison	73
19	Scatter Diagrams for Mechanism Simulations and BOM Data, Ozone Maxima	79
20	Scatter Diagrams for Mechanism Simulations and BOM Data, Time to Ozone Maxima	80
21	Scatter Diagrams for Two Versions of Demerjian Mechanism and BOM Data, Ozone Maxima	81
22	Scatter Diagrams for Two Versions of Demerjian Mechanism and BOM Data, Time for Ozone Maxima	81
23	Ozone Isopleths for the BOM Simulations	83
24	Ozone-Hydrocarbon Cross Sections at Constant NO_x for BOM Simulations	84
25	Ozone-NO_x Cross Sections at Constant Hydrocarbon for BOM Simulations	85
26	Comparison of Hydrocarbon and NO_x Ozone Cross Sections for BOM Simulations	86
27	The Regional Air Pollution Study Area at St. Louis	91
28	The Regional Air Monitoring Station UTM Co-ordinates	92
29	RAPS Major Point Sources	95
30	RAPS Grid System Overlay for Area Emissions Inventory	96
31	Trajectory Map, Day 159, June 7	101
32	Individual Trajectories, Day 159	102
33	Boxes Generated from Trajectories, Day 159	102
34	Trajectory Map, Day 160, Site 115, June 8	103
35	Individual Trajectories, Day 160, Site 115	104
36	Boxes Generated from Trajectories, Day 160, Site 115	104
37	TrajectoryMap, Day 160, Site 103, June 8	105
38	Individual Trajectories, Day 160, Site 103	106
39	Boxes Generated from Trajectories, Day 160, Site 103	106
40	Comparison of Individual Trajectories, Both Sites, Day 160	108

Figure		Page
41	Trajectory Map, Day 195, Site 114, July 13	109
42	Boxes Generated from Trajectories, Day 195	110
43	Trajectory Map, Day 201, July 19	111
44	Individual Trajectories, Day 201	112
45	Trajectory Map, Day 221, August 8	113
46	Individual Trajectories, Day 221	114
47	Trajectory Map, Day 238, August 25	115
48	Individual Trajectories, Day 238	116
49	Boxes Generated from Trajectories, Day 338	116
50	Trajectory Map, Day 261, September 17	117
51	Individual Trajectories, Day 261	118
52	Trajectory Map, Day 275, October 1	119
53	Boxes Generated by Inspection	120
54	Trajectory Map, Day 276, October 2	121
55	Ambient Data, Weighted Mean, Max and Min for Day 159 Trajectory, June 7	126
56	Ambient Data, Weighted Mean, Max and Min for Day 160/115 Trajectory, June 8	127
57	Ambient Data, Weighted Mean, Max and Min for Day 160/103 Trajectory, June 8	128
58	Ambient Data, Weighted Mean, Max and Min for Day 195 Trajectory, July 13	129
59	Ambient Data, Weighted Mean, Max and Min for Day 201 Trajectory, July 19	130
60	Ambient Data, Weighted Mean, Max and Min for Day 221 Trajectory, August 8	131
61	Ambient Data, Weighted Mean, Max and Min for Day 238 Trajectory, August 25	132

Figure		Page
62	Ambient Data, Weighted Mean, Max and Min for Day 261 Trajectory September 17	133
63	Ambient Data, Weighted Mean, Max and Min for Day 275 Trajectory, October 1	134
64	Ambient Data, Weighted Mean, Max and Min for Day 276 Trajectory, October 2	135
65	Example Segment of RAPS Gridded Inventory	137
66	Distribution of CO, NO_x, and HC Emissions for Selected RAPS Days	147
67	Carbon Distribution (Percent) of NMHC for Selected RAPS Days	147
68	Examples of Fitting Equal-Area Smooth Curve to Hourly Averaged Emission Values	149
69	Absolute Emisson Rates for CO, NO_x, NMHC used in Simple Trajectory Model Simulations, All Days	152
70	Effect of HC Composition and Concentration on Outdoor Smog Chamber Type Simulations with the Demerjian Mechanism	163
71	Effect of HC Composition and Concentration on Outdoor Smog Chamber Type Simulations with the Carbon Bond II Mechanism	164
72	Effect of Aldehyde Photolytic Rate with HC Composition and Concentration in Outdoor Smog Chamber Type Simulation with the Demerjian Mechanism	166
73	The Characteristic Growth Curve	170
74	Mixing Height Profiles, All Days	173
75	Dilution Rates Resulting From Selected Mixing Height Profiles	177
76	Relationship Between Ozone Aloft and Post-Inversion Breakup Ground Concentrations	178
77	MOSTM Simulation Results for NO_x, HC, CO, and O_3; All Days	183
78	Scatter-Diagram MOSTM Predictions and Ambient O_3 Maxima	197
79	Photochemical Simple Trajectory Model Simulation Results for NO, NO_2, and O_3; All Days	201
80	Scatter Diagrams: Mechanism Predictions and Ambient O_3 Maxima	217

Figure		Page
81	Scatter Diagrams: Mixing Height Predictions and Ambient O_3 Maxima	218
82	Effect of Increased Aldehyde Emission Fraction for Carbon Bond Mechanism; Day 275 (8)	221
83	Effect of Increased Aldehyde Emission Fraction for Carbon Bond Mechanism; Day 159	222
84	Effect of Increased Aldehyde Emisson Fraction for Carbon Bond Mechanism; Day 221	223
85	Effect of Increased Aldehyde Emissions Fraction: Effect of Changing From "OLD" to "NEW" Photolytic Rates; Day 261	225
86	Effect of Changing from "OLD" to "NEW" Photolytic Rates and Increasing Both the Radical Photolysis and Aldehyde Emissions Fraction; Day 275	226
87	Effect of Changing from "OLD" to "NEW" Photolytic Rates for Dodge Mechanism; Day 275	227
88	Effect of Changing Hydrocarbon Composition on Demerjian Mechanism's Simulation of Day 275	229
89	Effect of Changing Hydrocarbon Composition on Carbon Bond's Simulation of Day 275	231
90	Supplied Column Path for Day 238	234
91	Simulations with Different Trajectories; Day 238	237
92	Instantaneous Emission Rates Along Trajectories; Day 238	243
93	Supplied Column Path for Day 201	245
94	Simulations with Different Trajectories, Day 201	247
95	Instantaneous Emission Rates Along Trajectories, Day 201	253
96	Effects of Ozone Aloft on Simulations, Day 275	261
97	Effects of Ozone Aloft on Simulations, Day 159	262
98	Example of Locations for Simulations Used to Produce an Ozone Isopleth Surface	271
99	An Ozone Isopleth Surface (A); Surface Sliced at Constant NO_x (B); Surface Sliced at Constant HC(C); Simple Trajectory Model Simulation for Day (D); "+" Identification Coordinates of Initial Conditions and O_3 Maximum	272

Figure		Page
100	A Ozone-HC Cross Sections, October 1 Simulations	274
	B Ozone Isopleths, October 1 Simulations	275
	C Ozone-NO_x Cross Sections, October 1 Simulations	276
	D Ozone Isopleth and Cross Sections for CIT October 1 Characteristic Curve Simulation	277
	E Ozone Isopleths over Larger Range for Carbon Bond Simulations	278
101	A Ozone-HC Cross Sections, June 7 Simulations	280
	B Ozone Isopleths, June 7 Simulations	281
	C Ozone-NO_x Cross Sections, June 7 Simulations	282
	D Ozone Isopleths and Cross Section for CIT June 7 Characteristic Curve Simulation	283
102	The EKMA Procedure	286
103	Ozone-HC Fraction Plots for October 1 Simulations	289
104	Ozone-HC Fraction Plots for June 7 Simulations	290
105	Ozone Control Diagrams for October 4	293
106	Ozone Control Diagrams for June 7	294
107	Control Predictions by Day by Mixing Height, by Mechanism	295
108	Level III Simulation Profiles for Three RAPS Days with 250 m Initial Mixing Height	301
109	Level III Simulation Profiles for Three RAPS Days with 350 m Initial Mixing Height	302
110	D159 Level III Isopleth Diagrams and Ozone-HC Fraction Diagrams with 250 m Initial Mixing Height	310
111	D195 Level III Isopleth Diagrams and Ozone-HC Fraction Diagrams with 250 m Initial Mixing Height	311
112	D275 Level III Isopleth Diagrams and Ozone-HC Fraction Diagrams with 250 m Initial Mixing Height	312
113	Level III Isopleth Diagrams and Ozone-HC Fraction Diagrams with 350 m Initial Mixing Height for Three RAPS Days	313
114	Level III Ozone Reduction Diagrams for Three RAPS Days with 250 m Initial Mixing Height	318
115	Level III Ozone Reduction Diagrams for Three RAPS Days with 350 m Initial Mixing Height	319

Figure		Page
116	Effect of Increasing Simulation Time from 8 to 10 Hours for D275	324
117	Control Predictions by Model Level, by Day, by Mechanism	326
A.1	Comparison of Equal Area Histogram Algorithms Utilized by OZIPP and by UNC	333
A.2	Comparison of Equal Area Histogram Algorithms with OZIPP showing Strong Oscillation	334
B.1	Effect of Assumptions of Aldehyde Carbon Mole Fraction on EKMA for RAPS October 1, 1976	338
B.2	Effect of changing from a Level II to a Level III Application on EKMA for RAPS October 1, 1976	341
C	Simulation and Experimental Data Profiles for Bureau of Mines Study	343

List of Tables

Table		Page
1	Mathematical Equations of A Simple Trajectory Model	21
2	Nitrogen Balance at Ozone Maximum for Models and Data, August 8, 1977	31
3	Nitrogen Balance at Ozone Maximum for Models, June 19, 1978	33
4	Nitrogen Balance at Ozone Maximum for Models, September 18, 1976	35
5	The General Characteristics of the Selected Mechanisms	45
6	The Dodge Mechanism	47
7	The Demerjian Mechanism	50
8	The Carbon Bond II Mechanism	52
9	The California Institute of Technology Mechanism	55
10	Old and New Photolytic Rates at Selected Solar Zenith Angles	61
11	Photolytic Rates Used in Bureau of Mines Simulations	64
12	Hydrocarbon Species Characteristics in Each Mechanism	66
13	Factors Used in BOM Simulations	68
14	Bureau of Mines Model Simulation Results	74
15	Days from RAPS Database Selected for Simple Trajectory Model Simulations	94
16	Sample Ambient Data Printout	123
17	Initial Conditions of HC, NO_x, CO Chosen for Simulations	124
18	Sample Area Emission Inventory Printout	138
19	Sample Point Source Emissions Inventory Printout	139
20	Species Molecular Weights Used in Emissions Calcuation	140
21	Hydrocarbon Carbon Numbers Used in Emissions Calcuations	140

Table		Page
22	Sample Emissions Calculation for Point and Area Sources	143
23	Distributions of Emissions for Selected RAPS Days	145
24	Distributions of Emissions for the St. Louis AQCR	145
25	Carbon Distribution of NMHC for Selected RAPS Days	146
26	Computed Emissions Rates for Selected RAPS Days	150
27	HC Fractions for Each Mechanism	161
28	The Demerjian/Schere Characteristic Mixing Height Growth Curve	170
29	Mixing Height Patterns Used to Model Selected RAPS Days	172
30	Assumed Ozone Aloft Used in Models of Selected RAPS Days	179
31	Effects of Mixing Height Profile on the Contribution of Each Source to Final Concentrations in MOSTM Simulations, All Days	192
32	Ozone Maxima Predicted by MOSTM and PKSTM Using Four Mechanisms and Three Mixing Heights	216
33	Effects of Trajectory on Ozone Maxima, Day 238	241
34	Emission Rates and HC Fractions Resulting from Different Trajectory Assumptions, Day 238	242
35	Effects of Trajectory on Ozone Maxima, Day 201	251
36	Emission Rates and HC Fractions Resulting From Different Trajectory Assumptions, Day 201	252
37	Random Emissions Patterns and Total Mass of Emissions	255
38	Predicted Ozone Maxima Using Three Different Emissions Patterns	256
39	Deviations of Ozone Maxima Predicted from the Supplied Emission Pattern	257
40	Effect of Ozone Aloft on the Prediction of Ozone Maxima	259
41	Effects of Chemistry on Constant Ozone Aloft Survival	263
42	Effects of Chemistry on Variable Ozone Aloft Survival	264
43	EKMA Solution Points for October 1, 1976 Simulations	287

Table		Page
44	EKMA Solution Points for June 7, 1976 Simulations	288
45	Percent HC Reduction to Achieve 0.12 ppm O_3 Predicted by Models for October 1, 1976 and June 7, 1976	292
46	Level III Initial Conditions and Observed Ozone Maxima	299
47	Emission Densities for Level III Simulations	300
48	NMHC Composition Carbon Fractions for Level III Simulations	300
49	Predicted Ozone Maxima for Level III Simulations	303
50	Comparison of Initial and Emissions Mass for Level II and Level III Simulations	306
51	Level III % HC Control Estimates	315
52	Effect of Initial Aldehyde Fraction on O_3 Maxima for Selected Level III Simulations	321
B.1	EKMA Solution Points for October 1, 1976 (with Demerjian Mechanism)	339

GLOSSARY OF TERMS

EKMA - Empirical Kinetics Modeling Approach

A procedure applied to O_3 isopleth diagrams to estimate the impact of controlling organic and/or NO_x emissions on peak hourly O_3 concentrations. The method allows for scaling to permit use of isopleths which do not exactly match observed ambient conditions of maximum observed $[O_3]$, and initial [HC] and $[NO_x]$.

OZIPP - Ozone Isopleth Plotting Package

A plotting program which generates O_3 isopleths from results of repeated simulations using a simple trajectory model utilizing the Dodge mechanism.

SIP - State Implementation Plan

A report to the EPA from a state which describes what actions the state will take to meet National Ambient Air Quality Standards.

Mechanism - A representation of chemical processes thought to be necessary for O_3 formation; can be complex or simple; a mechanism is necessary for the estimation of the emissions control required to achieve the O_3 standard; example mechanisms are: Dodge, Demerjian, Carbon Bond II, and CIT.

BOM - Bureau of Mines database

A 1967-68 set of auto exhaust and NO_x constant light and temperature smog chamber experiments that were the basis for adjusting the Dodge mechanism

STM - Simple Trajectory Model

A model which is based on the assumption that an air parcel can be tracked for at least one day with simplifying assumptions of no horizontal exchange of mass, no vertical wind shear, and no vertical concentration gradients within the air parcel.

MOSTM - Meteorology Only Simple Trajectory Model

A simple trajectory model with no simulation of chemistry.

PKSTM - Photochemical Kinetics Simple Trajectory Model

A simple trajectory model with the functions to simulate photochemical systems that produce O_3.

RAPS - Regional Air Pollution Study

A 1975-76 EPA study centered in St. Louis and designed to collect data needed to test urban air quality simulation models.

MH - Mixing Height

The height to which complete mixing in the air parcel is assumed to occur; the height of the air parcel in the simple trajectory model.

LIN - Linear Mixing Height

The mixing height obtained from linear interpolation between soundings.

HP - Hand-picked Mixing Height

The mixing height estimated by a meterologist using surface temperatures and soundings.

CHAR - The "Characteristic Curve" Mixing Height

Technique developed by Demerjian and Schere (1980) for describing a mixing height profile.

NO_x - Nitrogen oxides

Refers to both nitric oxide (NO) and nitrogen dioxide (NO_2).

HC - Hydrocarbon

Usually refers to non-methane hydrocarbon in this text.

ALD - Aldehyde

Compounds containing a carbonyl group capable of photolyzing and producing radicals.

CO - Carbon monoxide

Level III - Refers to a simple trajectory model with a particular set of assumptions described in "Guideline for Use of City-Specific EKMA in Preparing Ozone SIPs". Model assumes trajectory path from mid-city to point of highest hour-average O_3 concentration; requires only county emission inventory, general wind data, and mid-city initial [HC] and [NO_x].

Level II - Refers to a simple trajectory model with a particular set of assumptions and guidelines described in "Data Collection for 1982 Ozone Implementation Plan Submittals." Model requires that a back-trajectory from point of highest hour-average O_3 concentration be calculated to morning position. A gridded emission inventory with HC composition detail adequate for the mechanism utilized is required.

Initial conditions of [HC] and [NO_x] are needed at the morning time and position of the air parcel. A comprehensive monitoring network is required for Level II.

DOD - Dodge Mechanism

An explicit mechanism for n-butane and propylene used in OZIPP.

DEM - Demerjian Mechanism

A highly compressed mechanism used in the Photochemical BOX Model.

CIT - California Institute of Technology Mechanism

A new lumped species mechanism for use in the CIT airshed model.

CB2 - Carbon Bond II Mechanism

A new mechanism based on bonding types used in SAI airshed model.

1.0 SUMMARY, CONCLUSIONS, RECOMMENDATIONS

1.1 SUMMARY

1.1.1 Purpose

The purpose of this study was to examine the effects of input choices and modeling methods likely to be used in "Level II" and "Level III"-type SIP applications on the predicted ozone precursor control requirements. A "Level II" analysis requires that a simple trajectory model incorporating effects of pathway, emissions, mixing height changes, entrainment from aloft, and chemistry be used to simulate days of high O_3 formation. The model is then used to generate an ozone isopleth diagram as a function of initial and emitted precursors from which precursor control requirements are estimated by procedures such as EKMA. A "Level III" analysis uses further simplifications of the inputs. It uses no actual trajectory information, center city initial conditions, and areawide averaged emissions to generate an isopleth diagram for use with EKMA procedure.

1.1.2 Need

Various methods for choosing the inputs to the simple trajectory model exist; different investigators make different choices. Two previous studies, one dealing mainly with the chemical mechanisms and one dealing mainly with the meteorological inputs, indicated that the effects of these choices might be large (Jeffries and Sexton, 1981, Gipson, 1980). This study combines both of these studies and extends the mechanism testing to include comparison with the entire Bureau of Mines auto-exhaust smog chamber database. A part of this database was used in developing the Dodge Mechanism incorporated in the current EPA calculation tool, OZIPP.

1.1.3 Approach

Four chemical mechanisms (Dodge, Demerjian, Carbon Bond II and CIT) were chosen for both smog chamber and ambient data comparisons (see Table 5, page 45 for mechanism details). Each mechanism was used to simulate the Bureau of Mines smog chamber database.

The ten RAPS days that had been selected for the previous EPA study were then simulated with an OZIPP-like, simple trajectory model incorporating each of the mechanisms for each of three choices of mixing height profiles. These were: 1) linear interpretation of the heights found from the three radiosonde soundings; 2) use of surface temperatures each hour to subjectively interpolate the soundings (called the "hand-picked" profile); and 3) calculated heights based on the "characteristic curve" of Demerjian and Schere (1980) and the morning and afternoon soundings. The first two of these had been used in the previous OAQPS study.

Selected days were then used to generate isopleth diagrams and these were subsequently used to perform EKMA control calculations.

Three of the ten days were selected for simulation with Level III assumptions using only the characteristic curve mixing height profiles. Isopleth diagrams were generated and subsequently used to perform EKMA control calculations.

The basic concept for these simulations was to use methods and procedures similar to those that might be used by state officials in making SIP calculations.

1.1.4 Results

The experimental uncertainties in the BOM database are greater than the differences in predictions among three of the four mechanisms (Demerjian, Dodge and Carbon Bond II), all of which have large differences in fundamental

assumptions. The fourth mechanism (CIT) did not adequately represent the BOM results at higher NO_x, but was reasonable at lower NO_x levels. The more recent, and presumably more kinetically correct mechanisms, suggest a stronger dependance of O_3 upon NO_x and HC changes than the older Dodge mechanism.

Thirty meteorological-only, simple trajectory model simulations were run: three mixing height profiles for each of ten days from the 1976 RAPS database. There was no chemistry in these simulations; they were used to examine the reasonableness of the meteorological, emission, and boundary condition input information used in the previous OAQPS study. Comparison of predicted CO, HC, and NO_x to ambient values suggested that there were substantial discrepancies for some days regardless of the mixing height profile used, and for others, poor predictions occurred for selected emissions-mixing height combinations. These results suggested that there would be non-mechanism related problems in simulating O_3 formation for as many as six of the days selected.

Ninety-six simple trajectory model simulations using standard assumptions were run: three mechanisms (Demerjian, Dodge, and Carbon Bond II) at each of three mixing height profiles for each of 10 days from the 1976 RAPS database; because of its poor results in the BOM simulations, the CIT mechanism was used for each of three mixing height profiles on only two of the ten days. As expected from the meteorological-only simulations many days' predictions were poor compared to ambient data.

The choice of the chemical mechanism and the mixing height profile can have a very large effect on O_3 prediction. For the highest observed O_3 day, October 1, 1976, the choice of mechanism and input assumptions resulted in a range of 5% overprediction to more than 70% underprediction for the linear mixing height profile. With the assumptions used in the simulations, the Carbon Bond II mechanism underpredicted eight of the 10 days by 50% or more and underpredicted nine days by more than 25% for all mixing height profiles.

Seven days were underpredicted by more than 25% for all mechanisms for the handpicked mixing height profile. On one day, however, it was the only profile that produced any reasonable result. Only two of the 96 simulations overpredicted the observed ozone; these were both for the Demerjian mechanism at the linear interpolated mixing height profile.

Twenty-five additional simulations were performed with the Carbon Bond II and Demerjian mechanisms to investigate their sensitivity to the input assumptions. On some days, the initial aldehyde concentration and aldehyde fraction in the emissions greatly affect the Carbon Bond mechanism's predictions. (These serve as radical sources in the mechanism.) Likewise, for an initial aldehyde fraction increase from 2% to 5%, the Demerjian mechanism's O_3 prediction increased by 20% for October 1, the high O_3 day. The Demerjian mechanism has O_3 + olefin chemistry that provides significantly more radicals than current theory suggests would occur. This probably incorrect chemistry serves as an enhanced radical source once O_3 formation starts and therefore improves the predictions. The Carbon Bond II mechanism uses a presumably more kinetically correct O_3 + olefin chemistry which results in a much reduced radical source by this path. The Carbon Bond mechanism is therefore more dependent upon aldehydes in the emissions than the Demerjian mechanism. The aldehyde fraction is very important for some days, not very important on other days and its effect varies with mechanism.

Twenty simulations using static smog chamber conditions, and 12 simple trajectory model simulations using Oct 1 conditions demonstrated the Demerjian and Carbon Bond II mechanisms' response to compositional changes in hydrocarbon classes within the emission inventories for the tne RAPS days. The mechanisms are very sensitive to compositional changes in hydrocarbon classes within the emission inventories for ten RAPS days; more than 80%

reduction in predicted O_3 occurred for the range of most olefin to most paraffin composition change with no change in HC concentration. Smog chamber data suggest that this response is excessive.

An additional 45 simple trajectory model simulations were used to investigate possible effects of trajectory choices (21 simulations), emission patterns (27 simulations), and ozone aloft profiles (18 simulations).

Simulations starting at 8 AM versus those starting at 7 AM or 6 AM generally result in better agreement between predictions and ambient data. This is because the usually higher, later initial conditions are being inputted based on ambient data instead of being dynamically generated by the correct combination of early morning emissions and early morning mixing heights. The 6 AM start on October 1, for example, resulted in a large over-prediction of the 8 AM NO_x and HC values for the handpicked and characteristic curve mixing heights.

No one mechanism nor one mixing height profile was superior at producing the "best fit" over all the days.

For the two best simulated days, October 1 and June 7, 1976, twenty ozone isopleth diagrams were generated using the simple trajectory models: for the Demerjian, Dodge, and Carbon Bond II mechanisms for the three mixing heights, and for the CIT mechanism for the characteristic curve mixing height. In addition to the isopleth diagrams, cross section diagrams showing O_3 as a function of HC at five constant NO_x levels and O_3 as a function of NO_x at five constant HC levels were produced. These figures show large differences among mechanisms, mixing heights, and days. The Dodge isopleths are characteristically u-shaped. The other mechanisms exhibit more v-shaped isopleths in which an isopleth may parallel a particular HC-to-NO_x ratio line.

The EKMA procedure for calculating ozone-precursor control requirements from isopleth diagrams was applied to the twenty isopleth diagrams described above. EKMA solutions were possible for only five of the ten isopleth diagrams produced for the highest O_3 day, October 1. That is, there was no intersection between the HC-to-NO_x ratio line and the ozone isopleth of interest on five isopleth diagrams. For mechanisms other than Dodge, the simple trajectory model simulation must be fairly close to the observed O_3 for an EKMA solution to be possible. This is because of the v-shaped nature of these isopleths and their tendency to parallel the observed HC-to-NO_x ratio line when the mechanism underpredicts. For the Demerjian mechanism, a small change in input assumptions (initial aldehyde fraction decreased from 5% to 2%) moved the EKMA solution point from 1.15 times the observed initial conditions to 2.1 times the observed initial conditions.

Control diagrams showing the percent ozone reduction as a function of percent hydrocarbon reduction at three NO_x control conditions were generated for the nine EKMA solutions. On October 1, the models predict nearly a linear ozone change for HC change and the percent change in O_3 is more than 1.5 times greater than the percent HC change. The predicted reductions required to achieve the O_3 standard are nearly twice as large for June 7 as for October 1, the day of highest O_3. This is because June 7 had 0.12 ppm O_3 aloft which resulted in 0.07 to 0.10 ppm O_3 entrained into the mixed layer; 52 to 72% of the entrained O_3 survived to add to the modelled maximum. October 1 had only 0.06 ppm O_3 aloft; only 0.01 to 0.04 ppm of this was added to the modelled O_3 maximum. The control diagram slopes on June 7 were less than one.

For four mechanisms, three mixing profiles and two days, where a solution was possible, the calculated Level II HC control requirements (with no change in NO_x) range from 15% reduction to 75% reduction. The most important factor

in the magnitude of the reduction is the amount of entrained O_3 from aloft relative to the amount of emissions generated O_3; this ratio is day specific. The second most important factor is the particular mechanism. The last factor is the mixing height profile.

Three of the ten RAPS days, October 1, June 7, and July 13 were selected for Level III simulations. Level III assumptions include use of the characteristic curve mixing height profile but with a minimum 8 AM mixing height of 250 meters. In addition to simulations with this minimum, each day was simulated with a 350 meter minimum for one mechanism. The Demerjian and Carbon Bond mechanisms were used. OAQPS/EPA supplied the Dodge mechanism results.

All Level III simulations overpredicted (by factors of 1.18 to 2.71) the O_3 maximum for the day. This is due to the assumptions in the Level III approach: (1) an origin in the center city has high initial conditions; (2) movement to outer stations is usually through higher emission areas than those in Level II trajectories; (3) high initial mixing heights increase the initial mass and decrease dilution and early emission contributions; and (4) average aldehyde initial and emissions fractions are higher than specific cases in the Level II approach. Because of these differences, all Level III isopleth diagrams provide an EKMA solution, in contrast to Level II isopleth diagrams for the same day, same mechanism where an EKMA solution was impossible or was very far out on each axis.

At Level II, the EKMA procedure most often required that existing initial conditions and existing emission inventories be scaled <u>upward</u> to obtain a solution while, at Level III, the EKMA procedure always required that these precursors be scaled downward to obtain a solution; the scale factors over both levels range from 2.10 to 0.29.

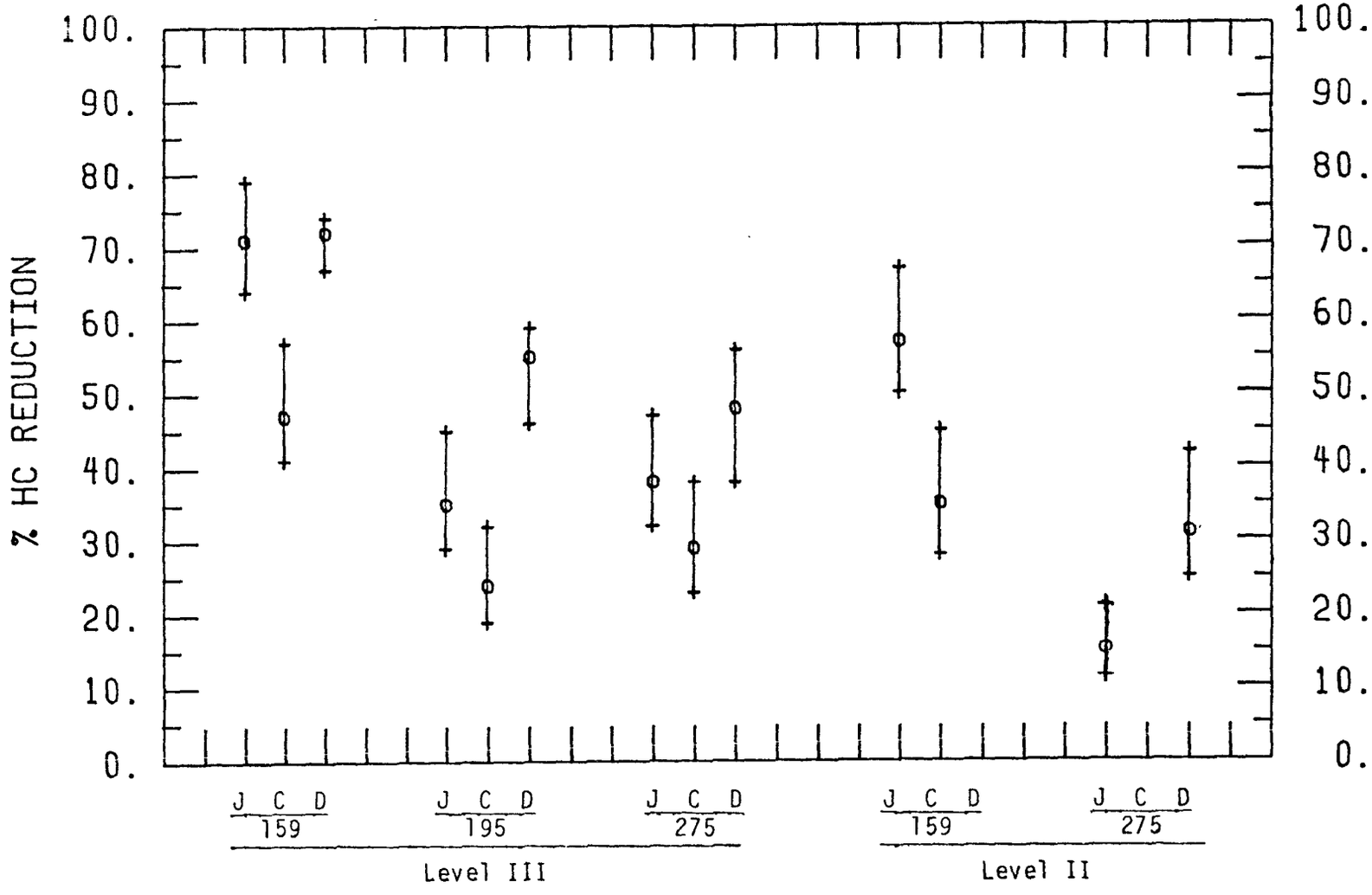

Figure 117. Control predictions by method by day by mechanism. J=Demerjian, D=Dodge, and C=Carbon Bond Mechanisms. 159=June 7; 195=July 13; 275=October 1. 0=no change in NO_x; upper range=-20% NO_x; lower range=+20% NO_x. Characteristic curve mixing height profile.

The control requirements predicted for three days, three chemical mechanisms, and two levels of modelling sophistication are shown in Figure 117, which has been repeated here. Summarizing Figure 117:

- The range of results is very large: 12% to 79% reduction.
- The largest difference among results is accounted for by the day modelled. The highest control requirement is not for the day with the highest observed O_x maximum, but was for the fifth highest day of the ten studied. This day had the highest O_3 aloft of the ten days investigated.
- Within a day, choice of mechanism is the next most significant factor. At Level III, mechanism substitution gave a ratio of 1.8 in control requirements; at Level II, mechanism substitution gave a ratio of 2.2 in control requirements. When it gives a solution, the Carbon Bond mechanism always predicts the lowest control requirement. The Dodge mechanism generally predicts the highest control requirement.
- For the same day, same mechanism, Level III control predictions were larger than Level II control predictions by as much as 2.2. to 1.

The effects of mixing height profiles on control predictions for the Level II approach is shown in Figure 107. At Level II, for the same day and same mechanism, changing the mixing height profile can result in control requirements differing by a factor of 1.47.

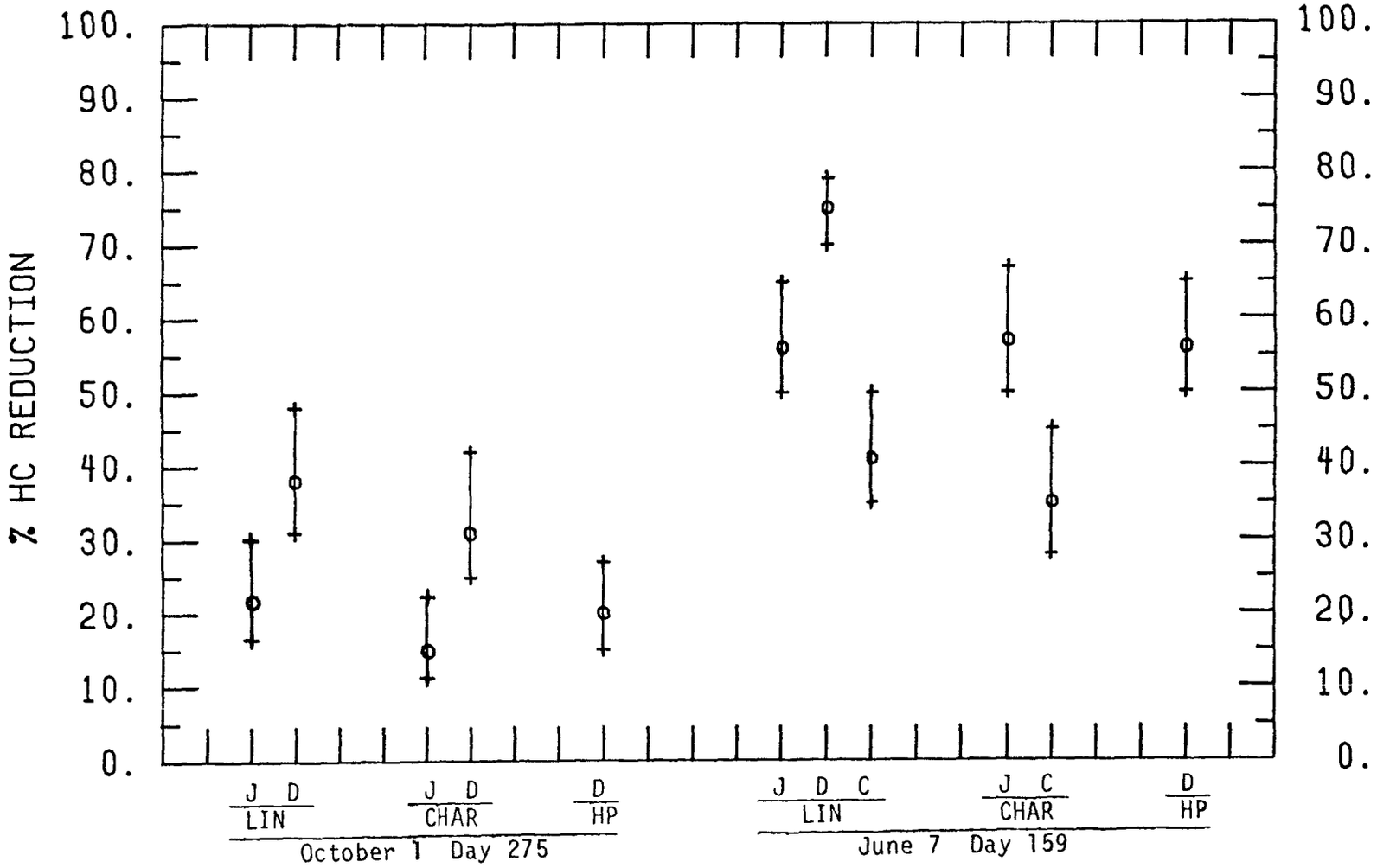

Figure 107. Control predictions by day by mechanism. J=Demerjian, D=Dodge, C=Carbon Bond Mechanisms. LIN=linear, HP=handpicked, CHAR=characteristic mixing height profiles.

1.2 CONCLUSIONS

The range of choices likely to be used by different investigators to perform a "Level II" or "Level III" state implementation plan ozone control calculation will result in substantial differences in calculated control requirements.

The range of choices include: which level of model sophistication to use; which days to model; which chemical representation to use; which representation of the extent of vertical mixing to use; which hydrocarbon composition to use; what assumptions to use for aldehyde emissions; what assumptions to use for O_3 aloft profiles; and what methods to use for calculating air parcel history and content.

Clearly, the present EPA documents provide inadequate guidance in these areas and it may be unreasonable to expect that EPA could provide the answers for each individual case.

It is not the "modelling approach" that is at fault in this situation. The model merely tells the user the outcome that would occur given his supplied descriptions and inputs; it is an outstanding tool for codifying and testing assumptions about the real world. What is inadequate, then, are the descriptions of the processes involved in O_3 formation and/or the input data used in this study that were related to these processes.

The chemical mechanisms used in this study are probably inadequate descriptions of the real atmospheric processes because they were not developed by comparison with databases which included the type and range of variations which apparently occur in the atmosphere. That is, none of the mechanisms have been tested against databases in which the hydrocarbon composition, including the aldehyde mole fraction, had been systematically varied, and in which dynamic dilution and injection of new reactants had

occurred, and in which dynamic addition of O_3 such as from entrainment aloft had occurred, or in which other factors similar to atmospheric processes had been used. These databases do not exist, thus modellers must use the 12-year old Bureau of Mines database. It will require years to develop the needed databases to insure that chemical mechanisms are giving adequate descriptions of the atmospheric chemical processes.

Based on meteorology only simulations, the methods of generating meteorological inputs to the simple trajectory model used in the previous OAQPS study and subsequently incorporated into this study are too simple to give adequate results for a range of days. Areas requiring work include: better methods to determine trajectories from surface wind data; better methods to incorporate point source emissions into the moving cell; and better methods to characterize the mixing process. These meteorological problems essentially invalidate any chemical mechanism results for the days affected.

The trajectories used in this study are more "jagged" and show greater regional variation than is likely in the real world. "Blending" functions, other than $1/r^2$, may be better at producing more consistent wind fields. Such a function might be $\exp(-ar^2)$ where "a" is an adjustable small number, say 0.01. More than three stations may be blended. Additional improvement may also result from allowing for more frequent variation in vectors (say every 15 minutes). The network pattern in RAPS may be inadequate in defining trajectories over the areas needed for examining O_3 formation.

In this study and the OAQPS study, point sources were treated like area sources. Agreement between ambient data and predictions could often be improved by assuming less dispersion of point sources. A simple point dis-

persion model applied to sources near the trajectory may significantly improve predictions.

Three mixing height soundings, without improved descriptions of atmospheric dynamic processes, are inadequate in describing the dilution experienced by the urban atmosphere. The characteristic curve is an improvement. However, it always gives the same rise rate regardless of atmospheric stability.

The results of this study are in disagreement with a fundamental assumption of the city specific EKMA method. The EKMA procedure is needed when the model predictions are not in agreement with observations. As stated in "Guidelines for Use of City-Specific EKMA in Preparing Ozone SIPs" (p. 4):

> ... sensitivity studies have shown that differences resulting from incomplete input data or gross assumptions employed by the model tend to exhibit proportional impacts on the positions of various ozone isopleths on an isopleth diagram. Thus, the model should perform satisfactorily when applied in a relative sense (e.g., to estimate a change in peak ozone accompanying changes in local precursor levels).

These sensitivity studies were conducted over a narrow range of conditions, varying only one factor at a time, with an inappropriate mixing height profile, using only one mechanism.

This study shows that the EKMA method, as a process for correcting the model's inadequate representation of O_3 formation, does not produce consistent results. In fact, using the EKMA procedure, it has been UNC's experience that the way to generate the lowest control requirement is to manipulate the model conditions to underpredict to the largest extent that still results in a possible EKMA solution. This moves the solution point away from the origin and gives an apparently greater effect for HC control. These results

imply that to be useful the models must give better absolute descriptions of the O_3 formation on each day or that more reliable and adequate methods for adjusting the model results when they do not describe the O_3 formation must be found.

1.3 RECOMMENDATIONS

- Allow SIP authors substantial freedom in modelling choices to find those that give the best description, and require extensive documentation and demonstration that the choices made were reasonable.

- Alternatives to EKMA as a procedure to deal with model predictions that are significantly different from atmospheric conditions, need to be investigated.

- Because of O_3 aloft assumptions, the day with the highest observed O_3 maximum may not be the day with the highest control requirement; the validity and consequences of these assumptions should be investigated fully. Some areas requiring further investigation are the effects of aloft profile assumptions, differential treatment of injected O_3 in chemical mecahnisms, and interaction of mixing height profile shapes with O_3 aloft profiles.

- Until descriptions that clearly are more adequate than those used herein are available, further Level II and Level III-type analysis should be performed with more than one chemical mechanism, and sensitivity to other major assumptions should be investigated as a requirement in the control calculation; in particular, at least ten days should be simulated.

- A new auto-exhaust smog chamber study using static and dynamic operating conditions and varying HC composition is needed to test mechanisms.

- A better wind-field model applied to the RAPS database is needed for trajectory determinations.

- A submodel for the wind-field model is needed to treat point source emissions.

- The characteristic curve for mixing height profiles should be made dependent upon more factors than the morning minimum and afternoon maximum mixing heights.

- Alternate methods for formulating the vertical mixing process in simple models should be investigated (e.g., as a dilution rate rather than a mixing height rise).

- Significant errors in some of the algorithms used in OZIPP need to be fixed. It is recommended that the code be substantially revised to increase its portability, flexibility, efficiency, and maintainability.

2.0 INTRODUCTION

2.1 THE REQUIREMENT FOR MODELLING

The National Ambient Air Quality Standard (NAAQS) for ozone (O_3) states that the expected number of days during a year with a maximum one-hour average ozone concentration above 0.12 parts per million (ppm) must be less than or equal to one. Because the NAAQS is widely violated, a significant number of localities will have to implement control programs to reduce ambient ozone levels. Therefore, methods are needed for determining the degree of emissions reductions of the ozone precursors, hydrocarbons and oxides of nitrogen, necessary to achieve the NAAQS. Because of the complex chemical and meteorological factors involved in ozone production mathematical simulation models are thought to provide the best methods for estimating the needed reductions.

In the November 14, 1979 Federal Register, EPA published a "Guide to Data Collection for 1982 State Implementation Plan Revisions" in which the data needs were divided into four levels "based upon four generic types of models: (1) photochemical dispersion models, (2) simplified trajectory models, (3) city-specific EKMA, and (4) standard EKMA." These are also referred to as "Level I", "Level II", "Level III", and "Level IV" methods.

Also included in the November 14 Federal Register was a list of anticipated levels of modeling for major urban areas: nine areas for Level I, ten areas for Level II, twenty-two areas for Level III, and none for Level IV.

A major investigation of the models expected to be used at Level I was already underway at EPA. Level II and Level III analyses were expected to

be based on EPA's Ozone Isopleth Plotting Package (OZIPP) used as a simple trajectory model and on EPA's Emperical Kinetics Modeling Approach (EKMA) applied to O_3 isopleth diagrams. Some assumptions, such as the mixing height profile, in OZIPP were somewhat arbitrary. Some of the assumptions underlying the EKMA procedure required further validation. Thus, OAQPS/EPA determined that further work was needed on these two methods.

2.2 MODELS OF INTEREST TO THIS STUDY

2.2.1 Simple Trajectory Models (STM)

Trajectory models are based on the concept of an "air parcel". An "air parcel" assumes that there is some continuity of identity for a body of air and therefore that this body can be followed or continuously identified within a given region. Field studies such as the Los Angeles Reactive Pollutant Program (LARPP) in which tetroons were used to "tag" air motion have indicated that the concept can be a reasonable representation of measured atmospheric events.

Simple means applying simplifying assumptions to complex atmospheric processes. The usual assumptions involved are: no horizontal exchange of mass; no vertical wind shear; and rapid vertical mixing of mass, i.e. no vertical concentration gradients. Thus the volume of air is a well mixed column that does not exchange material with adjacent columns. These simplifying assumptions allow a Lagrangian based mathematical model of the chemical and meteorological processes to be readily formulated. These sets of equations are relatively simple to solve and the input data requirements appear to be likewise simple. They therefore hold promise for providing useful calculating tools for state and local air pollution control officials faced with making decisions for State Implementation Plans (SIPs).

A simple trajectory model has the following components (see Figure 1): a) method of estimating where an air parcel is going or where it has been (i.e. determining a trajectory); b) a method of estimating the concentration and physical conditions along the estimated trajectory; c) a method of estimating the vertical extent of the air parcel (i.e. the mixing height) along the trajectory; d) a method of estimating the amount of material above the mixing volume that gets mixed into the air parcel as the mixing height rises; e) a method of estimating the magnitude and composition of emission sources encountered along the trajectory; f) a method for estimating the changes caused by chemistry along the pathway. The various methods may be in the form of separate computer programs or manual procedures. In the more complex models they may all be combined into one computer program. The various methods usually result in tables of values as a function of time. These tables then become input to a computer program designed to simulate chemical changes under various physical conditions. A major input to this program is a description of what chemical reactions are thought to take place in the urban atmosphere (a chemical mechanism).

The set of mathematical equations used in both EPA's OZIPP and the PKSTM program used herein are given in Table 1. In the programs, the tabular information discussed above is converted into a continuous function of time by fitting linear or non-linear functions to the table entries (for example, see the emissions plot in Figure 1). In Table 1, those fitted functions are: f, for the mixing height; g, for the concentrations aloft, and h for the emissions; the initial species concentrations and the functions that describe the chemical production and chemical loss of each species as functions of the other species are the other inputs. The latter functions are usually

Figure 1.

COMPONENTS OF A SIMPLE TRAJECTORY MODEL

Methods for Estimating:

- Trajectory

- Ambient Concentrations Along Trajectory

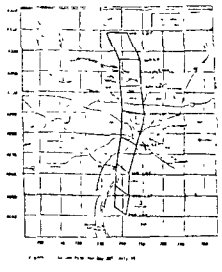

- Extent of Vertical Mixing

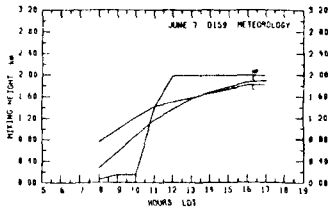

- Material Above Mixing Height

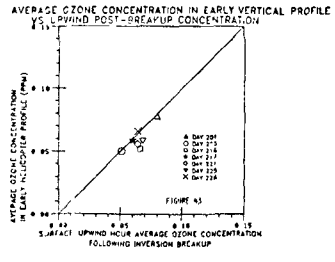

- Magnitude and Composition of Emission Sources

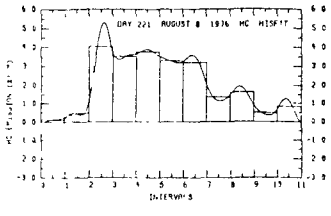

- Changes Caused by Chemistry

	NO2	--HV-->	1.00 NO	+ 1.00 O	
	O	------>	1.00 O3		
NO	+ O3	------>	1.00 NO2		
O3	+ NO2	------>	1.00 NO3		
O	+ NO2	------>	1.00 NO		
NO	+ NO3	------>	2.00 NO2		
NO3	+ NO2	------>	1.00 N2O5		
	N2O5	------>	1.00 NO2	+ 1.00 NO3	
	N2O5	------>	2.00 WHNO3		

Table 1. Mathematical Equations of A Simple Trajectory Model

$C_i \equiv$ the concentrations of the ith chemical species in the mixed volume at time = t

$C_i(@0) \equiv$ the initial concentration of the ith species in the mixed volume at time = 0

$C_i^{aloft} \equiv$ the concentration of the ith species <u>above</u> the mixed volume at time = t

$MH = f(t)$	mixing height at time = t
$\frac{dMH}{dt} = f'(t)$	rate of rise at time = t
$K_D = (\frac{1}{MH}) \frac{dMH}{dt}$	dilution rate at time = t
$\frac{dC_i}{dt}\Big\|_{dil} = -K_D C_i$	decrease in species C_i caused by mixing height rise
$C_i^{aloft} = g(t)$	concentration of species aloft at time = t
$\frac{dC_i}{dt}\Big\|_{ent} = + K_D C_i^{aloft}$	increase in species C_i caused by entrainment due to mixing height rise
$E_i = h(t)$	mass of species C_i emitted per unit time at time = t (concentration - height units)
$\frac{dC_i}{dt}\Big\|_{emis} = E_i/MH$	increase in species C_i caused by emissions into a mixing volume with unit area and height, MH, at time t
$P_i = func\ (C_j, j=1,n)$	production rate of species C_i due to chemical formation at time t
$L_i = func\ (C_j, j=1,n)$	loss rate constant for species C_i due to chemical reaction at time t
$\frac{dC_i}{dt}\Big\|_{chem} = P_i - L_i C_i$	increase or decrease in species C_i caused by chemical reactions of all species at time t

$$\frac{dC_i}{dt}\Big|_{TOTAL} = \frac{dC_i}{dt}\Big|_{dil} + \frac{dC_i}{dt}\Big|_{ent} + \frac{dC_i}{dt}\Big|_{emiss} + \frac{dC_i}{dt}\Big|_{chem}$$

SOLUTION:

$C_i = C_i(@0) + \int_0^t \frac{dC_i}{dt}\Big|_{TOTAL}$ numerical integration used to solve initial value, differential equation problem

constructed by the program by internally processing a reaction list such as that at the bottom of Figure 1. The rate of change of each species concentration can be generated by using all of these functions.

The concentrations of each species that would exist if the model (formulation and input data) gave proper descriptions of atmospheric events can be found by a numerical solution of these equations.

2.2.2 Control Calculations

Ozone Isopleth Diagrams. Once we have a simple trajectory model that presumably adequately describes atmospheric and chemical processes for a particular set of conditions, it is possible to simulate various emission control scenarios. The modelling computer programs can be easily modified to determine and display the maximum concentration outcomes from all possible emission control combinations within a given range (e.g. OZIPP, the Ozone Isopleth Plotting Package). That is, the trajectory model is run repeatedly with different combinations of emissions and a response surface, for O_3, is drawn as a function of initial and emission conditions. That is, all the conditions that generate the same maximum O_3 are connected together by a line. By comparing the coordinates of two locations on the diagram, the effects of various emission changes on the model's predicted O_3 can be quickly assessed.

Applications of EKMA. Given techniques for showing the effects of emission changes on STM's predicted O_3, how can these be translated into atmospheric control requirements? One procedure adopted by EPA is Empirical Kinetics Modelling Approach (EKMA). The fundamental assumption in EKMA is that an O_3-precursor response surface (an O_3 isopleth diagram) exhibits essentially constant relative shape. That is, it is assumed that two points

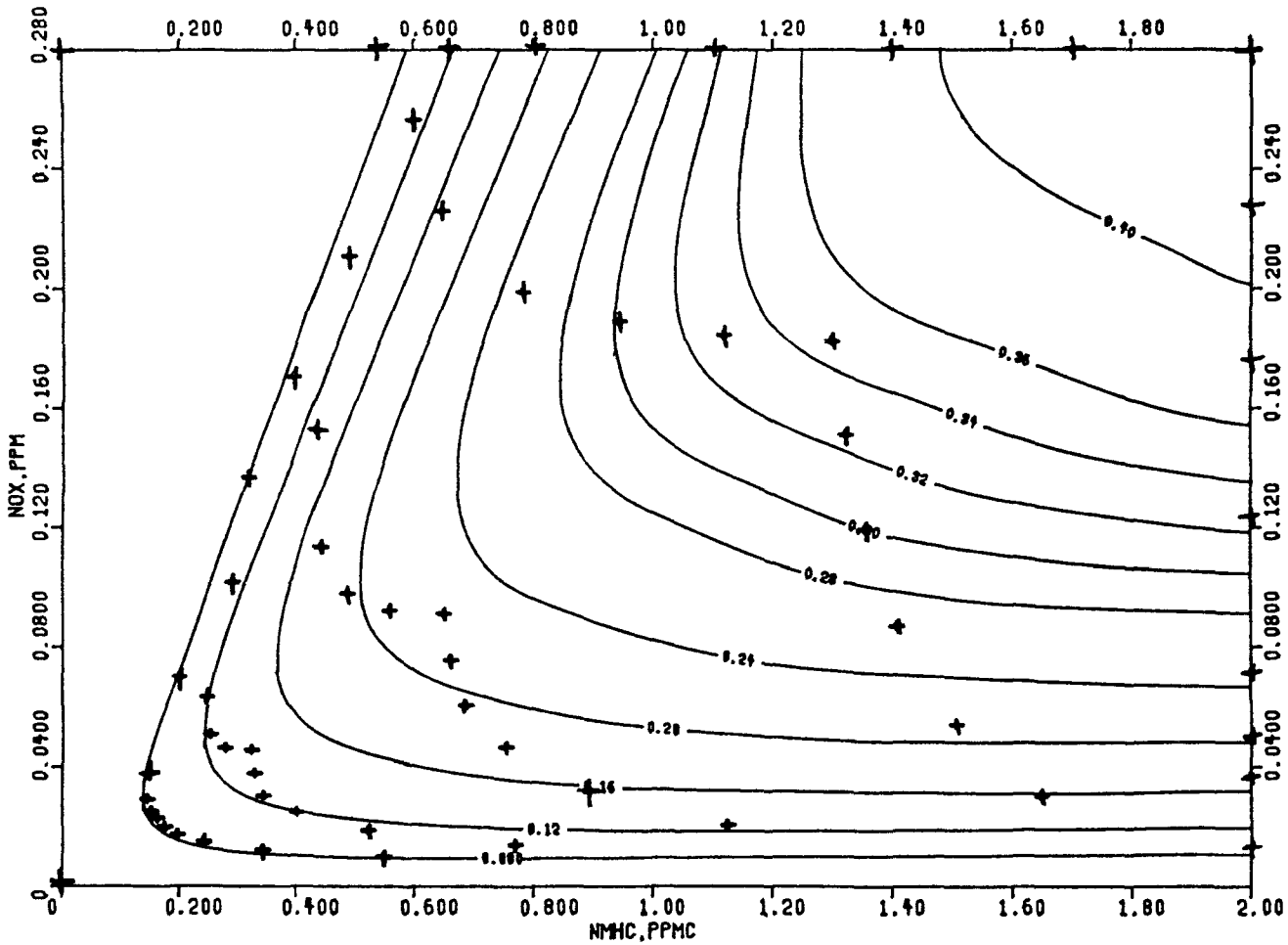

Figure 2. Standard Dodge isopleth diagram showing locations of simulations used to construct diagram.

on the surface move in a constant relative relationship to each other as the generating conditions of the surface are changed, therefore, it is not necessary to have an exact STM fit on a given day to calculate control requirements for the conditions of that day.

If a method is available for relating the observed ambient high O_3 concentration to some location on the O_3 isopleth surface, then because of the relative relationship assumption, the change in O_3 for change in precursors is assumed to be established. The EKMA procedure requires that the location of the starting point for control calculations on the surface is the intercept between the observed HC to NO_x ratio line and the isopleth equal to the observed ambient high O_3. For an isopleth surface developed from a STM, this point may be above, at, or below the actual coordinates of the precursor conditions for the day simulated. If the point is not at the actual coordinates, then the effect is to apply a linear scaling factor to the axes. An alternative might be to apply a linear scaling factor to the isopleth levels.

The EKMA procedure was primarily based upon the extrapolation of smog chamber data to the atmosphere. Its ability to perform under more realistic simulations of atmospheric conditions and different assumptions about the chemistry needed to be examined.

2.3 PURPOSE

Several methods for formulating the components of simple trajectory models and for estimating the input values to these models are in current use. Which of these formulations and input data generation methods are likely to give proper descriptions of atmospheric events and yet remain simple and reasonably available to local control agencies? Furthermore,

GIVEN: O_3 Daily Design Value = .24

Design NMOC/NO_x = 8:1

Anticipated Change in NO_x = -20%

Base case diagram shown below

FIND: Percent reduction in VOC emissions needed to reduce ozone from .24 to 0.12 ppm

SOLUTION:

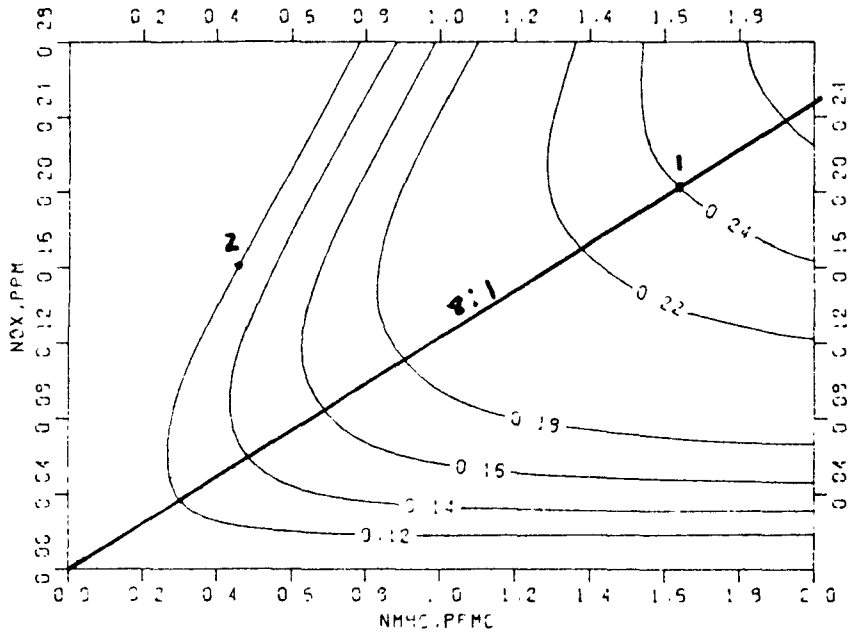

BASE CASE DIAGRAM, O3 ISOPLET = .12

STEP 1: The base case point is found by the intersection of the 8:1 NMOC/NO_x ratio line with the .24 ozone isopleth (Point 1) on the diagram. At Point 1, $(NMOC)_1$ = 1.64 and $(NO_x)_1$ = .205

STEP 2: The post-control NO_x coordinate is calcualted as follows:

$$(NO_x)_2 = (.205) \times (1 - \frac{20}{100}) = .164$$

STEP 3: The post-control point is located at the intersection of the .164 NO_x coordinate and the 0.12 ppm ozone isopleth (Point 2). At Point 2, $(NMOC)_2$ = 0.46

STEP 4: The VOC emission reduction is calculated as

$$\% \text{ reduction} = (1 - \frac{.46}{1.64}) \times 100 = 72\%$$

Figure 3. Example emission reduction calculation using a single ozone isopleth diagram

if choice is allowed, how are the results of control calculations likely to differ from those using the currently standard EPA techniques? Two previous studies (Jeffries and Sexton, 1980; Gipson, 1980), one dealing mainly with the chemical mechanisms and one dealing mainly with the meteorological inputs, indicated that the effects of this range of choices might be large.

The purpose of this study was to examine the effects of input choices and modeling methods likely to be used in "Level II"-type State Implementation Plan revision applications on the predicted ozone-precursor control requirements. A "Level II" analysis requires that a simple trajectory model incorporating effects of pathway, emissions, mixing height changes, entrainment from aloft, and chemistry be used to simulate days of high O_3 formation. The model is then used to generate an ozone isopleth diagram as a function of initial and emitted precursors from which precursor control requirements are estimated by procedures such as EKMA.

In the previous studies, some key areas were identified. Because the meteorological processes influence the concentration which determines the outcomes of the non-linear chemical processes, it was not possible to predict the combined effects of the processes previously studied. Two main areas were singled out, however.

Extent of Vertical Mixing. Dilution is a significant atmospheric process. In STM's the model volume is moving with the wind, does not exchange material with surrounding parcels, and therefore, dilution is caused only by increase in the height of the moving mixing volume.

Methods for estimating mixing heights and their temporal changes range from the application of statistical data (Holzworth,1972) when no other information is available to the use of an acoustical echo sounding equipment

which second by second echo-ranges the depth of the mixed layer. Different researchers generate different temporal profiles when given the problem of specifying the mixed layer. In the previous EPA study (Gipson, 1980) several likely-to-be-used methods were identified.

The effects of these choices on photochemical simple trajectory model predictions and on subsequent control calculations was a major concern for this study.

Chemical Mechanisms. A chemical mechanism is a collection of the pathways and their associated rates for the chemical transformations thought (by their developers) to be necessary to describe the chemical behavior of air pollutants. In collecting these pathways and in selecting the level of detail and nature of the representation, different researchers have made different choices. In addition, newer information often results in changed descriptions, so if a mechanism is submitted for publication, it frequently can be outdated before it actually appears. It is not surprising, therefore, that there is more than one mechanism intended for use in modeling urban air pollution chemistry.

Four mechanisms, their sources, and history of development will be presented in a later chapter. The majority of OAQPS/EPA control calculations have been made with the Dodge mechanism which was published in 1977. Even though it has some known kinetic deficiencies, it reportedly described the O_3 production of the Bureau of Mines auto exhaust smog chamber quite well. Several newer mechanisms are likely to be used for SIP calculations. The ability of these newer mechanisms to describe the Bureau of Mines database, as well as their ability to perform in ambient situations was of interest to EPA.

This study, therefore, was extended to include testing all the mechanisms by comparison with the entire Bureau of Mines auto exhaust smog chamber database, rather than the limited set used by Dodge (1977).

3.0 BACKGROUND AND APPROACH

3.1 PREVIOUS STUDIES

3.1.1 UNC Mechanism Study

As part of a previous study for EPA, (Jeffries and Sexton, 1980) UNC investigated the various descriptions of nitrogen chemistry used in six photochemical kinetics models. This was done by implementing each model and simulating identical situations. The test situations were based on three case days in the UNC outdoor smog chamber. Since ozone production does not depend upon absolute oxides of nitrogen concentrations, but rather upon a ratio of NO_2 to NO, mechanisms can predict reasonable ozone peaks while having significantly different chemistries for the nitrogen species. Nitrogen balances therefore can illustrate important differences among mechanisms. The results of these comparisons for three of the mechanisms that were tested will be described here. The three mechanisms are: the Dodge mechanism currently used in OZIPP and most likely to be used in Level II and Level III applications, the Carbon Bond II mechanism used in the SAI airshed grid model and still undergoing development on both UCR and UNC smog chamber data; and the Demerjian mechanism used in his Photochemical Box Model that has been applied in St. Louis and Houston simulations. These mechanisms will be described in more detail in Chapter 4.0.

The comparison was conducted by modeling increasing complex hydrocarbon systems with each model. These were: propylene (the August 8, 1977 experiment, Figure 4), a propylene-butane mixture (the June 19, 1978 experiment, Figure 6), a 13-component olefin-paraffin mixture (also June 19, 1978), and

real auto-exhaust (the September 18, 1976 experiment, Figure 8). The model predictions are reproduced here as Figures 5, 7, and 9. The nitrogen balances are given in Tables 3, 4 and 5.

Comparison of Figure 5 with Figure 4 and review of the data of Table 3 shows that the Carbon Bond mechanism is clearly much better at describing the August 8 propylene experiment. The Dodge mechanism incorrectly reproduces the O_3 and PAN greatly exceeds its measured concentration. The Demerjian mechanism also underpredicts the O_3 and incorrectly ends with 18% of the nitrogen as peroxynitric acid (HO_2NO_2).

For the June 19 propylene-butane experiment, the plots in Figure 7 show that the Dodge mechanism most nearly describes the NO_2 and O_3 profiles of Figure 6, the experimental data. Carbon Bond and Demerjian are nearly identical and both overestimate the O_3. Table 4 shows that Dodge makes far too much PAN and Demerjian again has a high (14%) prediction of peroxynitric acid.

In the auto-exhaust simulation of September 18, Carbon Bond and Demerjian mechanisms were again very similar in NO_2 and O_3 performance; both, however, underestimated the observed O_3. The Dodge predictions differ obviously from the observed data. The Carbon Bond mechanism predicts a substantial quantity of aromatic nitrates; again the Demerjian mechanism predicts an incorrect, large amount (12%) of peroxynitric acid. Likewise, Dodge predicts too much PAN, a characteristic of her mechanism since the PAN chemistry is now know to be incorrect.

A final set of simulations for the Carbon Bond II and Demerjian mechanism was based on the UNC smog chamber experiment of November 19, 1973, in which the hydrocarbon composition was drastically altered in the two

Table 2

Nitrogen Balance at Ozone Maximum for Models and Data, August 8, 1977.
Initial Conditions: 0.495 ppm NO_x, 1.5 ppmC propylene. (% nitrogen)

SPECIES	DATA	1) DODGE	2) CBII/VT	3) DERMJ
NO_2	8.2	0.00	5.42	5.24
NO	0.4	0.00	0.07	0.11
$WHNO_3$[a]	(24.4)	4.60	25.75	18.22
HNO_3	39.3	35.84	40.15	24.07
HO_2NO_2	-	-	-	17.77
RNO_3	-	-	3.08	3.57
PAN	27.6	60.04	25.54	30.95
TOTAL	100.0	100.00	100.01	99.93
O_3 max, ppm	>0.90	0.584	0.949	0.784

[a] $WHNO_3$ is formed from $N_2O_5 + H_2O$

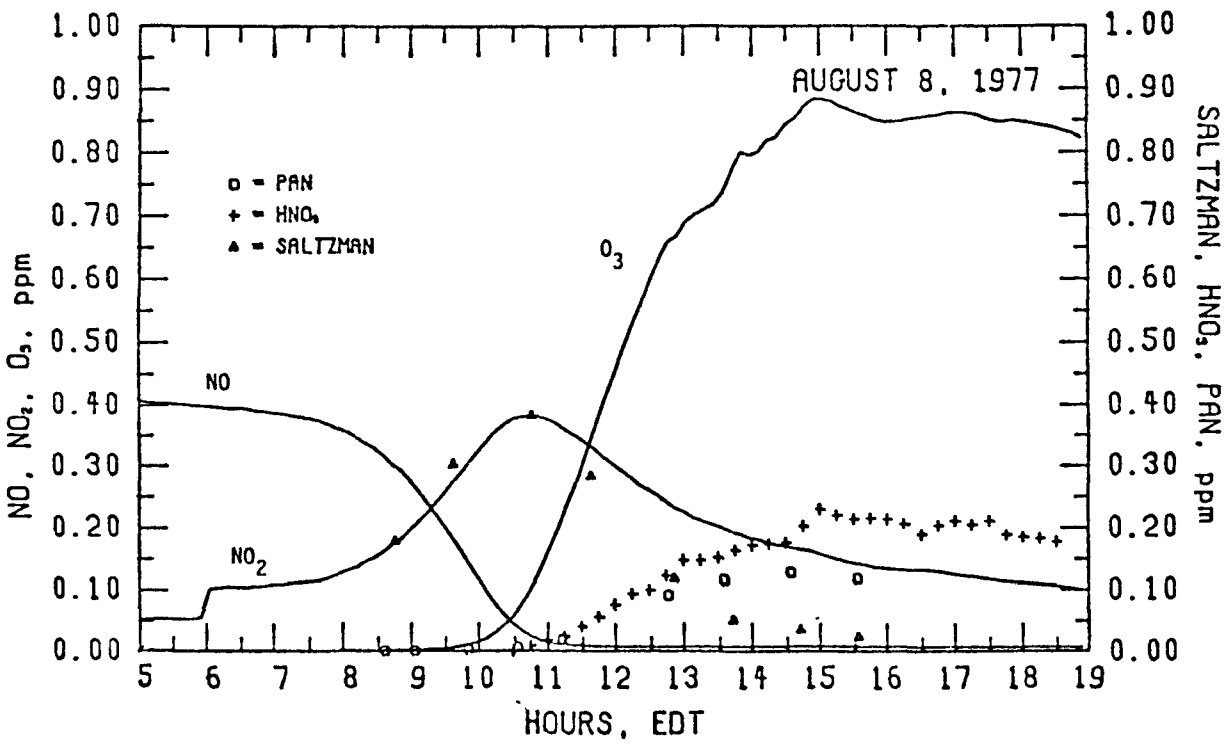

Figure 4

Experimental data from UNC outdoor smog chamber. Initial conditions: NO 0.395 ppm, NO_2 0.100 ppm, propylene 1.5 ppmC.

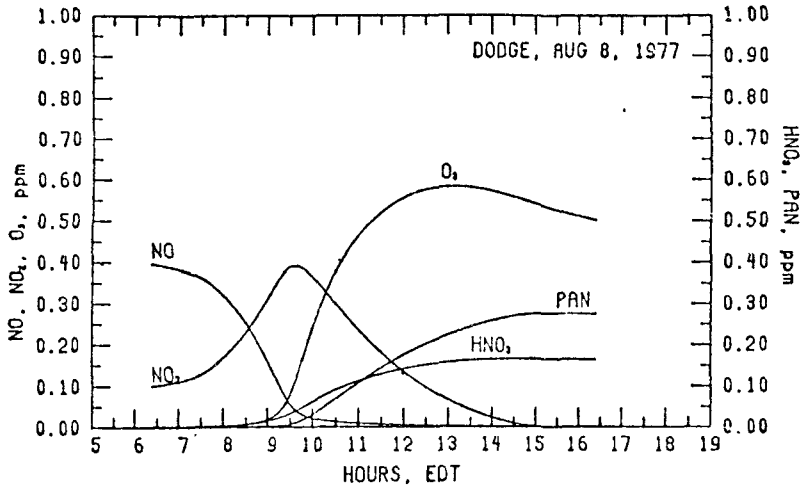

Simulation with DODGE mechanism. Initial conditions: NO 0.395 ppm, NO_2 0.100 ppm, O_3 0.1 ppb, H_2O $2x10^4$ ppm, HONO 2.5 ppb, propylene 0.56 ppmV; photolysis rates scaled to TSR for August 8.

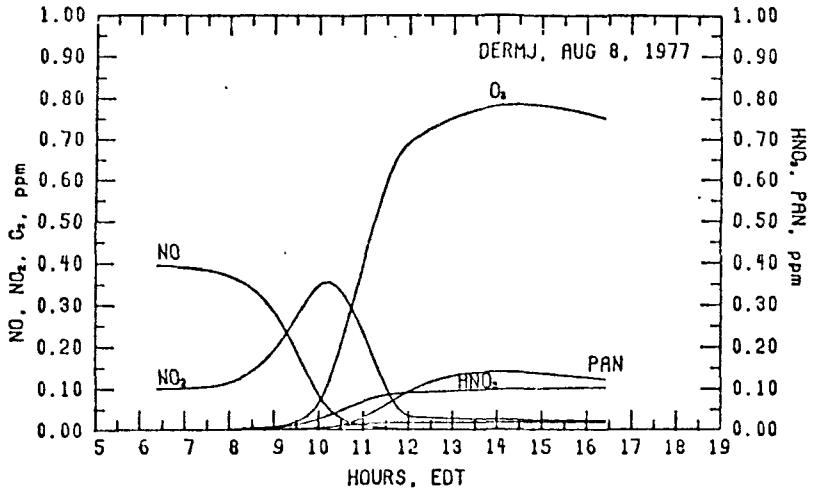

Simulation with DERMJ mechanism. Initial conditions: NO 0.395 ppm, NO_2 0.100 ppm, CO 0.4 ppm, H_2O $2x10^4$ ppm, HCl 0.56ppmV; photolysis rates scaled to TSR for August 8.

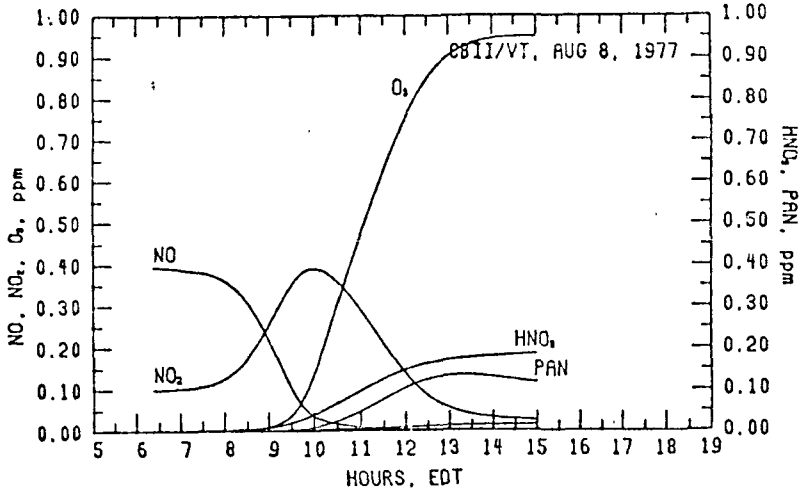

Simulation with CARBON BOND II mechanism using variable temperature. Initial conditions: NO 0.395 ppm, NO_2 0.100 ppm, CO 0.4 ppm, H_2O $2x10^4$ ppm, paraffin 0.56 ppmV, olefin 0.56 ppmV; photolysis rates scaled to TSR for August 8.

Figure 5. Models of August 8, 1977.

Table 3

Nitrogen Balance at Ozone Maximum for Models for June 19, 1978. Initial Conditions: 0.352 ppm NO_x, 2.07 ppmC propylene/butane; 0.352 ppm NO_x, 2.14 ppmC UNC mix.

SPECIES	DATA	1)DODGE	2)CBII/VT	3)DERMJ
NO_2	≤19	16.27	17.01	9.13
NO		0.45	0.23	0.19
$WHNO_3$		3.27	17.87	20.72
HNO_3		45.18	47.98	38.12
HO_2NO_2				14.22
RNO_3			4.86	2.30
PAN	≤24	35.17	12.07	15.78
TOTAL		100.34	100.02	100.45
O_3 max, ppm	0.435	0.476	0.645	0.626

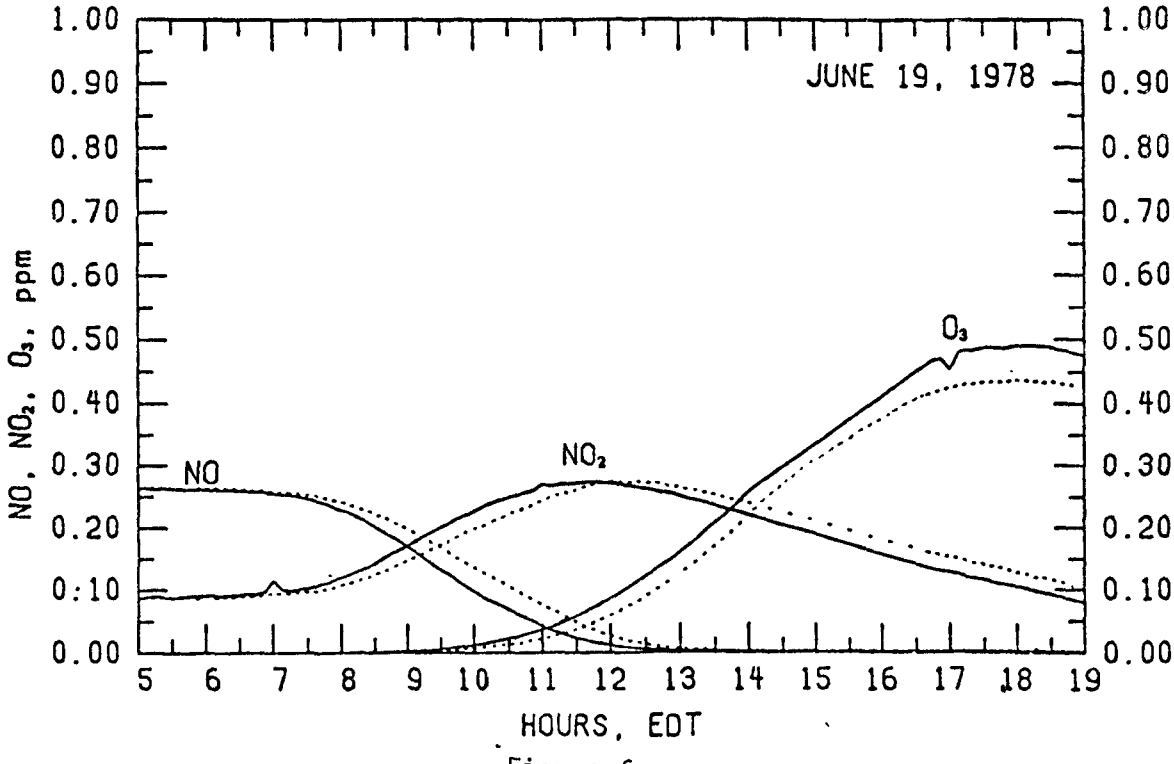

Figure 6

Experimental data from UNC outdoor smog chamber. Comparison of 25% propylene, 75% n-butane mixture (---), with 11 component mix (——). Initial conditions: NO 0.261 ppm, NO_2 0.091 ppm, HC 2.07 ppmV (---), HC 2.14 ppmV (——).

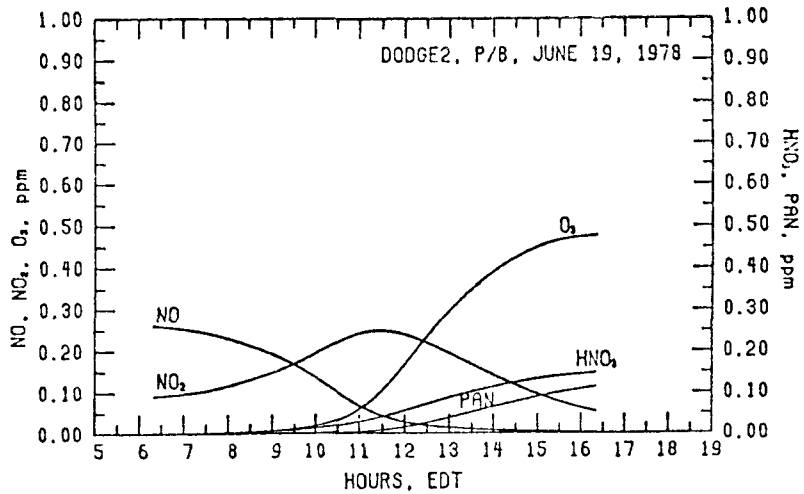

Simulation of propylene-butane experiment using DODGE mechanism. Initial conditions: NO 0.261 ppm, NO_2 0.091 ppm, CO 0.4 ppm, H_2O 2x10⁴ ppm, HONO 3.0 ppb, propylene 0.164 ppmV, butane 0.395 ppmV, photolysis rates scaled to TSR for June 19.

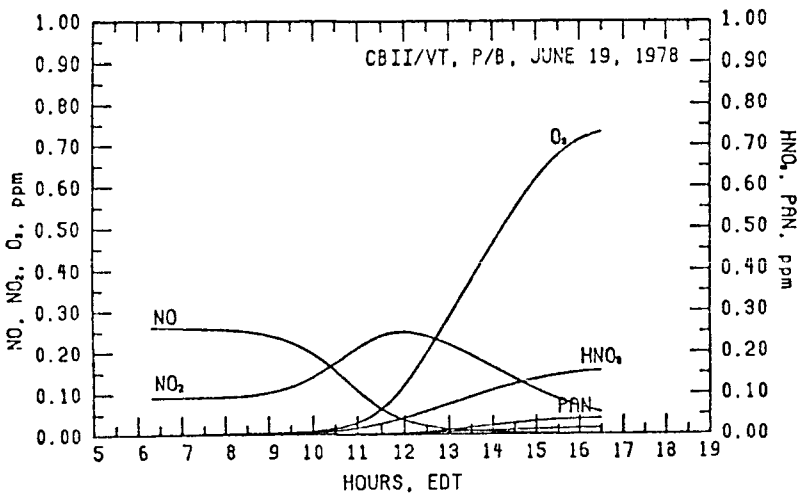

Simulation of propylene-butane experiment using CARBON BOND II mechanism with variable temperature. Initial conditions: NO 0.261 ppm, NO_2 0.091 ppm, CO 0.4 ppm, H_2O 2x10⁴ ppm, olefin 0.164 ppmV, paraffin 1.744 ppmV, photolysis rates scaled to TSR for June 19.

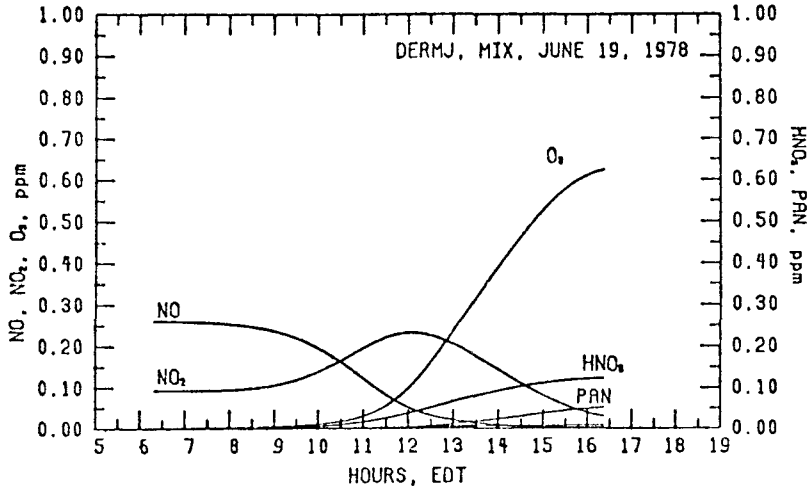

Simulation of mix experiment using DERMJ mechanism. Initial conditions: NO 0.261 ppm, NO_2 0.091 ppm, CO 0.4 ppm, O_3 0.1 ppb, H_2O 2x10⁴ ppm, HCl 0.274 ppmV, HC2 0.2497 ppmV, HONO 0.0 ppb; photolysis rates scaled to TSR for June 19.

Figure 7. Models of June 19, 1978.

Table 4

Nitrogen Balance at Ozone Maximum for Models, September 18, 1976. Initial Conditions: 0.340 ppm NO_x, 3.1 ppmC Auto Exhaust

SPECIES	DATA	1)DODGE	2)CBII/VT	3)DERMJ
NO_2	10	3.35	2.30	5.52
NO		0.05	0.03	0.07
$WHNO_3$		6.06	12.24	29.80
HNO_3		33.90	33.68	26.39
HO_2NO_2				12.29
RNO_3			5.15	2.18
ANO_3			34.23	
PAN	≤25	56.41	12.41	23.59
TOTAL	35	99.77	100.04	99.84
O_3 max,ppm	0.78	0.501	0.598	0.584

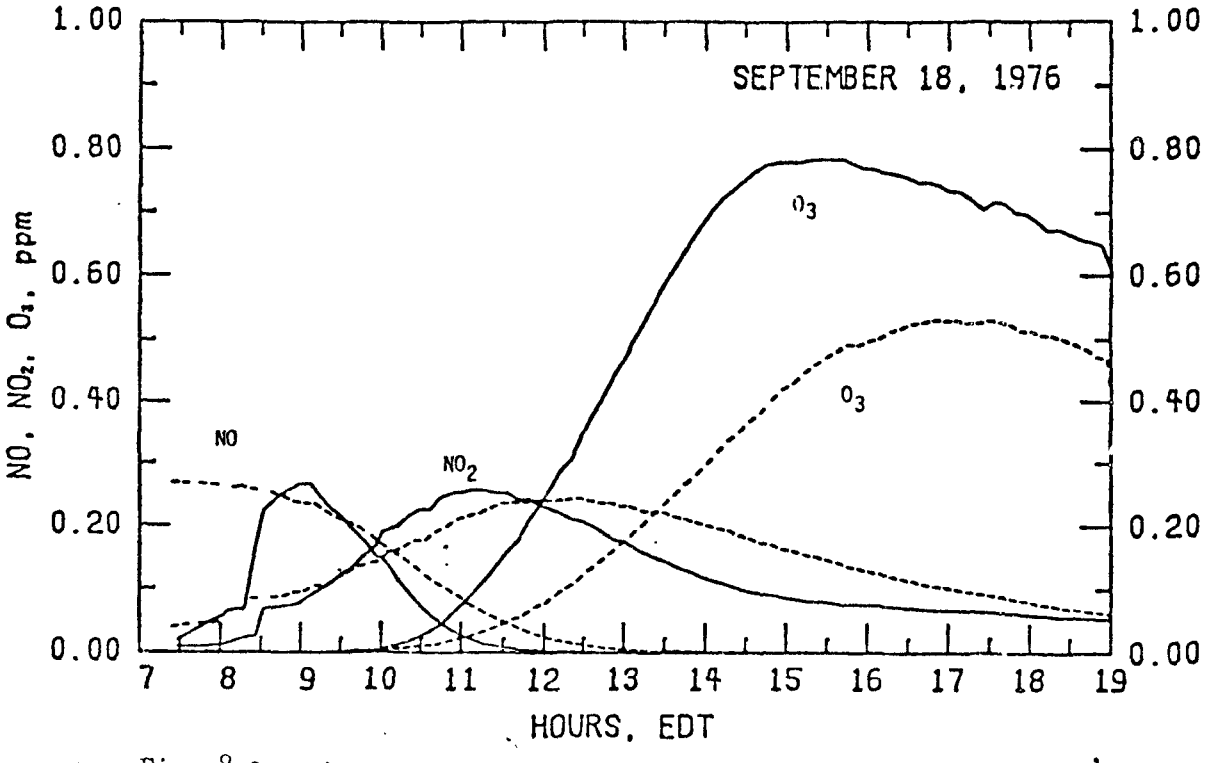

Fig. 8. Comparison of NO, NO_2 and O_3 profiles in dual run using auto exhaust as NMHC (___) and UNC urban mix as NMHC (---). Initial conditions: (___), NO_x: 0.34 ppm; NMHC: 3.1 ppmC; (---), NO_x: 0.33 ppm, NMHC: 3.1 ppmC.

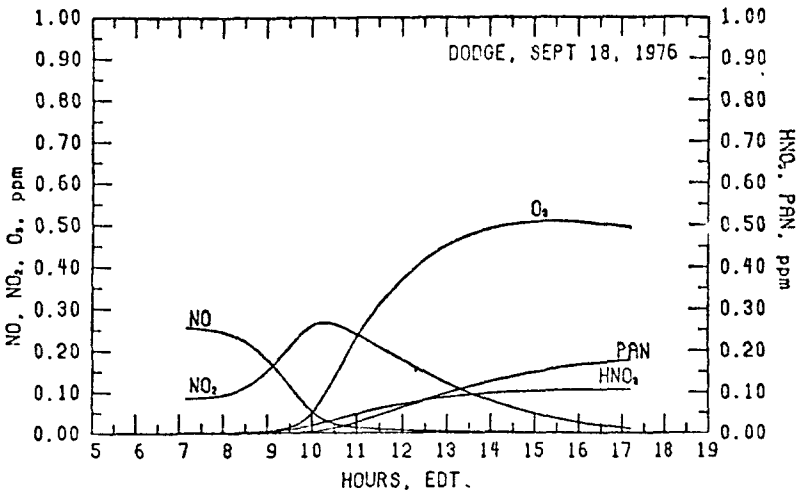

Simulation with DODGE mechanism. Initial conditions: NO 0.255 ppm, NO_2 0.085 ppm, O_3 0.1 ppb, H_2O $2x10^4$ ppm, propylene 0.258 ppmV, butane 0.581 ppmV, HCHO 0.100 ppmV; photolysis rates scaled to TSR for September 18.

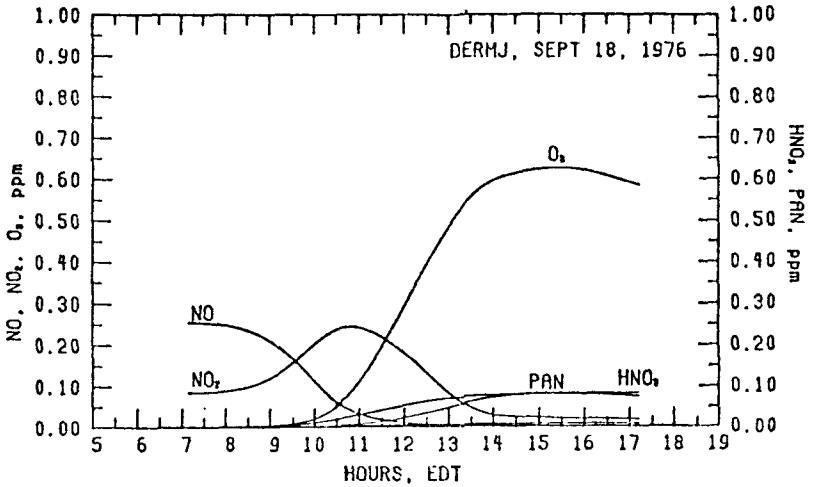

Simulation with DERMJ mechanism. Initial conditions: NO 0.255 ppm, NO_2 0.085 ppm, CO 0.4 ppm, H_2O $2x10^4$ ppm, HC1 0.2155 ppmV, HC2 0.1789 ppmV, HC3 0.1643 ppmV, HC4 0.1113 ppmV, photolysis rates scaled to TSR for September 18.

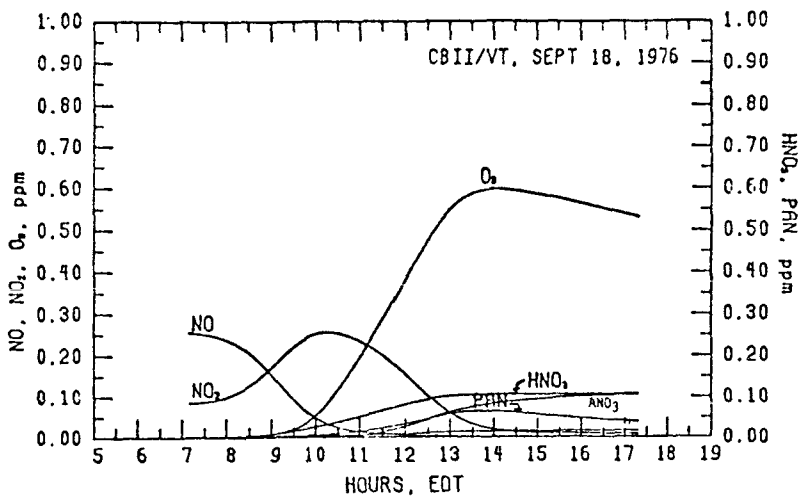

Simulation with CARBON BOND II using variable temperatures. Initial conditions: NO 0.255 ppm, NO_2 0.085 ppm, CO 0.4 ppm, O_3 0.1 ppb, H_2O $2x10^4$ ppm, olefin 0.051 ppmV, ethylene 0.051 ppmV, paraffin 1.953 ppmV, aromatic 0.124 ppmV, HCHO 0.115 ppmV; photolysis rates scaled to TSR for September 18.

Figure 9. Models of September 18, 1976.

chamber halves with little effect on O_3 production (see Figure 10). When this same kind of compositional change was simulated by the two mechanisms (Figure 11 and 12) large changes in O_3 were predicted. For the Carbon Bond mechanism, the effects reverse and increase with increasing concentration, whereas for Demerjian, the effect is decreased with increasing concentration.

Considering its overall behavior and its more recent development history, the Carbon Bond II mechanism would appear to be the more reasonably choice for describing the chemistry in urban simulations; it does, however, probably overrespond to hydrocarbon compositional changes. Except for its consistent overprediction (12% of the nitrogen) of peroxynitric acid, the Demerjian mechanism is quite close to the Carbon Bond mechanism. Both provide better descriptions than the older Dodge mechanism in these outdoor smog chamber comparisons.

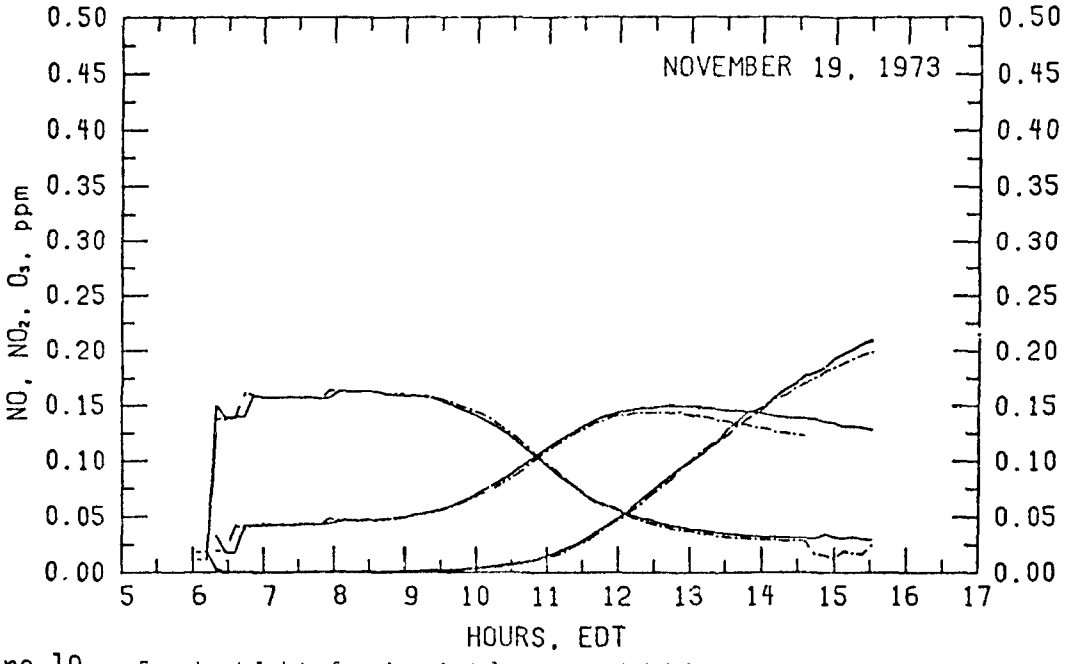

Figure 10. Experimental data for mix, mix-toluene run. Initial HC:
(——) 2.28 ppmC mix, 8.8% acetylene, 64.3% paraffins, 27.0% olefins, 0% aromatics;
(---) 2.34 ppmC mix, 5.3% acetylene, 38.9% paraffins, 16.3% olefins, 39.5% toluene.

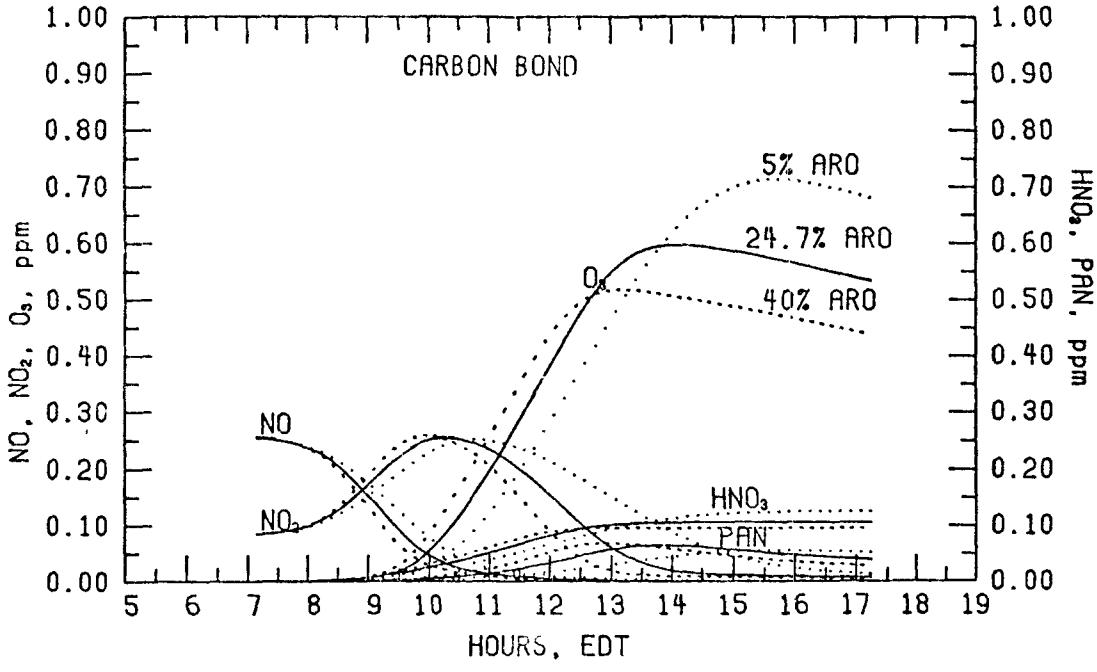

Figure 11a. Effects of compositional change on Carbon Bond II mechanism predictions. Initial HC: 3.1 ppmC.

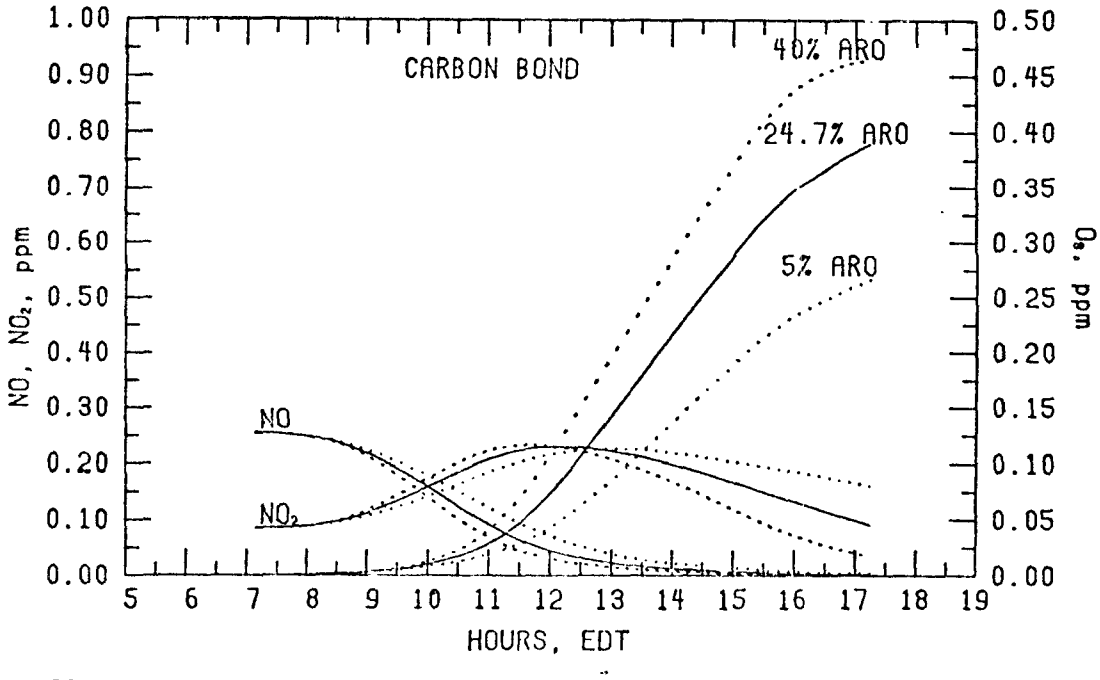

Figure 11b. Effects of compositional change on Carbon Bond II mechanism predictions. Initial HC: 1.5 ppmC.

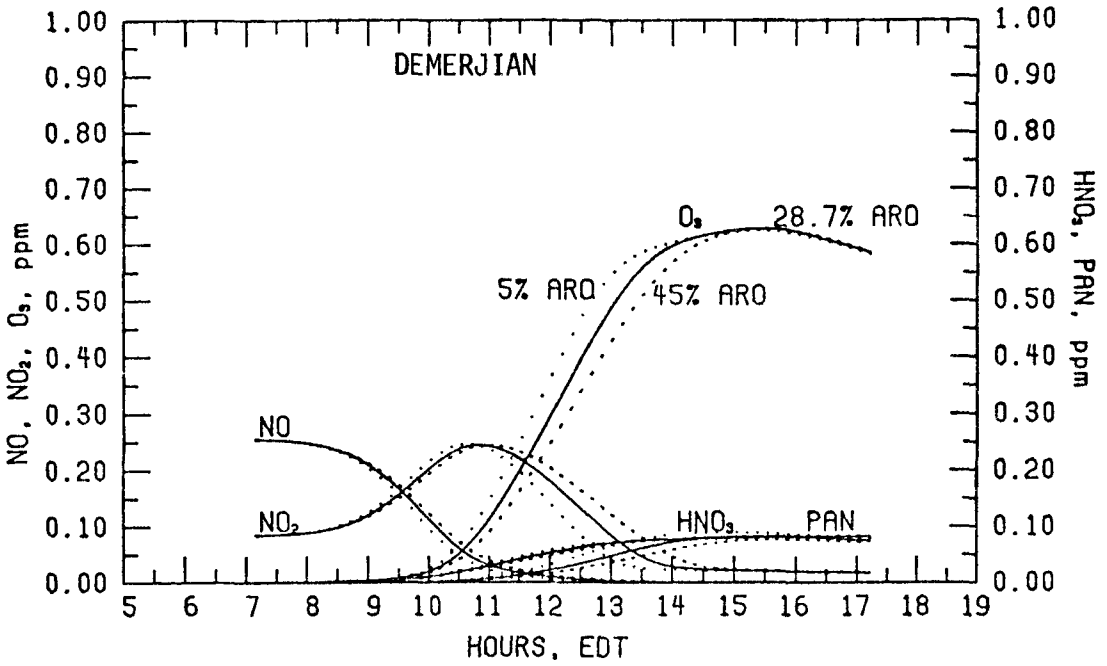

Figure 12a. Effects of compositional change on Demerjian mechanism predictions. Initial HC: 3.1 ppmC.

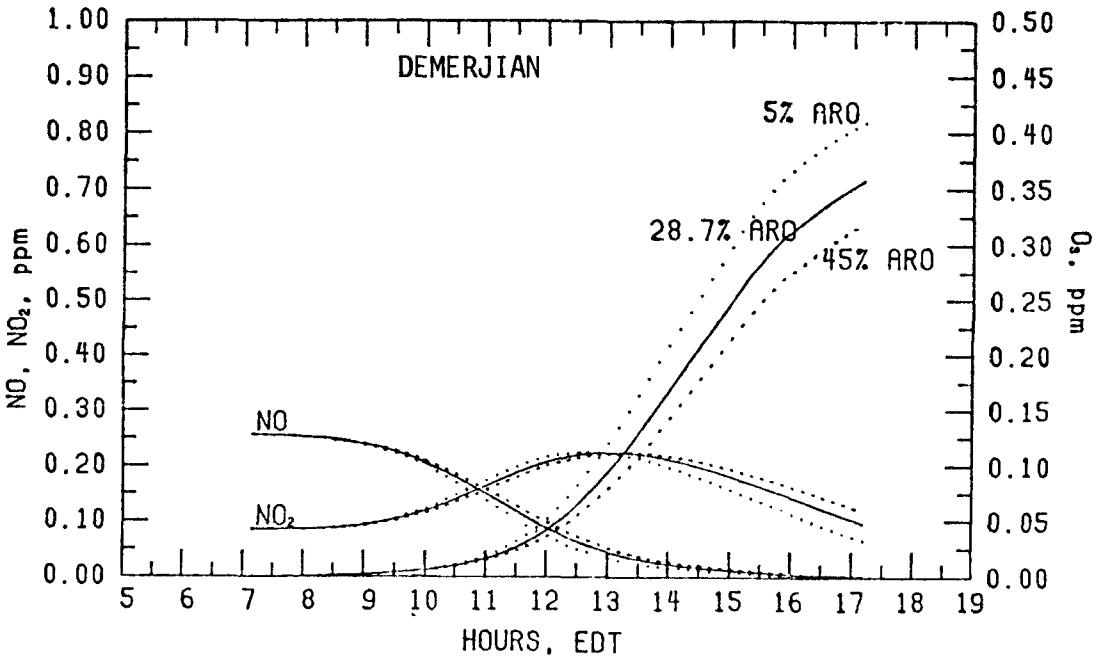

Figure 12b. Effects of compositional change on Demerjian mechanism predictions. Initial HC: 1.5 ppmC.

3.1.2 OAQPS/EPA OZIPP/EKMA Study

In early 1980 the Air Management Technology Branch of OAQPS conducted an evaluation of EKMA using the St. Louis RAPS database (Gipson, 1980). The purpose of the study was to assess how well the kinetics model imbedded in OZIPP (i.e. the Dodge mechanism) performs when atmospheric, rather than smog chamber data, were used for comparison. In the actual performance of of the study, OZIPP was operated as a "Level II" type model for ten days in St. Louis in 1976. The ambient data came from the RAPS database. In effect, the study was the prototype for Level II-type SIP revision model applications, and emphasis was placed on the models' ability to predict absolute ozone concentrations. A large number of methods for estimating input data had to be developed. Several specific computer programs to manipulate the extensive RAPS database were written and substantial amounts of

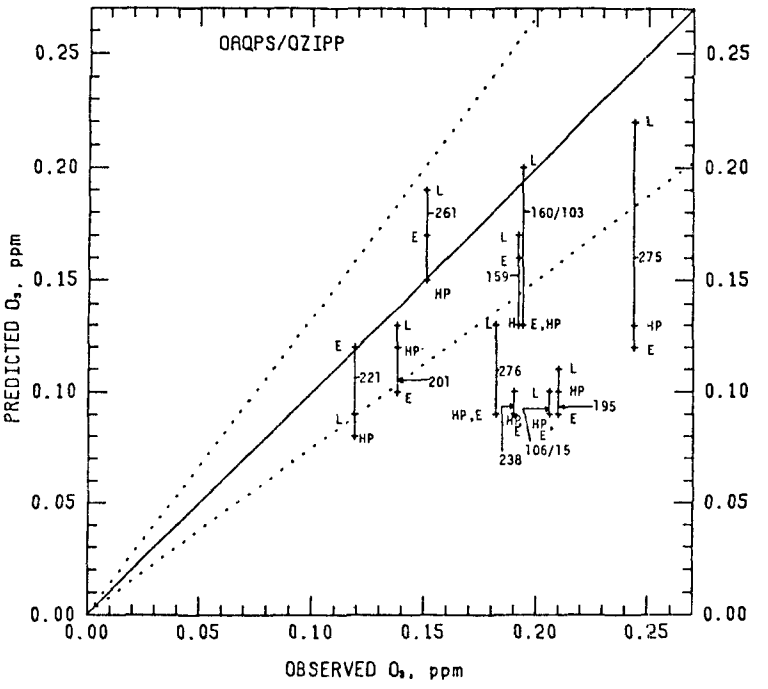

Figure 13. Scatter diagram for OAQPS OZIPP/DODGE simulation of RAPS days. See Table 15 for day identification. E=exponential, HP= hand-picked, and L=linear mixing height profiles.

data processing were performed for the ten selected days. The choices of the researchers were tempered, however, by the fact that the methods would have to be usable by state control agencies in performing SIP revisions.

The same ten RAPS days and much of the data already produced became the basis of the RAPS portion of this study. The procedures used to generate the data and the data themselves, therefore, will be presented in detail in Chapter 7.0.

One of the factors investigated in the OAQPS study was choice of mixing height profiles; the performance with the OZIPP default exponential dilution pattern was very poor. A linear interpolation method supposedly similar to that in the SAI airshed model and values determined by a meteorologist calculating from surface temperatures and soundings were the other methods. The peak O_3 and subsequent EKMA control calculations were found to be quite sensitive to the dilution pattern (see Figure 13). A conclusion was that a more appropriate mixing height profile method was needed and that other sensitivity studies would need to consider the mixing height specification problem.

It was difficult to judge how much of the underprediction problem that occurred on many days was associated with the Dodge chemistry. Combined with an assumption that different groups would choose different chemical mechanisms, the underprediction problems described above suggested that the study described herein was required to verify the effect of chemistry.

3.2 APPROACH

3.2.1 General Concept

Based on the previous described studies and other on-going developments, several mechanisms were considered: the Dodge mechanism, the Carbon Bond II mechanism, the Demerjian mechanism, the California Institute of

Technology mechanism (expected to be used in California's SIP), and an updated propylene-butane mechanism based on the most recent smog chamber work. The updated propylene-butane mechanism was deleted because of the extensive work that would be needed to determine a new propylene-butane carbon fraction split needed to model the BOM data.

Because the standard EPA method (OZIPP) used the Dodge mechanism and it had been validated against the BOM data, it was decided to compare all the mechanisms using the BOM conditions. Furthermore, it was decided to use all 31 BOM runs instead of the 14 used by Dodge in the 1977 study. In the BOM experiments, the light intensity was constant, and the chamber operation was static (i.e. all material present initially, no additions of material during the experiment and little dilution).

Because the information was readily available or could be determined by slight modifications of existing programs, the same days as were being studied in-house at OAQPS would be used for the ambient database. In the ambient RAPS data, the intensity and spectral distribution of the light changed, the hydrocarbon composition changed, the majority of the reactant was added throughout the day, and the dilution was often very large.

The exponential mixing height rise that is standard in OZIPP was determined by OAQPS to be unrealistic and they were seeking simple alternatives in their study. Two methods were being examined: a linear interpolation of soundings similar to that in the SAI airshed model and a method in which the mixing height was estimated each hour by surface temperatures and soundings. To these was added the "characteristic curve" method of Demerjian and Schere used in the photochemical box model.

This study, therefore, used four mechanisms, three mixing height profile methods, and two databases for comparison.

3.2.2 Project Tasks

1) Acquire BOM data base and determine assumptions necessary for modeling.
2) Simulate BOM experiments with mechanisms selected for study and compare.
3) Examine OZIPM program and deduce algorithms - write program for simple trajectory model with expanded (and corrected, if necessary) algorithms allowing for features and capabilities to aid in the study.
4) Determine for each mechanism how to convert emission inventory to inputs for each mechanism and provide documentation of this process.
5) Perform simulations along the trajectories with each of the mechanisms for each of ten days, the days and data to be supplied by EPA.
6) Compare mechanism simulations with each other.
7) Provide analysis of the results in 6 above which may require additional simulations and comparisons.
8) Generate isopleth diagrams for selected days and calculate control requirements for each mechanism for each day selected, for three choices of mixing height data.
9) Provide analysis of the results in 8 above which may require additional isopleth diagrams be generated for comparison.
10) Generate a report documenting the work performed and providing conclusions and recommendations.

4.0 CHEMICAL KINETICS MECHANISMS

4.1 SELECTION

Many mechanisms have been developed for modeling photochemical oxidant systems. Four mechanisms were selected for this study on the basis of the likelihood that they might be utilized in Level II or III applications.

The mechanisms selected were:

1) Dodge - currently used in OZIPP
2) Carbon Bond II - used in the SAI airshed grid model
3) Demerjian - used in the Photochemical Box model
4) California Institute of Technology - used in Cal Tech airshed model.

Each mechanism also reflects a different approach to representing the photochemical smog system. The Dodge mechanism consists of explicit chemistry of propylene and butane and NO_X, and is tuned to simulate the reactivity of urban NMHC mixtures by assuming the initial NMHC consists of a specific mixture of butane and propylene. The Carbon Bond II mechanism has reactions for carbon bond classes (i.e. sigma, pi, aromatic, and carbonyl) and an inorganic NO_X section. The Demerjian mechanism has reactions for HC classes (olefin, paraffin, aromatic, aldehyde) and inorganic NO_X chemistry. The CIT mechanism also uses hydrocarbon classes and is generally more explicit than Demerjian, with a separate set of ethylene reactions, and separate formaldehyde chemistry.

4.2 MECHANISM REACTIONS

Table 5 lists the characteristics of each mechanism. Besides the

Table 5. Mechanism Characteristics

ITEM	DODGE	CBII	DEMER	CIT[c]
Reactions:				
tot num	76	75	36	52
i/o[a]	23/53	14/61	19/17	25/27
temp[b]	0	6	0	11
H_2O[b]	3	1	1	1
light[b]	12	4	3	8
Species:				
total	36	30	23	26
i/o	12/24	9/21	12/11	13/13
major	C_3H_6, C_4H_{10}	PAR, OLE	HC1, HC2	ALK, OLE, ARO
organic	C_1-C_4 ald, MEK	ETH, CARB, ARO	HC3, HC4	ETH, HCHO, RCHO
N-species	NO_x, HNO_3 PAN, (HONO)	NO_x, HNO_3 PAN, RNO_3 $ARONO_3$	NO_x, HNO_3 PAN, HO_2NO_2 RNO_3, (HONO)	NO_x, HNO_3 PAN, HNO_4, RNO_4 RNO_3, HNO_2, RONO (HONO)
Chamber comparison:	BOM	UCR, UNC	BOM	UCR
Comments:	EKMA mechanisms	SAI airshed model mechanism	Photochemical Box model	CAL TECH airshed model mechanism

[a] number of inorganic/number of organic

[b] number of reactions with rate constants dependent on temperature, water vapor, or light intensity

[c] CIT, California Institute of Technology mechanism

differences mentioned above, these mechanisms also vary widely in the number of NO_X species represented and the number of water, temperature, and light dependent reactions.

Tables 6, 7, 8, and 9 list the mechanisms as actually represented in the models. Light dependent reactions are indicated by "HV" in the arrow of the reaction. Water dependent reactions are indicated with "H_2O" in parentheses before the reaction rate constant listed under the A factor column. Temperature dependent reactions have an activation energy value listed under the appropriate column.

The Dodge mechanism was obtained from the computer code for OZIPP. The other mechanisms were obtained from the developers directly. Instructions and guidance for mechanism use were obtained from publications and personal communication with the developers. Final verification was performed by matching supplied example simulations. Figures 14 and 15 are example verification model runs performed for the CIT mechanism. Figure 15 shows the simulations of chamber experiment SUR-119J (supplied by McRae) by both the CIT model and program and the UNC implemented model and program. The numerical results were identical to 4 decimal places. Figure 14 shows the chamber data and the simulation performed by the CIT mechanism with the UNC implemented model and program. These are identical to the results sent to us by McRae as an example of his mechanism.

The tests clearly indicated that each mechanism had been implemented correctly.

Table 6. The Dodge Mechanism

* * * \

Table 6. The Dodge Mechanism (continued)

28)	C3O2	+ ADD	------>	1.00 X	+ 1.00 C3O				1.000E+03	<1.000E+03>2
29)		X	------>	1.00 HCHO	+ 1.00 ALD2	+ 1.00 HO2			1.000E+05	<1.000E+05>1
30)	O3	+ PROP	------>	1.00 OH	+ 1.00 HO2	+ 1.00 ALD2			8.000E-03	<8.000E-03>2
31)	O3	+ PROP	------>	1.00 OH	+ 1.00 C2O3	+ 1.00 HCHO			8.000E-03	<8.000E-03>2
32)	OH	+ BUT	------>	1.00 SCO2					1.800E+03	<1.800E+03>2
33)	OH	+ BUT	------>	1.00 C4O2					1.800E+03	<1.800E+03>2
34)	C4O2	+ NO	------>	1.00 NO2	+ 1.00 C4O				1.800E+03	<1.800E+03>2
35)	SCO2	+ NO	------>	1.00 NO2	+ 1.00 SCO				1.800E+03	<1.800E+03>2
36)	C3O2	+ NO	------>	1.00 NO2	+ 1.00 C3O				8.000E+02	<8.000E+02>2
37)	C2O2	+ NO	------>	1.00 NO2	+ 1.00 C2O				1.800E+03	<1.800E+03>2
38)	MEO2	+ NO	------>	1.00 NO2	+ 1.00 MEO				1.800E+03	<1.800E+03>2
39)		C4O	------>	1.00 HCHO	+ 1.00 C3O2				7.500E+04	<7.500E+04>1
40)		SCO	------>	1.00 ALD2	+ 1.00 C2O2				1.000E+05	<1.000E+05>1
41)		C3O	------>	1.00 HCHO	+ 1.00 C2O2				8.000E+03	<8.000E+03>1
42)		C2O	------>	1.00 HCHO	+ 1.00 MEO2				4.000E+03	<4.000E+03>1
43)		C4O	------>	1.00 ALD4	+ 1.00 HO2				1.470E+05	<1.470E+05>1
44)		SCO	------>	1.00 MEK	+ 1.00 HO2				2.940E+05	<2.940E+05>1
45)		C3O	------>	1.00 ALD3	+ 1.00 HO2				1.050E+05	<1.050E+05>1
46)		C2O	------>	1.00 ALD2	+ 1.00 HO2				8.400E+04	<8.400E+04>1
47)		MEO	------>	1.00 HCHO	+ 1.00 HO2				8.400E+04	<8.400E+04>1
48)		HCHO	--UV-->						2.690E+00	<5.111E-03>1
49)		HCHO	--UV-->	2.00 HO2					1.000E+00	<1.900E-03>1
50)	OH	+ HCHO	------>	1.00 HO2	+ 1.00 CO				1.500E+04	<1.500E+04>2
51)		ALD2	------>						4.200E-06	<4.200E-06>1
52)		ALD2	--UV-->	1.00 MEO2	+ 1.00 HO2				5.700E-01	<1.083E-03>1
53)	OH	+ ALD2	------>	1.00 C2O3					1.500E+04	<1.500E+04>2
54)		ALD3	------>						6.000E-05	<6.000E-05>1
55)		ALD3	------>	1.00 C2O2	+ 1.00 HO2				2.500E-03	<2.500E-03>1
56)	OH	+ ALD3	------>	1.00 C3O3					4.500E+04	<4.500E+04>2
57)		ALD4	------>						6.000E-05	<6.000E-05>1

Table 6. The Dodge Mechanism (continued)

58)			ALD4	------>	1.00 C3O2	+ 1.00 HO2	1.900E-03	<1.900E-03>1
59)	OH	+	ALD4	------>	1.00 C4O3		4.500E+04	<4.500E+04>2
60)	C4O2	+	ADD	------>	1.00 X	+ 1.00 C4O	1.000E+03	<1.000E+03>2
61)	SCO2	+	ADD	------>	1.00 X	+ 1.00 SCO	1.000E+03	<1.000E+03>2
62)	NO	+	C4O3	------>	1.00 C3O2	+ 1.00 NO2	8.000E+02	<8.000E+02>2
63)	NO	+	C3O3	------>	1.00 C2O3	+ 1.00 NO2	8.000E+02	<8.000E+02>2
64)	NO	+	C2O3	------>	1.00 MEO2	+ 1.00 NO2	8.000E+02	<8.000E+02>2
65)	NO2	+	C4O3	------>	1.00 PAN		1.000E+02	<1.000E+02>2
66)	NO2	+	C3O3	------>	1.00 PAN		1.000E+02	<1.000E+02>2
67)	NO2	+	C2O3	------>	1.00 PAN		1.000E+02	<1.000E+02>2
68)	HO2	+	C4O2	------>			4.000E+03	<4.000E+03>2
69)	HO2	+	C3O2	------>			4.000E+03	<4.000E+03>2
70)	HO2	+	SCO2	------>			4.000E+03	<4.000E+03>2
71)	HO2	+	C2O2	------>			4.000E+03	<4.000E+03>2
72)	HO2	+	MEO2	------>			4.000E+03	<4.000E+03>2
73)	HO2	+	C4O3	------>			4.000E+03	<4.000E+03>2
74)	HO2	+	C3O3	------>			4.000E+03	<4.000E+03>2
75)	HO2	+	C2O3	------>			4.000E+03	<4.000E+03>2
76)			NR	------>	1.00 NR		1.000E-06	<1.000E-06>1

Table 7. The Demerjian Mechanism

```
* * * * * * * * * * * * * * * * * * * * * * * * * * M E C H A N I S M * * * * * * * * * * * * * * * * * * * * * * * * * * *
                    DERMERJIAN MECHANISM
NUM        REACTANTS                                    PRODUCTS                                          A FACTOR     ACT ENG     STD RATE  U
---  ------------------------  ---------------------------------------------------------------------  ----------  ----------  ------------
 1)                 NO2    --HV--> 1.00 NO     + 1.00 O                                                 1.000E+00               <5.000E-01>1
 2)                 O      ------> 1.00 O3                                                              4.200E+06               <4.200E+06>1
 3)          O3   + NO     ------> 1.00 NO2                                                             2.200E+01               <2.200E+01>2
 4)          O3   + NO2    ------> 1.00 NO3                                                             5.500E-02               <5.500E-02>2
 5)          NO3  + NO     ------> 2.00 NO2                                                             1.100E+04               <1.100E+04>2
 6)          NO3  + NO2    ------> 2.00 WHNO3                                          (H2O)            3.400E-03               <6.800E+01>2
 7)                 HNO2   --HV--> 1.00 HO     + 1.00 NO                                                 1.866E-01               <9.330E-02>1
 8)          HO   + CO     ------> 1.00 HO2    + 1.00 CO2                                               4.400E+02               <4.400E+02>2
 9)          HO2  + NO2    ------> 1.00 HNO2                                                            4.300E+00               <4.300E+00>2
10)          HO2  + NO     ------> 1.00 HO     + 1.00 NO2                                               1.200E+04               <1.200E+04>2
11)          HO2  + NO2    ------> 1.00 HO4N                                                            2.340E+03               <2.340E+03>2
12)                 HO4N   ------> 1.00 HO2    + 1.00 NO2                                               9.000E+00               <9.000E+00>1
13)          HO   + HNO2   ------> 1.00 NO2                                                             9.600E+03               <9.600E+03>2
14)          HO   + NO2    ------> 1.00 HNO3                                                            1.500E+04               <1.500E+04>2
15)          HO   + NO     ------> 1.00 HNO2                                                            1.200E+04               <1.200E+04>2
16)          HO2  + O3     ------> 1.00 HO                                                              4.000E+00               <4.000E+00>2
17)          HO   + O3     ------> 1.00 HO2                                                             8.700E+01               <8.700E+01>2
18)          HO2  + HO2    ------> 0.50 H2O2                                                            1.000E+04               <1.000E+04>2
19)          OLE  + O      ------> 1.00 RO2    + 1.00 ALD    + 1.00 HO2                                 5.100E+03               <5.100E+03>2
20)          OLE  + O3     ------> 1.00 RO2    + 1.00 ALD    + 1.00 HO2                                 1.700E-02               <1.700E-02>2
21)          OLE  + HO     ------> 1.00 RO2    + 1.00 ALD                                               3.700E+04               <3.700E+04>2
22)          PAR  + HO     ------> 1.00 RO2                                                             5.000E+03               <5.000E+03>2
23)                 ALD    --UV--> 0.50 RO2    + 1.50 HO2    + 1.00 CO                                  1.000E+00               <1.900E-03>1
24)          ALD  + HO     ------> 0.50 R1O2   + 0.50 HO2                                               2.200E+04               <2.200E+04>2
25)          RO2  + NO     ------> 1.00 RO     + 1.00 NO2                                               2.000E+03               <2.000E+03>2
26)                 RO     ------> 1.00 ALD    + 1.00 HO2                                               9.240E+02               <9.240E+02>1
27)          R1O2 + NO2    ------> 1.00 PAN                                                             2.100E+03               <2.100E+03>2
```

Table 7. The Demerjian Mechanism (continued)

28)	RO	+ NO2	------>	1.00 RNO3				1.200E+02	<1.200E+02>2
29)	RO2	+ O3	------>	1.00 RO				2.000E+00	<2.000E+00>2
30)	R1O2	+ NO	------>	1.00 RO2	+ 1.00 NO2			3.800E+03	<3.800E+03>2
31)		PAN	------>	1.00 R1O2	+ 1.00 NO2			1.100E-01	<1.100E-01>1
32)	ARO	+ HO	------>	1.00 R2O2	+ 2.00 ALD	+ 1.00 CO		2.000E+04	<2.000E+04>2
33)	R2O2	+ NO	------>	1.00 R2O	+ 1.00 NO2			2.000E+03	<2.000E+03>2
34)		R2O	------>	1.00 ALD	+ 1.00 HO2	+ 2.00 CO		2.100E+03	<2.100E+03>1
35)	R2O2	+ O3	------>	1.00 R2O				2.000E+00	<2.000E+00>2
36)	R1O2	+ O3	------>	1.00 RO2				2.000E+00	<2.000E+00>2
37)		NR	------>	1.00 NR				1.000E-06	<1.000E-06>1

Table 8. The Carbon Bond II Mechanism

* * * \

Table 8. The Carbon Bond II Mechanism (continued)

28)	PARC	+ X	------>					1.000E+05	<1.000E+05>2
29)	O	+ PARC	------>	1.00 MEO2	+ 1.00 OH			2.000E+01	<2.000E+01>2
30)	OH	+ PARC	------>	1.00 MEO2				1.500E+03	<1.500E+03>2
31)	O	+ ETHC	------>	1.00 MEO2	+ 1.00 HO2	+ 1.00 CO		6.000E+02	<6.000E+02>2
32)	O	+ ETHC	------>	1.00 CARB				6.000E+02	<6.000E+02>2
33)	OH	+ ETHC	------>	1.00 RBO2				1.200E+04	<1.200E+04>2
34)	O3	+ ETHC	------>	1.00 CARB	+ 1.00 CRIG			2.400E-03	<2.400E-03>2
35)	O	+ OLEC	------>	1.00 ACO3	+ 1.00 MEO2	+ 1.00 X		2.700E+03	<2.700E+03>2
36)	O	+ OLEC	------>	1.00 CARB				2.700E+03	<2.700E+03>2
37)	OH	+ OLEC	------>	1.00 RAO2				4.200E+04	<4.200E+04>2
38)	NO	+ RAO2	------>	1.00 NO2	+ 2.00 CARB	+ 1.00 HO2		1.200E+04	<1.200E+04>2
39)	NO	+ RBO2	------>	1.00 NO2	+ 2.00 CARB	+ 1.00 HO2		1.200E+04	<1.200E+04>2
40)	O3	+ OLEC	------>	1.00 CARB	+ 1.00 CRIG			8.000E-03	<8.000E-03>2
41)	O3	+ OLEC	------>	1.00 CARB	+ 1.00 MCRG			8.000E-03	<8.000E-03>2
42)	NO	+ CRIG	------>	1.00 NO2	+ 1.00 CARB			1.200E+04	<1.200E+04>2
43)	NO2	+ CRIG	------>	1.00 NO3	+ 1.00 CARB			8.000E+03	<8.000E+03>2
44)	CARB	+ CRIG	------>	1.00 OZD				2.000E+03	<2.000E+03>2
45)		CRIG	------>	2.00 HO2	+ 1.00 CO2			9.000E+01	<9.000E+01>1
46)		CRIG	------>	1.00 CO				6.700E+02	<6.700E+02>1
47)		CRIG	------>					2.400E+02	<2.400E+02>1
48)	NO	+ MCRG	------>	1.00 NO2	+ 1.00 CARB			1.200E+04	<1.200E+04>2
49)	NO2	+ MCRG	------>	1.00 NO3	+ 1.00 CARB			8.000E+03	<8.000E+03>2
50)	CARB	+ MCRG	------>	1.00 OZD				2.000E+03	<2.000E+03>2
51)		MCRG	------>	2.00 X	+ 2.00 MEO2			1.700E+02	<1.700E+02>1
52)		MCRG	------>	2.00 CO	+ 2.00 OH			1.700E+02	<1.700E+02>1
53)		MCRG	------>	2.00 HO2	+ 1.00 CARB	+ 1.00 CO		8.500E+01	<8.500E+01>1
54)		MCRG	------>	1.00 CO2	+ 1.00 MEO2	+ 1.00 HO2		4.250E+02	<4.250E+02>1
55)		MCRG	------>					1.500E+02	<1.500E+02>1
56)	O3	+ MEO2	------>	1.00 CARB	+ 1.00 HO2			5.000E+00	<5.000E+00>2
57)	O3	+ RAO2	------>	2.00 CARB	+ 1.00 HO2			2.000E+02	<2.000E+02>2

Table 8. The Carbon Bond II Mechanism (continued)

58)	O3	+ RBO2	------>	2.00 CARB	+ 1.00 HO2				5.000E+00	<5.000E+00>2
59)	HO2	+ ACO3	------>						4.000E+03	<4.000E+03>2
60)	HO2	+ MEO2	------>						4.000E+03	<4.000E+03>2
61)	OH	+ AROL	------>	3.00 ARPI	+ 1.00 HO2				6.000E+03	<6.000E+03>2
62)	OH	+ AROL	------>	1.00 HO2	+ 1.00 GLY	+ 1.00 X			1.600E+03	<1.600E+03>2
63)	OH	+ AROL	------>	1.00 OH	+ 1.00 GLY	+ 1.00 W			1.500E+04	<1.500E+04>2
64)	NO	+ ARPI	------>	1.00 NO	+ 1.00 CARB	+ 1.00 PARC			3.000E+01	<3.000E+01>2
65)	NO	+ ARPI	------>	1.00 NO2					1.500E+01	<1.500E+01>2
66)	NO3	+ ARPI	------>	2.00 CARB	+ 1.00 ARN				3.500E+04	<3.500E+04>2
67)	O3	+ ARPI	------>	3.00 AERO					6.000E-01	<6.000E-01>2
68)	CARB	+ W	------>						1.000E+05	<1.000E+05>2
69)		GLY	--HV-->	1.00 MEO2	+ 1.00 HO2	+ 3.00 ARPI			3.600E-02	<1.800E-02>1
70)	OH	+ GLY	------>	1.00 HO2	+ 3.00 ARPI	+ 1.00 CO			1.000E+04	<1.000E+04>2
71)		NR	------>	1.00 NR					1.000E-06	<1.000E-06>1

Table 9. The California Institute of Technology Mechanism

* M E C H A N I S M *

CAL TECH MECHANISM

NUM	REACTANTS		PRODUCTS				A FACTOR	ACT ENG	STD RATE U
1)		NO2	--HV--> 1.00 NO	+ 1.00 O			1.000E+00		<5.000E-01>1
2)		O	------> 1.00 O3				7.896E+05*EXP(5.100E+02/T)		<4.372E+06>1
3)	NO	+ O3	------> 1.00 NO2				3.050E+03*EXP(-1.450E+03/T)		<2.350E+01>2
4)	O	+ NO2	------> 1.00 NO				1.320E+04		<1.320E+04>2
5)	O	+ NO	------> 1.00 NO2				5.550E+02*EXP(5.840E+02/T)		<3.939E+03>2
6)	O	+ NO2	------> 1.00 NO3				3.580E+03		<3.580E+03>2
7)	O3	+ NO2	------> 1.00 NO3				1.740E+02*EXP(-2.450E+03/T)		<4.677E-02>2
8)	NO	+ NO3	------> 1.00 NO2	+ 1.00 NO2			2.720E+04		<2.720E+04>2
9)	NO2	+ NO3	------> 1.00 N2O5				2.190E+02*EXP(8.610E+02/T)		<3.938E+03>2
10)		N2O5	------> 1.00 NO2	+ 1.00 NO3			7.440E+15*EXP(-1.032E+04/T)		<6.854E+00>1
11)		N2O5	------> 1.00 HNO3	+ 1.00 HNO3		(H2O)	1.450E-05		<2.900E-01>1
12)	NO	+ OH	------> 1.00 HNO2				1.740E+04		<1.740E+04>2
13)		HNO2	--HV--> 1.00 OH	+ 1.00 NO			1.840E-01		<9.200E-02>1
14)	NO2	+ HO2	------> 1.00 HNO2				5.800E-02*EXP(1.006E+03/T)		<1.696E+00>2
15)	HNO2	+ OH	------> 1.00 NO2				9.590E+03		<9.590E+03>2
16)	NO2	+ HO2	------> 1.00 HNO4				5.730E+01*EXP(1.006E+03/T)		<1.676E+03>2
17)		HNO4	------> 1.00 HO2	+ 1.00 NO2			1.720E+15*EXP(-1.002E+04/T)		<4.365E+00>1
18)	NO	+ HO2	------> 1.00 NO2	+ 1.00 OH	+ 1.00 CON1		1.180E+04		<1.180E+04>2
19)	RO2	+ NO	------> 1.00 NO2	+ 1.00 RO	+ 1.00 CON2		1.180E+04		<1.180E+04>2
20)	RCO3	+ NO	------> 1.00 NO2	+ 1.00 RO2	+ 1.00 CON3		3.800E+03		<3.800E+03>2
21)	NO2	+ OH	------> 1.00 HNO3				1.500E+04		<1.500E+04>2
22)	OH	+ CO	------> 1.00 HO2				4.400E+02		<4.400E+02>2
23)		O3	--HV--> 1.00 O				7.188E-02		<3.594E-02>1
24)	O3	+ OH	------> 1.00 HO2				2.360E+03*EXP(-1.000E+03/T)		<8.233E+01>2
25)	O3	+ HO2	------> 1.00 OH				1.080E+02*EXP(-1.275E+03/T)		<1.497E+00>2
26)	HO2	+ HO2	------> 1.00 H2O2				3.700E+03		<3.700E+03>2
27)		H2O2	--HV--> 2.00 OH				2.560E-03		<1.280E-03>1

Table 9. The California Institute of Technology Mechanism (continued)

28)		HCHO	--HV-->	2.00 HO2	+ 1.00 CO	+ 1.00 NEW1	3.750E-03	<1.875E-03>1
29)		HCHO	--HV-->	1.00 CO			8.100E-03	<4.050E-03>1
30)	OH	+ HCHO	------>	1.00 HO2	+ 1.00 CO		1.389E+04	<1.389E+04>2
31)		RCHO	--HV-->	1.00 RO2	+ 1.00 HO2	+ 1.00 CO	3.100E-03	<1.550E-03>1
32)	OH	+ RCHO	------>	1.00 RCO3			2.671E+04	<2.671E+04>2
33)	ETH	+ OH	------>	1.00 RO2			1.168E+04	<1.168E+04>2
34)	ETH	+ O	------>	1.00 RO2	+ 1.00 HO2		1.219E+03	<1.219E+03>2
35)	OLE	+ OH	------>	1.00 RO2			5.952E+04	<5.952E+04>2
36)	OLE	+ O	------>	1.00 RO2	+ 1.00 RCO3		3.933E+04	<3.933E+04>2
37)	OLE	+ O3	------>	0.27 OH	+ 1.00 RCHO	+ 0.61 HO2	5.130E-02	<5.130E-02>2
38)	OLE	+ O3	------>	0.07 RO	+ 1.00 HCHO	+ 0.61 RO2	5.130E-02	<5.130E-02>2
39)	ALK	+ OH	------>	1.00 RO2			7.067E+03	<7.067E+03>2
40)	ALK	+ O	------>	1.00 RO2	+ 1.00 OH		1.210E+02	<1.210E+02>2
41)	OH	+ ARO	------>	1.00 RO2	+ 1.00 RCHO		1.539E+04	<1.539E+04>2
42)		RO	------>	1.00 RCHO	+ 1.00 HO2		2.000E+05	<2.000E+05>1
43)	RO	+ NO	------>	1.00 RONO			4.900E+04	<4.900E+04>2
44)		RONO	--HV-->	1.00 RO	+ 1.00 NO		5.000E-02	<2.500E-02>1
45)	RO	+ NO2	------>	1.00 RNO3			1.550E+04	<1.550E+04>2
46)	RO	+ NO2	------>	1.00 RCHO	+ 1.00 HNO2		1.550E+03	<1.550E+03>2
47)	RO2	+ NO2	------>	1.00 RNO4			5.500E+03	<5.500E+03>2
48)		RNO4	------>	1.00 NO2	+ 1.00 RO2		5.000E-01	<5.000E-01>1
49)	RO2	+ NO2	------>	1.00 RCHO	+ 1.00 HNO3		5.500E+00	<5.500E+00>2
50)	RO2	+ RO2	------>	2.00 RO			1.960E+02	<1.960E+02>2
51)	RCO3	+ NO2	------>	1.00 PAN			2.070E+03	<2.070E+03>2
52)		PAN	------>	1.00 NO2	+ 1.00 RCO3		4.770E+16*EXP(-1.252E+04/T)	<2.743E-02>1
53)		NR	------>	1.00 NH			1.000E-06	<1.000E-06>1

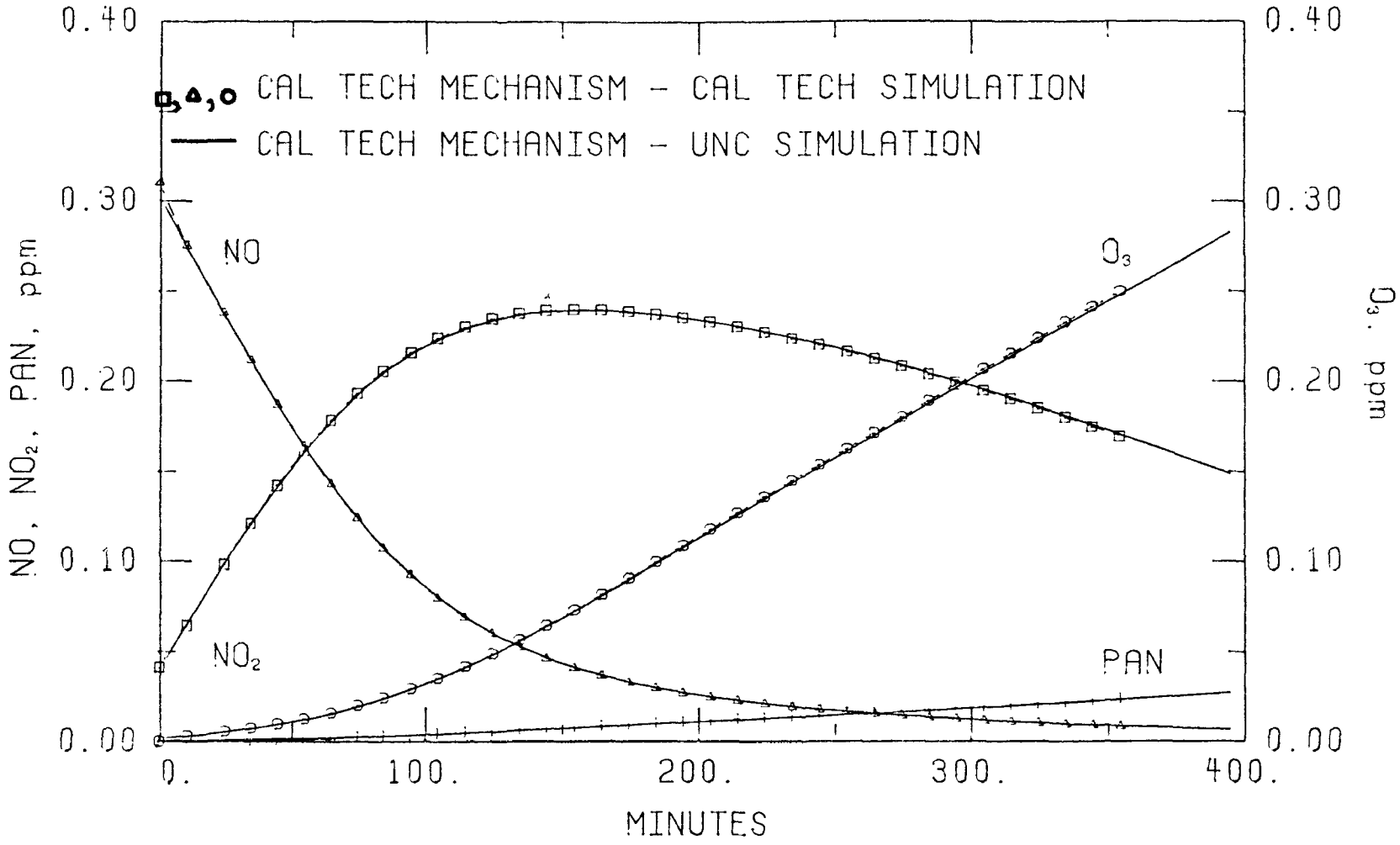

Figure 14. Comparison of California Institute of Technology simulation using the California Institute of Technology mechanism with UNC simulation using the California Institute Mechanism.

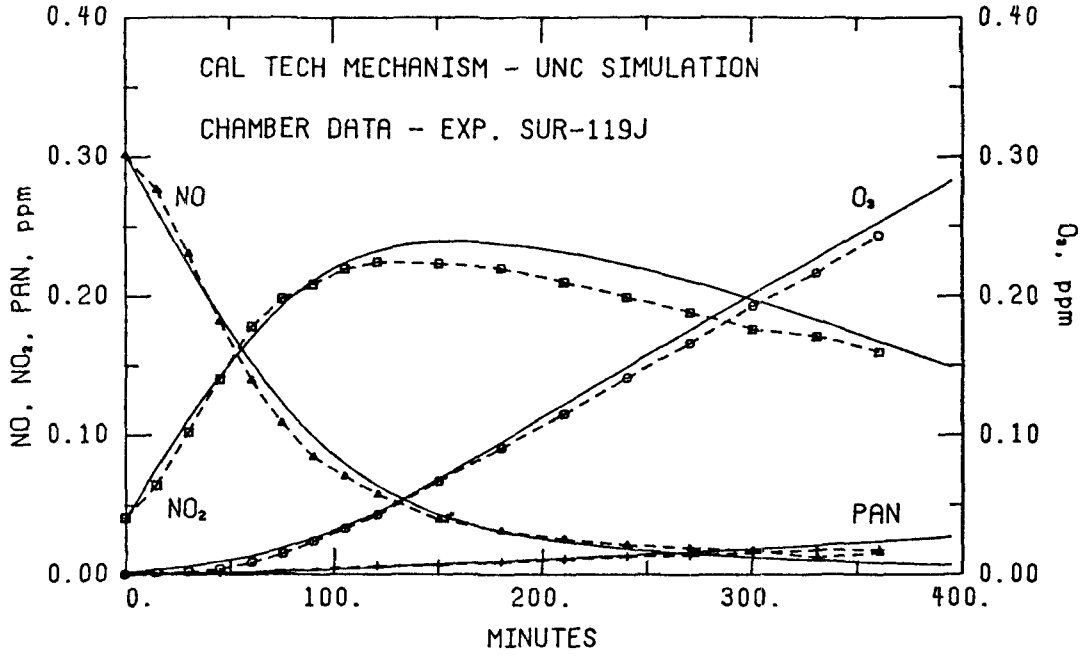

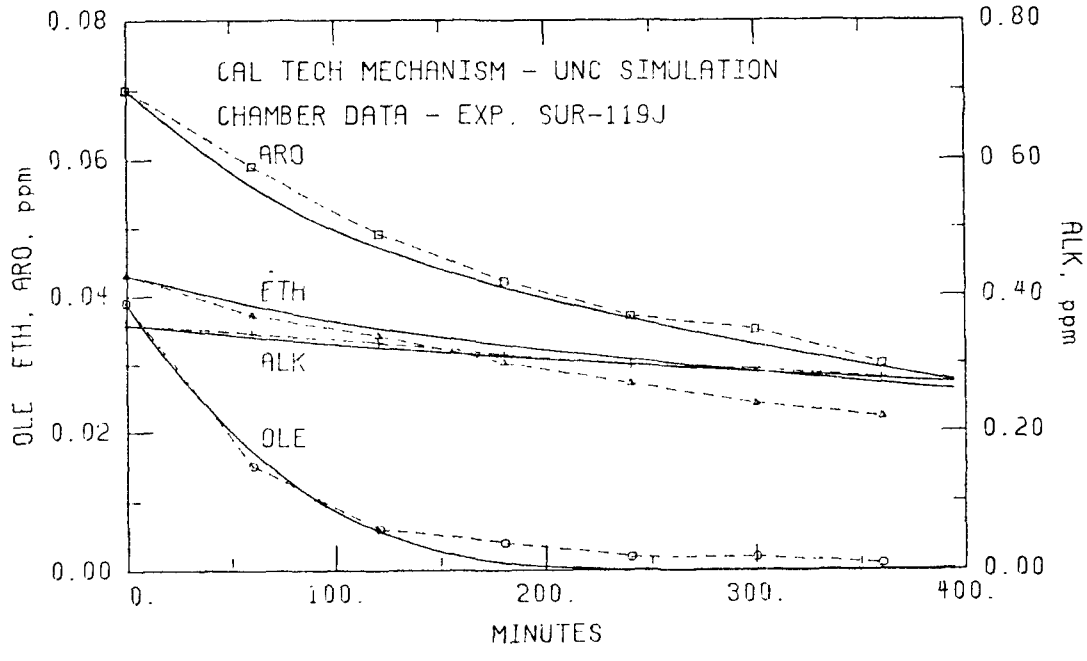

Figure 15. Simulation of University of California-Riverside smog chamber experiment SUR-119J with the CIT mechanism. Model results plotted as solid lines.

4.3 PHOTOLYSIS RATES

4.3.1 Introduction

In constructing generalized, simple mechanisms different investigators make different assumptions about the photolytic (and other) rates used. Since the photolytic reactions are the driving force of photochemical mechanisms, the choice of these rates can be critical; these rate choices are where "tuning" of mechanisms is often accomplished.

Demerjian and Schere (1976) first provided algorithms for computing theoretical rate constants for key photolyzing species. These rate constants are calculated from: 1) the theoretical actinic flux of sunlight as a function of wavelength and zenith angle; 2) the absorption crossection for each specie as a function of wavelength; and 3) the quantum yield for each specie for each photolytic process as a function of wavelength. The theoretical actinic flux is derived from a multilayer atmospheric scattering and absorption model with an assumed O_3 aloft, aerosol distribution, surface albedo, and no clouds. It is an expensive model to run; the output of this model is the usual starting point for all theoretical calculations. Data for items 2 and 3 are determined experimentally and are thus subject to frequent revision as techniques improve.

Dodge used Demerjian and Schere's 1976 values of photolytic rates when she developed her mechanism. When the Dodge mechanism was incorporated into the OZIPP program, the Demerjian and Schere code for calculating rate constants as a function of zenith angle, the theoretical actinic flux numbers, the absorption coefficients, and the quantum yields were built into the OZIPP program. These were the 1976 values. They can only be changed by changing the source code constants and recompiling the program.

In 1980 Demerjian, Schere, and Peterson published a set of new values of photolytic rates based upon new experimental values of absorption coefficients and quantum yields. Furthermore, these new values were to be used with the Demerjian mechanism and had been supplied to Whitten (Carbon Bond mechanism) and McRae (CIT mechanism).

UNC implemented new and more efficient computer code to compute photolytic rates. In this program, actual total solar radiation measurements can be used to adjust the theoretical actinic values before the rate calculation occurs and it is very simple to change absorption coefficients and quantum yields.

The OZIPP source computer code was used to obtain the values for use with the Dodge mechanism. Demerjian and Schere's new values were obtained directly from them.

Table 10 presents both the "new" values and the "old" (OZIPP) values for the common photolyzing species as a function of solar zenith angle. There are some significant differences in the formaldehyde (HCHO) photolysis rates. Both sets of values in Table 10 were used in the simulations performed herein.

The application of the data in Table 10, however is not straightforward because not all mechanisms include all these photolytic species and reactions. The photolytic reactions of O_3, HONO, and H_2O_2 are most often omitted. The photolytic reactions of aldehydes are often combined and/or adjusted by: 1) representing the aldehydes assumed to be present or to be important, by one or more general species; 2) assuming a certain composition of the aldehydes present; 3) assuming a representative set of rate constants for the composition assumed; and 4) adjusting the stoichiometry effecting the ratio of radical products/photolyzing species and the ratio of radical products/stable products for each photolyzing specie.

Table 10

New Values Computed by Demerjian (1980) and Old Values Computed by OZIPP for Photolytic Rates at Selected Solar Zenith Angles

(min^{-1}, values have been multiplied by 10^3)

Species	Zenith Angle (degrees) 0	10	20	30	40	50	60	70	78	86
NO_2, new	532.6	528.2	515.9	492.2	456.2	402.6	328.7	213.2	105.0	22.9
old	512.9	508.7	496.3	474.1	439.5	388.0	316.8	205.8	101.4	22.1
HONO, new	95.76	94.91	92.43	88.00	81.13	70.94	57.88	36.04	17.37	3.93
old	32.48	32.19	31.31	27.76	27.36	23.84	19.31	11.96	5.73	1.30
O_3[a], new	31.00	30.79	30.11	28.82	27.01	24.69	21.16	15.82	19.33	1.51
old	6.16	6.06	5.73	5.15	4.34	3.31	2.13	1.00	0.34	0.05
O_3[b], new	2.71	2.63	2.36	1.96	1.46	0.93	0.47	0.15	0.03	0.003
old	4.21	4.11	3.73	3.16	2.42	1.61	0.84	0.28	0.06	0.007
HCHO[c], new	2.23	2.20	2.09	1.90	1.62	1.27	0.86	0.43	0.16	0.03
old	2.14	2.11	2.01	1.85	1.61	1.30	0.92	0.49	0.20	0.04
HCHO[d], new	2.96	2.92	2.81	2.61	2.32	1.92	1.41	0.80	0.34	0.07
old	5.60	5.53	5.33	4.98	4.45	3.73	2.84	1.62	0.72	0.15
CH_3CHO, new	1.27	1.24	1.17	1.05	0.88	0.67	0.43	0.20	0.07	0.01
old	1.27	1.24	1.17	1.05	0.88	0.67	0.43	0.20	0.07	0.01
H_2O_2, new	0.54	0.53	0.50	0.46	0.40	0.32	0.23	0.12	0.05	0.01
old	1.63	1.61	1.55	1.44	1.28	1.07	0.81	0.46	0.20	0.04

a) $O_3 + h\nu \rightarrow O(^3P) + O_2$

b) $O_3 + h\nu \rightarrow O(^1D) + O_2$

c) $HCHO + h\nu \rightarrow HCO + H$

d) $HCHO + h\nu \rightarrow H_2 + CO$

The Dodge mechanism is an explicit mechanism in which the species represent themselves and the rate constants are generally those in Table 10 "old" values. For the Bureau of Mines simulations, Dodge assumed the light intensity and spectral distribution to be constant. The values of the photolytic rates were in the OZIPP computer code as constants. These were used for the Bureau of Mines Dodge simulations.

The copy of the Demerjian mechanism supplied to us included the rates used by Demerjian to model the Bureau of Mines data. In this mechanism there is a single aldehyde, therefore some choice of rate constants is needed.

A copy of the OZIPPM implementation of the Carbon Bond II mechanism and discussion of the values in Table 10 with Whitten led UNC to assume that essentially "old" values were used in the development of the Carbon Bond mechanism and some assumptions about mixtures are needed.

From the copy of the CIT mechanism supplied to UNC, it appears that the CIT mechanism used a mixture of "old" and "new" theoretical photolysis rate constants. For the Bureau of Mines simulations the values supplied in the simulation deck by McRae were used directly (except for the NO_2 photolysis rate).

4.3.2 Bureau of Mines Photolytic Rates

Table 11 summarizes the photolytic rates used in the Bureau of Mines simulations. There were two assumptions regarding the actual light itensity (see later discussion, Section 5.0). The Dodge assumption was used for all mechanisms and in addition the Demerjian assumption was used for his mechanism.

4.3.3 Simple Trajectory Model Photolytic Rates

For each RAPS day that was simulated, the appropriate values (old or new) from Table 10 were used in the UNC photolytic rate program to compute the

theoretical photolysis rates for each day. The total solar radiation was multiplied by an empirical scale factor determined by Saeger (1977) to be 0.40 $min^{-1}/(cal\text{-}cm^{-2}\text{-}min^{-1})$ for the NO_2 photolysis rate. These values were compared with the theoretically computed values and where necessary a daily correction for cloud cover and other atmospheric factors was computed. All mechanisms used the NO_2 photolysis rate derived from the actual sunlight measurements. Other rates were computed from Table 10 based theoretical rates and the daily correction factor from above.

For the Demerjian mechanism, a 50/50 average of the $HCHO^c$ and CH_3CHO "new" values in Table 10 was multiplied by the daily correction factor to give the ALD photolysis rate. The HONO photolysis rates were the "new" values in Table 10 scaled to the NO_2 photolysis rate.

For the Dodge mechanism, the $HCHO^c$ "old" photolysis rates in Table 10 were multiplied by the daily correction factor. For photolysis of $HCHO^d$ to stable products, Table 10 and the above corrected $HCHO^c$ rates were used for the HCHO photolysis to stable products. Likewise, for the photolysis of CH_3CHO to radicals, the 1000-1300 LDT average of the "old" CH_3CHO to $HCHO^c$ rates were used for the CH_3CHO photolysis rates. The fixed rate constants for the other aldehyde reactions were the same as those used for the BOM simulations (and in OZIPP). The other photolysis rates (O_3, H_2O_2, and HONO) were made dependent on the "observed" NO_2 photolysis rate with the ratios the same as those used for the BOM simulations.

For the Carbon Bond II mechanism, a 50/50 average of the $HCHO^c$ and CH_3CHO "old" values in Table 10 was multiplied by the daily correction factor to give the CARB photolysis to radicals. The CARB photolysis to CO was assumed to be all $HCHO \rightarrow CO + H_2$ and hence the rate was based on the "old" values of $HCHO^d$ in Table 10.

For the CIT mechanism all photolytic rate constants were varied with the diurnal NO_2 photolytic rate constant using the same ratios as utilized in the BOM simulations.

Table 11. Photolytic Rates Used in BOM Simulations

	RATE CONSTANT, min^{-1}				
Reaction	Demer	Dodge	Carbon Bond	CIT	Demer (Revised)
NO_2 →	0.434	0.35	0.35	0.35	0.35
HONO →	8.10-E2	0.133		6.44E-2	6.53E-2
RONO →				1.75E-2	
O_3 → O1D		9.49E-4			
O_3 → O3P		1.90E-2		2.52E-2	
H_2O_2 →		8.40E-4		8.96E-4	
HCHO → Rad		9.80E-4		1.31E-3	
HCHO → CO		3.00E-3		2.84E-3	
CH_3CHO → Rad		9.80E-4		1.09E-3	
CARB → Rad			9.10E-4		
CARB → CO			1.33E-3		
ALD → Rad	7.90E-4				6.37E-4
GLY → Rad			1.26E-2		

4.4 HYDROCARBON COMPOSITION INPUT CALCULATIONS

Mechanisms differ in many ways, including in the species used to represent the hydrocarbon present in the photochemical systems to be simulated. Hydrocarbon composition data usually need to be converted to the species representation used in each mechanism. The actual conversion depends on the degree of detail of the original HC composition data available, and the characteristics of each mechanisms' HC species as defined by the mechanism developer. The conversion calculations used by each mechanism utilized in this study are described in the following sections.

4.4.1 Dodge Mechanism

The Dodge mechanism uses a mix of butane and propylene to represent the hydrocarbon species present in a photochemical oxidant system. Dodge has determined for her mechanism that a carbon mole fraction of 75% butane and 25% propylene yielded a system which has a photochemical reactivity similar to that in the Bureau of Mines smog chamber experiments. The Dodge mechanism, therefore, does not utilize HC composition data, except for the aldehyde carbon mole fractions and aldehyde carbon numbers.

In the Bureau of Mines experiments, initial formaldehyde concentrations were determined for each run in the study, and the Dodge simulations of the BOM experiments utilized these initial conditions. The HC input values must be in units of ppmV, therefore the initial conditions for each HC specie are divided by the carbon number of the specie. The calculations are:

Prop (ppmV) = NMHC (ppmC)* 0.25/3.0
But (ppmV) = NMHC (ppmC)* 0.75/4.0
HCHO (ppmV) = measured initial HCHO

4.4.2 Demerjian Mechanism.

Demerjian mechanism used three HC classes (OLE, PAR, ARO) and one aldehyde specie to represent all aldehydes (Table 12). The Demerjian mechanism

TABLE 12
Mechanism Hydrocarbon Species Characteristics

Mechanism	Symbol	HC Species	Characteristics
Dodge	Prop	propylene	25% propylene/75% butane
	But	butane	represents urban ambient hydrocarbon reactivity
	HCHO	formaldehyde	explicit aldehydes of propylene and butane smog system
	ALD2	acetaldehyde	
	ALD3	propionaldehyde	
	ALD4	n-butyraldehyde	
Demerjian	OLE	olefin	olefin plus ethylene, carbon number=3
	PAR	paraffin	paraffin with four carbons and higher, carbon number=6
	ARO	aromatic	aromatics not including benzene, carbon number=8.1
	ALD	aldehydes	carbon number=1.0
CB2	OLEC	olefin double bond (C = C)	carbon number=2.0
	ETHC	ethylene	carbon number=2.0
	AROC	aromatic carbons	carbon number=6.0
	PARC	paraffin carbon	all paraffin carbons and all side chain carbons in olefins and aromatics carbon number=1.0
	CARB	carbonyl carbon (C=O)	carbon number=1.0
CIT	OLE	olefin	mole fraction weighted rate constant and carbon number olefin not including ethylene
	ETH	ethylene	
	ARO	aromatic	mole fraction weighted rate rate constant and carbon number aromatic
	ALK	alkane	mole fraction weighted rate rate constant and carbon number paraffins
	HCHO	formaldehyde	
	RCHO	aldehydes	not including formaldehyde

utilizes HC composition data of carbon mole fraction only. The carbon number for each HC and aldehyde class was defined by Demerjian. Ethylene was lumped into the olefin group. The characteristics of the mechanism HC species were based upon a generalized composition for the auto exhaust used in the Bureau of Mines experiments. The analysis generated by Demerjian is shown in Table 13.

Demerjian divided the carbon mole fraction by the carbon number in each class in Table 13 to obtain factors for converting NMHC (in ppmC units) to mechanism species concentrations in ppmV units. The equations are:

OLE (ppmV) = NMHC (ppmC)* 0.173/3.0
PAR (ppmV) = NMHC (ppmC)* 0.417/6.0
ARO (ppmV) = NMHC (ppmC)* 0.287/8.1
ALD (ppmV) = NMHC (ppmC)* 0.053/1.0

4.4.3 Carbon Bond II Mechanism

The Carbon Bond II mechanisms' HC species represent carbon bond types rather than hydrocarbon classes, with ethylene explicitly represented as the exception. The CARB specie represents the carbonyl carbon present in aldehydes, ketones and other oxygenates (Table 12 lists the species characteristics). Both carbon mole fraction and carbon number are needed in HC composition data. Each carbon bond type also has a defined carbon number (i.e., olefins: C = C has 2 carbons). Portions of each HC composition class are added to the paraffin carbon bond specie, depending on the extent that the HC composition carbon numbers are in excess of the corresponding carbon bond type carbon number. The fraction of the olefin portion (of the HC composition data), which is in ethylene, needs to be determined as well as the non-ethylene-olefin carbon number. For the BOM simulations, the ethylene fraction was known. The non-ethylene-olefin carbon number was determined to be 3.71. The formulas to determine the conversion factors are:

Table 13. Average Bureau of Mines Exhaust Composition (after Demerjian)

Component	Carbon Mole Fraction	Lumped Carbon Mole Fraction	Average Carbon No.
Ethane	.007		
Propane	-		
Acetylene	.063		
Benzene	.035		
Non-reactive		.105	3
Butanes	.034		
Pentanes	.107		
Hexanes & Heptanes	.088		
Octanes & Higher Order	.188		
Paraffins C_4 & Up		.417	6
Ethylene	.0720		
Propylene	.0457		
Butenes	.0419		
Pentenes & Higher Order	.0137		
Olefins		.173	3
Toluene	.1131		
M,P-Xylene	.0350		
O-Xylene	.0156		
Higher Order Alkyl Aromatics	.1233		
Aromatics		.2870	8
	TOTAL	0.982	
Aldehydes (not measured, estimated)		~0.053	1

OLEC (ppmV) = NMHC (ppmC)* 0.101/3.71
ETHC (ppmV) = NMHC (ppmC)* 0.072/2.0
AROC (ppmV) = NMHC (ppmC)* 0.287/8
PARC (ppmV) = NMHC *ppmC)* (0.417 +
(0.101/3.7 * 1.71) +
(0.287/8 * 2))
CARB (ppmV) = NMHC (ppmC)*(0.053/1.0)

4.4.4 California Institute of Technology (CIT) Mechanism

The CIT mechanism utilizes four HC species: olefine, ethylene, aromatic, and alkane, and two aldehyde species: formaldehyde and a general aldehyde species. (See Table 12). Both carbon mole fraction and carbon number data are required to implement this mechanism. The Demerjian HC composition analysis reported for the BOM study was reorganized slightly, to include ethane and propane into the alkane group, and benzene into the aromatics group. Ethylene was subtracted from the olefin value. To calculate carbon numbers for each general HC class, carbon numbers for each sub-classification shown in the BOM HC analysis needed to be approximated. The factors used for the CIT mechanism to simulate the BOM experiments are:

OLE (ppmV) = NMHC (ppmC)* 0.101/3.83
ETH (ppmV) = NMHC (ppmC)* 0.072/2.0
ARO (ppmV) = NMHC (ppmC)* 0.322/7.88
ALK (ppmV) = NMHC (ppmC)* 0.487/5.12

5.0 THE BUREAU OF MINES SIMULATIONS

5.1 THE BUREAU OF MINES DATABASE

The Bureau of Mines (BOM) auto exhaust database has been used for 12 years to validate relationships among NO_x, HC, and O_3. This database was generated by Basil Dimitriades during 1967-1968 at the Bureau of Mines Research Center at Bartlesville, Oklahoma.

At the time, the database was considered one of the best; it was reasonably complete, at concentrations close to those in the atmosphere, and most importantly it used real automobile exhaust. The study used only automobile exhaust from a 1963 automobile equipped with a 283 in^3 engine and used the 7-mode California cycle. Hydrocarbon concentrations were 0.25 and 5.0 ppmC and NO_x concentrations were 0.10 to 1.4 ppm. Thirty-one experiments were performed at approximately constant light intensity, temperature, and relative humidity. The experiments were six hours in duration.

The BOM data were obtained from Dimitriades in the form of copies of the hourly value printouts. These were plotted and Figure 16 is an example of two experiments. These are the first replicate run pair in the data set. Not included in the data set were other conditions, such as, the NO_2 photolytic rate, spectral distribution and accuracy of measurement systems. The previous Dodge study (1977) was used as a source of some of this information.

An isopleth-like view of the 31 BOM runs is shown in Figure 17. The runs are numbered in chronological order and the maximum O_3 produced is indicated for each point. Large numbers are used to order the seven duplicate run pairs. A scatter diagram comparing the duplicate ozone maxima is shown in Figure 18. In six of the seven pairs, the first run was substantially higher. The first six columns of Table 14 give the BOM information in numerical form.

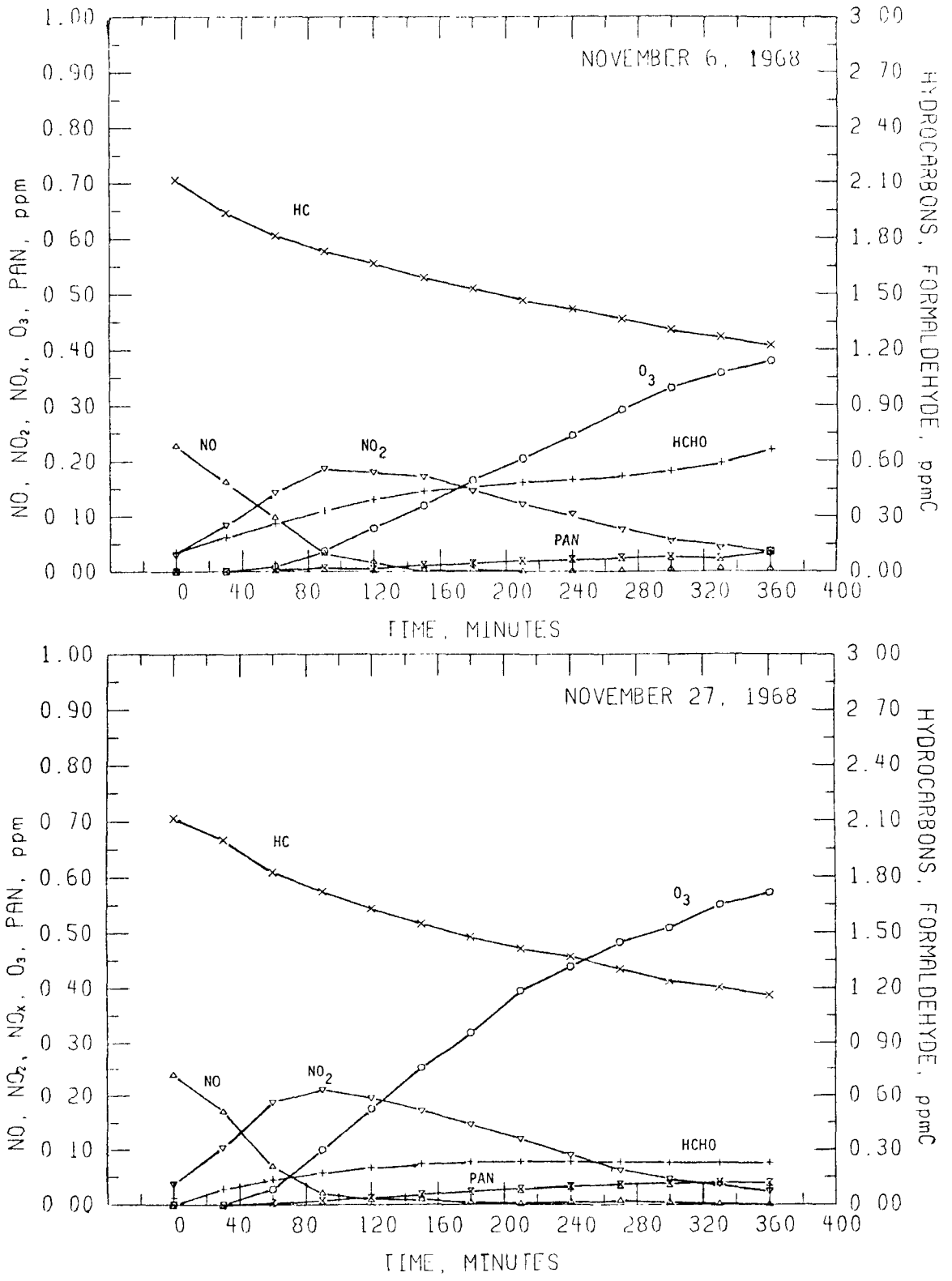

Figure 16. Examples of experimental data from the Bureau of Mines smog chamber auto exhaust data set. These were the first replicate pair of experiments (Nos. 1 and 8).

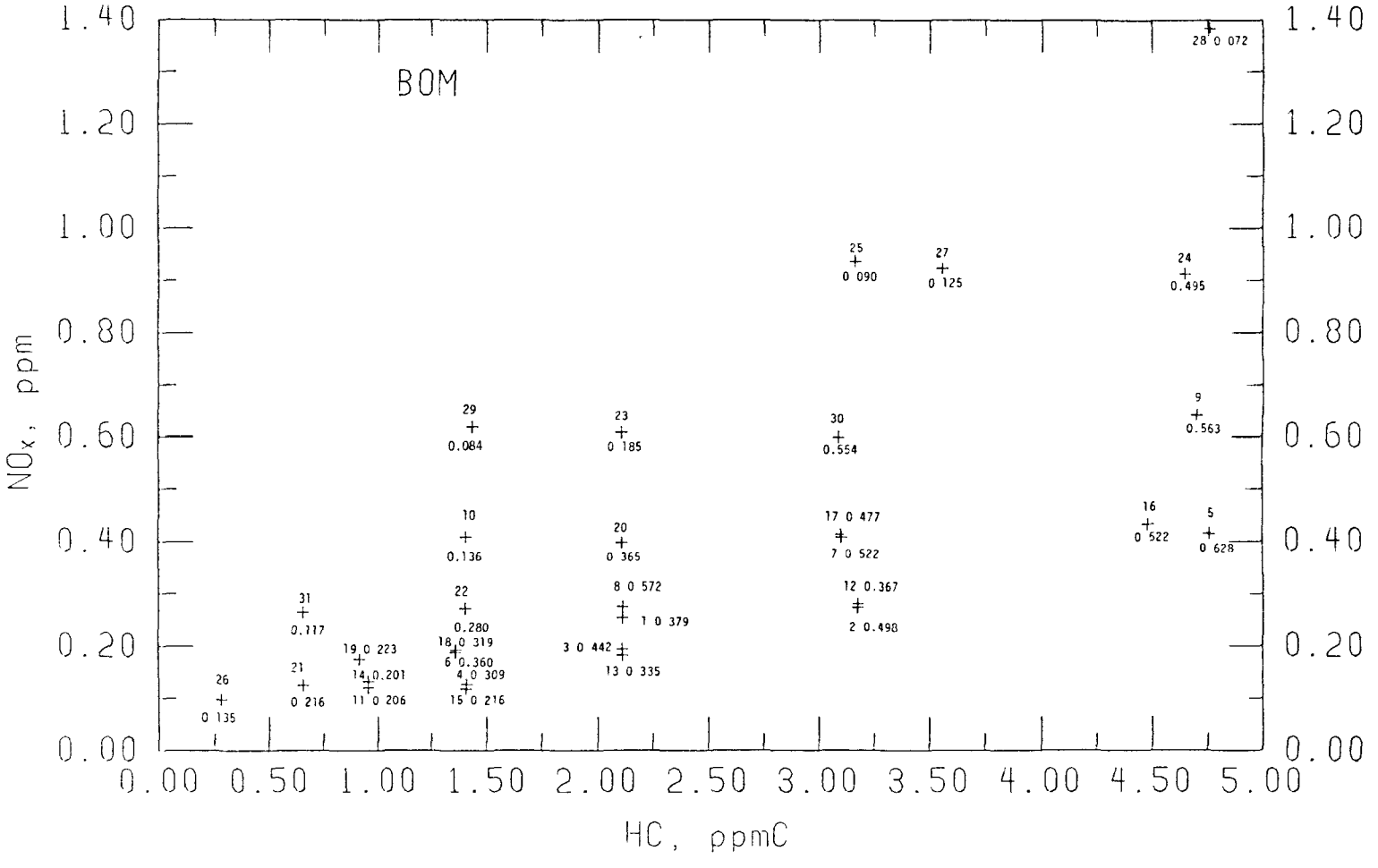

Figure 17. Bureau of Mines run locations and ozone maxima. The run numbers are identified in Table 14. Ozone maxima are reported values x 0.9.

In 1976 the BOM data were chosen as the basis for empirically adjusting the Dodge mechanism's propylene/n-butane fractions (the Dodge mechanism has no aromatics) to represent an appropriate O_3-reactivity. Subsequently, the Dodge mechanism and the assumptions of reactivity derived from the BOM data were incorporated into a computer program for producing O_3 isopleth diagrams (OZIPP). These isopleth diagrams are, in turn, used in an EKMA procedure to estimate HC reduction requirements for urban areas. The assumption is that the urban atmosphere has the same O_3-reactivity as the BOM smog chamber. The BOM HC composition, however, was high in aromatics compared to current emission inventories for urban areas.

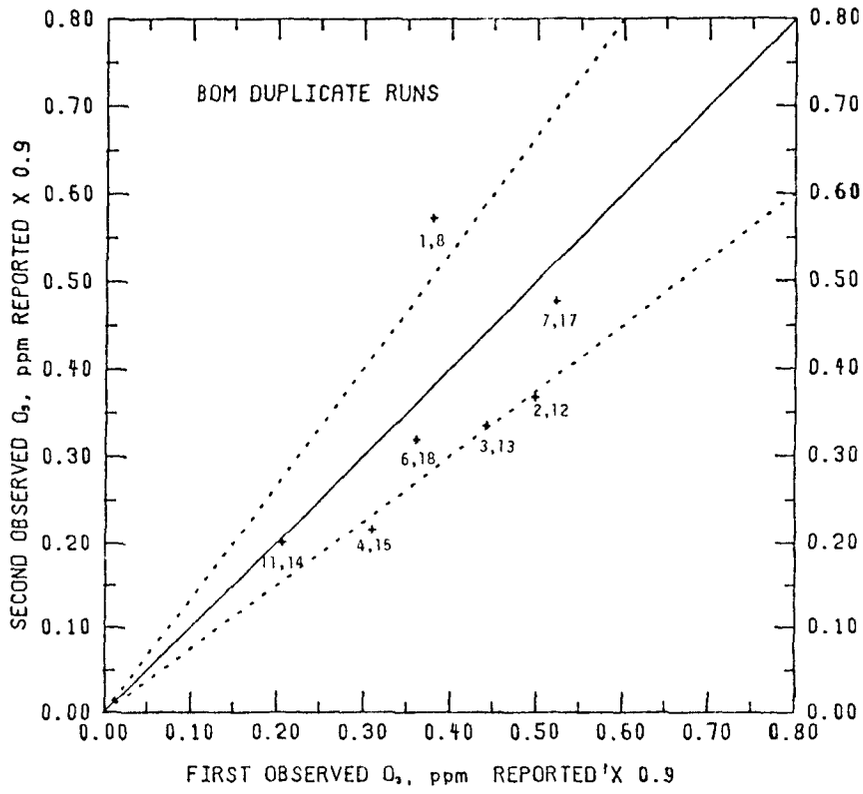

Figure 18. Bureau of Mines replicate run comparison. The run numbers are identified in Table 14. Dashed lines are ± 25%.

Table 14. Bureau of Mines Simulations

Num.		Day	HC	NO_x	O_3 max	Observed O_3max[b]	Observed Time	Modeled Dodge O_3 max	Dodge Time	Demerjian[c] O_3 max	Demerjian Time	Carbon O_3 max	Carbon Time	CIT O_3 max	CIT Time
1	5[a]	11/6/68	2.115	0.256	0.421	0.379	360	0.379	360	0.489	360	0.454	314	0.34	360
2	6	11/12/68	3.177	0.274	0.553	0.498	300	0.429	300	0.547	224	0.488	213	0.52	360
3	4	11/13/68	2.115	0.195	0.491	0.442	300	0.346	300	0.466	287	0.403	254	0.41	360
4	2	11/15/68	1.410	0.118	0.343	0.309	360	0.265	341	0.381	360	0.309	263	0.34	360
5		11/20/68	4.756	0.416	0.698	0.628	240	0.537	281	0.655	185	0.602	202	0.62	360
6	3	11/22/68	1.363	0.188	0.400	0.360	360	0.300	360	0.376	360	0.376	360	0.24	360
7	7	11/25/68	3.102	0.409	0.580	0.522	360	0.382	360	0.567	360	0.566	305	0.42	360
8	5	11/27/68	2.115	0.276	0.636	0.572	360	0.375	360	0.493	360	0.467	337	0.33	360
9		12/4/68	4.700	0.641	0.626	0.563	360	0.595	360	0.684	283	0.686	289	0.50	360
10		12/6/68	1.410	0.409	0.151	0.136	360	0.165	360	0.103	360	0.173	360	0.08	360
11	1	12/13/68	0.959	0.121	0.229	0.206	360	0.240	360	0.315	360	0.300	360	0.22	360
12	6	12/16/68	3.177	0.281	0.408	0.367	240	0.432	317	0.551	232	0.493	220	0.52	360
13	4	12/18/68	2.155	0.183	0.372	0.335	240	0.339	334	0.459	276	0.392	241	0.418	360
14	1	1/8/69	0.959	0.133	0.223	0.201	360	0.238	360	0.292	360	0.303	360	0.195	360
15	2	1/10/69	1.410	0.127	0.240	0.216	360	0.271	349	0.380	360	0.32	275	0.32	360
16		1/13/69	4.478	0.434	0.580	0.522	210	0.539	298	0.650	203	0.606	224	0.61	360
17	7	1/17/69	3.103	0.414	0.530	0.477	360	0.478	360	0.581	319	0.566	312	0.42	360
18	3	1/22/69	1.365	0.192	0.354	0.319	360	0.290	360	0.371	360	0.378	360	0.245	360
19		2/5/69	0.920	0.175	0.248	0.223	360	0.206	360	0.197	360	0.250	360	0.15	360
20		2/7/69	2.107	0.398	0.406	0.365	360	0.359	360	0.391	360	0.422	360	0.245	360
21		2/10/69	0.657	0.125	0.240	0.216	360	0.173	360	0.155	360	0.193	360	0.12	360
22		2/12/69	1.403	0.272	0.311	0.280	360	0.264	360	0.261	360	0.329	360	0.165	360
23		2/24/69	2.104	0.608	0.206	0.185	360	0.139	360	0.131	360	0.214	360	0.072	360
24		2/26/69	4.646	0.912	0.550	0.495	360	0.494	360	0.622	360	0.684	360	0.275	360
25		2/28/69	3.165	0.936	0.100	0.090	360	0.111	360	0.142	360	0.255	360	0.075	360
26		3/5/69	0.283	0.098	0.150	0.135	360	0.079	360	0.037	360	0.046	360	0.03	360
27		3/7/69	3.17/3.554	0.923	0.139	0.125	360	0.202	360	0.257	360	0.382	360	0.095	360
28		3/10/69	4.756	1.384	0.080	0.072	360	0.122	360	0.180	360	0.300	360	0.077	360
29		4/9/69	1.439	0.618	0.093	0.084	360	0.029	360	0.027	360	0.065	360	0.025	360
30		4/11/69	3.090	0.599	0.616	0.554	360	0.408	360	0.481	360	0.529	360	0.270	360
31		4/14/69	0.656	0.265	0.130	0.117	360	0.0442	360	0.028	360	0.053	360	0.025	360

[a]Replicate identification [b]Reported O_3 x 0.9 [c]Demerjian simulation use the revised mechanism

5.2 ASSUMPTIONS

Below is a list of key factors requiring assumption in the BOM modelling, the problem with each factor, the assumption made by previous BOM modellers (Dodge and Demerjian) and the choices made in this study.

Assumptions necessary to model the Bureau of Mines smog chamber database:

1) Light Intensity
   - only pseudo-first order NO_2 photolysis rate
   - Dodge assumed 0.35 min^{-1} photolysis rate for NO_2
   - Demerjian assumed 0.43 min^{-1} photolysis rate for NO_2
   - spectral distribution not measured assumed to be same as sunlight, but two different sets of quantum yields have been used (see Section 4.3, Table 10)
   - this study tested both assumptions for Demerjian (see Section 5.3), used "old" (OZIPP) values for Dodge, Carbon Bond, and CIT supplied values for CIT.

2) Temperature
   - wall temperature measured, air temperature gradients not characterized
   - assumed to be constant at 85^oF
   - this study assumed a constant temperature of 85^oF in all mechanisms

3) HC Composition
   - known to vary from test to test
   - detailed data not available during run
   - was assumed by Demerjian to be constant over range of experiments (see Section 4.4, Table 13)
   - Dodge "tuned" model composition fractions of n-butane and propylene to obtain good fit
   - this study accepted Demerjian's values and applied them in Carbon Bond and CIT (see Section 4.4)

4) O_3 Concentrations
   - known to be subject to interference
   - Dodge assumed true$[O_3]$ = 0.9 $[O_3]$ measured
   - Demerjian assumed true$[O_3]$ = $[O_3]$ measured
   - this study accepted Dodge assumption

5) Aldehyde Initial Values

- large variation in initial measured aldehyde to measured HC ratio
- Dodge assumed true aldehyde = measured[aldehyde]
- Demerjian assumed true aldehyde = 0.05 initial[NHMC]
- this study used Dodge assumption for Dodge and Demerjian's assumption for Demerjian, Carbon Bond and CIT simulations

6) Wall Effects and Background Reactivity

- Dodge assumed wall was a source of propylene
- Demerjian did not assume wall effects
- this study used Dodge's assumption for Dodge and Demerjian's assumption for Demerjian, Carbon Bond, and CIT simulations

5.3 SIMULATION RESULTS

Appendix C shows the NO, NO_2, PAN, and O_3 data and model predictions for each BOM run for each mechanism. In these plots the reported BOM O_3 values are used (i.e. the data were not adjusted) and the original Demerjian mechanism and light intensity assumptions were used. The simulated ozone maximum and the time of occurrence for each mechanism for each experiment are given in Table 14. Figure 19 shows the scatter diagrams for O_3 max for all four mechanisms. (In Figure 19, the second set of assumptions was used for the Demerjian mechanism.) These figures assume that the BOM O_3 was 90% of what was reported. Figure 20 shows the scatter diagrams for time to O_3 max.

These figures show that none of the four mechanisms is obviously superior. The CIT mechanism, however, had a large number of low predictions, late times, and more scatter than the others.

Runs 25, 27, and 28 for Carbon Bond and Demerjian were high compared to the Dodge mechanism. This was a direct consequence of the initial aldehyde assumptions for the simulations. Dodge assumed that the measured initial aldehyde was the actual aldehyde and Demerjian assumed that the aldehydes were proportional to the initial NMHC. UNC used Demerjian's assumption for Carbon Bond. For runs 25, 27, and 28 these assumptions resulted in a 5-fold difference in initial aldehydes (Dodge being less). Run 25 for Carbon Bond was resimulated with the same aldehyde as Dodge and the predicted O_3 was 2.5 times lower and similar to Dodge's prediction. These runs are at high NO_x concentrations and are very sensitive to radical sources and thus the results are more a reflection of the assumptions than of the mechanism behavior.

At the request of Demerjian, two sets of simulations were performed with the Demerjian mechanism. The first set used the rate constants from

the original mechanism (including some now known to be wrong) and an assumed light intensity equivalent to an NO_2 photolysis rate of 0.43 min^{-1}. The second set used lower rate constants for reactions 11 and 12 in Table 7 (the peroxynitric acid formation and decomposition reactions) resulting in less NO_2 loss and thus requiring a lower NO_2 photolysis rate to avoid overpredicting the O_3 formation. UNC assumed the same value for light intensity as Dodge had assumed (0.35 min^{-1}) for this second set of Demerjian simulations.

The scatter diagrams for these two sets are shown in Figure 21. The older rates and assumptions produced consistent overpredictions. The newer rates and assumptions still result in a slight overprediction. The BOM observed O_3 in these plots, however, is only 90% of the reported O_3 value (using the DODGE assumption). Therefore, if the reported O_3 is the true O_3 than the Demerjian predictions would be more centered on the data set. The newer rates and lower light intensity assumption were used for all subsequent work.

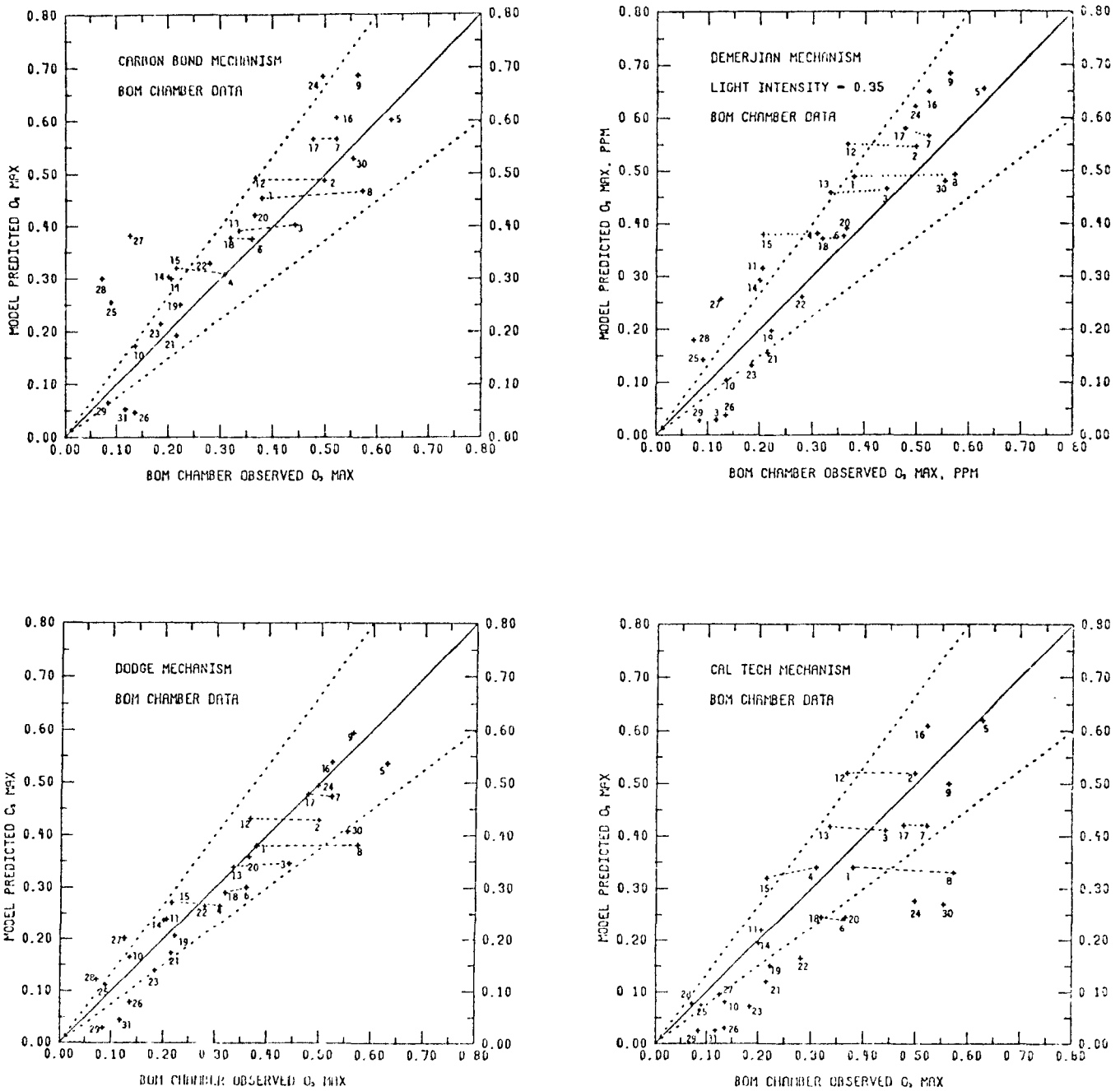

Figure 19. Scatter diagrams for mechanism simulations and BOM data, ozone maxima. Run numbers are identified in Table 14. Replicates are connected by broken line. Dashed lines are ±25%. It is assumed that the observed O_3 maximum is 90% of the oxidant value reported.

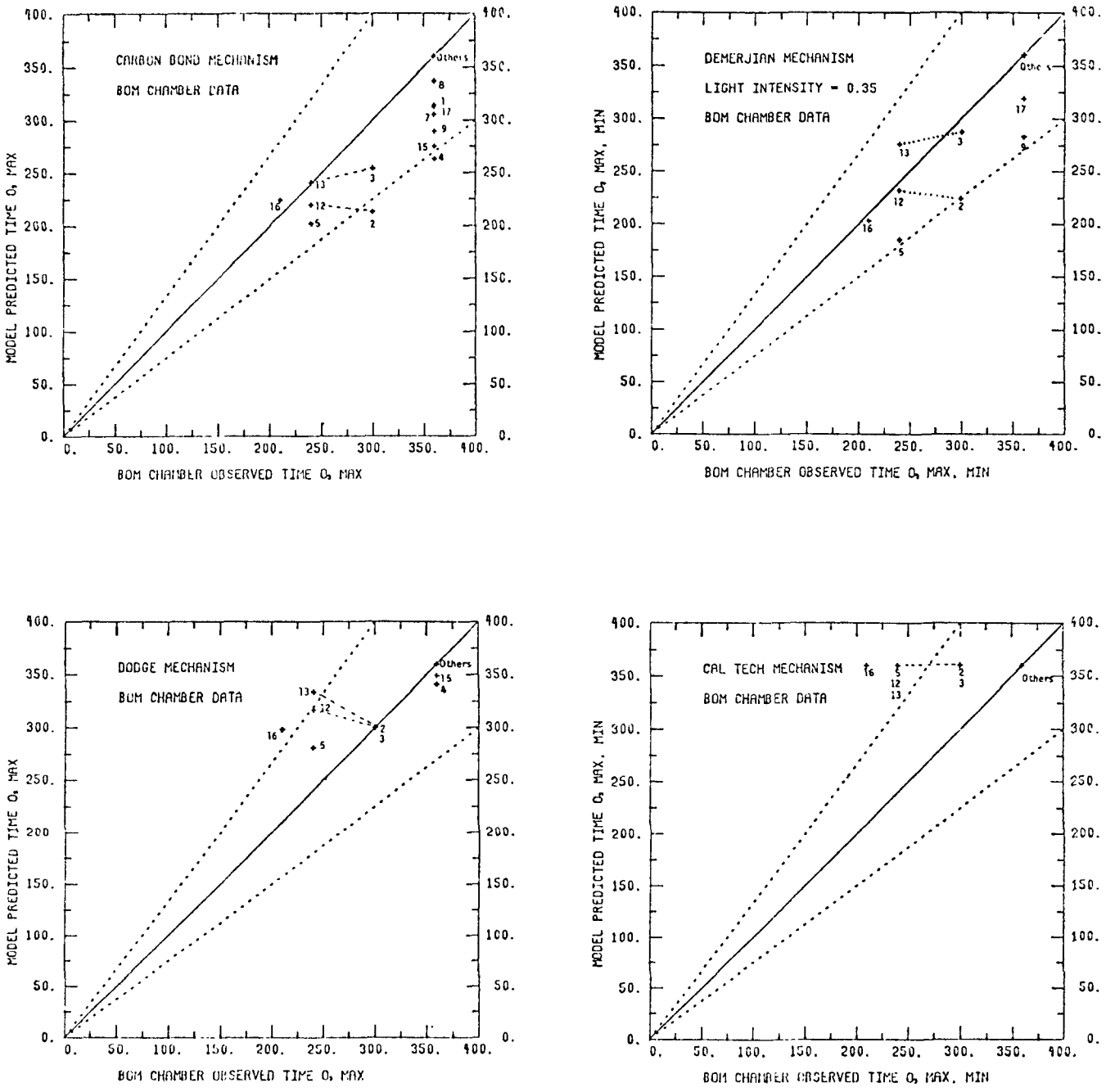

Figure 20. Scatter diagrams for mechanism simulations and BOM data, time to ozone maxima. Run numbers are identified in Table 14. Replicates are connected by broken lines. Dashed lines are ±25%.

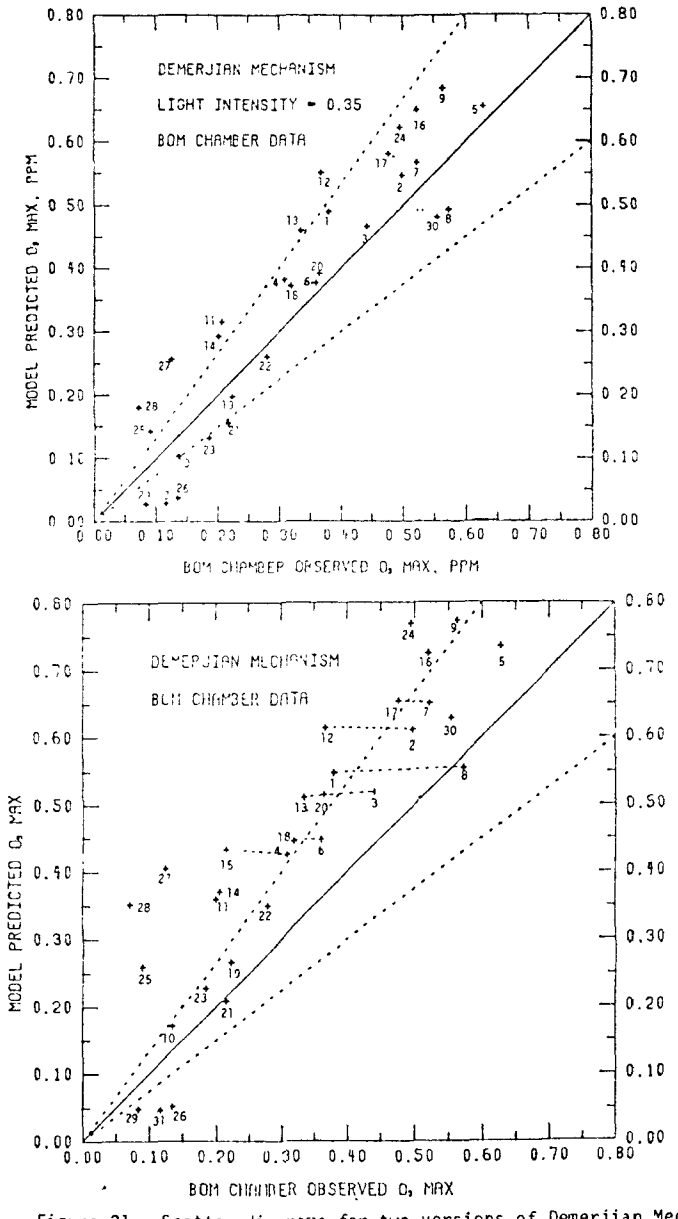

Figure 21. Scatter diagrams for two versions of Demerjian Mechanism and BOM data, ozone maxima.

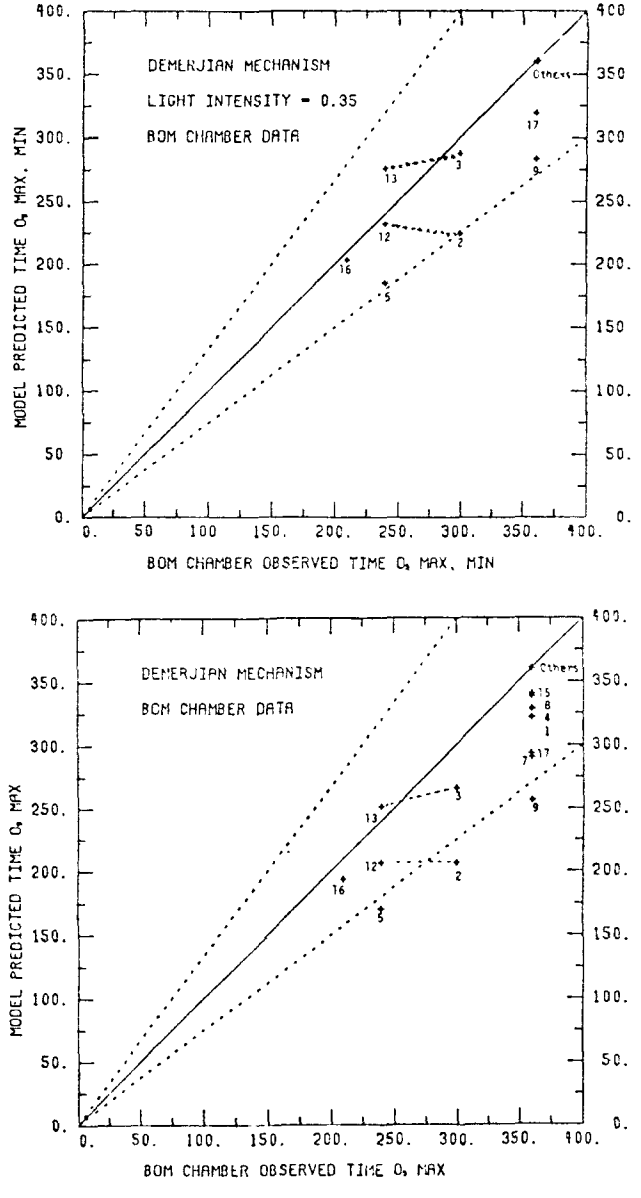

Figure 22. Scatter diagrams for two versions of Demerjian Mechanism and BOM data, time to ozone maxima.

5.4 BOM ISOPLETH AND CROSS SECTION DIAGRAMS

In addition to simulating the individual BOM runs, the mechanisms were used to generate isopleth diagrams for the BOM conditions. These are shown in Figure 23. The BOM datapoints have been superimposed on the isopleths.

The differences among the mechanisms are more evident in this figure. The HC-NO_x-ratio for maximum O_3 formation is much higher for the CIT mechanism than for the others which are reasonably similar. This accounts for the substantial number of underpredictions by the CIT mechanism. The top isopleth for Carbon Bond and Demerjian simulations is 0.65 ppm compared to 0.60 ppm for Dodge and CIT.

To obtain more insight into the differences among the mechanisms, cross sections of the O_3-precursor surface were generated at constant NO_x levels and at constant HC levels. These are shown in Figures 24 and 25. These figures suggest that Carbon Bond and Demerjian mechanisms are more sensitive to both HC and NO_x <u>change</u> than is Dodge. The CIT mechanism is <u>less</u> sensitive to HC change and <u>more</u> sensitive to NO_x change than the Dodge mechanism.

In Figure 26 all four mechanisms are compared in two sets of cross sectional diagrams, one at the maximum condition and one at lower, more urban-like conditions. Also shown at the lower conditions are BOM experimental datapoints and replicate experiments.

At NO_x above about 0.2 ppm the CIT mechanism is inconsistent with the other mechanisms and with the experimental data: it appears to be very inhibited by NO_x. An examination of the mechanism's reactions (Table 9) shows that one olefin molecule only gives one aldehyde molecule (the usual practice is two aldehydes) and that the aromatic molecules only produce a higher aldehyde which has a lower photolysis rate than formaldehyde. These

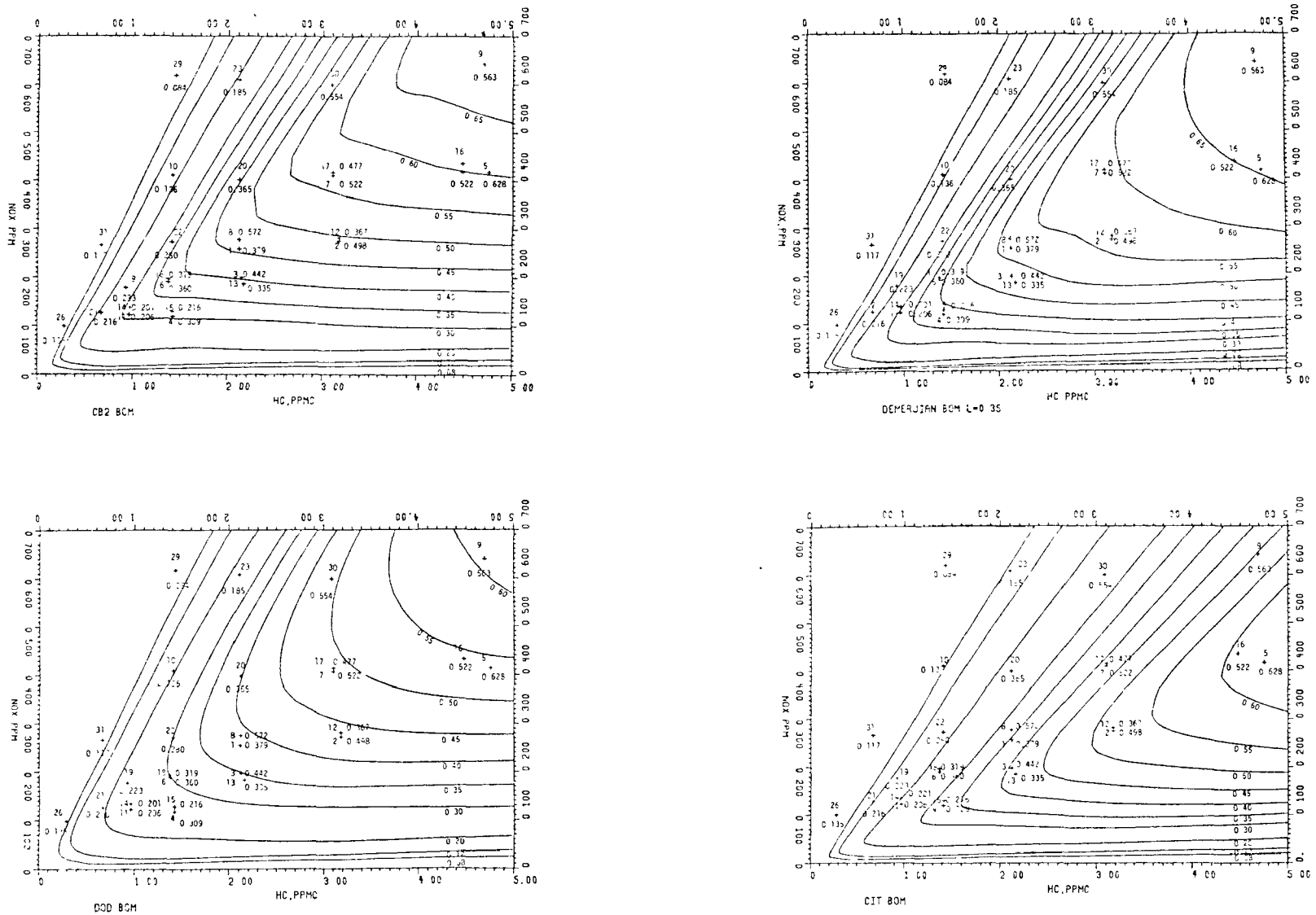

Figure 23. Ozone isopleths for the BOM simulations.

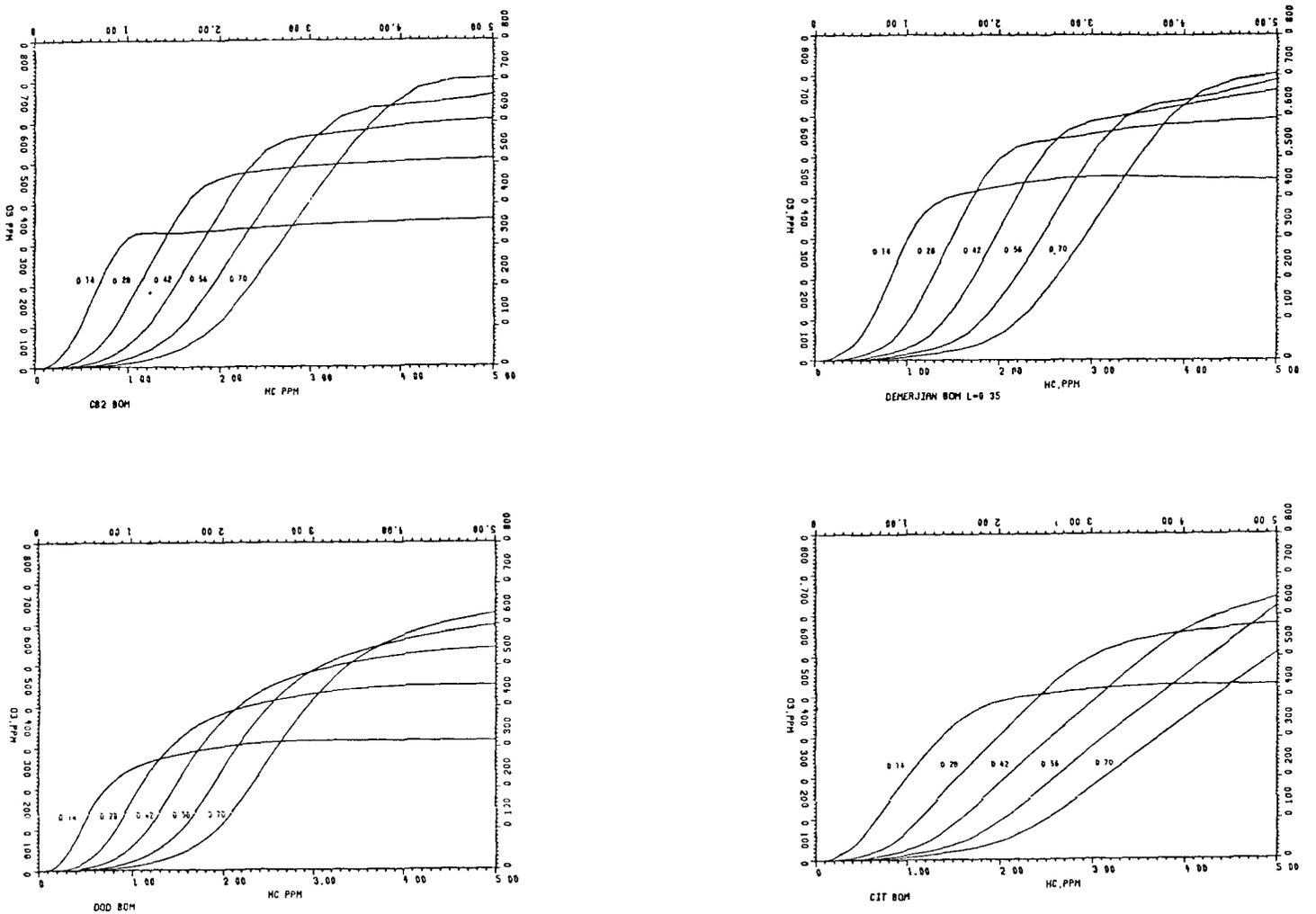

Figure 24. Ozone-hydrocarbon cross sections at constant NO_x for BOM simulations.

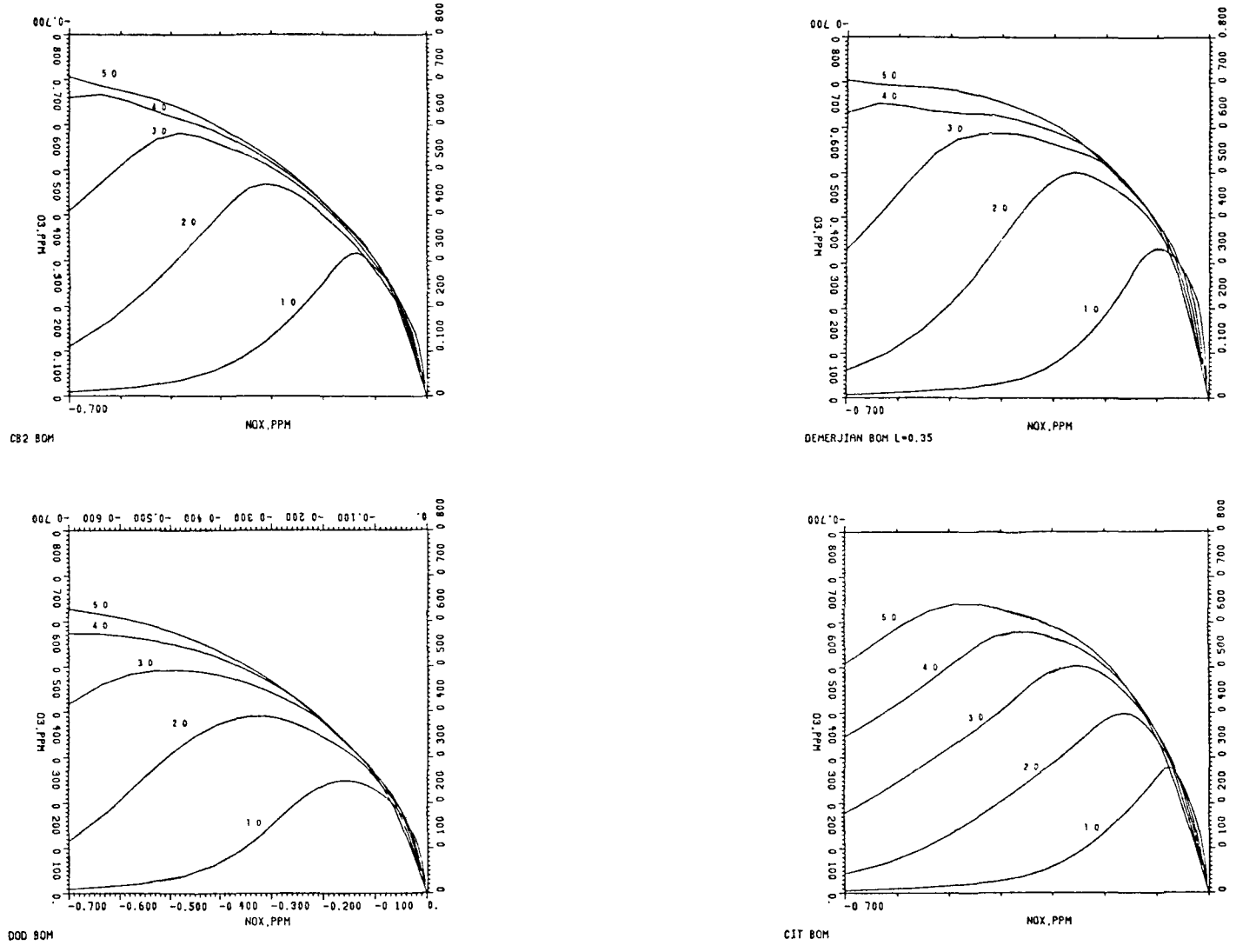

Figure 25. Ozone-NO_x cross sections at constant hydrocarbon for BOM simulations.

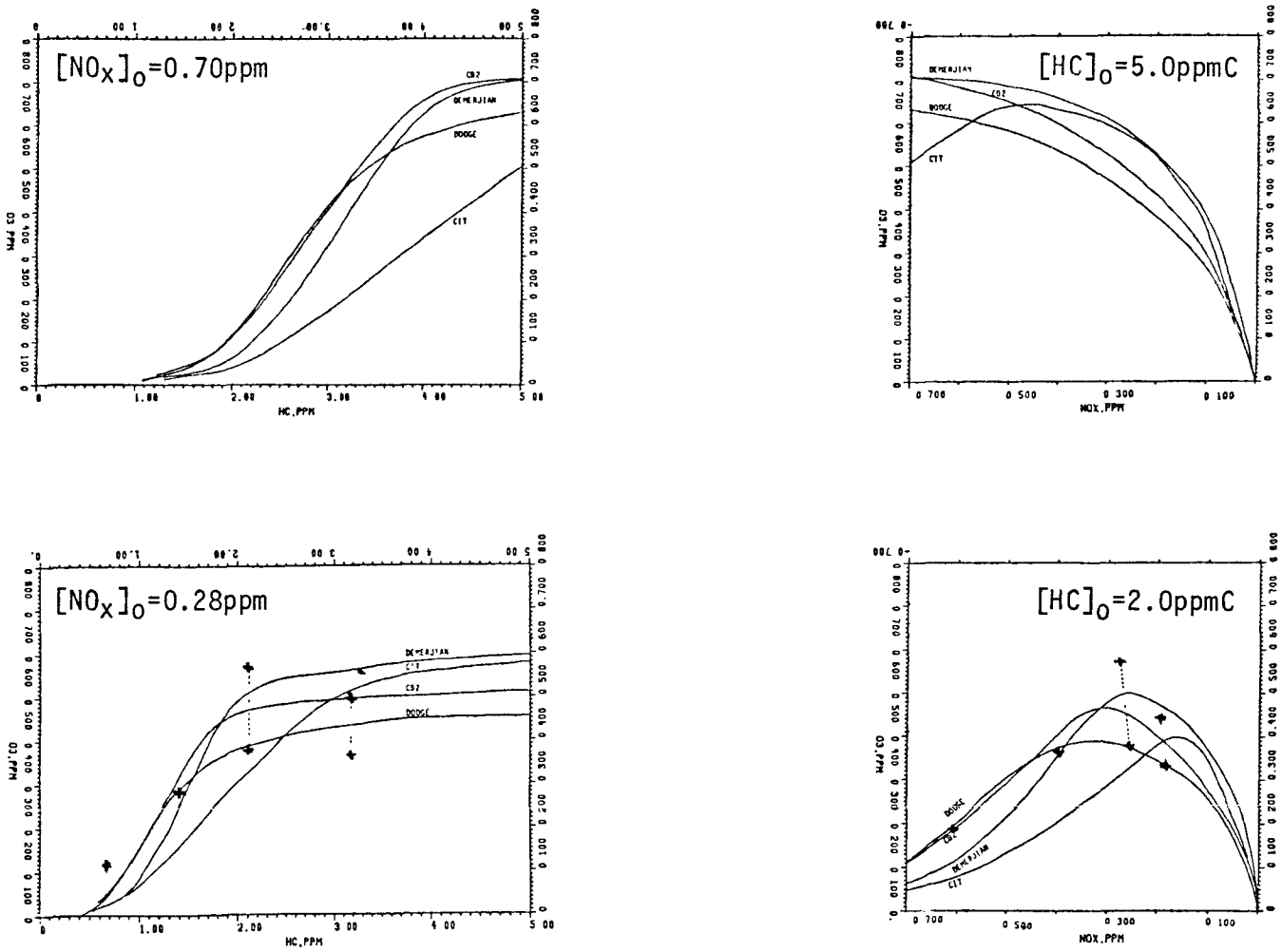

Figure 26. Comparison of hydrocarbon and NO_x ozone cross sections for BOM simulations. The + and +'s connected by broken lines are experimental points and replicates.

differences suggest that the initial reactivity in the mechanism would decrease very rapidly in the simulation. On the other hand, there would not be enough NO_x loss at high HC-to-NO_x ratios, so that although the O_3 may be reasonably predicted, the other secondary products would not be. Careful adjustment of the mechanism's rates and compositional inputs, however, could lead to good fits over a narrow range of conditions such as those shown in Figure 15.

In Figure 26 it can be seen that Carbon Bond and Dodge converge at low HC and at high NO_x for medium HC. Carbon Bond and Demerjian converge at high HC and at high NO_x for high HC. Compared to the experimental points, however, it would seem to be difficult to say which mechanism is a better description of BOM results.

5.5 SUMMARY

Four chemical mechanisms, potentially useful in photochemical simple trajectory models to calculate hydrocarbon and NO_x control requirements, have been compared with the Bureau of Mines auto exhaust database. The mechanisms were: the Dodge propylene-butane mechanism used in the OZIPP program; the Demerjian mechanism used in his photochemical box model; the Carbon Bond II mechanism (CB2) used in the SAI airshed grid model; the California Institute of Technology mechanism (CIT) designed for use in their airshed grid model.

The BOM database is the only complete and well documented set of auto exhaust smog chamber experiments. It does, however, contain enough uncertainties in experimental conditions, analytical methods, and replicate experiments that comparisons of models and data are not unambiguous. That is, the "noise" in the experimental results is greater than the differences shown among the Dodge, Demerjian, and Carbon Bond II mechanism simulations which have large differences in construction assumptions. At lower NO_x concentrations, this is also true for the CIT mechanism. At higher NO_x concentrations, the CIT mechanism O_3 reactivity falls significantly below that of the other three mechanisms and the BOM chamber. Thus, the suitability of the CIT mechanism for control strategy calculations at medium to high initial NO_x conditions may be questionable. Given the range of uncertainty in the BOM data (e.g. O_3 maxima and initial aldehydes) and the sensitivity of mechanisms to necessary assumptions, it is concluded that the Demerjian, Dodge, and CB2 mechanisms were all capable of providing adequate descriptions of the O_3 formation in the BOM chamber; the CB2 mechanism is probably slightly better at describing the other measured secondary products.

6.0 REGIONAL AIR POLLUTION STUDIES DATABASE: EPA SUPPLIED INFORMATION

6.1 GENERAL DESCRIPTION

The Regional Air Pollution Study (RAPS) was conceived early in 1970 to provide a rational, scientific basis for the management of air quality, as mandated by the Clean Air Act (as amended). The basic premise of the Act is that desired air quality standards can be obtained by setting appropriate emission standards. The development of Implementation Plans, called for by the Act, assumes that existing knowledge was at least minimally adequate for planning.

A basic tool for the development of air quality management is the simulation model, a mathematical description of the complex relationship between emissions, atmospheric dispersion and transformation, and ambient concentration. The development of any model presupposes: 1) a detailed understanding of the physical, chemical and meteorological process involved; and 2) availability of adequate emission data, meteorological information and measurements of ambient concentrations of the pollutants under investigation.

At the beginning of the RAPS study, a number of simulation models had been developed, but few -if any- had been verified in the field. The primary reason for this was the absence of an adequate database, which would contain accurate, high resolution data covering a sufficiently large area. Ambient data were available with adequate time resolution -one hour or less- but the stations providing such data were typically too few and improperly spaced to cover a given area. Meteorological data were usually available

only at very few points in a given area, such as an airport, where they were gathered for other purposes. Micrometeorological data related directly to ambient measurements were generally unavailable.

Emission inventories have been in existence for some years, and owing to the efforts of the National Air Data Branch of OAQPS, were being collected in a uniform, machine readable format known as National Emission Data System (NEDS). However, the NEDS inventory contained essentially only annual data, which cannot readily and reliably be converted to hourly values over the two year RAPS program period.

Clearly, what was needed as a first step in the development of a rational approach to the management of air pollution was an extensive, detailed data-base containing all these elements: emission, meteorological, and ambient data, with a resolution in time and space and an accuracy adequate to provide an input to simulation models.

The St. Louis Interstate Air Quality Control Region (AQCR 70) was chosen as the site for RAPS (Figure 27). The selection was based on the need to find a large city within the continental United States, which was away from oceans and mountains and which typified the coal-burning industrial nature of many urban areas, yet which lay in an extended region of rural country. Of the 33 Standard Metropolitan Statistical Areas larger than 400,000 population, St. Louis emerged as the clear choice based on the following criteria:

- Surrounding Area
- Heterogeneous Emission
- Area Size
- Pollution Control Program
- Historical Information
- Climate

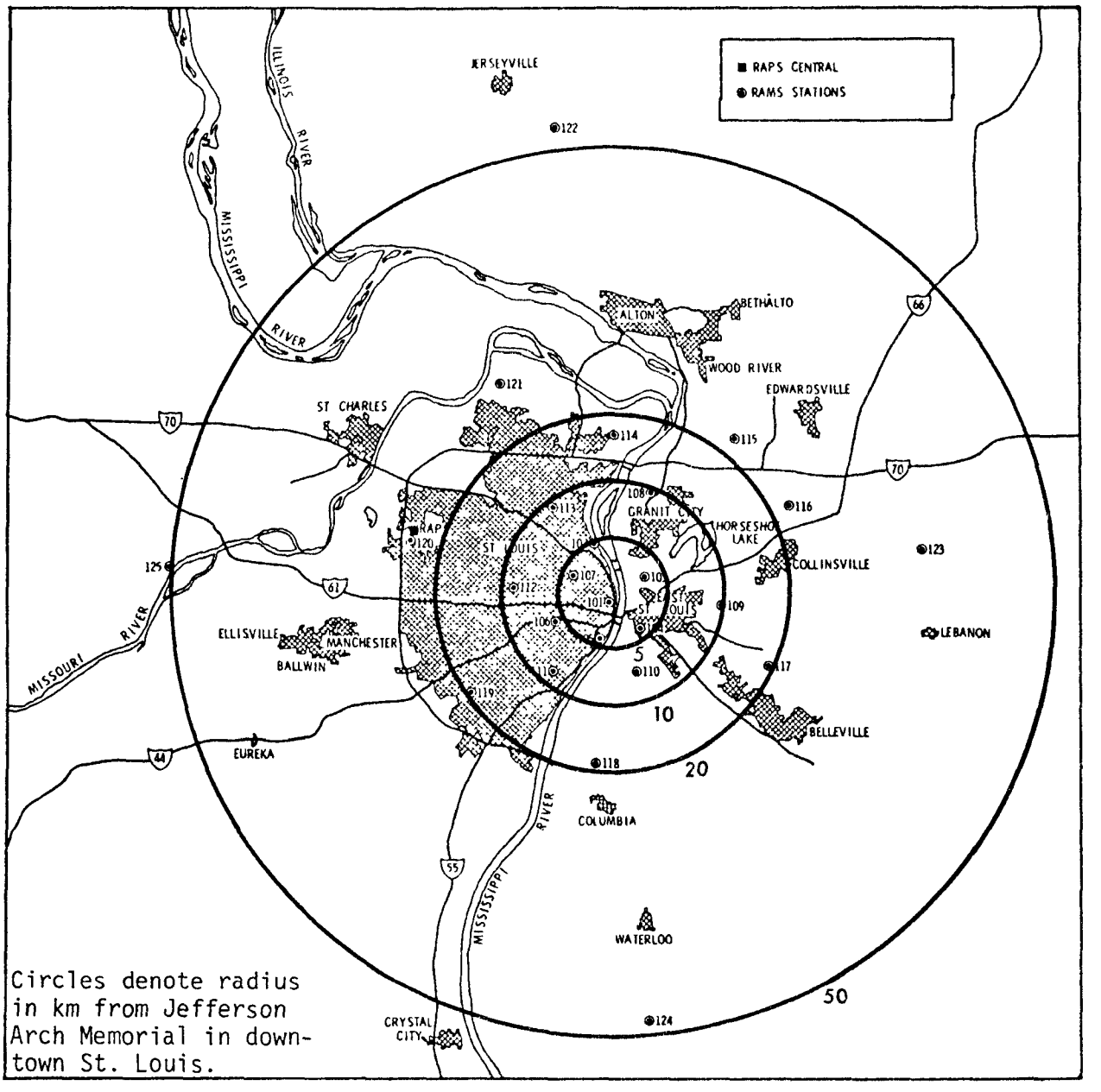

FIGURE 27. THE REGIONAL AIR MONITORING STATIONS NETWORK

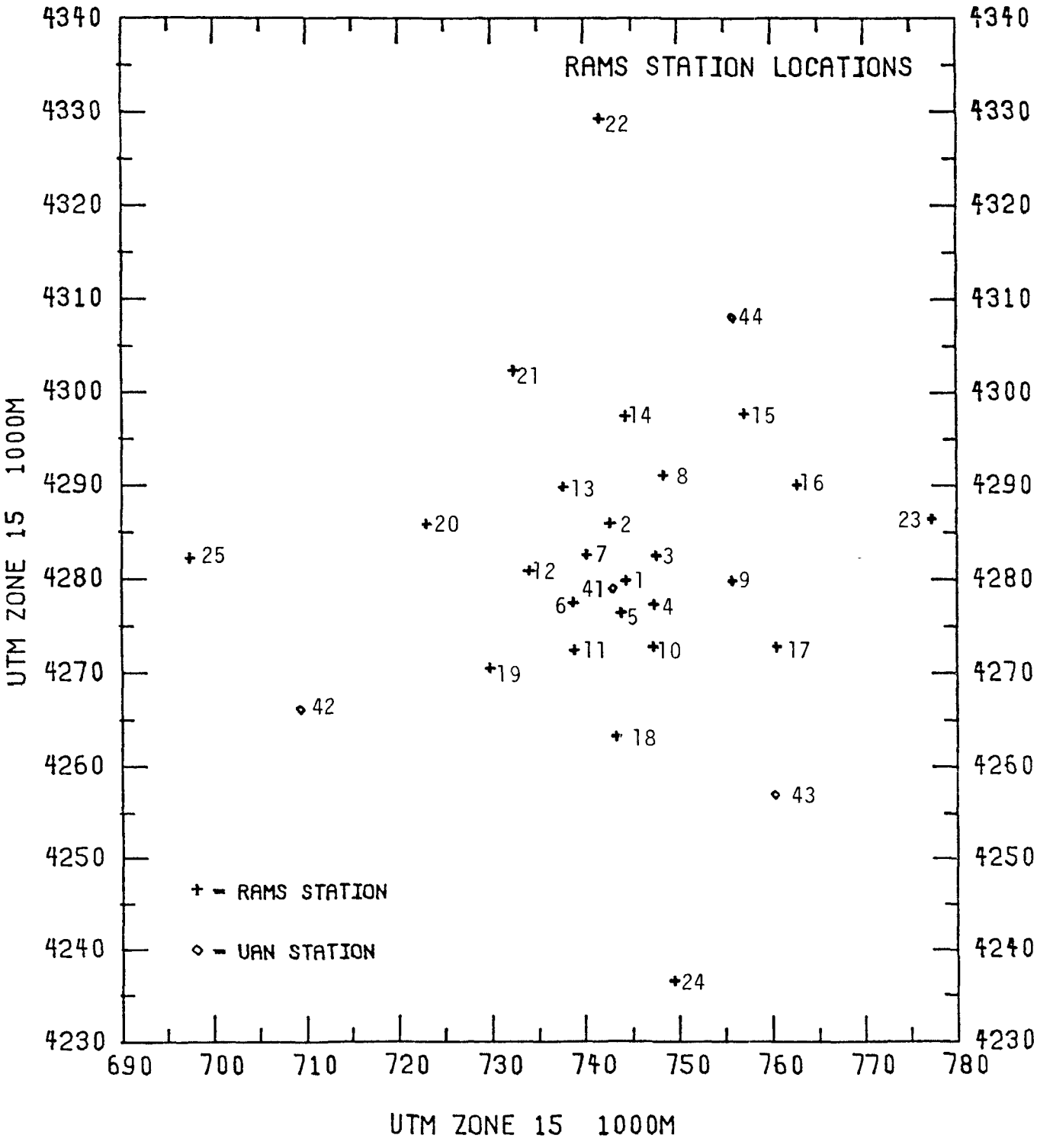

Figure 28. The Regional Air Monitoring Station UTM coordinates.

In the RAPS program 25 regional air monitoring stations (RAMS) were placed concentrically throughout the study region (see Figure 27). The stations, which were numbered 101 to 125, were thought to be located where they would not be unduly influenced by any one source or group of sources. The network was operated for two years, 1975 and 1976.

The RAPS database is maintained by EPA in several forms. Most readily available for each station are hourly average concentrations for: ozone, nitrogen dioxide, nitric oxide, total oxides of nitrogen, nonmethane hydrocarbons, sulfur dioxide, and carbon monoxide. Each station also measured wind speed, wind direction, and temperature; these too are available as hourly averaged values. The RAPS program also included an Upper Air Sounding Network (UASN). In this network, radiosondes were released three times per day, five times per week, at at least two stations. From these soundings a vertical temperature profile could be derived and the extent of atmospheric mixing could be estimated.

Figure 28 gives the locations of the RAMS stations and the four UASN stations on a UTM grid coordinate system (the RAMS stations have been numbered 1 to 25, the UASN stations are numbered 41 to 44). Station 1 was at the Arch. This plot will be the basis for showing the trajectories and emission areas in Section 7.1.2. The RAPS program also included a new and hourly resolved area and point source emissions inventory for a number of pollutants (Littman, 1979). Figure 29 identifies the major point sources. The area source inventory was spatially resolved using a variable-sized grid system in which the smallest grids were 1 km^2 and the largest were 100 km^2. The grid system is shown in Figure 30. A detailed section of the grid system near the center of the city will be shown later as Figure 65. Estimates of emission rates from both area and point sources are available by hour and by grid for any day in 1975 and 1976.

6.2 DAYS SELECTED

The days used in this study were the same days selected by OAQPS/EPA in their evaluation of EKMA (Gipson, 1980). These days were selected to include the days with the highest ozone levels and to include a range of atmospheric conditions (season, wind direction, mixing heights, ozone aloft, etc.). In addition, a few days with lower ozone concentrations were included to test for performance near the O_3 standard. Table 15 identifies the days selected.

Table 15. Model Test Days

Date	Julian Day	RAMS Site	Time of Peak O_3 Local Daylight Time	Peak O_3 Concentration, ppm
10/1/76	275	102	1500-1600	.24
7/13/76	195	114	1600-1700	.22
6/8/76	160	115	1700-1800	.22
6/7/76	159	122	1600-1700	.20
6/8/76	160	103	1400-1500	.19
8/25/76	238	115	1400-1500	.19
10/2/76	276	115	1700-1800	.19
9/17/76	261	118	1300-1400	.15
7/19/76	201	122	1300-1400	.15
8/8/76	221	125	1800-1900	.12

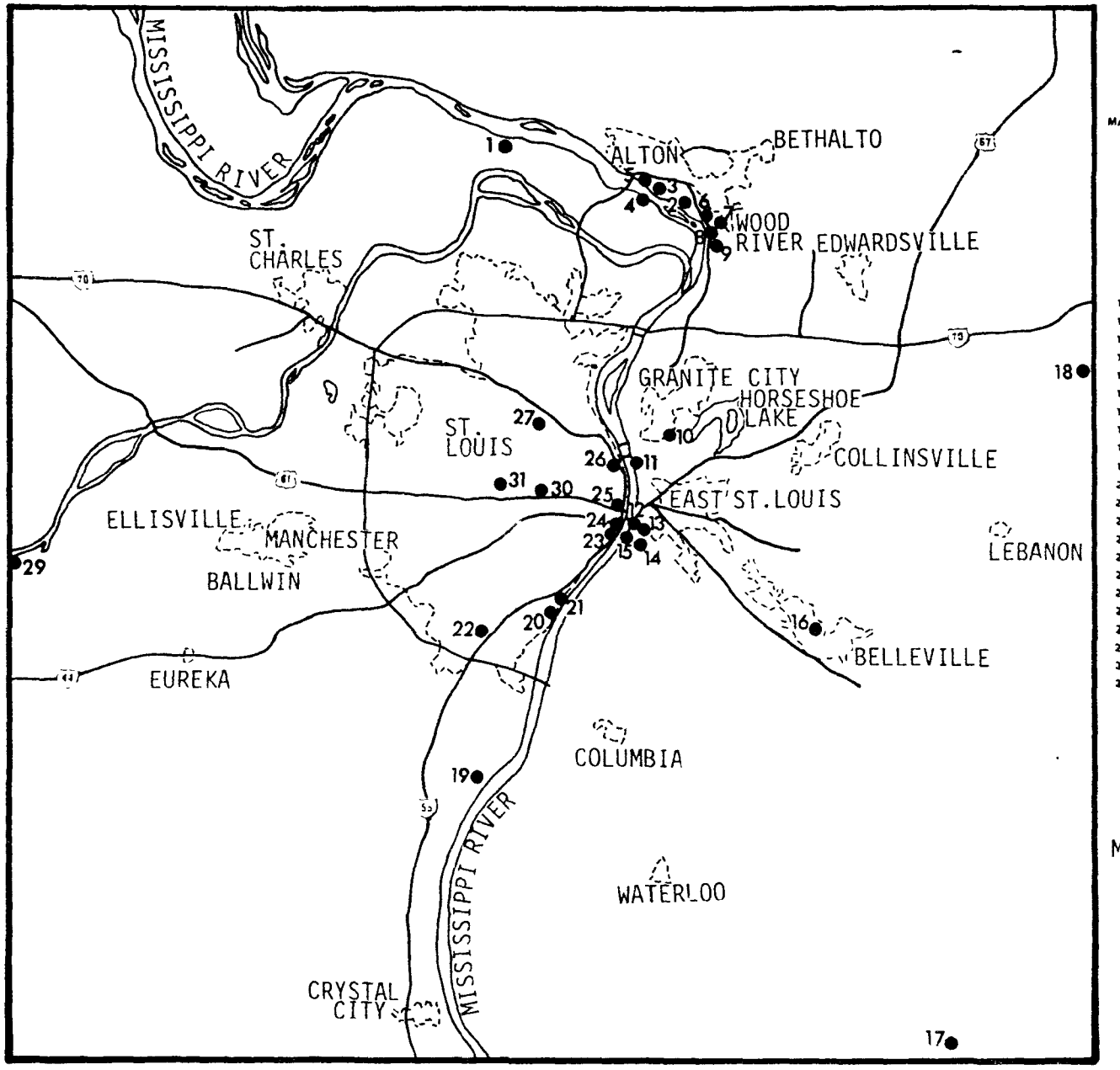

MAP NO	SOURCE
1	Union Electric – Sioux
2	Illinois Power – Wood River
3	Laclede Steel
4	Alton Box Board
5	Owens Illinois Glass
6	Amoco Oil Refinery
7	Shell Oil Refinery
8	Olin Co
9	Clark Oil Refinery
10	Granite City Steel
11	Union Electric – Venice
12	AMAX Zinc
13	Edwin Cooper
14	Monsanto – WG Krummrich
15	Union Electric – Cahokia
16	Stag Brewery
17	Illinois Power – Baldwin
18	Highland Electric
19	Union Electric – Meramec
20	N L Industries
21	Great Lakes Carbon
22	Alpha Cement
23	Anheuser Busch
24	Monsanto – J F Queeny
26	Union Electric – Ashley
26	PVO Int
27	General Motors
28	Missouri Portland
29	Union Electric – Labadie
30	Washington Univ – Euclid Sta.
31	Washington Univ – Campus

FIGURE 29. RAPS MAJOR POINT SOURCES

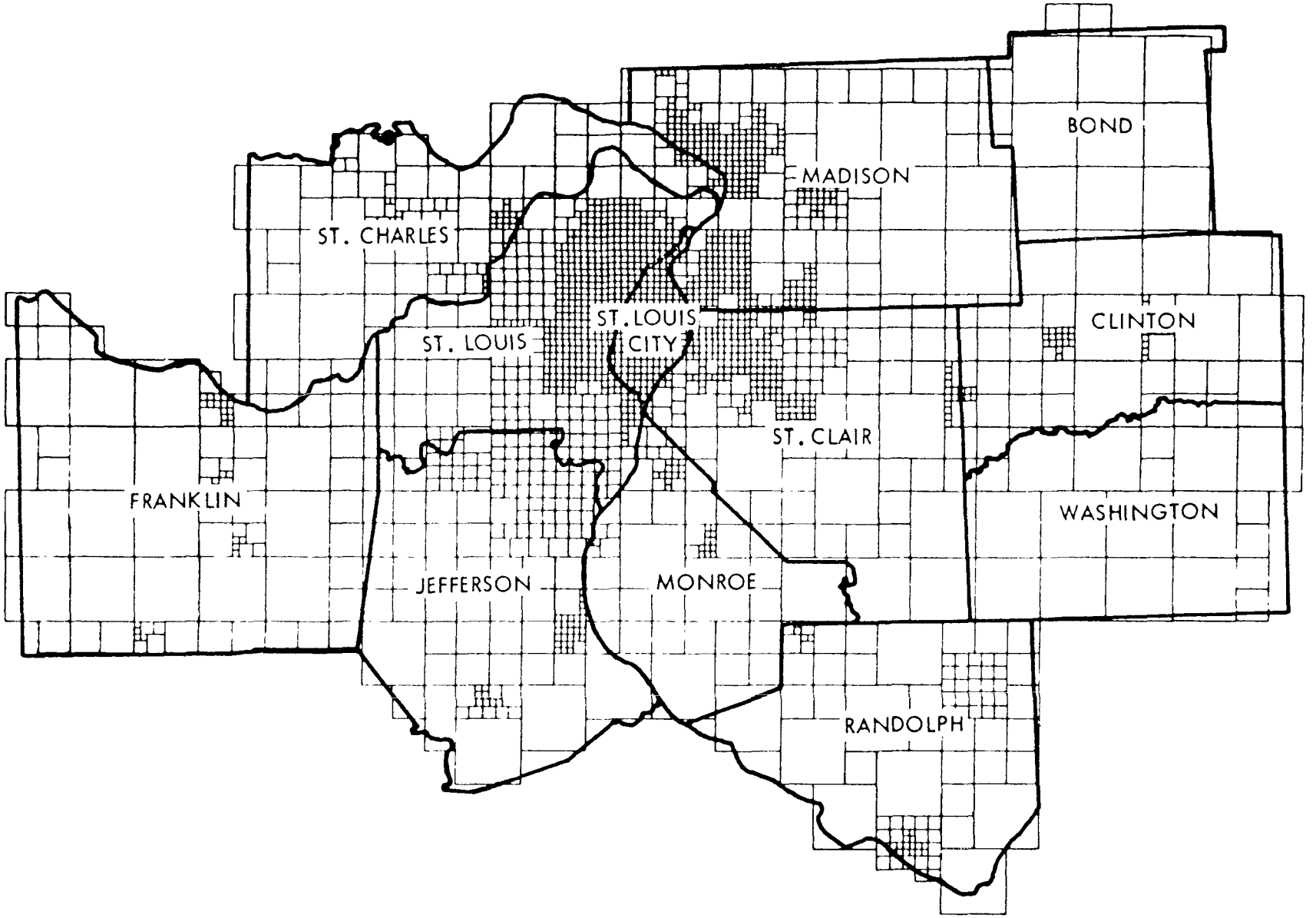

FIGURE 30. EXAMPLE OF RAPS GRID SYSTEM OVERLAY

6.3 INFORMATION SUPPLIED BY EPA

For each of the ten days during the 1976 RAPS study, EPA supplied to UNC the data used to run the DODGE model (OZIPP) and additional information that was needed for the different mechanisms. This information included:

a) trajectories for each day as both UTM coordinates and maps.

b) the emissions along the trajectory as used in the DODGE/OZIPP simulations and also in as much detail as is present in the emissions inventory.

c) the boundary conditions, both transport and aloft, used in all the DODGE simulations and the data used to generate these conditions.

d) the ambient concentrations estimated along each trajectory and the individual data points used to estimate these values.

e) the mixing height data used in the DODGE simulation and the sounding data used to generate this data.

f) example results of the DODGE/EKMA simulations for selected days and copies of each isopleth figure generated.

g) other data needed to accomplish the tasks.

7.0 INPUT DATA FOR SIMPLE TRAJECTORY MODELS FOR RAPS DAYS

7.1 TRAJECTORIES

7.1.1 Methods of Determining Trajectories

The determination of a trajectory is an implicit input to a simple trajectory model. An accurate trajectory is important because ambient data and emissions into the parcel are determined along its path. The first problem in determining the trajectory is to select the height at which it is to be determined. In most cases the 10-m wind is chosen; this is the usual observational height. Being in the surface layer, however, this height may not be the best one.

The surface layer is generally characterized by strong gradients of wind, temperature, and humidity. Thus a level in the higher mixed layer where the gradients are more uniform may describe the true winds more accurately. Measurements of these winds can be obtained using bistatic acoustic sounder, lidar, towers, balloons and aircraft.

In most cases the 10-m wind and possibly one or two rawinsonde observations may be available. From this information, models and smoothing techniques can give a mass consistent wind field from which a trajectory can be determined (Dickerson, 1978, Goodin, McRae and Seinfeld, 1980). The concept of a mass consistent wind field is important since in a convective boundary layer strong convergence can occur (Shreffler, 1978). The neglecting of the vertical wind component in a trajectory model can produce significant errors (Liu, Seinfeld, 1975).

An even more simple technique of calculating trajectories is to use a time averaged wind vector from the observing stations, weighing the closest stations to the point of interest by $1/r^2$.

If sufficient wind data are not available but there is sufficient atmosphere pressure data available for a region, then a wind flow may be estimated assuming a geostrophic balance. In an urban area, however, the difference in pressure measurement may not be resolvable within the accuracies of the instrumentation.

7.1.2 Trajectories for RAPS Days

The trajectories for the RAPS days were determined by OAQPS/EPA personnel and were supplied to UNC on request. The general procedure used by EPA was to perform backward trajectory calculations from the vicinity of the RAPS station with the high O_3, starting at the time of the observed high O_3. Two different computer programs were used depending upon station density (Gipson, 1980). In general, these programs performed a $1/r^2$ weighting of the three closest wind stations to generate a wind vector, then moved backwards along this vector and repeated the process.

Five trajectories were run for each site-day, one from the station itself and four displaced 5 Km North, South, East, and West around the station. As will be shown below, these trajectories sometimes converged, sometimes crossed, and sometimes diverged, leading to a large uncertainty in the initial location and path history of the air parcel.

Given the uncertainties in the trajectories, OAQPS/EPA personnel generated a "box" for each hour by connecting the extreme positions of the trajectories for that hour. Thus, the probable trajectory was assumed to be contained somewhere in the box. The "box" was used to select and average the emissions sources for that hour. This process will be described in the

next section. On some days, a bigger "box" was drawn around multiple hours of trajectories when little motion had taken place.

In the following discussion, the maps with boxes were supplied by OAQPS/EPA. They also supplied tables of trajectory and box coordinates. These have been plotted to more clearly demonstrate the basis of the calculations.

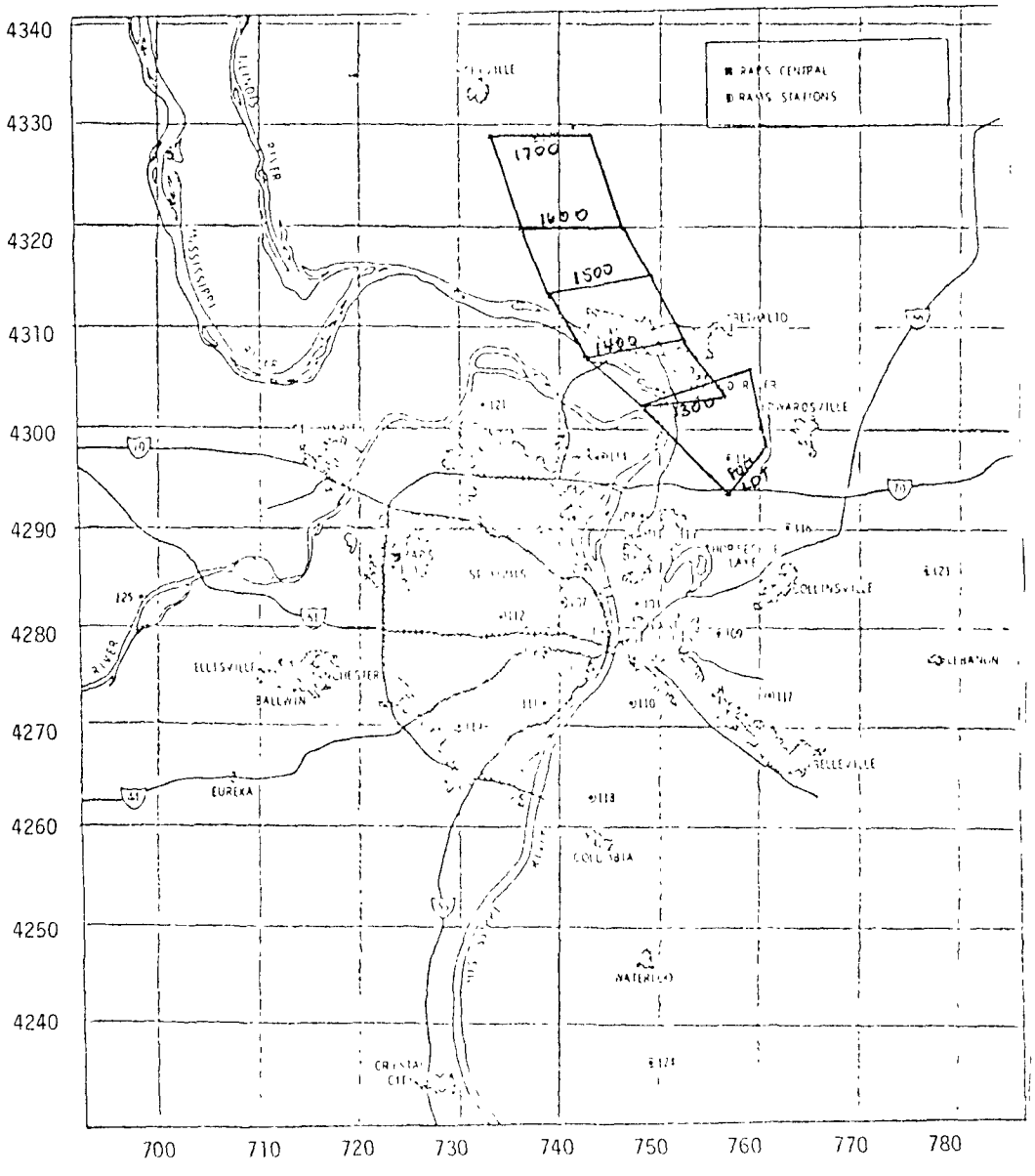

Figure 31. Trajectory for Day 159, June 7/Site 122

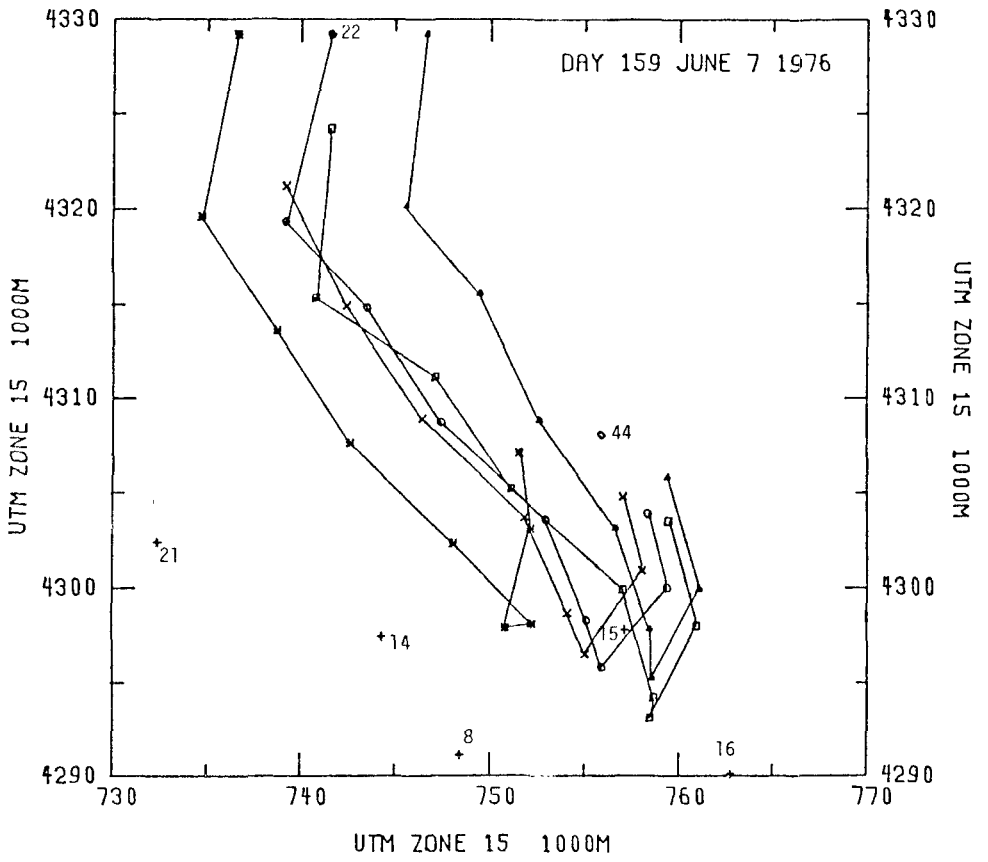

Figure 32. Individual trajectories, Day 159.

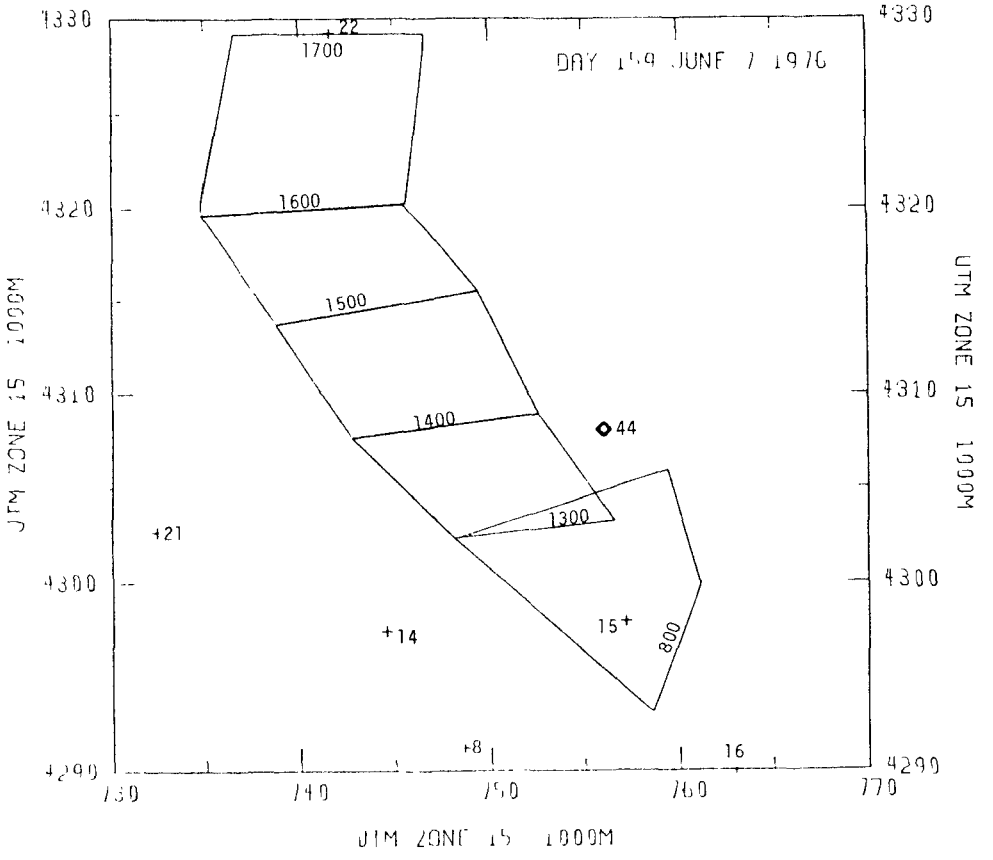

Figure 33. Boxes generated from trajectories, Day 159.

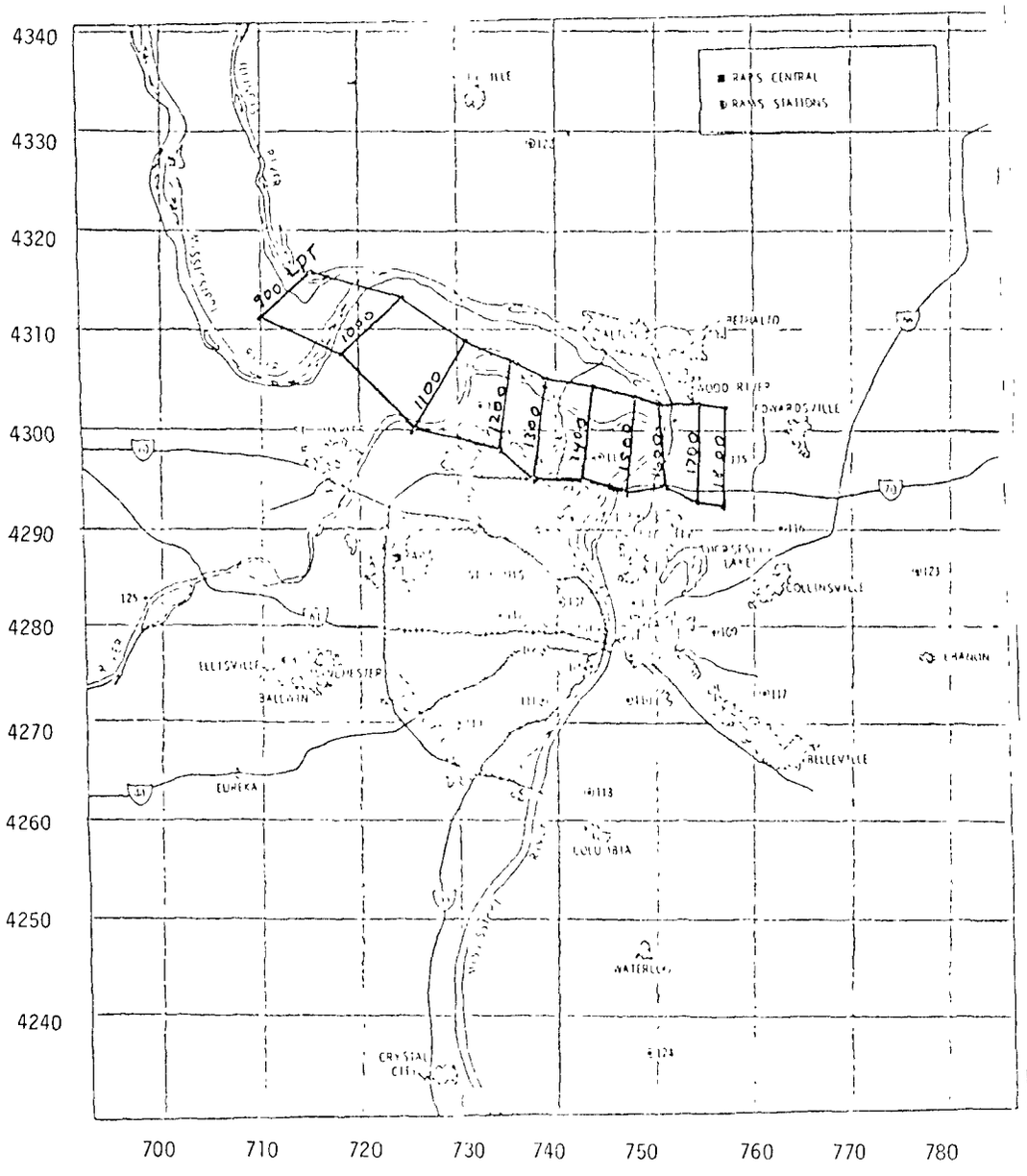

Figure 34. Trajectory for Day 160, June 8/Site 115

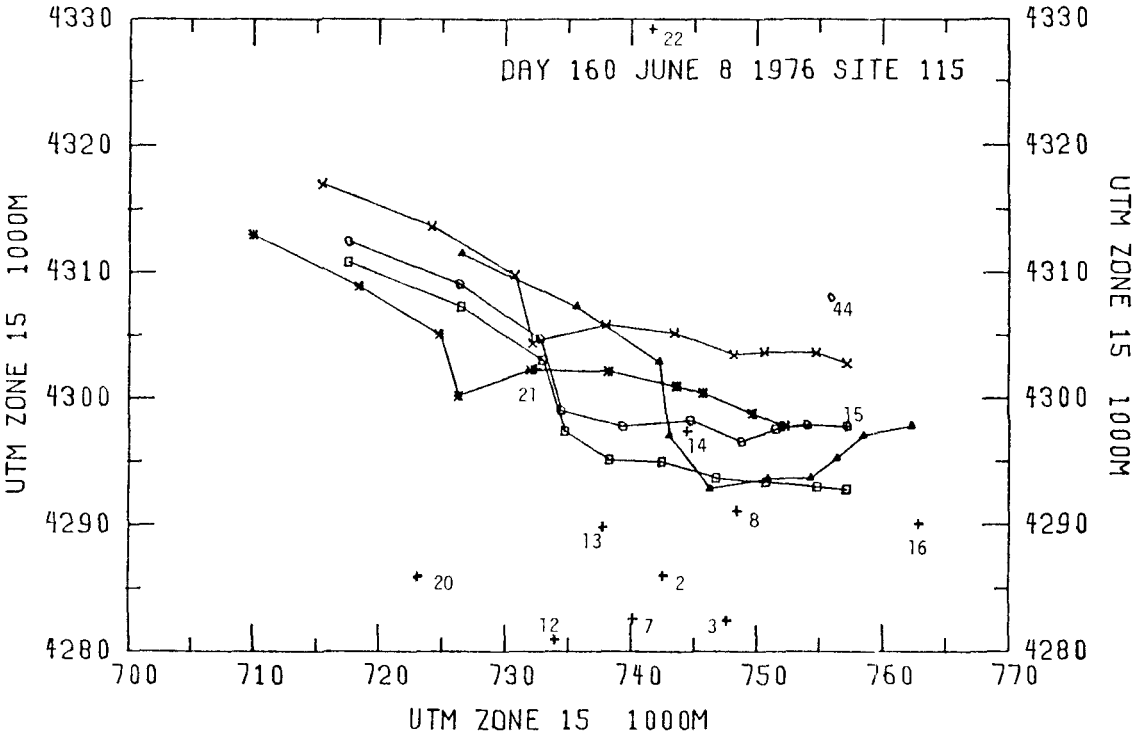

Figure 35. Individual trajectories, Day 160, Site 115.

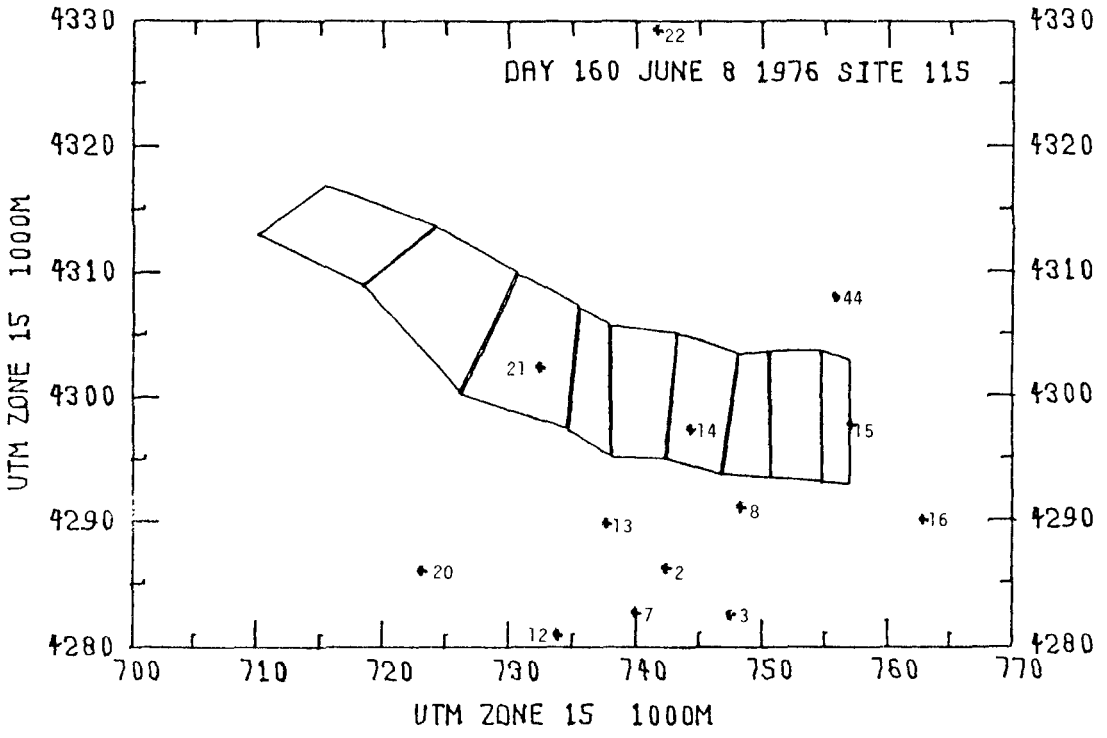

Figure 36. Boxes generated from trajectories, Day 160, Site 115.

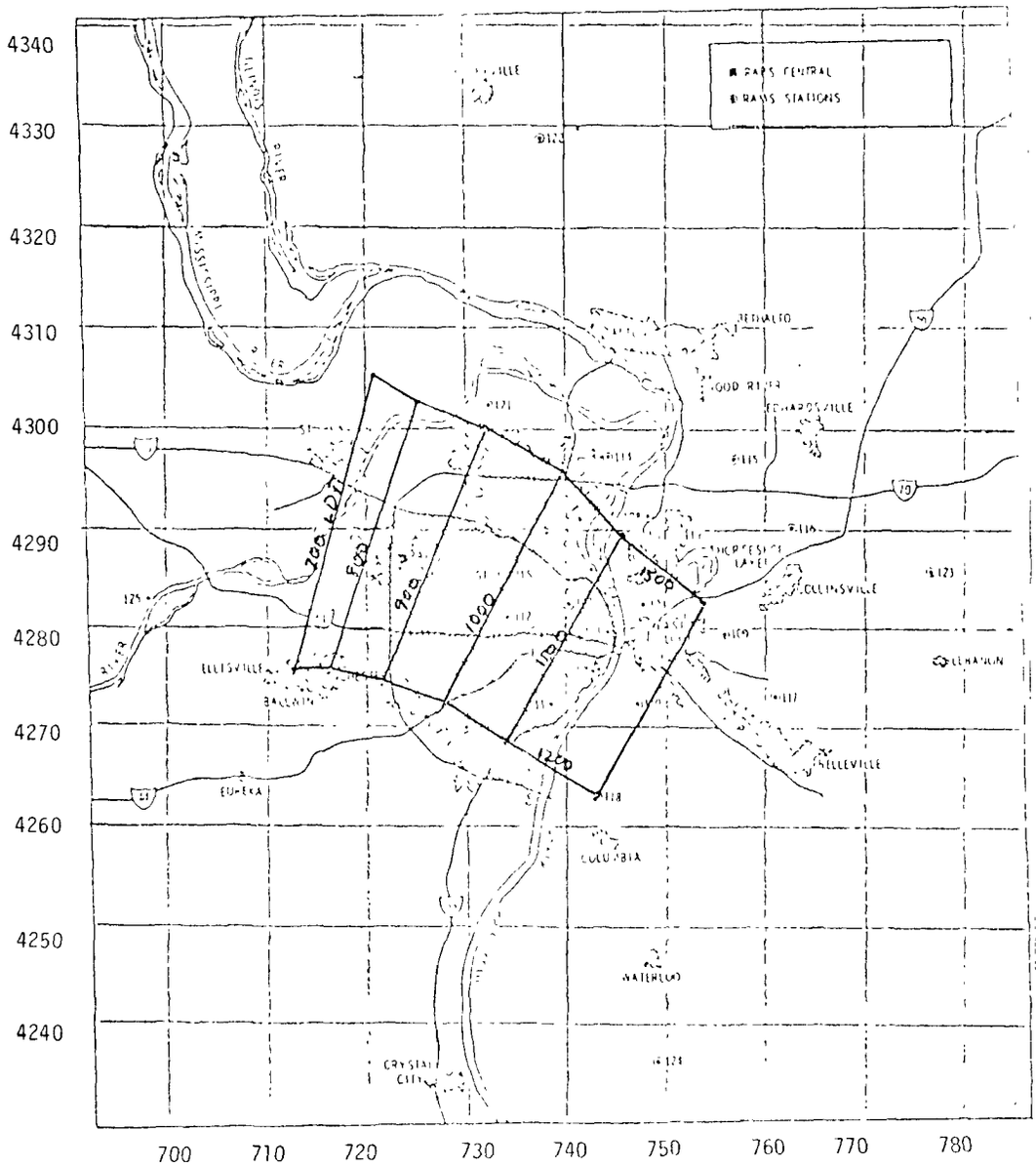

Figure 37. Trajectory for Day 160, June 8/Site 103

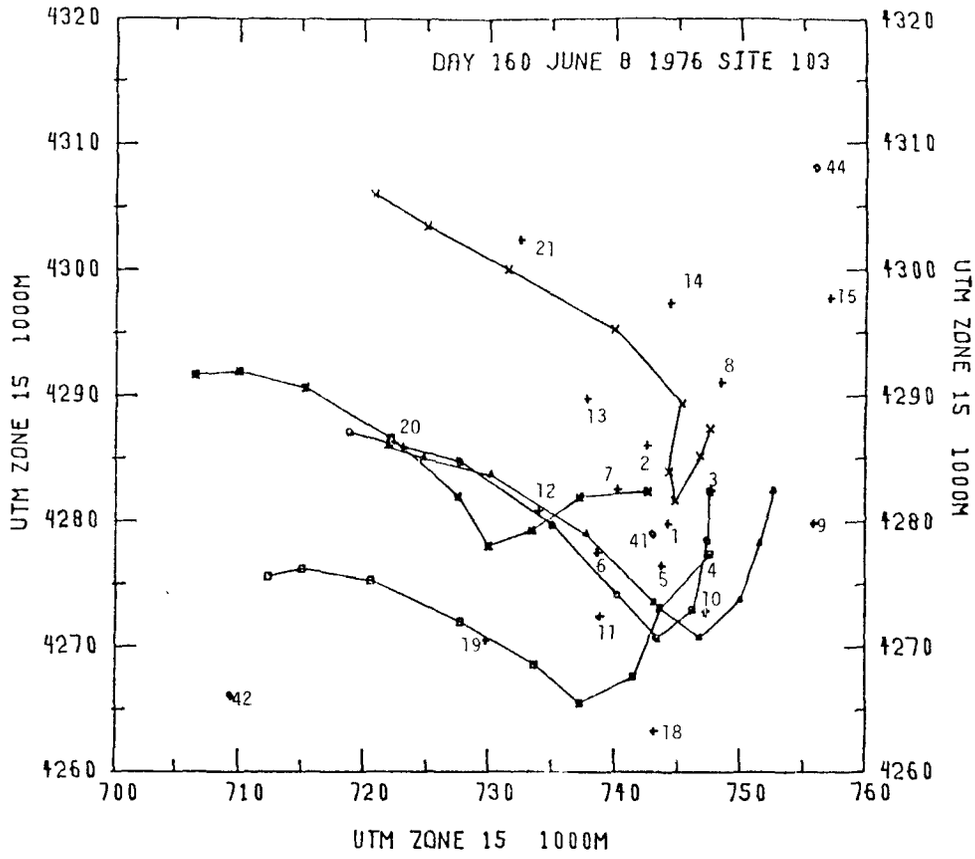

Figure 38. Individual trajectories, Day 160, Site 103.

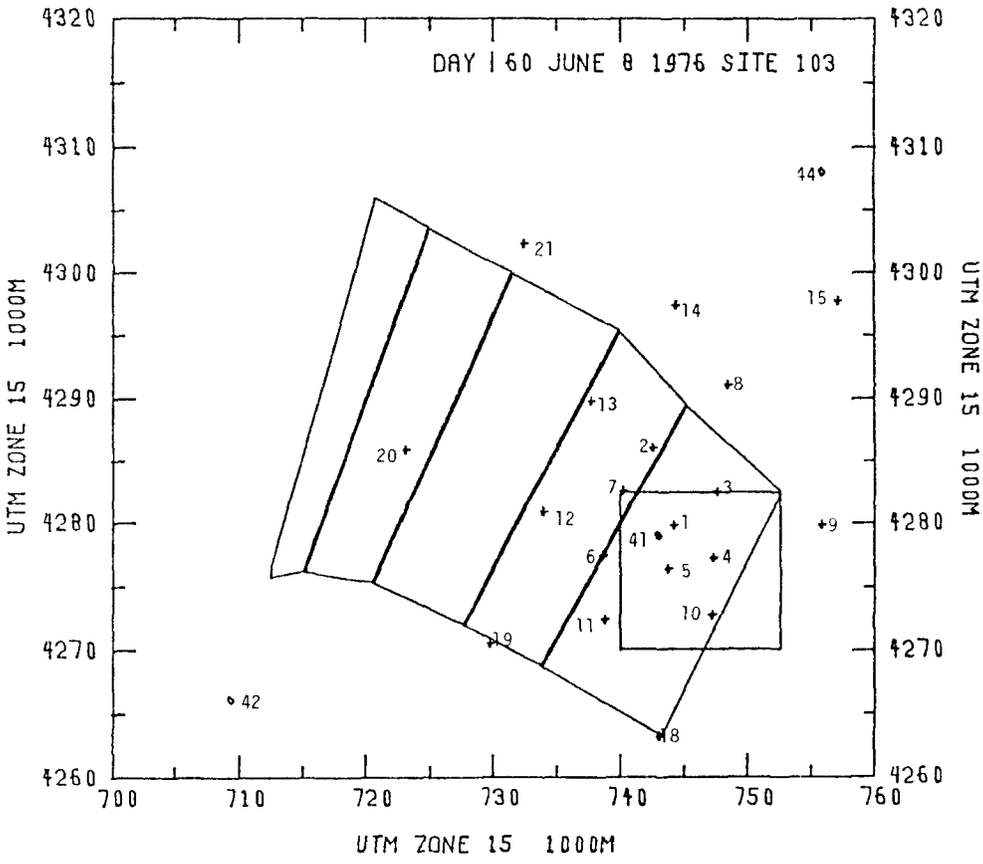

Figure 39. Boxes generated from trajectories, Day 160, Site 103.

D159 Trajectory. Figure 31 shows the map of the derived trajectory path for June 7. Figure 32 shows the coordinates of each backward trajectory for each hour and the nearest RAPS stations for which the wind and ambient data were derived. Figure 33 shows how the "boxes" were generated from the trajectories. Only one box was used for the first four hours of these trajectories.

D160/103 and D160/115 Trajectories. Two different sites were used on June 8, one in the center of the city (102) and one just north of the city (115). Trajectory calculations for these two sites illustrate some of the problems with the method used. The backward trajectories from site 115 (Figure 35) generally maintained about a 10 Km spread showing some narrowing from 10 am to 9 am. Most of the close wind stations were south of the trajectory. The 103 site, however, is surrounded by wind stations (Figure 38). After three hours of back calculations these trajectories diverge dramatically, ultimately becoming wider than the whole city!

Figure 40 shows both sets of trajectories on the same plot.

Other Days Trajectories. Maps, trajectories (where supplied) and "boxes" for other RAPS days used in this study are shown in Figures 41 to 54.

The trajectories and "boxes" for October 1 (Figures 52 and 53) were not done by computer program but were done by manual methods and detailed examination of data printouts (it was the first day to be studied by OAQPS). UNC was supplied no supporting documentation for the shapes and locations of the "boxes" shown in Figure 53. These boxes were used to select emissions sources.

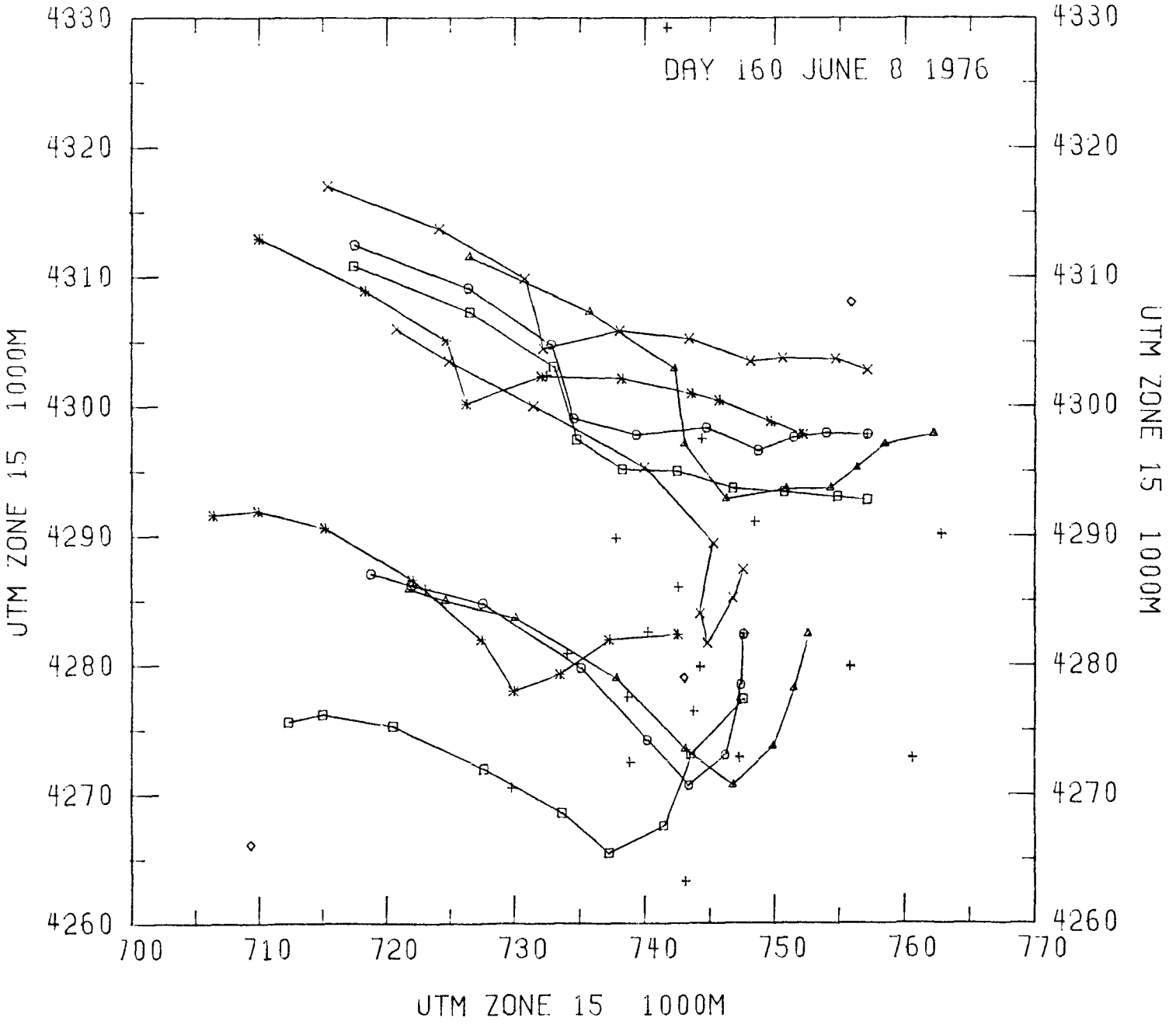

Figure 40. Comparison of individual trajectories, both sites, Day 160.

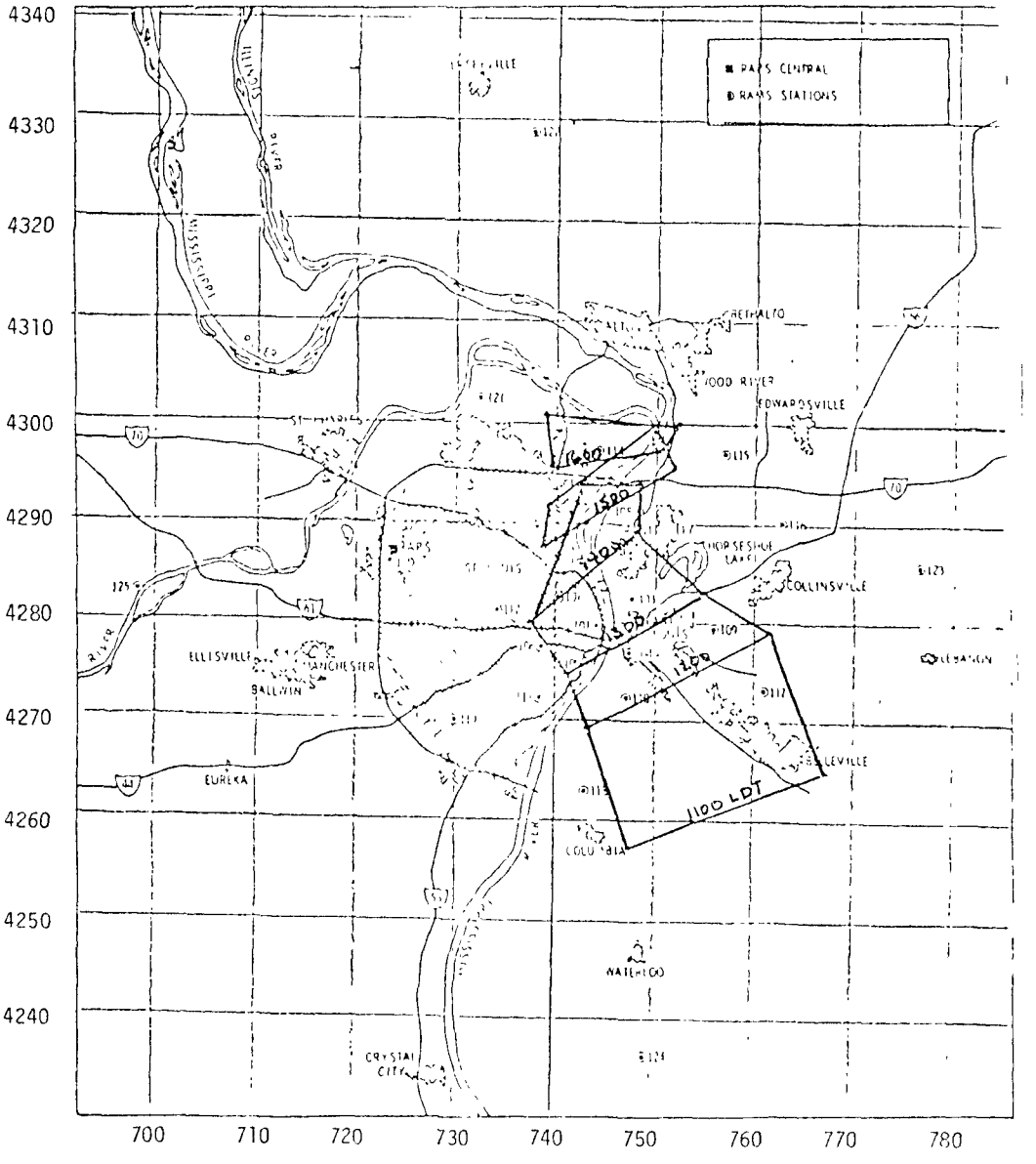

Figure 41. Trajectory for Day 195, July 13/Site 114

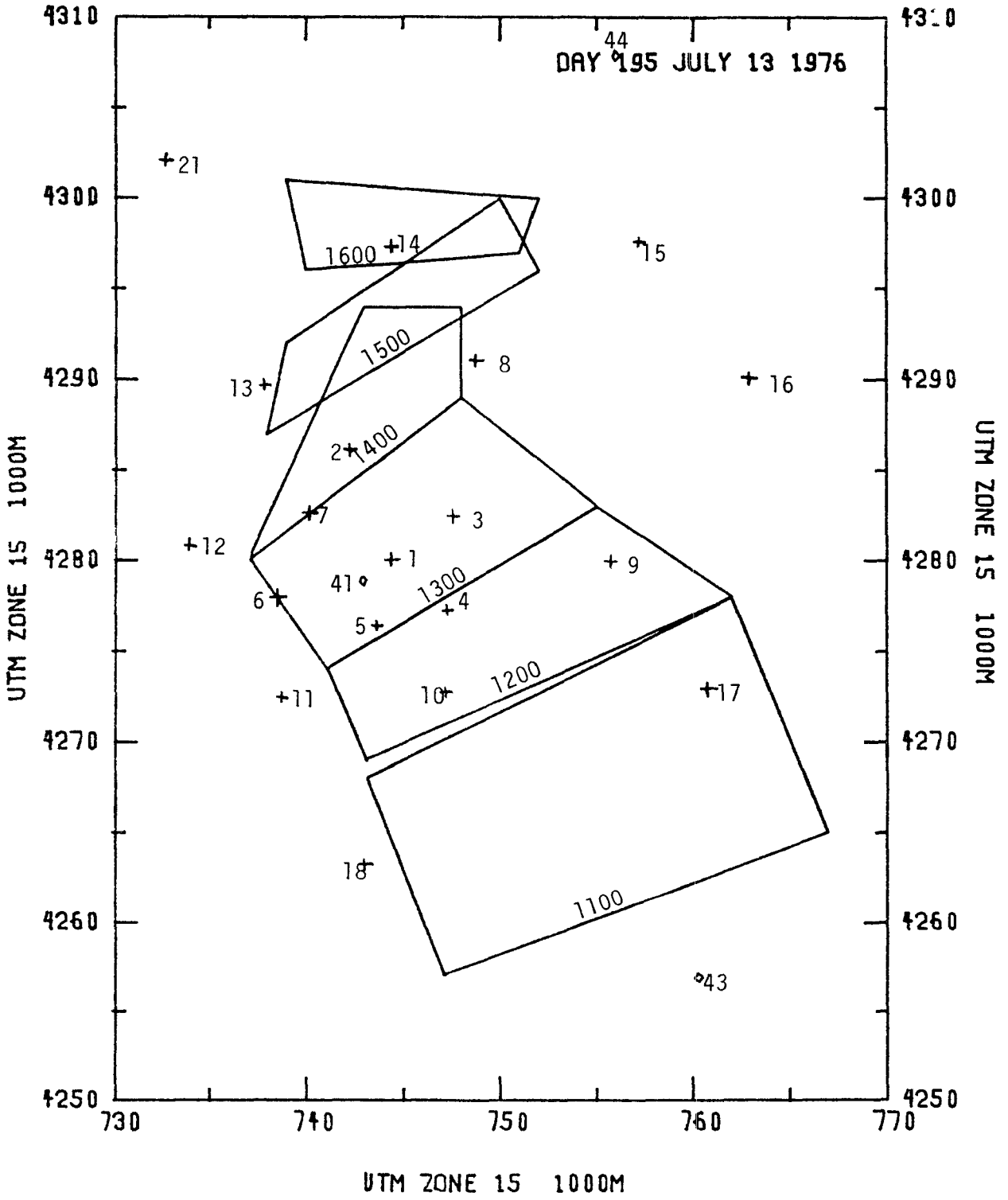

Figure 42. Boxes generated from trajectories, Day 195.

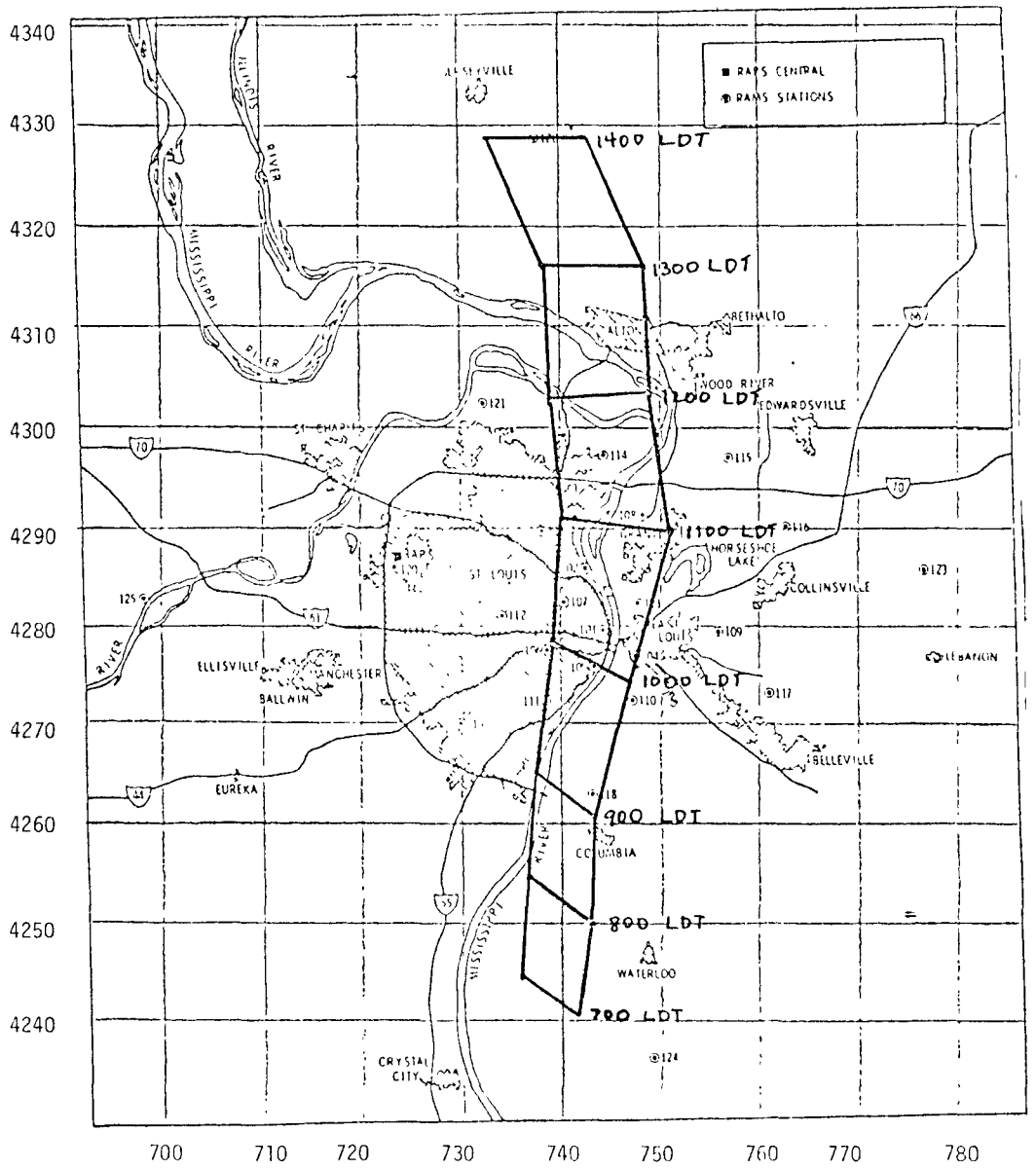

Figure 43. Column Path for Day 201, July 19

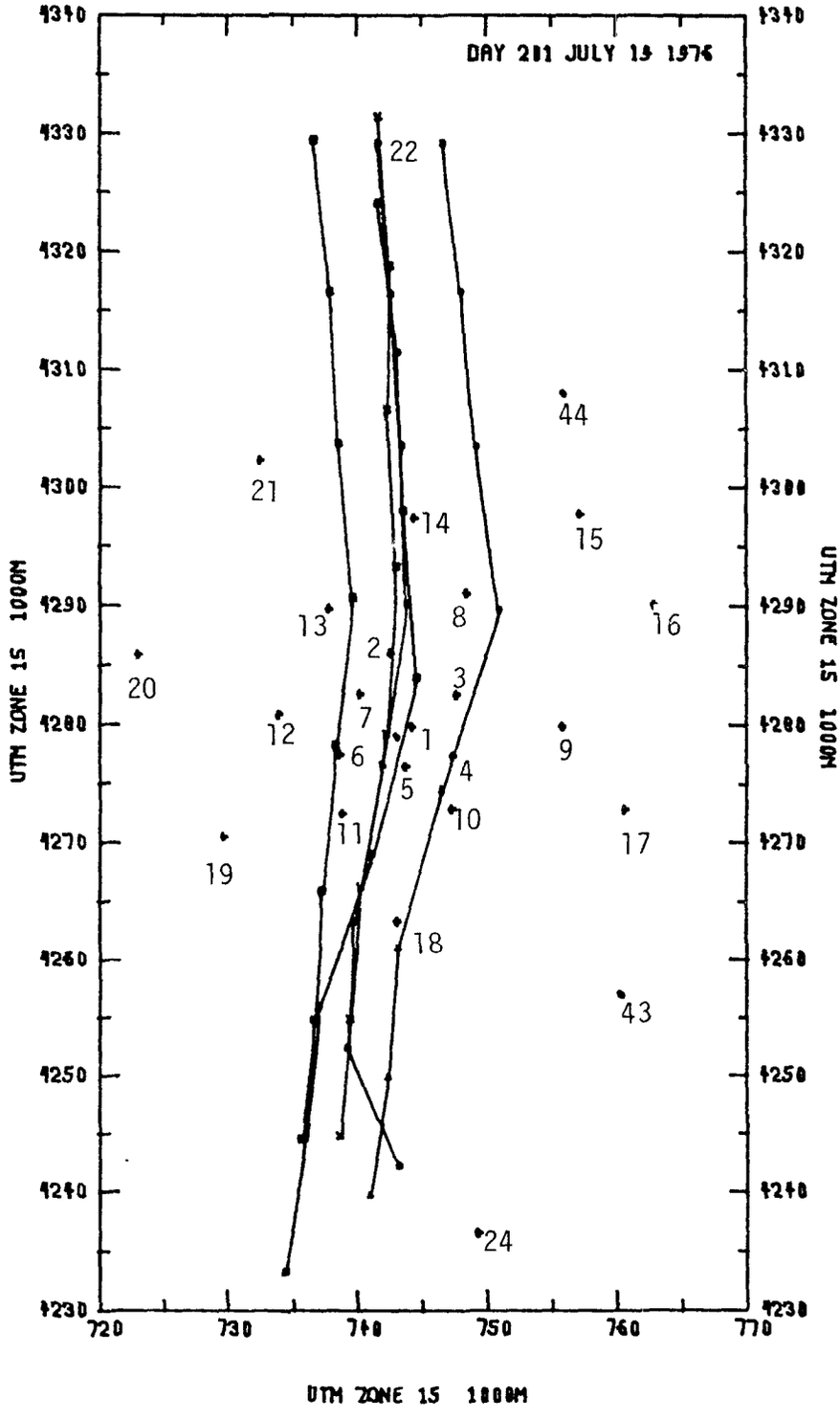

Figure 44. Individual trajectories, Day 201.

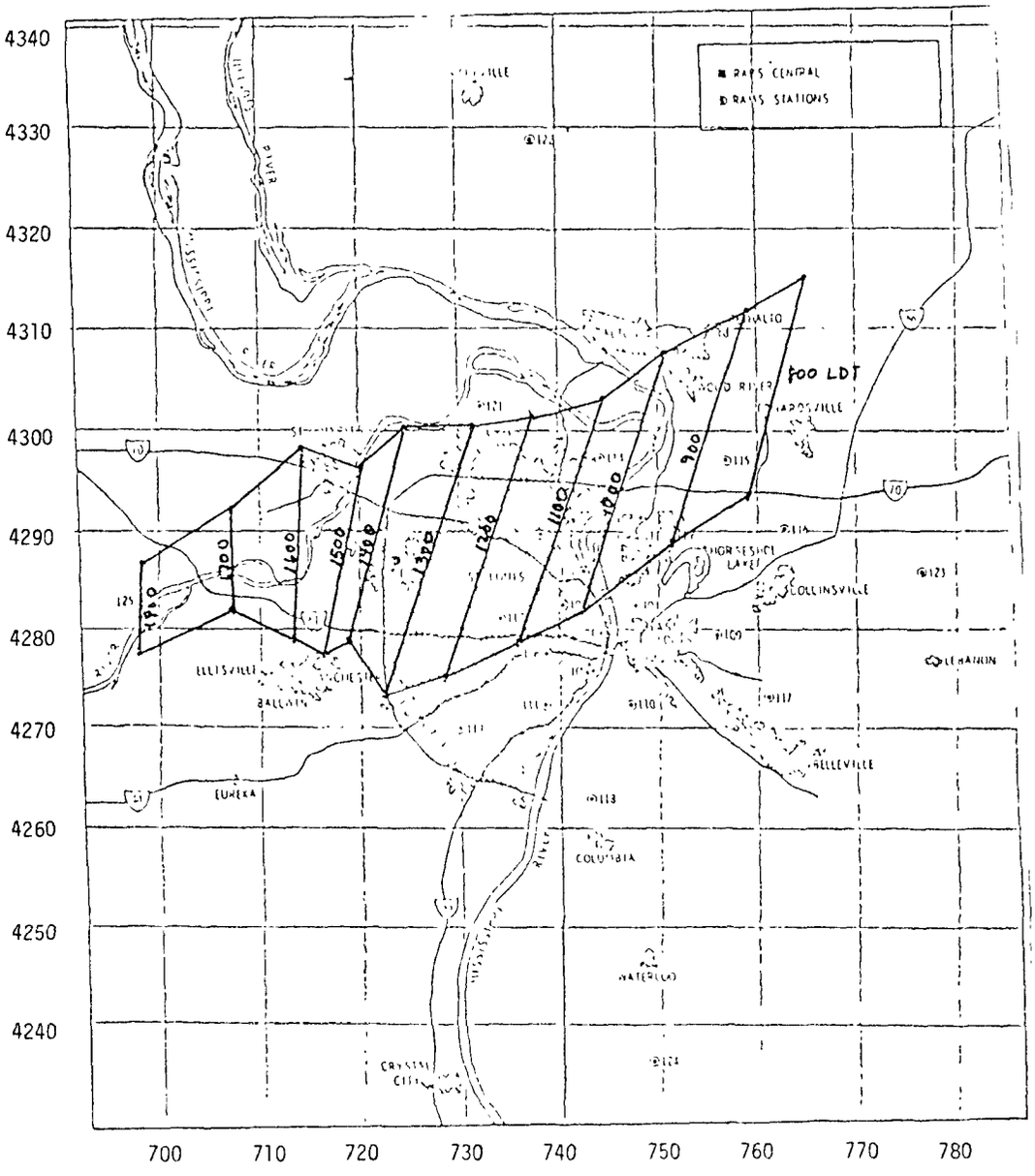

Figure 45. Trajectory for Day 221, August 8/Site 125

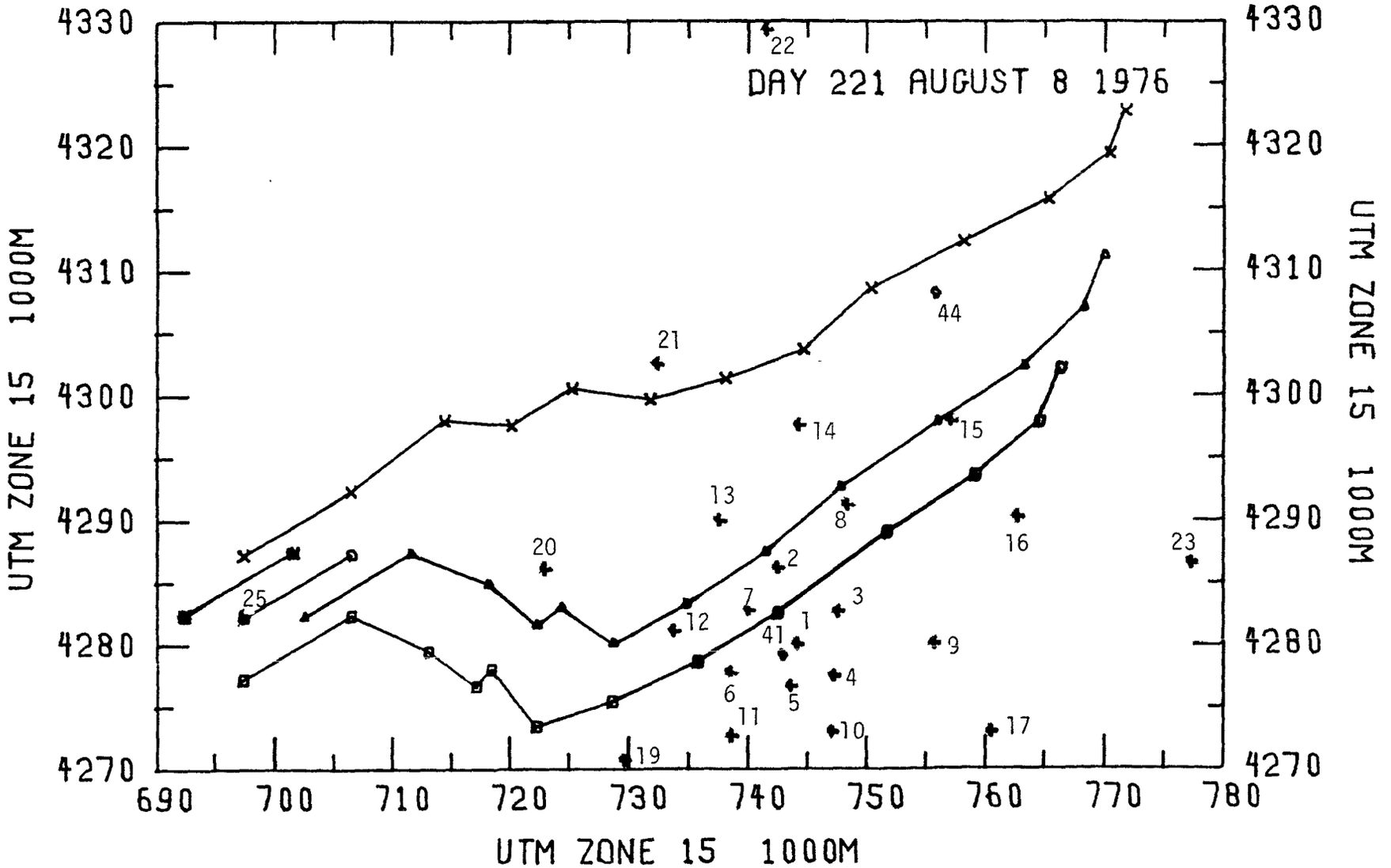

Figure 46. Individual trajectories, Day 221.

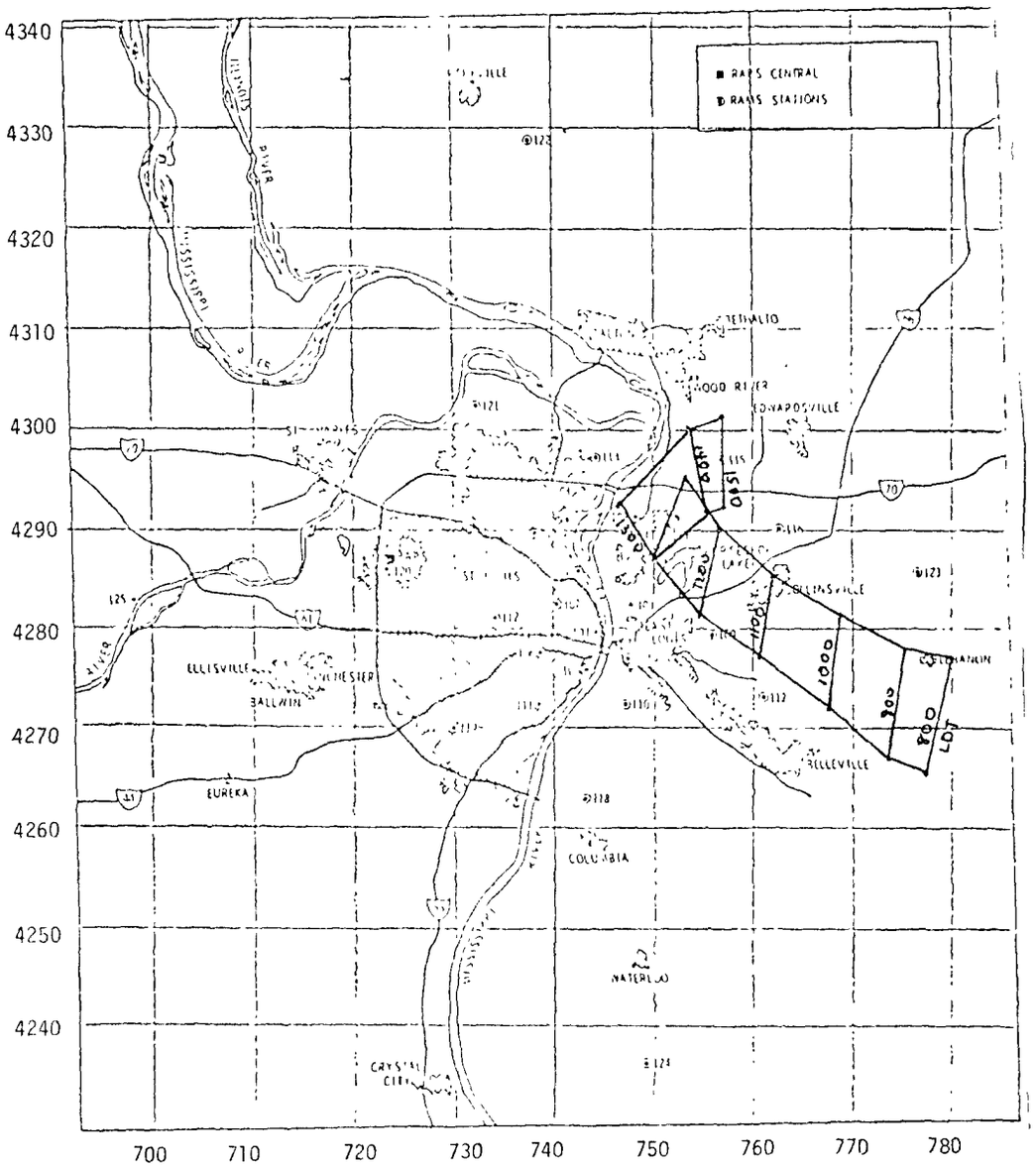

Figure 47. Trajectory for Day 238, August 25/Site 115

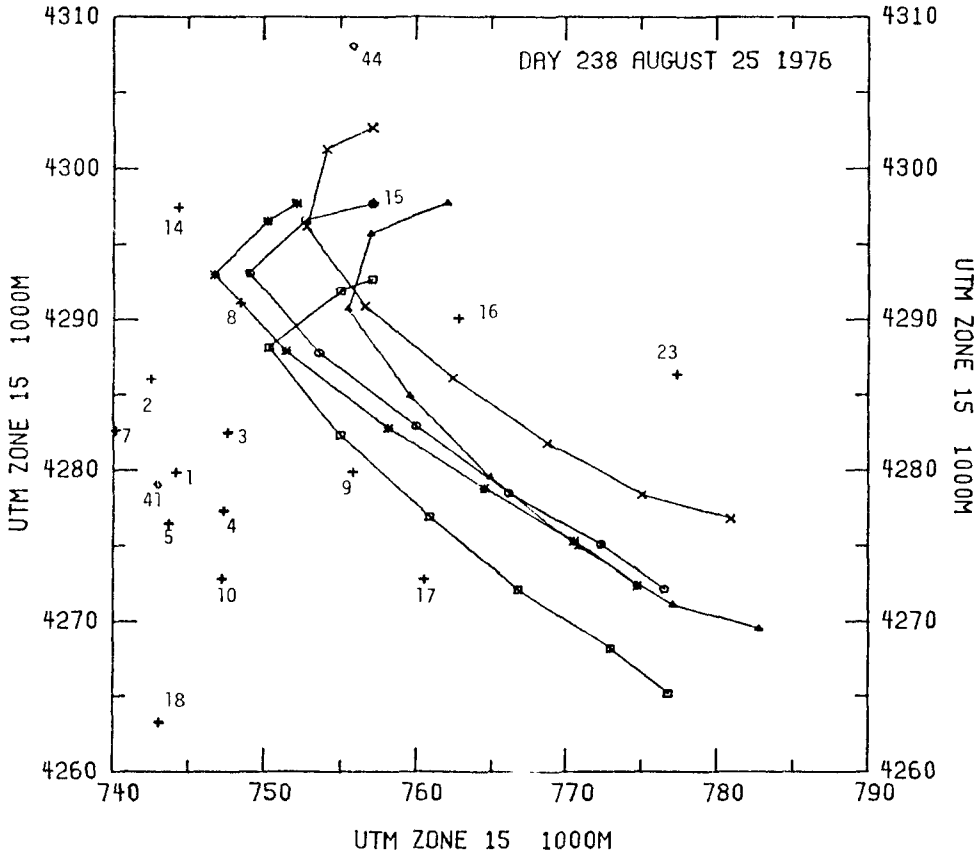

Figure 48. Individual trajectories, Day 238.

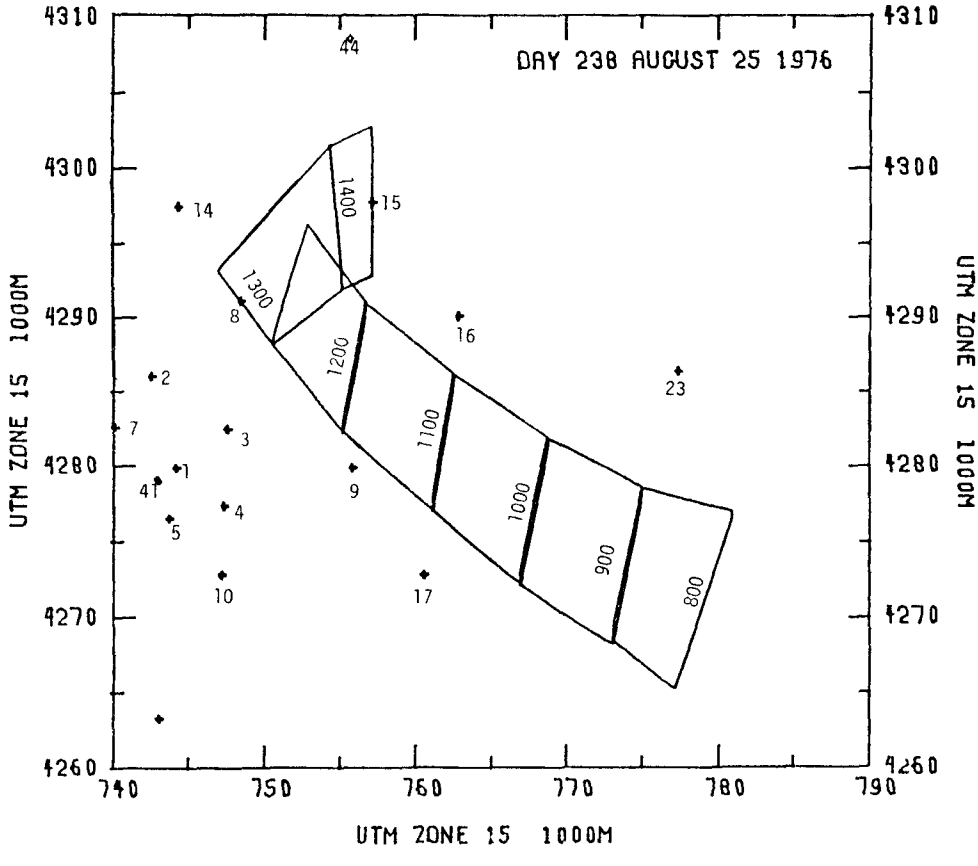

Figure 49. Boxes generated from trajectories, Day 238.

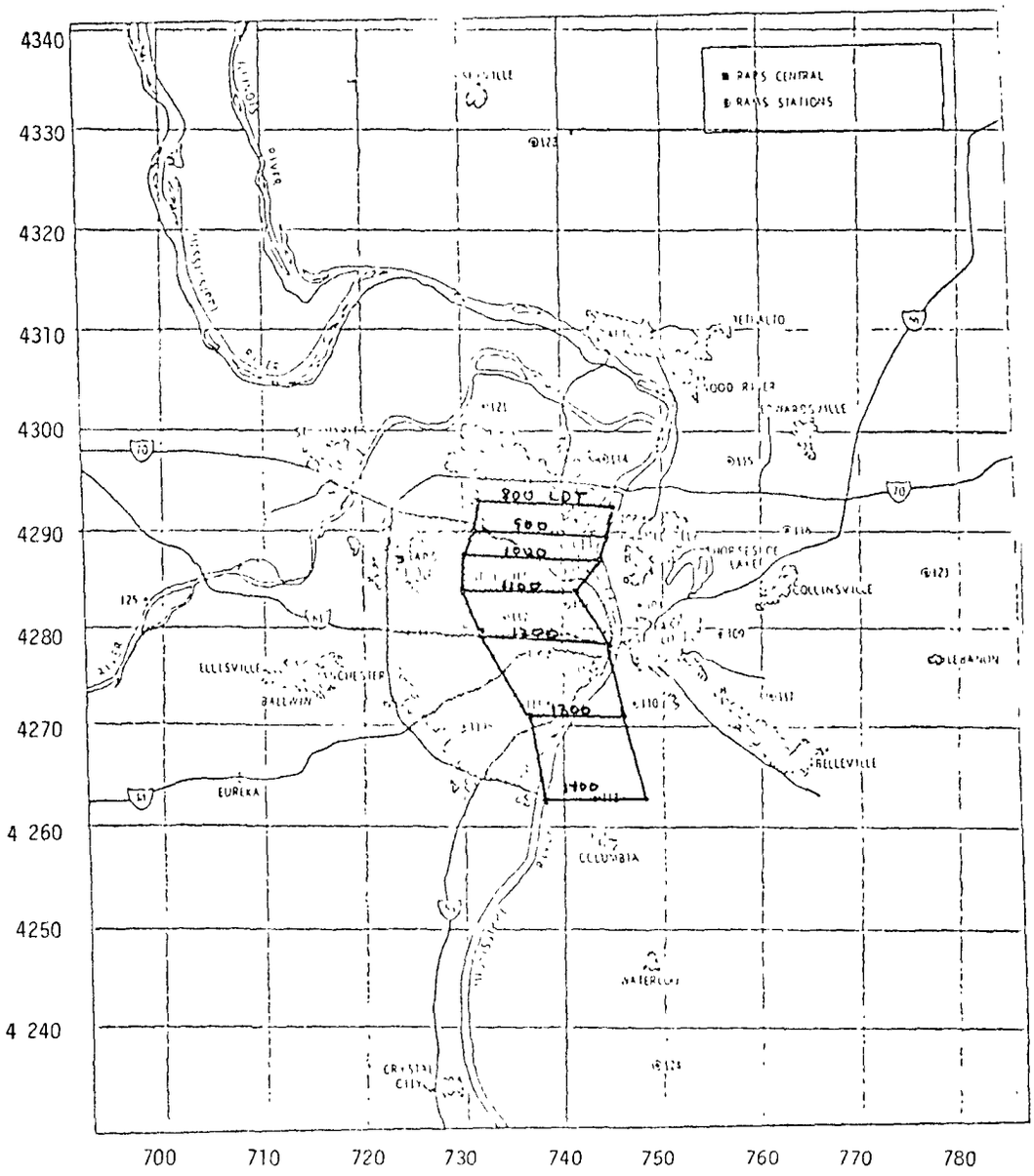

Figure 50. Trajectory for Day 261, September 17/Site 118

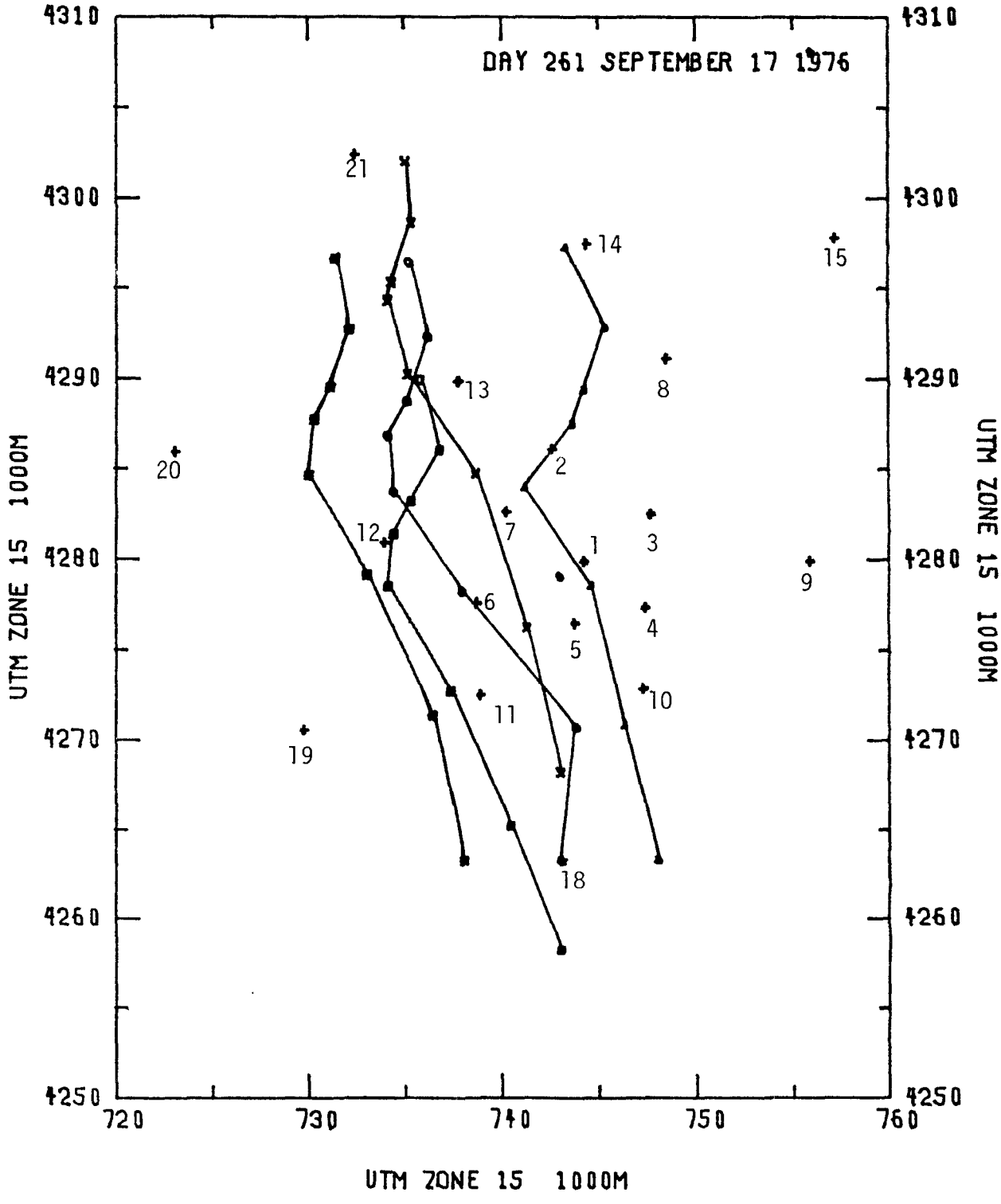

Figure 51. Individual trajectories, Day 261.

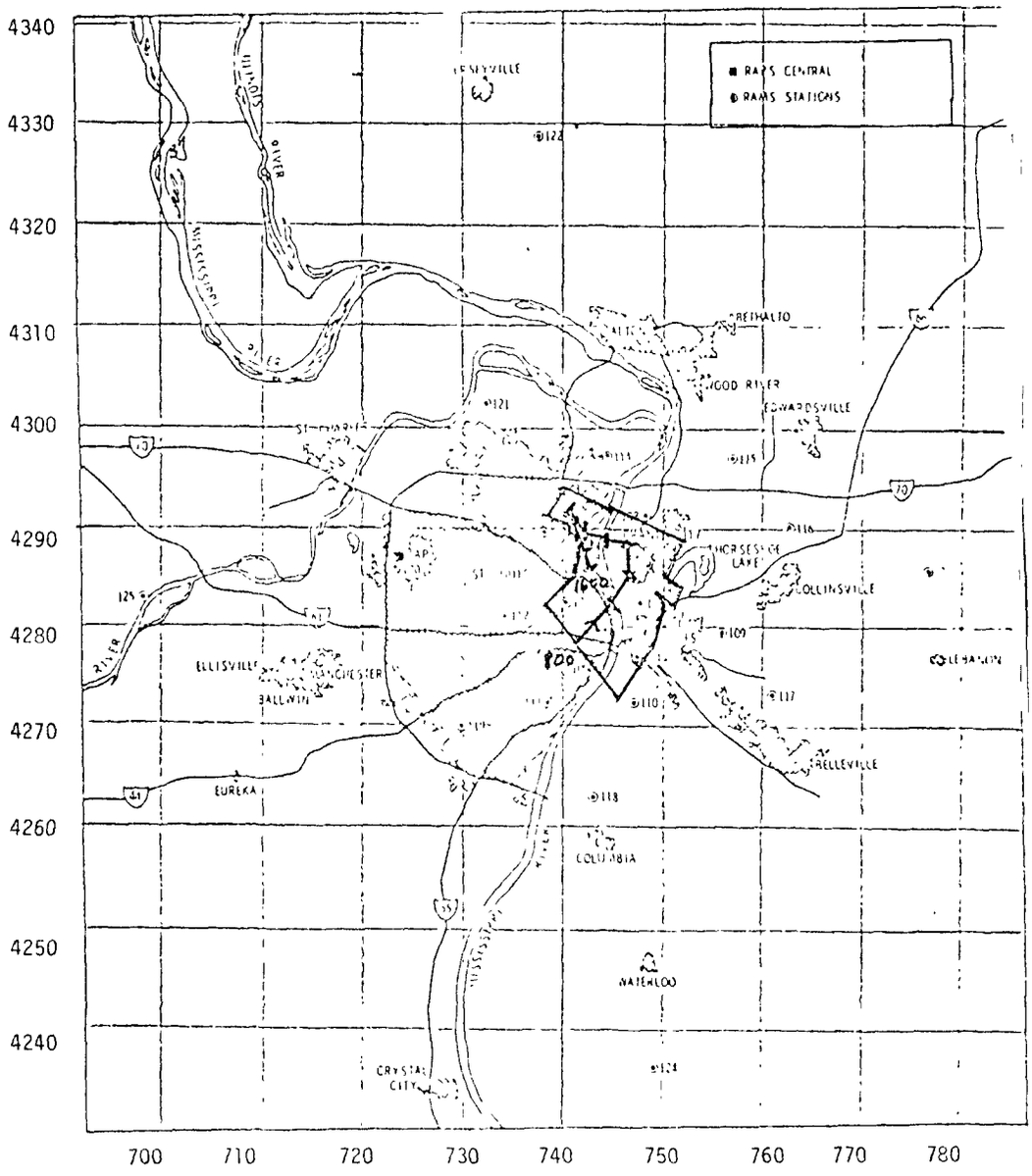

Figure 52 Trajectory for Day 275, October 1/Site 102

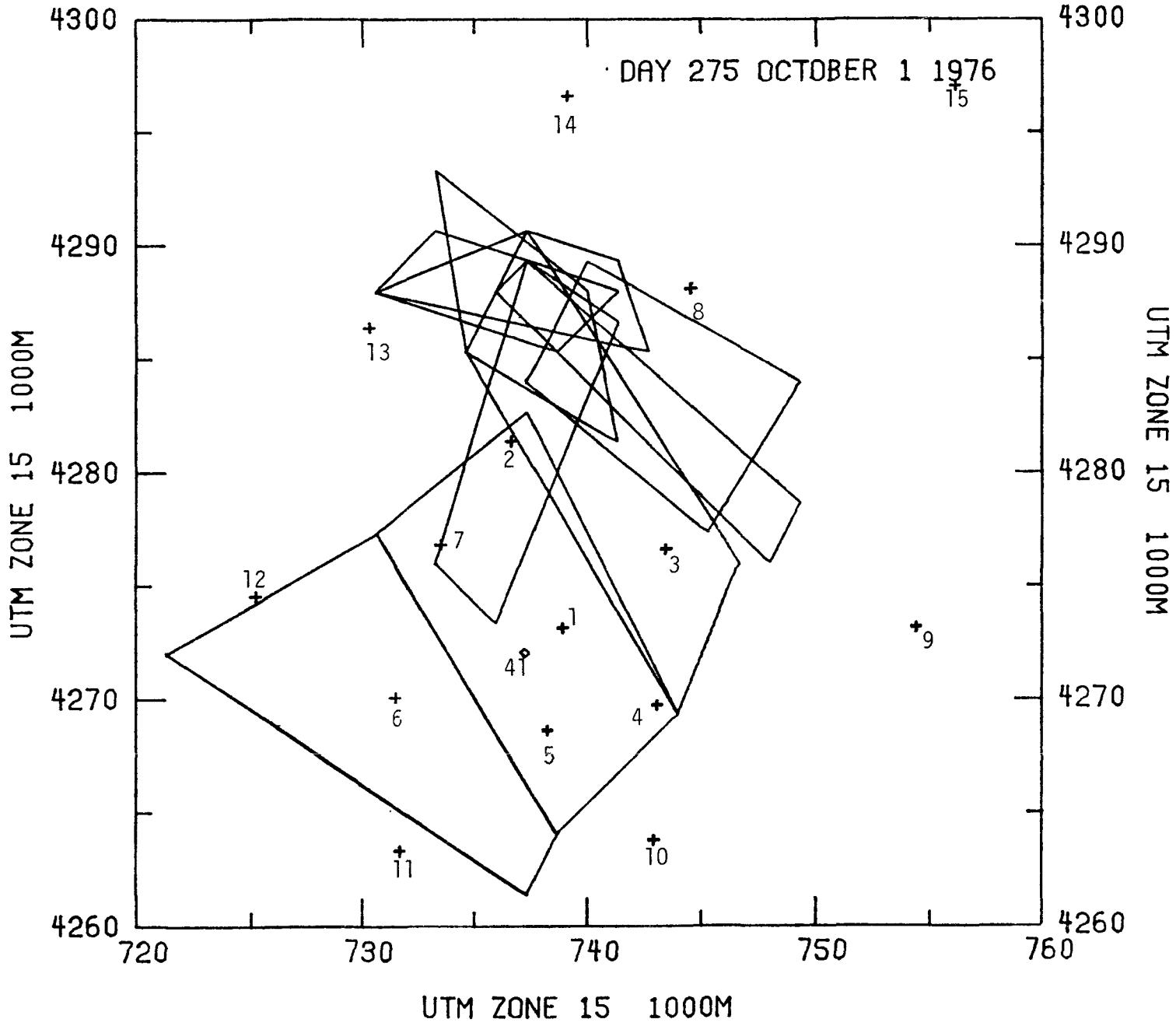

Figure 53. Boxes generated by inspection.

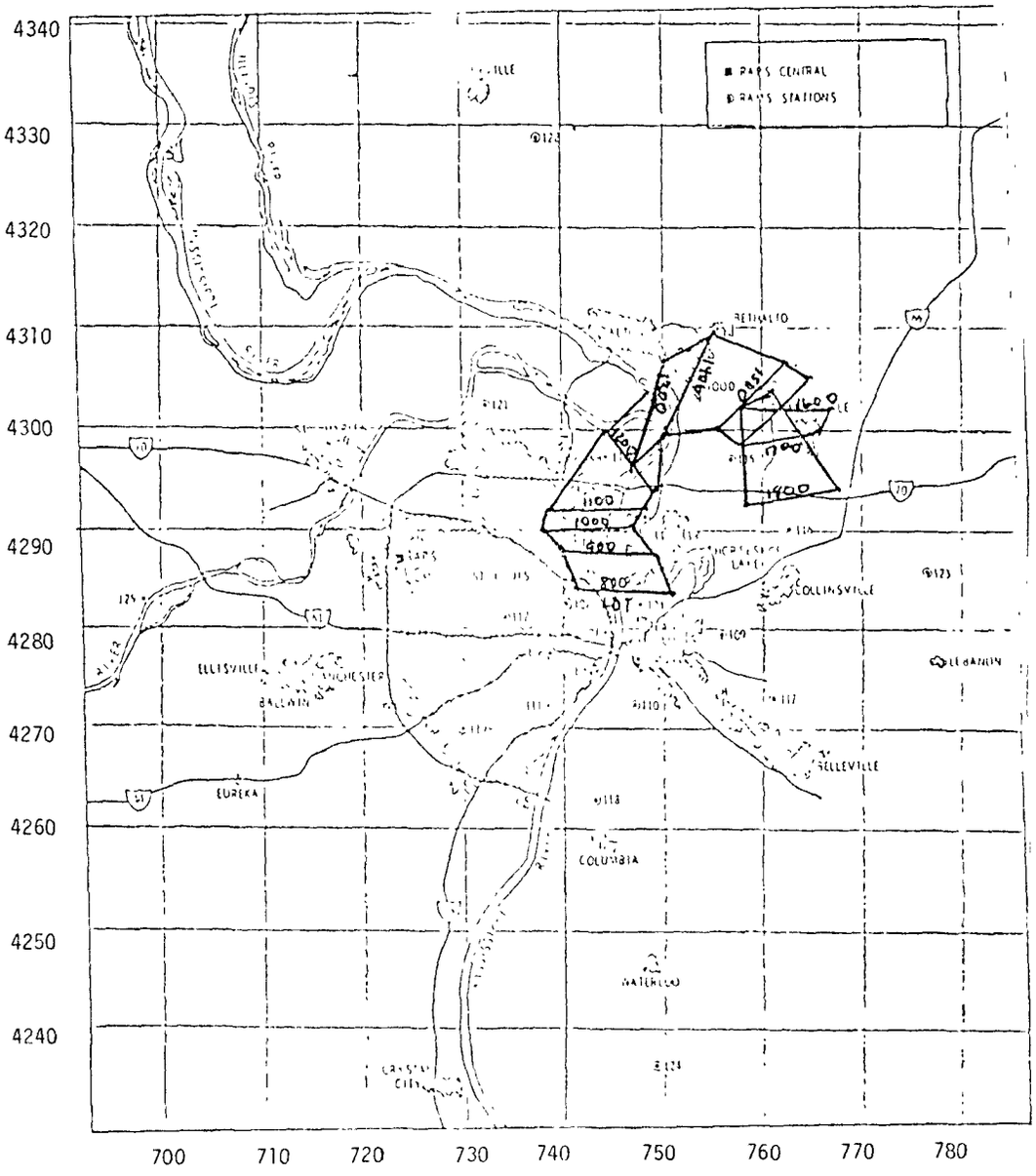

Figure 54 Trajectory for Day 276, October 2/Site 115

7.2 AMBIENT DATA ALONG TRAJECTORIES

The ambient data along the trajectories were supplied by OAQPS/EPA. An example of the ambient data printout is shown in Table 16. The table information was generated as follows. Given the midpoint of the trajectory path for each hour, the program searched the RAPS database for the three nearest RAMS station (see the second and third columns of Table 16). The hourly averaged concentration of each species and the number of minutes used to compute the average is shown in columns 4 to 7. The hourly average in the hour before and the hour after the calculating time were averaged to estimate the value on the hour. That is, to calculate the 0900 LDT values for O_3, the 0800-0900 LDT average and the 0900-1000 LDT average were averaged to give the value at 0900 LDT for each of the 3 closest stations. To estimate the probable value at the center line of the trajectories, the average values at the three closest stations were combined into a weighted average using the square of the reciprical of the distance between the trajectory location and the station location (column three, Table 16). This weighted average is shown in the last column in Table 16.

The average values for each day were used to select the simulation initial conditions. These values are given in Table 17.

Figures 55 to 64 show the ambient concentrations along the calculated trajectories as a function of time. Also included are the temperature and total solar radiation for each day. Three lines are shown in each plot. The solid line connects the $1/r^2$ weighted average points. The bottom dashed line connects the value from the station with the lowest value of the three used to compute the weighted average and the upper dashed line connects the value from the station with the highest value of the three used to compute the weighted average. The hourly averaged values are centered (plotted on

Table 16. Sample Ambient Data Printout

DAY 159 JUNE 7

TIME(LDT)

900

POLLUTANT	SITE	DIST(KM)	800-900		900-1000		AVERAGE	WT. AVERAGE
O3	15	2.52	.537-01	51	.942-01	59	.0739	
	16	11.84	.000	0	.000	0	[illegible]	
	8	12.45	.188-01	52	.344-01	60	.0366	.0725
NOX	15	2.52	[illegible]	51	.325-1	59	[illegible]	
	16	11.84	.406-01	44	.246-1	57	.0326	
	8	12.45	.971-01	52	.497-01	60	.0714	.0354
CO	15	2.52	.000	0	[illegible]		[illegible]	
	16	11.84	.489+00	46	.412+00	59	.45[illegible]5	
	8	12.45	.535+00	52	.318+00	6	.4267	.4392
NO	15	2.52	[illegible]	51	[illegible]	59	[illegible]	
	16	11.84	.765-2	44	.319-2	57	.0054	
	8	12.45	.292-1	52	.897-2	6	.0141	.0034
NO2	15	2.52	.33[illegible]-01	51	.298-1	59	.0314	
	16	11.84	.329-01	44	.218-1	57	.0272	
	8	12.45	.44 -01	52	.4[illegible]-1	6	.0524	.0320
NMHC	15	2.52	.790+00	23	.524+[illegible]	1	.5563	
	16	11.84	.409+00	46	.5[illegible]	59	.4577	
	8	12.45	.330+00	52	.217+[illegible]	55	.2702	.6353
TEMP	15	2.52	.203+02	52	.23[illegible]+2	59	21.5767	
	16	11.84	[illegible]	47	.231+[illegible]2	57	21.8527	
	8	12.45	.211+02	52	.235+2	60	22.3040	21.7078

Table 17

Simulation Initial Conditions

DAY	NMHC	NO	NO_2	O_3	CO
159	0.49	0.0082	0.029	0.034	0.731
160/103	0.26	0.0445	0.0121	0.011	0.484
160/115	0.10[a]	0.0105	0.0037	0.062	0.200
195	0.10[a]	0.0027	0.0028	0.059	0.115
201	0.10[a]	0.0052	0.0026	0.056	0.159
221	0.10[a]	0.0051	0.0047	0.016	0.185
238	0.22	0.011	0.0096	0.010	0.581
261	0.20	0.0199	0.0307	0.008	0.872
275/6	1.10	0.0265	0.0886	0.005	1.319
275/8	1.89	0.1466	0.0553	0.005	3.153
276	2.98	0.1219	0.3644	0.005	9.408

[a] assumed minimum value

the half-hour tic mark) and the average value between the hours is plotted on the hour tic mark. Because of the range of conditions for these 10 days, three different scale factors had to be used for NO_x, NMHC, and CO plots. The O_3 plots used one scale factor.

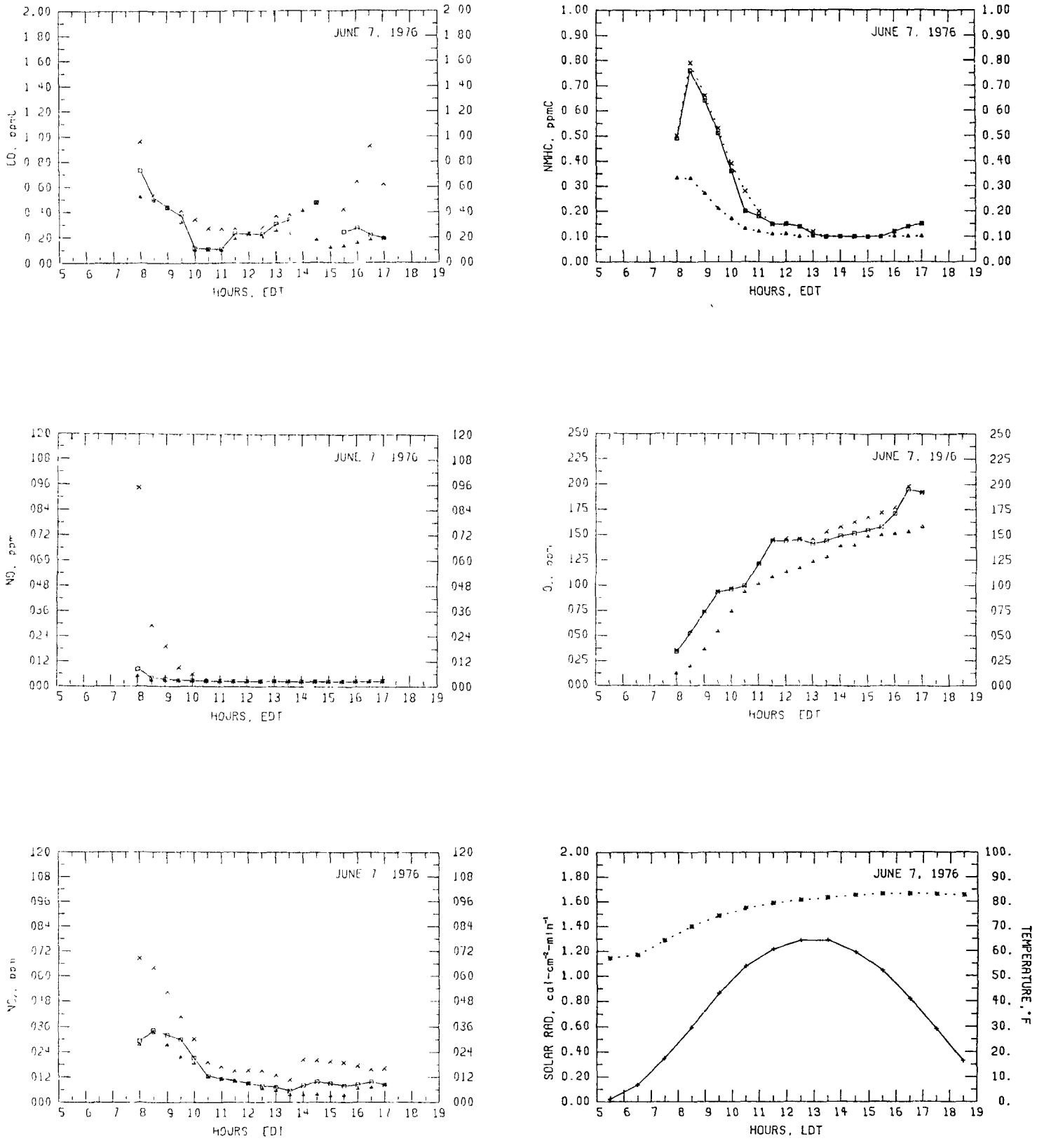

Figure 55. Ambient data, weighted mean, max and min for Day 159 trajectory.

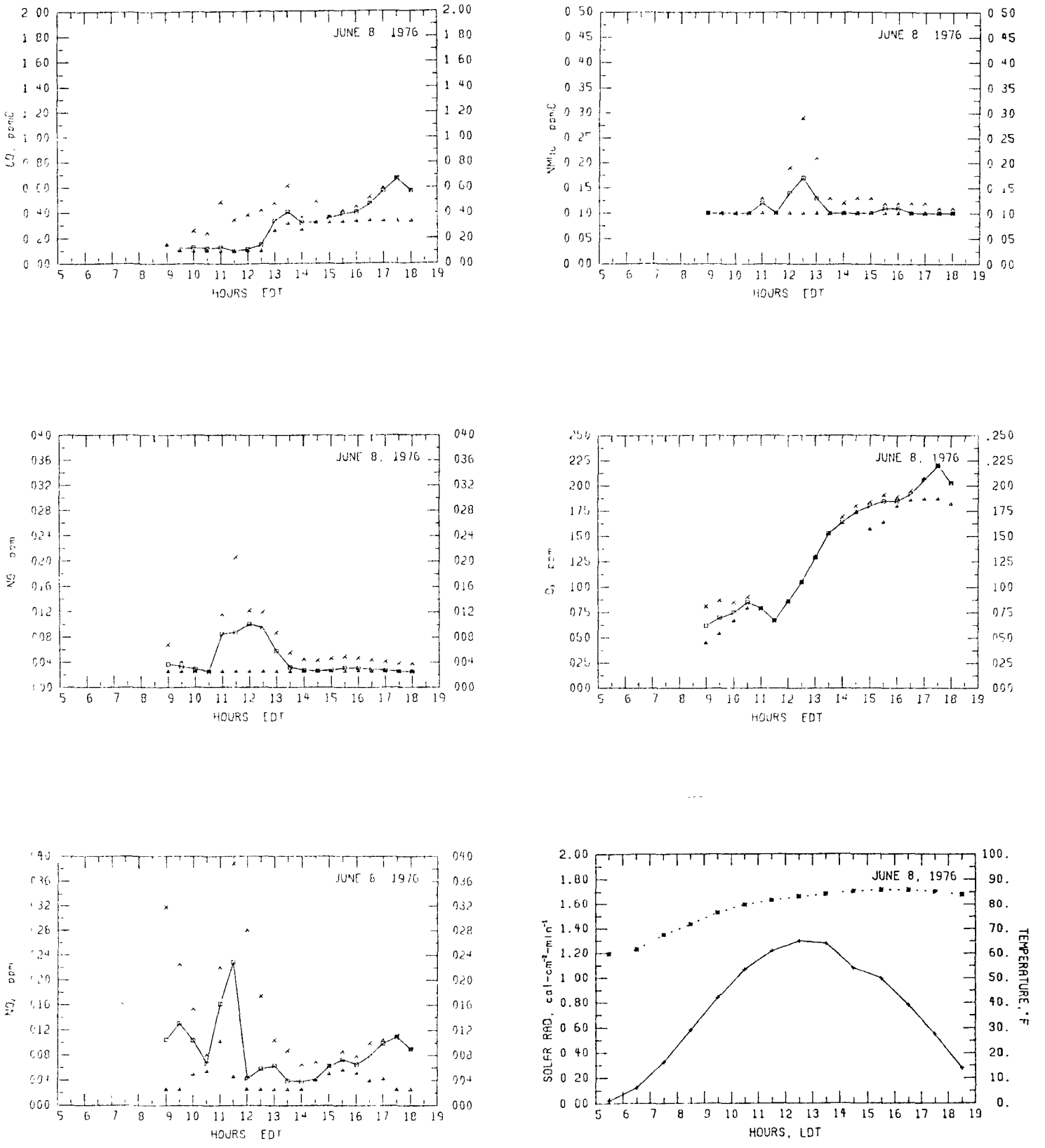

Figure 56. Ambient data, weighted mean, max and min for Day 160/115.

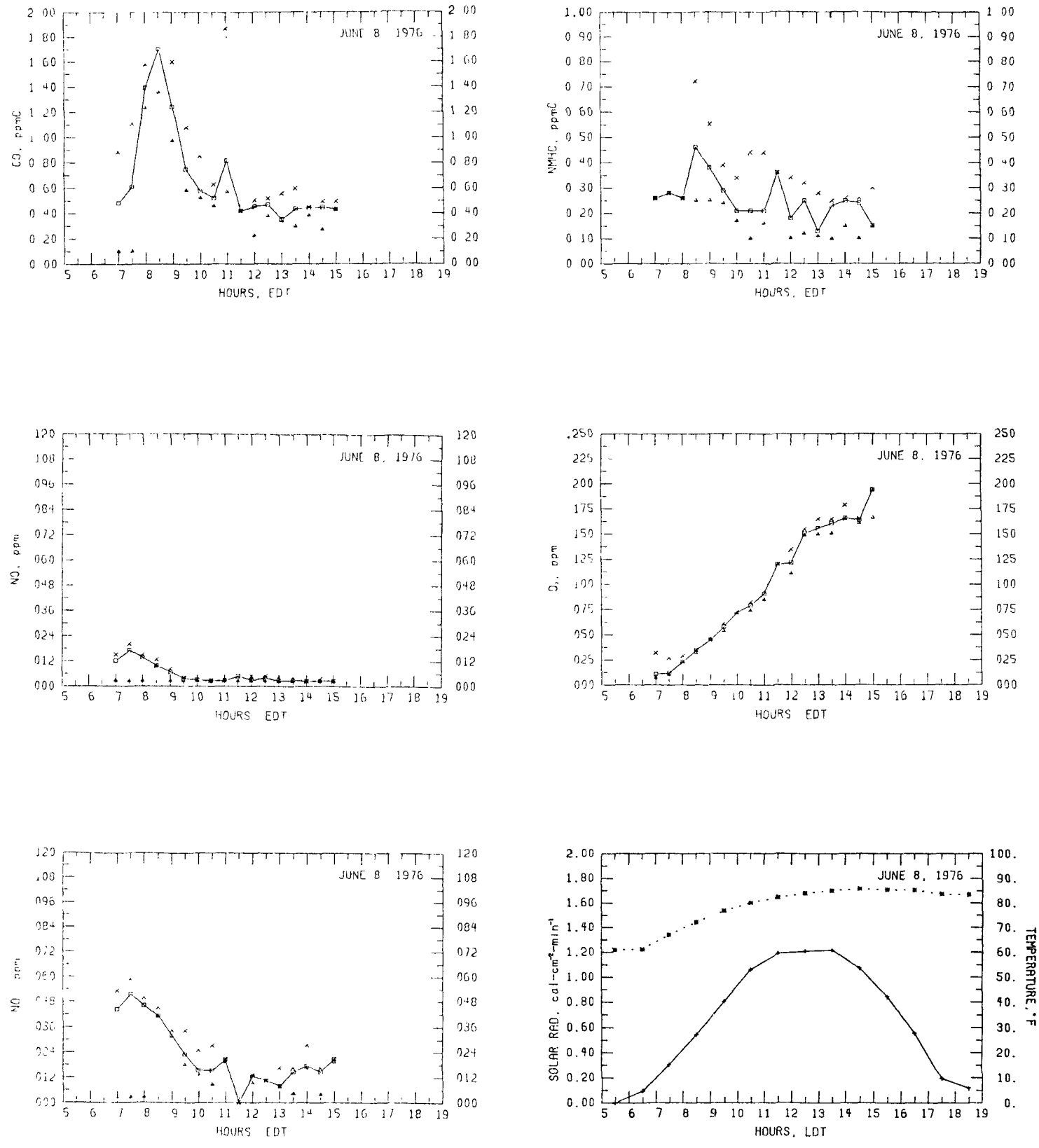

Figure 57. Ambient data, weighted mean, max and min for Day 160/103.

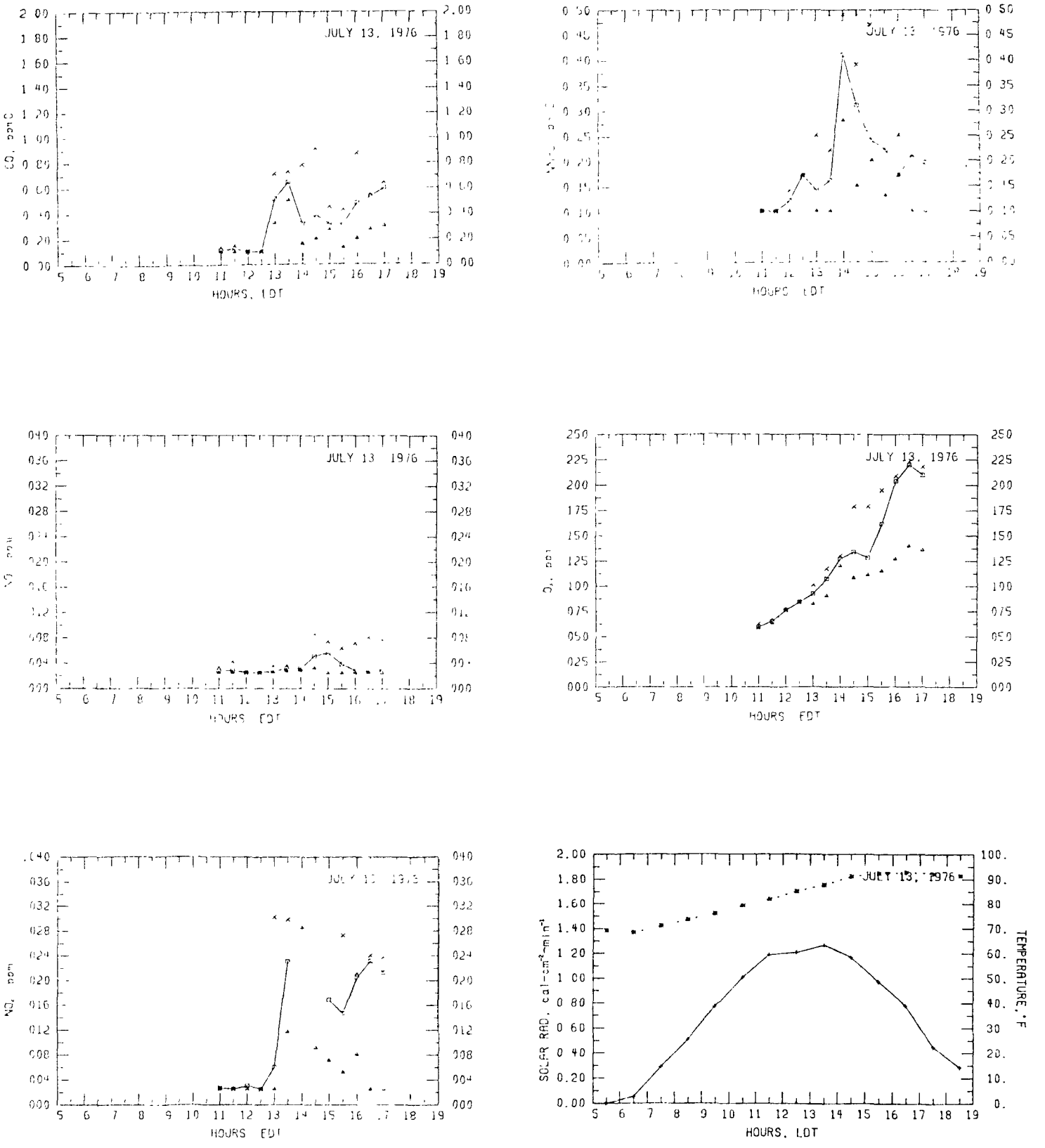

Figure 58. Ambient data, weighted mean, max and min for Day 195.

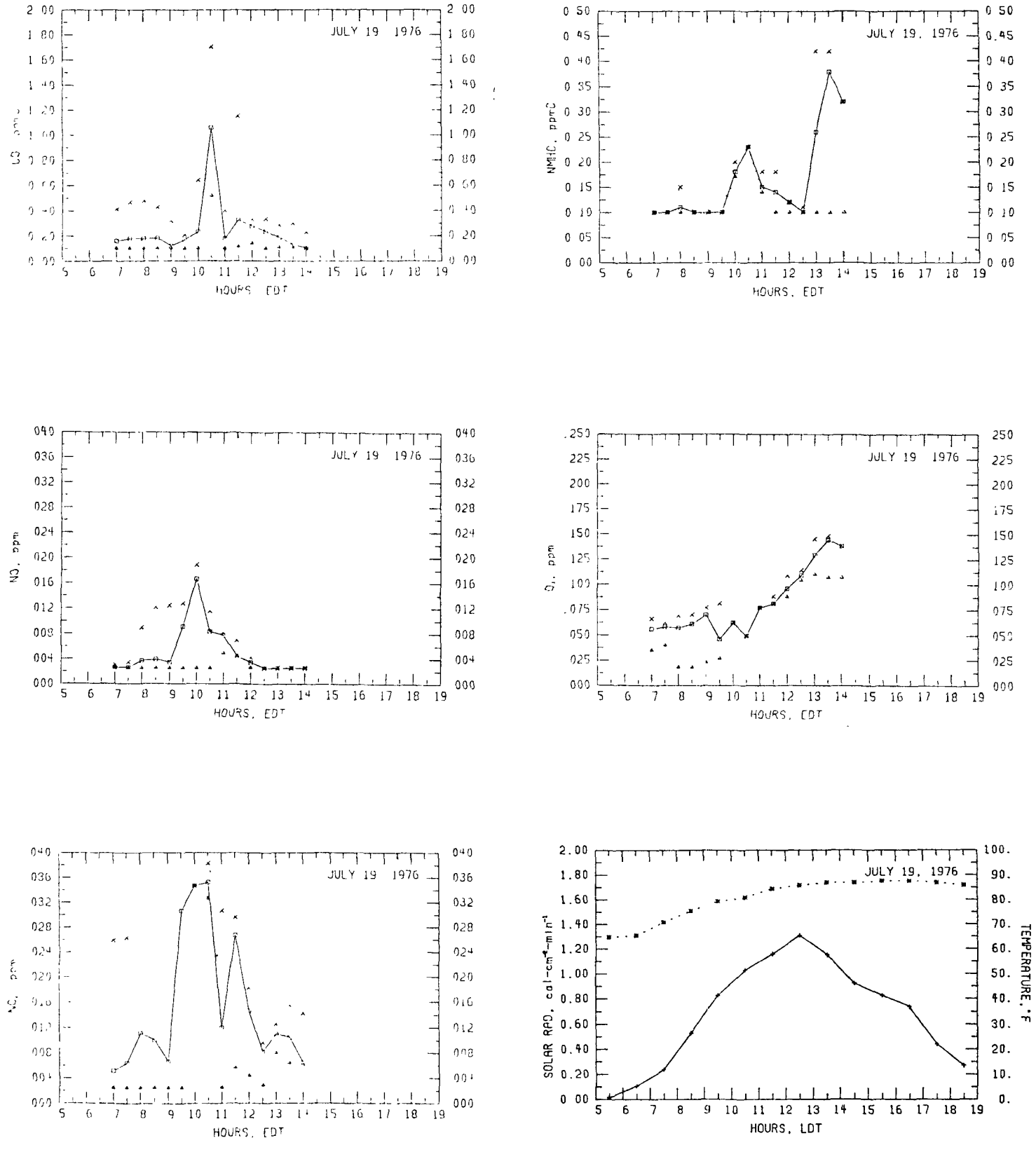

Figure 59. Ambient data, weighted mean, max and min for Day 201.

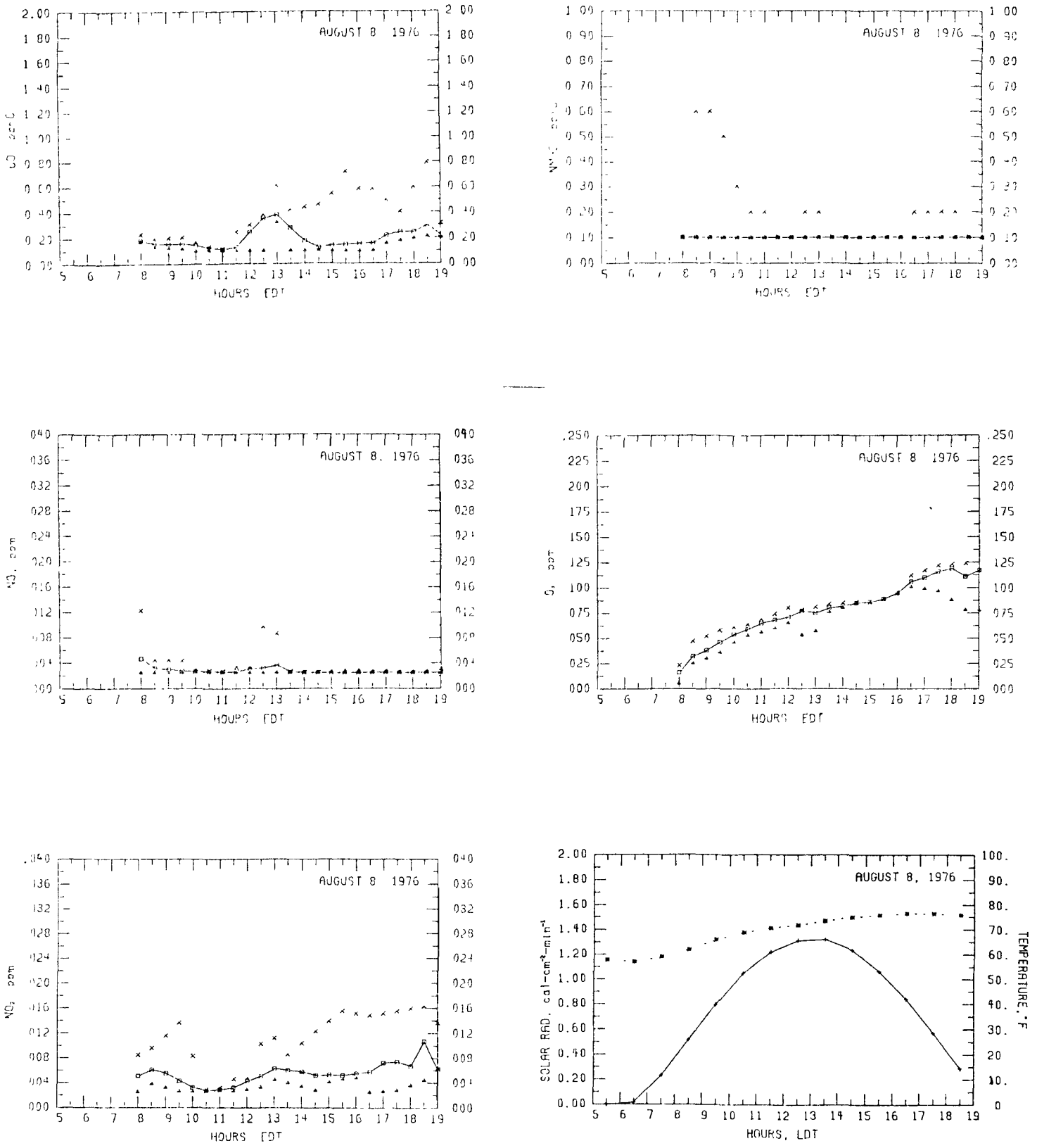

Figure 60. Ambient data, weighted mean, max and min for Day 221.

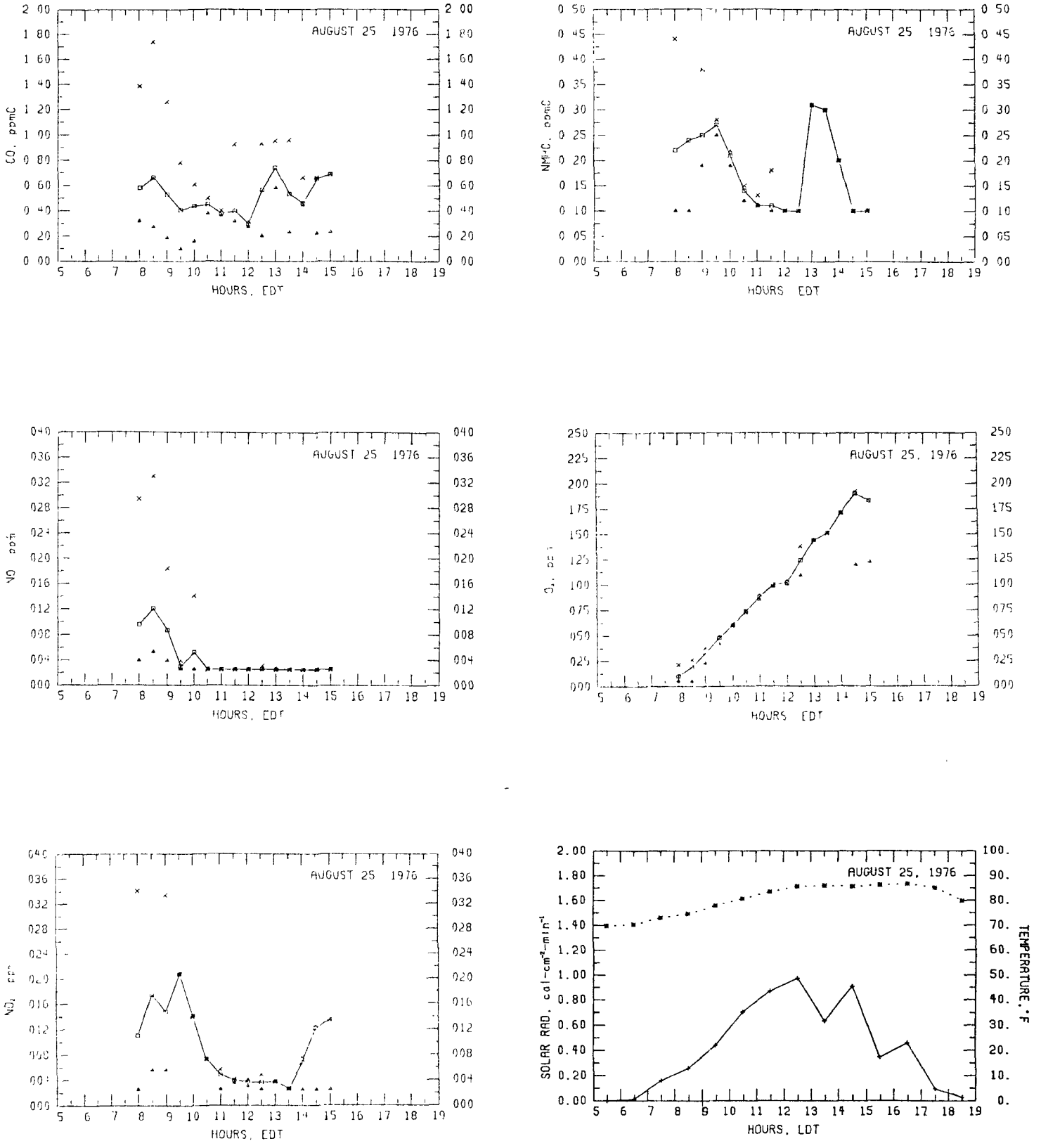

Figure 61. Ambient data, weighted mean, max and min for Day 238.

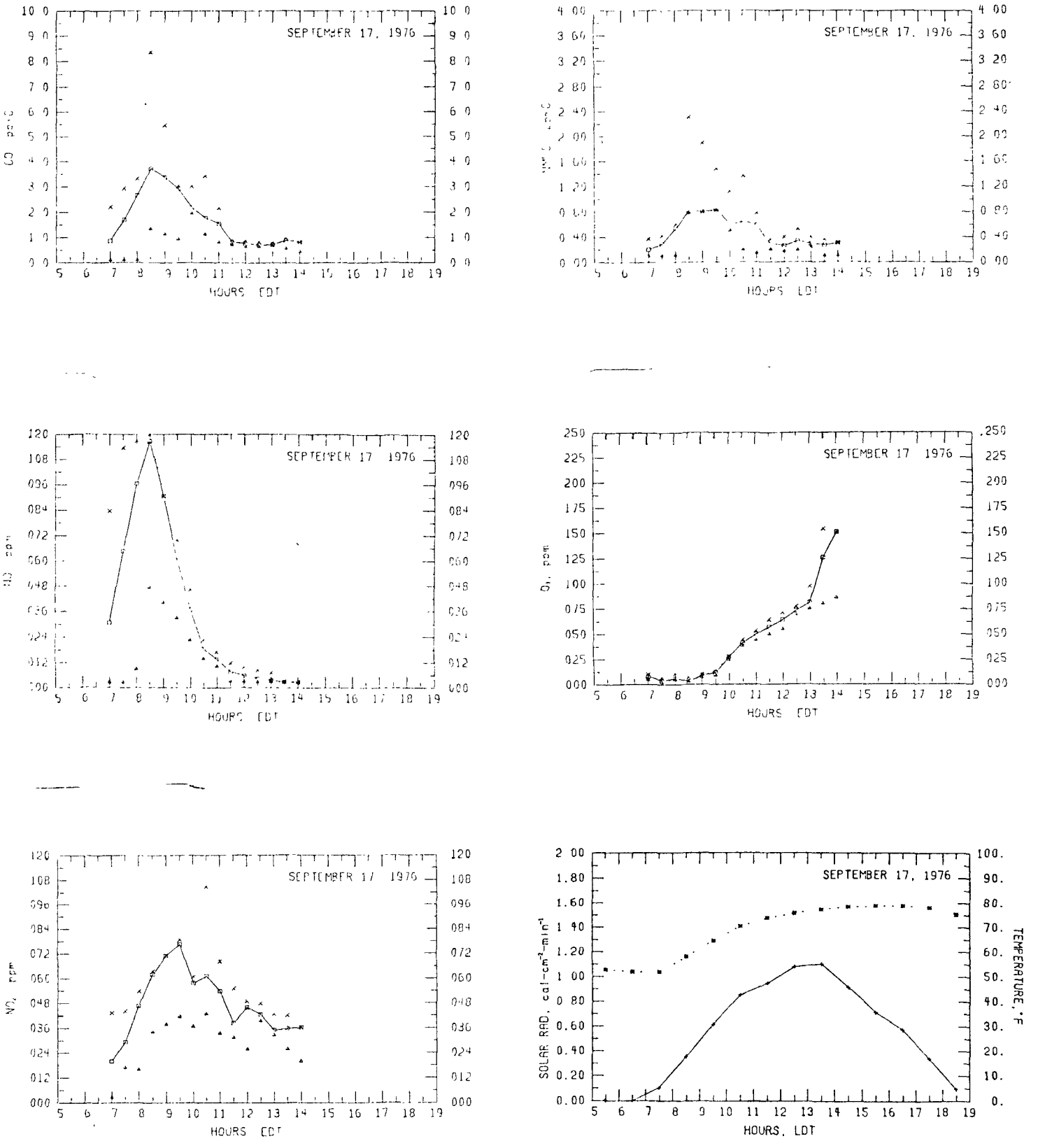

Figure 62. Ambient data weighted mean, max and min for Day 261.

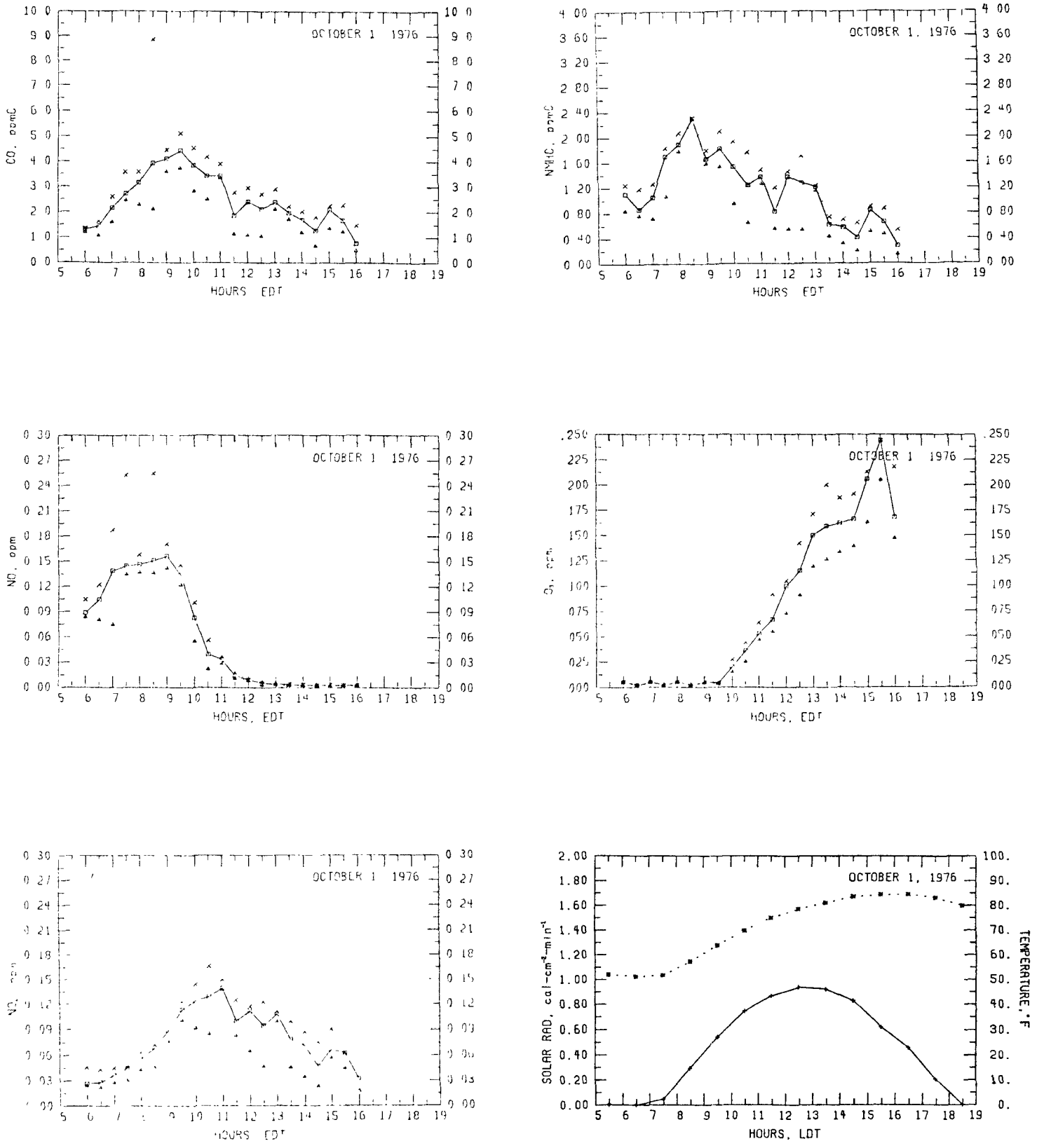

Figure 63. Ambient data, weighted mean, max and min for Day 275.

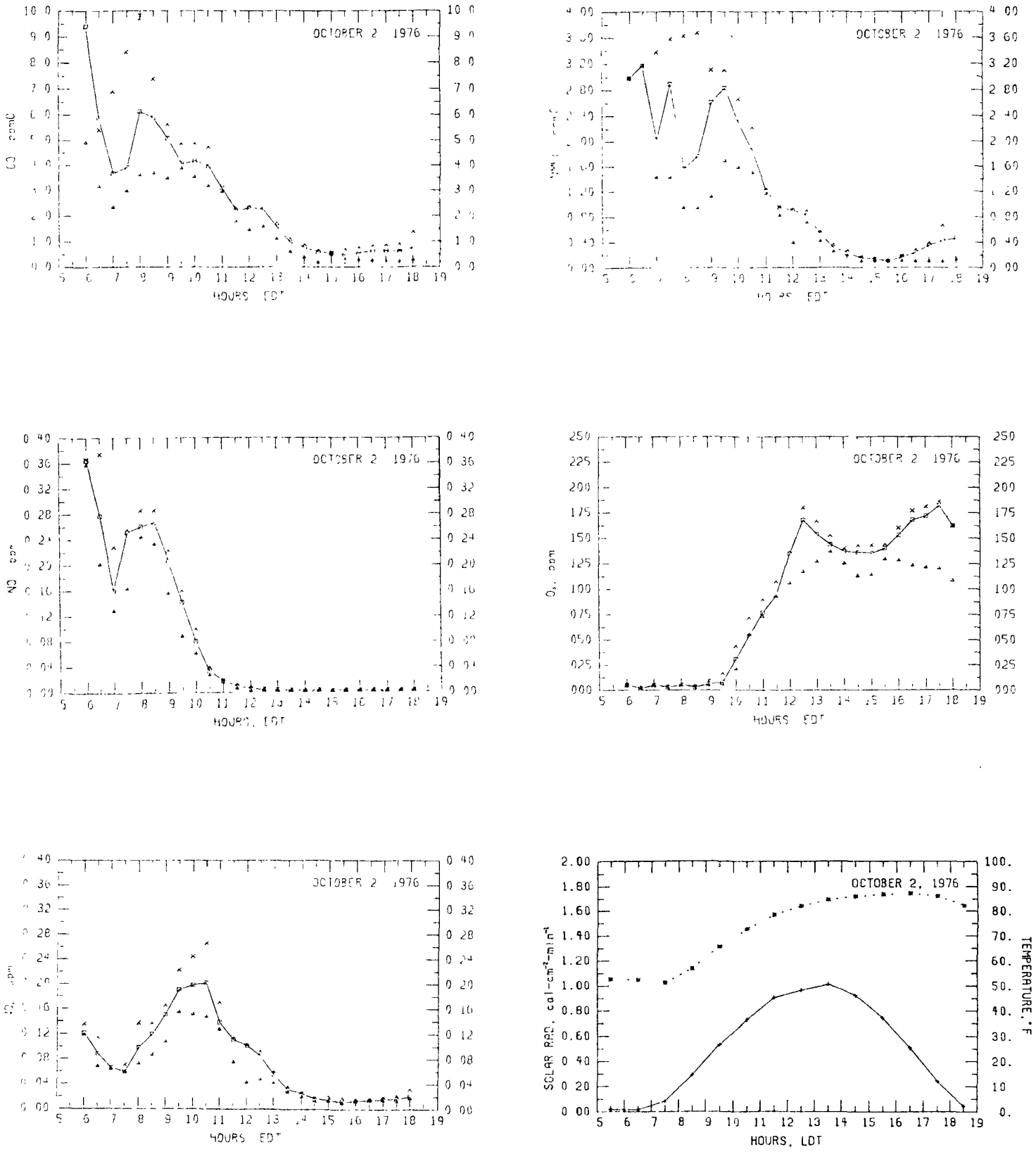

Figure 64. Ambient data, weighted mean, max and min for Day 276.

7.3 EMISSIONS ALONG TRAJECTORIES

7.3.1 Procedure for Processing Emissions

The procedure adopted by OAQPS/EPA for estimating emissions was to calculate an average emission rate over the entire uncertainty band of the trajectories for each hour. Thus the coordinates of the extreme trajectory locations at each hour were used to define the area over which the average would be computed. These areas were shown in Figures 31-54. A computer program was used to identify and process the emission inventory grid areas that fell inside each of these areas each hour. A detail of the grid near the center city (RAMS stations are plotted as *) is shown in Figure 65.

Table 18 is an example of the area source printout from the computer program for hour 10 (LST) of day 159, June 7, 1976. Listed are the grid squares that were totally or partially included in the trajectory area, their area, the fraction of the area included and the proportional amount of the emission rate for the pollutants. Table 19 is a printout for all the point sources that were in the area of trajectory between hour 10 (LST) and hour 11.

The emissions database used was the so-called "modellers tape" in which the hydrocarbon speciation of each of the source types has already been accounted for and the composition has been converted to an appropriately magnitude weighted, five level, lumped species inventory. These lumped species are: NR, non-reactive; PAR, paraffins; OLE, olefins; ARO, aromatics; and ALD, aldehydes. Tables 20 and 21 give the inventory average molecular weights and carbon numbers for the hydrocarbon species. These were obtained from Demerjian (1980).

In their in-house study (Gipson, 1980), OAQPS had converted the emissions to units relative to initial concentrations and initial mixing heights for use in the OZIPP program. In addition OAQPS had treated point sources as if

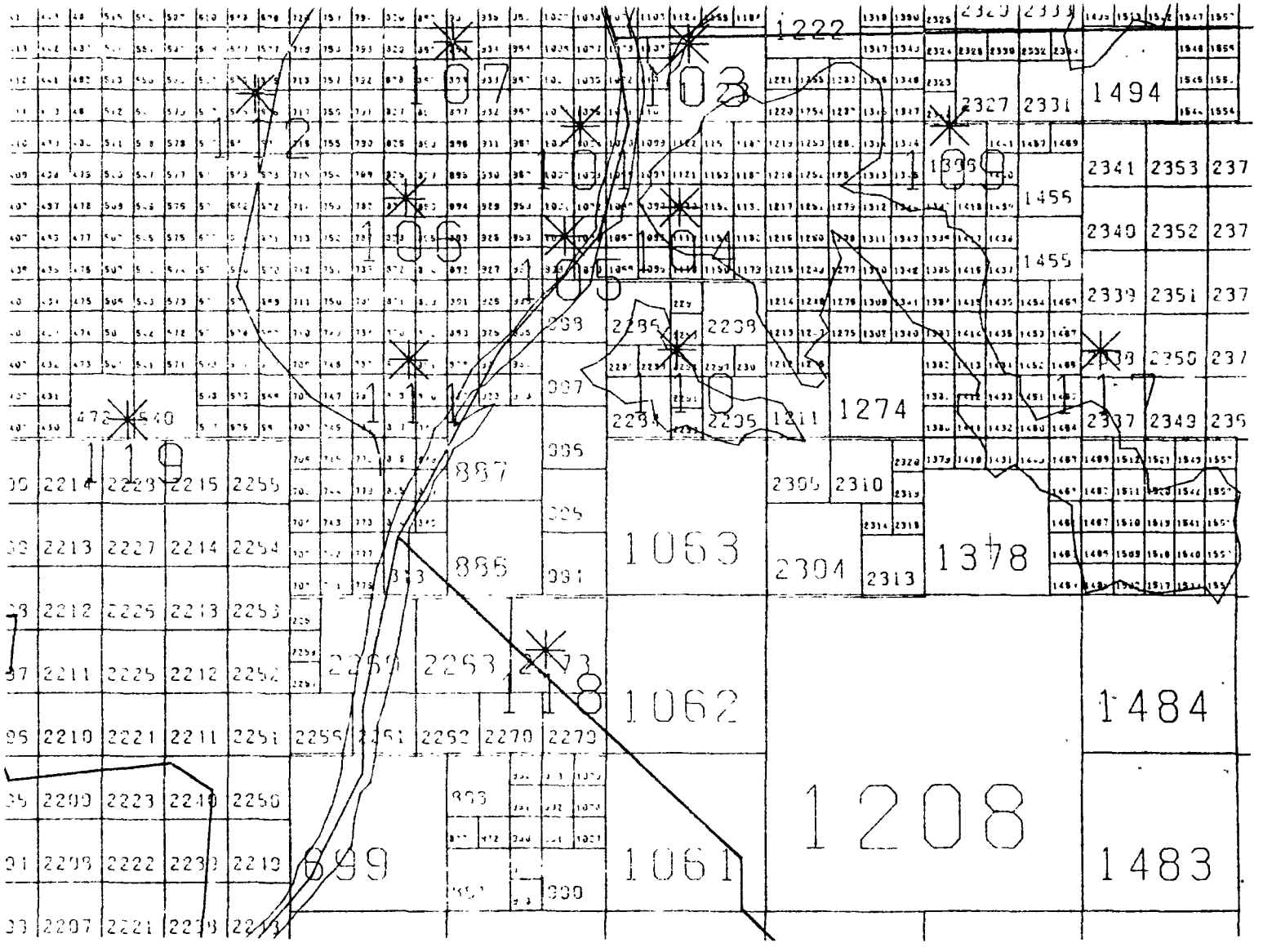

Figure 65. Example segment of RAPS gridded inventory.

Table 18. Sample Area Emission Inventory Printout

DAY 159 JUNE 7 — A R E A S O U R C E

HOUR	GRID	AREA (SQ KM)	FRACTION OF AREA WITHIN TRAJECTORY	AREA WITHIN TRAJECTORY (SQ KM)	CO EMISSIONS (KG/HR)	NOX EMISSIONS (KG/HR)	HC EMISSIONS (KG/HR)	HYDROCARBON SPECIES (G MOLE/HR) NON-REAC	PAR	OLE	ARO	ALD
10	1233	25	.327	8.18	154.524	16.873	22.227	210.9	120.9	193.1	28.3	36.4
10	1235	1	.986	.99	58.140	3.598	14.633	192.1	56.2	176.1	22.2	30.7
10	1236	1	.079	.08	4.935	.288	1.262	16.9	4.8	15.5	1.9	2.7
10	1266	1	1.000	1.00	80.695	5.878	10.608	117.6	54.7	109.2	13.5	17.9
10	1267	1	.383	.38	20.385	1.622	2.256	21.9	12.6	20.5	2.8	3.7
10	1294	1	1.000	1.00	6.059	1.429	1.044	7.4	5.9	6.8	1.4	1.9
10	1295	1	1.000	1.00	6.197	1.445	1.107	7.6	6.4	6.9	1.5	1.9
10	1296	1	1.000	1.00	3.889	1.586	1.181	6.6	6.5	5.8	1.8	2.3
10	1297	1	.702	.70	5.772	1.526	1.503	9.1	8.1	8.2	2.3	3.0
10	1330	1	1.000	1.00	5.660	.668	.831	6.2	5.3	5.6	1.0	1.0
10	1331	1	1.000	1.00	6.228	.925	1.949	10.0	13.0	7.6	2.4	1.6
10	1332	1	1.000	1.00	124.997	17.187	15.632	91.0	95.3	70.8	19.9	18.7
10	1333	1	.970	.97	71.570	7.890	13.772	77.3	90.5	57.9	16.2	11.4
10	1334	1	.051	.05	1.678	.146	.632	3.0	4.5	2.0	.7	.3
10	1352	1	1.000	1.00	34.949	2.774	5.673	56.1	31.1	50.6	7.1	8.2
10	1353	1	1.000	1.00	37.839	3.084	5.178	61.0	33.5	55.1	7.9	9.2
10	1364	1	1.000	1.00	33.755	3.227	4.396	40.2	25.4	37.5	5.4	6.9
10	1365	1	1.000	1.00	6.839	1.437	1.548	9.9	8.5	9.0	2.3	3.0
10	1366	1	.339	.34	13.513	1.029	4.681	28.3	31.0	21.1	5.4	3.2
10	1392	25	.109	2.72	29.361	5.823	3.503	41.8	51.4	31.2	8.9	5.1
10	1393	25	.935	23.38	35.073	11.715	12.171	56.1	80.0	39.4	15.3	11.2
10	1394	1	1.000	1.00	5.668	.672	1.640	8.4	11.5	6.2	1.9	1.0
10	1395	1	1.000	1.00	5.902	.690	1.715	8.8	12.0	6.5	2.0	1.0
10	1396	1	1.000	1.00	14.566	2.269	2.505	18.9	14.5	17.5	3.3	4.4
10	1397	1	1.000	1.00	6.720	.988	1.299	8.7	7.3	7.7	1.8	1.9
10	1398	1	.658	.66	32.557	2.541	9.834	64.9	63.6	50.6	11.4	7.7
10	1419	16	1.000	16.00	203.720	22.982	37.086	325.1	208.5	287.9	47.7	53.2
10	1420	1	.947	.95	5.774	.668	.923	6.6	6.0	5.8	1.2	1.0
10	1421	1	.029	.03	.176	.020	.051	.3	.4	.2	.1	.0
10	1442	9	.463	4.16	5.181	1.236	.720	5.3	4.2	4.7	1.0	1.1
10	2295	4	.035	.14	2.348	.059	.647	8.0	2.7	7.3	1.0	1.2
10	2299	1	.348	.35	21.714	.239	5.800	77.6	22.6	70.9	8.8	11.5
10	2302	4	.680	2.72	120.515	4.939	32.199	425.1	124.1	388.4	49.3	65.6
10	2303	1	.746	.75	4.959	.429	.971	5.9	6.2	5.1	1.5	.9
10	2308	1	1.000	1.00	46.985	3.393	4.942	49.3	28.4	46.2	5.8	7.5
10	2309	1	1.000	1.00	48.009	3.462	5.096	50.5	29.3	47.3	6.0	7.7
10	2343	4	.173	.69	1.191	.231	.421	1.9	2.9	1.3	.5	.2
10	2344	4	.467	1.87	3.995	1.459	1.433	6.9	9.4	5.2	1.7	1.6
10	2345	4	.262	1.05	21.793	2.035	3.453	35.0	18.2	31.9	4.4	5.7
10	2346	4	.024	.10	.175	.054	.027	.2	.1	.2	.0	.1
SUM	40			84.24	1293.993	138.487	242.556	2178.4	1327.9	1920.6	317.8	353.9
	EMISSION DENSITY (KG/HR SQ KM))				15.362	1.644	2.879					
	EMISSION DENSITY (KG MOLES/HR KM2)				.549	.036	.203					
	EMISSION DENSITY (G MOLES/HR KM2)							25.9	15.8	22.8	3.8	4.2

Table 19. Sample Point Source Emissions Inventory Printout

DAY 159 JUNE 7 — POINT SOURCE

HOUR	PLANT ID	STACK HEIGHT	CO EMISSIONS (KG/HR)	NOX EMISSIONS (KG/HR)	HC EMISSIONS (KG/HR)	HYDROCARBON SPECIES (G MOLE/HR) NON-REAC	PAR	OLE	ARO	ALD
10	1446801421	45	.000	.000	.000	.0	.0	.0	.0	.0
10	1446802436	17	.000	.000	3.556	11.6	38.7	14.2	.0	.0
10	1446802447	14	.000	.000	3.019	9.8	32.8	12.0	.0	.0
10	1446802448	12	.000	.000	2.037	6.5	21.8	8.0	.0	.0
10	1446802449	12	.000	.000	1.686	5.5	18.3	6.7	.0	.0
10	1446802450	12	.000	.000	1.686	5.5	18.3	6.7	.0	.0
10	1446802451	12	.000	.000	1.686	5.5	18.3	6.7	.0	.0
10	1446802460	14	.000	.000	2.185	2.6	16.0	3.4	1.9	.0
10	1446802461	14	.000	.000	2.185	2.6	16.0	3.4	1.9	.0
10	1446802462	15	.000	.000	5.517	6.6	40.5	8.5	4.8	.0
10	1446802532	24	.076	3.101	.120	10.2	.3	.3	.1	.3
10	1446802539	30	.047	1.612	.068	5.7	.2	.2	.1	.2
10	1446802510	30	.085	3.473	.134	11.4	.4	.4	.1	.4
10	1446802511	30	.066	2.728	.106	9.0	.3	.3	.1	.3
10	1446802512	30	.038	1.369	.050	4.3	.1	.1	.0	.1
10	1446802513	30	.132	5.214	.199	16.9	.5	.5	.2	.6
10	1446802514	54	.227	8.302	.344	29.2	1.0	1.0	.3	1.0
10	1446801468	4	.000	.000	45.738	56.2	343.0	71.9	41.0	.0
10	1446801465	22	.000	.000	20.518	66.9	223.2	81.8	.0	.0
10	1446801466	22	.000	.000	6.523	21.3	71.0	26.0	.0	.0
10	1446801467	22	.000	.000	10.733	35.0	116.8	42.8	.0	.0
10	1446801468	22	.000	.000	6.701	21.9	72.9	26.7	.0	.0
10	1446801469	22	.000	.000	8.717	28.4	94.8	34.8	.0	.0
10	1446801470	22	.000	.000	70.478	94.8	517.2	108.5	61.8	.0
10	1446801471	22	.000	.000	12.038	39.3	131.0	48.0	.0	.0
10	1446801472	22	.000	.000	24.491	79.9	266.5	97.7	.0	.0
10	1446801473	22	.000	.000	12.216	39.8	132.9	48.7	.0	.0
10	1446801474	22	.000	.000	8.302	27.1	90.3	33.1	.0	.0
10	1446801475	22	.000	.000	28.345	92.5	308.4	113.0	.0	.0
10	1446801476	22	.000	.000	4.050	13.2	44.1	16.2	.0	.0
10	1446801478	58	.000	.000	.000	.0	.0	.0	.0	.0
10	1446801479	45	.000	.000	.000	.0	.0	.0	.0	.0
10	1446801480	12	.000	.000	251.472	820.2	2735.9	1002.8	.0	.0
10	1446804201	45	.000	.000	.000	.0	.0	.0	.0	.0
10	1446804201	12	.000	.000	154.033	185.3	1139.4	237.1	135.0	.0
10	1446804101	12	.000	.000	136.658	164.4	1002.9	210.3	119.8	.0
TOTAL EMISSIONS (KG/HR)			7223.744	231.859	1355.757					
TOTAL EMISSIONS (KG MOLES/HR)			257.991	5.040	94.153					
TOTAL EMISSIONS (G MOLES/HR)						2791.8	11521.2	2993.0	703.0	10.0

Table 20. Species Molecular Weights

Species	Molecular Weight
HC	14.5
CH_4	16.0
NR	68.0
PAR	88.6
OLE	42.3
ARO	100.0
ALD	46.1

Table 21. Hydrocarbon Carbon Numbers

Species	Molecular Weight
CH_4	1.0
NR	3.0
PAR	6.3
OLE	3.0
ARO	7.1
ALD	2.0

they were area sources. That is, the summed point source emissions for each hour (the values at the bottom of Table 19) were divided by the total area of the "box" for the hour (the value near the bottom of Table 18). These averaged point source emissions were then summed with the area source emissions to give a single emissions value for each hour.

In this study, UNC decided to use absolute emission units of ppm-km/km^2-hr in the models instead of the relative units used by OAQPS. An emission rate of 0.25 ppm-km/hr would result in 0.25 ppm of material accumulating in a box 1 km^2 and 1 km high in one hour and would result in 0.50 ppm accumulating in a box 1 km^2 and 0.5 km high in one hour assuming no reaction of the material. The value is simply divided by the current mixing height to get the rate of change of concentration for a 1 km^2 box.

To be consistent with the OAQPS study, UNC decided to apply the same assumptions as OAQPS did to the point sources but to determine their contribution to the total emissions. The OZIPPM model program allows for a single emissions composition to be used for the entire day. To be consistent with this approach, UNC decided to compute this compositon from each day's trajectory's emission inventory.

To perform all the above tasks, a computer program was written. The program accepts as input the area and point source averaged emission values such as those at the bottom of Tables 18 and 19 in units of kg/hr or moles/hr. These are converted by use of the area, molecular weight, and average carbon number into ppm(C)-km/hr units.

The basic equations are:

$$Ei = (1000*factor/MWi)*(E_{supi}/A)$$

$$Ei = Ei*CNi$$

$$E_T = \Sigma Ei$$

where Ei = emission rate in ppm-km/hr for the ith species

factor = conversion from moles-km^2 to ppm-km (at 25°C)

factor = 24.46656×10^{-6}

MWi = molecular weight for the ith species

E_{supi} = supplied emission rate in units of kg/hr

A = area covered by trajectory in one hour (km^2)

CNi = carbon number for ith hydrocarbon species

Ei = emission rate in ppmC-km/hr for the ith hydrocarbon species

E_T = total emission rate in ppmC-km/hr for all hydrocarbons and aldehydes.

In addition the program computes the carbon fraction composition for each hours emissions and the running carbon fraction composition for point sources, area sources, and total emissions. An example printout for the 1100 LDT (1000 LST) hour of June 7, Day 159, is shown in Table 22. One printout page is produced for every hour of each day.

Table 22. Sample Emissions Calculation for Point and Area Sources

[illegible]
INITIAL MIXING HEIGHT: 0.204
INIT CO,NOX,HC: 7.000 0.037 0.500
HOUR: 11. AREA WITHIN TRAJECTORY KM**2: 84.24

	CO	NOX	HC	CH4	NR	PAR	OLE	ARO	ALD	ALD2	ALD3
AREA SOURCES											
KG/HR	1293.99	138.49	242.56								
MOL/HR					2178.40	1327.90	1920.60	317.80	353.90		
POINT SOURCES											
KG/HR	7223.74	231.86	1355.77								
MOL/HR					2791.80	11521.20	2993.00	703.00	10.00		
AREA,PPMKM	0.0134	0.0009	0.0049	0.0003	0.0003	0.0004	0.0006	0.0001	0.0001		
%	15.2	37.4	15.2	43.8	43.8	10.3	39.1	31.1	97.3		
run%	14.9	37.6	14.6								
POIT, PPMKM	0.0749	0.0015	0.0272	0.0004	0.0004	0.0033	0.0009	0.0002	0.0000		
%	84.8	62.6	84.8	56.2	56.2	89.7	60.9	68.9	2.7		
run%	85.1	62.4	85.4								
TOTL,PPMKM	0.0884	0.0023	0.0320	0.0007	0.0007	0.0037	0.0014	0.0003	0.0001		
TEPPAC	0.0167	0.0838	0.0849								
AREA											
PPMC					0.0009	0.0024	0.0017	0.0007	0.0000	0.0001	0.0001
CEPAC					0.1605	0.4109	0.2830	0.1108	0.0058	0.0116	0.0174
RUN CEPAC					0.1571	0.4220	0.2760	0.1107	0.0057	0.0114	0.0171
NMHC			0.0058								
POINT											
PPMC					0.0012	0.0211	0.0026	0.0014	0.0000	0.0000	0.0000
CEPAC					0.0461	0.7997	0.0989	0.0550	0.0000	0.0001	0.0001
RUN CEPAC					0.0461	0.7997	0.0989	0.0550	0.0000	0.0001	0.0001
NMHC			0.0264								
TOTAL											
PPMC					0.0022	0.0235	0.0043	0.0021	0.0000	0.0001	0.0001
CEPAC					0.0671	0.7285	0.1327	0.0652	0.0011	0.0022	0.0033
RUN CEPAC					0.0656	0.7335	0.1300	0.0648	0.0010	0.0021	0.0031
NMHC			0.0322								

7.3.2 Results of Emissions Calculations

Table 23 summarizes the calculated distribution of emissions among point and area sources for the 10 days; these values are illustrated in Figure 66. For comparison, Table 24 gives the distributions for the entire St. Louis area emissions inventory.

Figure 66 can be interpreted readily by reviewing the location of major point sources, Figure 29, and the trajectory paths for the days. The trajectories for days 159 and 160/15 were both north of the central business district (CBD) and spent significant time near the Alton/Wood River group of point sources. The trajectories for days 160/3, 221, and 261, which have similar distributions in Figure 66, were all west of CBD, and day 238 was east of CBD, areas reasonably low in major point sources. Days 195, 201, and 275, which also have similar distributions in Figure 66, had trajectory paths near the CBD (stations 101, 103, and 109). Day 276 was northeast of the CBD.

Since the point sources were uniformly distributed into the entire trajectory area for one hour, it is difficult to estimate whether their influence has been over or under estimated. For example, a large point source located just inside the upwind edge of a trajectory "box" contributes for nearly an hour in advance to its being encountered. On the other hand, it is dispersed over the entire box volume (in effect, it diffuses "upwind") thus greatly reducing its contribution to areas near it. Sometimes point sources located 20 km perpendicular to the trajectory could make significant contributions to a given hour's emissions.

Table 25 gives the computed percent carbon distribution among the five nonmethane hydrocarbon classes in the emission inventory for point sources, area sources and the total for the ten trajectory paths. The total percen-

Table 23

Distributions of Emissions for Selected RAPS Days
(Percent)

Day	Date	CO		NO_x		HC	
		Area	Point	Area	Point	Area	Point
160/3	Jun 8	89.8	10.2	86.9	13.1	81.6	18.4
160	Jun 8	53.9	46.1	72.0	28.0	64.5	35.5
159	June 7	25.1	74.9	34.6	65.4	27.8	72.2
221	Aug 8	90.1	9.9	84.3	15.7	78.7	21.3
261	Sept 17	94.5	5.5	90.5	9.5	76.0	24.0
201	Jul 19	78.6	21.4	58.7	41.3	81.5	18.5
195	Jul 13	85.7	14.3	66.0	34.0	85.8	14.2
276	Oct 2	47.3	52.7	65.1	34.9	84.5	15.5
275	Oct 1	73.7	26.3	62.8	37.2	88.1	11.9
238	Aug 25	99.7	0.3	83.0	17.0	65.7	34.3

TABLE 24. TOTAL EMISSIONS FOR THE ST. LOUIS AQCR (TONS PER YEAR)

	Particulates	SO_2	NO_X	HC	CO
Point Sources (% of Total)	45,224 (3%)	1,007,530 (97%)	322,730 (72%)	47,610 (23%)	164,331 (11%)
Area Sources (% of Total)	1,299,782 (97%)	30,813 (3%)	125,567 (28%)	157,204 (77%)	1,325,556 (89%)
Total	1,345,006	1,038,334	448,297	204,814	1,489,887

Table 25. Carbon Distribution of NMHC from Emission Inventory for Selected RAPS Days (percent)

Day	Date	Source	NR	PAR	OLE	ARO	ALD	Fraction of Total
159	June 7	Area	13.7	50.2	22.3	11.2	2.95	27.8
		Point	5.1	79.6	10.2	5.1	0.00	72.2
		Total	7.7	70.6	13.9	7.0	0.82	
160/103	June 8	Area	11.2	57.0	17.4	12.4	2.09	81.6
		Point	3.8	46.4	4.2	45.6	0.07	18.4
		Total	9.9	55.1	15.2	17.9	1.72	
160/115	Jun 8	Area	15.3	44.3	26.1	11.3	3.07	64.5
		Point	4.7	80.1	10.1	5.0	0.00	35.5
		Total	12.0	55.5	21.1	9.3	1.98	
195	July 13	Area	12.0	54.3	19.1	12.4	2.31	85.8
		Point	10.1	47.5	5.3	37.0	0.00	14.2
		Total	11.7	53.4	17.4	15.5	1.98	
201	July 19	Area	11.8	54.3	18.7	12.8	2.38	81.5
		Point	12.0	45.9	6.0	36.0	0.00	18.5
		Total	11.8	52.9	16.6	16.7	1.94	
221	Aug 8	Area	15.6	42.0	28.9	10.1	3.43	78.7
		Point	4.8	79.0	7.5	8.6	0.69	21.3
		Total	13.7	48.3	25.1	9.9	2.86	
238	Aug 25	Area	6.8	75.5	10.1	6.6	1.01	96.4
		Point	75.9	11.1	5.3	4.2	3.03	3.6
		Total	6.75	75.5	10.1	6.6	1.08	
261	Sept 17	Area	11.6	55.0	18.6	12.7	2.21	76.0
		Point	4.0	56.1	1.8	38.1	0.00	24.0
		Total	10.0	55.2	15.0	18.1	1.68	
275	Oct 1	Area	11.8	55.5	18.4	12.0	2.29	88.1
		Point	15.2	39.0	6.8	38.9	0.00	11.9
		Total	12.2	53.7	17.2	14.9	2.02	
276	Oct 2	Area	15.2	44.2	26.2	10.6	4.05	84.5
		Point	5.3	78.0	4.1	12.5	0.00	15.5
		Total	14.0	48.5	23.3	10.8	3.42	

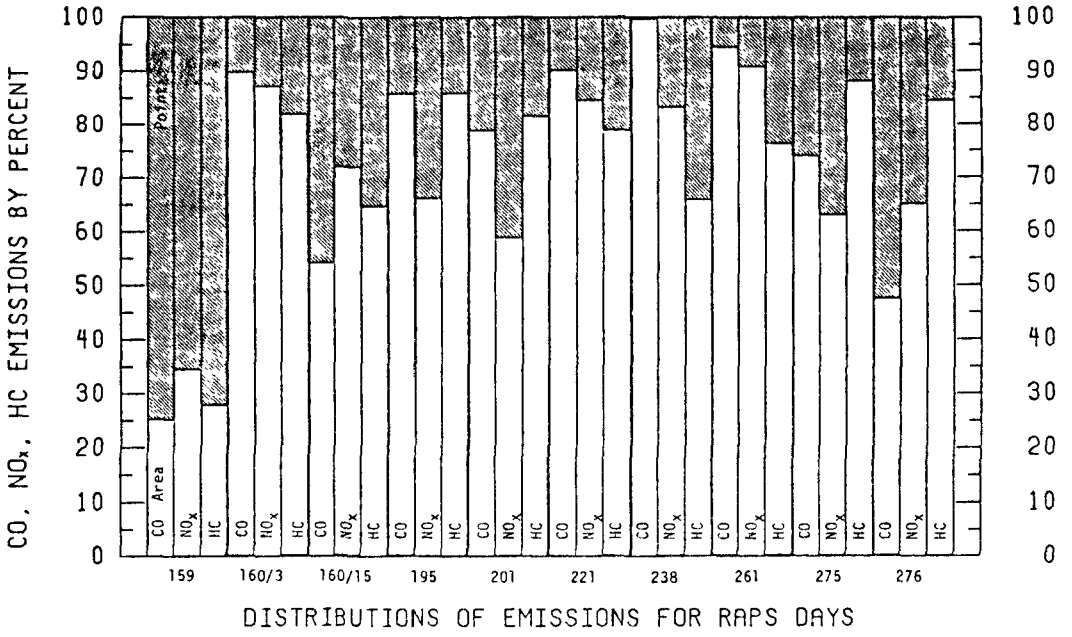

Figure 66. Distribution of CO, NO_x, and HC emissions for trajectory paths through the RAPS emission inventory.

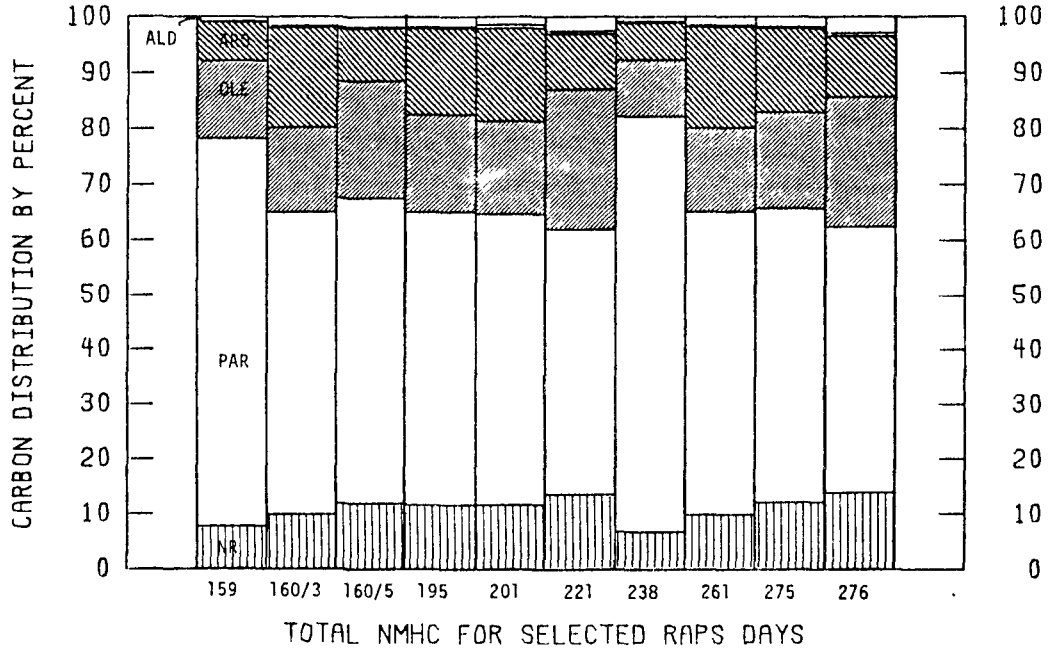

Figure 67. Carbon distribution (percent) of NMHC for trajectory paths through the RAPS emission inventory.

tages are plotted in Figure 67. Day 238 (Aug 25), in which the trajectory came from east of the CBD and curved north, had the highest paraffin fraction, 75%. Day 221 (Aug 8), in which the trajectory came from northeast of the CBD, swept through the city and ended west of the CBD, had the highest olefin carbon fraction, 25%. Day 261 (Sept 17), in which the trajectory started slightly north of the CBD and went south, had the highest aromatic fraction, 18%. The significance of these compositional changes will be examined more fully in later sections (see 7.3.4 and 8.3).

The computed hourly averaged emissions rates for each selected day are given in Table 26. These rates exhibit significant changes from hour to hour and the solution methods in the computer programs (such as the Gear routine in OZIPP and PKSTM) do not work well with such changes.

One method for dealing with this problem is to substitute a smoothly changing curve for the hourly averaged values. Figure 68 shows an example of NO_x and HC hourly averaged emission values and a smooth curve fitted through these values. An important criterion for such a curve is that the average emission computed from the curve each hour must be equal to the original constant hourly value. Another way of stating this requirement is that when the average hourly values are plotted in a histogram-like plot, then the area under the smooth curve each hour must be equal to the area of the histogram bar each hour.

The algorithm for producing these equal-area, smooth-curve histogram fits is not simple. Unfortunately, the algorithm in the OZIPP program does not always work properly and sometimes it produces negative emissions rates; this was true for several days in this study. Appendix A discusses the problem more fully and describes an algorithm developed by UNC to solve the problem without giving negative rates.

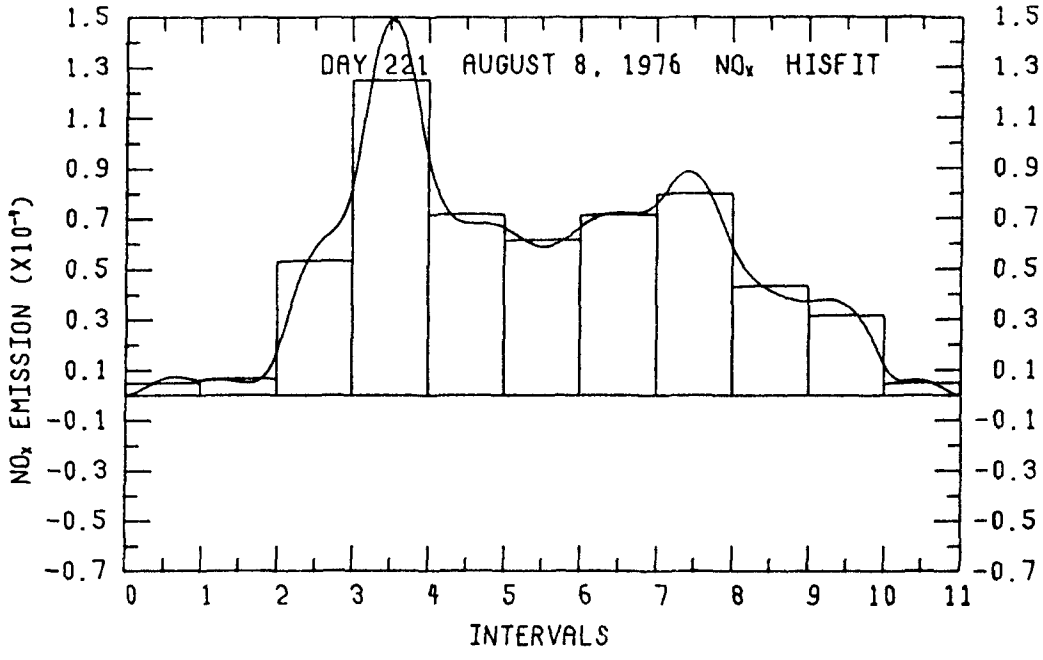

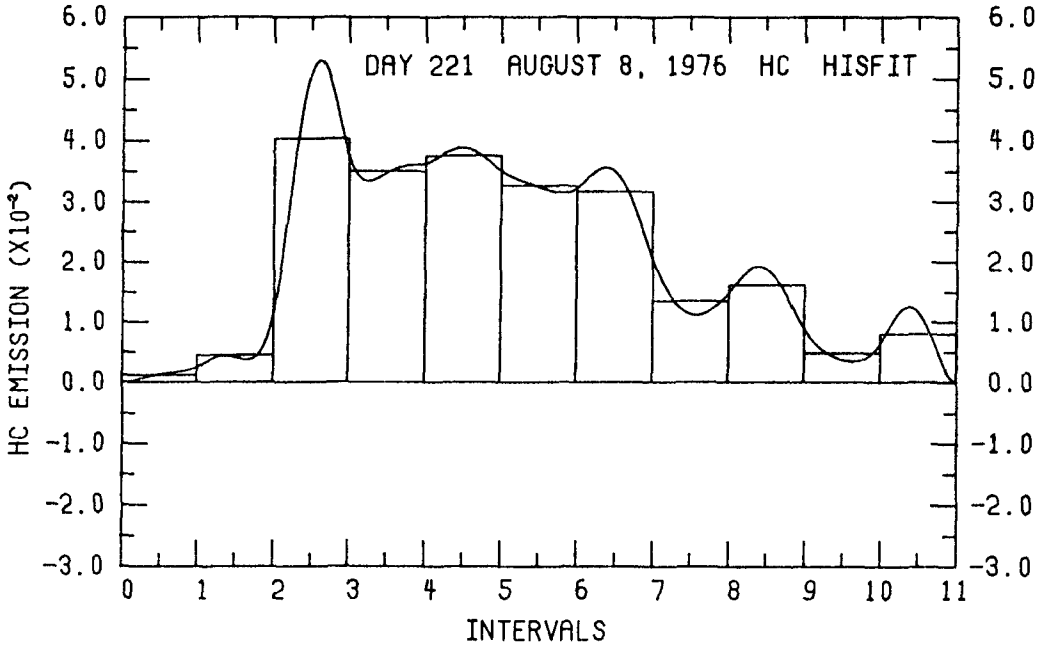

Figure 68. Examples of fitting equal-area smooth curve to hourly averaged emission values.

Table 26

Computed Emissions Rates for Selected RAPS Days

	DAY 159		
LDT	CO	NO_x	HC
0800	0.0885	0.0025	0.0316
0900	0.0876	0.0023	0.0319
1000	0.0875	0.0023	0.0319
1100	0.0883	0.0024	0.0321
1200	0.0888	0.0024	0.0322
1300	0.0567	0.0174	0.0322
1400	0.0202	0.0012	0.0131
1500	0.0052	0.0040	0.0030
1600	0.0016	0.0002	0.0005

	DAY 160/103		
LDT	CO	NO_x	HC
0700	0.0278	0.0032	0.0115
0800	0.0618	0.0056	0.0306
0900	0.0798	0.0050	0.0461
1000	0.1117	0.0099	0.0706
1100	0.1012	0.0097	0.0508
1200	0.1095	0.0092	0.0601
1300	0.1073	0.0091	0.0596
1400	0.1140	0.0095	0.0612

	DAY 160/115		
LDT	CO	NO_x	HC
0900	0.0071	0.0002	0.0033
1000	0.0076	0.0002	0.0038
1100	0.0153	0.0005	0.0098
1200	0.0275	0.0015	0.0179
1300	0.0246	0.0015	0.0157
1400	0.0184	0.0008	0.0094
1500	0.0266	0.0012	0.0120
1600	0.1782	0.0050	0.0578
1700	0.0099	0.0008	0.0027

	DAY 195		
LDT	CO	NO_x	HC
1100	0.0164	0.0011	0.0092
1200	0.0437	0.0056	0.0319
1300	0.1695	0.0185	0.0657
1400	0.0673	0.0067	0.0408
1500	0.0576	0.0054	0.0250
1600	0.0244	0.0010	0.0121

	DAY 201		
LDT	CO	NO_x	HC
0700	0.0009	0.0002	0.0007
0800	0.0055	0.006	0.0023
0900	0.0698	0.0074	0.0373
1000	0.1459	0.0127	0.0663
1100	0.0311	0.0048	0.0141
1200	0.0261	0.0060	0.0104
1300	0.0035	0.0003	0.0027

	DAY 221		
LDT	CO	NO_x	HC
0800	0.0021	0.0003	0.0006
0900	0.0040	0.0004	0.0027
1000	0.0586	0.0033	0.231
1100	0.0556	0.0075	0.0182
1200	0.0707	0.0043	0.0182
1300	0.0592	0.0037	0.0168
1400	0.0577	0.0044	0.0519
1500	0.0343	0.0048	0.0067
1600	0.0280	0.0026	0.0077
1700	0.0088	0.0019	0.0024
1800	0.0067	0.0003	0.0040

	DAY 238		
LDT	CO	NO_x	HC
0800	0.0043	0.0005	0.0055
0900	0.0057	0.0004	0.0050
1000	0.0101	0.0006	0.0063
1100	0.0194	0.0014	0.0094
1200	0.0198	0.0014	0.0119
1300	0.0199	0.0015	0.0104
1400	0.0084	0.0007	0.0035

	DAY 261		
LDT	CO	NO_x	HC
0700	0.0960	0.0069	0.0376
0800	0.0987	0.0085	0.0401
0900	0.0905	0.0057	0.0598
1000	0.1071	0.0077	0.1070
1100	0.1493	0.0116	0.0737
1200	0.1805	0.0147	0.0834
1300	0.0315	0.0037	0.0145

	DAY 275		
LDT	CO	NO_x	HC
0600	0.0533	0.0048	0.0302
0700	0.1979	0.0188	0.0082
0800	0.2198	0.0184	0.1075
0900	0.0413	0.0113	0.0278
1000	0.1770	0.0077	0.0135
1100	0.1089	0.118	0.0243
1200	0.0432	0.0088	0.0258
1300	0.0735	0.0128	0.0257
1400	0.0539	0.0110	0.171
1500	0.1187	0.0092	0.0465

	DAY 276		
LDT	CO	NO_x	HC
0600	0.0379	0.0114	0.0172
0700	0.0327	0.0084	0.0138
0800	0.2691	0.0062	0.0113
0900	0.1235	0.0034	0.0180
1000	0.0514	0.0085	0.108
1100	0.0220	0.0018	0.0061
1200	0.0074	0.0006	0.0010
1300	0.0166	0.0012	0.0046
1400	0.0138	0.0009	0.0032
1500	0.0027	0.0003	0.0007
1600	0.0092	0.0007	0.0027
1700	0.0060	0.0005	0.0016

units are ppm(C)-km/km^2-hr

Figure 69 illustrates, on the same scales, the emissions rates used in the UNC simulations. The equal-area histogram fitting procedure was applied to the values in Table 26 to produce the rates plotted in Figure 69.

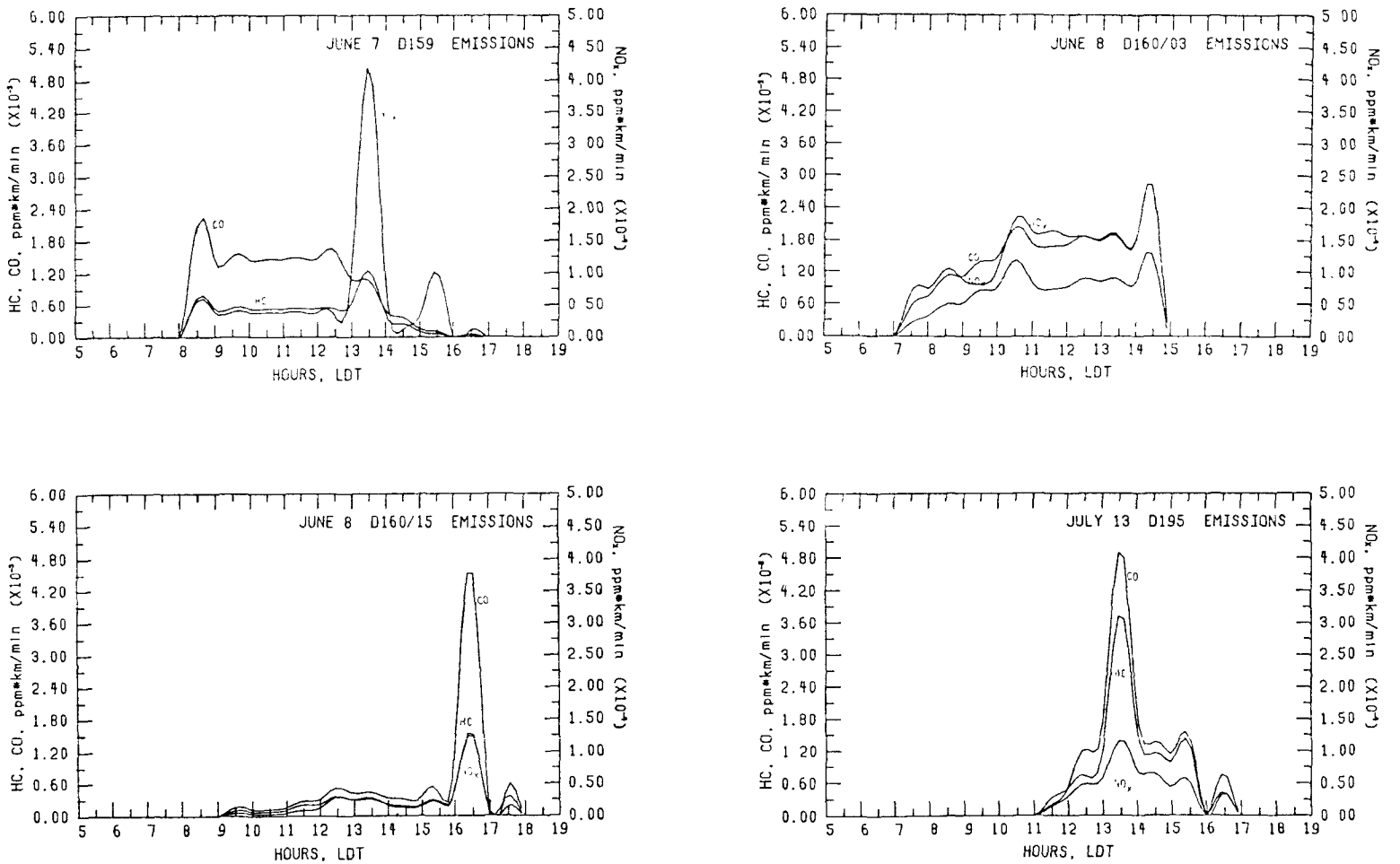

Figure 69. Absolute emission rates for CO, NO_X, NMHC used in simple trajectory model simulations, all days.

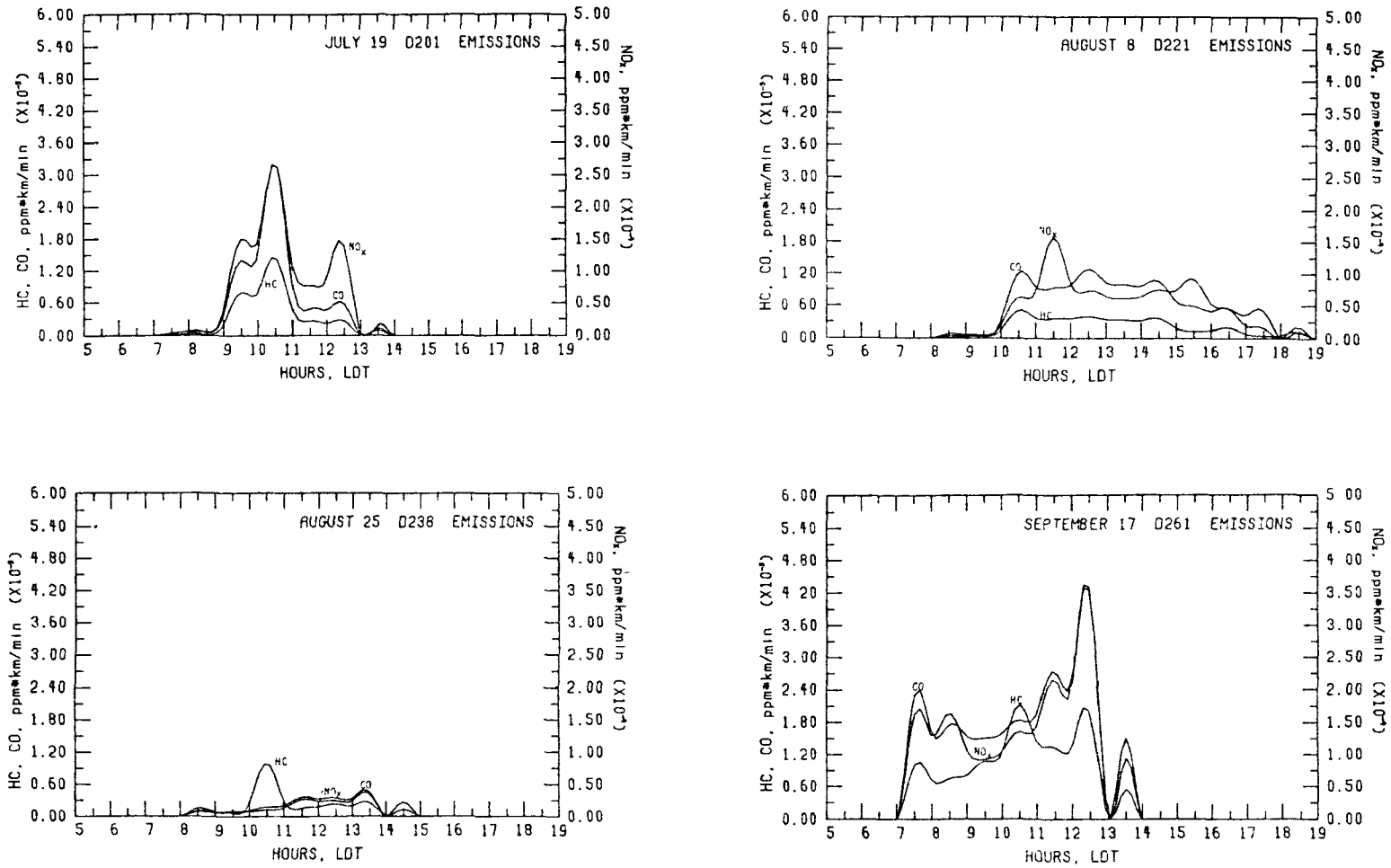

Figure 69. Absolute emission rates for CO, NO_X, NMHC used in simple trajectory model simulations, all days. (continued)

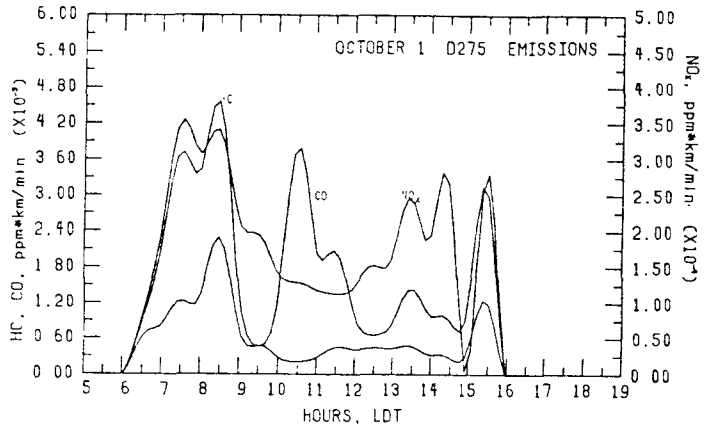

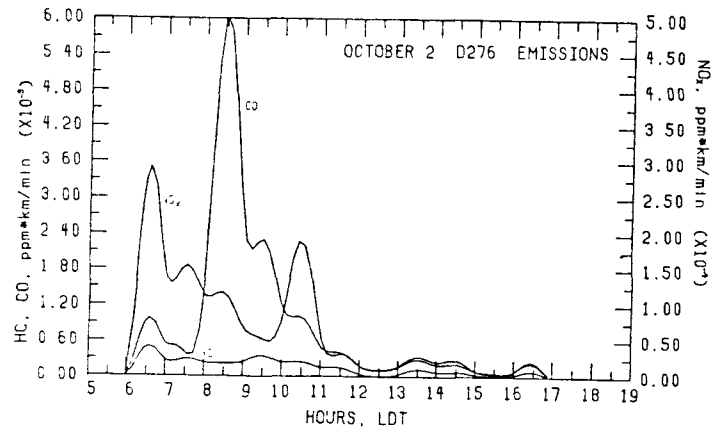

Figure 69. Absolute emission rates for CO, NO_x, MNHC used in simple trajectory model simulations, all days. (continued)

7.3.3 Method of Treating HC Composition in Each Mechanism

Mechanisms differ in the number and characteristics of the species used to represent the hydrocarbons present in the photochemical systems to be simulated. Hydrocarbon composition data available from the RAPS emission inventory (see Table 25 and Figure 66) usually needed to be converted to the appropriate representation used in each mechanism. The actual conversion depends on the characteristics of each mechanisms' hydrocarbon species as defined by the mechanism developer.

In simple trajectory models, HC composition data are utilized in calculating emission composition along the path, in addition to calculation of the initial morning HC concentrations.

The HC concentrations needed internally in the model are in ppmV. The values for each HC specie used in the mechanism are calculated by multiplying the measured NMHC value from RAPS (or the NMHC values calculated from emission inventory) times the calculated carbon mole fraction for each specie, divided by the determined carbon number for each specie. The conversion calculations used in this study for each mechanism will be described. Table 27 lists the HC fractions.

7.3.3.1 Dodge Mechanism. The Dodge mechanism used a mix of butane and propylene to represent the hydrocarbon species present in a photochemical oxidant system. Dodge had determined that a carbon mole fraction of 75% butane and 25% propylene yielded a system which had a photochemical reactivity equivalent to the Bureau of Mines smog chamber experiments. The Dodge mechanism, therefore, does not utilize HC composition data.

In the standard OZIPP program the assumption has been made that aldehyde fraction would be 5%: 2% formaldehyde and 3% acetaldehyde.

Species	Fraction	Carbon No.
Prop	0.25	3.0
But	0.75	4.0
HCHO	0.02	1.0
ALD2	0.03	2.0

7.3.3.2 Demerjian Mechanism. The Demerjian mechanism uses three HC classes (OLE, PAR, ARO) and one aldehyde species to represent all aldehydes. The Demerjian mechanism utilizes HC composition data of carbon mole fraction only. The carbon number for each HC and aldehyde class is defined by Demerjian. Therefore, the RAPS carbon number data in Table 21 is not utilized. Ethylene is included in the olefin group. These conditions allow direct use of the RAPS emission inventory derived carbon mole fractions (Table 25). These fractions were utilized for initial condition determinations as well as for the emission fractions.

Species	Fraction	Carbon No.
OLE	RAPS OLE	3.0
ALK	RAPS PAR	6.0
ARO	RAPS ARO	8.1
ALD	RAPD ALD	1.0

7.3.3.3 Carbon Bond II Mechanism. The Carbon Bond II mechanism's HC species represent carbon bond types rather than hydrocarbon classes, with ethylene explicitly represented as the exception. The CARB specie represents the carbonyl carbon present in aldehydes, ketones and other oxygenates. Both carbon mole fraction and carbon number are needed from the RAPS HC composition data. Each carbon bond type also has a defined carbon number (e.g., olefins: C = C has 2 carbons). Portions of each HC composition class are added to the paraffin carbon bond specie, depending on the degree that the HC composition carbon numbers exceed the corresponding carbon bond type carbon number. The carbon mole fraction of the olefin portion (of the HC composition data) which

is ethylene needs to be determined (or assumed), as well as the non-ethylene-olefin carbon number. For this study both a 50/50 or 33/66 ethylene/olefin carbon mole fraction was used. Little effect was observed when one split was substituted for the other. The carbon number for OLE as determined in the St. Louis emission inventory was 3.0. Since the carbon number for ethylene is 2.0, the eth/ole split and the inventory carbon number determine the carbon number for ole without ethylene. The formula below is used to calculate the Carbon Bond II's Olefin # from the RAPS total Olefin fraction (includes ethylene) and the assumed ethylene fraction/total olefin fraction ratio (E).

$$\text{CBII Olefin \#} = \frac{1 - E}{\left(\frac{1}{(\text{RAPS Ole \#})} - \frac{E}{2}\right)}$$

% Ethylene carbon / % Olefin carbon	Eth #	Ole #	Inventory Total Olefin #
50/50	2.0	6.0	3.0
33/66	2.0	4.0	3.0

The carbon number for Ole in the CB2 mechanism is 2.0. Therefore to arrive at the CB2 emission fraction for olefin from the St. Louis inventory: $(\frac{eth}{ole} = 1/3)$.

$$\text{CB2 ole frac} = \frac{(1 - \frac{eth}{ole})(\text{ole carbon frac particular day})}{\text{4.0 carbons/inventory olefin}} \times 2.0$$

The initial olefin value is: $\text{CB2 init olec} = \frac{\text{NMHC} * \text{CB2 ole frac}}{2.0}$

Likewise for ethylene:

$$\text{CB2 eth frac} = \frac{(\frac{eth}{ole}) \times (\text{ole frac St. Louis})}{2.0} \times 2.0$$

and

$$\text{CB2 init ethc} = \frac{\text{NMHC x CB2 eth frac}}{2.0}$$

The aromatic carbon number is 7.1 in the emission inventory and 6.0 in the CB2 mechanism.

Therefore,

$$\text{CB2 aromatic frac} = \frac{\text{(arom frac St. Louis)}}{7.1} \times 6.0$$

$$\text{CB2 init aroc} = \frac{\text{NMHC x CB2 aromatic frac}}{6.0}$$

The aldehyde carbon number is 2.0 in the emission inventory and 1.0 in the CB2 mechanism: the carbonyl carbon atom (CARB). Therefore

$$\text{CB2 CARB frac} = \frac{\text{(ald frac St. Louis)}}{2.0} \times 1.0$$

$$\text{CB2 init CARB} = \frac{\text{NMHC x CB2 CARB frac}}{1.0}$$

The paraffin carbon number is 1.0 in the CB2 mechanism. Therefore the St. Louis fractin for paraffin can be used directly. However, several other species contain paraffin carbon atoms in side chains which must be added to the paraffin class.

The number of carbon atoms over two in the average olefin molecule are added to the paraffin fraction. The carbon atoms in the aromatic side chains are added. The carbon atoms in excess of the carbonyl carbon in the aldehydes are also added to the paraffin fraction.

Therefore

$$\text{CB2 par frac} = \text{(par fraction St. Louis)} + \frac{(4.0-2)(1-\frac{\text{eth}}{\text{ole}})\text{(ole frac St. Louis)}}{4.0}$$

$$+ \frac{(7.1-6)(\text{aro frac St. Louis})}{7.1}$$

$$+ \frac{(2.0-1.0)(\text{ald frac St. Louis})}{2.0}$$

$$\text{CB2 init par} = \frac{\text{NMHC} \times \text{CB2 par frac}}{1.0}$$

The non reactives were treated as follows:

$$\text{CB2 NR frac} = \frac{\text{NR frac St. Louis}}{3.0} \times 3.0$$

$$\text{CB2 init NR} = \frac{\text{NMHC} \times \text{CB2 NR frac}}{3.0}$$

7.3.3.4 California Institute of Technology (CIT) Mechanism. The CIT mechanism utilizes four HC species: olefin, ethylene, aromatic, and alkane, and two aldehyde species: formaldehyde and a general aldehyde species. Both carbon mole fraction and carbon number data are required to implement this mechanism.

Generally the RAPS emission inventory derived HC carbon mole fractions can be used directly with the CIT mechanism. However, the fraction of the RAPS Olefin fraction which is ethylene must be determined or assumed. A 50/50 split was assumed for the Ethylene/Total olefin fraction ratio for the Level II simulations (The BOM autoexhaust analysis indicates 42% of Olefin is ethylene). Therefore, the carbon number for the non-ethylene olefin fraction must be approximated. The value used for this study was 4.0. Also the HCHO/RCHO fraction needs to be determined or assumed, as well as the carbon number for RCHO. A value of 33%/66% was assumed. Since the aldehyde carbon number determined from the emission inventory was 2.0, the carbon number for RCHO was assumed to be 2.5.

Species	Fraction	Carbon No.
OLE	(non-ethylene olefin factor)	RAPS OLE
used 4.0		RAPS non-ethylene olefin
ETH	(1 - non-ethylene olefin factor)	RAPS OLE 2.0
ALK	RAPS PAR	RAPS PAR
ARO	RAPS ARO	RAPS ARO
HCHO	1/3 (RAPS ALD)	1.0
RCHO	2/3 (RAPS ALD)	2.5

Table 27. Hydrocarbon Composition Fractions for the Ten RAPS Days

Species	Carbon Number	D159	D160/3	160/15	D195	D201	D221	D238	D261	D275	D276
					DEMERJIAN						
PAR	6.0	0.706	0.551	0.555	0.534	0.529	0.483	0.755	0.552	0.537	0.485
OLE	3.0	0.139	0.152	0.211	0.174	0.166	0.251	0.101	0.150	0.172	0.233
ARO	8.1	0.070	0.179	0.093	0.155	0.167	0.099	0.066	0.181	0.149	0.108
ALD	1.0	0.0082	0.0172	0.0198	0.0198	0.0194	0.0286	0.0108	0.0168	0.0202	0.0342
					CARBON BOND						
PARC	1.0	0.7556	0.6237	0.6321	0.6114	0.6061	0.5754	0.7959	0.6259	0.6275	0.5771
ETHC	2.0	0.0695	0.0760	0.1055	0.0870	0.0830	0.1255	0.0505	0.0750	0.0573	0.1165
OLEC	2.0	0.0347	0.0380	0.0528	0.0435	0.0415	0.0628	0.0253	0.0375	0.0573	0.0583
ARDC	6.0	0.0592	0.1513	0.0786	0.1310	0.1411	0.0837	0.0558	0.1530	0.1259	0.0913
CARB	1.0	0.0041	0.0086	0.0099	0.0099	0.0097	0.0143	0.0054	0.0084	0.0101	0.0171
					CIT						
ALK	6.3	0.0706								0.537	
OLE	4.0	0.0695								0.0925	
ETH	2.0	0.0695								0.0925	
ARO	7.1	0.070								0.149	
HCHO	1.0	0.0027								0.0067	
RCHO	2.5	0.0055								0.0135	

7.3.4 Sensitivity of Demerjian and Carbon Bond II Mechanisms to RAPS Ambient HC Composition in Smog Chamber Type Simulations

Figures 70 and 71 show simulations of BOM-type outdoor smog chamber experiments at 0.2 ppm NO_x and 1.0 or 2.0 ppmC NMHC initially, using the Demerjian and CB2 mechanisms and four HC compositions: 1) BOM auto exhaust, 2) RAPS D261, 3) RAPS D221, and 4) RAPS D238.

The compositions of the BOM exhaust and the three RAPS days, representing the days of highest aromatic, olefin, and paraffin fractions were:

Day	NR	PAR	OLE	ARO
261	0.100	0.552	0.150	0.181
221	0.137	0.483	0.251	0.099
238	0.0675	0.755	0.101	0.066
BOM	0.105	0.417	0.173	0.287

Each figure shows simulations performed with a single mechanism. In each figure, columns show the same initial NMHC concentration and each row shows a different HC composition.

Generally the BOM composition yielded the highest predicted O_3 concentrations for a given mechanism and initial NMHC condition. Although the two mechanisms agreed within 20% for both levels of initial HC utilizing the BOM auto exhaust composition, the mechanisms respond differently to changes of composition. The CB2 mechanism, for example, predicted that the high aromatics day (D261) at 2.0 ppmC NMHC, would produce as much O_3 as the CB2 2.0 ppmC BOM-composition system, while the Demerjian mechanism shows a substantially reduced O_3 yield for the same change in composition. The same change in composition would also have a dramatic effect at the 1.0 ppmC initial level, with the Demerjian mechanism again showing the greatest effect, yielding less than half the O_3 than predicted by the CB2 mechanisms.

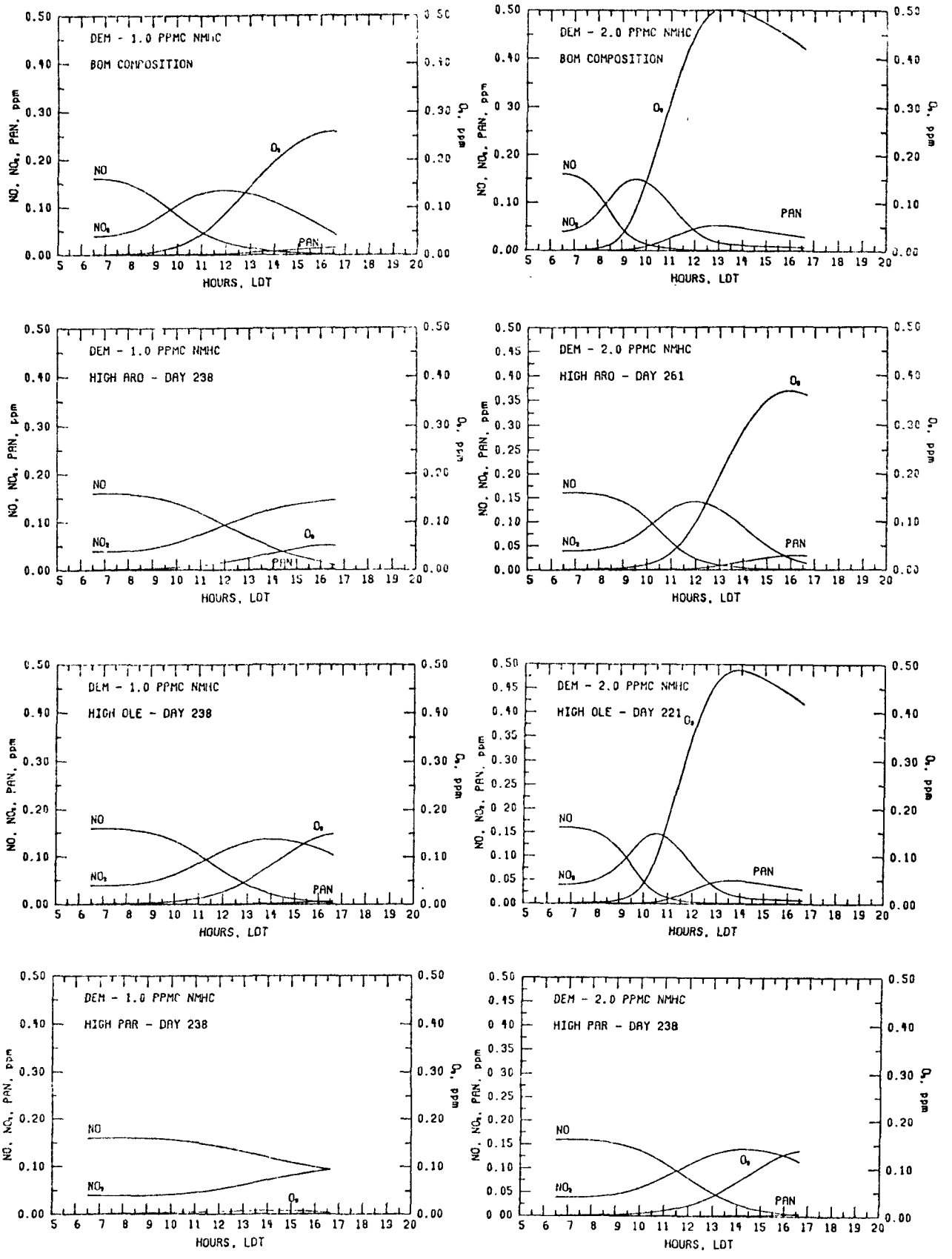

Figure 70. Effect of HC composition and concentration on outdoor smog chamber type simulations with the Demerjian Mechanism.

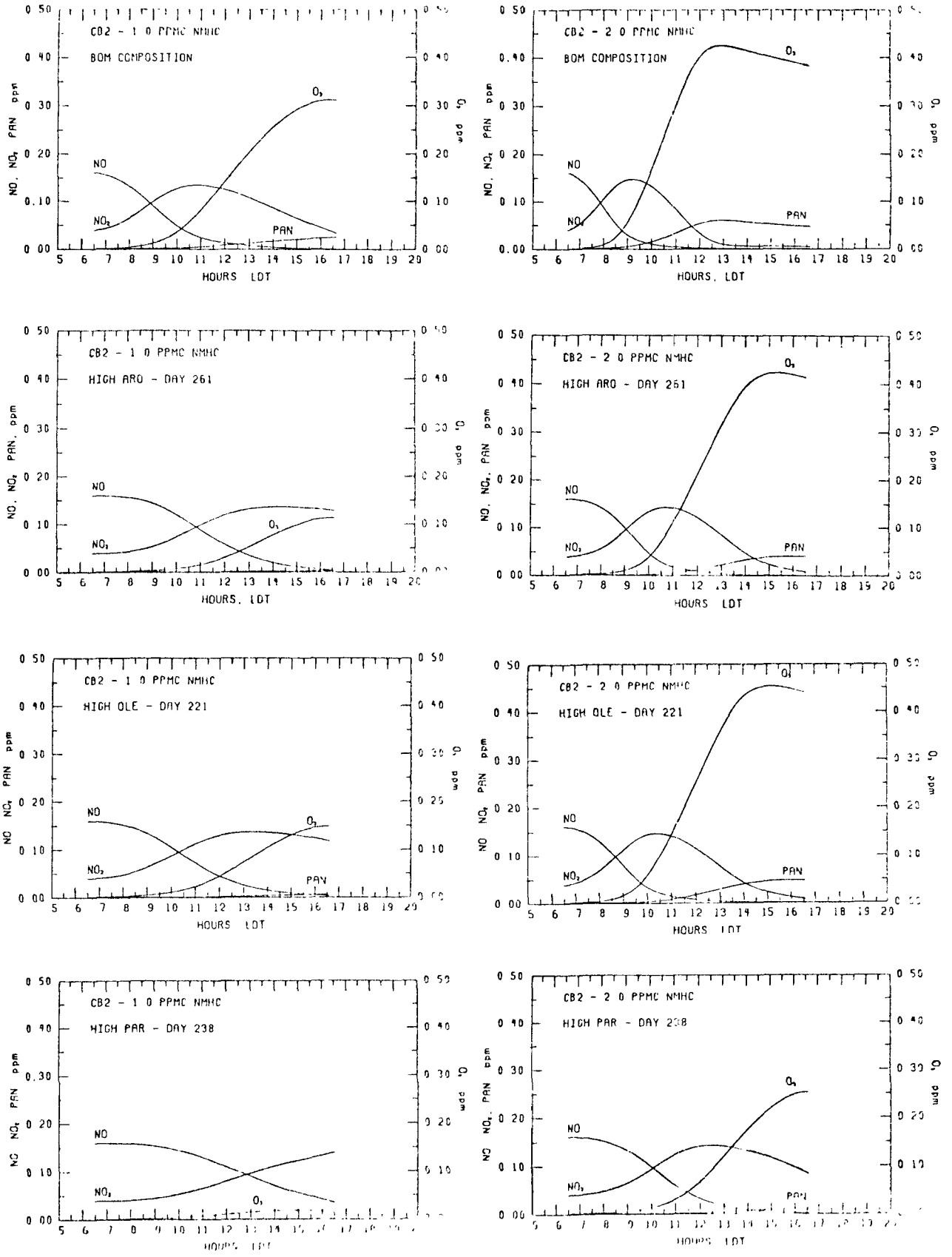

Figure 71. Effect of HC composition and concentration on outdoor smog chamber type simulations with the Carbon Bond II Mechanism.

The switch from BOM composition to the high OLE day composition (D221) also illustrates the difference in directional results. Both mechanisms at the 1.0 ppmC NMHC system showed similar decreases in O_3 yield, but at the higher 2.0 ppmC level systems the Demerjian mechanism indicated that the high OLE would be slightly less reactive system than the BOM composition system and the CB2 would be slightly more reactive than predicted with the BOM composition.

Similar effects are seen with the high PAR day (D238). The initial 1.0 ppmC NMHC system predictions were most dramatic for both mechanisms.

Figure 72 shows the effect of changing from a summer to fall (October) distribution of photolytic rates, for the Demerjian mechanism at 2 ppmC initial HC. The aldehyde photolysis rate constants change most dramatically: decreasing about 40%. There is little effect shown for the more reactive HC compositions (BOM and high olefin) but there is considerable effect in the high paraffin composition. Similar studies with the Carbon Bond II mechanism showed less of an effect and are not shown here.

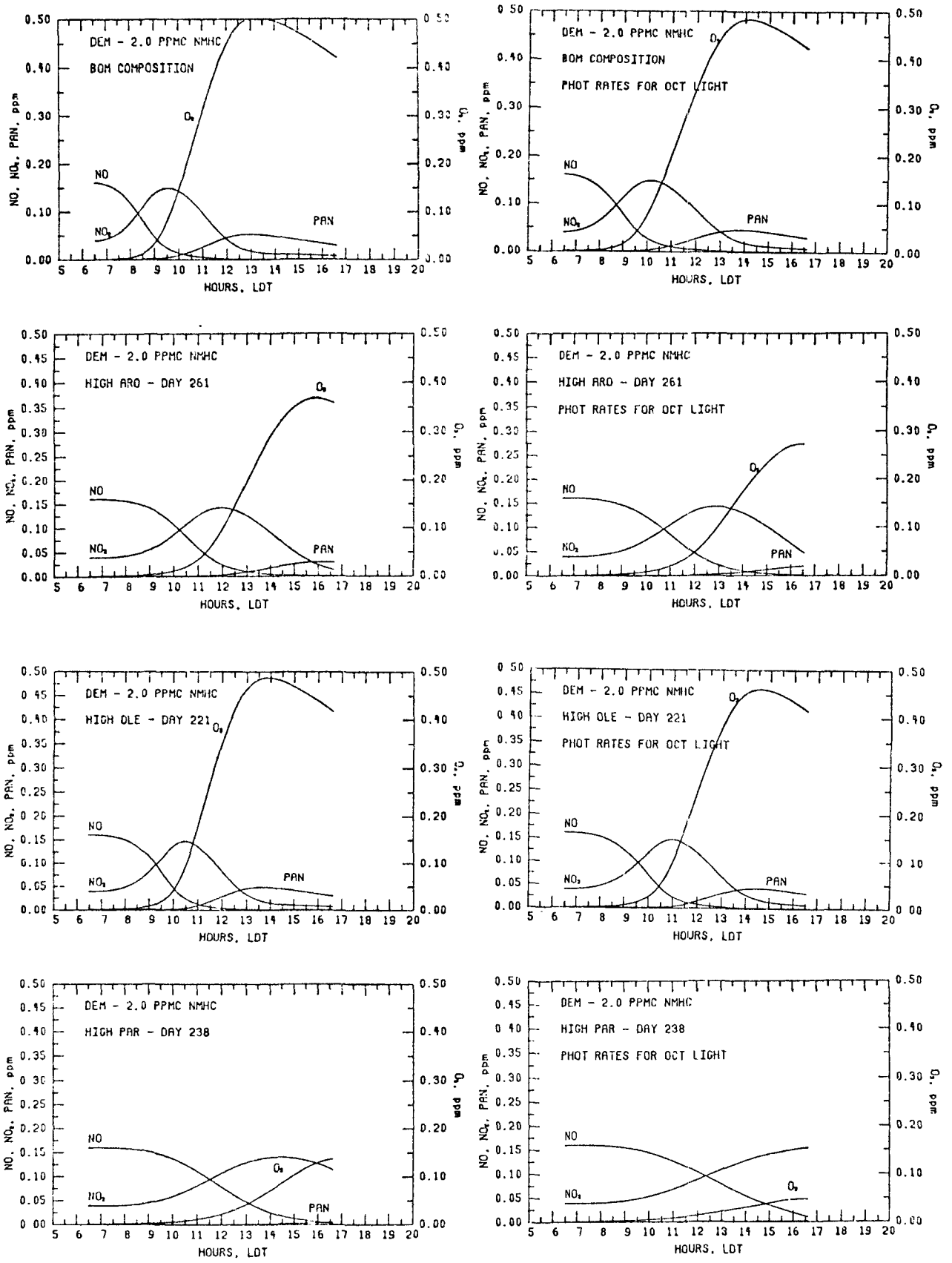

Figure 72. Effect of aldehyde photolytic rate with HC composition and concentration in outdoor smog chamber type simulation with the Demerjian Mechanism.

7.4 MIXING HEIGHT PROFILES

The atmospheric boundary layer (ABL) is generally classified by its stability. The classification systems generally involve the depth of the ABL, h and the Obukhov length (a buoyancy length scale), L. Using this system,the atmosphere can be divided into three general categories: unstable or convective, neutral or near neutral, and stable. The convective boundary layer is usually observed during the daytime over land while stable boundary layers are generally observed during the nighttime. The neutral or near neutral boundary layer is rarely seen over land, except for momentary episodes during the transition from the daytime to the nighttime boundary layer and vice versa.

In convective boundary layer regime, the buoyant production of turbulence dominates over the mechanical production. The convective boundary layer is characterized by three layers, a mixed layer, a transition layer and a cloud layer. The mixed layer is characterized by a uniform mean velocity profile, with no significant vertical gradients. This is due to a large amount of mixing. The transition layer is slightly stable due to the entrainment downward of warmer and drier air from the cloud layer. The transition layer occurs around the height of the capping inversion, in which there is a noticeable jump in the wind speed across the inversion, with significant wind shears in the cloud layer above. The wind velocity in the mixed layer is nearly geostrophic (Yamada, 1976).

The simplest methods to determine the depth of the boundary, h, are direct measurements, i.e., using Sondar (acoustic sounder) and Lidar (the

optical equivalent of radar). The echoes detected by a monostatic acoustic sounder are produced entirely by temperature fluctuations; with a bistatic system the echoes are produced by both wind and temperature fluctuations. The principal scattering sources for lidar echoes are aerosols and light molecules. During the daytime, these direct measuring devices may not have enough power to reach the top of the boundary layer. Other direct measurements include turbulence sensors mounted on research aircraft, high towers or on tethered balloons. These provide a means of measuring h directly. Generally, these types of turbulence measurements are rarely made. More often, the ABL depth is estimated from the measured temperature and humidity profiles obtained from radiosonde observations.

If direct measurements are not available then climatic or historical methods must be relied on. These generally involve the use of an early morning radiosonde observation from the nearest National Weather Service Radiosonde station. Proposed methods include Holzworth (1972), Benkley and Schulman (1979) and EPA (1981).

During the nighttime, the boundary layer becomes stable, and the depth reaches a minimum. The ABL is generally identified with a surface inversion. The height defined by the observed mean potential temperature profile may not correspond to the actual height of the ABL due to turbulent exchanges -- thus the need for direct measurements.

The boundary layer height is highly variable in both time and space. This is due to horizontal roll vortices and convective cells. Thus, the average height of the interface between the turbulent ABL and the free atmosphere should be determined by the averaging or smoothing of continuous data; a single sounding can only give an instantaneous value (Arya, 1979).

Methods for choosing mixing height profiles given radiosonde data are

likely to vary from investigator to investigator. One objective of this study was to examine how sensitive the control requirements might be to some likely-to-be-used methods for estimating the mixing height profiles.

The method that is built in to OZIPP assumes an exponential rise between the 8 A.M. mixing height and the afternoon mixing height. The reason is simple: this profile results in a constant dilution rate. It is an inadequate representation of the ABL behavior, however, and was not used in this study.

In the OAQPS EKMA study (Gipson, 1980), two alternative mixing height profile methods were explored. The first method, Linear, consisted of a simple linear interpolation between the mixing height calculated from the near-sunrise sounding and the mixing height calculated from the late-morning soundings and between the late-morning mixing height and that calculated from the afternoon sounding. In the second method, Handpicked, the hourly mixing heights were manually calculated by a meteorologist using the same three soundings and hourly surface temperatures. It was decided to include these two methods in this study. The data for the ten days were supplied by OAQPS/EPA.

The third mixing height profile method used in this study was the Characteristic curve method. The method is based upon a piecewise curve thought to describe the characteristics of the mixing height rise. The numerical values for the curve were derived from detailed data from about 40 days in the RAPS study by Schere and Demerjian (1980). Table 28 gives the numerical values of the curves break points and Figure 73 shows the normalized curve plotted. The curve has been normalized by fraction of total growth in the mixing height versus fraction of the total daylight period. Use of the curve requires the sunrise mixing height and the maximum afternoon

Table 28. The Demerjian/Schere Characteristic Mixing Height Growth Curve

Interval:	= 1	2	3	4	5	6	7	8	9
Fraction of day:	= 0.0	0.07	0.14	0.33	0.50	0.70	0.90	1.0	2.0
Fraction of growth:	= 0.0	0.02	0.10	0.588	0.85	1.00	1.00	0.5	0.5
Growth rate:	= 0.286	1.143	2.526	1.588	0.750	0.0	-5.0	6.0	0.0

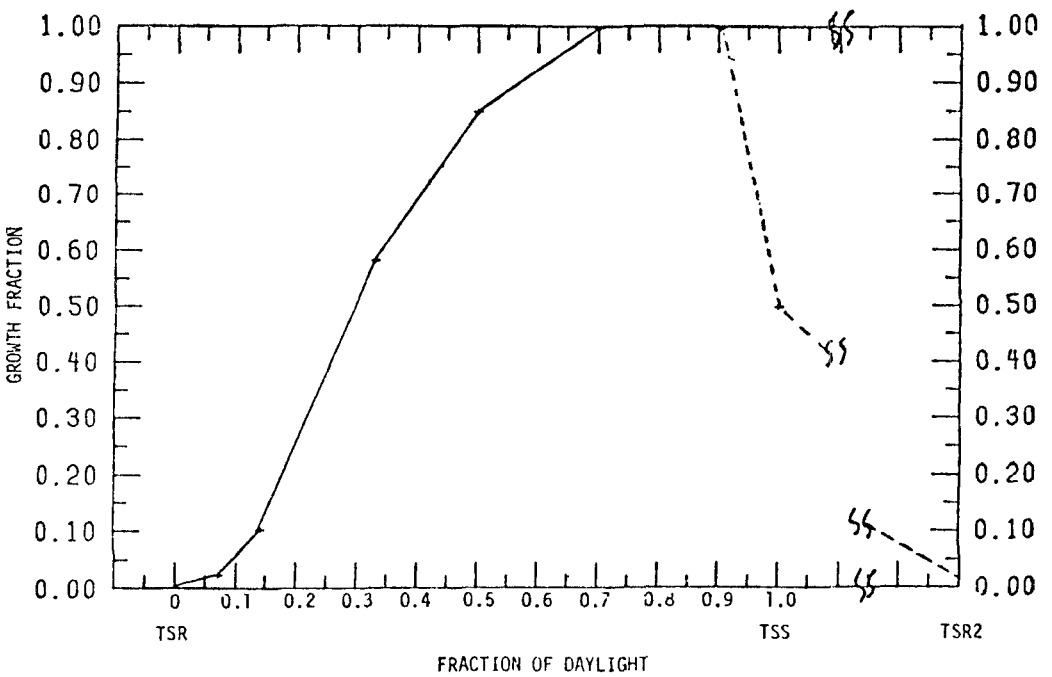

Figure 73. The characteristic growth curve.

mixing height. The maximum mixing height is assumed to occur at 70% of the total daylight period. Note that 10% of the growth occurs in 14% of the day and that 85% of the growth occurs in 50% of the day. Morning and afternoon mixing heights for use with the curve were supplied by OAQPS/EPA.

Table 29 lists the hourly values of mixing height for all three methods for the ten days studied.

The effect of a mixing height rise, assuming uniform mixing to the mixing height, is three-fold: 1) the volume of the "box" is bigger and the same mass in a bigger volume means a decrease in concentration, i.e., dilution; 2) the rate of increase of concentration due to emissions is less because the volume is bigger; and 3) material that was above the mixing height is entrained into the mixed layer and is diluted uniformly throughout. As described in Table 1, the first and third effects are implemented in the model as a dilution rate while the second effect is accounted for by dividing the emissions rate by the current mixing height.

To calculate a dilution rate, the rate of change of the mixing height is needed, as well as the mixing height; that is, the dilution rate is given by: $k_d = \frac{1}{h} \frac{dh}{dt}$, where k_d = dilution rate, h = mixing height

To obtain a smooth and continuous value for the mixing height and its rate of change, rational spline functions with variable tension were used to fit the values in Table 29. The resulting mixing height profiles must be monotonically increasing functions, that is, the derivative must be zero or positive everywhere. The mixing height values were initially fitted with a low tension which results in a cubic spline-like fit. If the derivatives anywhere were negative, the fit was repeated with increasing tension until the derivatives were positive everywhere. The resulting curves for each of the

Table 29

Mixing Height Patterns Used to Model Selected RAPS Days
(km)

DAY 159 - June 7			
LST	Linear	H.P.	Char.
0800	0.754	0.050	0.272
0900	0.987	0.145	0.574
1000	1.220	0.151	0.883
1100	1.421	1.400	1.172
1200	1.499	1.990	1.367
1300	1.578	1.990	1.561
1400	1.656	1.990	1.685
1500	1.734	1.990	1.777
1600	1.812	1.990	1.869
1700	1.812	1.990	1.890

DAY 160/103 - June 8			
LST	Linear	H.P.	Char.
0700	0.080	0.050	0.134
0800	0.080	0.050	0.269
0900	0.100	0.050	0.563
1000	0.120	0.105	0.866
1100	0.150	0.145	1.149
1200	0.250	2.090	1.339
1300	0.420	2.090	1.529
1400	0.630	2.090	1.651
1500	0.880	2.090	1.740

DAY 160/115 - June 8			
LST	Linear	H.P.	Char.
0900	0.080	0.105	0.563
1000	0.100	0.145	0.866
1100	0.150	2.090	1.149
1200	0.290	2.090	1.339
1300	0.450	2.090	1.529
1400	0.660	2.090	1.651
1500	0.900	2.090	1.740
1600	1.130	2.090	1.830
1700	1.130	2.090	1.852
1800	1.130	2.090	1.852

DAY 195 - July 13			
LST	Linear	H.P.	Char.
1100	0.440	0.494	1.198
1200	0.464	0.795	1.372
1300	0.762	0.951	1.547
1400	1.061	1.251	1.651
1500	1.359	1.351	1.733
1600	1.657	1.351	1.815
1700	1.853	1.351	1.826

DAY 201 - July 19			
LST	Linear	H.P.	Char.
0700	0.437	0.110	0.131
0800	0.437	0.110	0.257
0900	0.564	0.400	0.541
1000	0.691	0.750	0.839
1100	0.818	1.250	1.118
1200	0.900	1.600	1.305
1300	1.100	1.610	1.493
1400	1.200	1.610	1.607

DAY 221 - August 8			
LST	Linear	H.P.	Char.
0700	0.437	0.110	0.131
0800	0.437	0.110	0.257
0900	0.564	0.400	0.541
1000	0.691	0.750	0.839
1100	0.818	1.250	1.118
1200	0.900	1.600	1.305
1300	1.100	1.610	1.493
1400	1.200	1.610	1.607

DAY 238 - August 25			
LST	Linear	H.P.	Char.
0800	0.509	0.050	0.204
0900	0.654	0.110	0.411
1000	0.800	1.045	0.654
1100	1.067	1.050	0.884
1200	1.148	1.250	1.037
1300	1.228	1.335	1.1189
1400	1.309	1.400	1.278
1500	1.389	1.450	1.350
1600	1.389	1.550	1.419
1700	1.389	1.550	1.419
1800	1.389	1.550	1.419
1900	1.389	1.550	1.419

DAY 261-September 17			
LST	Linear	H.P.	Char.
0700	0.268	0.050	0.103
0800	0.445	0.050	0.166
0900	0.621	0.110	0.383
1000	0.798	0.310	0.712
1100	0.974	1.105	1.035
1200	1.128	1.105	1.242
1300	1.220	1.105	1.449
1400	1.311	1.105	1.549

DAY 275 - October 1			
LST	Linear	H.P.	Char.
0600	0.064	0.050	0.100
0700	0.120	0.050	0.100
0800	0.177	0.050	0.109
0900	0.233	0.100	0.163
1000	0.289	0.150	0.257
1100	0.346	0.390	0.351
1200	0.411	0.490	0.410
1300	0.504	0.620	0.469
1400	0.597	0.800	0.497
1500	0.690	0.890	0.524
1600	0.784	0.890	0.533

DAY 276 - October 2			
LST	Linear	H.P.	Char.
0600	0.062	0.050	0.100
0700	0.062	0.050	0.100
0800	0.397	0.050	0.159
0900	1.066	0.100	0.486
1000	1.400	0.200	1.061
1100	1.735	0.350	1.634
1200	2.070	0.750	1.996
1300	2.404	3.150	2.350
1400	2.739	3.150	2.521
1500	2.739	3.150	2.692
1600	2.739	3.150	2.739
1700	2.739	3.150	2.739
1800	2.739	3.150	2.739

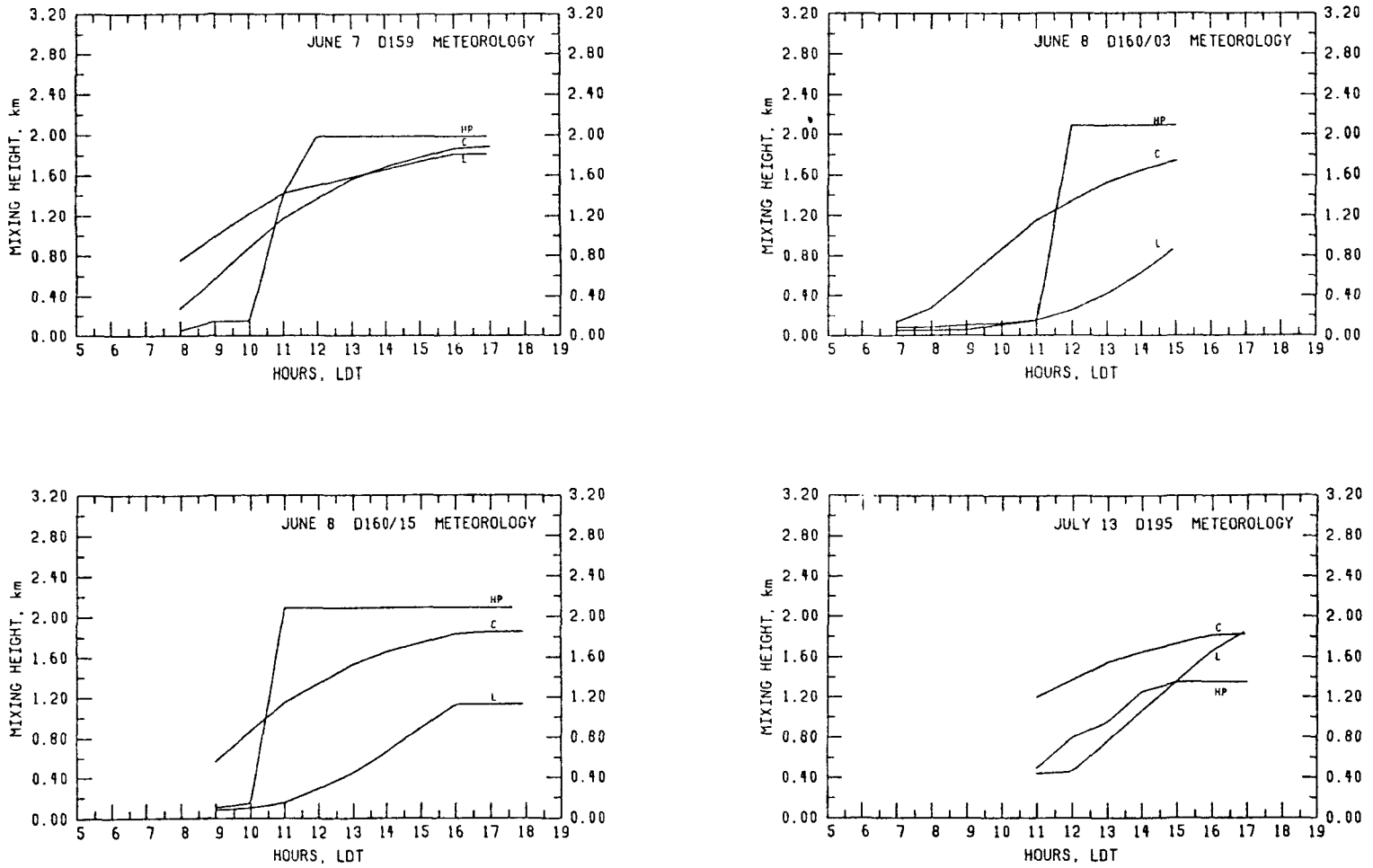

Figure 74. Mixing height profiles, all days. L=linear, HP=handpicked, and C=characteristic curve.

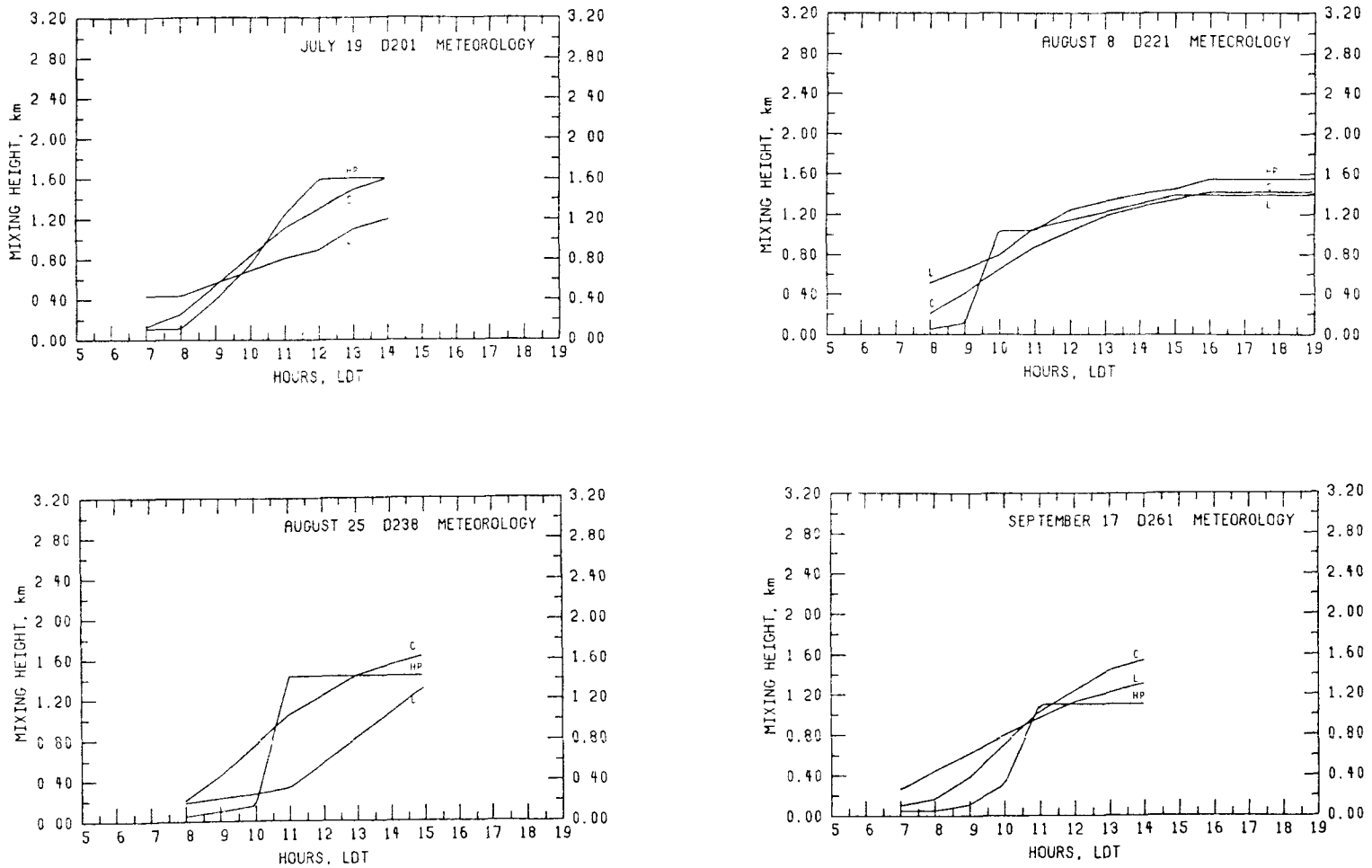

Figure 74. Mixing height profiles, all days. (continued)

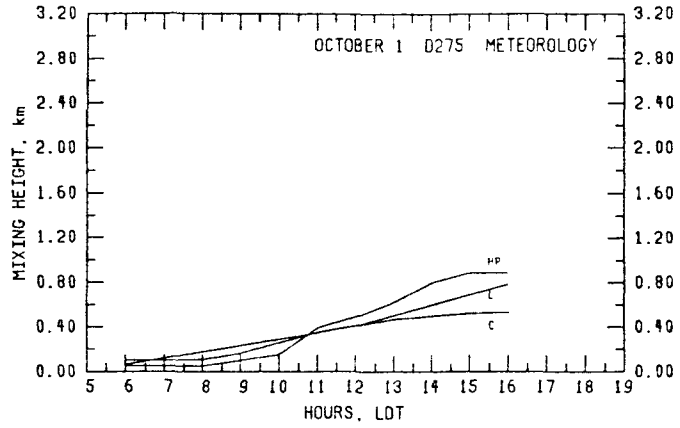

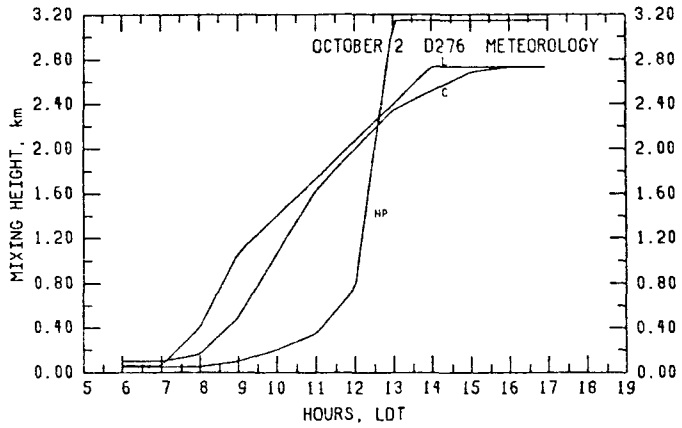

Figure 74. Mixing height profiles, all days. (continued)

profile methods(linear, handpicked, and characteristic curve) for each of the days are shown in Figure 74, all on the same scale.

The different methods of estimating the mixing height profile do produce large temporal differences in the profiles.

In the solution of the model it is the dilution rate, rather than the mixing height itself, that is of interest. As has been explained, both the height and the rate of change determine the dilution rate. Thus, if the rate of change is constant, then the dilution rate will decrease over time. If this period is followed by one in which the rate changes, then the dilution rate can rapidly increase before decreasing again. To illustrate this process, the dilution rates resulting from the three profiles for two days are shown in Figure 75. Obviously, the different dilution patterns will have a strong influence on the concentration profiles. Such discontinuities in dilution probably do not occur in the real world.

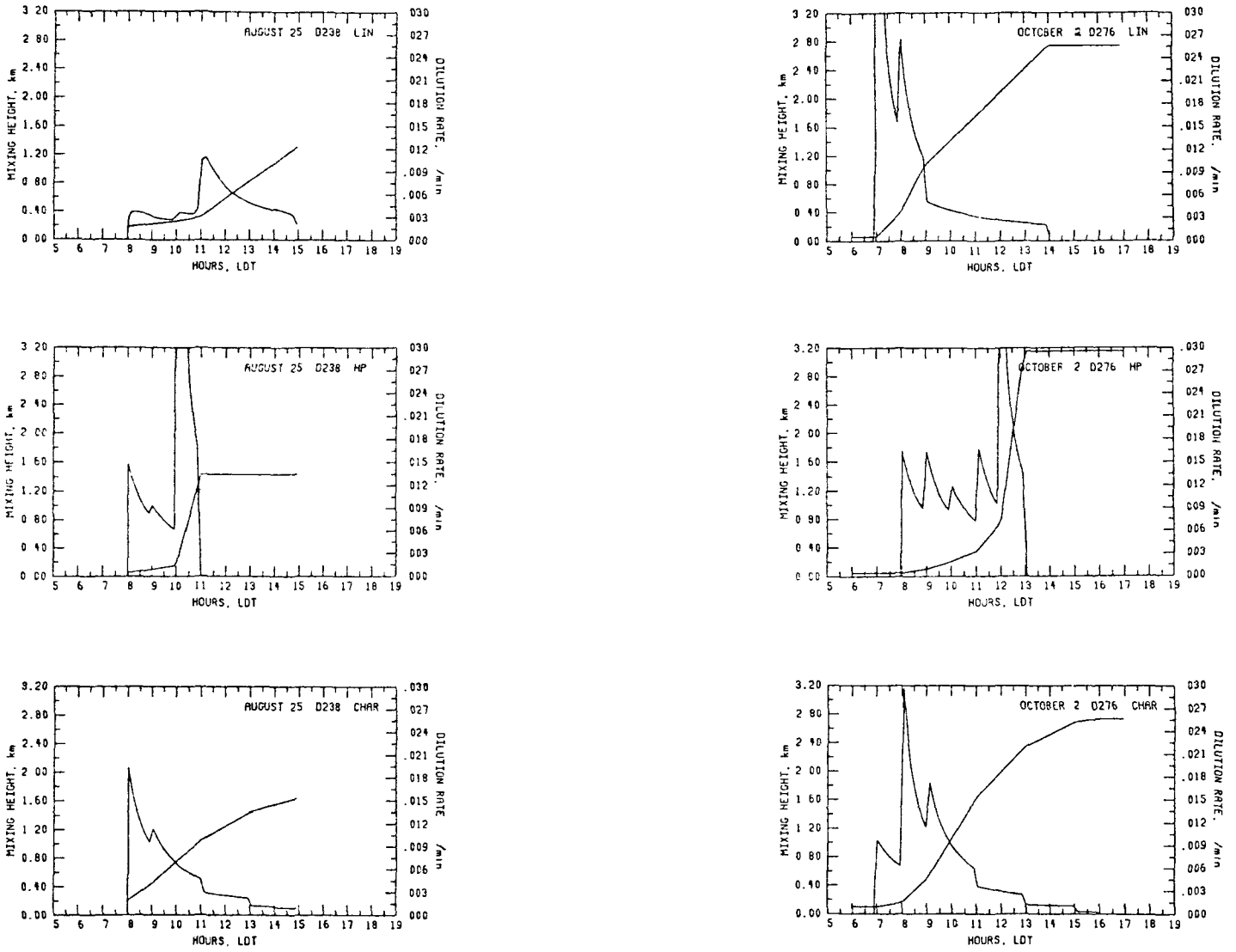

Figure 75. Dilution rates resulting from selected mixing height profiles.

7.5 OZONE ALOFT

The last data needed to perform the simulations are estimates of O_3 aloft or ozone that is above the mixing height in the morning that would be entrained into the mixed layer as the mixing height rises. Direct measurements of this value are rare. It has been shown that there is a relationship between the average O_3 aloft as measured by helicopters and subsequent reading of surface O_3 monitors following inversion breakup. One example of this relationship is shown in Figure 76 (Evans, 1979). The recommended procedure for estimating the O_3 aloft values is described in the EPA guidance document (EPA, 1981). The procedure basically consists of using O_3 measurements from surface monitoring sites upwind of the city during the first hour after breakup of the nocturnal inversion as an estimate of the ozone aloft. This technique was used by OAQPS/EPA to estimate the O_3 aloft values for the days studied herein; these studies were supplied to UNC and are listed in Table 30.

In addition to O_3 aloft, all simulations assumed a natural background value of 0.20 ppm carbon monoxide aloft.

Figure 76. AVERAGE OZONE CONCENTRATION IN EARLY VERTICAL PROFILE VS UPWIND POST-BREAKUP CONCENTRATION

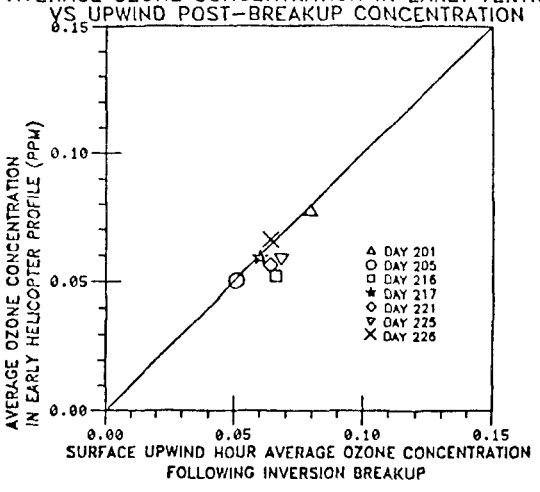

Table 30

Assumed Ozone Aloft Used in Models
of Selected RAPS Days
(ppm)

Day	Concentration
159 - June 7	0.12
160 - June 8	0.09
195 - July 13	0.07
201 - July 19	0.08
221 - August 8	0.07
238 - August 25	0.09
261 - September 17	0.06
275 - October 1	0.06
276 - October 2	0.08

8.0 RAPS SIMULATIONS WITH SIMPLE TRAJECTORY MODELS

8.1 METEOROLOGY-ONLY SIMPLE TRAJECTORY MODEL SIMULATIONS OF RAPS DAYS

8.1.1 Brief Description

The Meteorology-Only Simple Trajectory Model (MOSTM) has no chemistry. That is, the concentrations of the species of interest are effected by the initial concentrations, their boundary values (the concentrations transported and entrained in the mixed layer) and their emissions; all of which are diluted as the mixing height rises. Thus, the rate of change in the concentration is prescribed by the equation:

$$\frac{dC_i}{dt} = -\frac{1}{h}\frac{dh}{dt} C_i + \frac{1}{h}\frac{dh}{dt}(FRA_i\ CA_i) + \frac{E_i}{h}$$

where,

$\frac{dC_i}{dt}$	is the rate of change of the concentration of the ith species
$\frac{1}{h}\frac{dh}{dt}$	is the dilution rate
h	is the mixing height
C_i	is the concentration of the ith species
FRA_i	is the fraction aloft of the ith species at time t
CA_i	is the concentration aloft of the ith species
E_i	is the emission flux of the ith species

A meteorology-only simulation gives an indication of the reasonableness of the input data. If the precursors are not predicted correctly, then the O_3 is not likely to be predicted correctly. Since adding chemistry to the simulation acts as a sink for NO_x and HC and a source for O_3, the predictions of NO_x and HC concentrations in MOSTM should be greater than the observed concentrations along the trajectory. Carbon monoxide predictions should be close to the ambient data if the emissions and mixing height data were accurate. The magnitude of O_3 aloft entrainment can also be seen. When the meteorology-only simulation underpredicts the observed NO_x and HC concentrations, the input data should be reexamined.

8.1.2 Results of MOSTM Simulations

Figure 77 shows the model predictions as solid lines and the ambient data that were shown in Figures 55 - 64 are shown here as symbols and dashed lines. One mixing height profile was used for each row and a single day is in each column. One page shows the NMHC and CO predictions and the facing page shows the NO_x and O_3. Remember that the O_3 model predictions are the result of initial concentrations and entrainment from aloft as the mixing height rises and that, since there was no chemistry, there is no reaction of the NO with the O_3.

In the June 7 (D159) model predictions, the first column of Figure 77, the only differences in input data were the three mixing height profiles (see Figure 74). These do result in significant differences among the simulations. In the LIN simulation, the CO is nearly constant at about 0.7; in the HP (handpicked) simulation, the CO decreases sharply then rises to a peak greater than 1 ppm and then falls to about 0.4 ppm; in the CHAR simulation the CO decreases slowly all day.

A comparison of the emission pattern for this day (Figure 69) with the

mixing height profiles (Figure 74) reveals the causes of these different predictions. The highest CO emissions were for the 8-9 A.M. hour; from 9 to 13 the emissions were almost constant and they decreased after 1300 LDT.

The linear mixing height profile was the highest at 8 and it changed only a small amount over the 8-9 hour. The dilution caused by the rise was almost exactly compensated for by the emissions so the concentration did not change very much. After 9, the CO emissions decreased and likewise the dilution rate decreased all day, resulting in little change in the CO concentration.

The HP mixing height profile was the lowest at 8 and it tripled its height in 8-9 hour, resulting in a factor of three dilution for the initial CO concentration. This was more than compensated for by the CO emissions. Even though these were the same magnitude as in the LIN case, they went into a volume that was initially 15 times smaller and at 0900 LDT, was still six times smaller. Thus, the emissions into this smaller volume were able to rapidly increase the CO concentration. In the hour from 10 to 11, however, the volume increased by nearly a factor of 10, resulting in a rapid and dramatic decrease in CO concentration. After 1100 LDT, there was no change in mixing height and therefore no dilution. The CO emissions into the large volume were able to slightly increase the CO concentration.

Since the CHAR mixing height profile is in between the LIN and HP it exhibits some characteristics of both. Its initial height and rate of rise prevents the large increase in CO concentration that was seen in the HP case. The dilution rate, however, is larger than in the LIN case, resulting in a rapid initial drop. Because the initial volume was smaller than in the LIN case, less CO mass was present, even though both simulations had the same

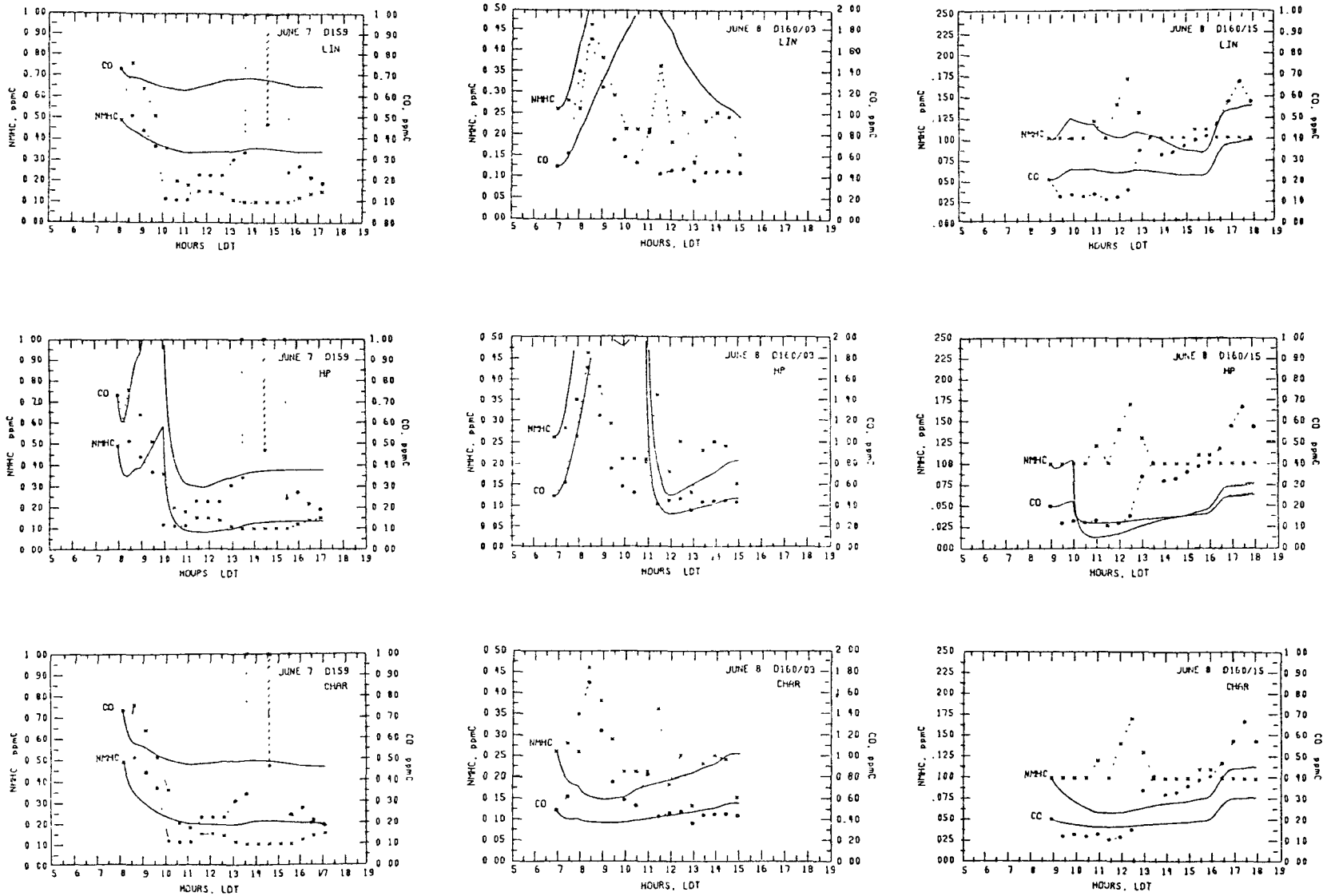

Figure 77. MOSTM simulation results for NO_x, HC, CO, and O_3, all days. Solid lines are model predictions.

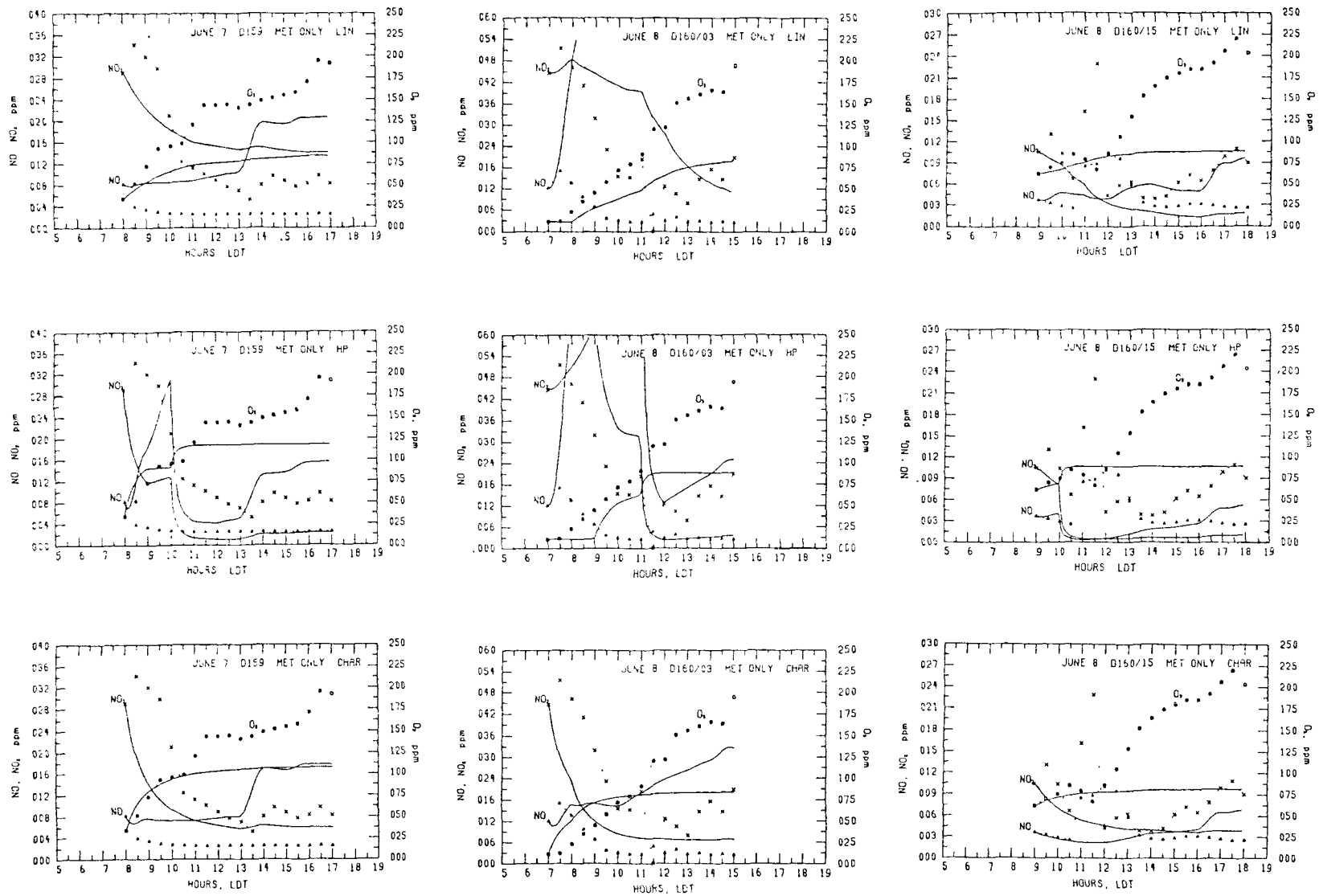

Figure 77. continued

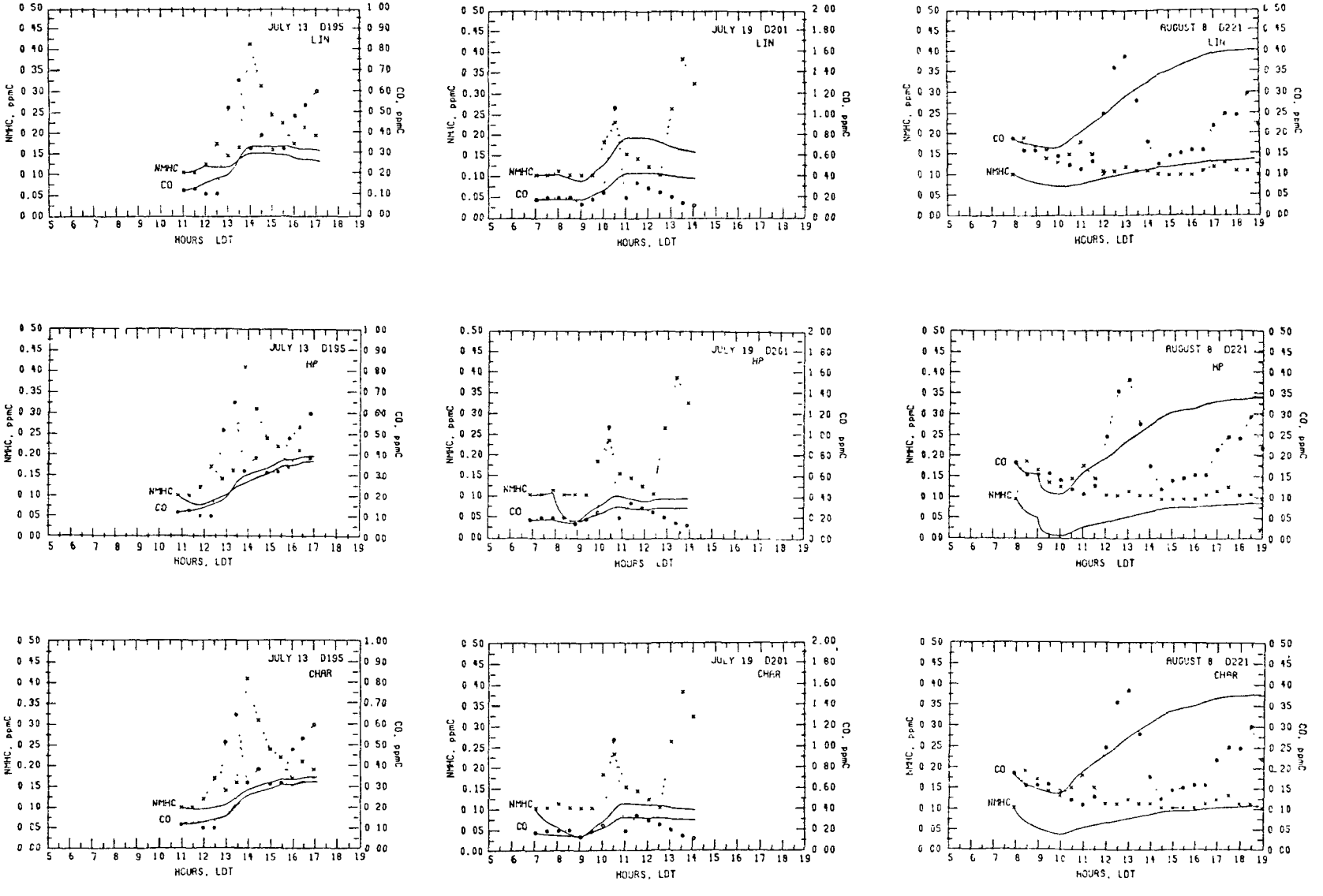

Figure 77. continued.

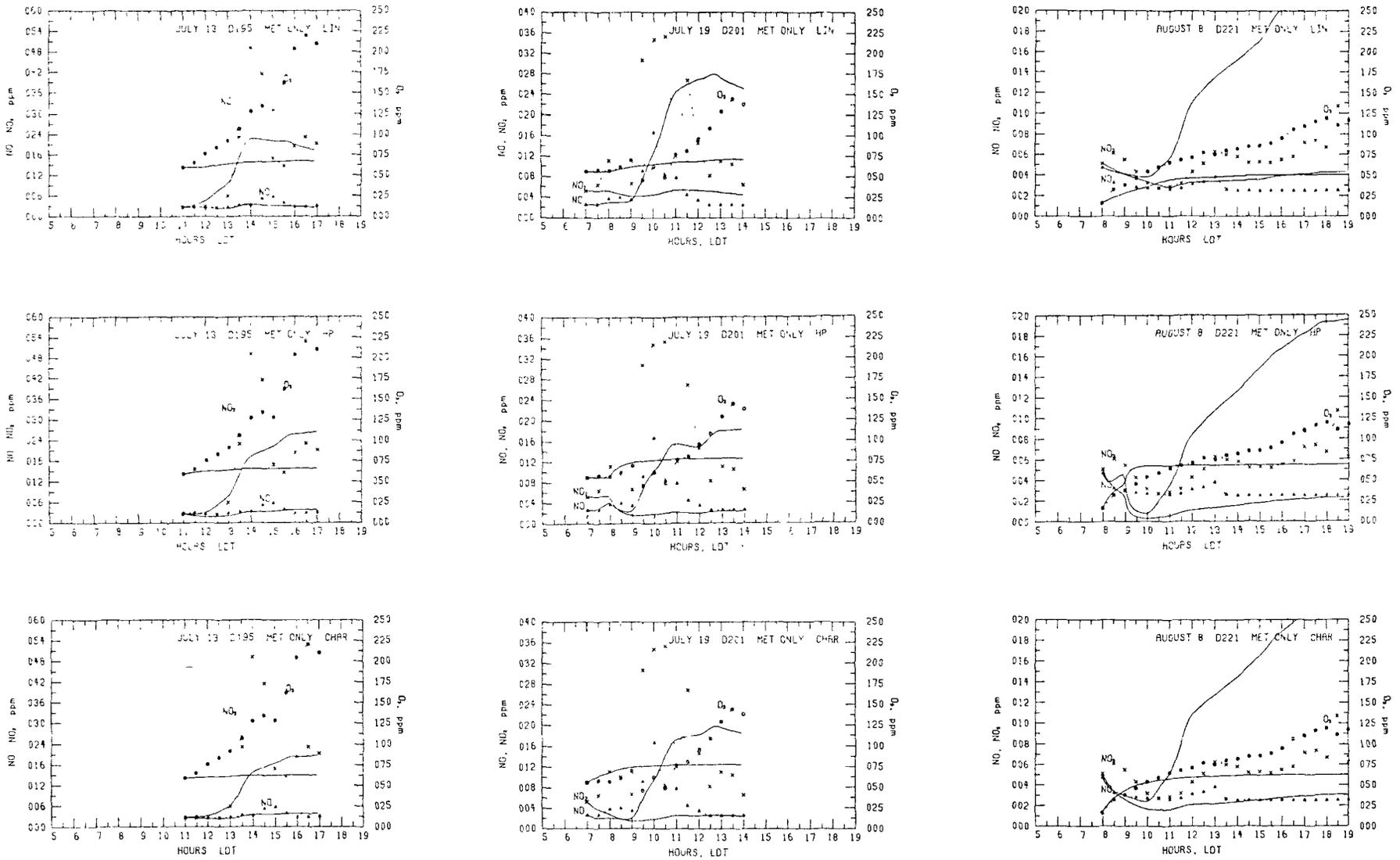

Figure 77. continued

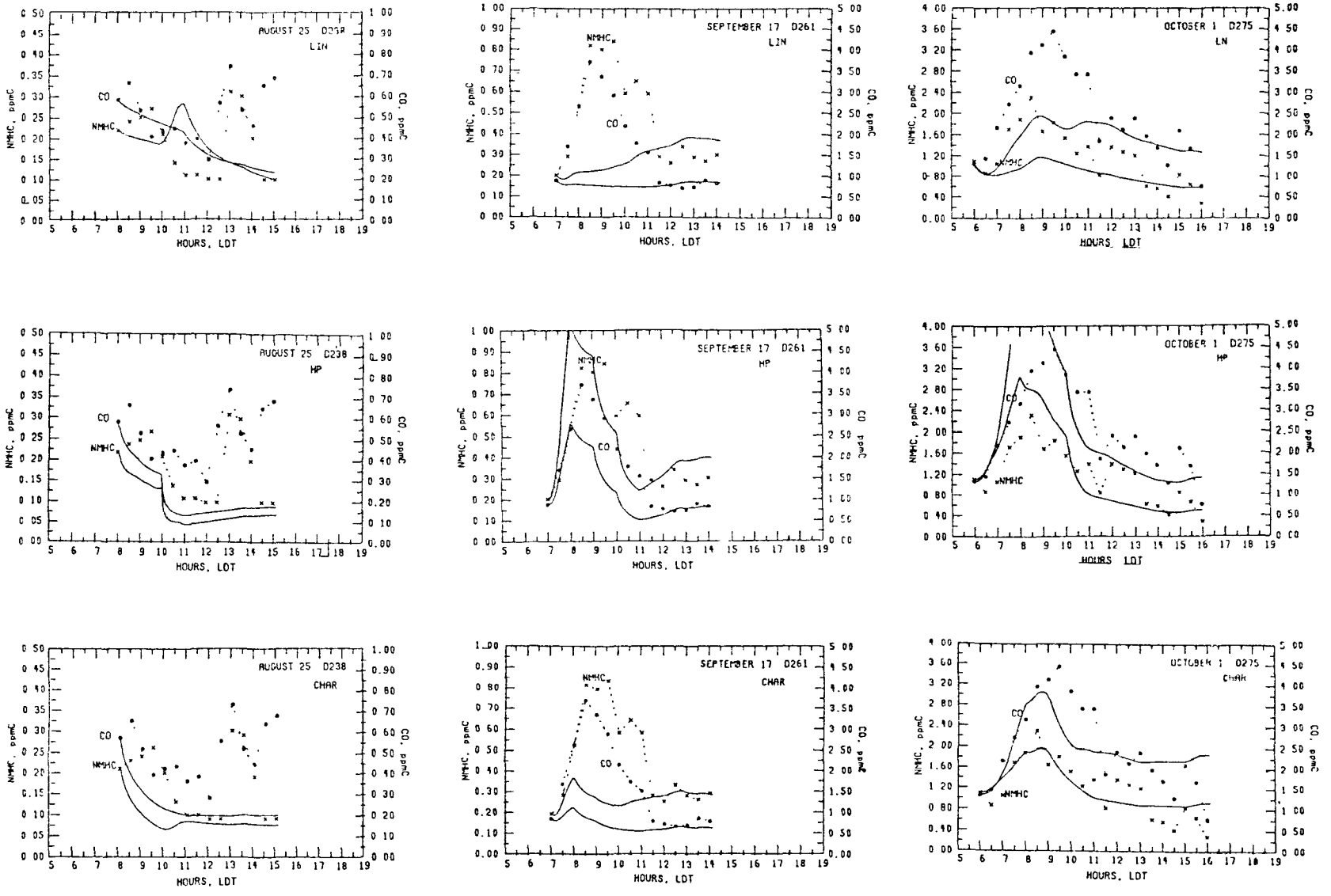

Figure 77. continued.

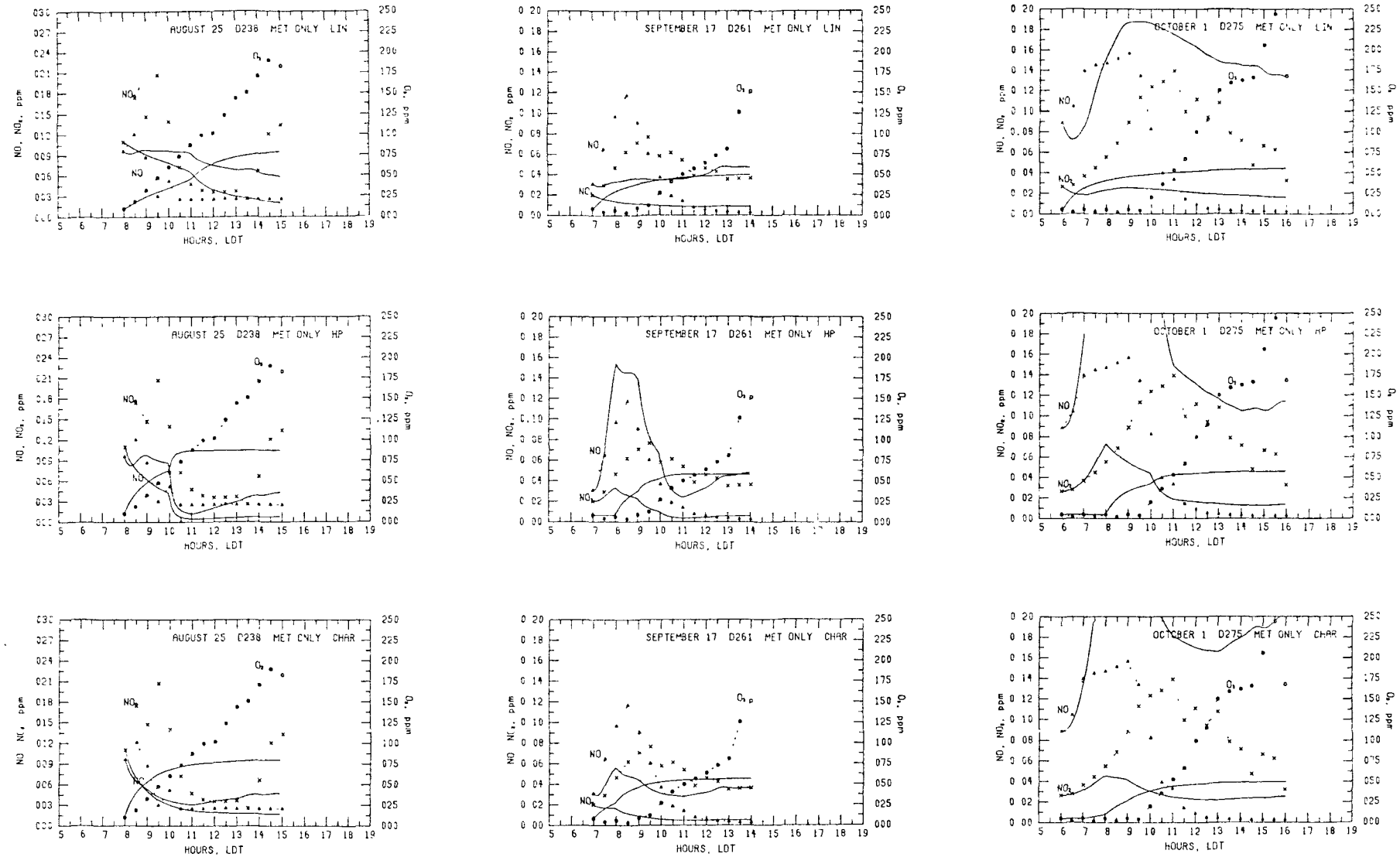

Figure 77. continued

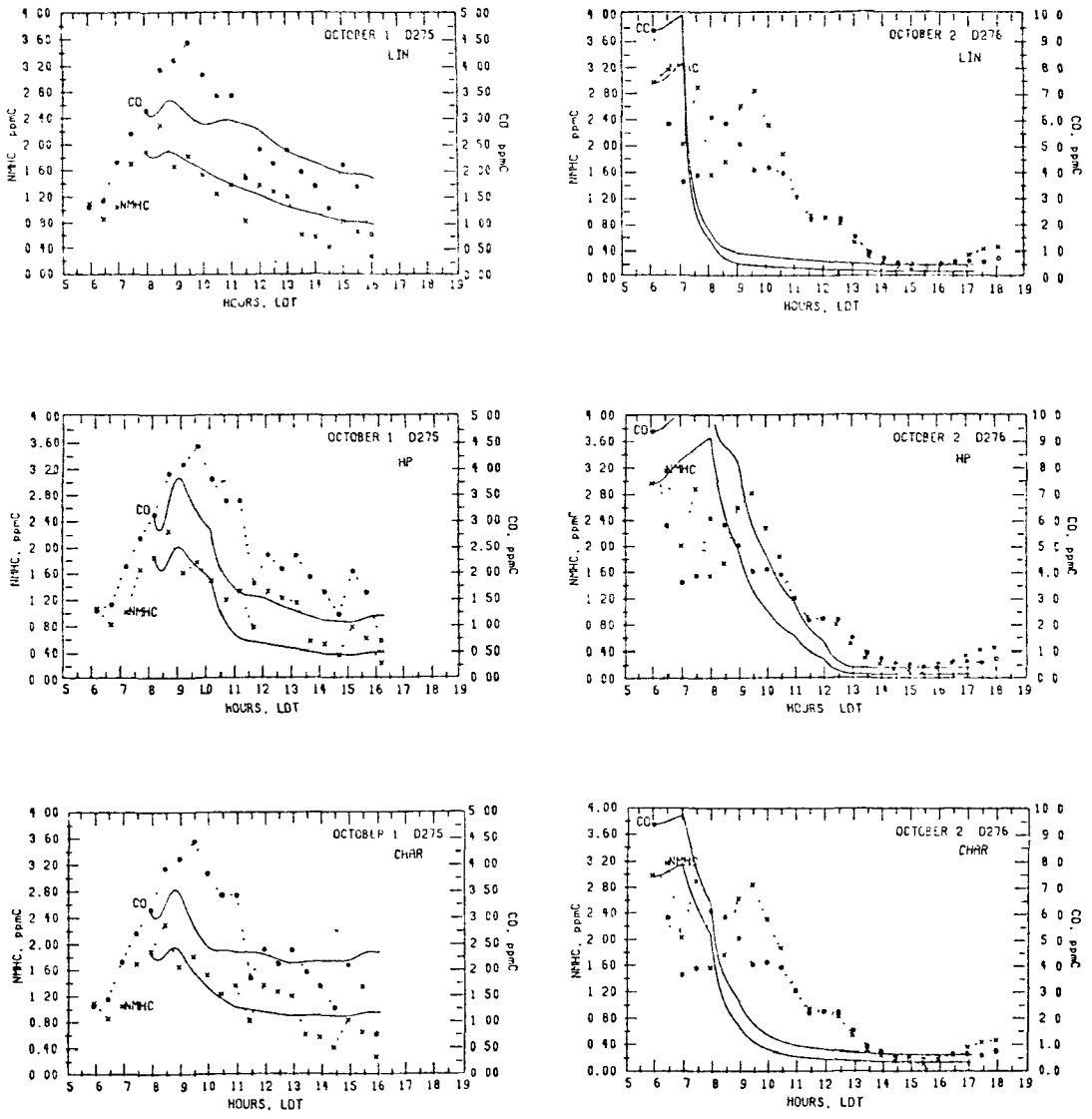

Figure 77. continued.

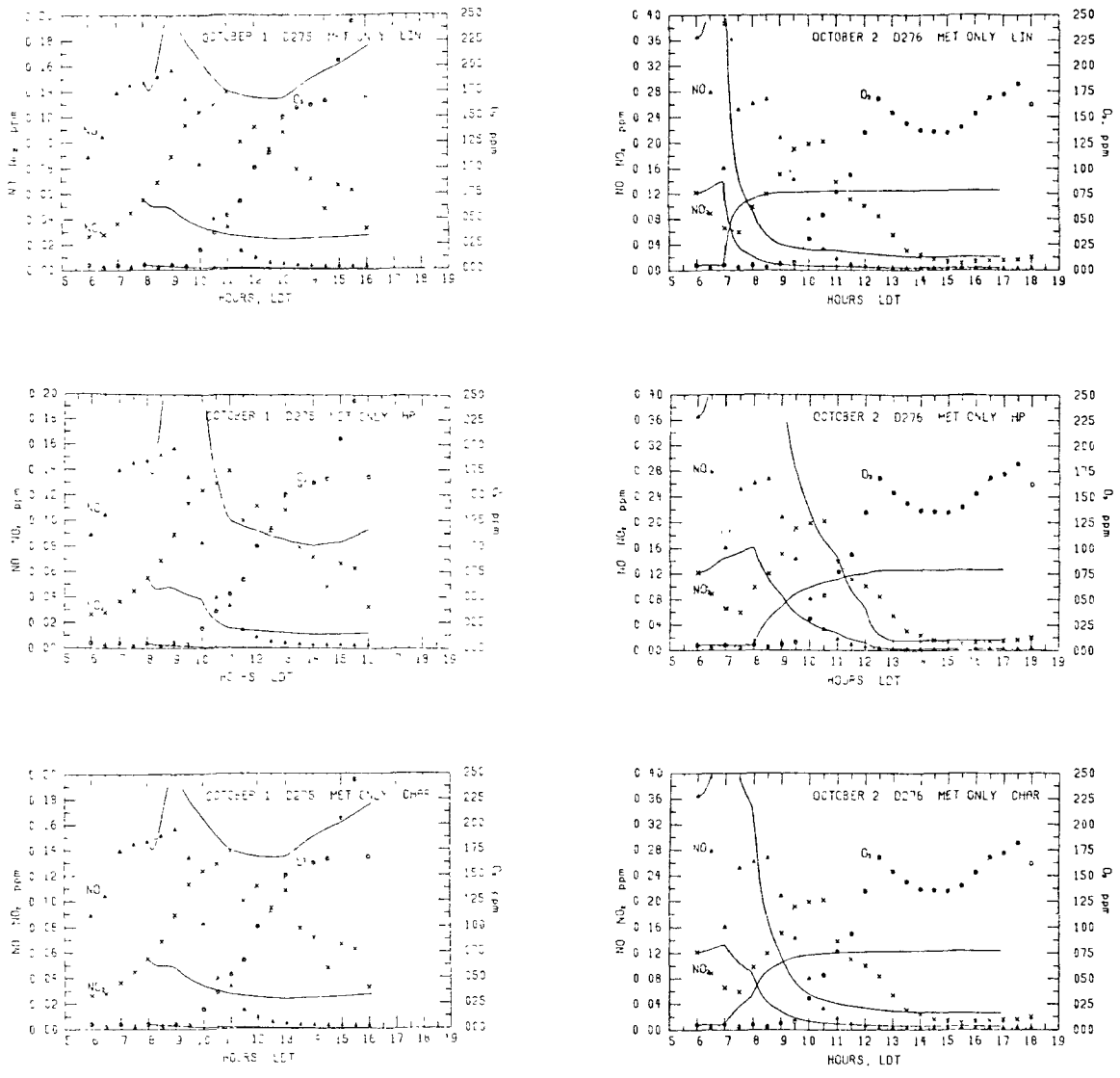

Figure 77. continued

initial CO concentration. The final volumes, however, were similar, therefore, the concentration was less in the CHAR simulation.

To aid in these interpretations, Table 31 has been prepared. In MOSTM simulations there are three sources of mass: initial material, emissions, and material aloft that is entrained. There are no losses of mass, only increase in volume which results in decrease of concentrations (mass/unit volume). MOSTM keeps track of how much of the final concentration resulted from which process; these values are shown in Table 31. For Day 159 (June 7), for example, 46.6% of the final CO concentration was the result of the initial amount of CO specified. That is, if there had been no emissions and no CO aloft, the final CO concentration would have been 0.304 ppm.

The amount of material that results from entrainment varies with mixing height profile (see Table 31). This is because the ratio of the difference between final and initial heights to the final height is quite different for each mixing height profile. That is, the mass of ozone at the end of the simulation is given by:

$$\text{ozone mass} = [O_3]_f * MH_f = [O_3]_{AL} * (MH_f - MH_i) + [O_3]_i * MH_i$$

where, $[O_3]_f$ = final ozone concentration in mixed region

$[O_3]_{AL}$ = aloft ozone concentration (assumed constant)

$[O_3]_i$ = initial ozone concentration in mixed region

MH_f = mixing height final

MH_i = mixing height initial

Table 31. Effects of Mixing Height Profile on the Contribution of Each Source to Final Concentrations in MOSTM Simulations, All Days

Day 159
(ppm)

Mixing Height Profile	Species	INITIAL Amount	INITIAL Percentage	EMISSIONS Amount	EMISSIONS Percentage	ENTRAINMENT Amount	ENTRAINMENT Percentage	Final Concentration
Linear	CO	0.304	46.6	0.290	44.4	0.058	9.0	0.652
	NO	0.003	16.6	0.017	83.4	0.000	0.0	0.021
	NO2	0.012	86.3	0.002	13.7	0.000	0.0	0.014
	HC	0.023	14.9	0.130	85.1	0.000	0.0	0.152
	O3	0.014	16.8	0.000	0.00	0.070	83.2	0.084
Handpicked	CO	0.018	4.8	0.264	69.5	0.098	25.7	0.380
	NO	0.000	1.3	0.016	98.7	0.000	0.0	0.016
	NO2	0.001	29.5	0.002	70.5	0.000	0.0	0.003
	HC	0.001	1.2	0.118	98.9	0.000	0.0	0.119
	O3	0.001	0.7	0.000	0.0	0.117	99.3	0.118
Characteristic	CO	0.105	22.5	0.278	59.3	0.086	18.3	0.469
	NO	0.001	6.7	0.017	93.3	0.000	0.0	0.018
	NO2	0.004	69.5	0.002	30.5	0.000	0.0	0.006
	HC	0.008	5.9	0.124	94.1	0.000	0.0	0.132
	O3	0.005	4.6	0.000	0.0	0.103	95.5	0.108

Day 160 Site 103
(ppm)

Mixing Height Profile	Species	INITIAL Amount	INITIAL Percentage	EMISSIONS Amount	EMISSIONS Percentage	ENTRAINMENT Amount	ENTRAINMENT Percentage	Final Concentration
Linear	CO	0.044	4.7	0.810	85.7	0.091	9.6	0.945
	NO	0.001	1.7	0.063	98.3	0.000	0.0	0.064
	NO2	0.004	36.8	0.007	63.2	0.000	0.0	0.011
	HC	0.003	0.6	0.460	99.5	0.000	0.0	0.463
	O3	0.001	1.2	0.000	0.0	0.082	98.8	0.083
Handpicked	CO	0.002	2.6	0.341	75.6	0.098	21.7	0.450
	NO	0.000	1.1	0.026	98.9	0.000	0.0	0.027
	NO2	0.001	2.7	0.003	73.3	0.000	0.0	0.004
	HC	0.001	0.4	0.194	99.6	0.000	0.0	0.194
	O3	0.000	0.3	0.000	0.0	0.088	94.7	0.118
Characteristic	CO	0.037	6.9	0.410	76.0	0.092	17.1	0.539
	NO	0.001	2.9	0.032	97.1	0.000	0.0	0.033
	NO2	0.003	49.4	0.004	50.7	0.000	0.0	0.007
	HC	0.002	1.0	0.233	99.0	0.000	0.0	0.235
	O3	0.001	1.0	0.000	0.0	0.083	99.0	0.084

Table 31. continued

Day 160 Site 115

Mixing Height Profile	Species	INITIAL Amount	INITIAL Percentage	EMISSIONS Amount	EMISSIONS Percentage	ENTRAINMENT Amount	ENTRAINMENT Percentage	Final Concentration
Linear	CO	0.014	3.7	0.279	72.3	0.093	24.1	0.386
	NO	0.000	2.7	0.009	97.3	0.000	0.0	0.010
	NO2	0.001	41.7	0.001	58.2	0.000	0.0	0.002
	HC	0.001	0.6	0.129	99.4	0.000	0.0	0.130
	O3	0.000	5.0	0.000	0.0	0.084	95.0	0.088
Handpicked	CO	0.010	3.9	0.151	59.0	0.095	37.1	0.256
	NO	0.000	3.6	0.005	96.4	0.000	0.0	0.005
	NO2	0.001	48.5	0.001	51.5	0.000	0.0	0.001
	HC	0.001	0.8	0.770	99.2	0.000	0.0	0.011
	O3	0.003	3.5	0.000	0.0	0.086	96.5	0.089
Characteristic	CO	0.061	20.2	0.170	56.6	0.079	23.2	0.301
	NO	0.001	16.5	0.006	83.5	0.000	0.0	0.007
	NO2	0.003	83.5	0.001	16.5	0.000	0.0	0.004
	HC	0.004	4.3	0.079	95.7	0.000	0.0	0.082
	O3	0.019	23.1	0 000	0.0	0.063	76.9	0.082

Day 195

Mixing Height Profile	Species	INITIAL Amount	INITIAL Percentage	EMISSIONS Amount	EMISSIONS Percentage	ENTRAINMENT Amount	ENTRAINMENT Percentage	Final Concentration
Linear	CO	0.027	8.9	0.205	66.4	0.076	24.7	0.308
	NO	0.001	3.5	0.019	96.5	0.000	0.0	0.019
	NO2	0.001	23.1	0.002	77.9	0.000	0.0	0.003
	HC	0.003	2.5	0.106	97.5	0.000	0.0	0.108
	O3	0.014	20.8	0.000	0.0	0.053	79.2	0.067
Handpicked	CO	0.042	10.9	0.281	72.7	0.063	16.4	0.386
	NO	0.001	3.9	0.025	96.1	0.000	0.0	0.027
	NO2	0.001	25.2	0.003	74.8	0.000	0.0	0.004
	HC	0.004	2.9	0.150	97.2	0.000	0.0	0.149
	O3	0.022	32.7	0.000	0.0	0.044	67.3	0.066
Characteristic	CO	0.075	23.8	0.208	65.4	0.034	10.8	0.318
	NO	0.002	8.9	0.019	91.1	0.000	0.0	0.021
	NO2	0.002	44.9	0.002	55.1	0.000	0.0	0.004
	HC	0.008	6.6	0.107	93.4	0.000	0.0	0.115
	O3	0.039	61.7	0.000	0.0	0.024	38.4	0.063

Table 31. continued

Day 201

Mixing Height Profile	Species	INITIAL Amount	INITIAL Percentage	EMISSIONS Amount	EMISSIONS Percentage	ENTRAINMENT Amount	ENTRAINMENT Percentage	Final Concentration
Linear	CO	0.058	16.2	0.236	66.0	0.064	17.8	0.357
	NO	0.001	3.8	0.024	96.2	0.000	0.0	0.025
	HO2	0.002	41.5	0.003	58.6	0.000	0.0	0.005
	HC	0.004	3.5	0.117	96.5	0.000	0.0	0.121
	O3	0.020	28.6	0.000	0.0	0.051	71.4	0.0071
Handpicked	CO	0.011	3.9	0.176	62.8	0.093	33.3	0.280
	NO	0.000	1.0	0.018	99.0	0.000	0.0	0.018
	NO2	0.000	15.1	0.002	84.9	0.000	0.0	0.002
	HC	0.001	0.9	0.087	99.1	0.000	0.0	0.088
	O3	0.004	4.9	0.000	0.0	0.075	95.1	0.078
Characteristic	CO	0.013	4.6	0.176	62.7	0.092	32.7	0.281
	NO	0.000	1.2	0.018	98.8	0.000	0.0	0.018
	NO2	0.001	17.5	0.002	82.5	0.000	0.0	0.002
	HC	0.001	1.1	0.087	48.9	0.000	0.0	0.088
	O3	0.005	5.9	0.000	0.0	0.074	94.2	0.078

Day 221

Mixing Height Profile	Species	INITIAL Amount	INITIAL Percentage	EMISSIONS Amount	EMISSIONS Percentage	ENTRAINMENT Amount	ENTRAINMENT Percentage	Final Concentration
Linear	CO	0.068	16.6	0.278	67.9	0.063	15.5	0.409
	NO	0.002	7.4	0.022	92.6	0.000	0.0	0.023
	NO2	0.002	43.8	0.002	56.2	0 000	0.0	0.004
	HC	0.004	4.2	0.097	95.8	0.000	0.0	0.102
	O3	0.006	11.7	0.000	0.0	0.044	88.3	0.050
Handpicked	CO	0.006	1.7	0.249	70.8	0.097	27.5	0.352
	NO	0.000	0.8	0.019	99.2	0 000	0.0	0.020
	NO2	0.000	7.1	0.002	92.9	0 000	0.0	0.002
	HC	0.000	0.4	0.087	99.6	0 000	0.0	0.088
	O3	0.001	0.8	0.000	0.0	0 068	99.2	0.068
Characteristic	CO	0.027	6.9	0.272	70.8	0.086	22.3	0.304
	NO	0.001	3.1	0.021	96.9	0.000	0.0	0.022
	NO2	0.001	23.8	0.002	76.2	0.000	0.0	0.003
	HC	0.002	1.9	0.095	98.3	0 000	0.0	0.097
	O3	0.002	0.037	0.000	0.0	0.060	96.3	0.062

Table 31. continued

Day 238

Mixing Height Profile	Species	INITIAL Amount	INITIAL Percentage	EMISSIONS Amount	EMISSIONS Percentage	ENTRAINMENT Amount	ENTRAINMENT Percentage	Final Concentration
Linear	CO	0.081	34.6	0.067	28.6	0.086	36.8	0.234
	NO	0.001	23.0	0.005	77.0	0.000	0.0	0.006
	NO	0.002	75.5	0.001	24.5	0.000	0.0	0.002
	HC	0.003	4.7	0.068	95.3	0.000	0.0	0.071
	O3	0.001	1.8	0.000	0.0	0.078	98.2	0.079
Handpicked	CO	0.020	11.4	0.061	34.3	0.097	54.3	0.1778
	NO	0.000	7.6	0.004	92.4	0.000	0.0	0.004
	NO2	0.000	45.8	0.001	54.2	0.000	0.0	0.001
	HC	0.001	1.3	0.062	98.7	0.000	0.0	0.063
	O3	0.000	0.4	0.000	0.0	0.087	99.6	0.087
Characteristic	CO	0.072	33.6	0.053	25.1	0.088	41.3	0.213
	NO	0.001	24.9	0.004	75.1	0.000	0.0	0.05
	NO2	0.001	77.4	0.000	22.6	0.000	0.0	0.002
	HC	0.003	5.1	0.054	94.8	0.000	0.0	0.057
	O3	0.001	0.5	0.000	0.0	0.079	98.5	0.080

Day 261

Mixing Height Profile	Species	INITIAL Amount	INITIAL Percentage	EMISSIONS Amount	EMISSIONS Percentage	ENTRAINMENT Amount	ENTRAINMENT Percentage	Final Concentration
Linear	CO	0.078	21.4	0.575	69.0	0.080	9.6	0.833
	NO	0.006	13.4	0.041	86.6	0.000	0.0	0.047
	NO2	0.004	47.5	0.005	52.5	0.000	0.0	0.009
	HC	0.005	1.4	0.331	98.6	0.000	0.0	0.336
	OC	0.002	3.3	0.000	0.0	0.048	96.7	0.049
Handpicked	CO	0.040	4.8	0.682	83.5	0.010	11.7	0.817
	NO	0.001	2.8	0.048	97.1	0.000	0.0	0.049
	NO2	0.001	14.5	0.005	85.6	0.000	0.0	0.006
	HC	0.001	0.3	0.393	49.7	0.000	0.0	0.394
	O3	0.000	0.6	0.000	010	0.057	99.4	0.058
Characteristic	CO	0.058	9.1	0.048	76.3	0.093	14.6	0.638
	NO	0.002	5.6	0.034	94.4	0.000	0.0	0.036
	NO2	0.001	25.8	0.004	74.2	0.000	0.0	0.005
	HC	0.002	0.5	0.280	99.5	0.000	0.0	0.282
	O3	0.001	10.9	0.000	0.0	0.056	99.1	0.057

Table 31. continued

Day 275 @ 8 am

Mixing Height Profile	Species	INITIAL Amount	INITIAL Percentage	EMISSIONS Amount	EMISSIONS Percentage	ENTRAINMENT Amount	ENTRAINMENT Percentage	Final Concentration
Linear	CO	0.712	38.4	1.067	57.5	0.077	4.2	1.856
	NO	0.033	25.1	0.099	74.9	0.000	0.0	0.132
	NO2	0.013	53.3	0.011	46.7	0.000	0.0	0.0234
	HC	0.043	10.4	0.368	89.6	0.000	0.0	0.411
	O3	0.001	2.4	0.000	0.0	0.045	97.6	0.048
Handpicked	CO	0.177	14.6	0.940	77.6	0.094	7.8	1.211
	NO	0.008	8.7	0.087	91.3	0.000	0.0	0.095
	NO2	0.003	24.4	0.010	75.6	0.000	0.0	0.013
	HC	0.011	3.2	0.324	96.8	0.000	0.0	0.335
	O3	0.000	0.5	0.000	0.0	0.057	1.0	0.057
Characteristic	CO	0.645	28.1	1.569	68.4	0.080	3.5	2.293
	NO	0.030	17.1	0.145	82.9	0.000	0.0	0.175
	NO2	0.011	41.3	0.016	58.7	0.000	0.0	0.027
	HC	0.039	6.7	0.541	93.3	0.000	0.0	0.580
	O2	0.001	2.1	0.000	0.0	0.048	97.9	0.049

Day 275

Mixing Height Profile	Species	INITIAL Amount	INITIAL Percentage	EMISSIONS Amount	EMISSIONS Percentage	ENTRAINMENT Amount	ENTRAINMENT Percentage	Final Concentration
Linear	CO	0.108	6.8	1.387	87.4	0.092	5.8	1.587
	NO	0.007	5.4	0.126	94.6	0.000	0.0	0.133
	NO2	0.002	13.4	0.014	86.6	0.000	0.0	0.016
	HC	0.006	1.3	0.493	98.7	0.000	0.0	0.500
	O3	0.000	0.7	0.000	0.0	0.055	99.3	0.056
Handpicked	CO	0.074	5.3	1.222	87.9	0.094	6.8	1.391
	NO	0.005	4.3	0.111	95.7	0.000	0.0	0.1556
	NO2	0.002	10.8	0.012	89.2	0.000	0.0	0.014
	HC	0.004	1.0	0.435	99.0	0.000	0.0	0.439
	O3	0.000	0.5	0.000	0.0	0.057	99.5	0.057
Characteristic	CO	0.248	10.5	2.041	86.1	0.081	3.4	2.369
	NO	0.017	8.3	0.185	91.8	0.000	0.0	0.202
	NO2	0.005	19.5	0.021	80.5	0.000	0.0	0.026
	HC	0.015	2.0	0.726	98.0	0.000	0.0	0.740
	O3	0.001	1.9	0.000	0.0	0.049	98.1	0.050

Table 31. continued

Day 276

Mixing Height Profile	Species	INITIAL Amount	INITIAL Percentage	EMISSIONS Amount	EMISSIONS Percentage	ENTRAINMENT Amount	ENTRAINMENT Percentage	Final Concentration
Linear	CO	0.213	40.5	0.215	40.9	0.010	18.6	0.526
	NO	0.008	36.7	0.014	63.3	0.000	0.0	0.0223
	NO2	0.003	63.5	0.002	36.5	0.000	0.0	0.004
	HC	0.008	17.6	0.037	82.4	0.000	0.0	0.045
	O3	0.000	0.1	0.000	0.0	0.078	99.9	0.078
Handpicked	CO	0.149	34.3	0.187	43.0	0.098	22.6	0.435
	NO	0.006	31.8	0.012	68.2	0.000	0.0	0.018
	NO2	0.002	58.4	0.001	41.6	0.000	0.0	0.003
	HC	0.006	14.7	0.032	85.3	0.000	0.0	0.038
	O3	0.000	0.0	0.000	0.0	0.079	99.9	0.079
Characteristic	CO	0.344	52.4	0.215	32.9	0.096	14.7	0.655
	NO	0.013	48.3	0.014	51.7	0.000	0.0	0.028
	NO2	0.004	73.7	0.002	26.3	0.000	0.0	0.006
	HC	0.013	25.6	0.037	74.4	0.000	0.0	0.050
	O3	0.000	0.2	0.000	0.0	0.077	99.8	0.077

Thus, for the LIN case for Day 159, the O_3 concentration resulting from entrainment was 0.070 ppm with $[O_3]_{AL}$ = 0.12 ppm and $(MH_f - MH_i)/MH_f$ = 0.58, while for the HP case $(MH_f - MH_i)/MH_f$ = 0.97, resulting in 0.117 ppm O_3 from entrainment. In examining the plots in Figure 77, it is evident that the detail in the ambient data is not always simulated very well by the model. For example, the CO ambient data for Day 159 shows some very sharp spikes in the afternoon(1330 to 1530 LDT) that do not occur in any of the models. The NMHC data exhibits similar rapid jumps for June 8 (D 160/03) and in the morning the NO_x shows a quadrupling of concentration in one hour. Particularly bad cases are July 13 and July 19, where the trajectories presumably went through the center of town and a dense part of the RAMS network. It is evident from the simulations in Figure 77 that the emissions and mixing height data for these two days are not consistent with the ambient data. This is especially troublesome on July 19 which should be an ideal case for a simple trajectory model approach. The July 19 case will be examined in detail later in this report (Section 8.3.3 and 8.3.4). The oversimplistic treatment of point sources and the large amount of "noise" in the trajectory leading to spacial averages of the area emissions may be major causes of the poor agreement.

8.1.3 Summary of MOSTM Simulations

Based on meteorology-only simulations the days expected to perform poorly in the photochemical simulations are: June 8, D160/15; July 13, D195; July 19, D201; August 25, D238; LIN and CHAR for Sept 17, D261; starting at 0600 LDT on October 1, D275; and LIN and CHAR of October 2, D276. More than one-half of the test cases appear to be so poorly characterized by input data that they are probably not suitable for examining the effects of chemical mechanism choices on controls.

8.2 PHOTOCHEMICAL SIMPLE TRAJECTORY MODEL SIMULATIONS OF RAPS DAYS

8.2.1 Brief Description

The Photochemical Kinetics Simple Trajectory Model (PKSTM) is a substantially expanded OZIPP-like model more suitable for research use. The equations solved by the model were given in Table 1. Special features of the model include:

- easy entry of different chemical mechanisms
- easy entry of photolytic processes
- use of variable temperature and temperature dependent rate constants
- use of variable humidity and water vapor dependent rate constants
- allows for CO emissions
- allows for CO aloft (constant or variable)
- allows for variable O_3 aloft
- use of absolute emission units
- use of smooth, equal-area emission histogram fits
- use of smooth mixing height fits
- simple, fast solution algorithms
- large amount of output information
- simple repeat functions for isopleth diagram generation.

Of course the model incorporates all of the processes included in the meterology-only (MOSTM) model and adds to these the processes needed to represent the chemistry.

Each of the 10 days was simulated with each of the three mixing height profiles (linear, hand picked, or characteristic) with each of three mechanisms (Demerjian, Dodge, or Carbon Bond). Because of its performance on the Bureau of Mines smog chamber, the CIT mechanism was used to simulate

June 7 (D159) and October 1 (D275) only.

8.2.2 Results of PKSTM Simulations

The comparison of predictions and ambient data for all days is shown in Figure 79. Figure 79 shows one day per page, a single mixing height per row, and a single mechanism per column. The top row is always the linear (LIN) mixing height profile results; the bottom row is always CHAR. The order from left-to-right is always the Demerjian (DEM), Dodge (DOD), and Carbon Bond II (CB2) mechanisms results. The CIT simulations appear on a separate page by themselves.

Only the NO, NO_2, and O_3 data are shown since the CO data would be essentially the same as the MOSTM simulations already shown. Of course, the mechanisms do not use NMHC, but represent individual molecules of various hydrocarbon species. These were not plotted because there would be no ambient data for comparison.

June 7 D159. As expected from the MOSTM simulations, this day was reasonably well simulated by all four mechanisms. Of course this day had 0.12 ppm O_3 aloft and significant quantities of O_3 were entrained.

June 8 D160/03. Only DEM and DOD CHAR simulations were close to ambient data.

June 8 D160/15. As expected from MOSTM results, no simulations were satisfactory.

July 13 D195. As expected from MOSTM results, no simulations were satisfactory.

July 19 D201. As expected from MOSTM results, no simulations were satisfactory. Although the DEM and DOD LIN simulated O_3 values were similar to the ambient data for the first few hours, the failure to track

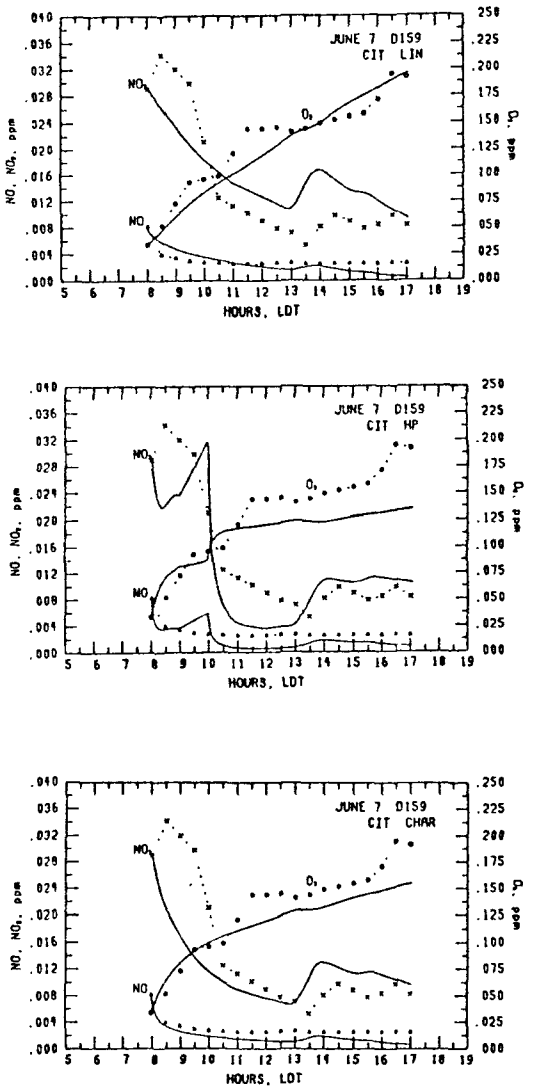

Figure 79. Photochemical simple trajectory model simulation results for NO, NO_2 and O_3, all days.

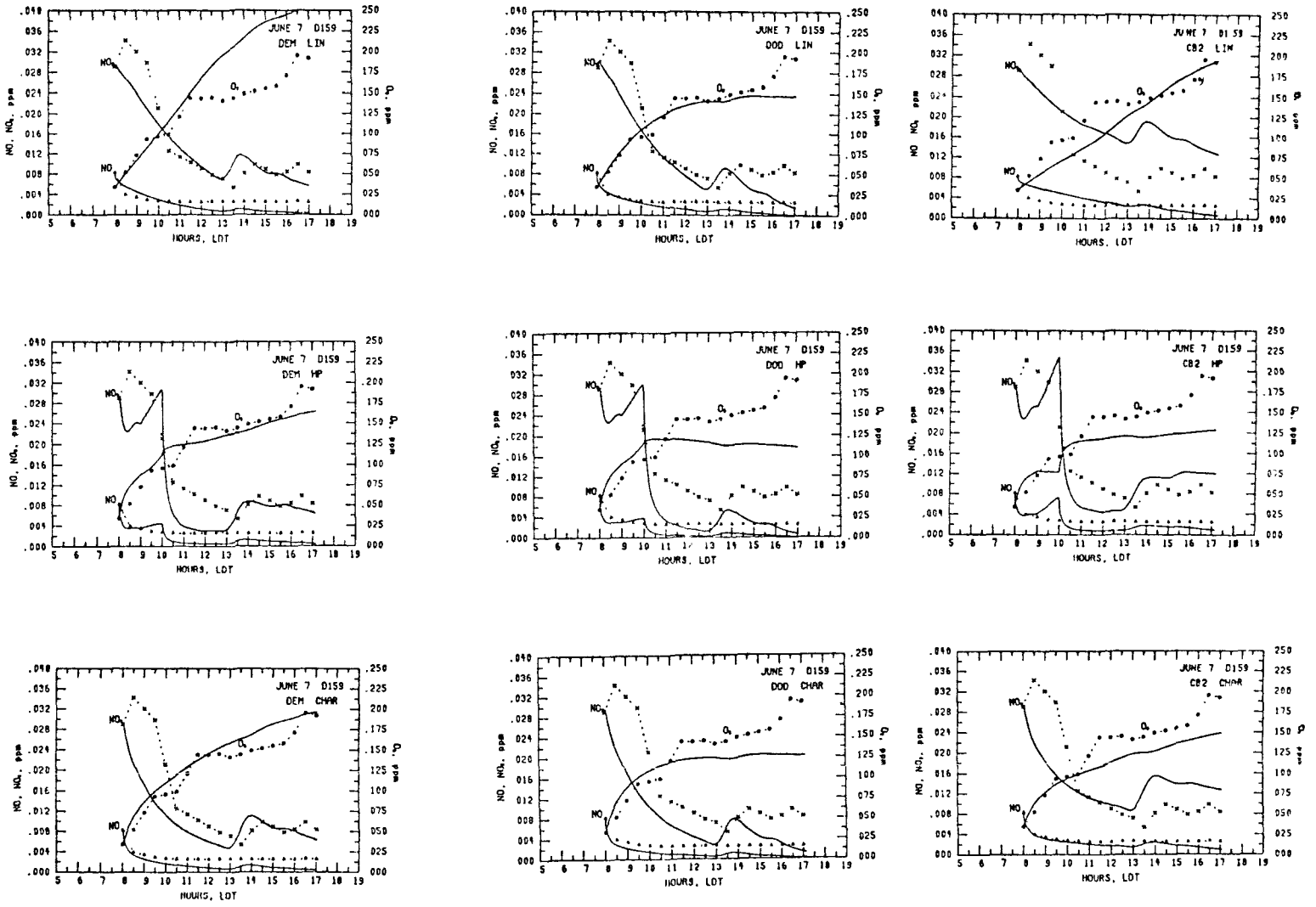

Figure 79. continued.

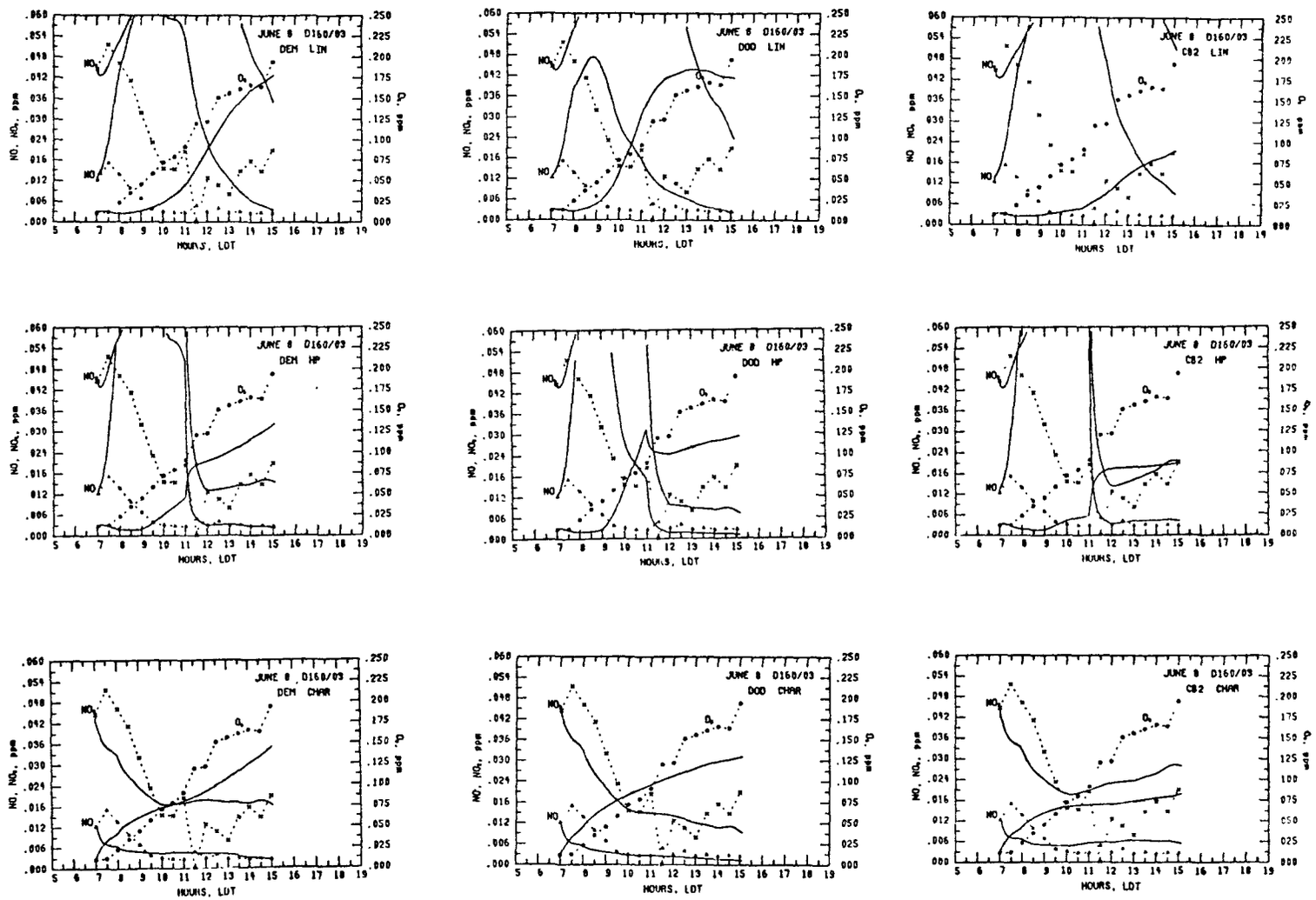

Figure 79. continued.

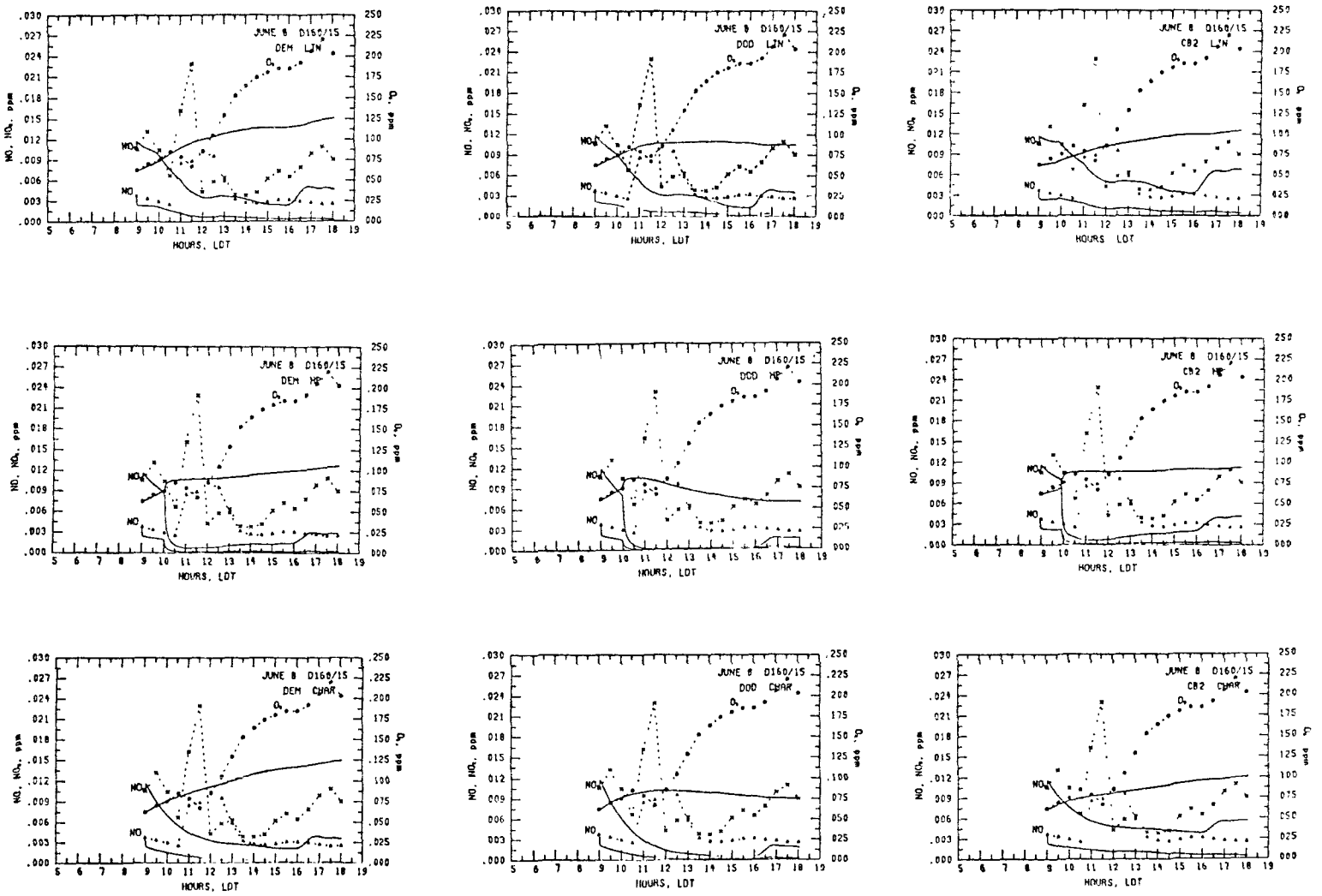

Figure 79. continued.

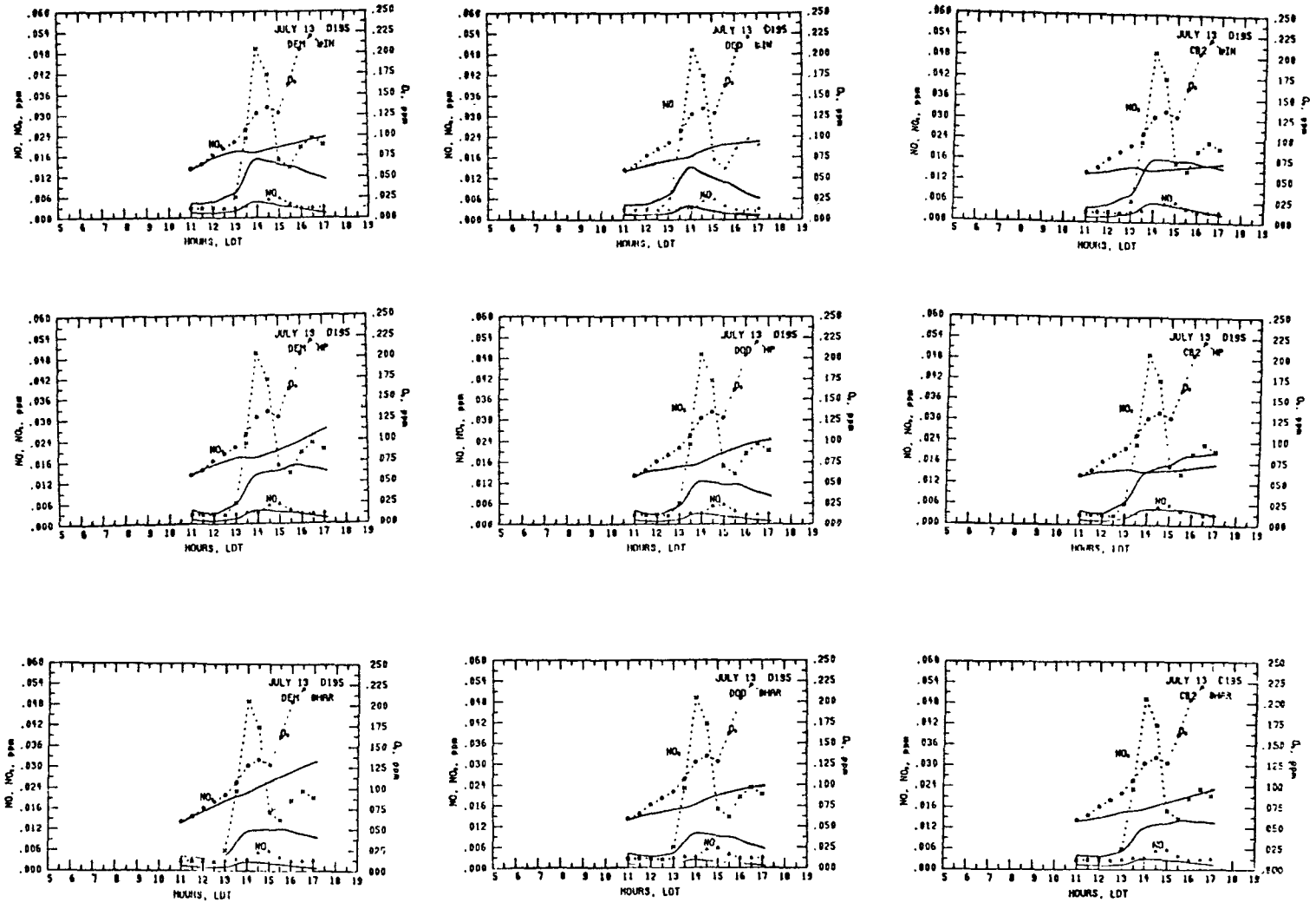

Figure 79. continued.

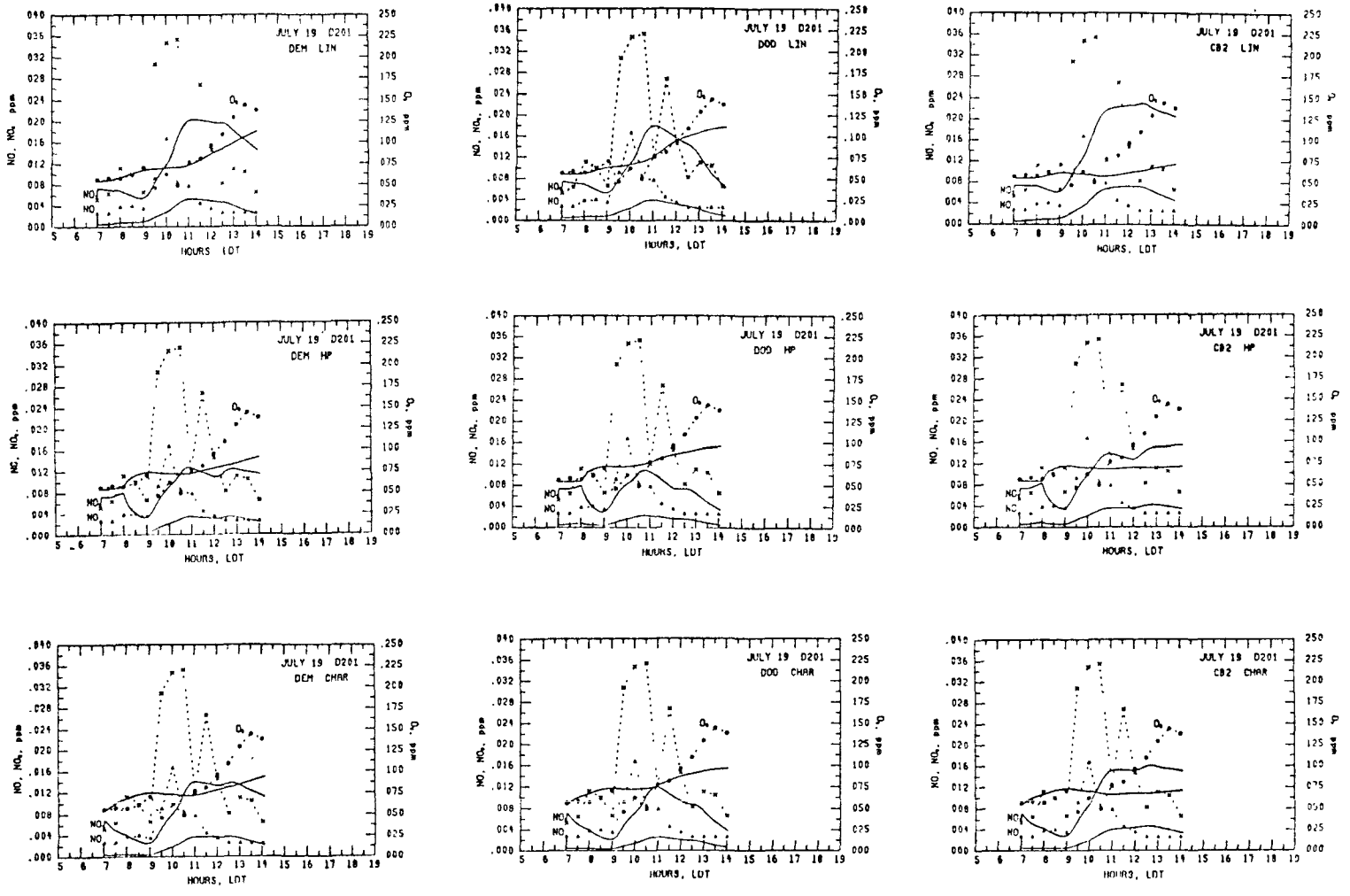

Figure 79. continued.

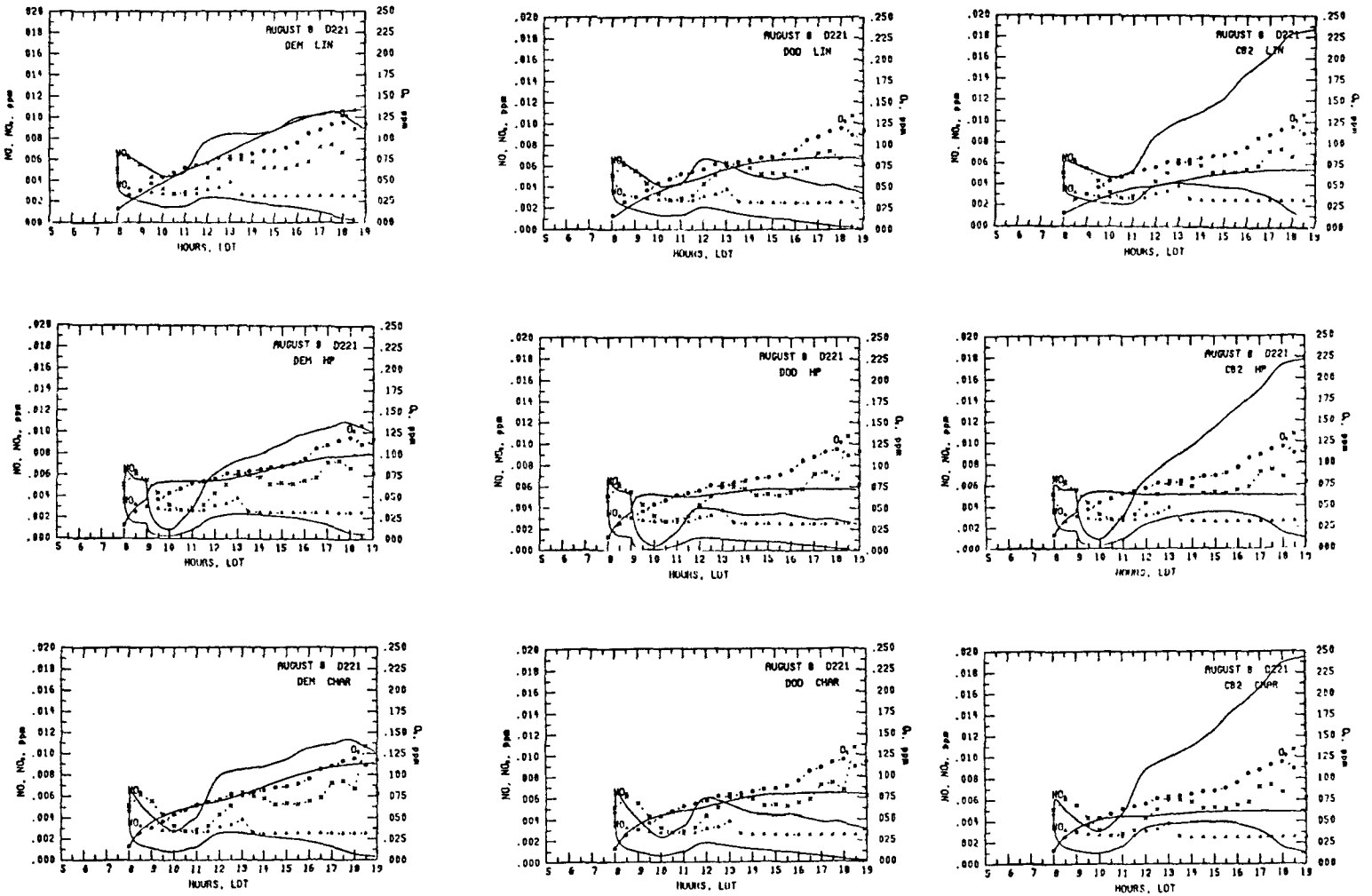

Figure 79. continued.

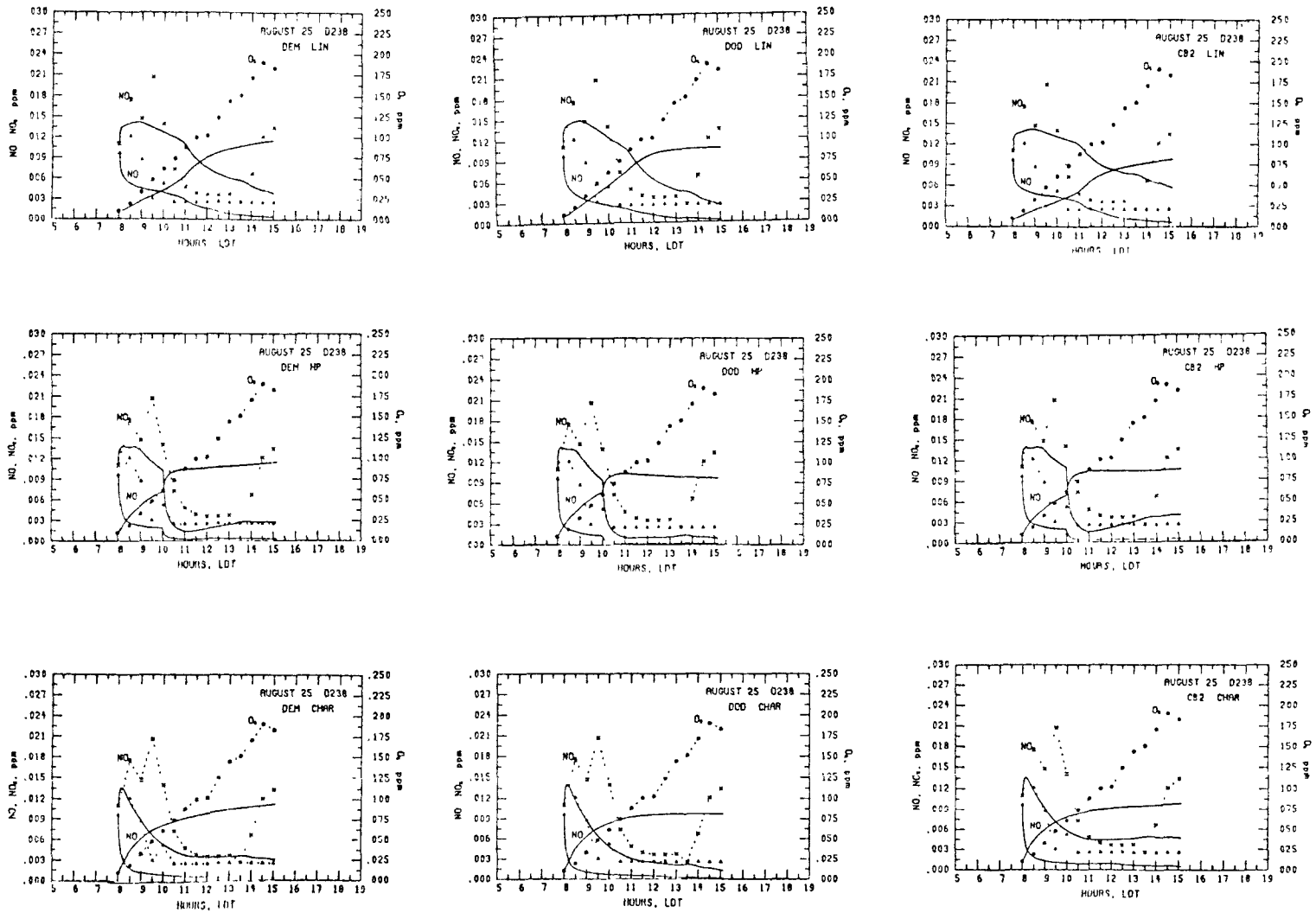

Figure 79. continued.

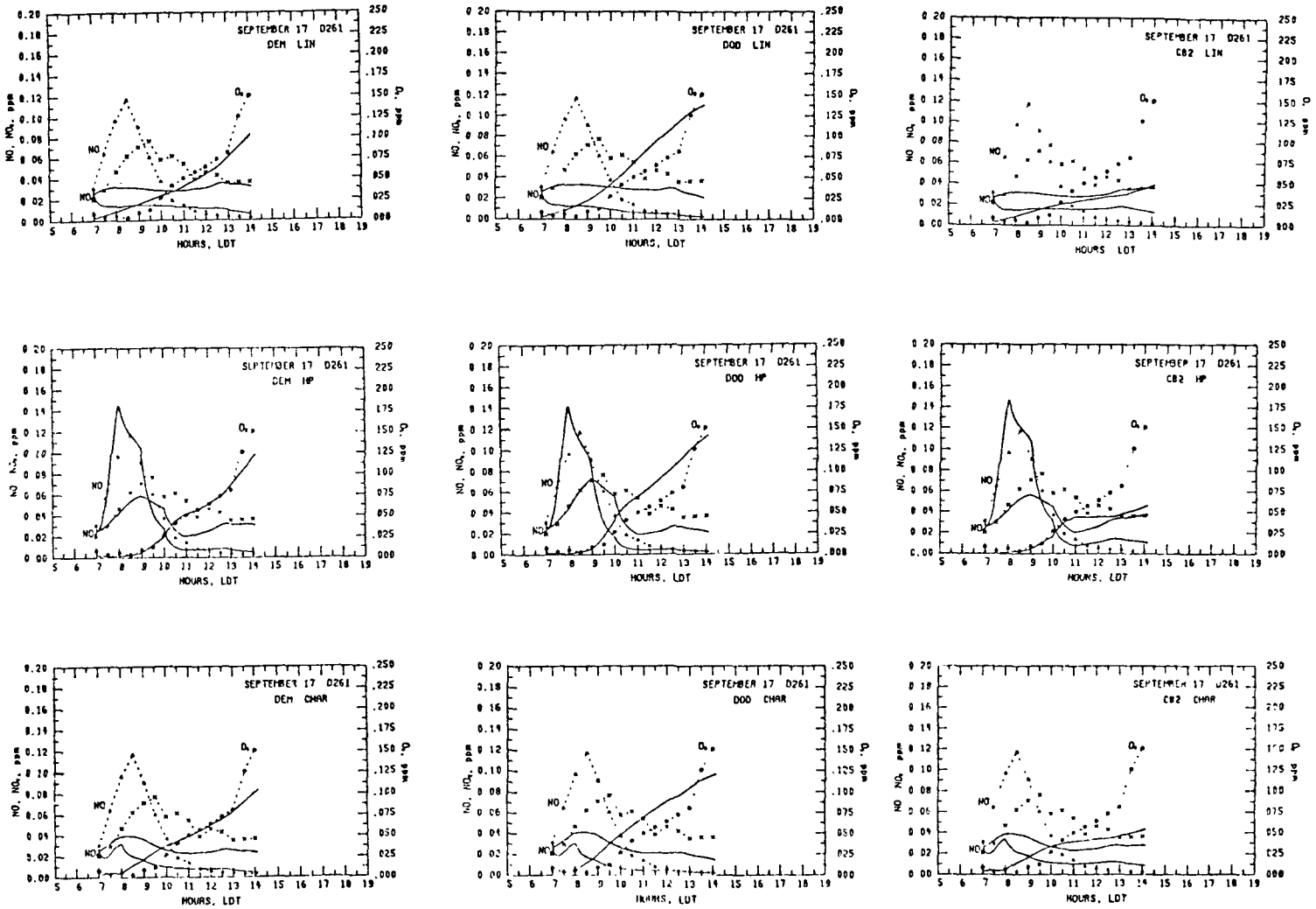

Figure 79. continued.

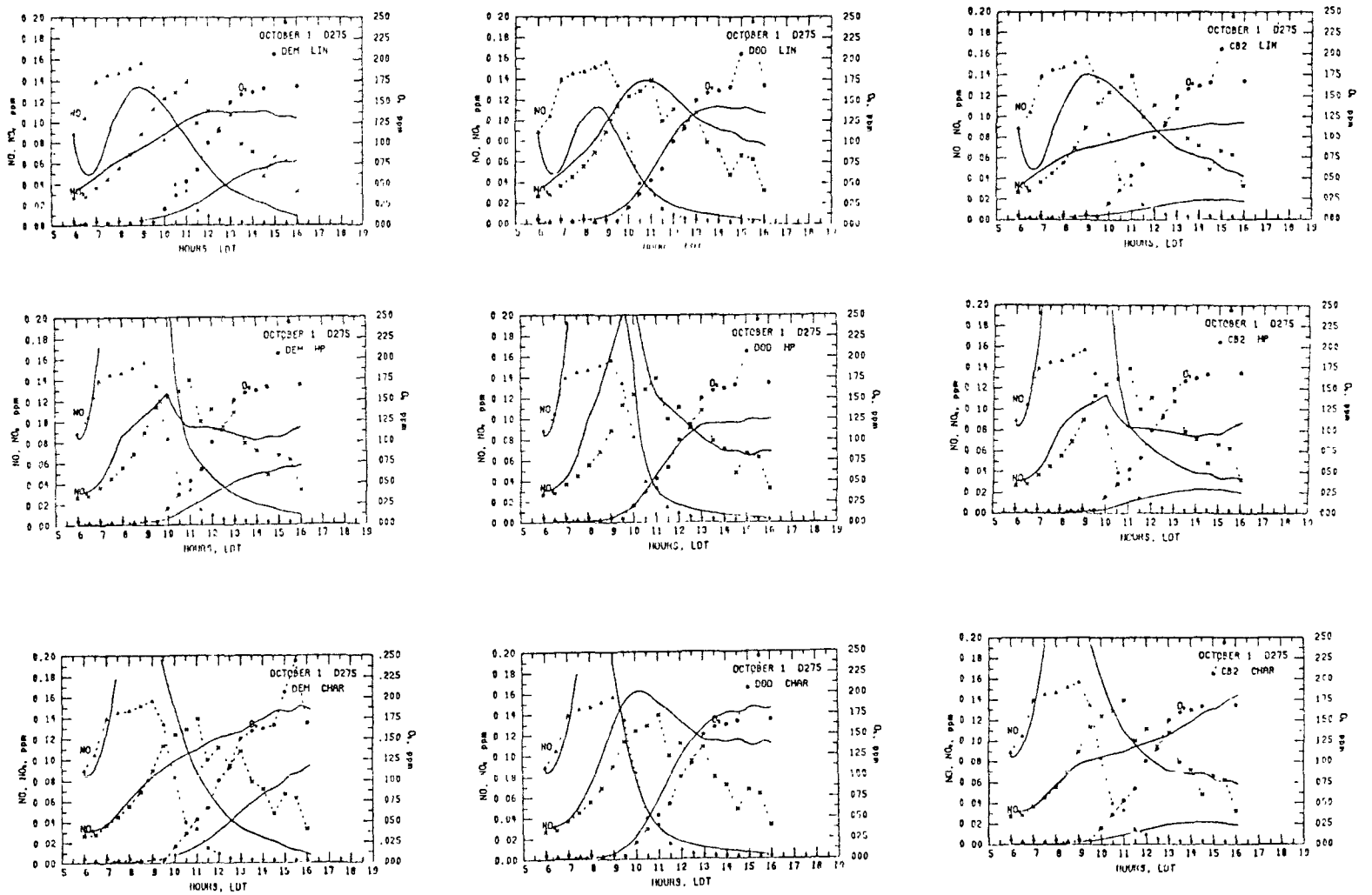

Figure 79. continued.

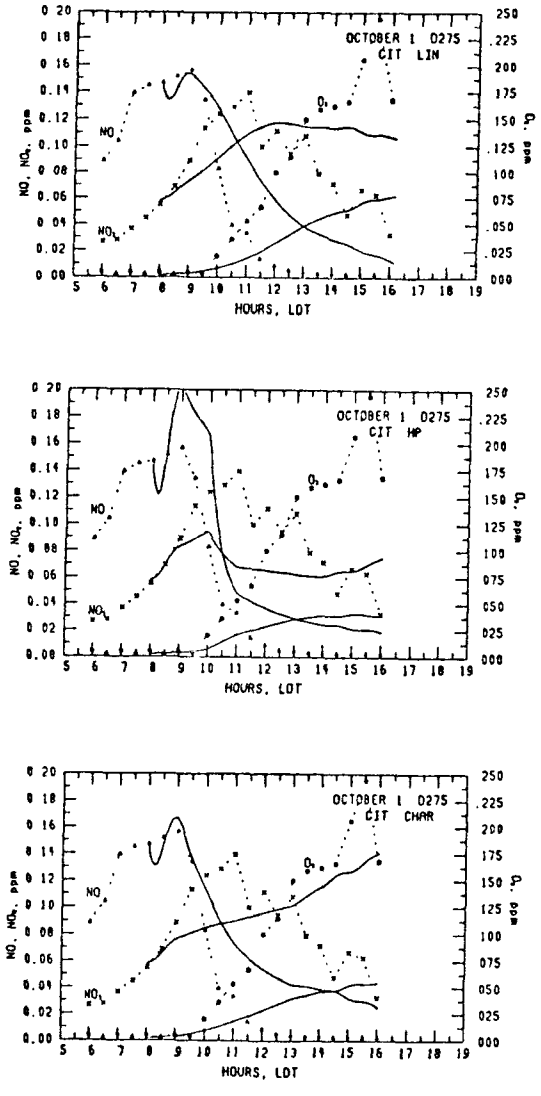

Figure 79. continued.

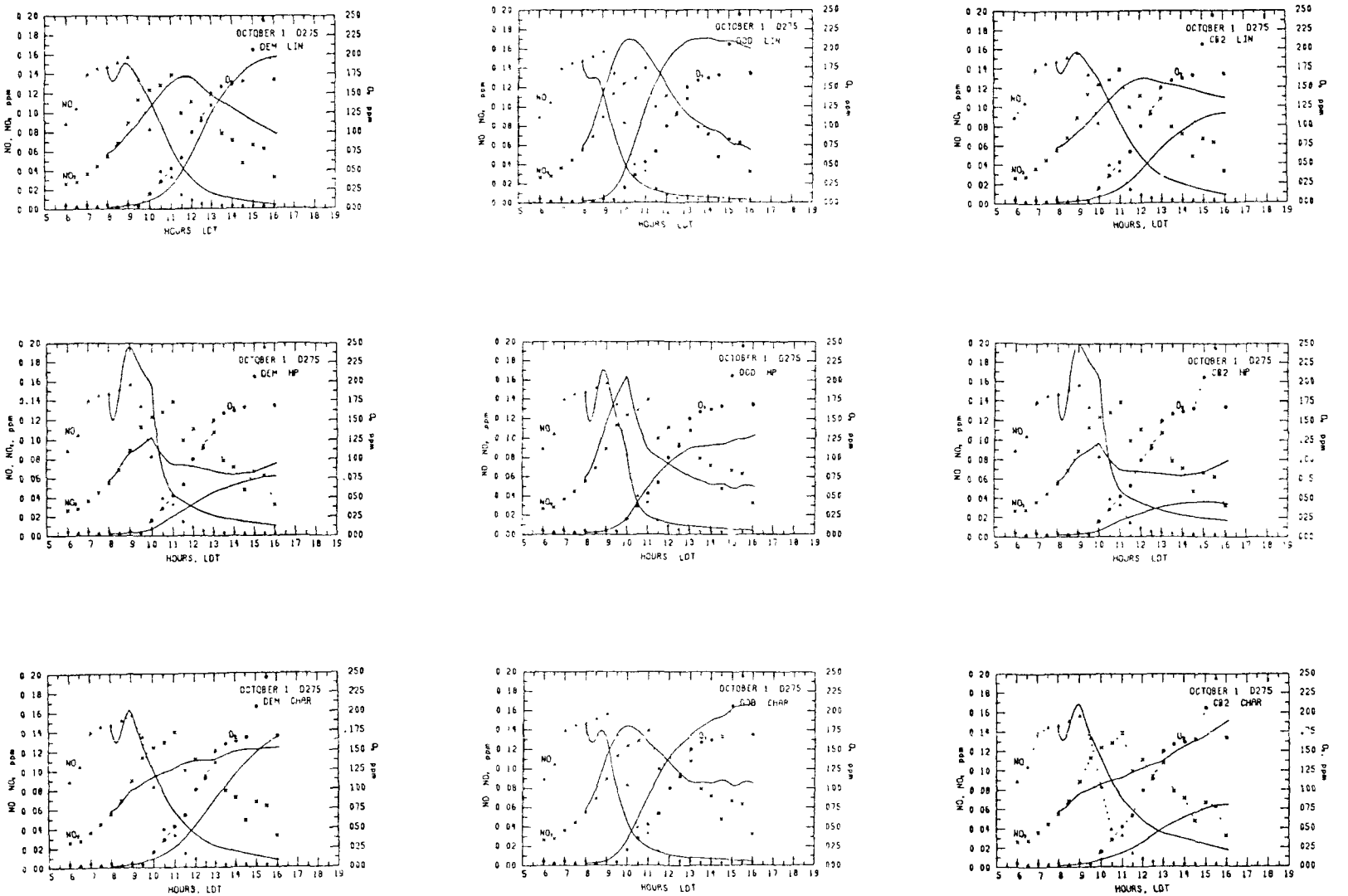

Figure 79. continued.

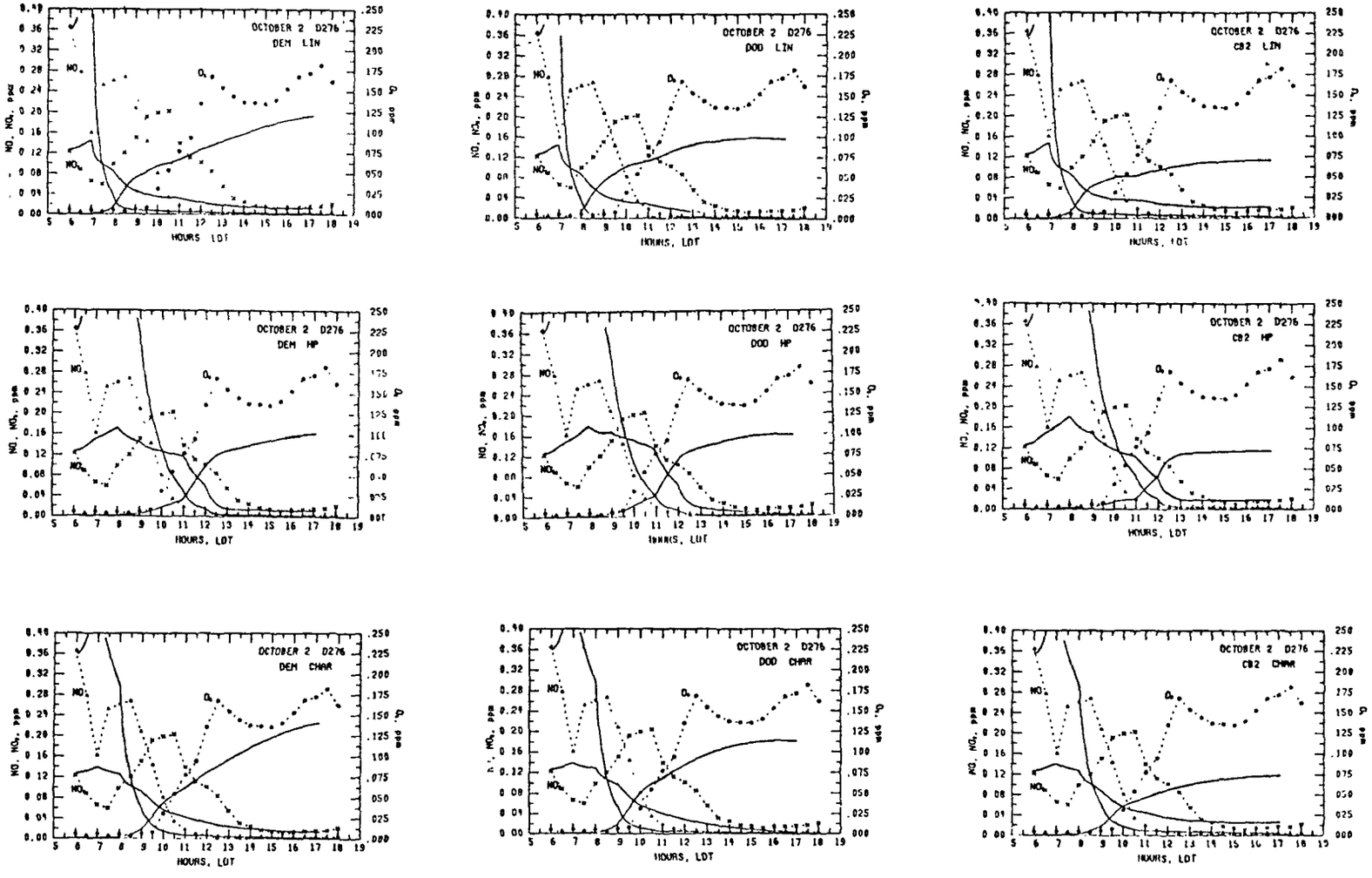

Figure 79. continued.

the NO_x and NMHC for this day suggest that the actual processes for this day were not well represented.

August 8 D221. The MOSTM results suggested that this day had potential for being reasonably simulated. DEM simulations were reasonable; DOD simulations were slightly low; and CB2 failed to remove the NO_2 and form O_3.

August 25 D238. The MOSTM results showed that the afternoon CO, NMHC, and NO_x were poorly predicted. Since the NO_x and HC rise in the 13-1500 LDT period was not predicted, the O_3 predictions were significantly low.

Sept. 17 D261. As suggested by the MOSTM the hand picked mixing height profile appears to be the most appropriate for this day. Both DEM and DOD predicted not only the O_3 but also the NO, NO_2, and NMHC (and the shape for CO) very closely. CB2 did not make much O_3 in the afternoon.

Oct. 1 D275 at 6AM. The early start on this day is a good test of having to simultaneously match the mixing height and its rise with the emissions rates. The MOSTM LIN simulation suggested that CO would not be predicted well. The HC and NO_x values, considering chemical losses, might be a little low. The HP MOSTM results gave large NO_x overpredictions and the CHAR simulation also gave a somewhat smaller but still large 8-9 morning spike.

In the PKSTM simulations, only DOD for CHAR was able to produce a reasonable simulation.

Oct. 1 D275 at 8 AM. This was the high O_3 day. Comparison of the 8 AM simulations with the 6 AM simulations shows significant differences. A major difference is that the 8 AM initial NO is specified in this

simulation (and is therefore correct) whereas it was computed from two hours of meteorology, emissions, and chemistry in the 6 AM starting simulation. DEM and DOD did reasonably well; CB2 was lower. This was the second day simulated with the CIT mechanism. As expected from the high NO_x initial conditions and the BOM simulation results, the CIT mechanism performed poorly on this day.

Oct. 2 D276 at 6 AM. The MOSTM simulations suggested that the mixing heights specified for this day resulted in too much dilution and that the NO_x emissions used were inappropriate for the 8-11 LDT period. As shown in the PKSTM these problems resulted in too little mass to continue the O_3 production.

8.2.3. Summary of PKSTM Simulations

Table 32 summarizes the ozone maxima predictions by the photochemical kinetics simple trejectory model for the eleven selected days. Figures 80 and 81 are scatter diagrams organized by mechanism and by mixing height profiles. See Section 8.4 for discussion of "fits".

Table 32. Ozone Maxima Predicted by MOSTM and PKSTM Using Four Mechanisms and Three Mixing Height Profiles for RAPS Days (ppm O_3)

Day	Obs	MHP	MOSTM	PKSTM DEMER	PKSTM DODGE	PKSTM CARB BOND	PKSTM CIT
159	0.192	L	0.084	0.2519	0.1478	0.1970	0.1963
June 7		HP	0.118	0.1642	0.1143	0.1320	0.1348
		C	0.108	0.1965	0.1279	0.1540	0.1534
160/03	0.194	L	0.083	0.1782	0.1822	0.0904	
June 8		HP	0.084	0.1338	0.1221	0.0876	
		C	0.084	0.1457	0.1300	0.0825	
160/15	0.206	L	0.088	0.1258	0.0872	0.1046	
June 8		HP	0.089	0.1059	0.0564	0.0935	
		C	0.082	0.1245	0.0747	0.1006	
195	0.210	L	0.067	0.0982	0.0937	0.0719	
July 13		HP	0.066	0.1127	0.1022	0.0756	
		C	0.063	0.1325	0.0988	0.0986	
201	0.138	L	0.071	0.1127	0.1107	0.0717	
July 19		HP	0.078	0.0918	0.0954	0.0706	
		C	0.078	0.0933	0.0962	0.0709	
221	0.119	L	0.050	0.1337	0.0851	0.0721	
Aug 8		HP	0.068	0.1002	0.0732	0.0628	
		C	0.062	0.1137	0.0807	0.0651	
238	0.190	L	0.079	0.0960	0.0888	0.0820	
Aug 25		HP	0.087	0.0951	0.0864	0.0875	
		C	0.080	0.0943	0.0811	0.0823	
261	0.151	L	0.049	0.1032	0.1382	0.0491	
Sept 17		HP	0.058	0.1227	0.1425	0.0580	
		C	0.057	0.1042	0.1210	0.0545	
275/6	0.244	L	0.056	0.0783	0.1429	0.0241	
Oct 1		HP	0.057	0.0708	0.1254	0.0297	
		C	0.050	0.1175	0.1820	0.0270	
275/8	0.244	L	0.048	0.1970	0.2138	0.1160	0.0771
		HP	0.057	0.0772	0.1298	0.0450	0.0385
		C	0.049	0.1680	0.2100	0.0808	0.0546
276	0.181	L	0.078	0.1206	0.0990	0.0709	
Oct 2		HP	0.079	0.1012	0.0997	0.0723	
		C	0.077	0.1399	0.1138	0.0739	

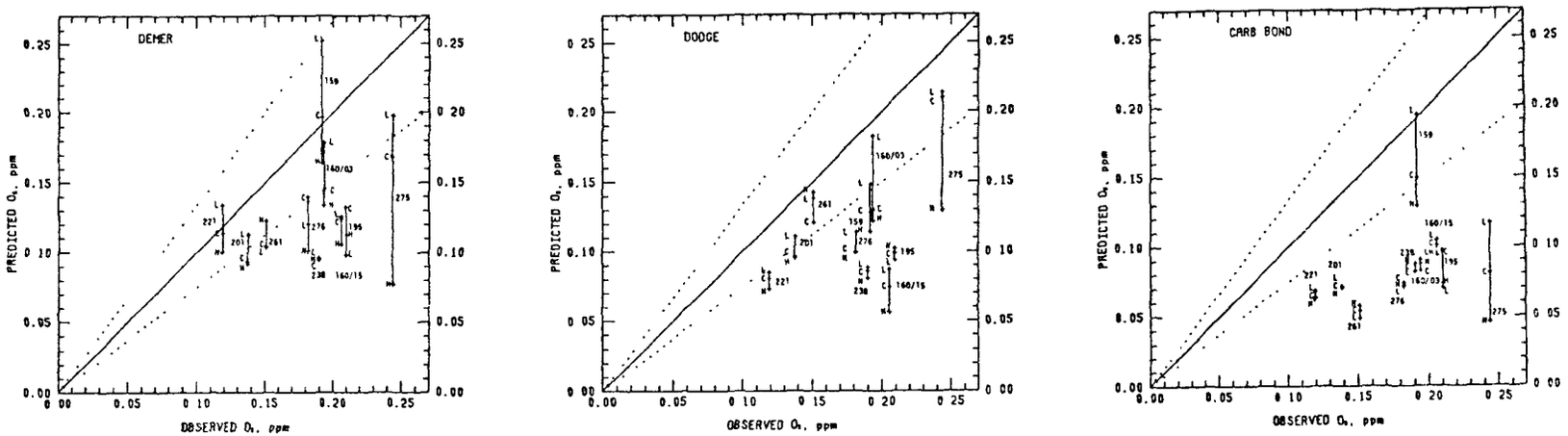

Figure 80. Scatter diagrams: mechanism predictions and ambient O_3 maxima by mechanisms. Dashed lines are $\pm$ 25%. L=linear, HP=handpicked, and C=characteristic mixing height profile.

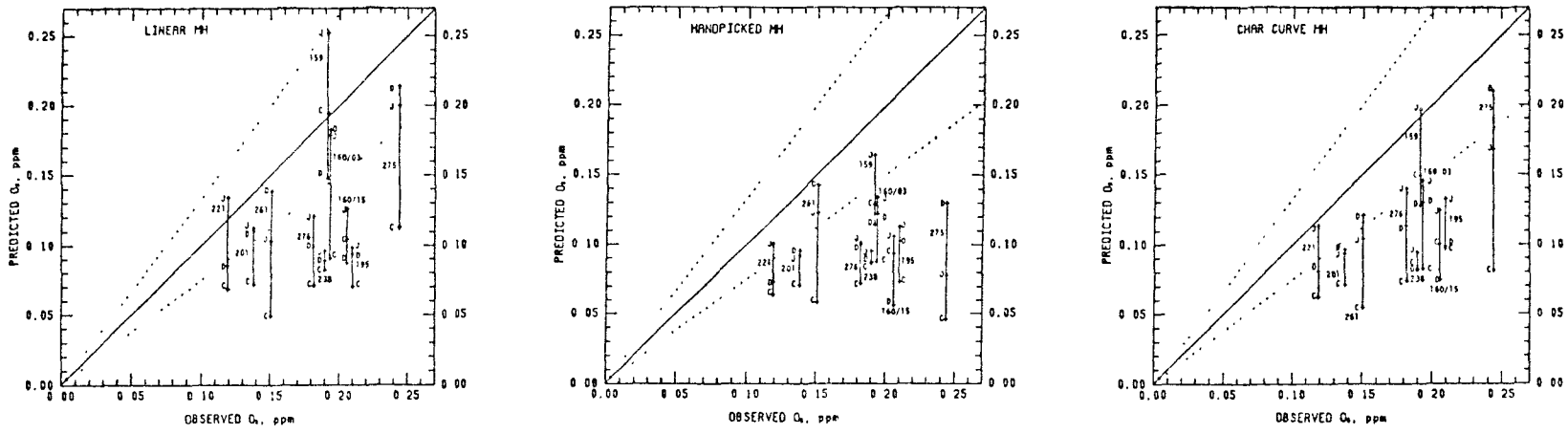

Figure 81. Scatter diagrams: mechanism predictions and ambient O_3 maxima by mixing heights. Dashed lines are $\pm$ 25%. J=Demerjian, D=Dodge, and C=Carbon Bond Mechanism.

8.3 RESPONSE OF SELECTED PHOTOCHEMICAL SIMULATIONS TO DIFFERENT INPUT ASSUMPTIONS

8.3.1 Carbon Bond and Demerjian Mechanism's Response to Increased Aldehyde Emissions.

In the RAPS emission inventory (Table 25), aldehydes represented from 0.8% to 3% of the carbon for the days included in this study. The OZIPP program with the Dodge mechanism assumes that aldehydes are 5% of the NMHC and this assumption was maintained in this study for the Dodge mechanism. The aldehyde fraction in the emission inventory may be a highly uncertain number; there were no systematic aldehyde measurements conducted in RAPS. Aldehydes are significant radical sources in the chemical mechanisms.

The Carbon Bond mechanism performed very well in the Bureau of Mines smog chamber simulations in which Demerjian's value of ~5% aldehydes was used and it performed poorly in the RAPS simulations in which ~2% aldehydes were used. Furthermore, Demerjian had assumed an average aldehyde carbon number of about one for the BOM data and the RAPS emission inventory average aldehyde carbon number was reported by Demerjian as being about 2.0. In the Demerjian mechanism this shift is not important since there is no real effort to have carbon accountability in the Demerjian mechanism. In the Carbon Bond mechanism, where carbon accountability is a feature, this shift could be critical. The extra carbon on the aldehyde would have to be counted as a paraffin carbon in CB2 and thus the actual number of photolytic carbons would be decreased by a factor of two when compared to Demerjian's mechanism in which the single aldehyde species represents some combination of 1-carbon, 2-carbon, and higher-carbon number aldehydes. For Carbon Bond then, the difference in assuming that the aldehyde carbon number is one or two repre-

ents a doubling of the amount of carbon that is carbonyl and thus a photolytic source of radicals.

In Figure 82, the October 1, D275/8 standard Carbon Bond simulation is compared to a Carbon Bond simulation in which the aldehyde initial and emission carbon fractions have been doubled. Although the simulation predictions remain under the observed O_3, there is a substantial improvement in the predictions. Other simulations, not shown here, with higher aldehyde fractions show that large aldehyde fraction assumptions can give nearly perfect fits, suggesting that for this day the Carbon Bond mechanism is a little short of radicals.

A similar experiment was conducted with the Demerjian mechanism. In Figure 83, the October 1, D275/8 standard Demerjian simulation is compared to a Demerjian simulation in which <u>only</u> the <u>initial</u> aldehyde carbon fraction was increased from 2.0% to 5.0%; the emission aldehyde carbon fraction remained at 2.0%. The effect was dramatic; the O_3 maximum increased by 20%! The cause for this large response will be discussed below.

The effect of increased aldehydes was tested on a day that was modelled well by Carbon Bond with the standard assumptions, June 7, D159. In Figure 84, the standard Carbon Bond simulation is compared to one in which <u>both</u> the initial and the emission aldehyde carbon fraction had been increased from 0.82% to 5%, a fivefold increase. Less than a ten percent effect on O_3 maxima was observed. However, this day had 0.12 ppm O_3 aloft and October 1 had only 0.06 ppm O_3 aloft.

The reaction of aloft O_3 with emissions can serve as a radical source. The addition of two radical sources does not have a linear effect in mechanisms; if there are sufficient radicals, the effect of a second source may not be very discernible. Furthermore, a detailed analysis of the October 1 simu-

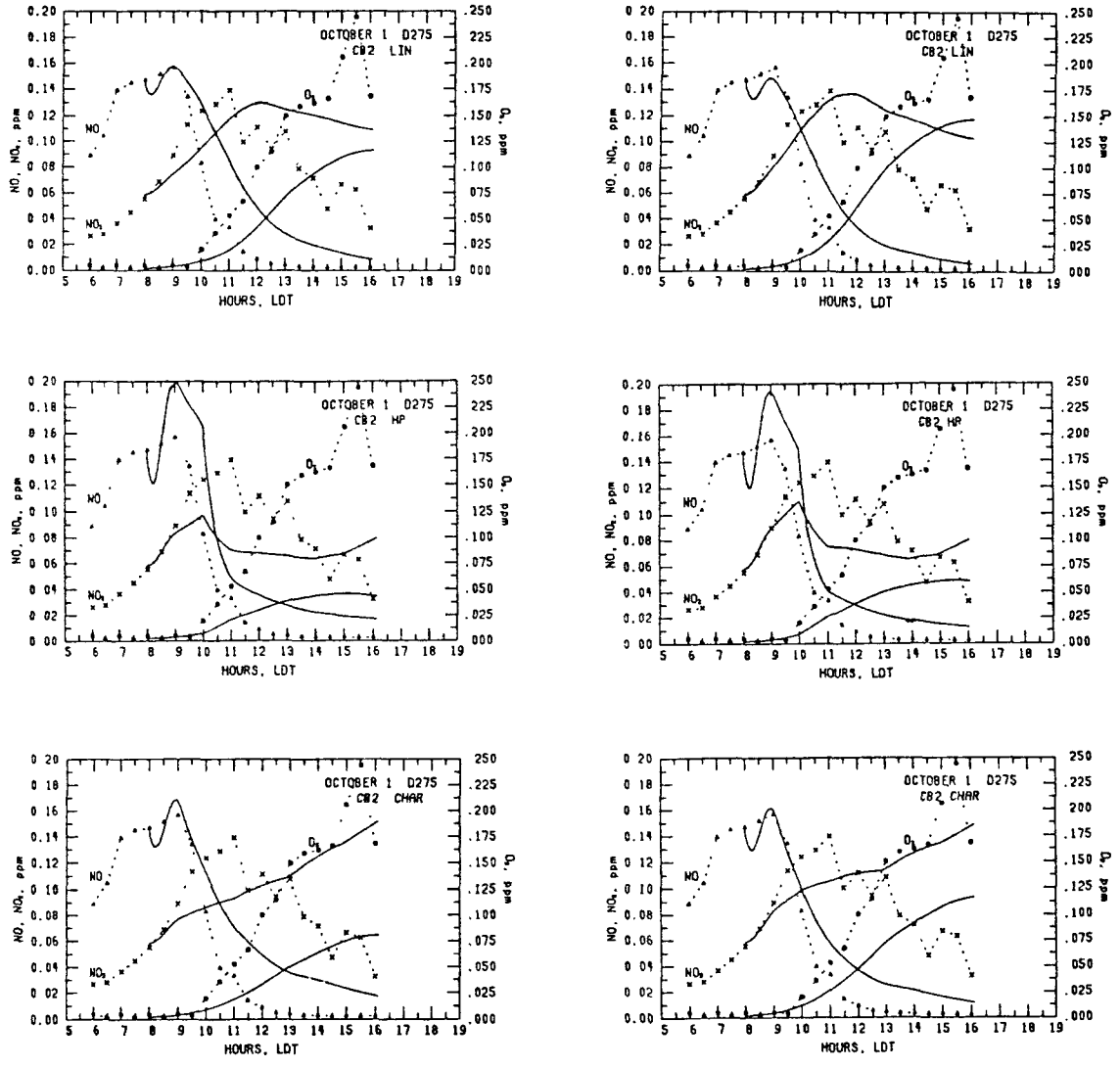

Figure 82. Effect of doubling the aldehyde fractions for Carbon Bond II mechanism for October 1, 1976 RAPS simulation beginning at 8 a.m. Increased aldehyde in right column.

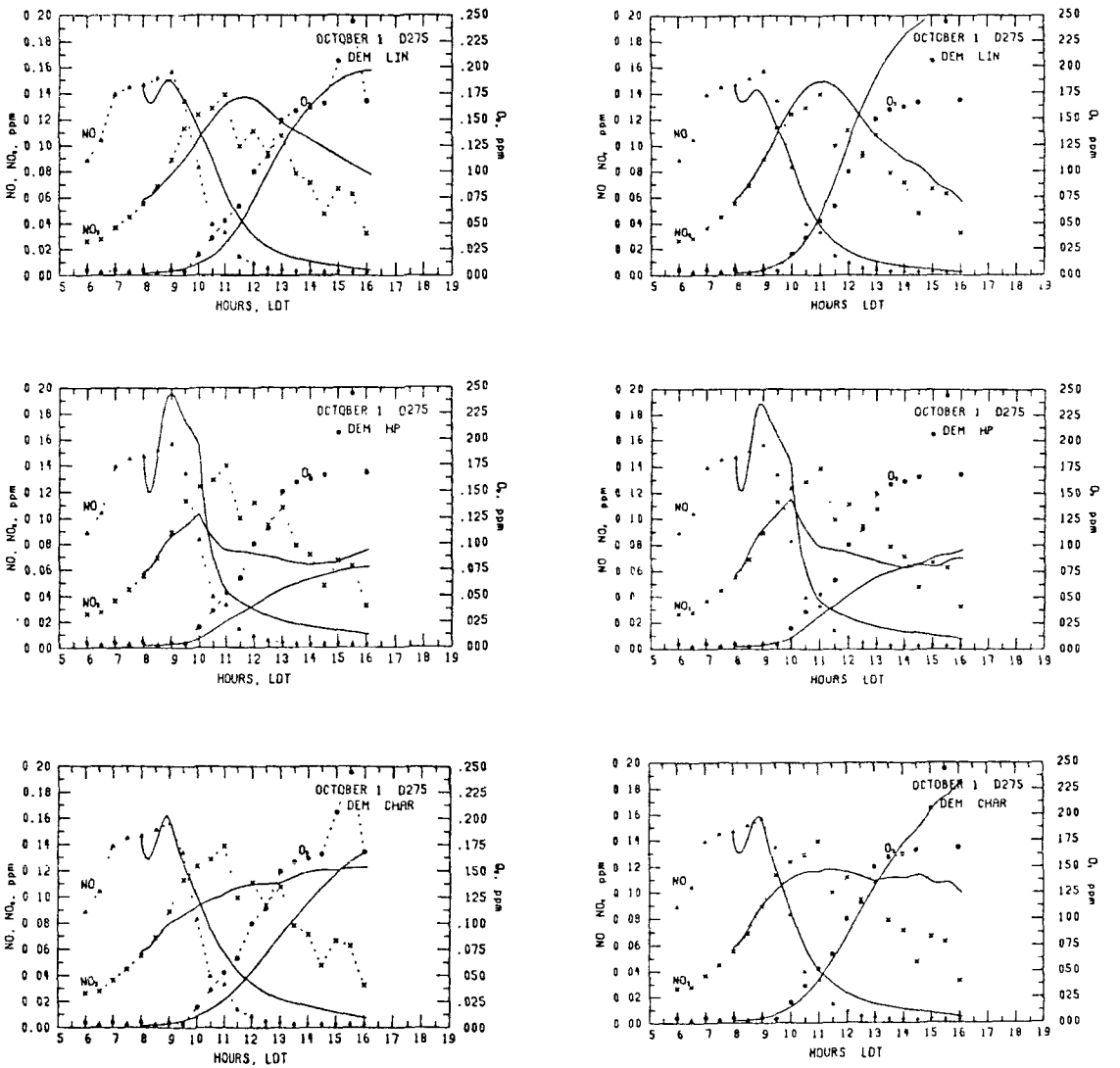

Figure 83. Effect of using 5% initial aldehyde fraction for Demerjian mechanism for October 1, 1976 RAPS simulation beginning at 8 a.m. 5% on the right.

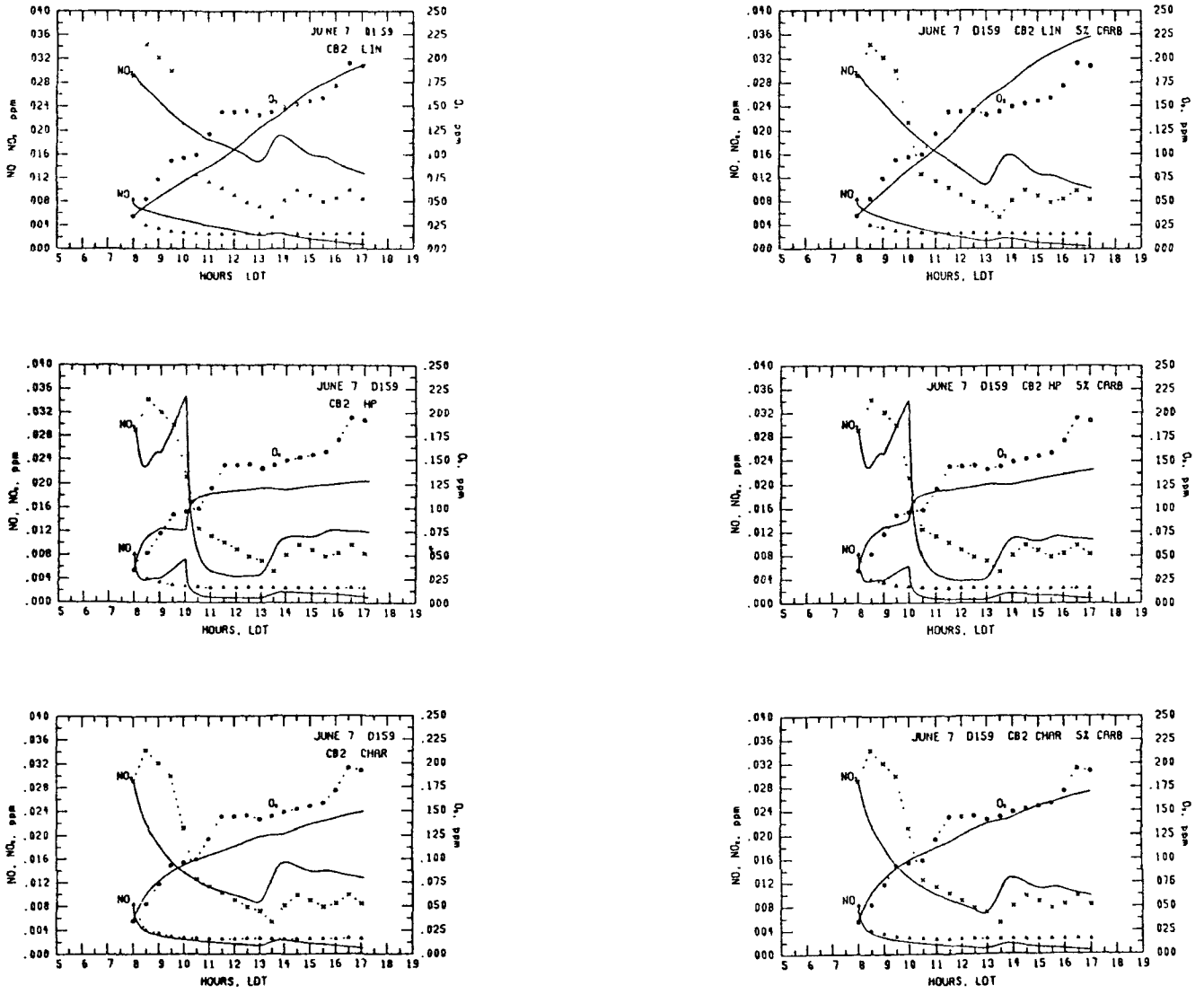

Figure 84. Effect of increased aldehyde emission fraction for Carbon Bond II mechanism for June 7, 1976 RAPS simulation.

lations showed that in the Demerjian mechanism the O_3 + OLE reaction (Reaction 20, Table 7) gives two radicals (one RO_2 and one HO_2) and is a significant source of new radicals (~5% of the radicals) for this mechanism. The Carbon Bond mechanism, on the other hand, uses newer (and presumably more kinetically correct) O_3 + OLE chemistry in which the radical yield is only about 0.1 (compared to Demerjian's 2.0) and this process is <u>not</u> a significant source of radicals (<0.1% of the radicals) in the CB2 mechanism. There is an additional radical source in the Carbon Bond mechanism and it is photolysis of unique carbonyl products resulting from aromatic reactions. Demerjian has no unique carbonyl aromatic products; aromatics are treated similar to olefins with an extra standard aldehyde being produced.

Thus, for Demerjian, once O_3 production begins and olefins are present in the hydrocarbon emissions, new radicals are abundantly available to sustain the O_3 production process. This may not be a good representation of the actual process.

Extra aldehydes are not always adequate to improve the Carbon Bond mechanism's performance. Figures 85 and 86 compare standard Carbon Bond simulations to those with increased aldehyde emissions; not much improvement occurred for these days which were simulated better by the other mechanisms.

For the Dodge mechanism, the aldehyde emission fraction assumption is constant. As was shown in Table 10, however, new photolytic rate data are available which, if used, might affect the radical production in the Dodge simulations. Figure 87 compares the standard Dodge October 1, D275/8 simulation using the original ("OLD") photolytic rates from the OZIPP program with a simulation using the newer photolytic rates ("NEW"). The effect was very small.

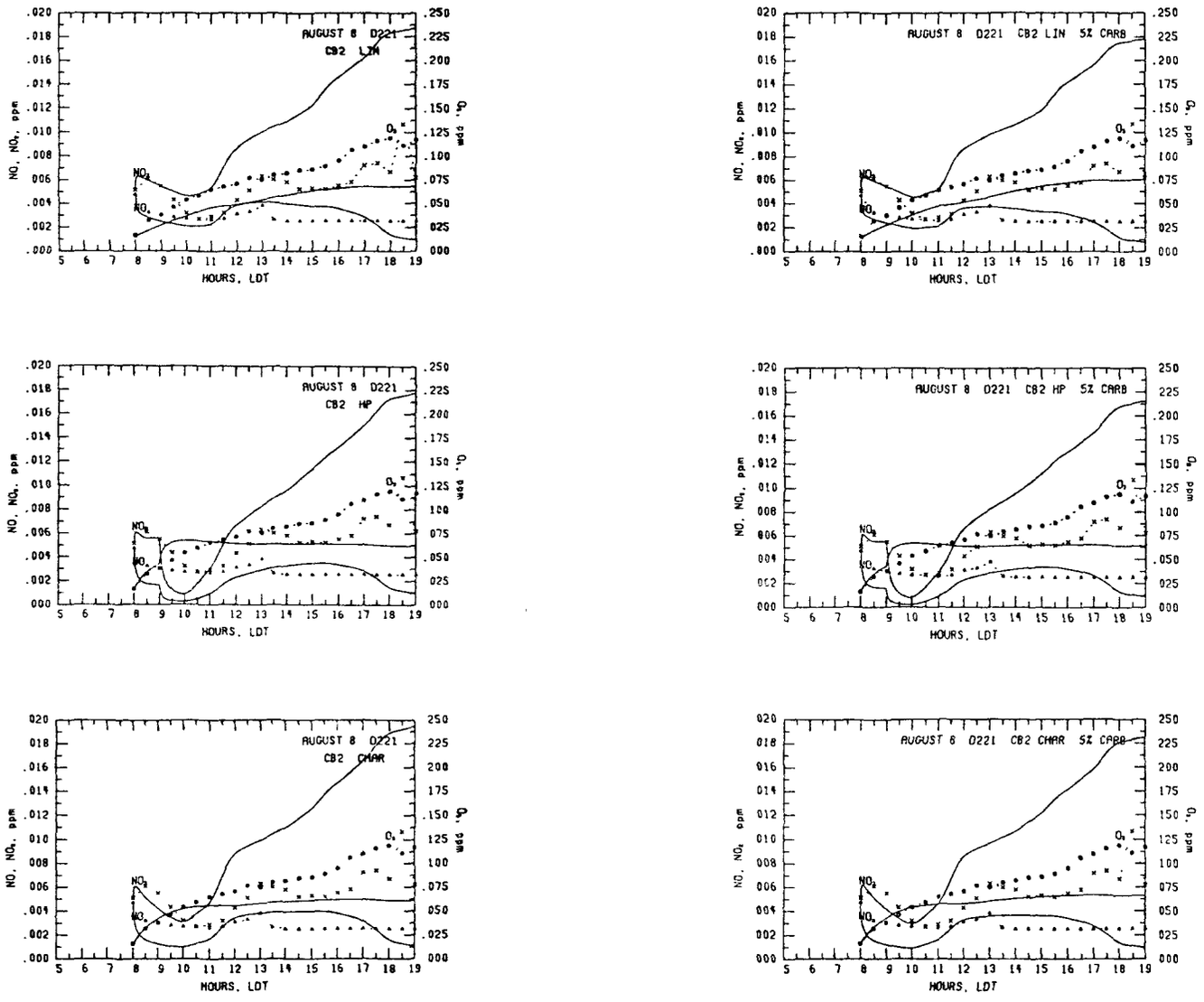

Figure 85. Effect of increased aldehyde emission fraction for Carbon Bond II mechanism for August 8, 1976 RAPS simulation.

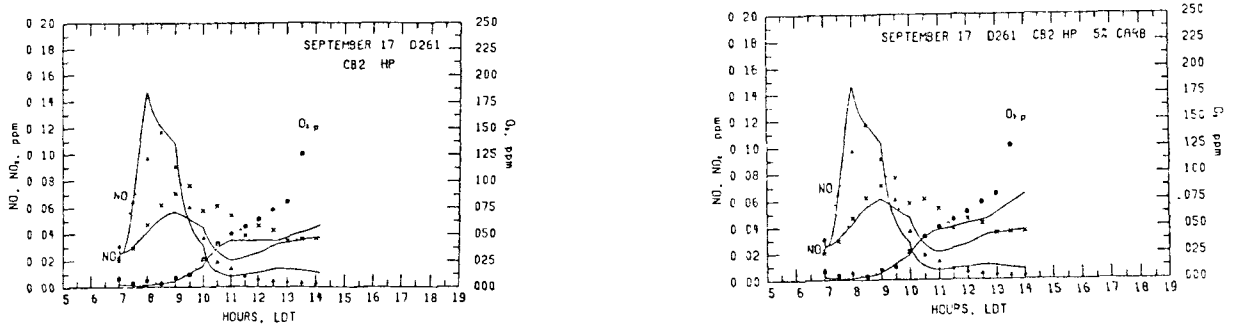

Figure 86. Effect of increased aldehyde emissions fraction from 1.68% to 5% for Day 261 for the Carbon Bond Mechanism.

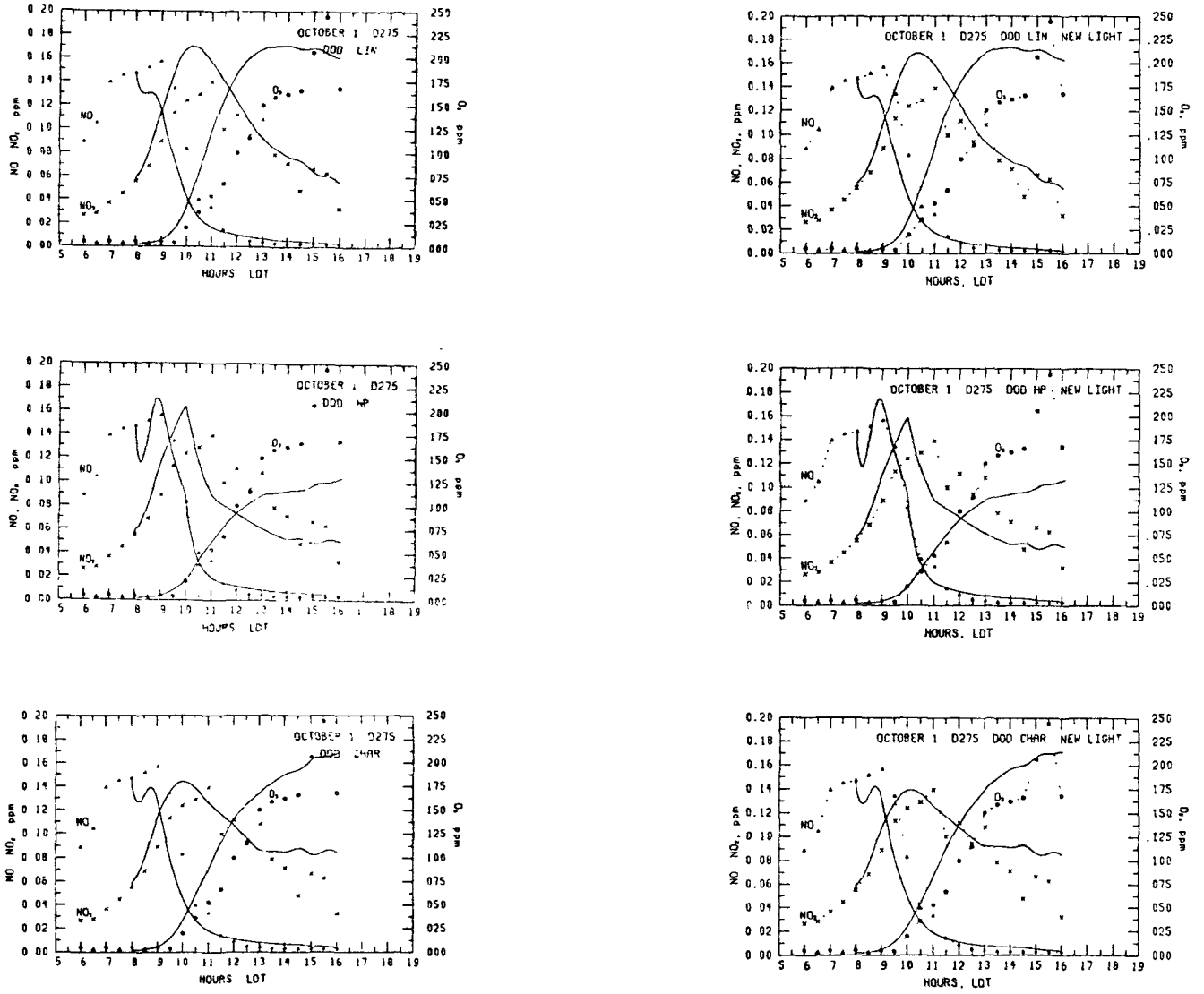

Figure 87. Effect of "old" and "new" photolytic rates for Dodge Mechanism for October 1, 1976 RAPS simulation.

8.3.2 Demerjian and Carbon Bond Mechanism Response to Hydrocarbon Compositional Changes

The Carbon Bond mechanism did well in the Bureau of Mines smog chamber simulations in which the aromatics carbon fraction was nearly 30%, the aldehyde carbon fraction was assumed to be about 5%, and the aldehyde carbon number was assumed to be one. The mechanism did poorly in the RAPS simulations in which the aromatics carbon fraction was 6% to 18%, the aldehyde carbon fraction was 0.8% to 3%, and the aldehyde carbon number was 2.0.

The effect of switching from an aldehyde carbon number of 2.0 to an aldehyde carbon number of 1.0 has already been demonstrated and discussed (Figure 82). The effect of using the BOM HC composition in the RAPS October 1 simulation will now be investigated. To see the effects of composition changes only, all simulations assumed an aldehyde carbon number of 1.0.

The left column of Figure 88 shows the October 1 simulation using the October 1 HC composition and an aldehyde carbon number of 1.0; this is the same as the right column of Figure 82. The center column of Figure 88 shows the October 1 simulation with the BOM HC composition but using the October 1 aldehyde emission carbon fraction and an aldehyde carbon number of 1.0. The right column of Figure 88 shows the October 1 simulation with the BOM composition and the BOM aldehyde carbon fraction (5%) and an aldehyde carbon number of 1.0. The simulations with the full BOM assumptions nearly perfectly fit this day.

The HC compositional change was (% carbon):

	NR	PAR	OLE	ARO	ALD
Oct. 1	12.2	53.7	17.2	14.9	2.0
BOM	10.5	41.7	17.3	28.7	5.3

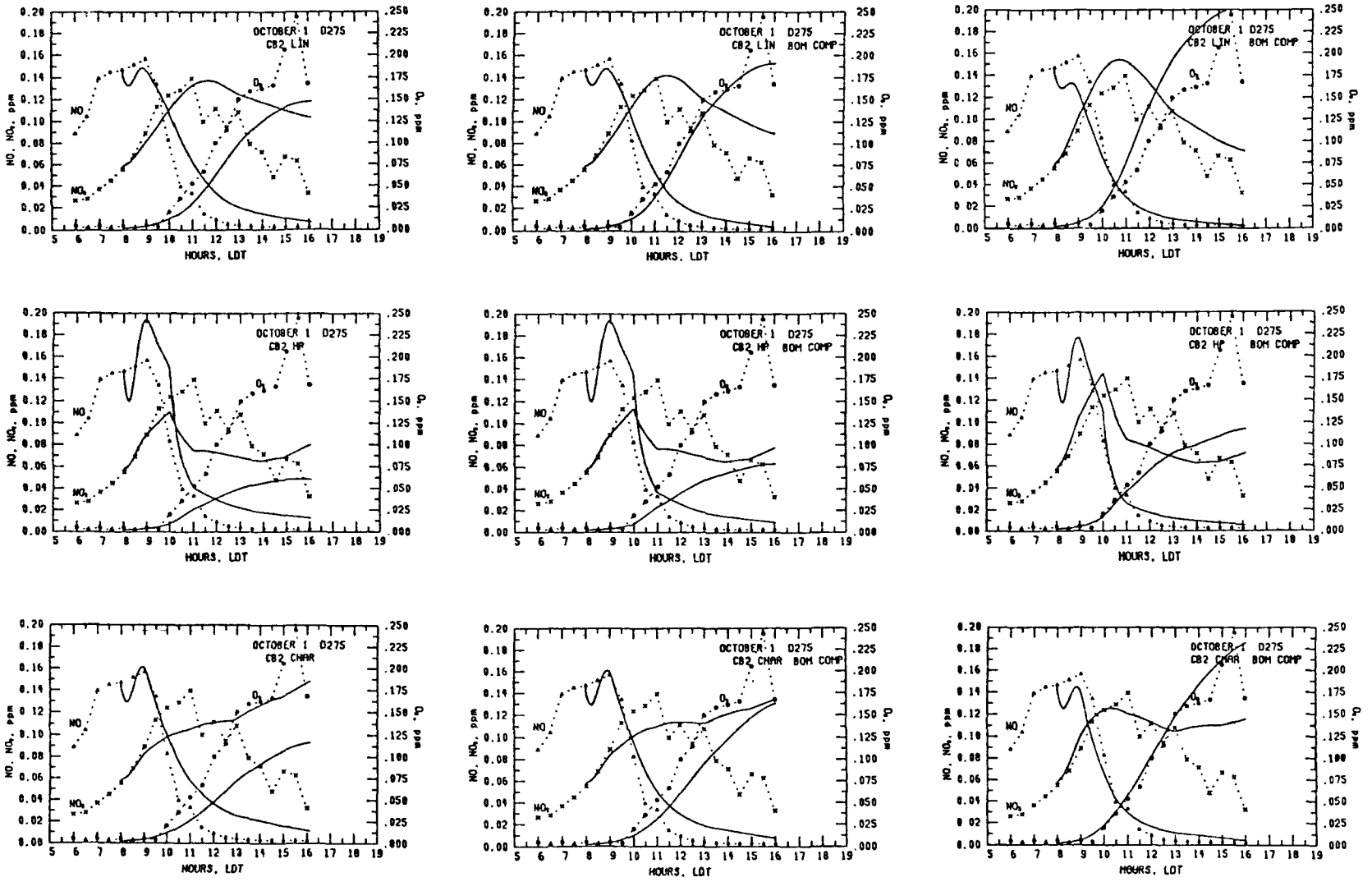

Figure 88. Effect of changing from HC composition of October 1, 1976 to Bureau of Mines composition at 2% aldehydes (center) and 5% aldehydes (right).

That is, about 12% of the carbon was shifted from paraffins to aromatics between the simulations.

The change in O_3 resulting from the various assumptions were (ppm O_3):

Composition	Oct. 1	Oct. 1	BOM	BOM
Aldehyde Fraction	0.020	0.020	0.020	0.053
Ald. Carb. No.	2.0	1.0	1.0	1.0
Mixing Height:				
LIN	0.116	0.147	0.192	0.252
HP	0.045	0.060	0.079	0.118
CHAR	0.081	0.117	0.164	0.233

That is, the Oct. 1 to BOM compositional change increased the O_3 by 0.045 ppm (31% increase) and the Oct. 1 to BOM change with BOM aldehydes increased the O_3 by 0.105 ppm (71% increase). The total change in going from standard Oct. 1 conditions to full BOM conditions, however, increased the O_3 by 0.135 ppm (117%). As described above, aromatic products are significant sources of radicals for the Carbon Bond II mechanism and it has some difficulties in dealing with these RAPS days with low aromatic content as determined from the emission inventory and the trajectory paths.

Another demonstration of HC compositional effects on mechanism predictions, similar to that discussed in Section 7.3.4, is shown in Figure 89. The left column is the standard Demerjian Oct. 1, D275/8 simulation from Figure 79. The center column shows the effect of substituting the HC composition fractions from the day with the highest olefin content (August 8, Day 221) for the October 1 HC composition fractions. The right column shows the effect of substituting the HC composition fractions from the day with the highest paraffin content (August 25, Day 238) for those of October 1. This compositional change was (% carbon):

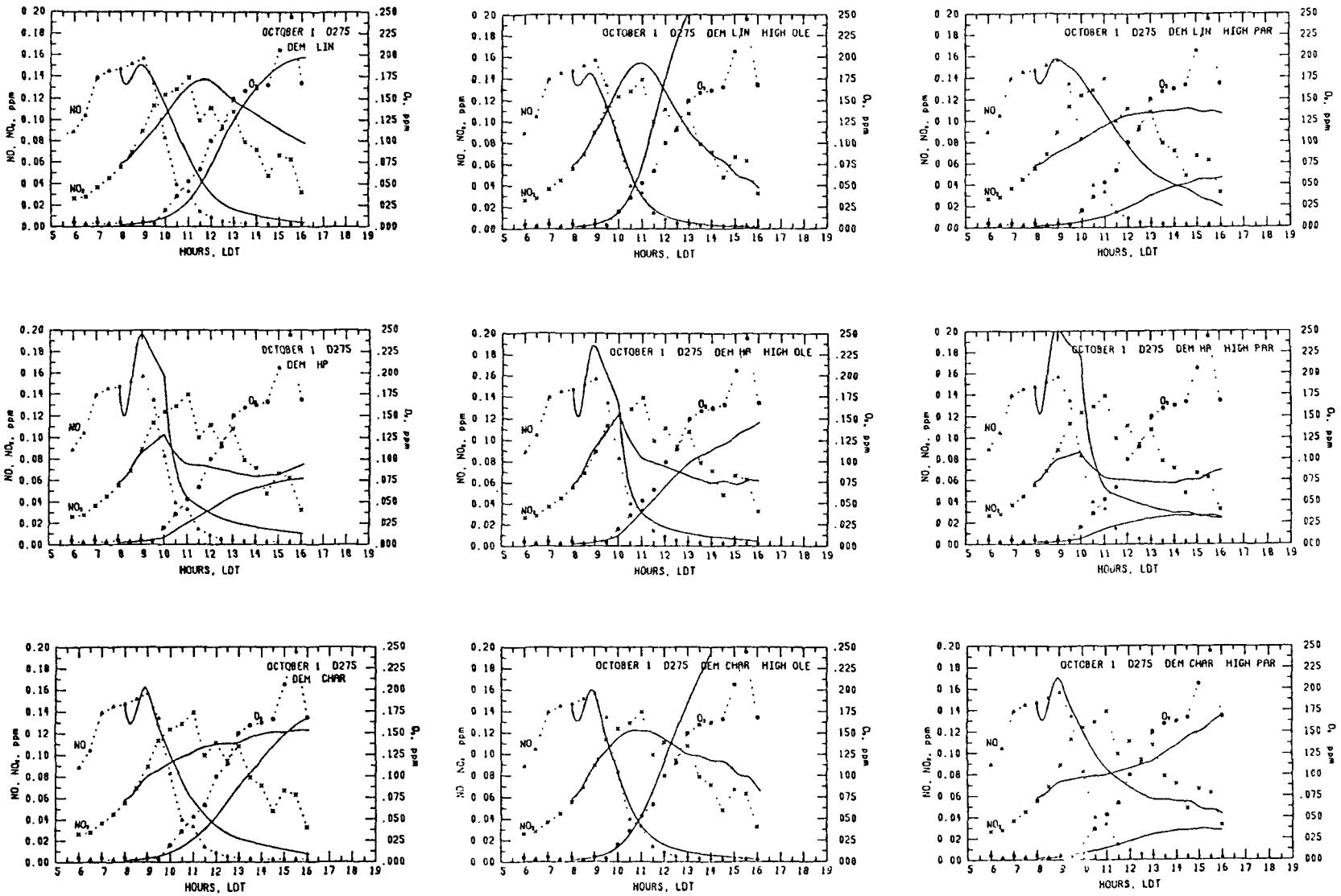

Figure 89. Effect of changing the HC composition from October 1 values to August 8 (high olefin) to August 25 (high paraffin) values for Demerjian Mechanism in the October 1, 1976 RAPS simulation.

	NR & PAR	OLE	ARO	ALD
Oct. 1	65.9	17.2	14.9	2.0
Aug. 25	86.0	10.0	6.6	1.0

These modelling results suggest that the control strategy for St. Louis would be to replace 15% of the olefin and aromatic carbon with paraffin carbon and have no reduction in total emissions; smog chamber data, however, suggests that this would not be true.

8.3.3 Effects of Trajectory Assumptions for Selected Days

The purpose of this section is to show the effects of emission pattern variations that might result from trajectory assumptions. The emission rate pattern is determined by the column path of the air parcel. The column path is defined as the area over which the emission rates are determined. For this study the column path was defined by the area encompassed by five back trajectories from the site of observed ozone maximum. Since the meteorological parameters are assumed to be uniform throughout the urban area, the emission rate pattern variations show the effects of column path variations.

To examine the effects of different emission rate patterns two approaches will be taken. First days 238 and 201 will be examined, since each exhibited similar ozone profiles for the three different mixing height profiles when modeled with the three different chemical mechanisms (see Figure 79 of section 8.2). The other approach is to see the effects of altering the pattern of the hourly emission rates while keeping the total amount of the emitted mass constant.

Day 238 - August 25. The column path from the supplied information is repeated as Figure 90. The back trajectories from the site of the highest ozone maximum indicate that the column enters the RAPS data region from the southeast then turns approximately 90°, just southeast of the Wood River-Alton point source region (see Figure 29). Figure 91 shows the modelled and ambient concentrations of NO_x, O_3, CO and HC. The ambient concentrations of these species along the column path are plotted as the dashed lines. These represent the weighted average concentrations from the three closest monitoring sites to the centerline of the column path. The solid lines represent the predicted concentration of the species by the Demerjian, (DEM)

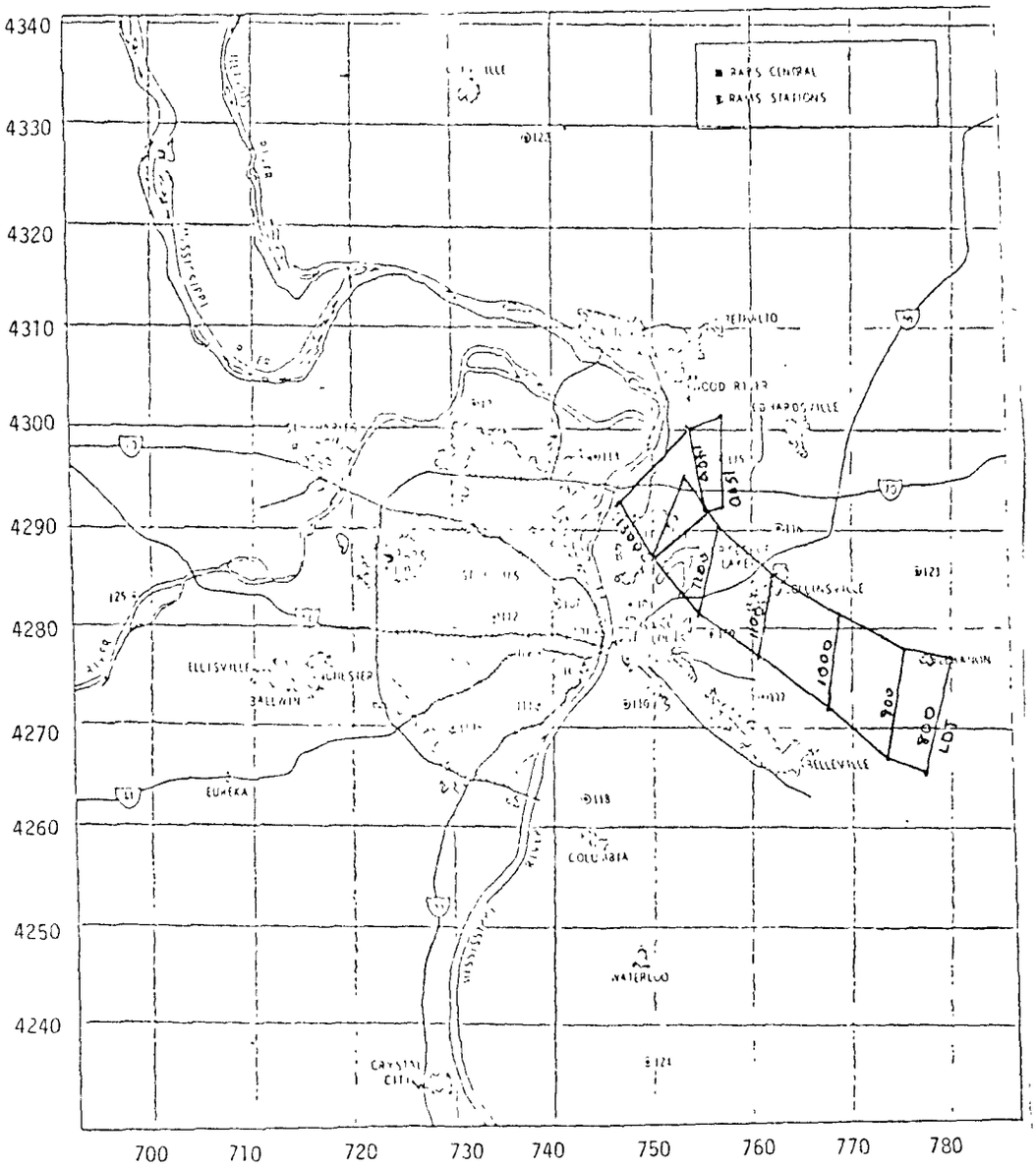

Figure 90. Trajectory for Day 238, August 25/Site 115

mechanism.

Since the ozone maximum predicted by all three mechanisms for the three different mixing height profiles was considerably less than the observed ozone for the day (0.190 ppm), and since the CO concentration is so poorly predicted, one can assume that the emission pattern of the column path reaching the observation station is different than that used in the model run.

For Day 238, August 17, three alternative column paths were examined:

A. The first, T1, uses the centerline trajectory of the supplied column path and places a two kilometer box around it, one km radius. Figure 91 shows that the ozone predicted varies little from the supplied column path. Table 33 contains a list of the ozone predicted for each column path. Table 34 contains the emission rates in units of ppm-km used for each column path, Figure 92 represents the instantaneous fit of these emission rates. The emission rates for T3 and TH column paths were selected from the emission rates from the supplied column path for Day 201.

Notice the rise in ambient NO_x concentration in Figure 91, during the last hour and a half, and the rise and fall of the hydrocarbon and CO concentration (also in Figure 91), during the last three hours of the simulation. These changes in the ambient concentrations are not predicted using either the supplied or T1 column paths.

B. The T3 column path considers a discontinuous column path, during the last three hours of the simulation. The column path considered does not curl around from the southeast, but comes down from the northwest passing

through the Wood River-Alton Point source region, Figure 29. The T3 emission rates consist of the T1 rates for the first four hours and the major emissions from the Wood River-Alton region for the last three hours of the simulation.

Using this discontinuous column path, the DEM mechanism predicts much more ozone than either the supplied or the T1 column paths, Table 33. The NO_2 peak is now present, Figure 91, and the ozone concentration profile appears to be best predicted using the characteristic or handpicked mixing height profiles. A hydrocarbon peak is predicted, but in an excessive amount, while the CO concentration is not modeled well.

C. Since there was promise from the T3 results,a hypothetical column path was determined passing through the Wood River-Alton region, TH. The TH column path was constructed from a straight line hypothetical path through this region using a two kilometer wide box surrounding this line. The emission rates for the TH column path consist of the T1 emission rates for the first four hours and these new rates for the last three hours. Figure 91 and Table 33 show that this column path is an inadequate description of the processes occurring on this day. The NO_2 levels are excessive; while the hydrocarbon and CO predictions are better, they do not agree with the observed ambient data.

The turning of the wind back trajectories in the region of the observed ozone maximum may indicate a convergence zone just outside the center city. If this is the case then the air parcels reaching this region came from many paths. To adequately establish if this was the case a more detailed wind field analysis must be performed. The determination of a column path is not a simple process, as established by the TH column path selection.

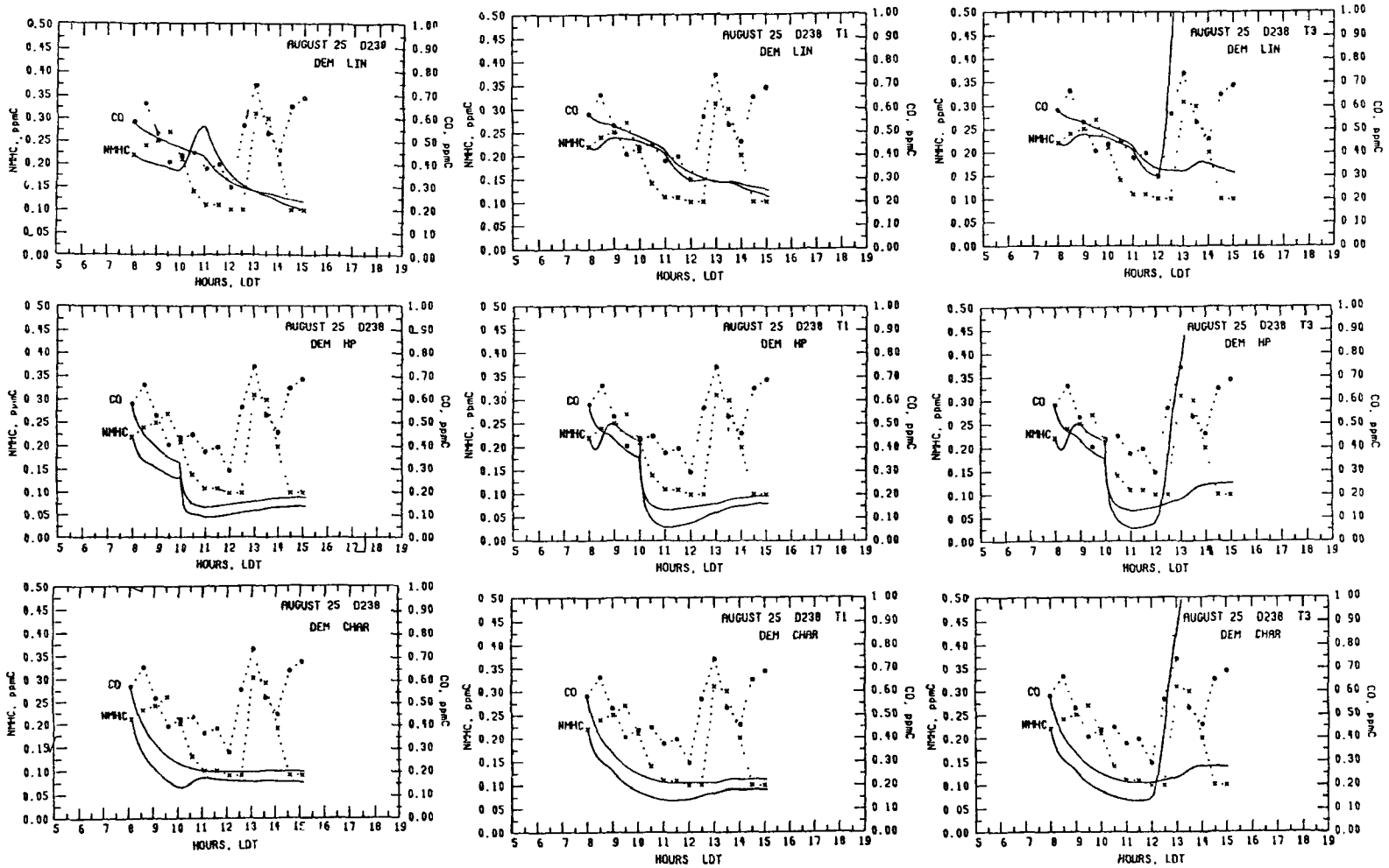

Figure 91. Simulations with different trajectories, Day 238.

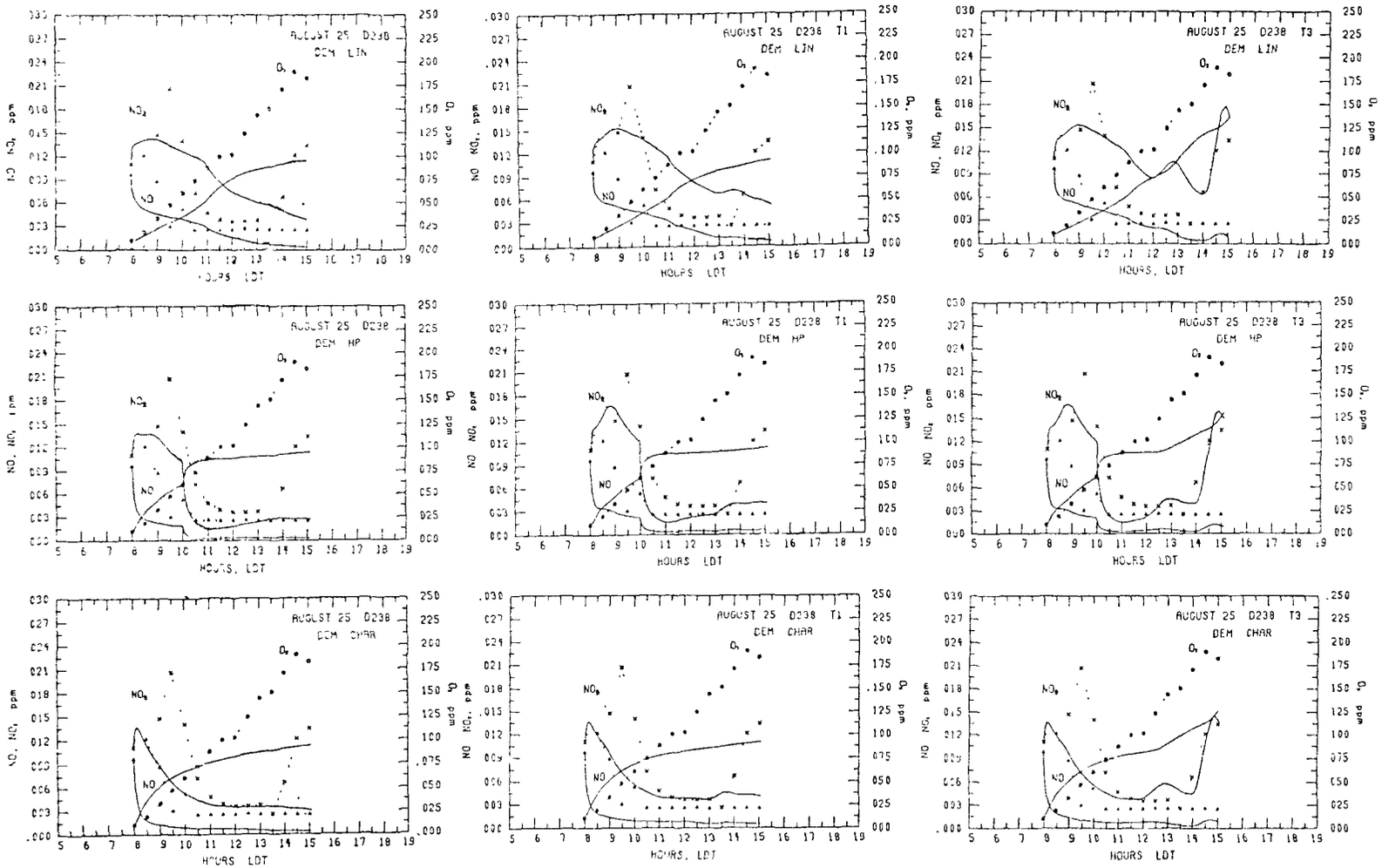

Figure 91. continued.

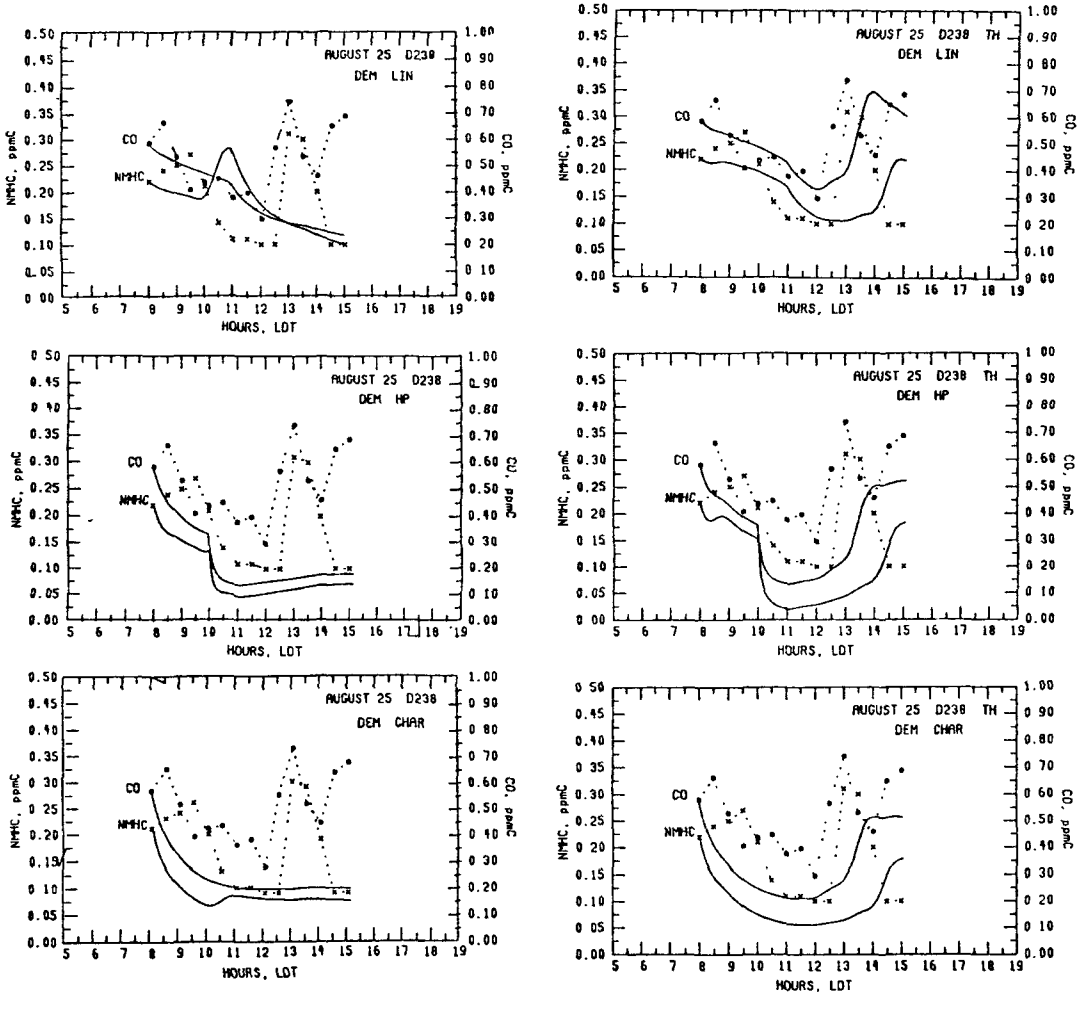

Figure 91. continued.

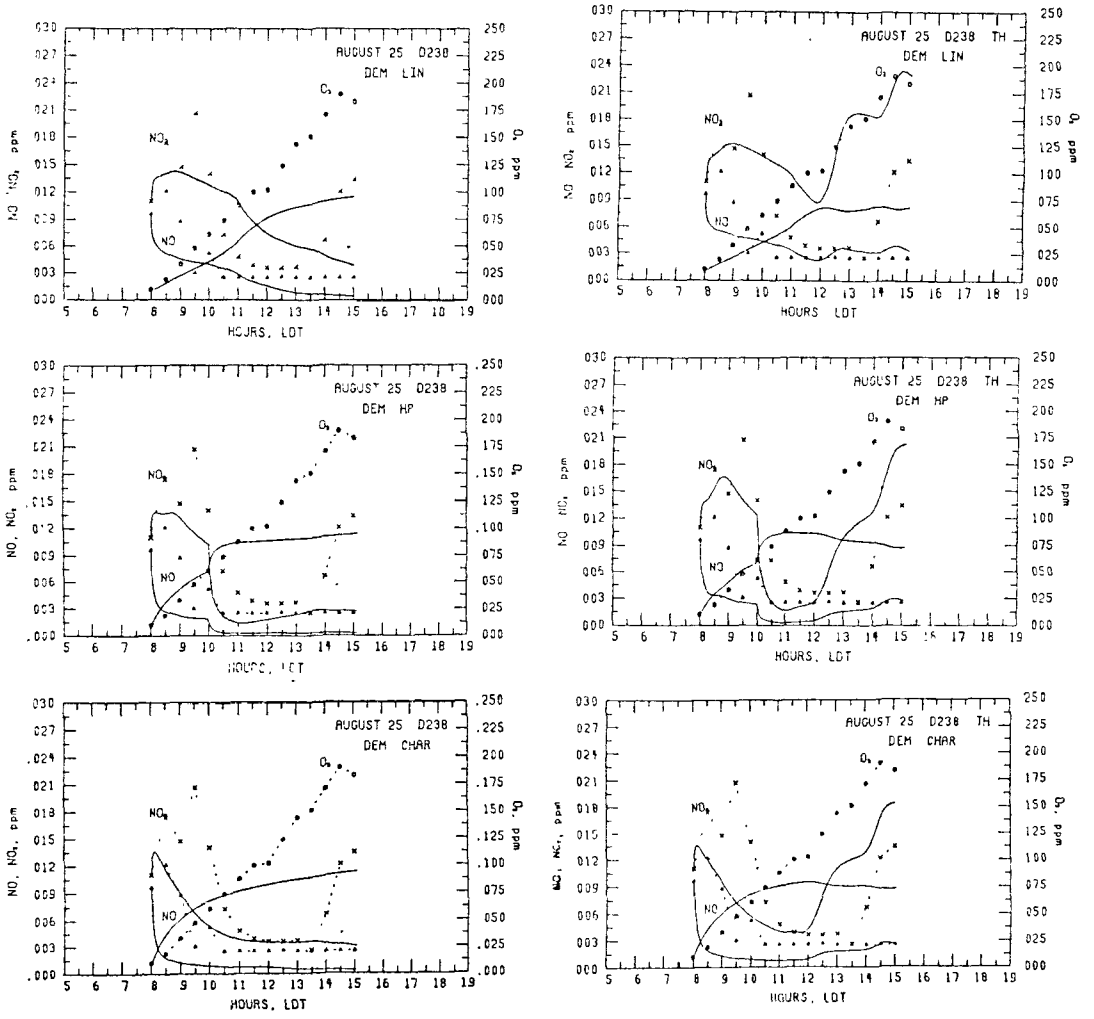

Figure 91. continued.

Table 33. Effects of Trajectory on Ozone Maxima; Day 238

DAY 238

Observed ozone = 0.190 ppm

Trajectory / Mixing height profile	Sup	T1	T3	TH
Linear	0.095	0.092	0.137	0.068
Handpicked	0.095	0.093	0.130	0.086
Characteristic	0.095	0.092	0.127	0.079

DAY 238

CO Emissions

Traj. Time	Sup	T1	T3	TH
8-9	0.0043	0.0081	0.0081	0.0081
9-10	0.0057	0.0060	0.0060	0.0060
10-11	0.0101	0.0063	0.0063	0.0063
11-12	0.0194	0.0213	0.0213	0.0213
12-1	0.0198	0.0193	0.0483	0.1061
1-2	0.0199	0.0369	0.0923	0.4049
2-3	0.0084	0.0127	0.0032	0.0151

NO_x Emissions

Traj. Time	Sup	T1	T3	TH
8-9	0.0005	0.0009	0.0009	0.0009
9-10	0.0004	0.0004	0.0004	0.0004
10-11	0.0006	0.0005	0.0005	0.0005
11-12	0.0014	0.0016	0.0016	0.0016
12-1	0.0014	0.0012	0.0055	0.0126
1-2	0.0015	0.0030	0.0116	0.0053
2-3	0.0007	0.0011	0.0248	0.0141

HC Emissions

Traj. Time	Sup	T1	T3	TH
8-9	0.0036	0.0080	0.0080	0.0080
9-10	0.0050	0.0047	0.0047	0.0047
10-11	0.0426	0.0040	0.0040	0.0040
11-12	0.0102	0.0092	0.0092	0.0092
12-1	0.0124	0.0201	0.3025	0.0239
1-2	0.0112	0.0135	0.2573	0.0488
2-3	0.0040	0.0049	0.1571	0.1753

DEM Fractions

OLE	0.1010	0.1669	0.1669	0.0515
PAR	0.7550	0.5895	0.5895	0.6656
ARO	0.0660	0.1095	0.1095	0.2145
NR	0.0675	0.1121	0.1121	0.0618
AID	0.0108	0.0220	0.0220	0.0066

Table 34. Emission Rates and Hydrocarbon Fractions Resulting From Different Trajectory Assumptions, Day 238

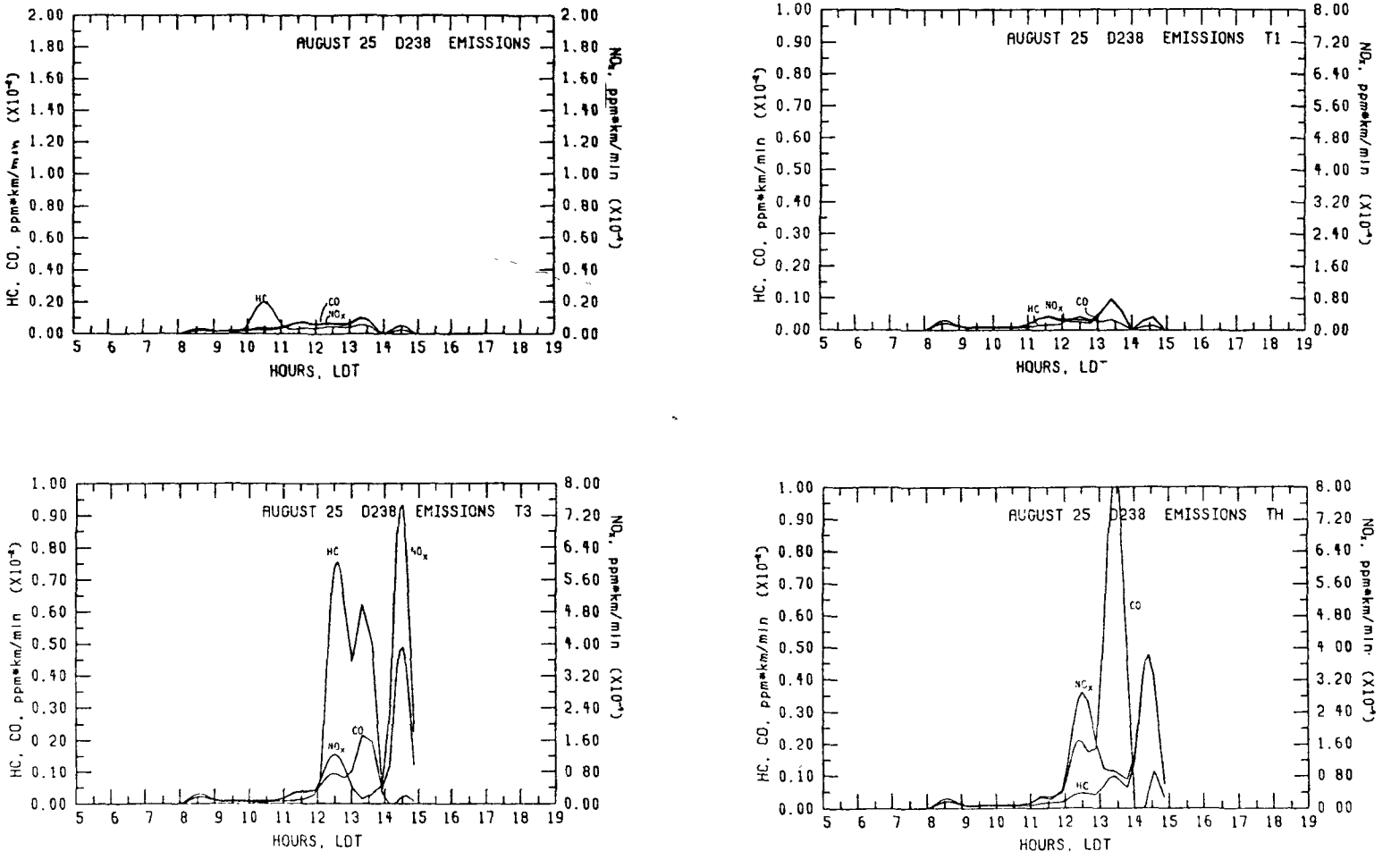

Figure 92. Instantaneous Emission Rates Along Trajectories; Day 238

Day 201 - July 19. The column path for this day from the supplied information is shown in Figure 93. On this day, the column path runs north-south through the city from the south. In comparison with Figure 29, note that the supplied column path encompasses the two major clusters of point sources in the RAPS database, the St. Louis-East St. Louis region and the Wood River-Alton region.

Again the dotted lines in Figure 94 represent the ambient concentration interpolated along the centerline of the column path, and solid lines represent the predicted concentrations by the Demerjian mechanism. For the supplied column path, neither the Demerjian (shown), Dodge, or Carbon Bond II mechanisms did well in predicting the ozone maximum. For the three different mixing height profiles the results were very similar for each mechanism. The observed ozone maximum on this day was 0.144 ppm. Again different emission patterns or column paths will be examined to see their effects on the ozone prediction.

For day 201, July 19, three alternative column paths were examined.

A. The first, T1, uses the centerline trajectory of the supplied column path and places a two kilometer box around it, one kilometer radius. Table 35 and Figure 94 indicate that the predicted ozone concentration was not any better than the predicted concentration using the supplied column path. The predicted ozone precursor concentrations (Figure 94) for the T1 column path, do not agree with the observed ambient concentrations for this day. In determining the emission rates for this column path, two point sources were encountered in the region, but their locations could not be established from the information at hand. The T1 column path does not consider either of the sources to be within the column path. The remaining two column paths consider both of the point sources to be within the column

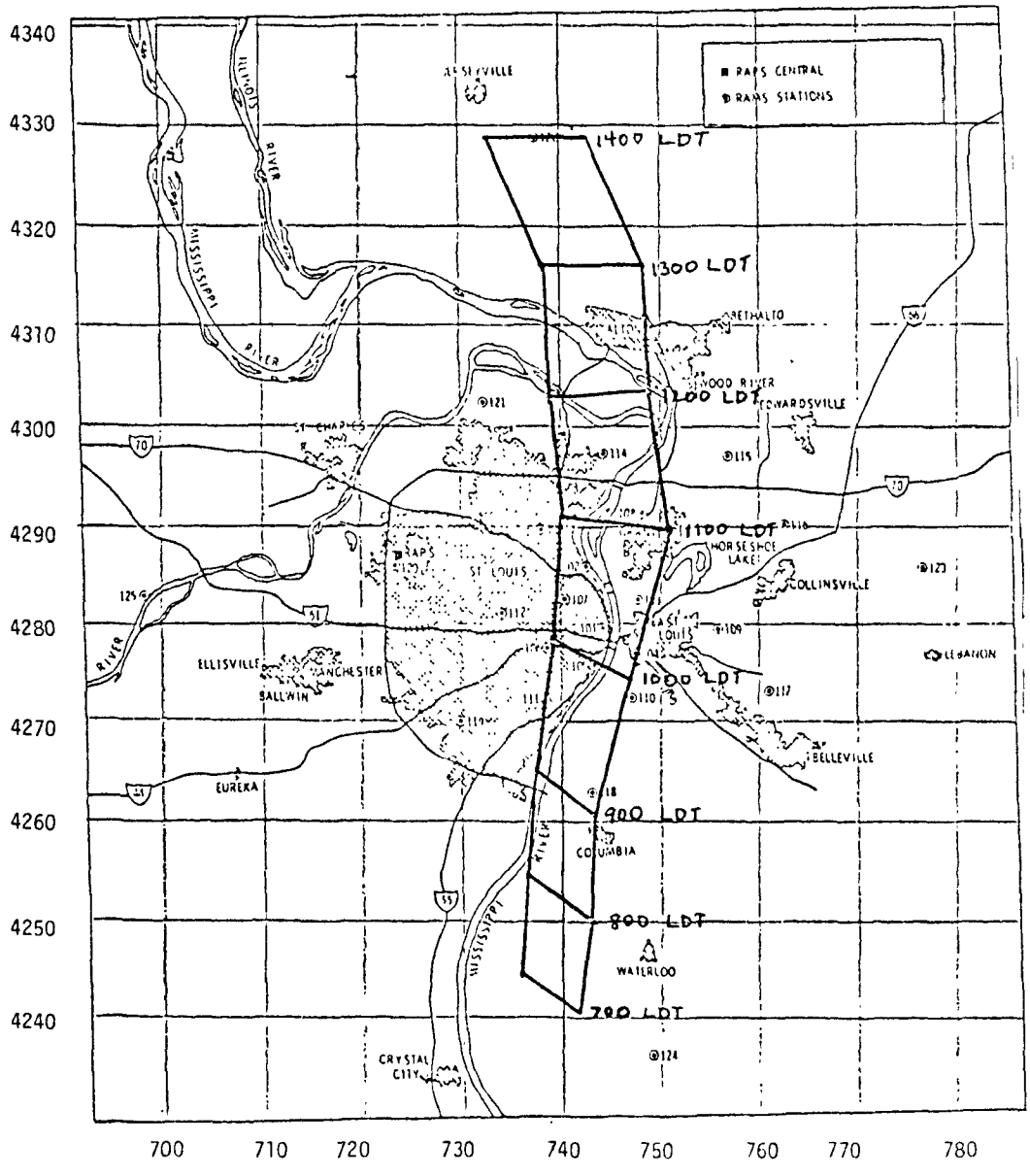

Figure 93. Column Path for Day 201, July 19.

path. Both of these point sources are hydrocarbon sources only. With their inclusion into the column path, the hydrocarbon fractions for the DEM mechanism are shifted. The column path TAB is the T1 column path for emission rates, with these new hydrocarbon fractions. Table 35 and Figure 94 indicate that shifting to these new fractions has a small effect on the predicted concentrations.

The remaining two column paths are a variation of the T1 column path. The emission rates represent levels which were increased or decreased slightly, based upon the comparison of the predicted concentrations with the observed ambient concentrations.

B. In the column path TA, the emission rates for the hour between 10 and 11 were increased five fold from the T1 emission rates. Table 35 and Figure 94 show that the ozone predicted is much closer to the observed concentration than either the T1 or the supplied column paths. The ozone concentration is overpredicted with the linear mixing height profile. Figure 94 shows that the prediction of the precursor concentrations are also overpredicted, with the greatest overprediction for NO_2.

C. In the column path TB, the emission rate for the oxides of nitrogen was decreased by approximately 15% from the TA column path, Figure 95. This decrease causes the model to predict an increased ozone maximum. The ozone concentration predicted using the handpicked and characteristic mixing height profiles increases to a level which is very close to the observed maximum; with the linear mixing height profile, the predicted ozone concentration also increases by 10%.

The fact that the predicted ozone concentration rose by 10% with a 15% decrease in oxides of nitrogen emissions indicates that the timing and/or the mass of the emission rates is important to the amount of ozone predicted.

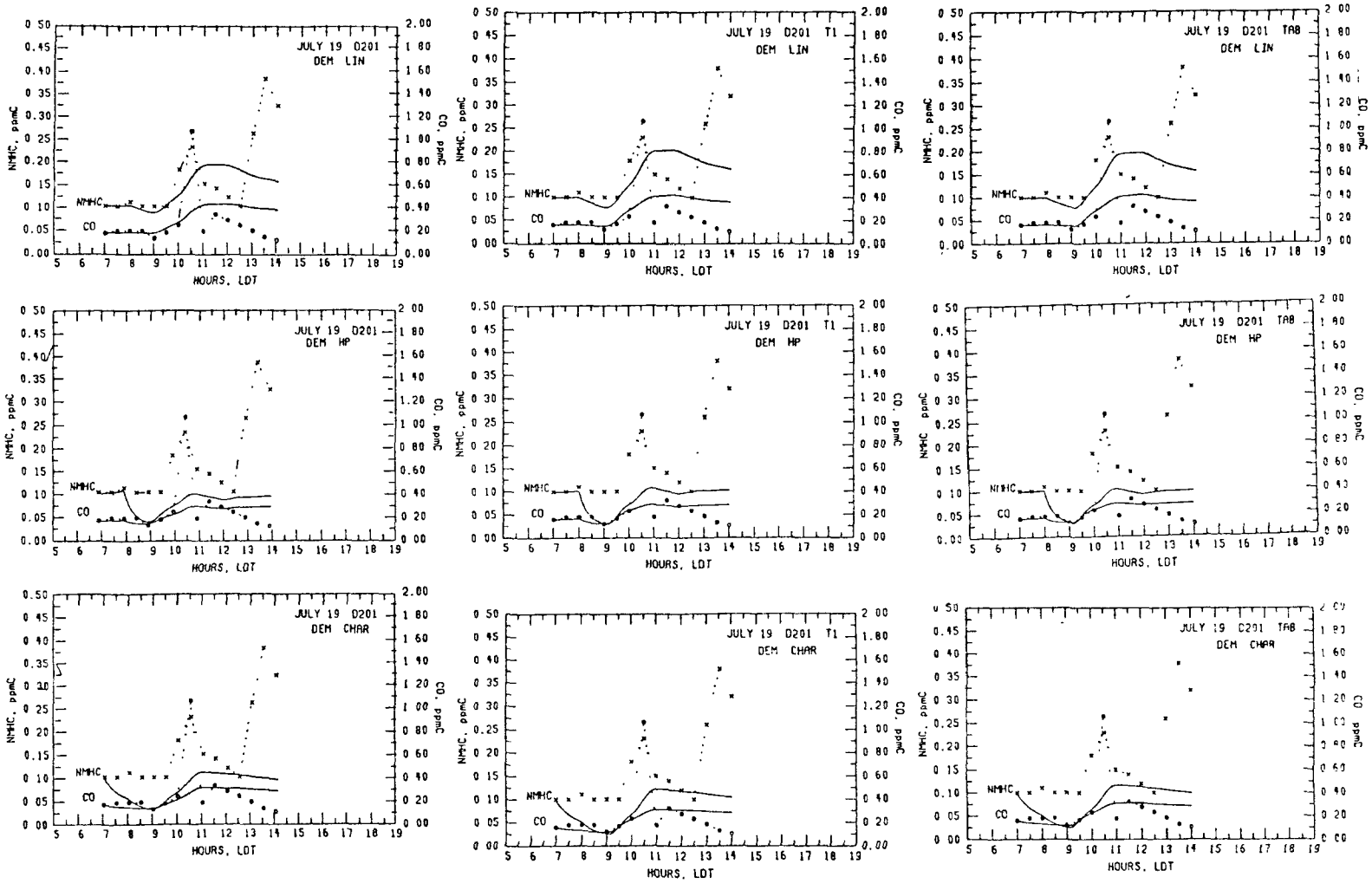

Figure 94. Simulations with different trajectories; Day 201.

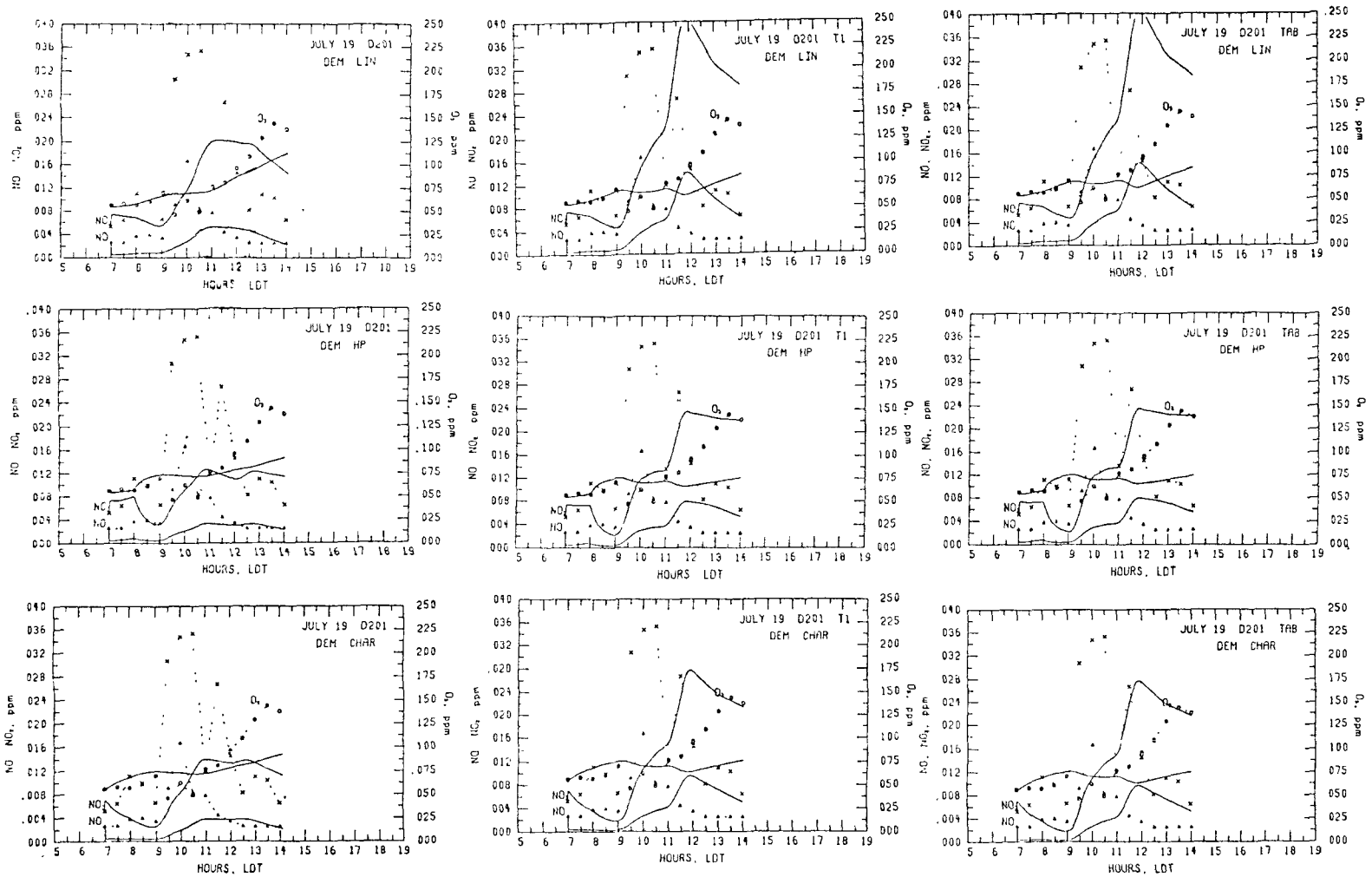

Figure 94. continued.

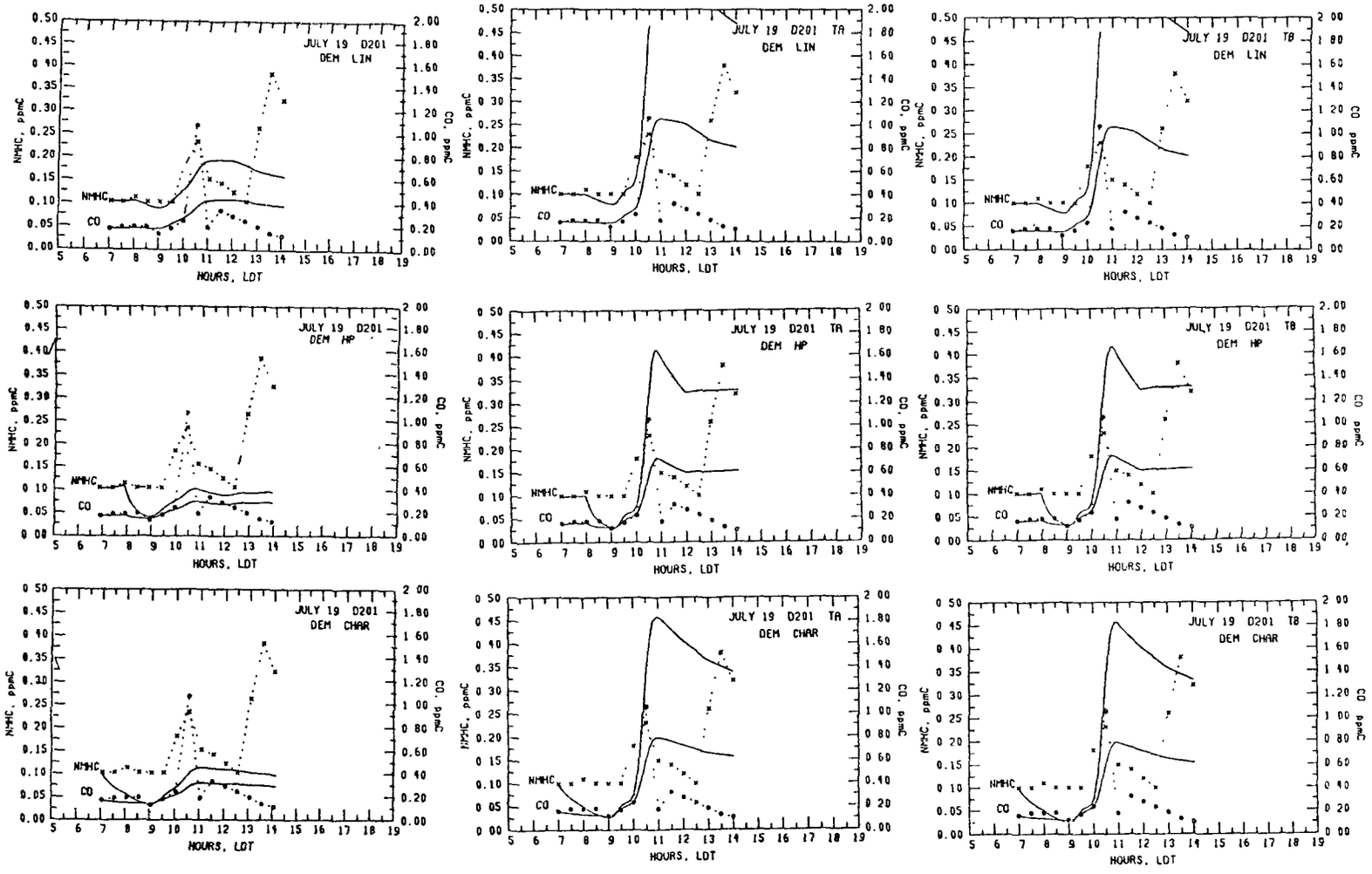

Figure 94. continued.

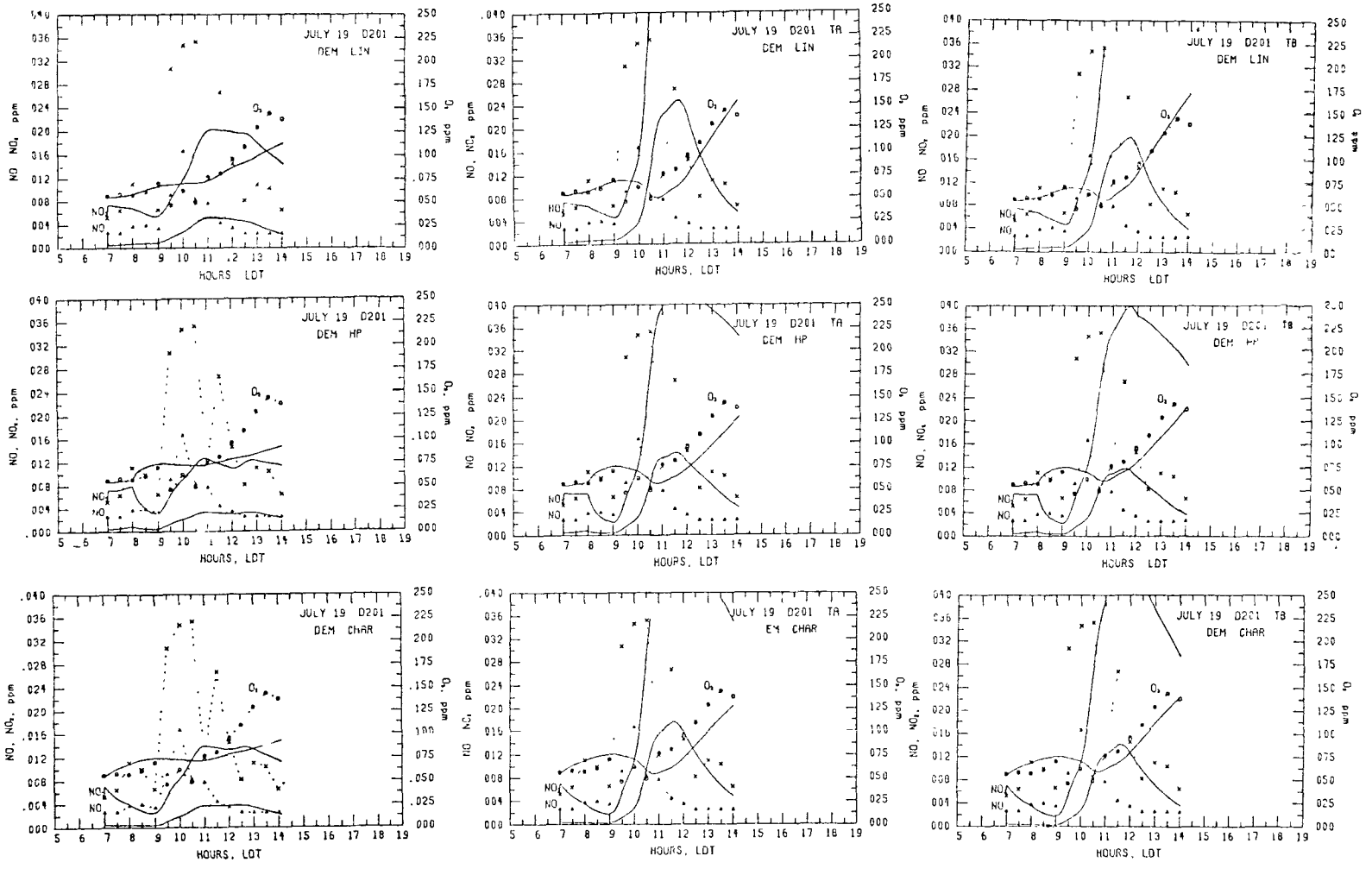

Figure 94. continued.

Table 35

Effects of Trajectory on Ozone Maxima, Day 201

DAY 201

Observed ozone = 0.144 ppm

Trajectory Mixing height profile	S	TI	TAB	TA	TB
Linear	0.113	0.086	0.084	0.154	0.172
Handpicked	0.091	0.076	0.074	0.128	0.140
Characteristic	0.093	0.077	0.076	0.128	0.141

Table 36
Emission Rates and HC Fractions Resulting from Different Trajectory Assumptions, Day 201

DAY 201

CO Emissions

Traj. Time	Sup	T1	TA	TB
7-8	0.0009	0.0006	0.0006	0.0006
8-9	0.0055	0.0012	0.0012	0.0012
9-10	0.0697	0.0966	0.0966	0.0966
10-11	0.1459	0.1295	0.6475	0.6475
11-12	0.0311	0.0374	0.0374	0.0374
12-1	0.0261	0.0173	0.0173	0.0173
1-2	0.0035	0.0043	0.0043	0.0043

HC Emissions

Traj. Time	Sup	T1	TA	TB
7-8	0.0007	0.0002*	0.0002	0.0002
8-9	0.0026	0.0006	0.0006	0.0006
9-10	0.0389	0.0419[A]	0.0459	0.0459
10-11	0.0676	0.0789[B]	0.4549	0.4549
11-12	0.0160	0.0174	0.0174	0.0174
12-1	0.0117	0.0113	0.0113	0.0113
1-2	0.0027	0.0012	0.0012	0.0012

NO_x Emissions

Traj. Time	Sup	T1	TA	TB
7-8	0.0002	0.0001	0.0001	0.0001
8-9	0.0006	0.0002	0.0002	0.0002
9-10	0.0074	0.0105	0.0105	0.0105
10-11	0.0127	0.0117	0.0585	0.0500
11-12	0.0048	0.0296	0.0296	0.0296
12-1	0.0061	0.0009	0.0009	0.0009
1-2	0.0003	0.0004	0.0004	0.0004

DEM Fractions

OLE	0.1660	0.1723*	0.1632[A,B]	0.1632
PAR	0.5290	0.5610	0.5747	0.5747
ARO	0.1670	0.1280	0.1302	0.1302
NR	0.1180	0.1199	0.1143	0.1143
AID	0.0194	0.0188	0.0176	0.0176

*considers neither unknown Location Point Sources

[A,B]considers both unknown Location Point Sources

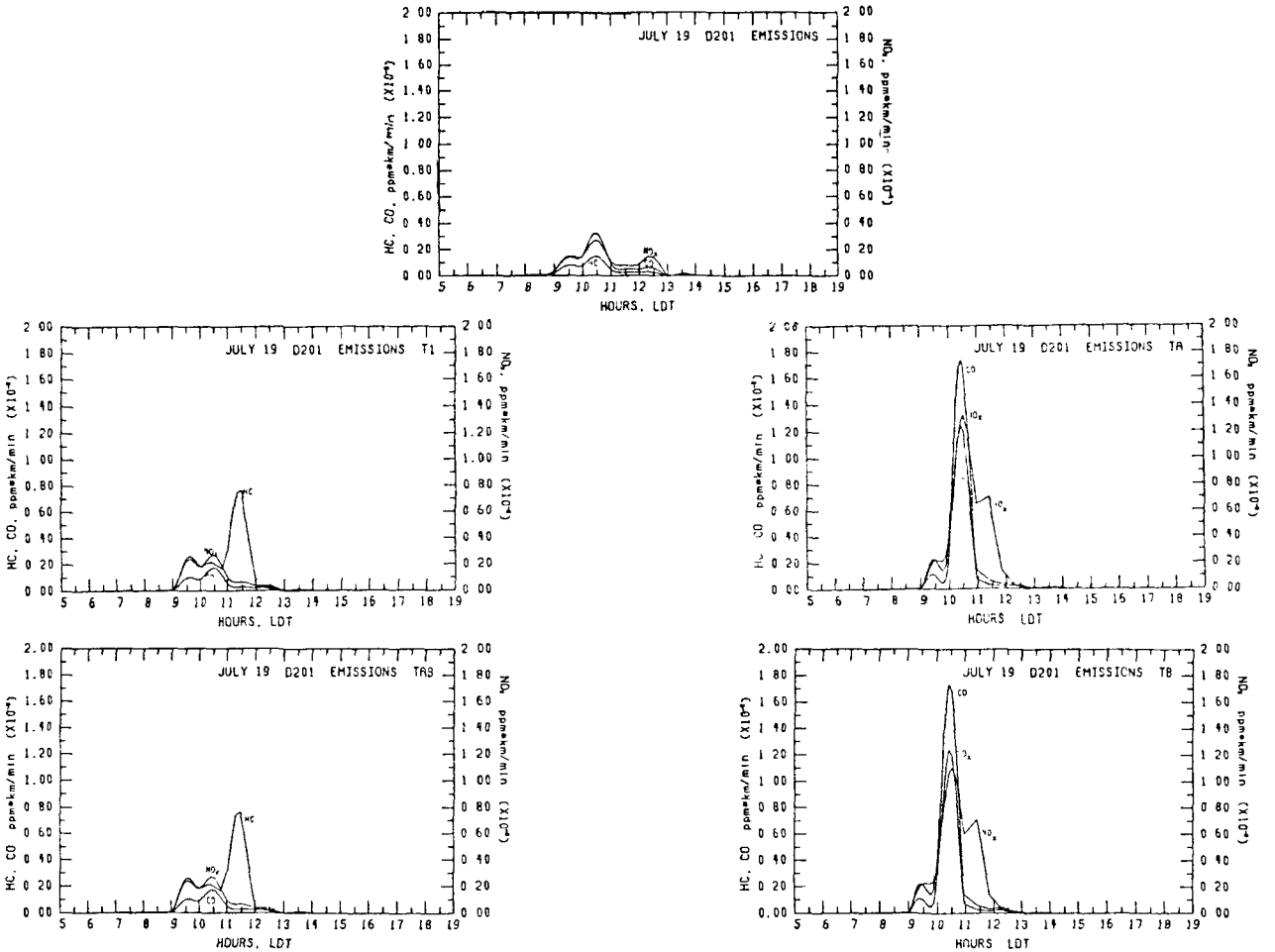

Figure 95. Instantaneous emission rates along trajectories.

8.3.4 Effects of Emissions Pattern for Selected Days

The purpose of this section is to examine the effects of changing the pattern of the emission rates while keeping the total emission mass constant.

On three days, Day 159-June 7, Day 261-September 17, and Day 275-October 1 starting at 8 o'clock, three different emission patterns were examined. The emission rate patterns were determined using a random number table. Each hour's emission rate was assigned a value corresponding to the hour of its occurrence, the first hour being one, the second, two, etc. (Table 37). Then these numbers were reordered by going down the random number table until all the numbers had appeared. Table 37 indicates the order of the emission rates for the three different patterns, A, B, and C, and the total emission mass in ppm-km for the three days.

Day 159, June 7 is the day with the lowest oxides of nitrogen emissions while day 275 starting at 8 AM has the highest. Both of these days have similar hydrocarbon emission rates. The results are shown in Table 38. Table 39 shows the absolute and relative deviations as percent of each emission pattern from the supplied pattern. Day 275 shows the largest deviations while day 159 has the smallest deviations.

The results suggest that the order in which the column path intersects the emission inventory is important.

8.3.5 Effects of Ozone Aloft Assumptions

The purpose of this section is to examine the effects of two different ozone aloft profiles on the predicted ozone maximum. Three days from the St. Louis RAPS study will be used to examine the effects, using the Demerjian chemical mechanism.

The two profiles are a constant profile and a variable profile. In the constant ozone aloft profile a constant concentration of ozone is entrained into the mixed layer for a given mixing height rise. For the variable ozone

Table 37

Random Emissions Patterns and Total Mass of Emissions

Pattern	Hour Order of Emissions								
Supplied	1	2	3	4	5	6	7	8	9
A	3	4	5	8	6	3	7	1	9
B	5	3	6	4	7	9	1	2	8
C	3	6	4	9	8	5	2	1	7

	CO	NO_x	HC
Day 159, June 7	0.5248	0.0346	0.2347
Day 261, September 17	0.7535	0.0589	0.4344
Day 275, October 1 at 8 AM	0.8364	0.0859	0.2884

Table 38

Predicted Ozone Maximum Considering Three Different Emission Patterns

		Emission Pattern			
Day 159, June 7 Mixing Height Profile		Sup	A	B	C
	Linear	0.252	0.248	0.243	0.239
	Handpicked	0.164	0.157	0.157	0.152
	Characteristic	0.197	0.104	0.189	0.184
Day 261, September 17 Mixing Height Profile					
	Linear	0.103	0.118	0.113	0.119
	Handpicked	0.123	0.136	0.137	0.137
	Characteristic	0.104	0.118	0.114	0.115
Day 275, October 1 at 8 am Mixing Height Profile					
	Linear	0.261	0.233	0.228	0.238
	Handpicked	0.096	0.070	0.067	0.070
	Characteristic	0.234	0.186	0.179	0.189

Table 39

Deviations of Ozone Maximum Prediction from the Supplied Emission Pattern

	Emission Pattern		
	A	B	C
Day 159, June 7			
Mixing Height Profile			
Linear	-0.004*	-0.009	-0.0013
	1.59	3.57	5.16
Handpicked	-0.0007	-0.0007	-0.012
	4.27	4.27	7.32
Characteristic	-0.093	-0.0008	-0.013
	47.21	4.06	6.60
Day 261, September 17			
Mixing Height Profile			
Linear	0.015	0.010	0.016
	14.56	9.71	15.53
Handpicked	0.013	0.014	0.014
	10.57	11.38	11.38
Characteristic	0.014	0.010	0.011
	13.46	9.62	10.58
Day 275, October 1 at 8 AM			
Mixing Height Profile			
Linear	-0.028	-0.033	-0.023
	10.73	12.64	8.81
Handpicked	-0.026	-0.029	-0.026
	27.08	30.21	27.08
Characteristic	-0.048	-0.055	-0.045
	20.51	23.50	19.29

*The top number represents the absolute deviations, calculated as difference in ozone maximum between the variation pattern and the supplied pattern. The lower number represents the relative deviation, represented as percent; computed as absolute deviation divided by the predicted ozone maximum from the supplied emission pattern.

aloft profile, the concentration of ozone entrained into the mixed layer depends on the fraction of the total rise of the mixing height for that day. The fractional multiplier is prescribed by the equation:

$$FAL = 2FR^3 - 3FR^2 + 1$$

where FAL is the fraction of the aloft concentration

FR is the fractional rise in mixing height, given by the current mixing height minus the initial mixing height divided by the total rise in mixing height for that day.

As one might expect, the maximum ozone concentration decreases as the concentration of ozone entrained into the mixed layer decreases, i. e. a constant aloft profile provides the greatest entrained concentration, and the variable aloft profile provides a lesser concentration, Table 40.

The constant aloft profile is considered in Table 41. The first column represents the effective concentration of the entrained ozone. This was determined by subtracting the maximum ozone concentration with ozone aloft from the maximum ozone concentration using the constant ozone aloft profile. The second column represents the concentration of the ozone entrained considering only dilution, i. e. no chemistry. The third column can be interpreted as the effect of chemistry on the entrained ozone concentration, expressed as a percentage. A value of zero indicates the entrained ozone concentration is not affected by chemistry. For the three days examined, no pattern of the affect of chemistry with respect to the different mixing height profiles can be determined. For day 261, the ozone maximum is enhanced by the chemistry and the entrainment ozone, with the characteristic mixing height profile.

Table 40

Variation of Ozone Aloft on the Prediction of Ozone Maximum

		Aloft Profile	
	Constant	Variable	None
Day 159, June Mixing Height Profile			
Linear	0.252	0.232	0.215
Handpicked	0.164	0.117	0.072
Characteristic	0.197	0.159	0.123
Day 261, September 17 Mixing Height Profile			
Linear	0.103	0.081	0.067
Handpicked	0.123	0.096	0.070
Characteristic	0.104	0.072	0.058
Day 275, October 1 at 8 am Mixing Height Profile			
Linear	0.261	0.241	0.218
Handpicked	0.095	0.070	0.053
Characteristic	0.233	0.209	0.193

The results from using a variable aloft profile are presented in Table 42. The three columns contain the same information as in Table 41, considering a variable ozone aloft profile. Again no pattern can be determined with respect to the mixing height profile.

In comparing the days for the two different aloft profiles, specifically days 159 and 275, a trend of the effects of chemistry are similar, with the magnitudes being close in most cases. For day 261, the enhancement of the ozone maximum with constant ozone aloft profile was not reproduced with the variable aloft profile.

In conclusion, the predicted ozone maximum decreases as less material is entrained from aloft, while the effects of chemistry on this entrained ozone vary widely between days and mixing height profiles.

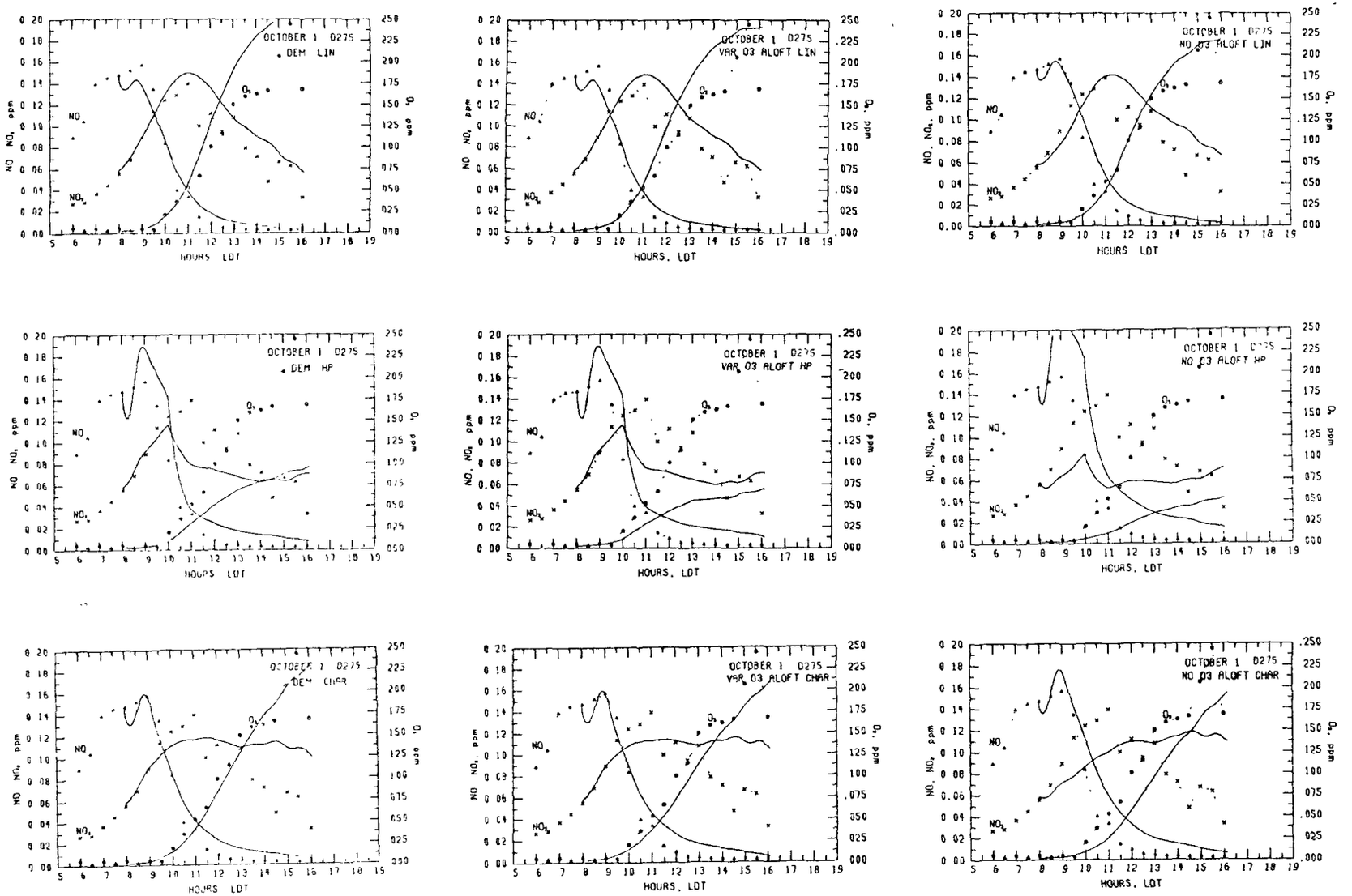

Figure 96. Effects of ozone aloft on simulations, Day 275.

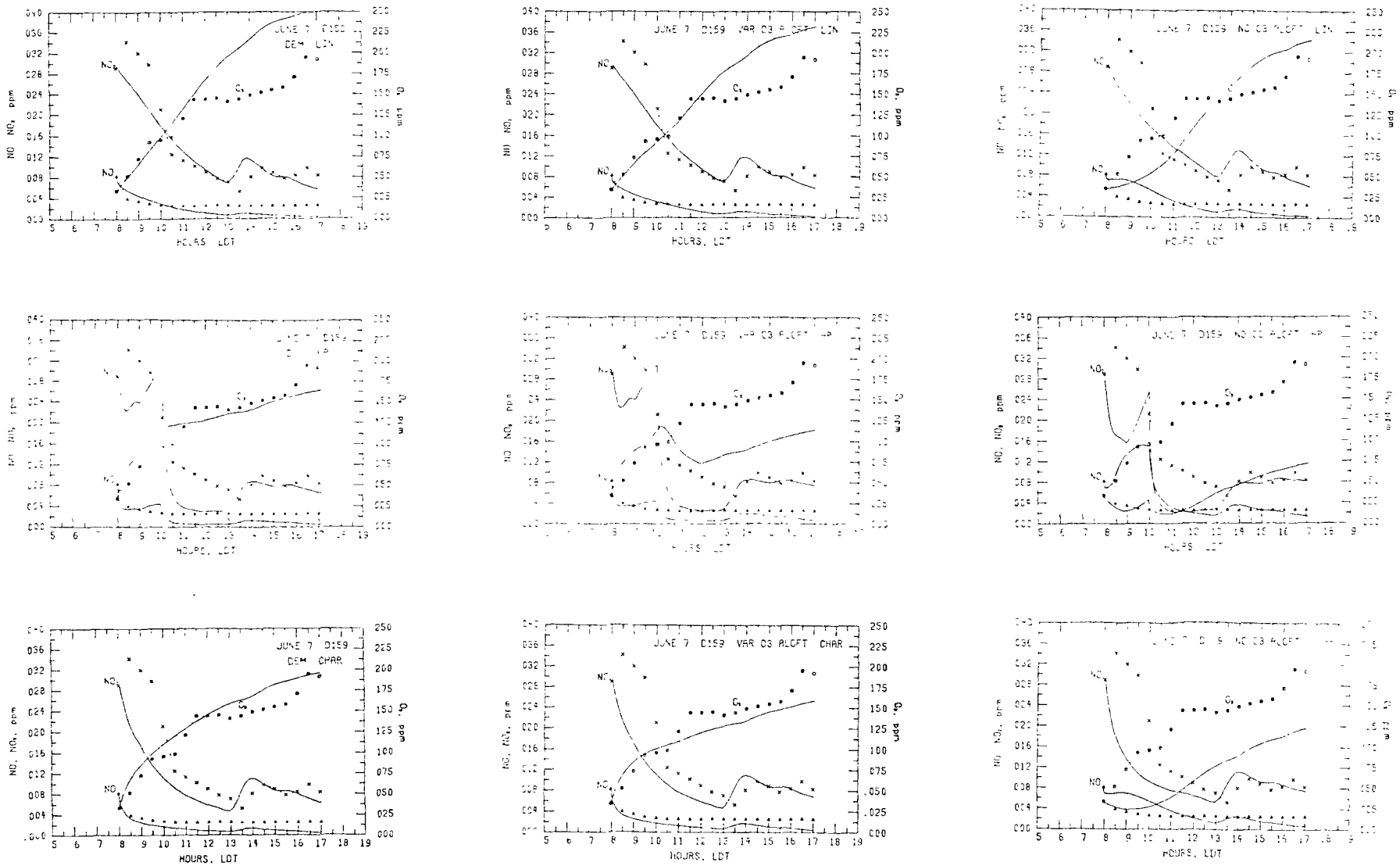

Figure 97. Effects of ozone aloft on simulations, Day 159.

Table 41

Effects of Chemistry on a Constant Ozone Aloft Profile

Day/Mixing Height Profile	Effective[A] Entrained Ozone Conc	Entrained[B] Ozone Conc (dilution only)	Percentage of[C] the Entrained Ozone Survival
Day 159, June 7			
Linear	0.037	0.070	52.9
Handpicked	0.092	0.117	78.6
Characteristic*	0.074	0.108	71.8
Day 261, September 17			
Linear	0.036	0.048	75.0
Handpicked*	0.053	0.057	93.0
Characteristic	0.058	0.056	103.6
Day 275, October 1 at 8 AM			
Linear*	0.043	0.045	95.6
Handpicked	0.042	0.057	73.7
Characteristic*	0.040	0.048	83.3

(A) Computed as the difference between the predicted ozone maximum with no ozone aloft from the predicted ozone maximum using the constant ozone aloft profile.

(B) Considers only the effect of dilution on the entrained ozone.

(C) Computed as A/B *100.

*Good prediction of ozone maximum (See PKSTM Section).

Table 42

Effects of Chemistry on a Variable Ozone Aloft Profile

Day/Mixing Height Profile	Effective[(A)] Entrained Ozone Conc	Entrained[(B)] Ozone Conc	Percentage of[(C)] the Entrained Ozone Survival
Day 159, June 7			
Linear	0.017	0.035	48.6
Handpicked	0.045	0.058	77.6
Characteristic*	0.036	0.051	70.6
Day 261, September 17			
Linear	0.014	0.024	58.3
Handpicked*	0.026	0.029	89.7
Characteristic	0.014	0.028	50.0
Day 275, October 1 at 8 AM			
Linear*	0.023	0.023	100.0
Handpicked	0.017	0.028	60.7
Characteristic*	0.016	0.024	66.7

(A) Computed as the difference between the predicted ozone maximum with no ozone aloft from the predicted ozone maximum using the variable ozone aloft profile.

(B) Considers only the effect of dilution on the entrained ozone.

(C) Computed as A/B *100.

*Good prediction of ozone maximum (See PKSTM Section).

8.4 SUMMARY

In analyzing the RAPS data and in generating input data and reference data for photochemical simple trajectory models, significant uncertainties were encountered. Although used in this study, the simple inverse distance weighing of hourly wind data at the closest RAPS stations was judged not adequate for defining the origin and history of air arriving at a particular station. In some cases this procedure resulted in variations of origin that encompassed the whole city of St. Louis; thus divergence and convergence problems were significant. A mass conservative wind field model should be developed for the RAPS database and trajectories determined from this model.

The three closest RAPS stations to the assumed trajectory location at each hour often showed large differences in measured concentrations resulting in uncertainties in starting concentrations and in values along the trajectories.

The uncertainties in the trajectories and the conceptual basis of the simple trajectory model lead to an averaging technique for the emissions inventory that resulted in a large uncertainty for the contributions of point sources. Hence a significant amount of "tuning" could be necessary for any particular day. A sub-model in the above proposed wind field model could provide better treatment of the impact of significant point sources.

The calculated composition of hydrocarbons along the trajectories had the following ranges (in percent carbon): 6.7 to 14.0, nonreactive; 4.8 - 75.5, paraffin; 10.1 to 25.1, olefin; 6.6 to 18.1, aromatic; 1.08 to 2.86, aldehydes. There are no smog chamber databases in which the hydrocarbon composition has been systematically varied in a complex mixture to test or develop chemical mechanisms. The Dodge and Demerjian mechanisms were both developed on the BOM auto exhaust composition. The CB? and CIT mechanism were developed on synthetic mixture smog chamber experiments.

For the Demerjian and Carbon Bond II mechanisms, in static diurnal light simulations, changing the hydrocarbon composition over the ranges given above without changing the hydrocarbon concentration resulted in O_3 decreases of more than a factor of 5 (80% reduction). A few UNC outdoor smog chamber experiments indicate that the models greatly overrespond to compositional changes in complex mixtures.

Significant uncertainties existed in calculating the mixing height profiles. Typically, soundings were taken at 0500, 1100, and 1700 LDT. In this study, three techniques for converting these soundings to temporal variation in mixing height, and thus dilution rates, were compared. The first method was a linear interpolation between the soundings. The second was to have a meteorologist examine each day and generate a "handpicked" mixing height profile. The third method was the application of Demerjian and Schere's Characteristic Curve developed for their photochemical box model. Each of these profiles were used for each mechanism for each day.

A meteorology-only simple trajectory model (MOSTM), that is, a model incorporating initial conditions, emissions, mixing height rise, and entrainment from aloft but excluding any chemistry, was used to examine the reasonableness of the non-chemistry assumptions, especially mixing heights and emissions patterns.

MOSTM simulation results were that: a) the "handpicked" mixing height profile generally gave poor results for most days in that it was usually too low, too long, resulting in too high early concentrations and then rose too fast, resulting in too much dilution and low final concentrations; b) the probable parcel pathways were poorly represented by the "trajectory boxes" used and therefore the emission input figures are inadequate for June 8, Site 15, July 13, July 19, and the last 2 hours of August 25. A mass

balance for each species in MOSTM simulations showed that: a) 4-47% of CO mass, 2-25% of NO_x mass, and 1-15% of HC mass was the result of material present initially, b) 44-86% of CO mass, 83-98% of NO_x mass, and 85-99% of HC mass was due to emissions, and c) 9-24% of the CO mass was entrained from aloft. This suggests that the chemistry should be emission dominated.

A photochemical simple trajectory model (PKSTM), equivalent to the OZIPP "calculate" mode but having more flexibility, was used to simulate the ten RAPS days. There were 9 simulations for each day: three mechanisms at each of three mixing height profiles. The mechanisms were Demerjian, Dodge, and CB2. Only June 7 and October 1

were simulated with the CIT mechanism because of its previous poor performance on the BOM simulations.

PKSTM Results. Different chemistries do give large differences in results for the same conditions of emissions and meteorology. The CB2 mechanism generally predicted the lowest O_3 values, the DODGE mechanism generally predicted a middle value, and the DEM mechanism generally predicted the highest value.

For four days, O_3 was underpredicted by more than 25% by all mechanisms for all mixing height profiles. On a fifth day such underprediction also occurred for all mechanisms for the handpicked and characteristic mixing height profiles. These underpredictions are associated with very poor predictions of observed NO_x and HC concentrations. The MOSTM simulations had already suggested that these days had problems with the trajectories and possibly the large averaging process applied to the emissions.

For three days, including the days with the highest and lowest observed O_3, O_3 was overpredicted from 2 to 23% by the DEM mechanism for the linear

mixing height profile. These same three days were predicted within ±5% for the DEM mechanism and the characteristic mixing height profile. The other two days were underpredicted by 10-15% by the DEM mechanism for the linear and characteristic mixing height profile.

On different days different combinations of mechaniams and mixing height profiles gave the "best fits" using the standard assumptions. Slight modification in the standard assumptions can dramatically improve the fits. Below is a summary of "best fits" based on examination of CO, NMHC, NO_x and O_3 profiles:

Using Standard Assumptions

Day	Mechanism	Mixing Height	Comment
159	DEMER	CHAR	CB2 LIN also good;
160/03	DEMER	CHAR	LIN better in O_3, but NO_2 bad; CO bad
160/15			None good
195			None good
201	DEMER,DODGE	LIN	O_3 18% low and NO_2 bad; HC bad at end
221	DEMER	CHAR	NO_2 probably within measurement error (lowest day); missed HC peak
238			None good
261	DODGE,DEM	HP	DEM low on O_3, but better shape
275/6am	DODGE	CHAR	O_3 25% low but good shape until last hr.; CO good
275/8am	DEMER	LIN	O_3 19%, low but good shape until last hr.; CO bad
276/6am			None good

Using Modified Assumptions

Day	Mechanism	Mixing Height	Comments
275/8	DEMER	CHAR	5% initial ald gives excellent fit.
275/8	CARB BOND	CHAR	BOM HC composition including aldehyde gives excellent fit
238		LIN	Modification of trajectory/emissions still 25% low only DEM tested
201		HP	Modification of trajectory/emissions only DEM used

9.0 ISOPLETHS AND CONTROL CALCULATIONS

9.1 OZONE ISOPLETHS GENERATED FROM PHOTOCHEMICAL SIMPLE TRAJECTORY MODEL SIMULATIONS

The purpose of generating an O_3 isopleth diagram is to illustrate how the simple trajectory model's maximum predicted O_3 varies as a function of increases and decreases in HC and NO_x initial conditions and emission values. To accomplish this, the trajectory models in the previous chapter were run repeatedly; in each run, the HC and NO_x initial concentrations and the emissions of the standard run were multipled by scale factors. Figure 98 shows an example of the locations of the run points as a function of initial condition of HC and NO_x. These initial conditions also represent the emissions since the same factor was used for each. That is, when the initial conditions were halved, so were the emission values.

When all of the simulations had been run, a bicubic spline surface was fitted to the maximum O_3 and initial conditions. The locations of points of constant O_3 were found by interpolation over this surface. These isopleths are shown as a "level set" by viewing the surface from above ((A) in Figure 99). To aid in comparison, the surface was also "sliced" and its cross-section shown for various conditions (the dotted lines in (A) of Figure 99). Figures will be presented for O_3 as a function of HC 1.0, 0.8, 0.6, 0.4, and 0.2 of maximum NO_x and as a function of NO_x at the same values of maximum HC ((B) and (C) of Figure 99). The location of the ambient data point, that is, the initial ambient HC, initial ambient NO_x, and maximum ambient O_3, is shown on the diagrams as a "+" ((D) and arrows of Figure 99).

Ten isopleth surfaces were done for each of two days: the Demerjian,

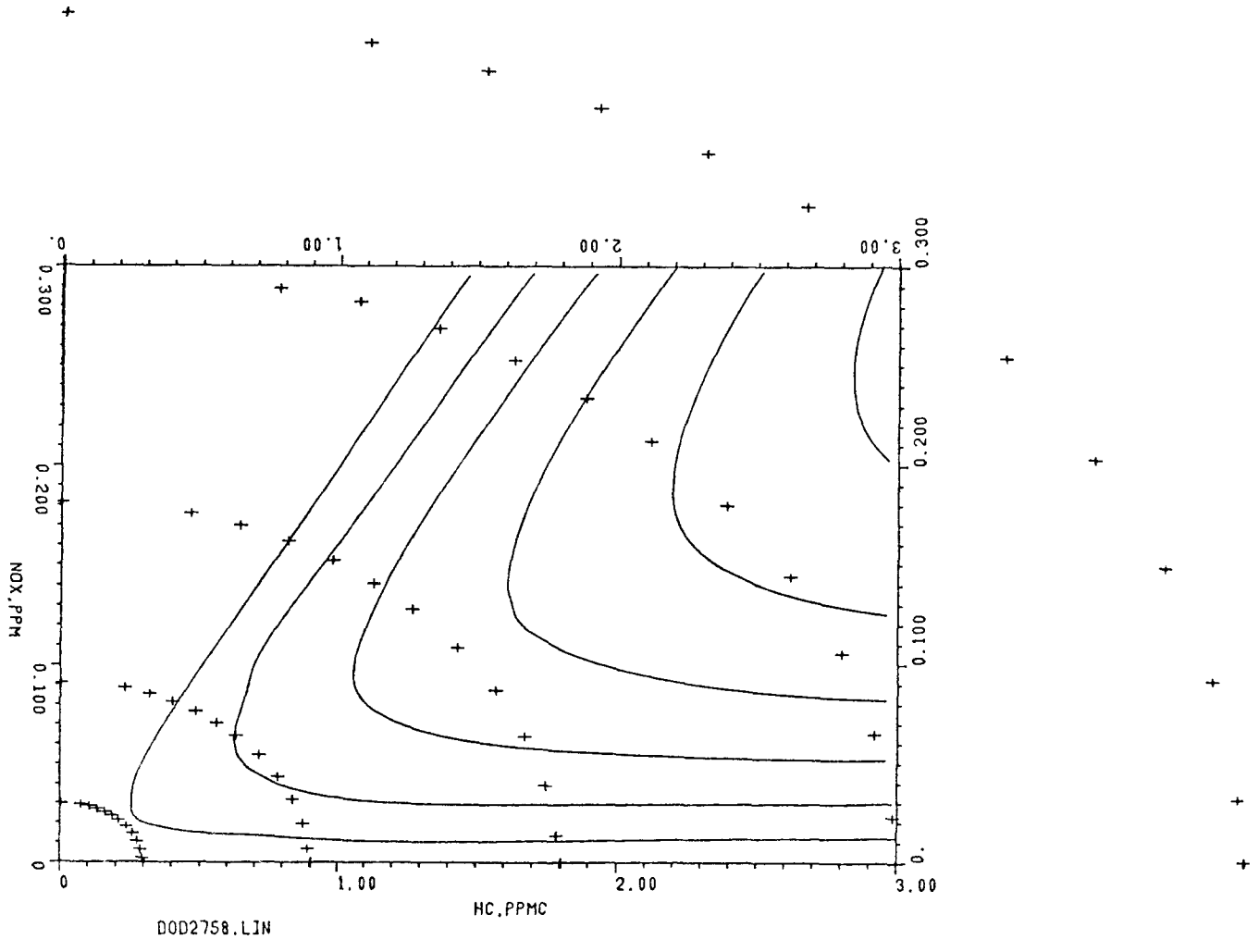

Figure 98. Example of Locations for Simulations Used to Produce an Ozone Isopleth Surface

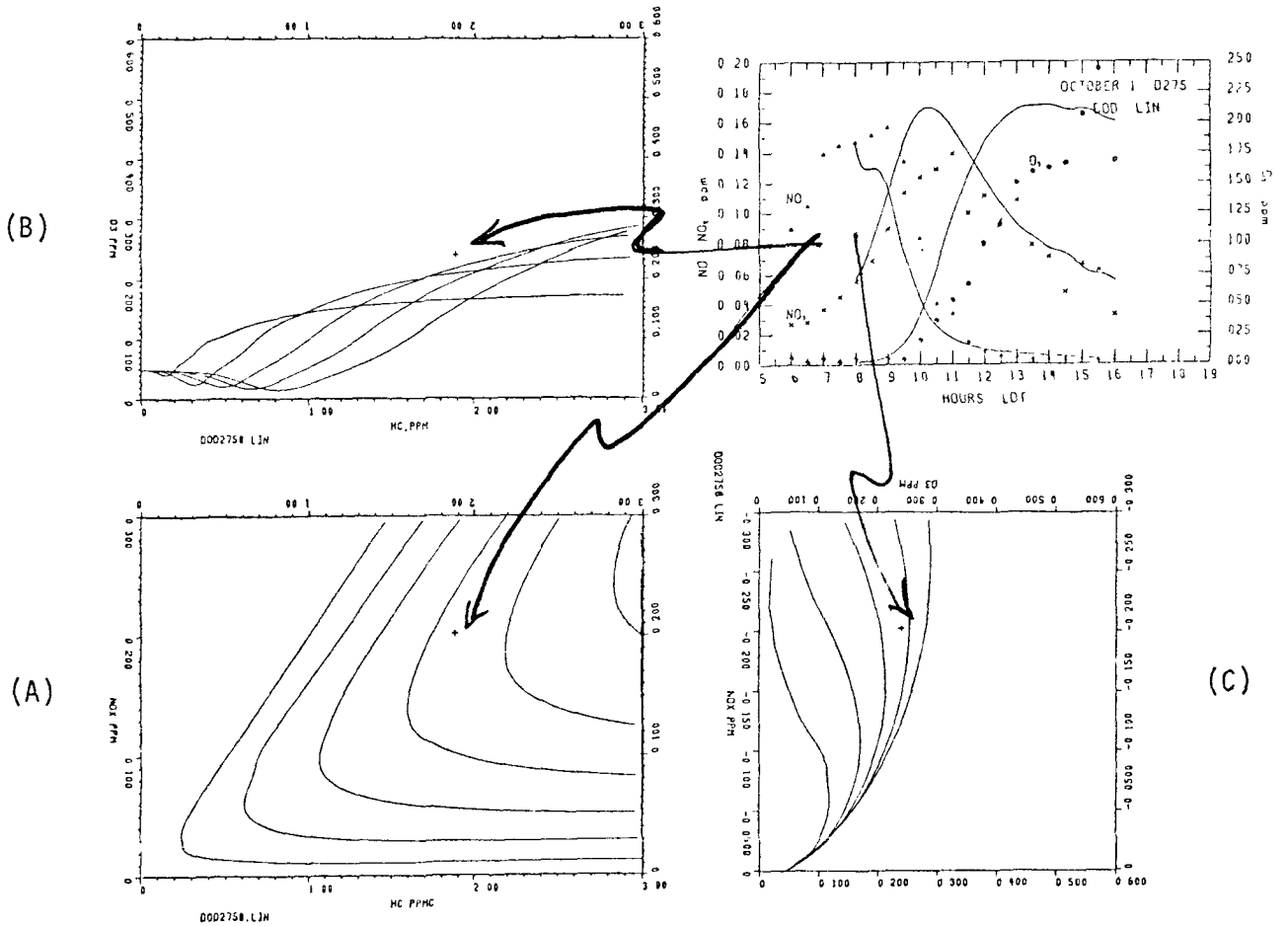

Figure 99. An Ozone Isopleth Surface (A); Surface Sliced at Constant NO_x (B); Surface Sliced at Constant HC (C); Simple Trajectory Model Simulation for Day (D); "+" Identifies Coordinates of Initial Conditions and O_3 Maximum.

Dodge, and CB2 mechanism at each of three mixing height profiles and the CIT mechanism at the characteristic curve mixing height profile, for October 1, 1976, Day 275 at 8 am and for June 7, 1976, Day 159. October 1 was the high O_3 day for the year (0.244 ppm O_3). The initial HC-to-NO_x ratio was 9.4 and the emissions HC-to-NO_x ratio (determined for MOSTM simulation) was 3.35. Of the ten days studied, June 7, 1976 had the highest initial HC-to-NO_x ratio, 13.2, and the highest O_3 aloft (0.12 ppm). It was also the only day simulated well by all mechanisms. The isopleth levels used were: 0.08, 0.12, 0.20, 0.24, 0.28, 0.30, 0.32, 0.34 and 0.40.

The results for October 1, Day 275, are shown in Figure 100 A,B,C,D, E. Recall that this day was underpredicted by DEM2758.LIN simulation, was underpredicted slightly by DEM2758.CHAR simulation, was underestimated about 10% by both the DOD2758.LIN and .CHAR simulations, and was underpredicted greatly by all other simulations (all .HP, all CB2, and CIT.CHAR).

In Figure 100B, there are obvious large difference in the isopleths for different mechanisms-mixing height combinations, even where there were less obvious differences among the PKSTM simulations. The Demerjian, Carbon Bond, and CIT mechanisms have "steeper" sides than the Dodge mechanism. That is, the O_3 formation is more responsive to HC and NO_x in these mechanisms than in the Dodge mechanism. The response to NO_x is so great in the CB2 and CIT mechanisms that they cannot simulate this day. At low NO_x, they exhibit a higher O_3 dependence on HC than Dodge and therefore have more, and more closely spaced, isopleths than Dodge.

The "flatness" in response to HC and NO_x gives the Dodge isopleths a characteristics "U" shape. The other mechanisms have more "V" shaped isopleths. These shapes have important implications for EKMA control calculations which will be discussed in the next section. The U-shaped isopleths

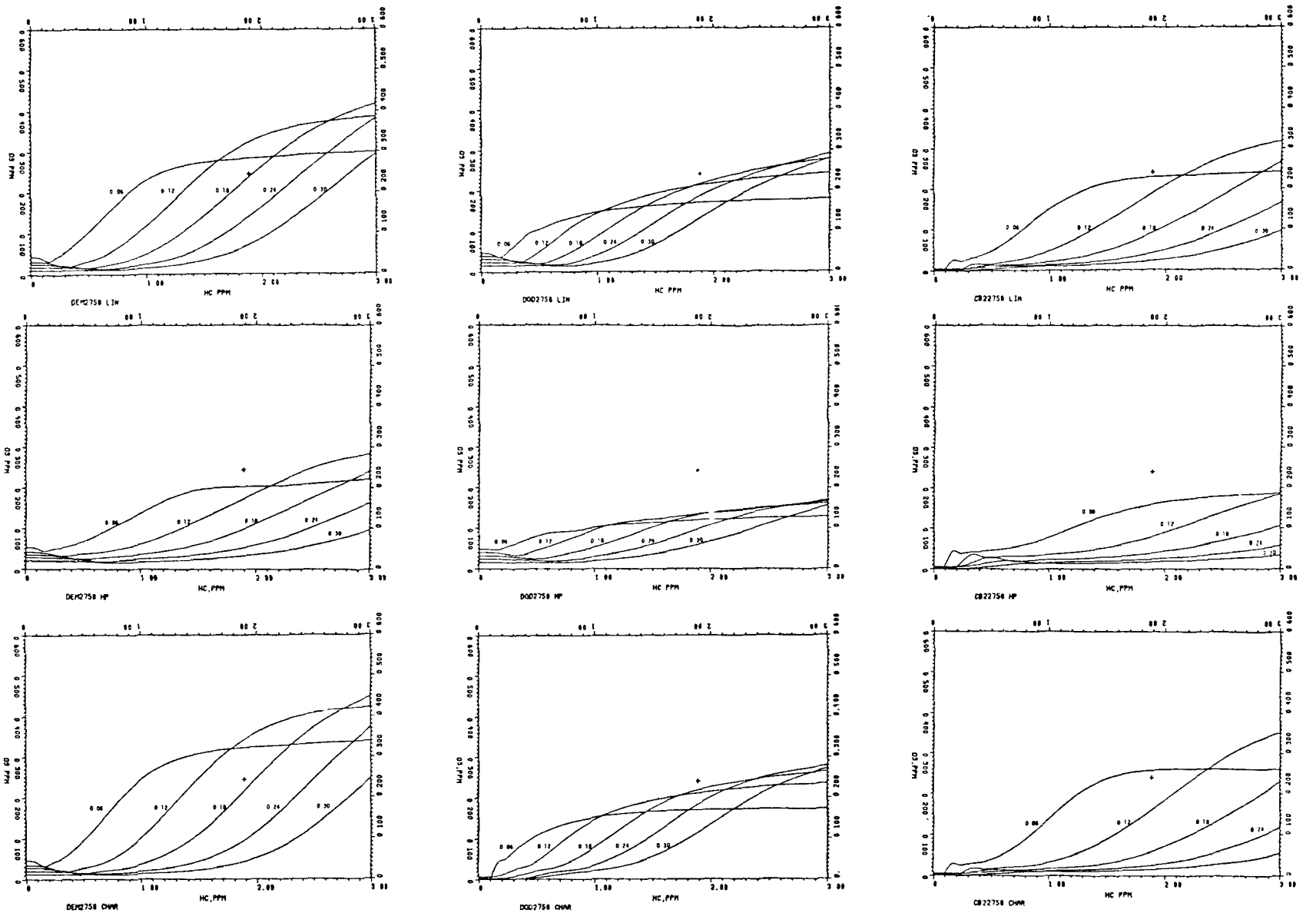

Figure 100A. Ozone-HC cross sections, October 1 simulations.

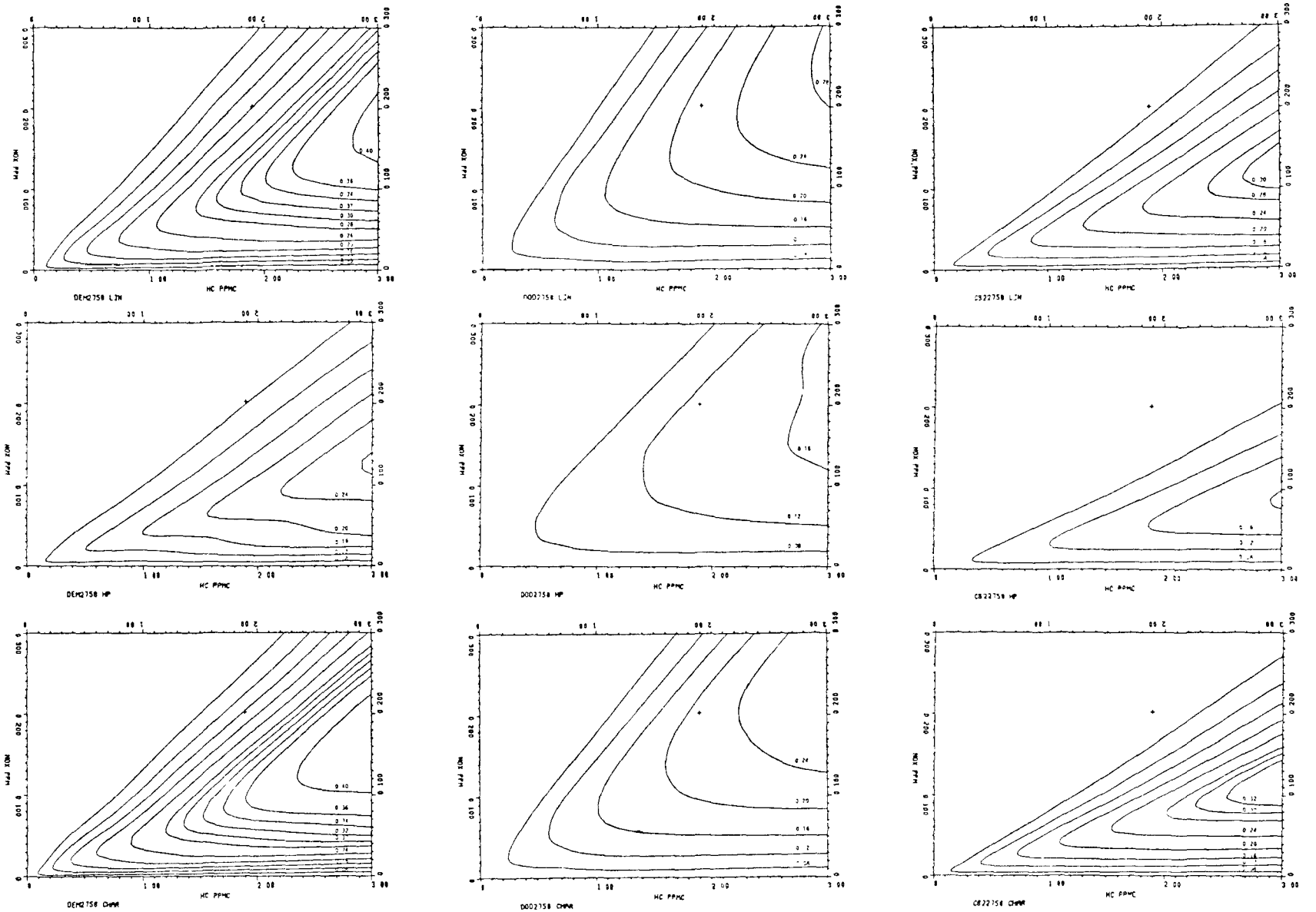

Figure 100B. Ozone isopleths, October 1 simulations.

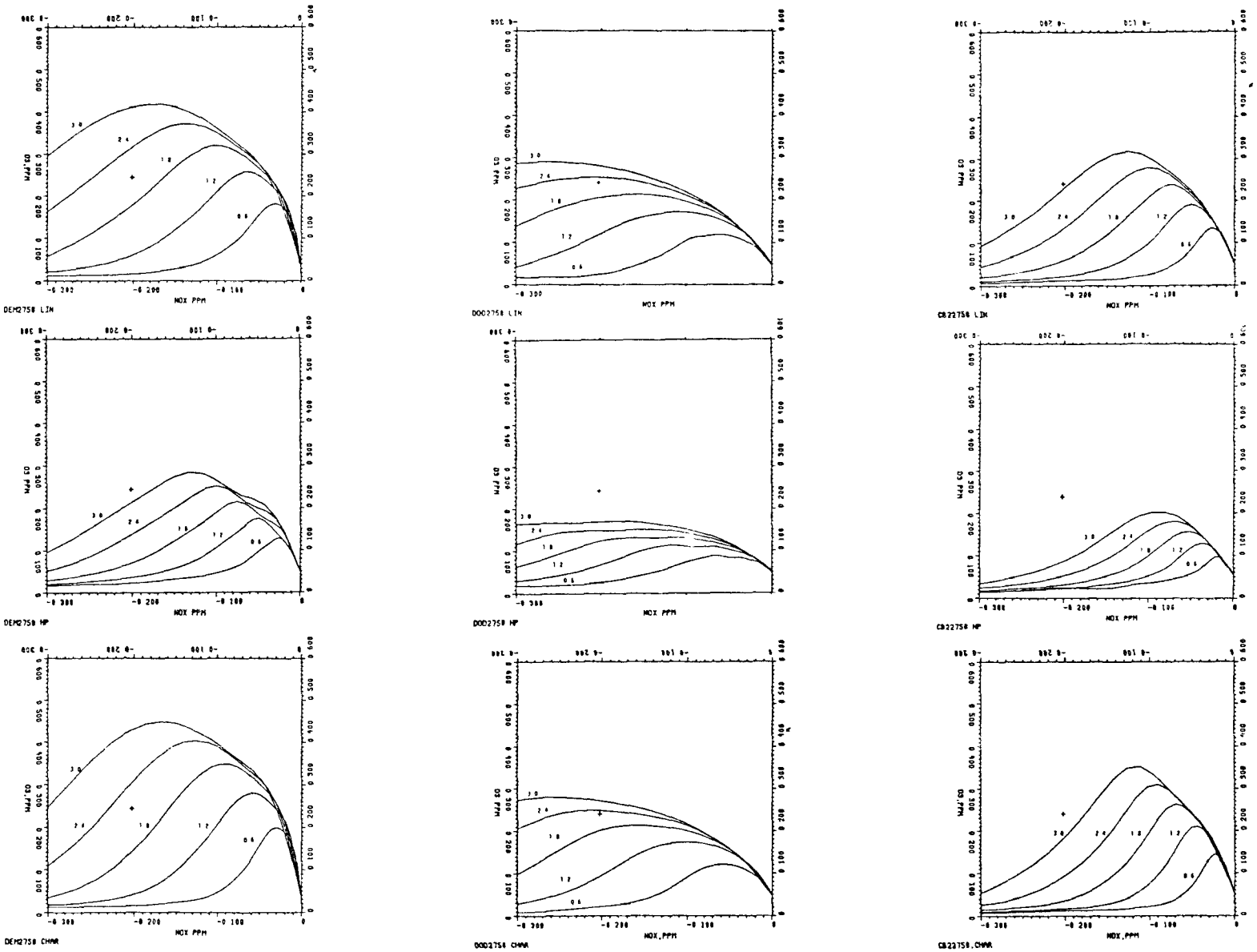

Figure 100C. Ozone-NO_x cross sections, October 1 simulations.

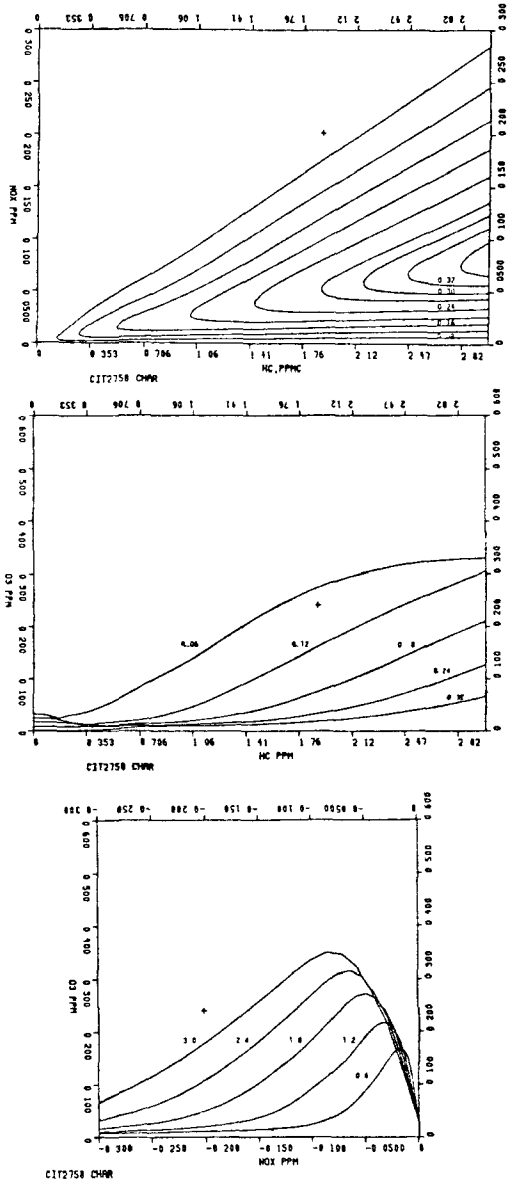

Figure 100D. Ozone isopleths and cross sections for CIT October 1 characteristic curve simulations.

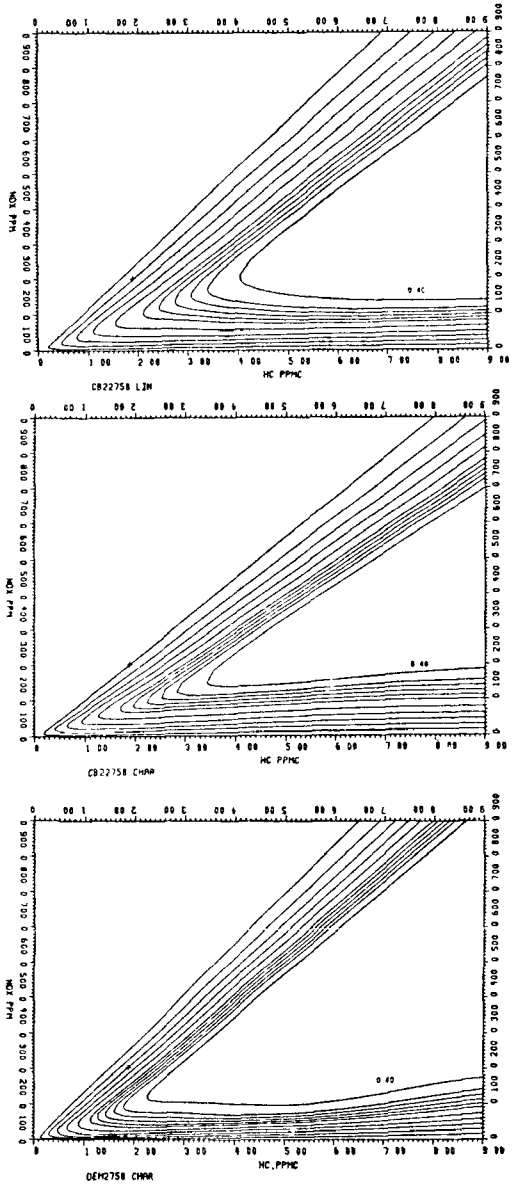

Figure 100E. Ozone isopleths over larger range for Carbon Bond and Demerjian October 1 simulation.

generally "spread" as the HC and NO_x inputs are increased, that is, the isopleth location moves to lower and higher HC-to-NO_x ratios with increasing HC and NO_x values. The V-shaped isopleths, however, tend to parallel a particular HC-to-NO_x ratio as the HC and NO_x inputs are increased, that is a particular O_3 value may never occur at a particular HC-to-NO_x ratio no matter how much HC and NO_x input is used. Figure 100E illustrates CB2 isopleths over a larger range of HC and NO_x than those of Figure 100B. It is evident that the fifth isopleth (0.24 ppm O_3) will never intercept a line drawn through the origin and the "+" which marks the HC and NO_x for October 1. Therefore, mechanisms which exhibit V-shaped isopleths must predict the observed O_3 maximum for present emission conditions (the PKSTM simulation) within reasonably narrow limits (maybe $\pm$10 or 15%) if a standard EKMA procedure is going to be used.

The results for June 7, 1976, Day 159, are shown in Figure 101A,B,C,D. This day was overpredicted by DEM159.LIN simulation, predicted within 5% by DEM159.CHAR, CB2159.LIN, and CIT159.LIN simulations, and was 12% underpredicted by DEM159.HP, was 25% underpredicted by the DOD159.LIN, CB2159.CHAR, and CIT159.CHAR simulations. The rest were more than 25% underpredicted.

The first observation to be made about the June 7th isopleths is that the Demerjian handpicked isopleth is missing. There was apparently a closed isopleth for this condition and the computer code to find isopleths on the O_3 response surface was not designed to deal with closed isopleths, therefore, no surface was depicted.

The second observation is that the O_3 value at the origin was nearly 0.10 ppm O_3 for most surfaces. This is because of the very large value of O_3 aloft on this day. Since the upper left and lower right simulations (zero HC, 0.07 NO_x and 1.0 HC and zero NO_x) interacts with the entrained O_3

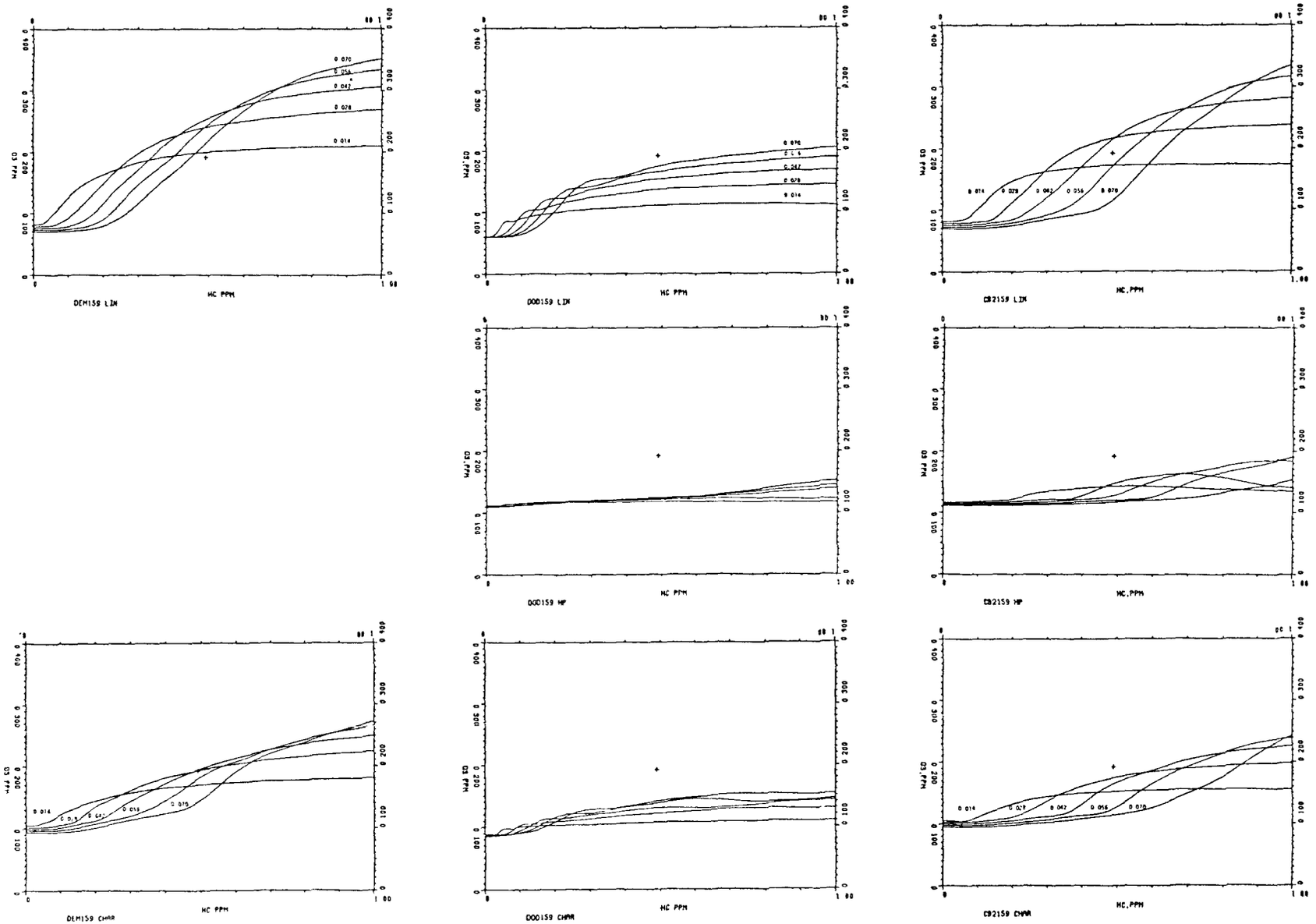

Figure 101A. Ozone-HC cross sections, June 7 simulations.

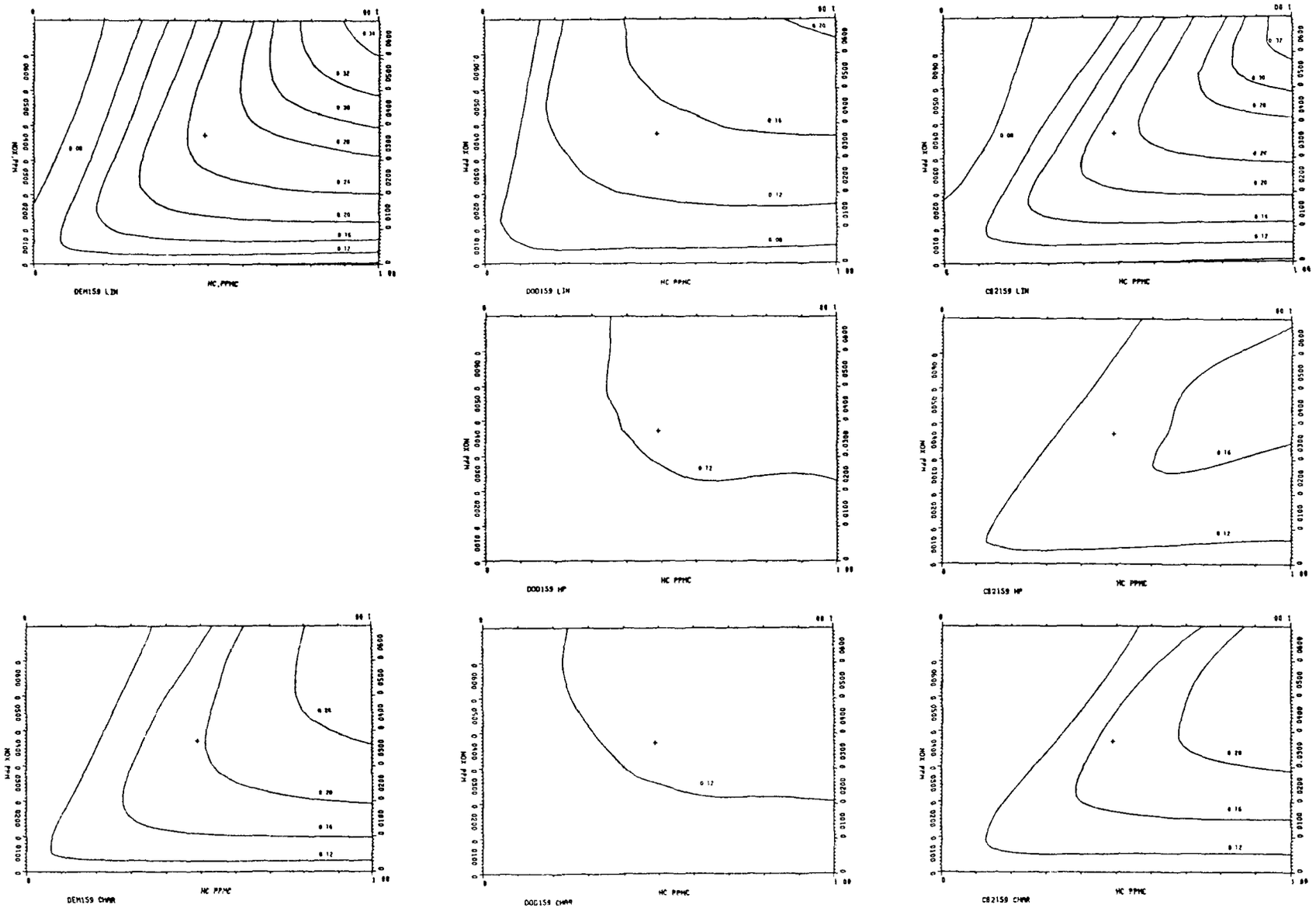

Figure 101B. Ozone isopleths, June 7 simulations.

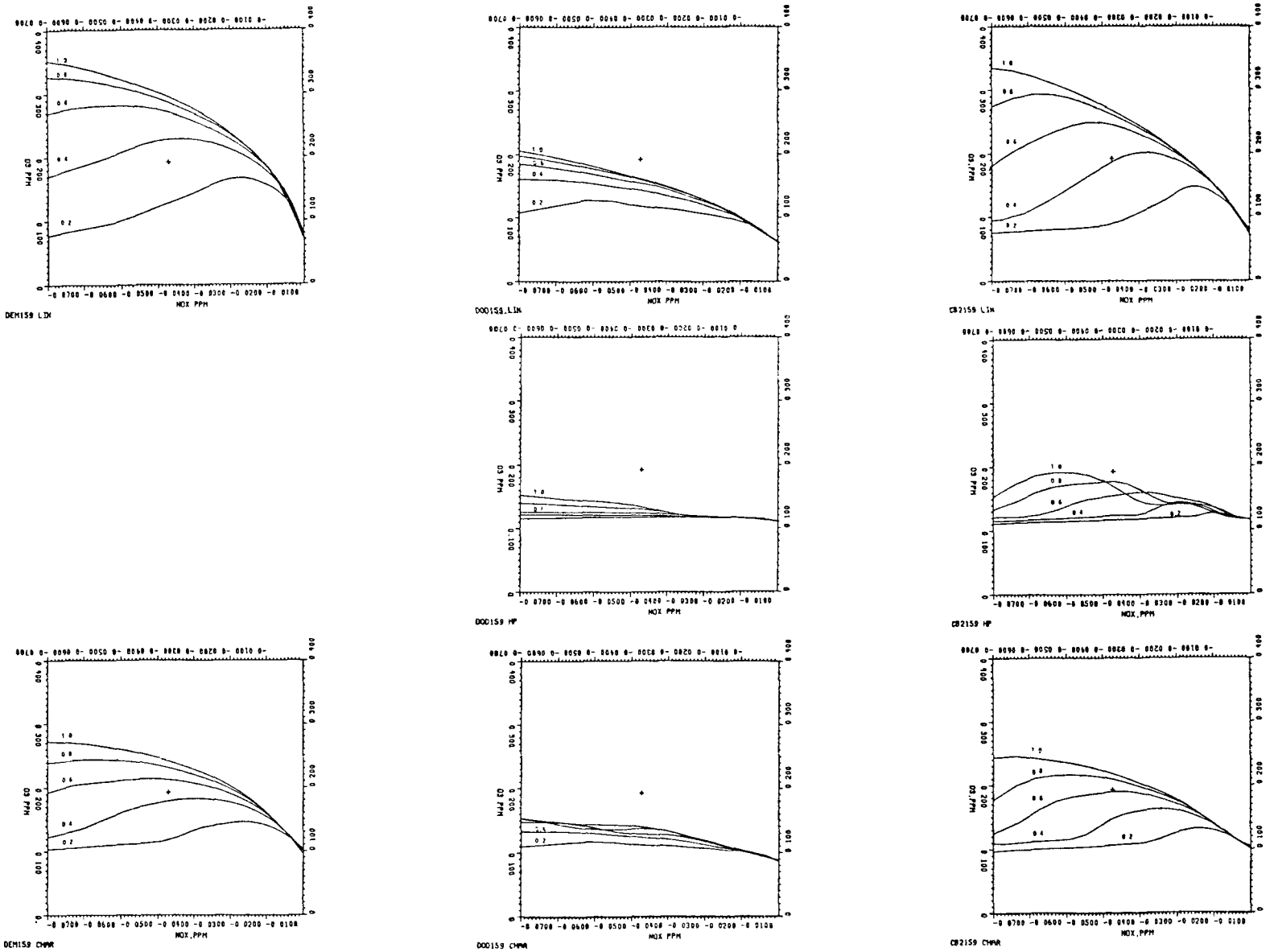

Figure 101C. Ozone-NO_x cross sections, June 7 simulations.

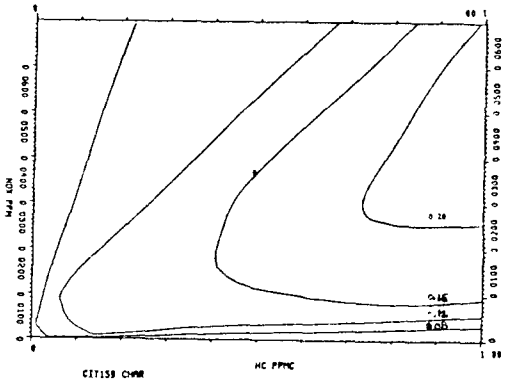

Figure 101D. Ozone isopleth for CIT June 7 characteristic curve simulation.

differently for each mechanism, the O_3 values in the corners are different. This same isopleth surfaces have a 0.08 ppm O_3 isopleth that intercepts the edge and some have no 0.08 ppm O_3 isopleth at all. Because of a high O_3 photolysis reaction (R23 in Table 9) in the CIT mechanism, it consumes O_3 near the origin (Figure 101D), resulting in a 0.08 ppm O_3 isopleth that only touches the HC axis.

The Dodge surfaces exhibit almost no response to HC and only a low response to NO_x. That is, the O_3 vs HC at constant NO_x cross-section plots (Figure 101A),the lines are nearly horizontal but do show increasing O_3 (only slightly for HP and CHAR), increasing constant NO_x levels. As in the isopleths for Day 275, the Demerjian and CB2 surfaces show a much stronger dependence upon both HC and NO_x than the Dodge surfaces.

On Day 275, the LIN surfaces are very similar in appearance to the CHAR surfaces. On Day 159, the LIN surfaces and the CHAR surfaces differ substantially in appearance. These similarities and dissimilarities will be examined further in the EKMA control calculation discussion.

Although somewhat affected by the high O_3 aloft values, the U-shaped versus the V-shaped character of the Dodge versus the Demerjian and CB2 isopleths is still evident. It is expected, therefore, that if the upper right corner values of DOD159.HP and DOD159.CHAR were made high enough, the corner O_3 value would exceed 0.20 ppm O_3, the value needed for an EKMA type calculation for Day 159. These high concentration simulations were not done.

9.2 OZONE CONTROL CALCULATIONS FROM PKSTM ISOPLETHS AND EKMA PROCEDURE

The isopleths in the previous section show the effects of emission changes on simple trajectory model's O_3 predictions. The Emperical Kinetics Modelling Approach (EKMA) is a method for translating the models' response to emission changes into atmospheric control requirements.

Stated in its simplest form, the EKMA procedure is (Figure 102): a) to find the point of interception between a radial line at the initial HC-to-NO_x ratio and the isopleth for the ambient O_3 maximum for this day; b) divide the values on the NO_x axis by the NO_x values at the point of intercept; c) draw a line at constant NO_x through the intersection point, draw a line on which NO_x increased 20% for 50% HC decrease, and draw a line on which NO_x decreased 20% for 50% HC decrease; d) the values of O_3 along these lines as a function of HC fraction are assumed to represent the O_3 values in the atmosphere as a function of ambient HC emission reductions.

Note that in the example in Figure 102, the model was not perfect. That is, the DOD2758.LIN PKSTM simulation, with our best estimates of initial concentrations (0.202 ppm NO_x and 1.89 ppmC HC) and HC NO_x emissions, only produced 0.214 ppm O_3 instead of the observed 0.244 ppm O_3 (observed-to-predicted ratio 1.14). The EKMA solution point occurred at 2.38 ppmC HC and 0.254 ppm NO_x, a ratio of calculated-to-observed initial conditions and emissions of 1.26. In other words, the model's emissions had to be increased by 26% to get 14% more O_3. These increased emissions become the starting point for the control calculations. Following down the O_3-HC fraction line of Figure 102D shows that 0.12 ppm O_3 is reached at a HC fraction of 0.62, that is, to achieve the O_3 standard with no change in NO_x, a 38% reduction in HC is required by this model.

The EKMA solution technique was incorporated into the isopleth generation

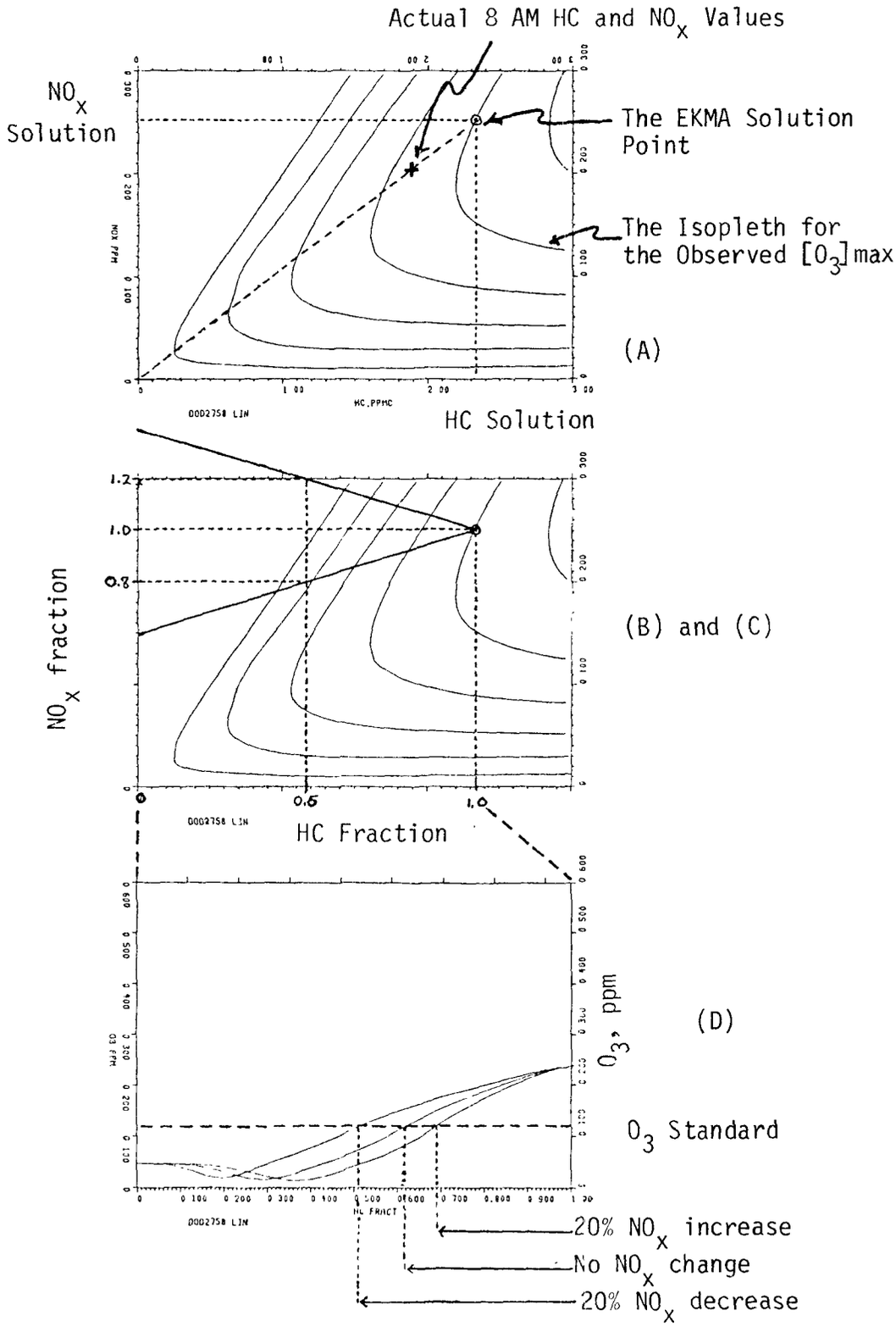

Figure 102. The EKMA Procedure

Table 43. EKMA Solution Points for October 1, 1976 Simulations

Ambient Values[a]		
HC	NO_x	O_3
1.89	0.202	0.244

Mixing Height Profile	DEMERJIAN					DODGE					CARBON BOND				
	PKSTM[b]		EKMA SOLN[b]			PKSTM		EKMA SOLN			PKSTM		EKMA SOLN		
	O_3	r1[c]	HC	NO_x	r2[c]	O_3	r1	HC	NO_x	r2	O_3	r1	HC	NO_x	r2
Linear	0.197	1.239	2.703	0.289	1.43	0.214	1.14	2.333	0.249	1.234	0.068	3.60		-NS-	
HP	0.077	3.16		-NS-[d]		0.130	1.88		-F-		0.033	7.41		-NS-	
Char	0.168	1.452	3.969	0.424	2.10	0.210	1.162	2.439	0.261	1.290	0.041	5.95		-NS-	

[a] All HC units are ppmC, all NO_x and O_3 units are ppm

[b] PKSTM means the photochemical simple trajectory model results
EKMA means the Emperical Kinetics Model approach

[c] r1 is the ratio of ambient value O_3 to PKSTM predicted O_3
r2 is the ratio of EKMA calculated initial conditions to ambient values

[d] -NS- means no solution possible; -NF- means solution not found

Table 44. EKMA Solution Points for June 7, 1976 Simulations

Ambient Values		
HC	NO_X	O_3
0.49	0.037	0.192

Mixing Height Profile	DEMERJIAN					DODGE					CARBON BOND				
	PKSTM		EKMA SOLN			PKSTM		EKMA SOLN			PKSTM		EKMA SOLN		
	O_3	r1	HC	NO_X	r2	O_3	r1	HC	NO_X	r2	O_3	r1	HC	NO_X	r2
Linear	0.252	0.762	0.283	0.021	0.578	0.148	1.30	0.831	0.063	1.696	0.194	0.99	0.371	0.028	0.757
HP	0.164	1.17	no isopleth possible			0.114	1.68	-NF-			0.129	1.49	-NS-		
Char	0.196	0.98	0.477	0.036	0.973	0.128	1.50	-NF-			0.149	1.29	0.672	0.051	1.371

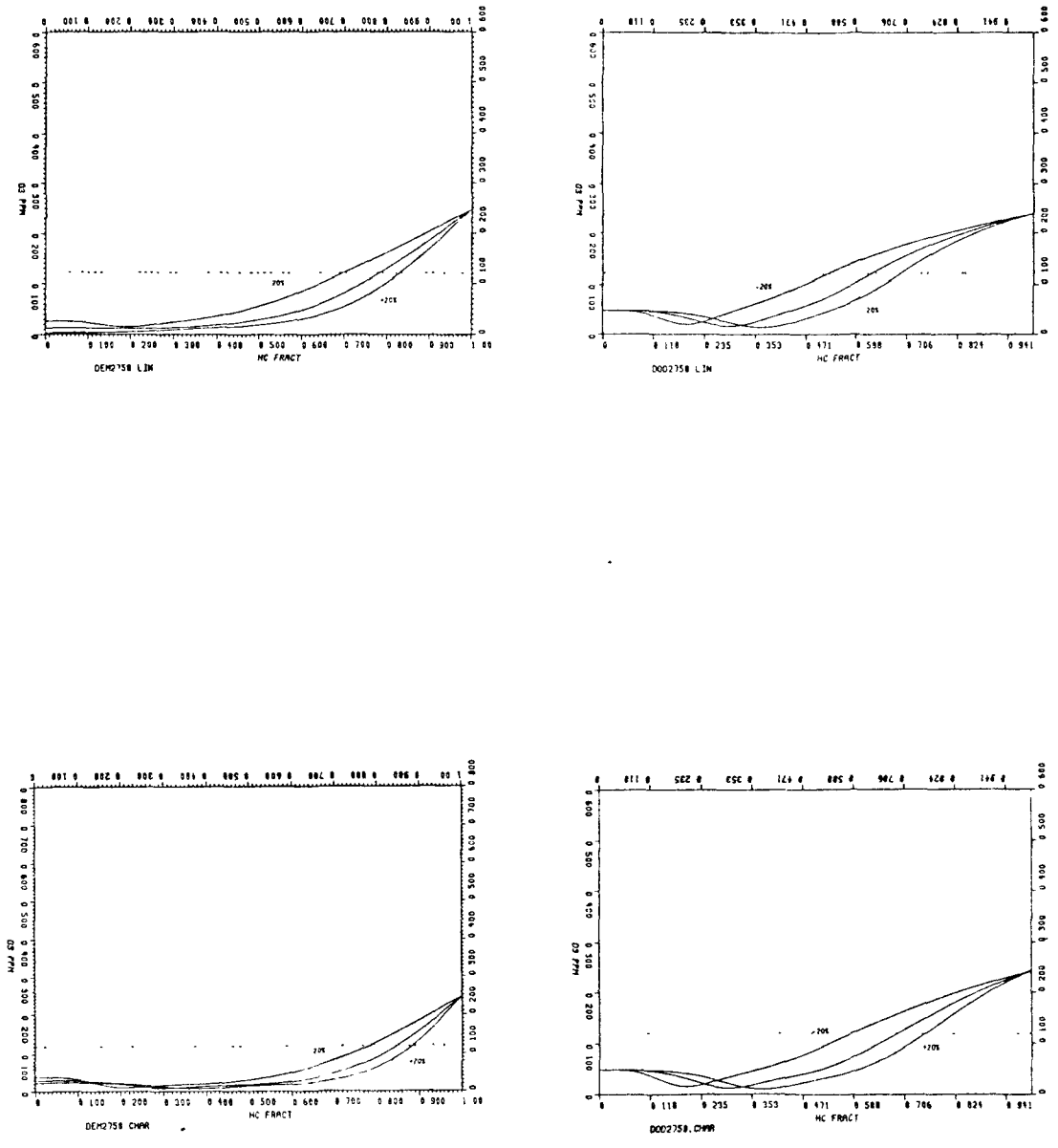

Figure 103. Ozone-HC fraction plots for October 1 simulations.

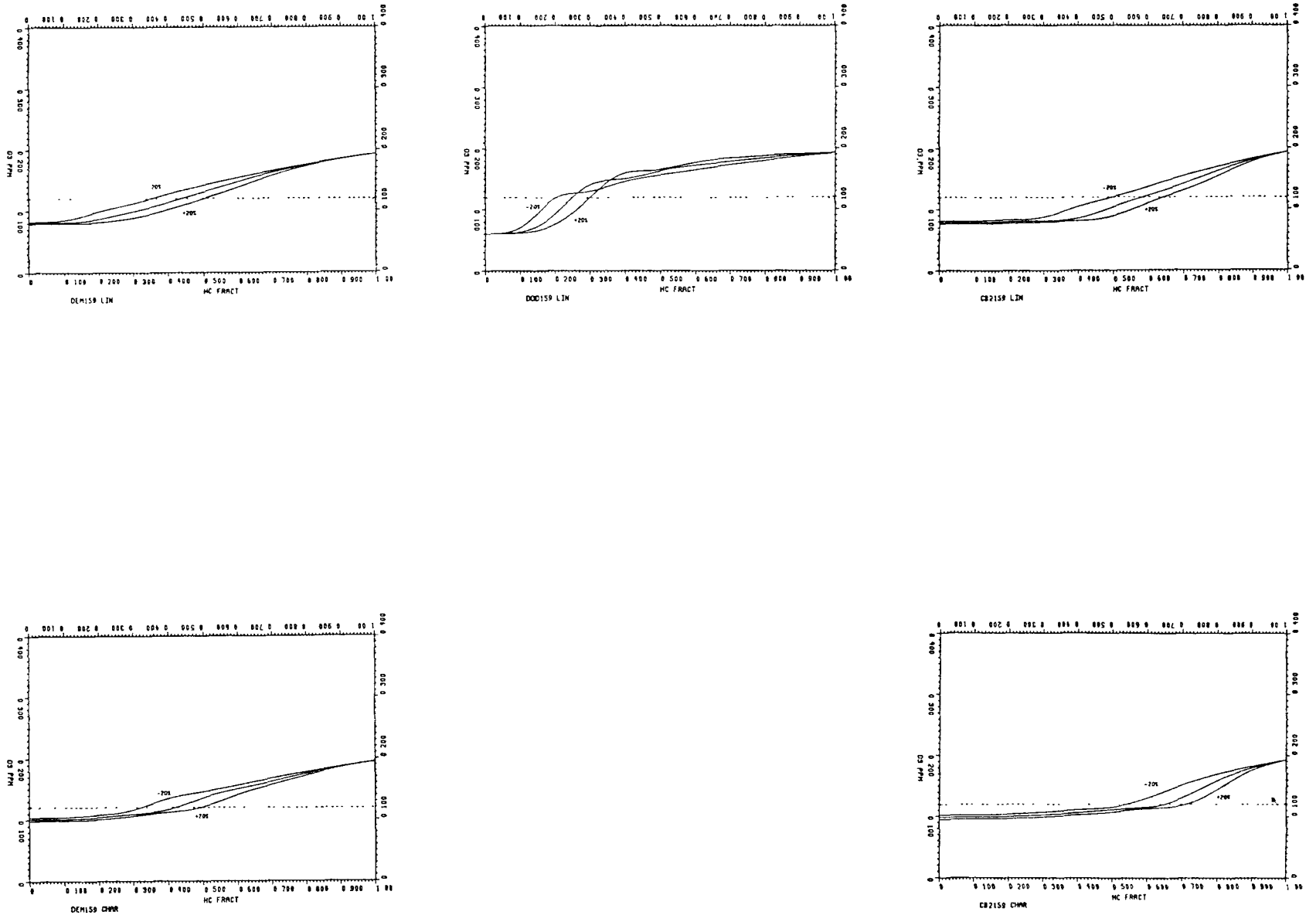

Figure 104. Ozone-HC fraction plots for June 7 simulations.

program, so that the EKMA solution point could be found and O_3-HC fraction plots automatically produced. The procedure was applied to the ten isopleths for October 1 (Day 275) and the nine isopleths for June 7 (Day 159) and the results are shown in Table 43 and 44 and Figures 103 and 104. As had been indicated in the isopleth discussion of the previous chapter, not all isopleths produced solutions, and some could not, even if 100 times the initial conditions were used.

The data in Figures 103 and 104 have been converted into control diagrams, that is, plots of percentage O_3 reduction versus percentage HC reduction, and these are shown in Figures 105 to 106. The HC reduction necessary to achieve the 0.12 ppm O_3 value are summarized in Table 45 and in Figure 107.

From Figure 107 it is evident that the most important factor in the amount of HC reduction needed was the choice of day. Day 159 (June 7) was not the day of highest O_3; it was the day with maximum O_3 aloft (0.12 ppm). This O_3 aloft is not reduced by emissions reductions in the same manner that O_3 produced from emissions is reduced by emissions reductions. This resulted in "flatter" ozone control diagrams (Figure 106).

The next most important factor in the amount of HC reduction needed was the chemical mechanism used. When it could give a solution, the Carbon Bond mechanism gave the least HC reduction needed (other conditions the same). The Demerjian mechanism, when it could give a solution, always required less HC reduction than Dodge (other conditions the same).

The third most important factor was the choice of mixing height profiles. The characteristic curve profile, in general, required less HC reduction than the linear profile. Except for the Dodge mechanism, solutions were not possible with the handpicked profile. For the Dodge mechanism, the hand-

Table 45 . Percent HC Reduction to Achieve 0.12 ppm O_3 Predicted by Models for October 1, 1976 and June 7, 1976

Mixing Height Profile	Demerjian			Dodge			Carbon Bond		
	-20% NO_x	0% NO_x	+20% NO_x	-20% NO_x	0% NO_x	+20% NO_x	-20% NO_x	0% NO_x	+20% NO_x
October 1									
Linear	30	22	17	48	38	31		-NS-	
HP		-NS-		27	20	15		-NS-	
CHAR	22	15	12	42	31	25		-NS-	
June 7									
Linear	65	56	50	79	75	70	50	41	35
HP		-NS-			56			-NS-	
CHAR	67	57	50		-NF-		45	35	28

[a] -NS- means no solution possible

-NF- means no solution found in concentration range

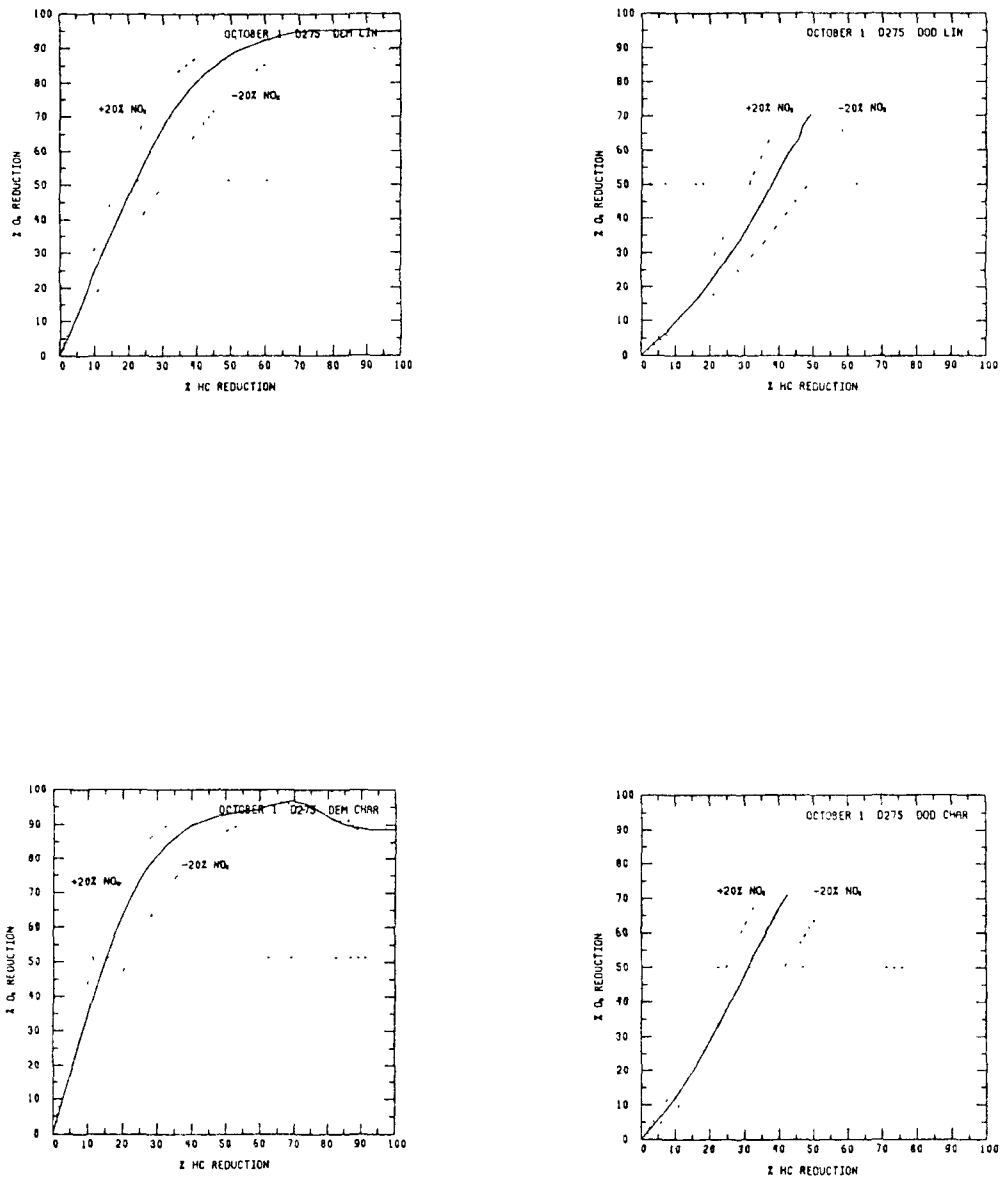

Figure 105. Ozone control diagrams for October 1. Dashed line is reduction needed to reach 0.12 ppm O_3.

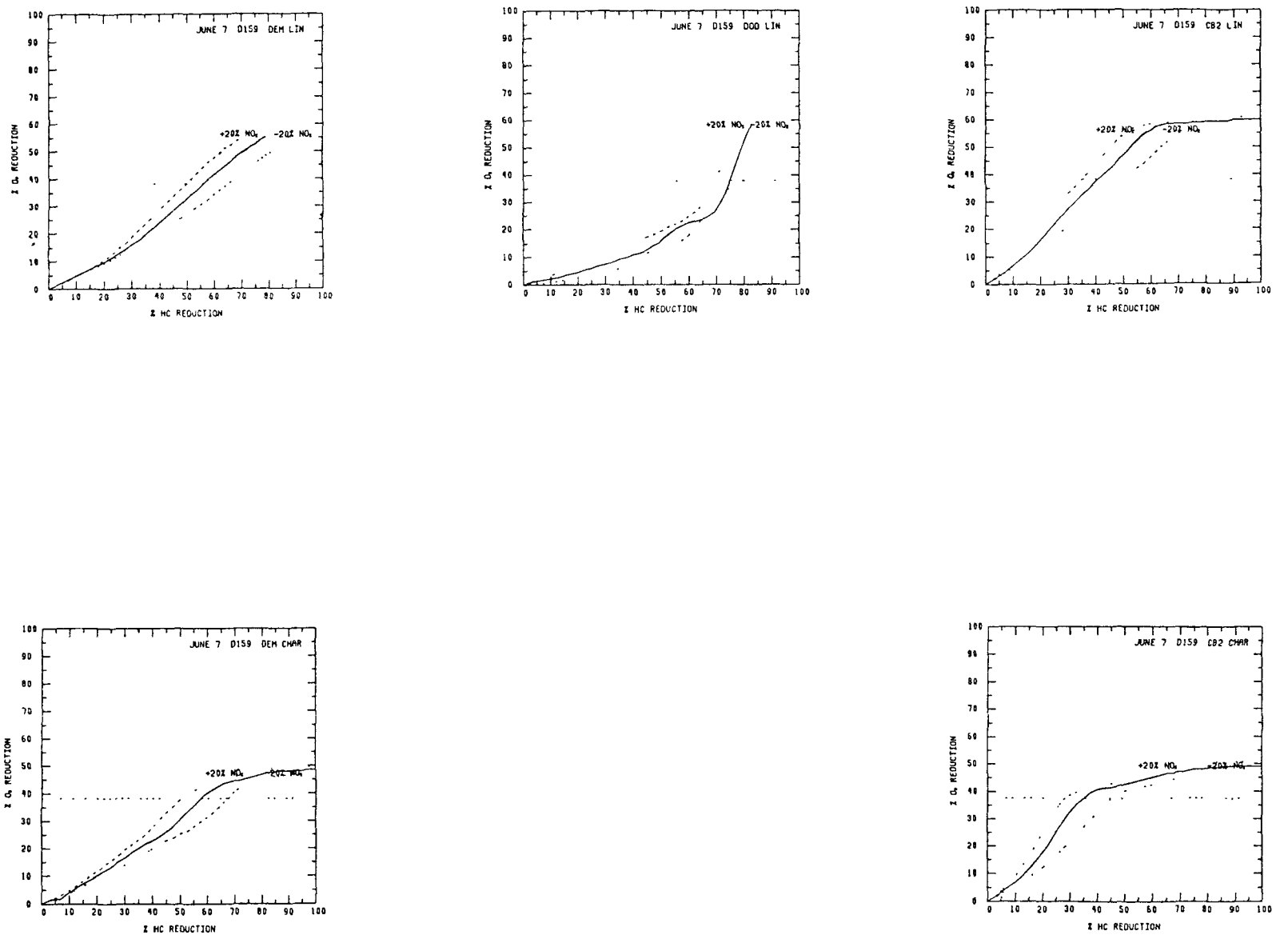

Figure 106. Ozone control diagrams for June 7. Dashed line is reduction needed to reach 0.12 ppm O_3.

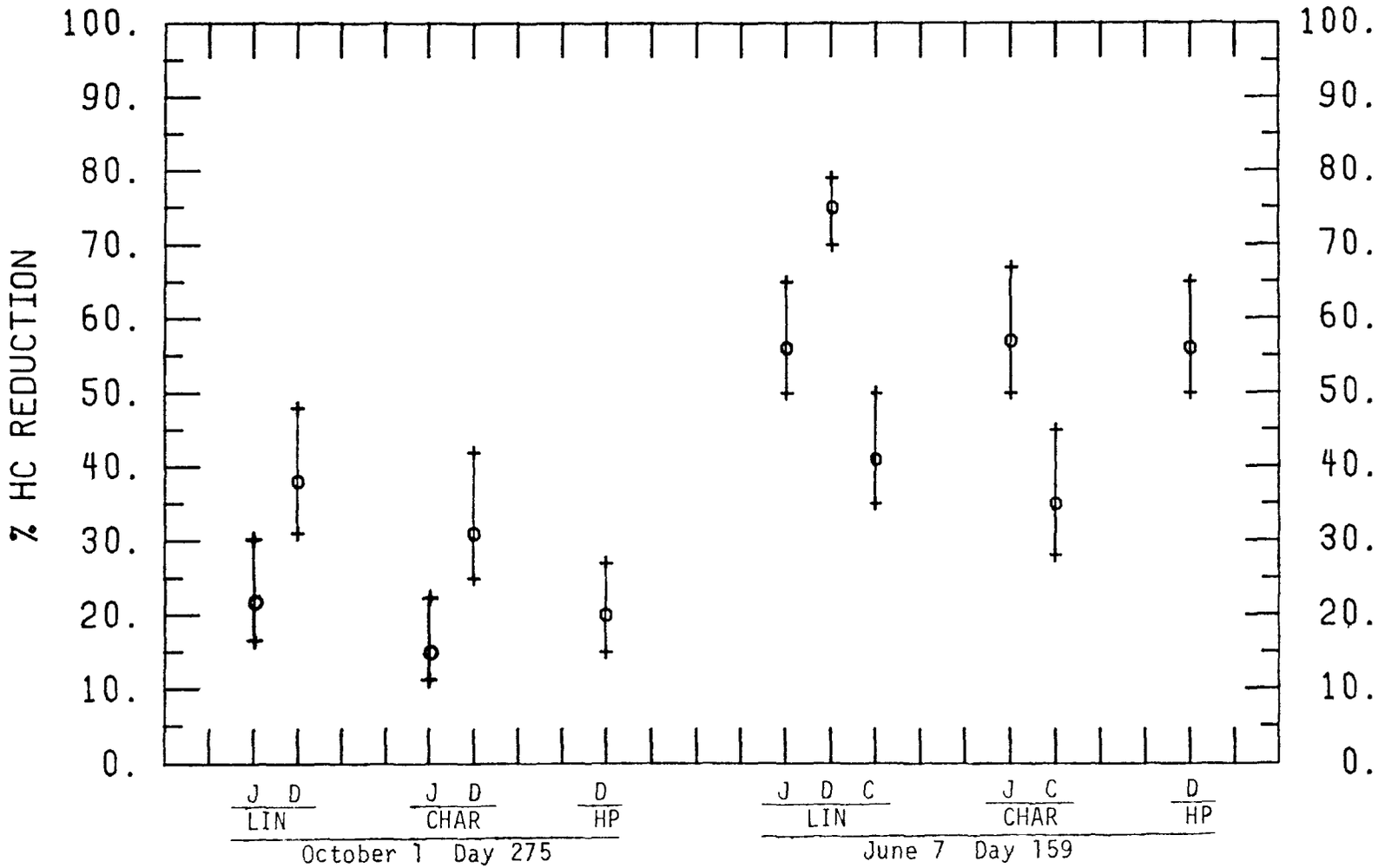

Figure 107. Control predictions by day by mechanism. J=Demerjian, D=Dodge, C=Carbon Bond Mechanisms. LIN=linear, HP=handpicked, CHAR=characteristic mixing height profiles.

picked profile gave lower control requirements than the other profile. These solution points, however, were often at very large HC and NO_x concentrations.

10.0 RAPS SIMULATION WITH LEVEL III MODEL

A Level III analysis has much less stringent data requirements than a Level II analysis because of simplifying assumptions inherent in the Level III model. The Level III model assumes that the air parcel containing the measured O_3 maximum originated in mid-city at 8:00 am, traveled in a straight path at a uniform speed such that the parcel would arrive at the monitoring station at the time that the ozone maximum was measured. Therefore a back trajectory need not be calculated and an extensive wind direction-speed monitoring network is not required. Wind direction data is only required to insure positive identification of the correct downwind monitoring station. A gridded emission inventory is not required. Only city or county wide average emissions are utilized, since the actual trajectory is not determined.

The air quality data requirements are also much less for Level III. Only three O_3 monitoring sites and one or two THC/CH_4 and NO_x monitoring sites are recommended, as compared to the 7-11 O_3 and 4-6 THC/CH_4 and NO_x sites recommended for Level II modeling.

Control requirements are estimated using procedures described in EPA 1981. These are estimated using the ozone design value and prevailing 6-9 am $NMHC/NO_x$ ratio to identify a starting point on the isopleth diagram.

10.1 LEVEL III INPUTS AND CONDITIONS

Three of the ten days previously simulated with the Level II approach were picked to be simulated with the Level III approach: D159, D195, and

D275. Only the Demerjian and Carbon Bond II mechanisms were used. Level III isopleths utilizing the Dodge mechanism for these days were supplied by OAQPS/EPA.

As explained in the EPA EKMA guidance document (EPA 1981), Level III assumptions include an initial morning 8:00 am mixing height of 250 meters. Additional simulations and isopleths were performed with the Demerjian mechanism with assumed initial mixing heights of 350 meters for comparison. Only the characteristic curve for mixing height profile was utilized. In each case, the measured final mixing heights were used in the characteristic curve calculation. The input data were supplied by OAQPS/EPA.

The initial conditions of NMHC and NO_x, the observed O_3 maxima, the initial and final mixing heights, and the assumed county/hr path for each day are given in Table 46. The county emission densities are given in Table 47. The NMHC distribution and carbon fractions are shown in Table 48. The latter values were recommended by Demerjian (personal communication, 1981).

For comparison with Level II simulations (Figure 79), Figures 108 and 109 show the plots of NO, NO_2, and O_3 profiles along the assumed trajectories for each simulation. Note that two mixing heights (250 meters and 350 meters) were used for the Demerjian simulations.

Table 49 lists the O_3 maxima predicted for each simulation, the observed O_3 maxima for the day, and the ratio of the two values. Also included in Table 49 are the Level II simulations results for comparison with the Level III results.

An important point is that although the Level II simulations end at the time (hour) of the observed O_3 maximum the guidance suggests that Level III simulations be commonly performed for 10 hours regardless of the time of

Table 46. Initial Conditions and Observed $[O_3]$ Max for Level III Simulations

Item	D159	D195	D275
$[NMHC]_o$, ppm	1.79	0.26	1.90
$[NO_x]_o$, ppm	0.205	0.048	0.236
$[O_3]$ max , ppm	0.192	0.210	0.244
Max Time	1700	1700	1600
$[O_3]$ aloft , ppm	0.12	0.074	0.06
Init Mix Ht. , m	250,350	250,350	250,350
Final Mix Ht. , m	1900	1800	900

Trajectory

Hour			
800	St. Louis City	St. Louis City	St. Louis City
900	"	"	"
1000	"	"	"
1100	St. Louis Co.	"	"
1200	St. Charles Co.	"	"
1300	"	"	"
1400	Madison Co.	"	"
1500	"	"	"
1600	Jersey Co.	St. Louis Co.	"

Table 47. Area Wide Emission Densities for Level III Simulations

County	Kg-mole/ (Km^2-hr) HC	Kg-mole/ (Km^2-hr) NO_x	ppm(C)-Km/hr HC	ppm(C)-Km/hr NO_x
St. Louis City	2.716	0.465	0.06641	0.011362
St. Louis County	0.533	0.148	0.01305	0.003634
Madison	0.163	0.044	0.00406	0.002254
St. Charles	0.070	0.092	0.00174	0.001058
Jersey	0.014	0.003	0.00029	0.000092

Table 48. NMHC Compositional Carbon Fraction[a] for Morning Initial Conditions and Emissions for Level III Simulations (from Demerjian 1981)

Species	Initial	Emissions	Avg. Carbon Number
NR	0.12186	0.12791	3.0
OLE	0.18195	0.19089	3.0
PAR	0.43596	0.47965	6.3
ARO	0.18549	0.17054	7.1
ALD	0.07478	0.03101	2.0

[a]To obtain ppmV for each class, multiply total NMHC in ppmC units by fraction and divide by average carbon number.

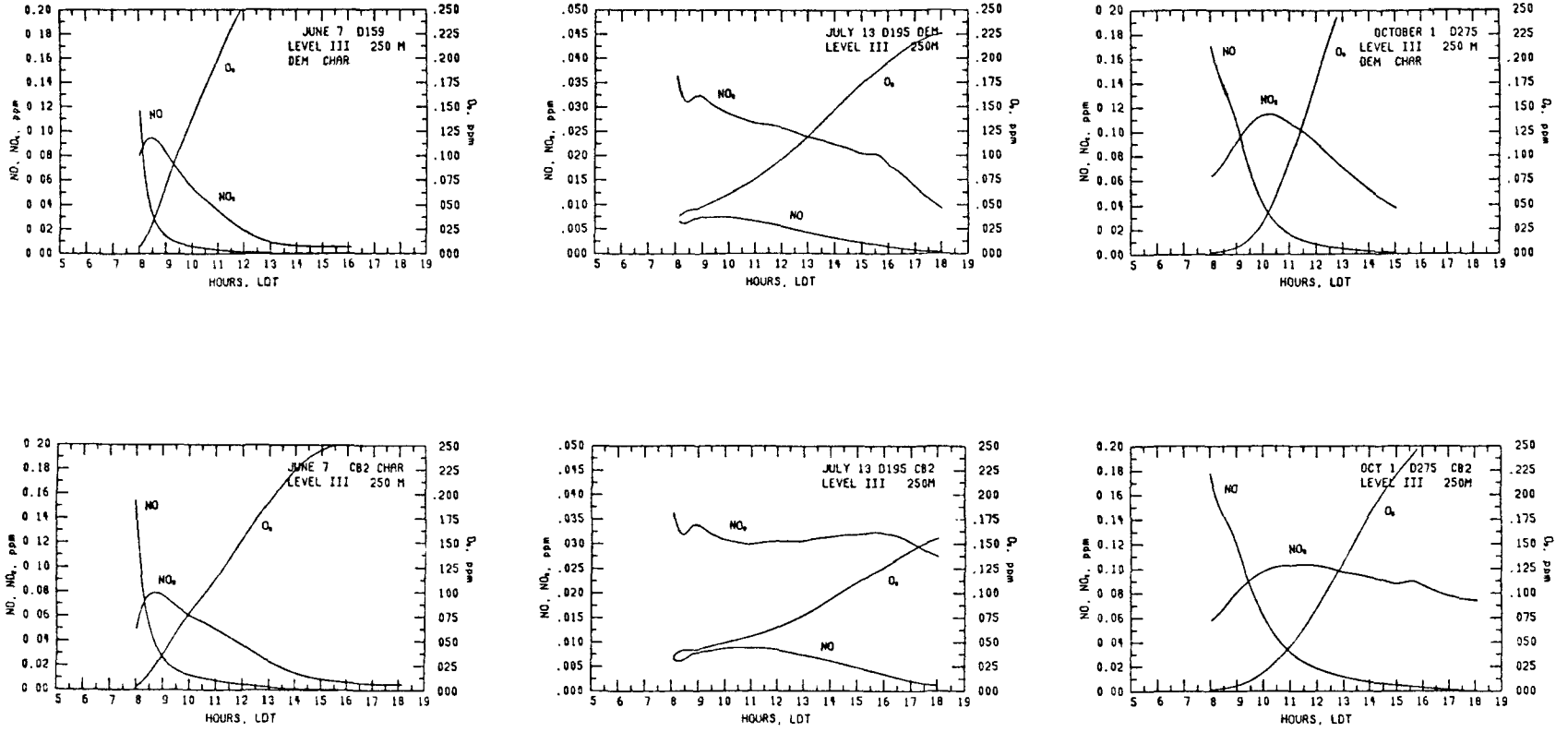

Figure 108. Level III simulations for three RAPS days (159, 195, and 275) using 250 m initial mixing height for Demerjian and Carbon Bond II mechanisms.

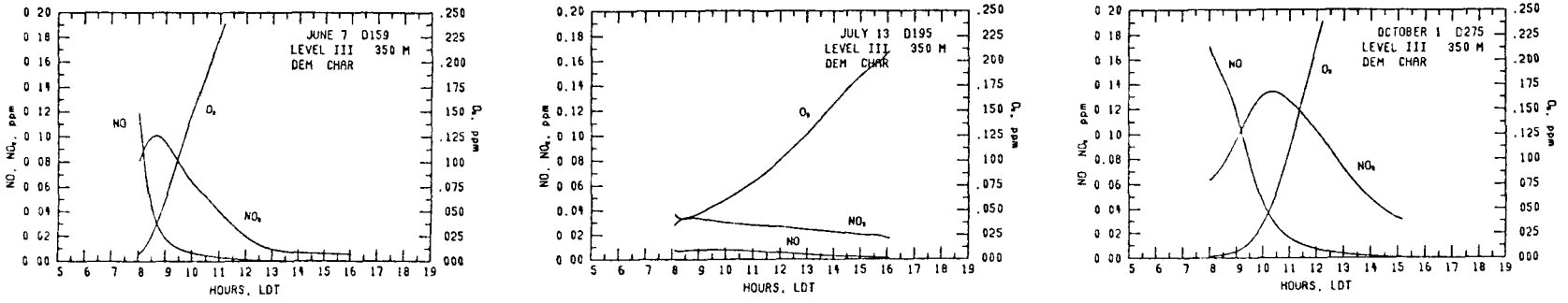

Figure 109. Level III simulations for three RAPS days (159, 195, and 275) using 350 m initial mixing height for Demerjian mechanism.

Table 49. Ozone Maxima Predicted in Level III Simulations of Selected RAPS Days. Comparison with Level II Simulations

Item	June 7 (159)		July 13 (195)		Oct 1 (275)	
ACTUAL DATA						
$[O_3]$ max, ppm	0.192		0.210		0.244	
Time max	1700		1700		1600	
LEVEL III SIMS.						
DEM/250 M[a]						
$[O_3]$ pred	0.302		0.216	0.226	0.418	0.418
Time pred	1700		1700	1800	1600	1800
R1[c]	0.636		0.972	0.929	0.584	0.584
CB2/250 M[a]						
$[O_3]$ pred	0.260	0.262	0.143	0.156	0.250	0.282
Time pred	1700	1800	1700	1800	1600	1800
R1	0.738	0.733	1.469	1.346	0.976	0.865
DEM/350 M[a]						
$[O_3]$ pred	0.332		0.210		0.458	
Time pred	1700		1700		1600	
R1	0.578		1.00		0.533	
LEVEL II SIMS.						
DEM/CHAR[b]						
$[O_3]$ pred	0.197		0.133		0.168	
Time pred	1700		1700		1600	
R1	0.975		1.579		1.452	
CB2/CHAR						
$[O_3]$ pred	0.154		0.097		0.081	
Time pred	1700		1700		1600	
R1	1.247		2.165		3.012	

[a] Code is DEM = Demerjian Mechanism; CB2 = Carbon Bond II Mechanism number after / is initial mixing height in meters; characteristic curve used in all level III simulations.

[b] Code is same as in a; CHAR = characteristic curve using individual day's initial mixing height.

[c] R1 is ratio of actual day's O_3 to simulation predicted O_3.

the observed O_3 maximum. Therefore, Table 49 lists two sets of values for some simulations to indicate the effects of the extra time.

10.2 DISCUSSION OF DAILY SIMULATIONS

Level III simulations predicted much higher $[O_3]$ max than the Level II counterparts (see Table 49). Only one simulation, CB2/D195 underpredicted the observed $[O_3]$ maximum. For the Level II simulations of these three days, only one (D159, a day dominated by high O_3 aloft) was overpredicted (the Demerjian mechanism, by ~2%).

There are three major reasons for these results:

1) Level III simulations start in center city with 250 meter mixing heights and maximum center-city concentrations resulting in more mass initially present than in Level II;
2) the average hourly emissions of HC and NO_x are often higher in Level III simulations than average emission values in Level II simulations, because the assumed trajectories start in a high emissions density region; and
3) differences occurred in assumptions of emission inventory composition in Level III as compared to Level II.

Initial concentrations in Level III simulation are commonly higher than Level II since it is assumed that the trajectory originates in the middle of the city. The morning mixing height assumed (250 m) is often higher than the morning mixing height used in Level II. These conditions tend to result in greater amounts of mass initially present in the Level III air parcel. This can be illustrated by conversion of the initial conditions for HC and NO_x and the assumed mixing height into equivalent emission terms

(i.e. ppm-km units) and comparison of the values with the post 8 am emissions. This has been done in Table 50. The table shows that two of the Level III simulations are clearly initial condition dominated (D159 and D275).

Since the Level III approach assumes that the trajectory travels from mid-city straight to the downwind station which measured the $[O_3]$ max, the average hourly emissions of HC and NO_x can be higher than average emissions in Level II simulations (D195 in Table 50). This would be especially true when the trajectory in the Level II simulations traversed the edge of the city as was the case for D195. Consequently, Level III simulations can have more mass input from emissions into the parcel than Level II simulations.

The third reason for differences between these Level III and Level II simulations is related to the emission inventory assumptions of these two versions. Level II simulations require a rather extensive emission inventory. Level III does not. It has been shown that the aldehyde fraction of both the initial HC concentrations and consequent emissions is a key parameter in the photochemistry represented in this study. The Level II inventory provided aldehyde fractions which were used in the Level II simulations. The fraction ranged from ~1-3% for the 10 days studied. These may be rather low values. The fact is, however, that the inventory was conducted and these values were reported. A Level III simulation does not require an extensive inventory, but rather uses county wide average data. It is not probable that an inventory of this type would include satisfactory aldehyde data. Therefore this value would need to be approximated.

Based on his extensive knowledge of the emissions inventory for St. Louis, Demerjian estimated the values given in Table 48. He used morning, ambient, detailed hydrocarbon analysis to aid in estimating the initial conditions.

Table 50. Comparison of Initial and Emission Mass for Level II and Level III Simulations

			NMHC, ppmC-Km			NO_x, ppm-Km		
Day	Sim	MHi	conc*MHi	Average Emission	Total Emission	conc*MHi	Average Emission	Total Emission
159	II	272	0.133	0.026	0.234	0.010	0.0038	0.0346
	III	250	0.448	0.025	0.224	0.081	0.0049	0.0441
	III	350	0.627					
195	II	1100	0.120	0.031	0.185	0.006	0.0064	0.0383
	III	250	0.065	0.060	0.544	0.012	0.0105	0.0945
	III	350	0.091					
275	II	109	0.206	0.036	0.288	0.022	0.011	0.0856
	III	250	0.475	0.066	0.531	0.059	0.011	0.0909
	III	350	0.665					

The morning initial aldehyde fraction is an estimate made by Demerjian. These values were used in the Level III simulations herein.

D159

Discussion for June 7. The observed $[O_3]$ max was 0.192 ppm. Table 49 gives the Level II and III simulation O_3 maxima. Both Carbon Bond II and Demerjian mechanisms were used with a 250 m initial morning mixing height and the Demerjian mechanism was also used with a 350 m mixing height. All the Level III simulations overpredicted (36-73%) while only Demerjian overpredicted at Level II (~2%); and CB2 underpredicted in the Level II simulation by 20%. The reasons for these differences in simulations are readily explained. The overriding factor for D159 was the difference in the assumed initial location and initial conditions of HC and NO_x. The initial mixing height in both cases were almost identical: 250 m in Level III and 272 m in Level II (characteristic curve). The initial HC, however, was 0.49 ppmC for the Level II simulation and 1.79 ppmC for the Level III because of the differences in the assumed starting point of the trajectories (see Figure 31). The NO_x initial conditions were also higher by a factor of ~5.5 The emissions in both simulations were almost identical (because the trajectory traveled very far). Therefore the Level III simulation predicted more O_3 than the Level II simulation because of more mass initially in the system. The same effect can be seen between the two DEM simulations. The 350 m simulation made 0.332 ppm O_3 as opposed to 0.302 ppm at the 250 m initial mixing height. These simulations also show that for the Level III approach DEM produces more O_3 than CB2 (e.g. 0.302 ppm vs 0.260 ppm at 250 m initial height).

D195

Discussion for July 13. This day illustrates the range of assumptions possible in switching between Level II and Level III approaches. This range makes it difficult to compare. The Level II trajectory analysis for this day (Figure 41) shows that the parcel originated in the far south east of the city, so much so that the earliest hour that can be assigned a position is 1100 LDT (with an initial mixing height = 1198 m). The Level III assumption, however, originates the parcel in the center of St. Louis with 250 m at 0800 LDT. The initial conditions (concentration and mixing height) were such that in either case, the mass they contributed was low. Thus, this day is dominated by emissions, both for Level II and Level III approaches. But since the Level III trajectory originates in the city, the emission's contribution to the Level III simulation is much greater than the emission's contribution to the Level II simulation. Hence, for the Level III simulations, the Demerjian mechanism predicted 1.03 times the observed ozone maxima; the CB2 mechanism predicted 0.68 times the observed. For the Level II simulations, the Demerjian mechanism predicted 0.63 times the observed; the CB2 mechanism predicted 0.46 times the observed ozone maxima.

D275

Discussion for October 1. Both effects, greater emissions and greater initial mass, played a part in Day 275 DEM and CB2 simulations. Both of the simulations predicted greater $[O_3]$ maxima in the Level III than Level II simulations. Initial concentrations were nearly the same at the two different levels. The Level II initial mixing height, however, was 109 m (for Characteristic curve). Therefore the initial condition has ~2.5 times

the mass in the Level III simulation as in the Level II simulation. Also in the Level II simulation the trajectory was on the eastern border area of the city. Therefore the Level III emissions resulted in more than twice the mass input into the parcel.

The resulting difference between Level II and Level III in $[O_3]$ max prediction is most dramatic for this day. The observed was 0.244 ppm. In the Level II simulation with characteristic curve, the Demerjian simulation yielded 0.168 and the CB2 simulation 0.081 ppm O_3. The O_3 maxima for Level III simulations were: (DEM/250 m) 0.418 ppm; (DEM/350 m) 0.45 ppm; and (CB2/250 m) 0.250 ppm.

A basic difference therefore between the Level II and Level III approaches, is that the Level III assumptions often result in more total mass being injected into the system than Level II assumptions, resulting in more ozone predicted in Level III than in Level II simulations. The increased aldehyde initial condition and emissions factor also has a major impact on these simulations.

10.3 ISOPLETH DIAGRAMS AND EKMA CONTROL CALCULATIONS FOR LEVEL III SIMULATIONS

Isopleth diagrams for the Level III simulations for use with the EKMA procedure were obtained in the same manner as for the Level II simulations. Figures 110 to 113 show the isopleth diagrams and O_3 as a function of relative HC for three levels of NO_x control for the three days simulated with the Level III approach. Table 51 lists the %HC reduction estimates obtained by EKMA procedure. Finally, plots of $\%O_3$ reduction vs %HC reduction estimates for these Level III simulations are presented as Figures 114 and 115.

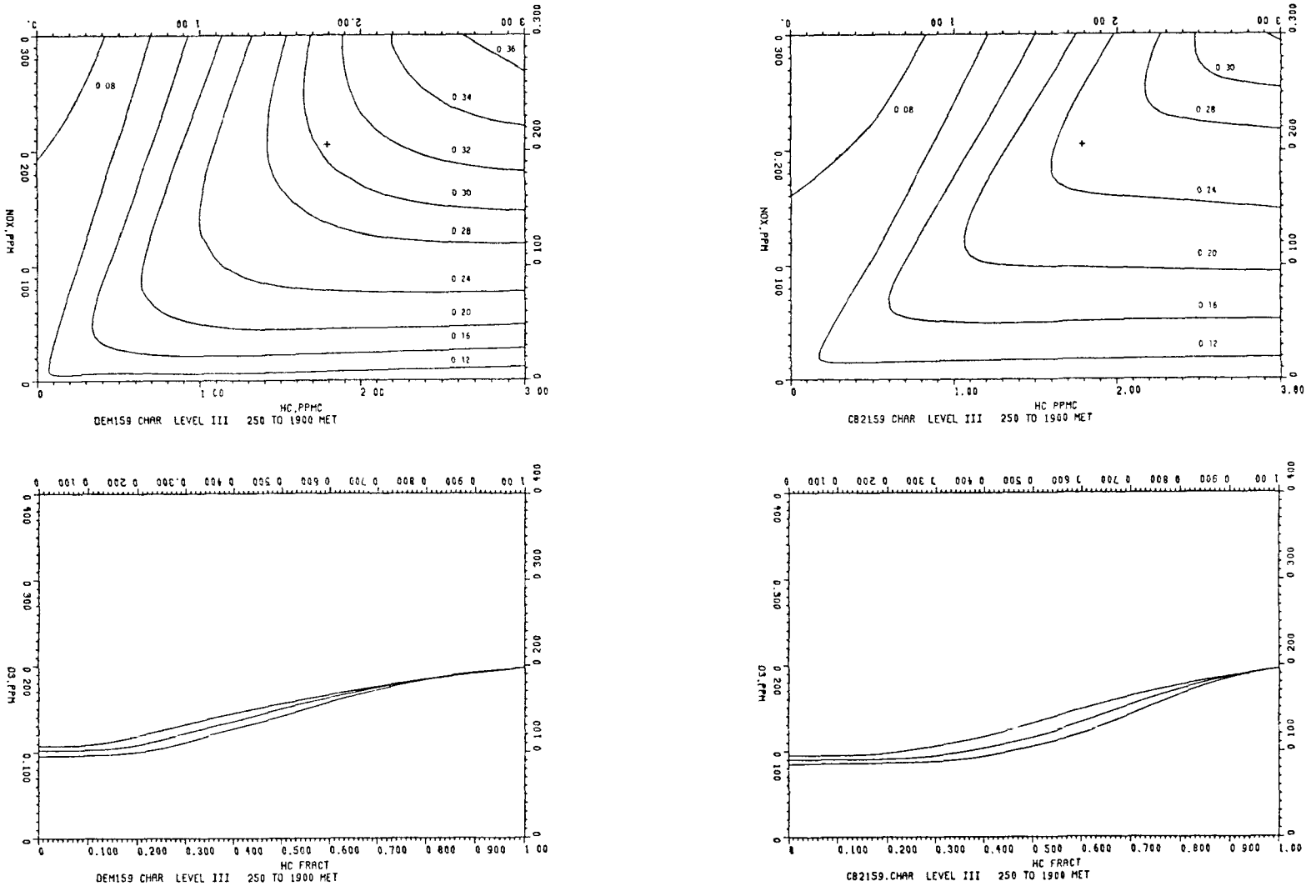

Figure 110. Ozone isopleth diagrams and ozone-HC fraction diagrams for June 7, 1976 (Day 159) Level III simulation assuming 250 meter initial mixing height for both the Demerjian and Carbon Bond II mechanism.

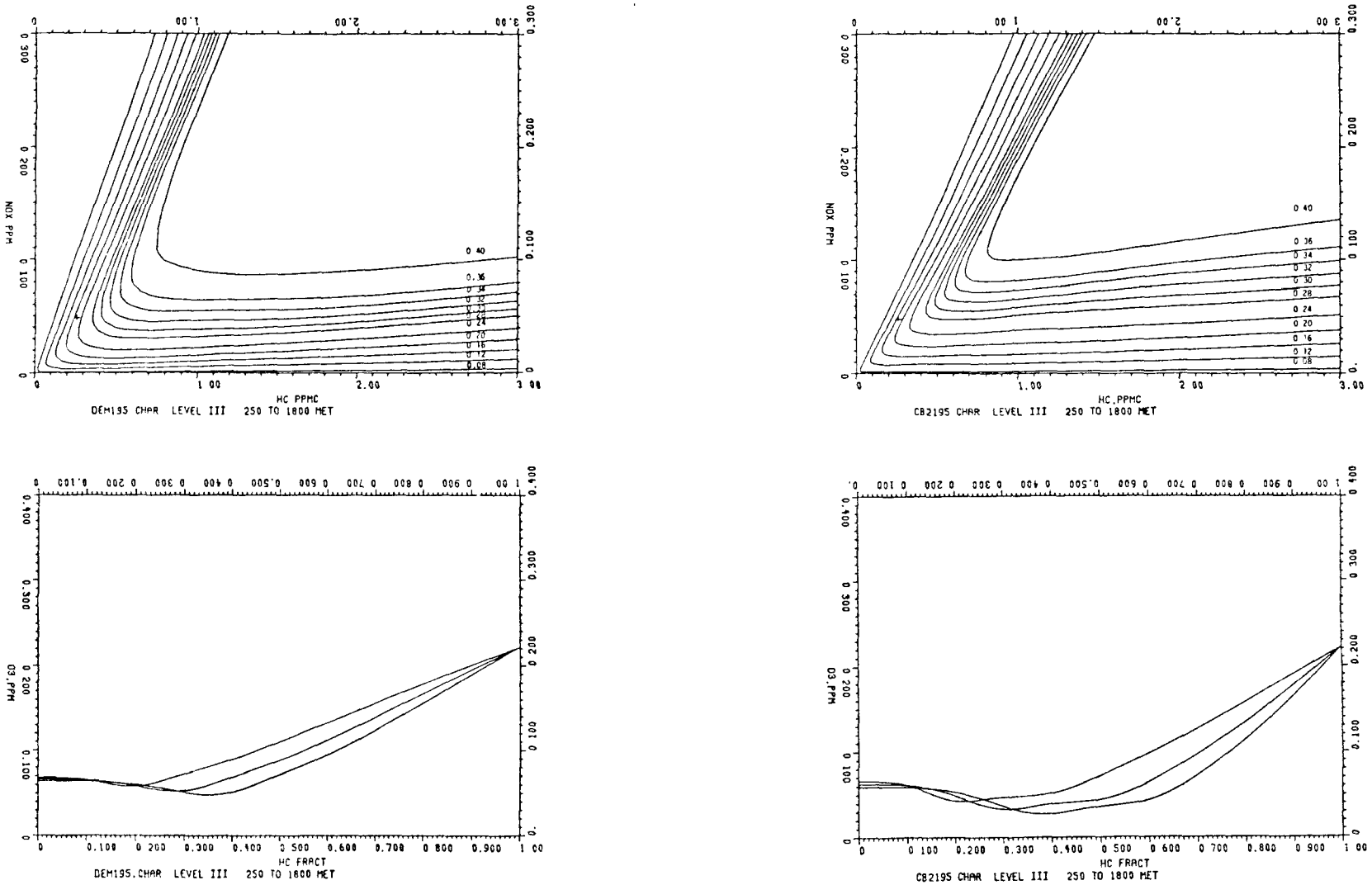

Figure 111. Ozone isopleth diagrams and ozone-HC fraction diagrams for July 13, 1976 (Day 195) Level III simulation assuming a 250 m initial mixing height for both the Demerjian and Carbon Bond II mechanism.

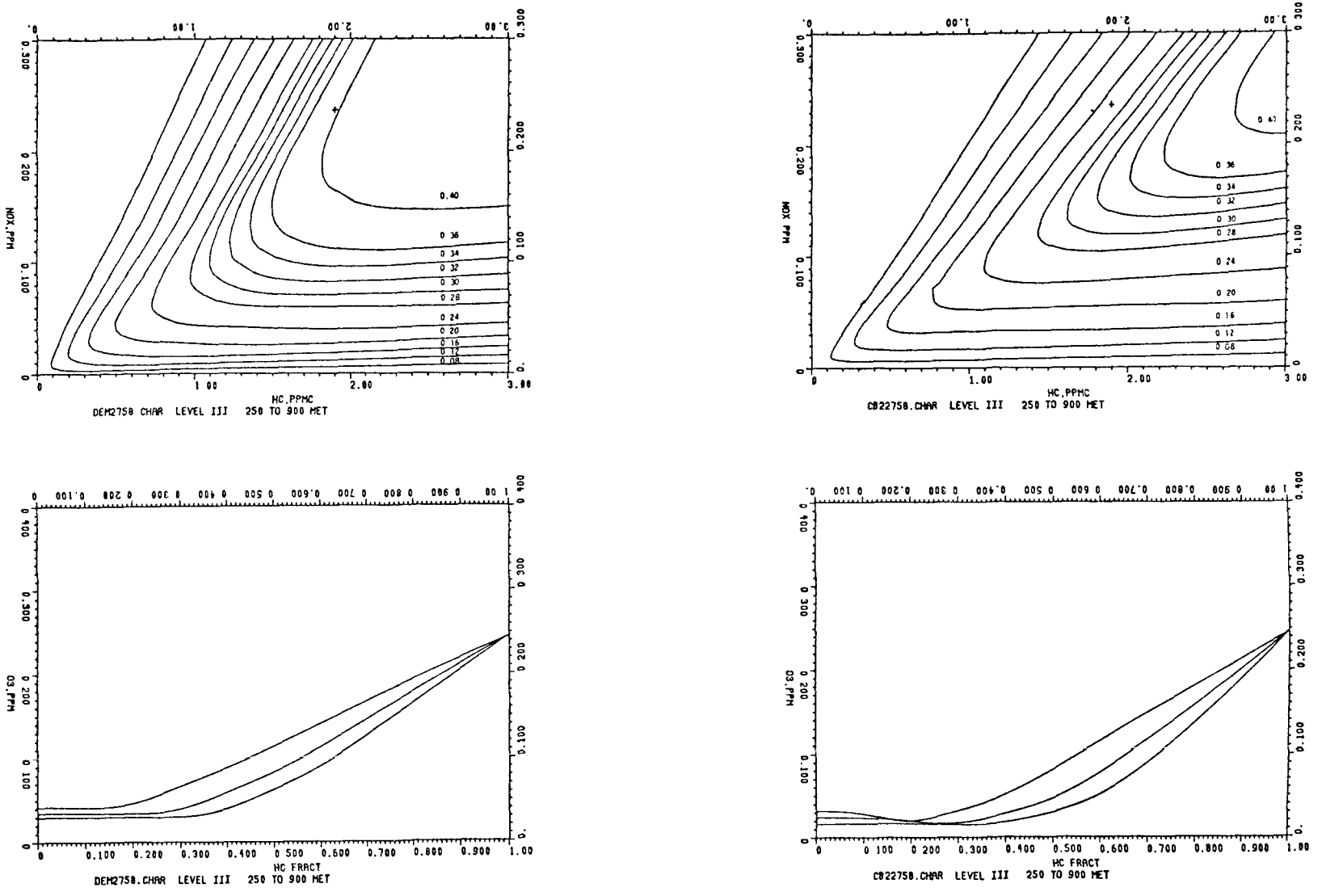

Figure 112. Ozone isopleth diagrams and ozone-HC fraction diagrams for October 1, 1976 (Day 275) Level III simulation assuming a 250 m initial mixing height for both the Demerjian and Carbon Bond II mechanism.

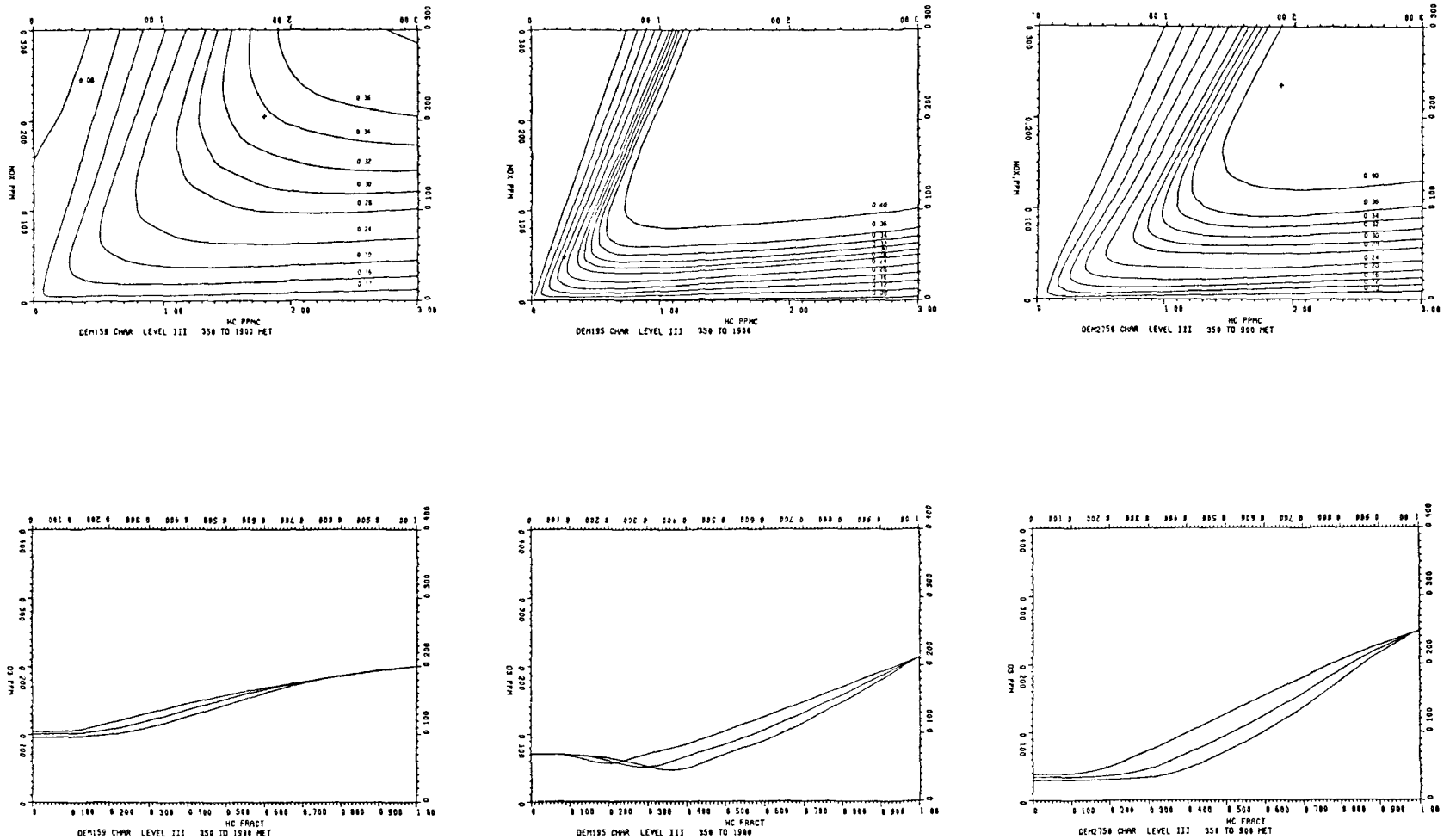

Figure 113. Ozone isopleth diagrams and ozone-HC fraction diagrams for Level III simulations assuming 350 meter initial mixing height for June 7, July 13, and October 1976 using the Demerjian mechanism.

10.3.1 Discussion of June 7, D159

Figure 110 shows the isopleth diagrams and O_3-HC fraction diagrams for the Demerjian mechanism and the Carbon Bond II mechanism simulations starting at 250 m initial mixing height. Figure 113 shows the Demerjian mechanism simulation starting at 350 m initial mixing height. It should be recalled that all three simulations overpredicted the observed ambient O_3 maximum. The EKMA solution points were lower than the measured initial HC and NO_x for all three isopleths: the DEM simulations were about 1/3, and CB2 were about 1/2 of initial HC and NO_x. D159 has the highest O_3 aloft values: 0.120 ppm and results with diagrams showing only a portion of the 0.08 ppm isopleth line. The O_3 value at the origin was greater than 0.080 ppm.

Although the DEM/250M and 350M isopleth diagrams do appear different, the EKMA procedure when applied to each resulted in remarkably similar HC control estimates, 79.6 and 77.6% for a -20% change in NO_x (Table 52). The CB2/250M isopleth diagram resulted in a much lower control estimate: 57.3% (-20% NO_x). For the Level II simulations the HC emission reduction for the corresponding conditions were much less. DEM Level II was 67% reduction and Level III was 79.6% reduction; CB2 Level II was 45% reduction and Level III was 57.3% reduction.

10.3.2 Discussion of July 13, D195

Figure 111 shows the Demerjian and the Carbon Bond II 250 m isopleth diagrams prepared for this day. This day can be compared with D275 in that the absolute emissions rates were the same except for the last hour.

Table 51. Level III %HC Control Estimates

		NO_x Control		
Day	Mech/Mix Ht	-20%	0%	+20%
159	DEM/250	79	71	64
	DEM/350	78	69	64
	CB2/250	57	47	41
	Dodge/250	74	72	67
275	DEM/250	47	38	32
	DEM/350	53	42	34
	CB2/250	38	29	23
	Dodge/250	56	48	38
195	DEM/250	45	35	29
	DEM/350	43	34	29
	CB2/250	32	24	19
	Dodge/250	59	55	46

The initial HC values, however, were 7.5 times less than Day 275. Also the final mixing height for D195 (1800 m) is twice that of Day 275 (900 M). The O_3 aloft was similar for the two days.

The isopleth diagrams for these days were plotted on axis with the same magnitudes used for D159 and D275. The isopleths suggest that this day would produce ozone dramatically. What must be remembered is that the emissions as well as the initial conditions are multiplied in generating the diagrams. Therefore at the point on the D195 isopleth diagram which matches the initial conditions of D275 (1.9 HC, 0.236 NO_x) the emissions are 7.5 times as great as the design point emission rate (observed initial conditions and emissions). This is a great amount of material compared to the X1 emission rate which is of course at the design point of D275.

Of further interest is that the control estimates for the DEM/250M day 195 (44.6%) closely match those of DEM/250M day 275 (47.4%) while the 350 m control estimates differ: DEM 195/305M was 42.6% and DEM 275/350 M was 52.5% reduction.

The isopleth diagram generated with the CB2 mechanism (250 m), which appears to be similar to the DEM isopleth diagram for this day, yielded a significantly lower control estimate (32.2% vs 44.6% for -20% NO_x).

10.3.3 Discussion of October 1 , D 275

Figure 11 shows the isopleth diagram and the O_3-HC fraction diagrams for the Demerjian and Carbon Bond II simulations using 250 m initial mixing height. This day contrasts with D159 in that the initial conditions on this day were similar to those of D159, yet the emissions were much larger on D275. This was true in the absolute sense and the effect was

further enhanced by the 900 m final height on D275 compared to the 1900 m final mixing height on D159. These factors resulted in Day 275 having more O_3 producing ability for both DEM and CB2 mechanisms than on Day 159.

Since the DEM/250M simulation predicted much more than the CB2/250M simulation the isopleth diagrams also show similar trends.

On the DEM/250M isopleth diagram, the EKMA solution point was found at 52% less than the day's initial condition and on the CB2/250M isopleth diagram the EKMA solution point was found at 8% less than the day's initial conditions. In spite of these differences in absolute predictions, the EKMA HC control estimates are 38.2% for CB2 and 47.4% for DEM (at 250 m and -20% NO_x reduction). The DEM/350M isopleth diagram, like the day's simulation, predicts the most ozone formation for this day's conditions. The EKMA control estimate using this isopleth diagram is only 5% more (52.5%) than that using the DEM 250 M isopleth diagram.

10.3.4 Discussion of O_3 Reduction Diagrams

Figures 114 and 115 show the percent O_3 reduction as a function of the percent HC reduction for the Demerjian and Carbon Bond II mechanisms for the three days simulated. Except for June 7, Day 159, which had 0.12 ppm O_3 aloft, the results suggest a greater than 1:1 control effect. That is, a given %HC reduction results in more than that % reduction in O_3 (e.g. a 25% HC reduction gives a 50% O_3 reduction).

The ratio of % O_3 reduction to %HC reduction is about 2:1 for Carbon Bond II and about 1.3:1 for Demerjian (independent of initial mixing height) in the Level III simulations with small amounts of O_3 aloft. For Day 159 with 0.12 ppm O_3 aloft, the ratios are less than one (i.e. 0.8:1 for Carbon Bond II and 0.5:1 for Demerjian). Recall that in the Level II

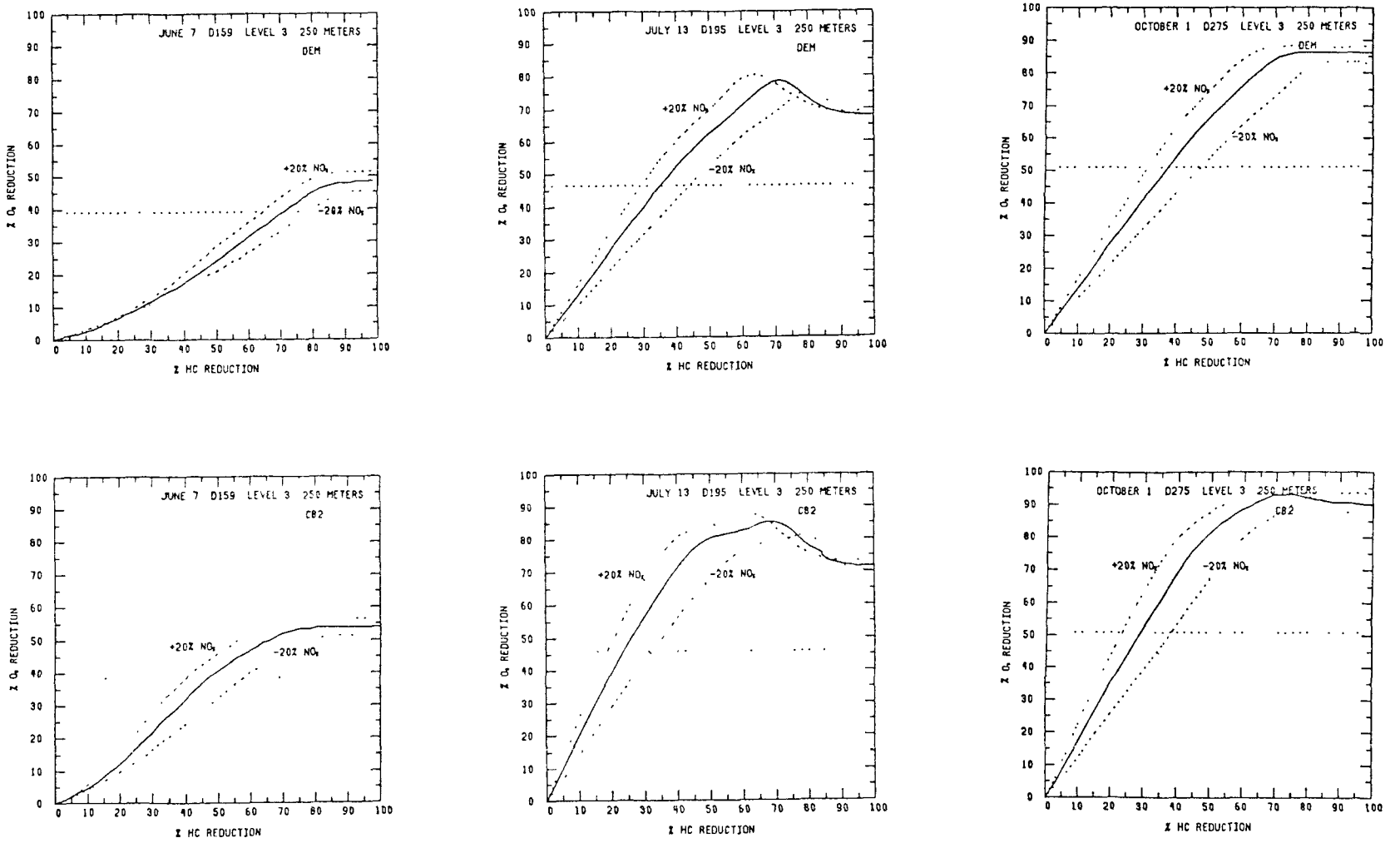

Figure 114. Ozone reduction diagrams for Demerjian and Carbon Bond II simulations using 250 m initial mixing height. Dashed horizontal line is the reduction needed to give the O_3 standard (0.12 ppm).

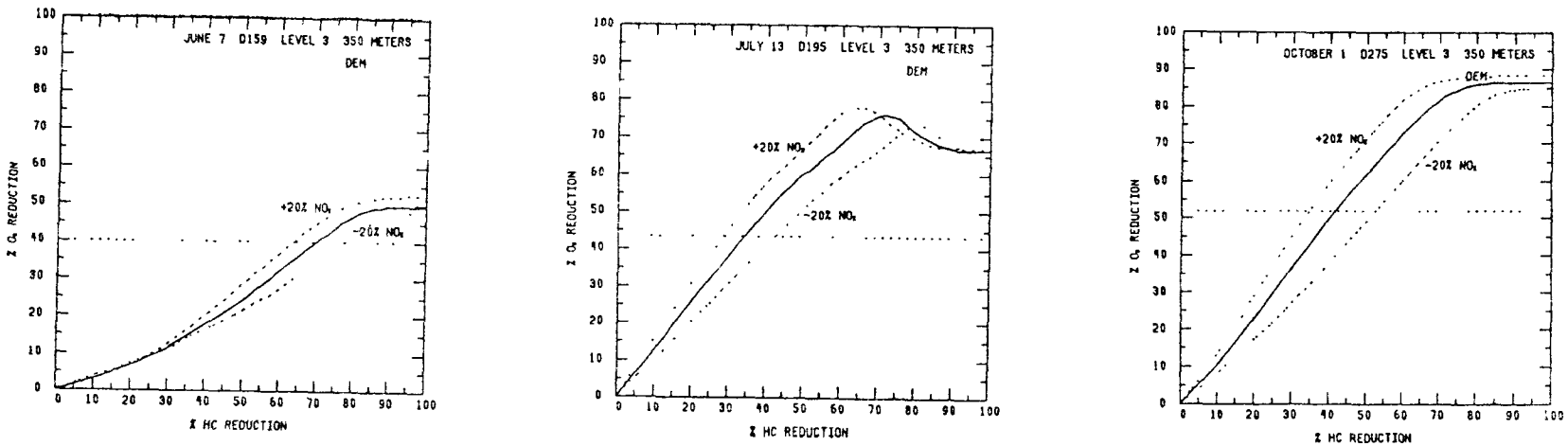

Figure 115. Ozone reduction diagrams for Demerjian simulations using 350 m initial mixing height. Dashed horizontal line is the reduction needed to give the O_3 standard (0.12 ppm).

simulations for Day 275, the ratio was about 2:1 for Demerjian characteristic curve and that the Carbon Bond mechanism gave no solution because of under prediction (the Dodge simulation ratio was about 1.6:1). For Level II simulations of Day 159, the ratio was about 0.7:1 for Demerjian and 1:1 for Carbon Bond II. Thus it appears that the Carbon Bond II mechanism consistently suggests greater sensitivity of ozone to HC control than either Demerjian or Dodge and that this sensitivity is more than (up to twice) that of simple linear roll back.

10.3.5 Effect of Initial Aldehyde Fraction

It was stated earlier that the Level III approach does not require more than a county-wide emission inventory. Aldehydes are generally not well characterized in these inventories and therefore must be approximated by the modeler.

Based on suggestions by Demerjian, values of 3% Carbon and 8% Carbon were used for the ALD emissions fractions and ALD initial conditions fractions in this study. A value of 3% for the aldehyde carbon fraction marks the upper limit of the values determined from detailed emission inventory calculations for the 10 days studied in the Level II section. It is a reasonable value.

In the Level II discussion, the effects of variation of the aldehyde fraction on the simulations of certain days were demonstrated. To examine the effect for the simpler Level III approach, two level III simulations with the Demerjian mechanism were redone with an aldehyde fraction for the iniital conditions equal to the emissions aldehyde fraction: a change from 8% to 3%. The results are shown in Table 52.

Table 52. Effect of Initial Aldehyde Fraction on O_3 Maximum for Level III Simulations with Demerjian Mechanism

Day	$[O_3]$ max for 8% Initial Ald., ppm	$[O_3]$ max for 3% Initial Ald., ppm	Ratio 3% to 8%
275	0.418	0.359	0.859
195	0.216	0.208	0.963

The magnitude of the effect of the variation on $[O_3]$ maxima depends on the relative contribution of the initial conditions to the total mass of pollutants emitted into the parcel, hence a sizable effect for Day 275 and a small effect for Day 195, which was dominated by emissions.

The aldehyde fraction effects the O_3 maximum concentration mainly on the left-hand side of the ridge on an isopleth diagram. For those days in which the EKMA solution points are located on this left-hand side, the effects of aldehyde initial carbon fraction on the HC reduction are probably minimal. For those days in which the solution points are on the right-hand side (which is not much effected by aldehyde fraction) the crossing of the ridgeline in a control calculation will probably result in a significant effect on the HC reduction required.

10.3.6 Effect of Simulation Length on Control Requirements

The guidance supplied by EPA implies that Level III simulations (for isopleth generation) would commonly be performed for a 10 hour day, regardless of the time that the $[O_3]$ max was measured. For example, the days simulated by the Level III approach in this study (D159, D195, D275) had maximum ozone concentrations measured during the 9th or 8th hour (after 0800 LST). Emissions data were supplied only for the 8 or 9 hours it

took to reach the maximum measured (see Table 46). The Dodge isopleths generated by OAQPS for these days used 10 hours of simulation time and 8 or 9 hours of emissions data and used zero emissions for the extra one or two hours until the end of the 10-hour simulation period. Isopleth diagrams generated in this report for the Demerjian or Carbon Bond II mechanisms used the actual time to $[O_3]$ max, 8 or 9 hours, depending on the RAPS day in question. Concern for the possible effects from these additional assumptions (10 hour default run time and zero emissions past supplied data) suggested that simulations should be compared with these different conditions. Five additional simulations and an additional isopleth were obtained. These additional simulations are reported in Table 49 as the second column under each day.

For D159 and D195, simulations were performed for an additional hour (nine to ten hours). The one simulation for D159 using the CB2 mechanism showed only a 1% increase in O_3 maximum indicating that the O_3 profile had almost peaked at 1700.

Two simulations were performed for D195 using both the DEM and CB2 mechanisms. DEM showed a 5% increase and CB2 showed a 9% increase.

Two simulations showing the most dramatic effects were performed for D275. The DEM mechanism shows that the O_3 peak is closer to 1600, so that the effect of simulating an additional two hours actually yields a lower final O_3 maximum. The CB2 mechanism, however, having not reached O_3 maximum at 1600, yields a 13% higher O_3 maximum after simulation for an additional two hours (0.250 to 0.282 ppm).

For Level III, the effect of simulation time is important not for absolute $[O_3]$ predictions but for the HC reduction estimates obtained

from different isopleths generated for a day using different simulation times. To obtain the greatest possible effect, one isopleth diagram was generated with the conditions showing the largest change in O_3 maximum in the tests just described: CB2 for D725, simulating 10 rather than 8-hours.

The isopleth and O_3 reduction diagrams for these two conditions are shown in Figure 116. The isopleths on the left-side of the ridge have been shifted to the left (the initial condition point occurs between 0.28 and 0.30 instead of between 0.24 and 0.28) for the longer simulation. The control diagrams, however, are essentially identical. For no change in NO_x, the required HC reductions are 29.0 and 29.8% for 8 and 10 hours of simulation. The EKMA solution points, however, are on the left-hand side of the ridgelines and an effect might occur if the EKMA solution points were on the right-hand side and the required HC reduction crossed the ridgeline.

10.4 SUMMARY OF LEVEL III SIMULATION RESULTS

The Level III simulations predicted higher O_3 maxima than the Level II simulations. This is due to the assumptions in the Level III approach; a trajectory originating in mid-city has higher initial conditions, higher emissions and hence more mass in the air parcel. Assumptions of initial mixing height and the aldehyde fraction are also parameters that effect the magnitude of the ozone maxima in the Level III approach.

Figure 117 is a graphic summary of the control requirements predicted by three mechanisms (Demerjian, Carbon Bond II, and Dodge) for three RAPS days (159, 195, and 275) using a Level III modeling approach as described in the recent EPA draft guidance (EPA, 1981). Included in Figure 117 are

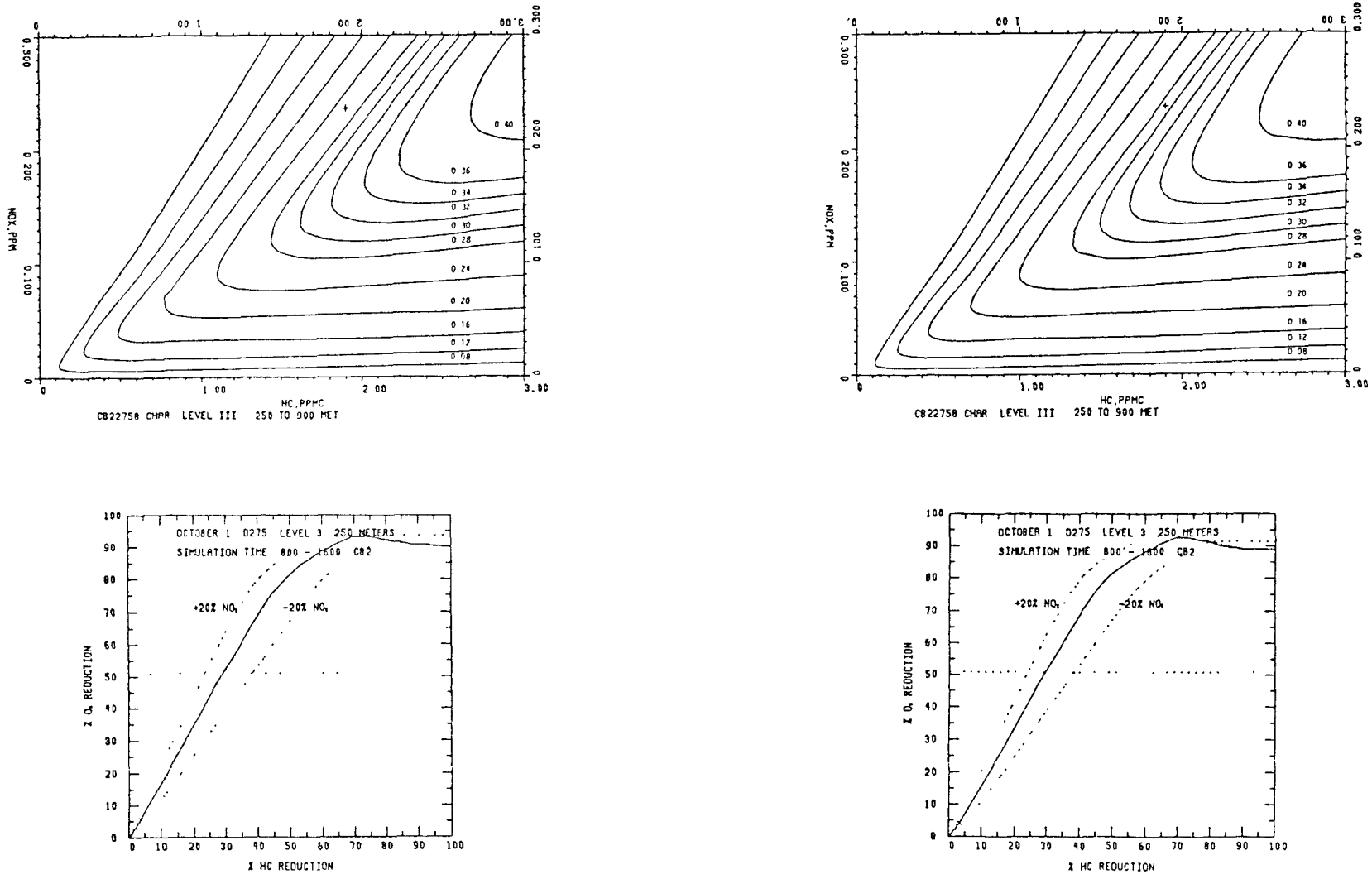

Figure 116. Effect of increasing simulation time from 8 to 10 hours with no additional emissions for the Carbon Bond II mechanism for October 1, 1976 (Day 275).

the control requirements predicted in the Level II modeling study (see Chapter 9 for comparison).

The Carbon Bond II mechanism always gives the lowest control requirement by a substantial margin (ratios of CB2 to DEM are 0.66:1, 0.67:1, and 0.70:1, and ratios of CB2 to Dodge are 0.65:1, 0.43:1, and 0.56:1 for days 159, 195, and 275). This mechanism is the newest, most complex, and most validated mechanism of the four studied. Except for Day 159 in which the Demerjian and Dodge control requirements were similar, Demerjian always gave lower control requirements than Dodge at both Level III and II. For the days studied, Dodge always gives the highest control requirement.

Secondly, regardless of mechanism, the Level III control requirement predicitons are significantly higher than Level II predictions (ratios of Level III to Level II requirements are 2.4:1, 1.5:1, and 1.3:1 for Demerjian, Dodge, and CB2).

Level III, like Level II, gives the maximum control requirement not for the day with the highest observed O_3 maximum, but for the day with the maximum O_3 aloft and a lower contribution from local emissions.

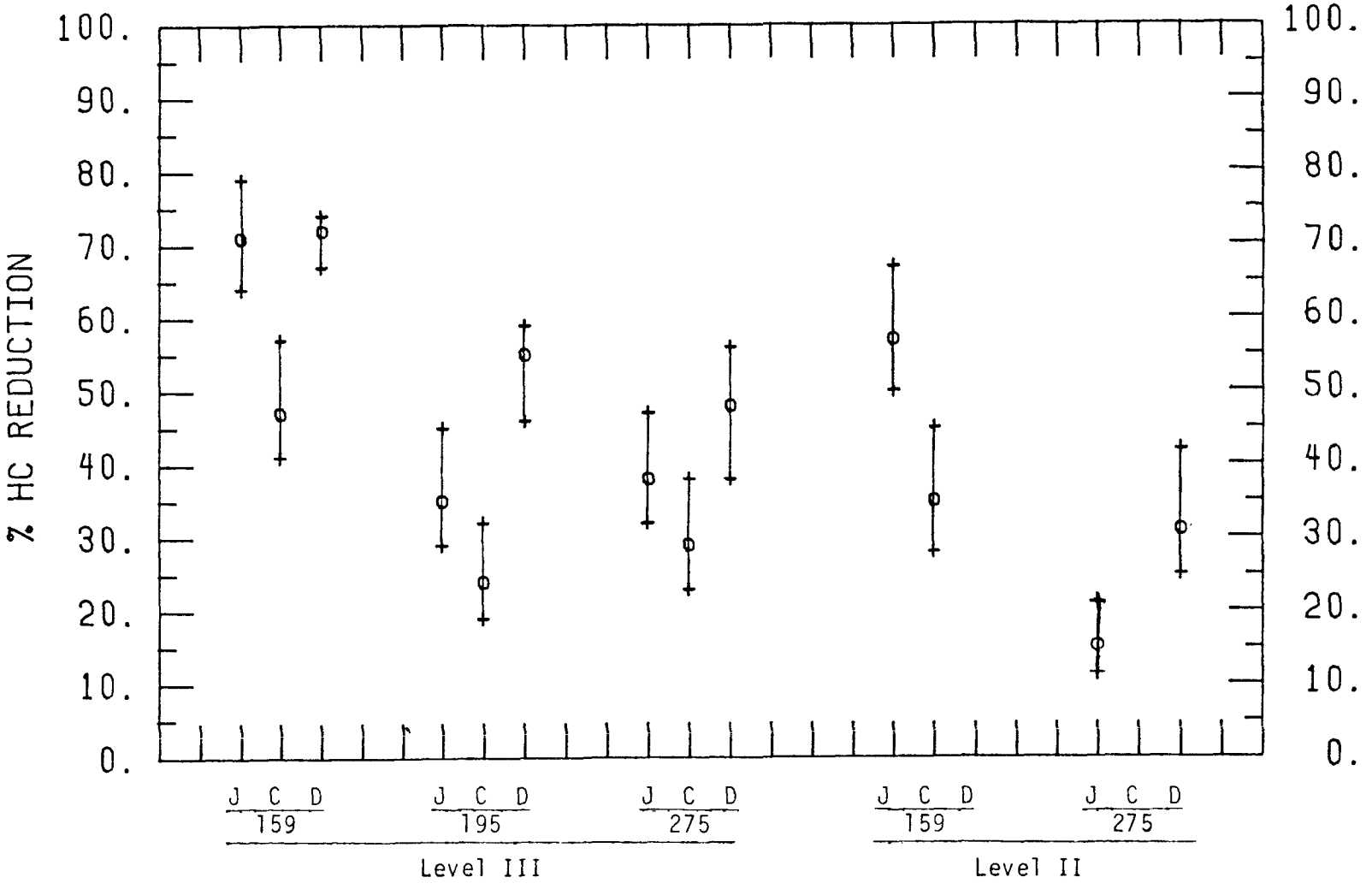

Figure 117. Control predictions by method by day by mechanism. J=Demerjian, D=Dodge, and C=Carbon Bond Mechanisms. 159=June 7; 195=July 13; 275=October 1. 0=no change in NO_x; upper range=-20% NO_x; lower range=+20% NO_x. Characteristic curve mixing height profile.

References

1. Uses, Limitations, and Technical Basis of Procedures for Quantifying Relationships Between Photochemical Oxidants and Precursors, EPA-450/2-77-021a, U. S. Environmental Protection Agency, Research Triangle Park, North Carolina, November 1977.

2. Arya, S.P.S. (1979) Atmospheric Boundary Layers, to be published in Engineering Meteorology, Elsevier.

3. Benkley, C.W., L. L. Schulman (1979) "Estimating Hourly Mixing Depths from Historical Meteorological Data," JAM, Vol. 18, pp. 772-78.

4. Demerjian, K. L., K. L. Schere (1979) Applications of a Photochemical Box Model for Ozone Air Quality in Houston, Texas, In Proceedings: Ozone/oxidants Interactions with the Total Environment II, Oct. 14-17, Houston, Texas, pp. 414-21.

5. Demerjian, K. L. and K. L. Schere (1976) personal communication.

6. Demerjian, K. L. (1980) personal communications.

7. Demerjian, K. L., K. L. Schere and J. Peterson (1980) "Theoretical Estimates of Actinic (Spherically Integrated) Flux and Photolytic Rate Constants of Atmospheric Species in the Lower Troposphere," Advances in Environmental Science and Technology, Vol. 10, John Wiley and Sons, New York, New York.

8. Demerjian, K. L. (1981) personal communication.

9. Dickerson, M. H. (1978) MASCON - A Mass Consistent Atmospheric Flux Model for Regions with Complex Terrain, JAM, Vol. 17, pp. 241-53.

10. Dodge, M. C. (1977) Combined Use of Modeling Techniques and Smog Chamber Data to Derive Ozone-Precursor Relationships EPA-600/3-77-001b.

11. Dodge, M. C. Effect of Selected Parameters on Predictions of a Photochemical Model EPA-600/3-77-048, U. S. Environmental Protection Agency, Research Triangle Park, North Carolina, June 1977.

12. Evans, R. B. (1979) The Contribution of Ozone Aloft to Surface Ozone Maxima, Ph.D. Thesis, University of North Carolina, Chapel Hill, NC.

13. Federal Register, "Data Collection for 1982 Ozone Implementation Plan Submittals" Nov. 14, 1979, 44, (221) 65669-65670.

14. Gipson, G. L. (1980) personal communication: OAQPS study.

15. Gipson, G. L., W. Freas, R. Kelly, E. Meyer (1981) Guideline for Use of City-Specific EKMA in Preparing Ozone SIPs, EPA-450/4-80-027, U. S. Environmental Protection Agency, Research Triangle Park, N.C., March 1981.

16. Goodin, McRae, Seinfeld (1980) An Objective Analysis for Construction Three Dimensional Urban Scale Wind Fields, JAM, Vol. 19, pp. 98-108.

17. Holzworth, G. C. (1972) Mixing Heights, Wind Speeds, and Potential for Urban Air Pollution throughout the Contiguous United States, AP-101, USEPA Research Triangle Park, NC.

18. Jeffries, H. E. and K. G. Sexton (1981) Modeling Aspects of Nitrogen oxides Using Smog chamber data, in workshop proceedings on Formation and Fate of Atmospheric Nitrates, EPA-600/9-81-025, U. S. Environmental Protection Agency, Research Triangle Park, NC.

19. Jeffries, H. E., J. E. Sickles, M. Saeger, and M. A. Carpenter "Experimental Determination of the Specific Photolysis Rate of Nitrogen Dioxide," Draft Final Report, Bruce Gay, Jr., Project Officer, Environmental Protection Agency, Research Triangle Park, NC, Feb. 1981.

20. Littman, F. E. (1979) "Regional Air Pollution Study: Emission Inventory Summarization", EPA-600/4-79-004, Rockwell International Creve Coeur, Mo.

21. Liu, M. K., J. H. Seinfeld (1975) On the Validity of Grod and Trajectory Models of Urban Air Pollution, Atm. Env., Vol. 9, pp. 555-74.

22. Schere, K. L. and K. L. Demerjian (1980) personal communication: characteristic curve.

23. Shreffler, J. H. (1978) Detection of Centripetal Heat Island Circulation from Tower Data in St. Louis, BLM, Vol. 15, pp. 229-42.

24. Spath, H. Translated by Hoskins, W. D., H. W. Sager (1974) Spline Algorithms for Curves and Surfaces, UTILTAS Mathematica Publishing Incorporates, Winnipge.

25. Whitten, G. Z. and H. Hugo User's Manual for Kinetics Model and Ozone Isopleth Plotting Package, EPA-600/8-78-014a, U. S. Environmental Protection Agency, Research Triangle Park, NC, July 1978.

26. Whitten, G. A. and H. Hugo U. S. Environmental Protection Agency, EPA-600/8-78-014b, Research Triangle Park, NC, July 1, 1978.

27. Whitten, G. Z., J. P. Killus, and H. Hugo Modeling of Simulated Photochemical Smog with Kinetic Mechanisms, EPA-600/3-80-028a, U. S. Environmental Protection Agency, Research Triangle Park, NC, February 1980.

28. Yamad, T. (1976) On the Similarity Functions A, B, and C of the Planetary Boundary Layer, JAS, Vol. 33, pp. 781-93.

APPENDIX A

THE HISFIT ALGORITHM: AN AREA TRUE HISTOGRAM FUNCTION

Appendix A

The HISFIT Algorithm: An Area-True Histogram Function

It is frequently desirable to represent a series of interval histogram values as a smooth function having the area-true property. Consider a series of n intervals and associated histogram values h_1, h_2 .. h_n. We define e_0, e_1 .. e_n to be the abscissa values (x) at the edges of the intervals. Thus e_1 .. e_{n-1} are common edges, e_0 and e_1 are the edges of the first interval, e_1 and e_2 are the edges of the second interval and so on. For any abscissa value x we assume the function produces an ordinate value y. Then the function is defined to be smooth (differentiable):

$$\lim_{\varepsilon \to 0} f^P(e_{k+\varepsilon}) = \lim_{\varepsilon \to 0} f^P(e_{k-\varepsilon}) = y_k^P \quad (p = 0,1 \text{ and } k = 1..n-1)$$

The area true property may be expressed as:

$$\int_{e_{k-1}}^{e_k} f_k(x)dx = h_k(e_k - e_{k-1}) \qquad (k = 1 .. n)$$

An algorithm for finding the coefficients of a fourth degree spline with these properties is presented in Späth (1974).In the present situation, negative function values are physically meaningless and so we must ensure that the function has no negative values. Cubic splines (as originally used in OZIPP) have fewer degrees of freedom and when a cubic spline is constrained to have no negative values, very poor fits often result. Oscillating histogram values also lead to poor fits with excessive over- and under- shoot. Comparative examples are presented in Figures A1 and A2 below.

The STAIR algorithm (Späth, 1974) solves the equation system over a domain given the ordinate values at the edges and boundary values for the first derivative. Thus a solution domain consists of a contiguous series of intervals a, a+1,...,b ($1 \leq a \leq b \leq n$), the given ordinate values at the edges y_{a-1}, y_a, .., y_b and the two boundary values dy_{a-1} and dy_b.

It was discovered that some histograms resulted in spline functions having negative values when the solution domain is the entire histogram. In particular when either of the ratios:

$$\frac{h_k}{h_{k+1}} \quad \text{or} \quad \frac{|dy_k|}{|dy_{k+1}|}$$

is too large or too small, negative function values result. In either case, we control the maximum (minimum) value of the first derivative at the various edges. Examining the histogram, we apply a heuristic to find those edges which are likely to have an excessively large (or small) first derivative, and we break the solution domain at those points. Each such edge then becomes a common boundary for two solution domains, and we can define the edge first derivative as a boundary condition such that the resulting function has no negative values. Any $h_k = 0$ must always be a boundary of at least one solution domain.

HISFIT finds the minimum set of solution domains and defines the ordinate and boundary values as follows:

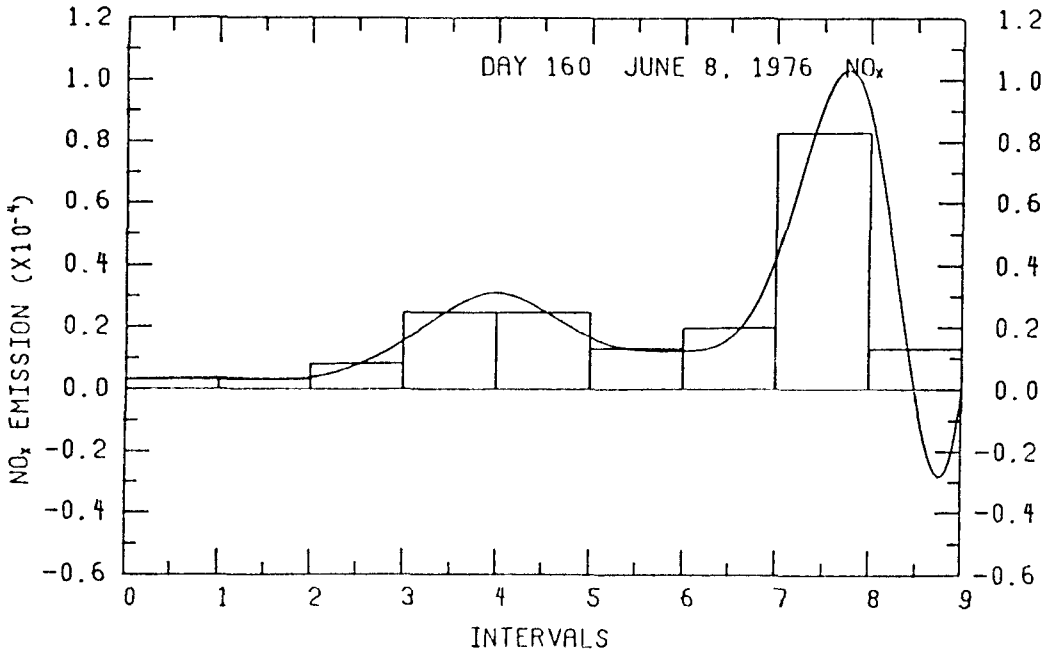

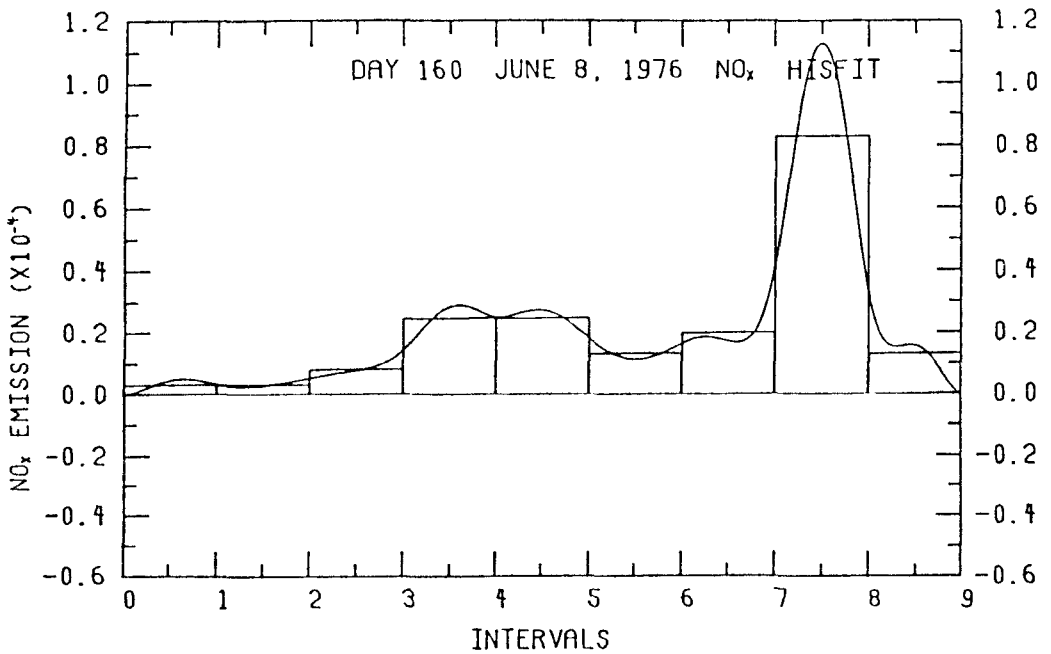

Figure A.1. Comparison of equal area histogram fit as produced by OZIPP algorithm giving negative area (top) and by HISFIT algorithm (bottom).

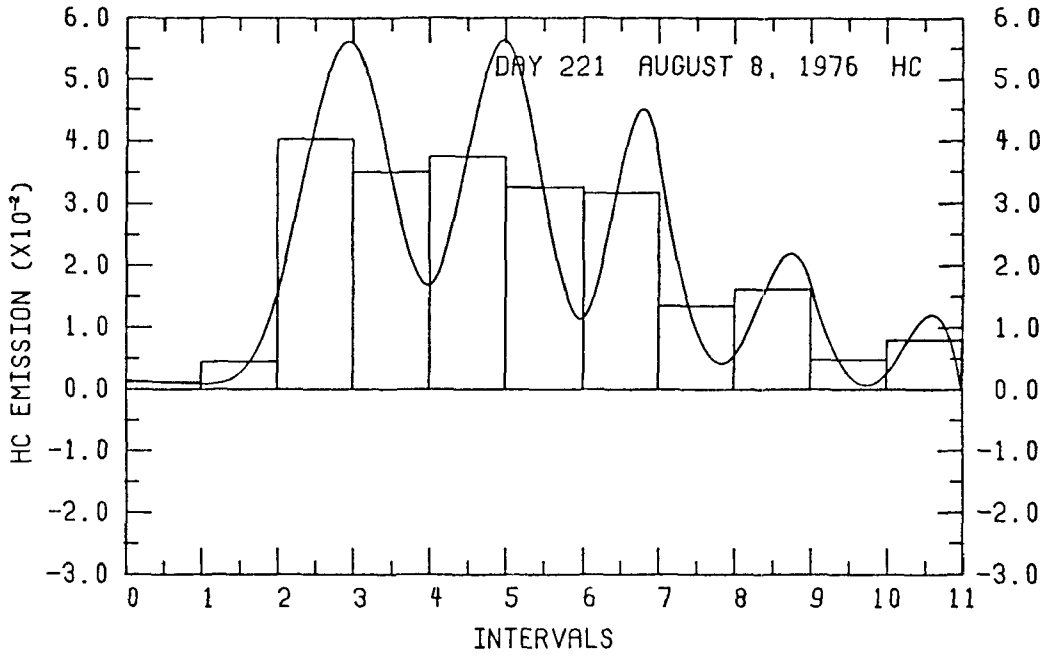

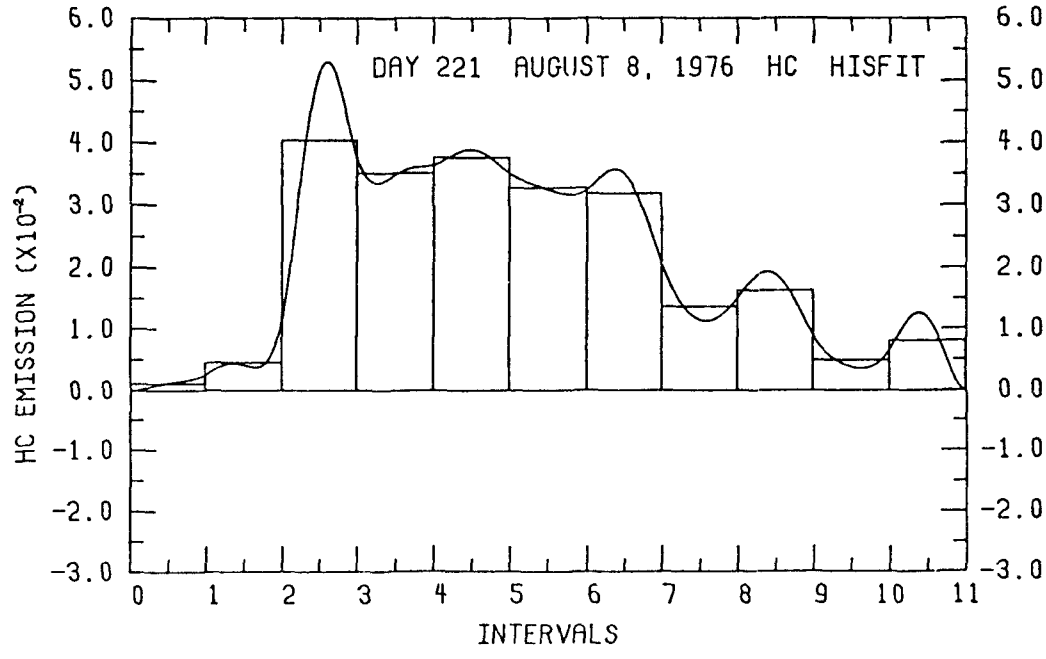

Figure A.2. Comparison of equal area histogram fit as produced by OZIPP algorithm showing strong oscillation (top) and by HISFIT algorithm (bottom).

$$\left.\begin{array}{l} h_k = 0 \\ \text{or} \\ h_{k+1} = 0 \end{array}\right\} \qquad \left\{\begin{array}{l} y_k = 0 \\ \\ dy_k = 0 \end{array}\right.$$

$$5.01 > \frac{h_{k+1}}{h_k} > \frac{1}{5.01} \qquad y_k = \begin{cases} \left(\frac{h_{k+1}}{h_k}\right)^{0.5} h_k , & h_{k+1} \geq h_k \\ \left(\frac{h_k}{h_{k+1}}\right)^{0.5} h_{k+1} , & h_k > h_{k+1} \end{cases}$$

$$\left.\begin{array}{l} \frac{h_{k+1}}{h_k} \geq 5.01 \\ \text{or} \\ \frac{h_k}{h_{k+1}} \geq 5.01 \end{array}\right\} \qquad \begin{array}{l} y_k = \begin{cases} 2.5\ h_k , & h_{k+1} > h_k \\ 2.5\ h_{k+1} , & h_k > h_{k+1} \end{cases} \\ \\ dy_k = \begin{cases} 5.25\ h_k\ (e_k - e_{k-1}) , & h_{k+1} > h_k \\ -5.25\ h_k\ (e_k - e_{k-1}) , & h_k > h_{k+1} \end{cases} \end{array}$$

It is assumed that $h_{n+1} = 0$. There are two alternative assumptions about the value of h_0. In one case (mode = 0) we assume $h_0 = 0$. Otherwise (mode = 1), we assume $h_0 > h_1$ and we set $y_0 = 2\ h_1$ and $dy_0 = -y_0/(e_1 - e_0)$.

APPENDIX B

SPECIAL EKMA COMPARISONS

APPENDIX B

Special EKMA Comparisons.

EKMA is a technique which is used to obtain HC control estimates from O_3 isopleth diagrams which do not necessarily agree in the absolute sense to the observed atmospheric conditions to which the isopleth diagram is being applied. EKMA is a scaling procedure; it is not needed for isopleth diagrams which agree with the observed precursors and O_3 values. In simple models or models with gross assumptions, the absolute agreement is generally poor and EKMA provides a means of estimating control requirements for these cases.

This study has shown that assumptions made by modelers can have an effect on the calculated control requirements. The validity of EKMA and the effect of incomplete and assumed data has been considered by the EPA (1980):

> "...Sensitivity studies have shown that differences resulting from incomplete input data or gross assumptions employed by the model tend to exhibit proportional impacts on the positions of various ozone isopleths on an isopleth diagram. Thus, the model should perform well when applied in a relative sense..."

Some results from this study tend to disagree with the above conclusion. Figure B.1 shows the results of two applications of the Level II approach to D275 October 1, 1976 (RAPS) with the Demerjian mechanism and the characteristic curve mixing height. The carbon mole fraction for aldehydes needs to be determined for both the emissions into the air parcel along the trajectory and the initial conditions of NMHC. Each row of Figure B.1 shows the simulation and observed profiles for NO, NO_2, and O_3 for the day, the isopleth generated, and the final $\%O_3$ reduction-%HC reduction plot obtained with the EKMA procedure (the horizontal dashed line shows the % O_3 reduction needed to obtain the 0.12 ppm level). Row A used the emission inventory value of 2.02% carbon mole fraction for aldehydes for both emissions and

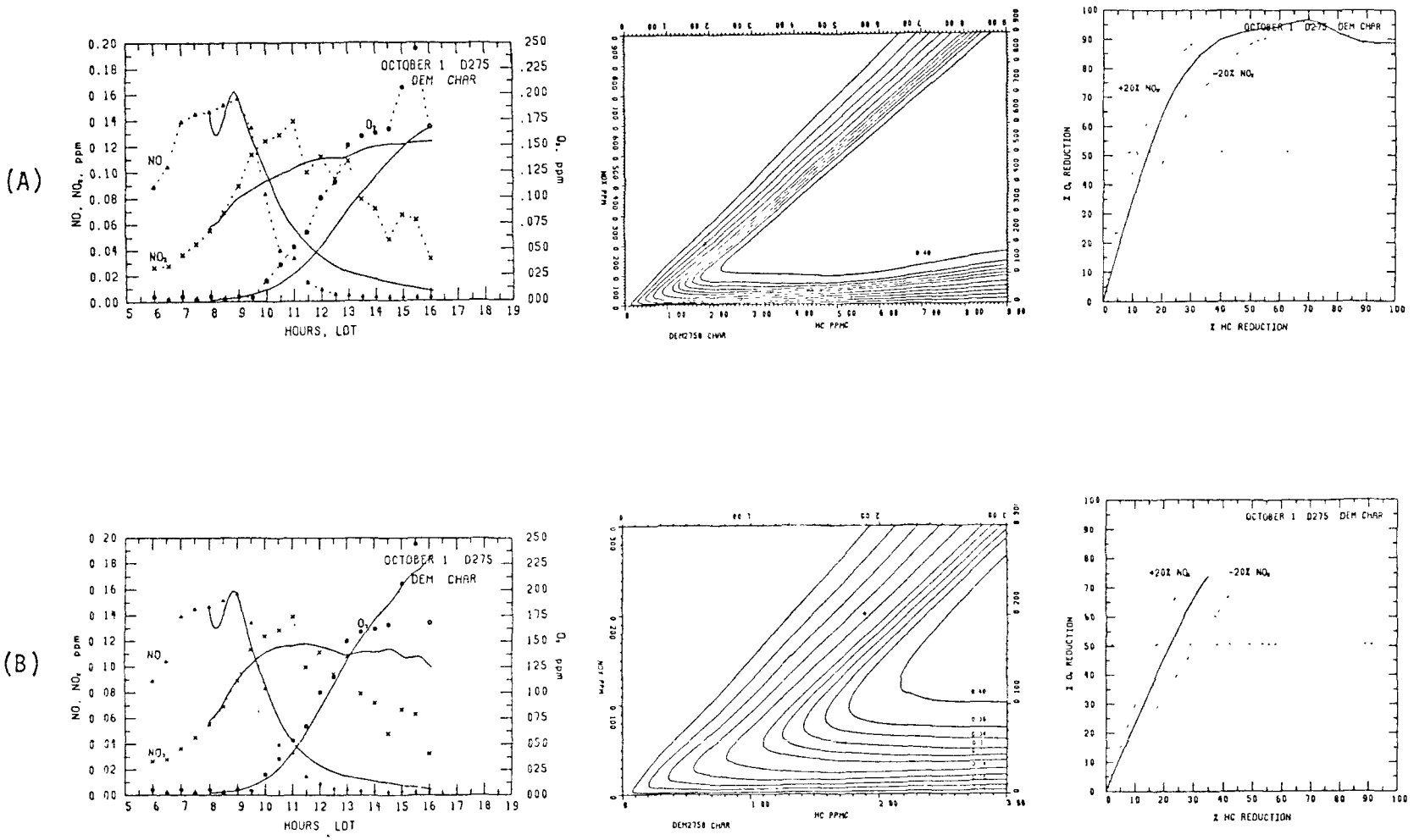

Figure B.1. The effect of changing the aldehyde carbon mole fraction of initial NMHC from 2.02% (A) to 5.0% (B) on the EKMA control solution for a Level II application to October 1, 1976 (Demerjian mechanism and characteristic curve mixing height).

Table B.1. EKMA solution points for October 1, 1976 simulation (Demerjian Mechanism).

Condition	O_3[a]	r_1[b]	HC	NO_x	r_2[c]
ambient values	0.244	--	1.89	0.202	--
2% simulation	0.168	1.452	3.969	0.424	2.10
5% simulation	0.234	1.04	2.174	0.232	1.15

[a] all HC, NO_x, and O_3 units are ppm.

[b] r_1 is the ratio of ambient value O_3 to simulation predicted value.

[c] r_2 is the ratio of EKMA calculated initial conditions to ambient values.

initial NMHC. Row B used the emission inventory value for the emissions, but used a value of 5.0% for the initial conditions of NMHC. It can be seen that not only the simulation profiles and isopleth diagrams changed considerably, but that the EKMA calculated control requirements changed considerably as well. The change in scale on the isopleth diagram was necessary to obtain an EKMA solution for the upper set of conditions. The numeral values are shown in Table B.1. The solution point moved from 15% more initial and emitted HC and NO_x to 110% more initial and emitted HC and NO_x, and the control requirement went from 15% to 22%, a ratio of 1.47.

Figure B.2 shows again two approaches to estimating control requirements to D275 October 1, 1976. Row A is a Level II application and Row B is a Level III application. The different assumptions for each Level has been described in this report. Approximately the same mechanism (CB2), emissions, initial conditions, O_3 aloft, and final mixing height were used on both applications for this day. The basic difference lies in the initial mixing height assumed (Level II 109 m, Level III 250 m) and the NMHC carbon mole fractions assumed for emissions and initial conditions (see report for discussion). Not only are the simulation profiles and isopleth diagrams drastically different, but while an EKMA solution was obtained from the Level III approach, no solution at all was possible with the Level II approach.

(A)

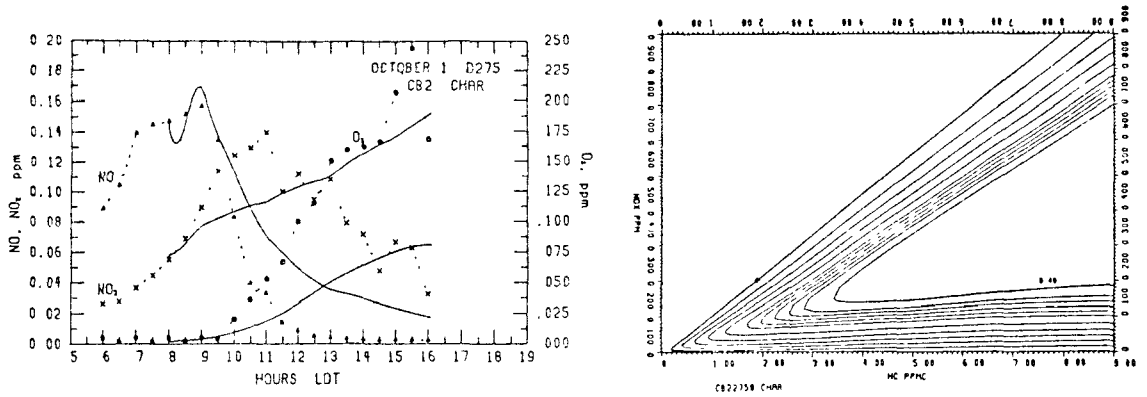

NO SOLUTION

(B)

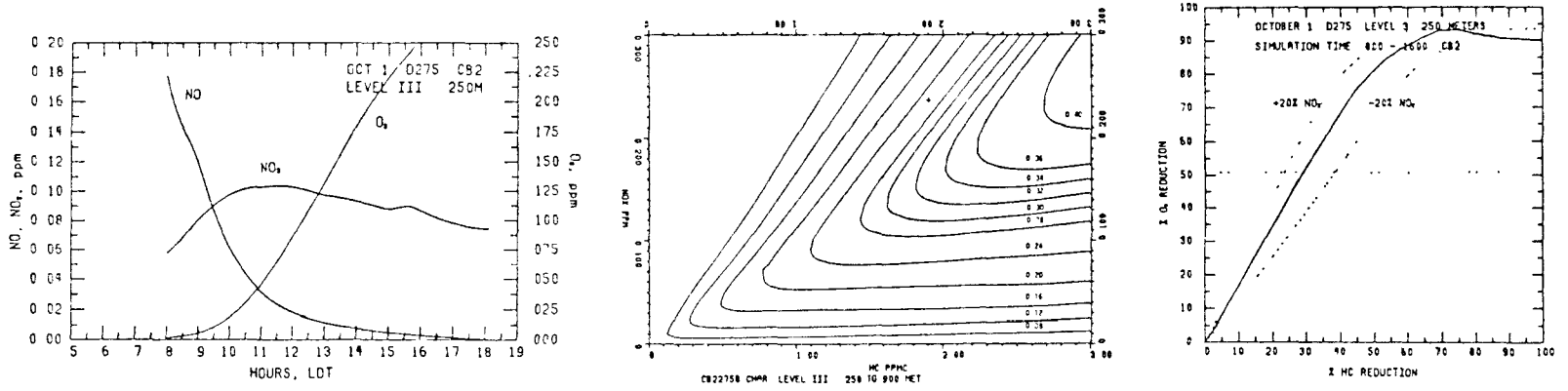

Figure B.2. The effect of changing from a Level II (A) to a Level III (B) application on the EKMA control solution for October 1, 1976 (Carbon Bond Mechanism and characteristic curve mixing height).

APPENDIX C

SIMULATIONS OF INDIVIDUAL BUREAU OF MINES EXPERIMENTS USING CARBON BOND, DEMERJIAN, DODGE, AND CIT MECHANISMS

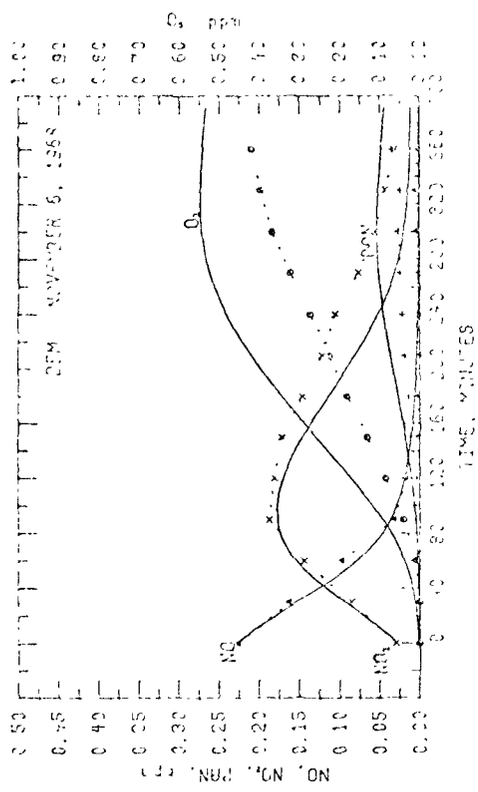
O₃, ppm
NO, NO₂, PAN, ppm
TIME, MINUTES
NO
NO₂
PAN
O₃

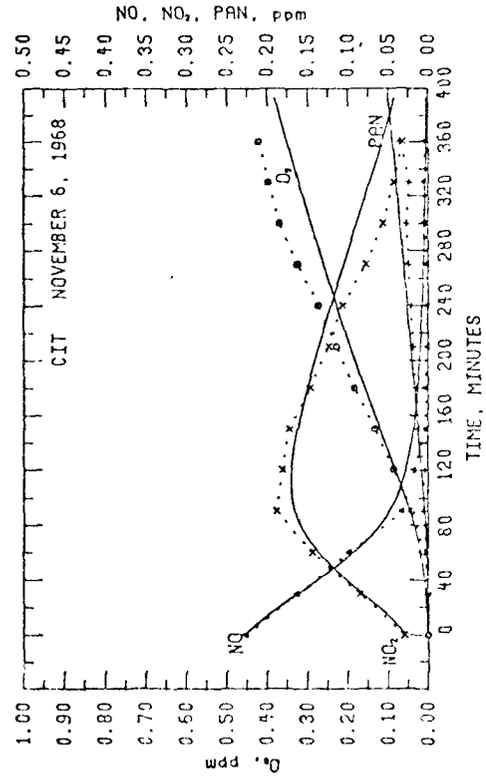
NO, NO₂, PAN, ppm
O₃, ppm
CIT NOVEMBER 6, 1968
TIME, MINUTES
NO
NO₂
PAN
O₃

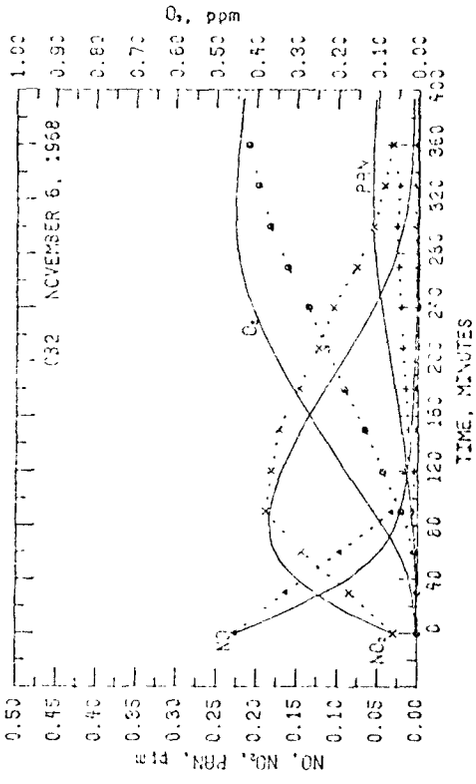
O₃, ppm
NO, NO₂, PAN, ppm
C32 NOVEMBER 6, 1968
TIME, MINUTES
NO
NO₂
PAN
O₃

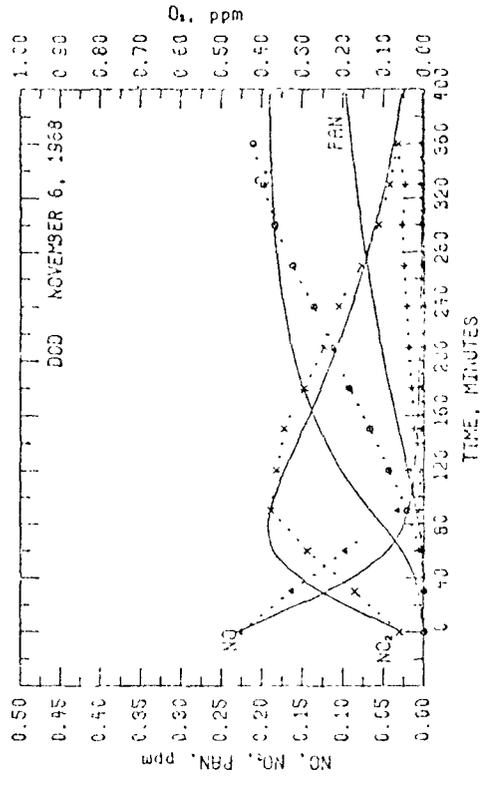
O₃, ppm
NO, NO₂, PAN, ppm
DCD NOVEMBER 6, 1968
TIME, MINUTES
NO
NO₂
PAN

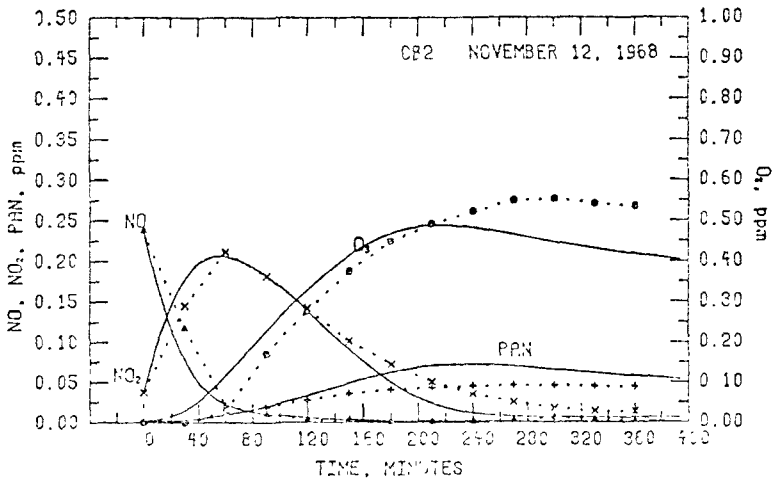
CB2 NOVEMBER 12, 1968
NO, NO₂, PAN, ppm
O₃, ppm
NO
NO₂
O₃
PAN
TIME, MINUTES

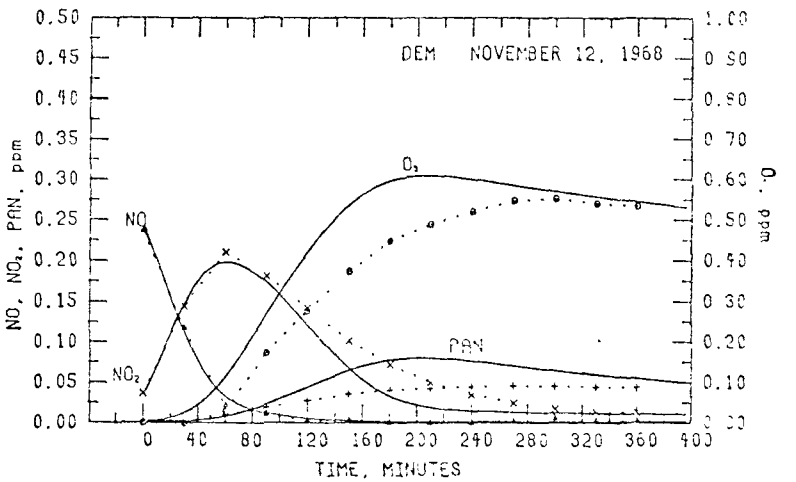
DEM NOVEMBER 12, 1968
NO, NO₂, PAN, ppm
O₃, ppm
NO
NO₂
O₃
PAN
TIME, MINUTES

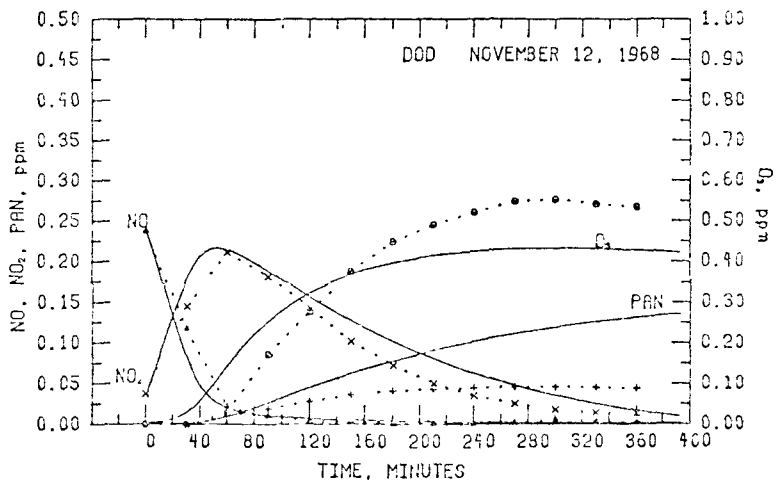
DOD NOVEMBER 12, 1968
NO, NO₂, PAN, ppm
O₃, ppm
NO
NO₂
O₃
PAN
TIME, MINUTES

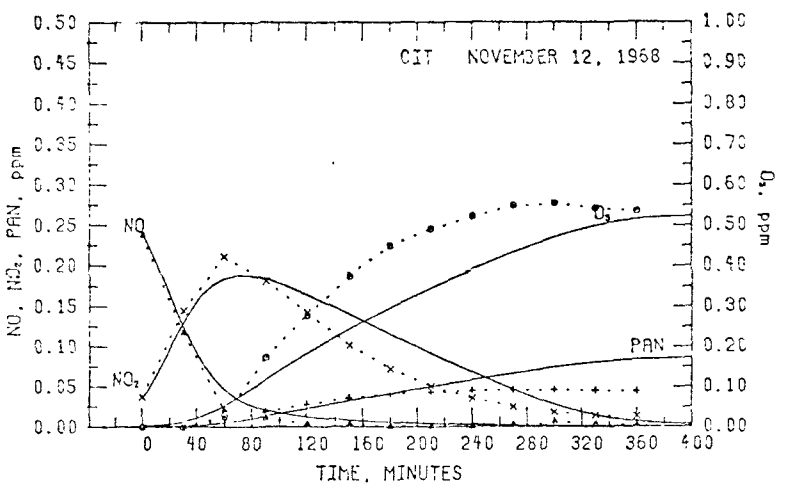
CIT NOVEMBER 12, 1968
NO, NO₂, PAN, ppm
O₃, ppm
NO
NO₂
O₃
PAN
TIME, MINUTES

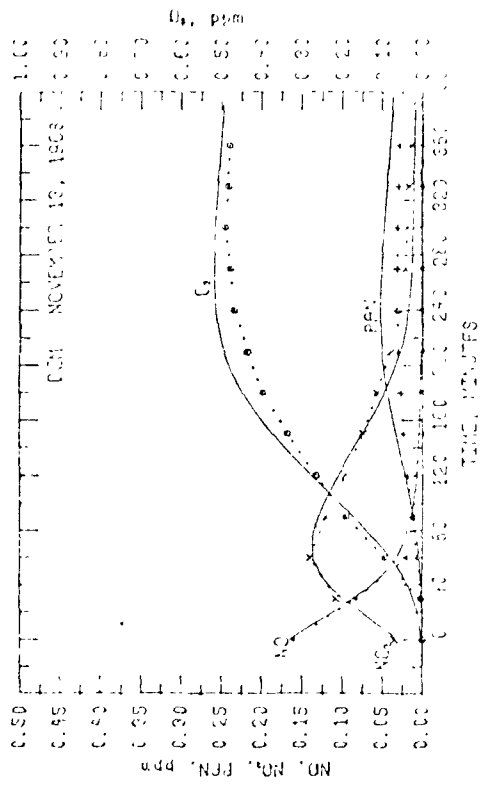
CIT NOVEMBER 13, 1968
O_3, ppm
NO, NO_2, PAN, ppm
TIME, MINUTES
O_3
PAN
NO
NO_2

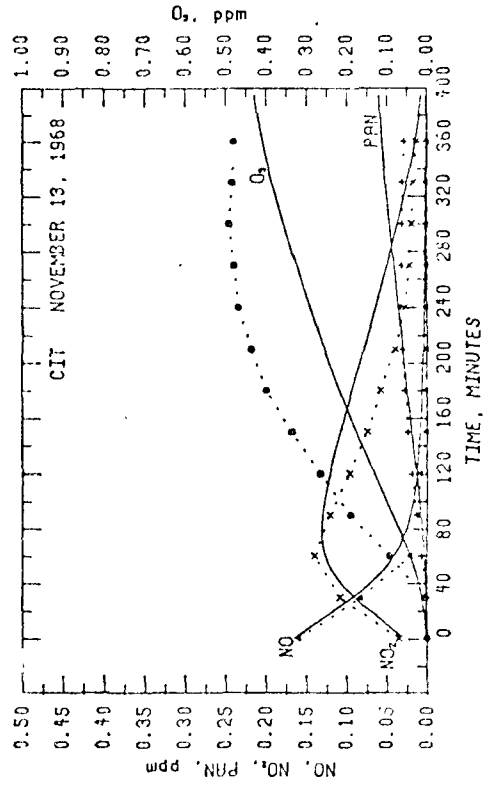
CIT NOVEMBER 13, 1968
O_3, ppm
NO, NO_2, PAN, ppm
TIME, MINUTES
O_3
PAN
NO
NO_2

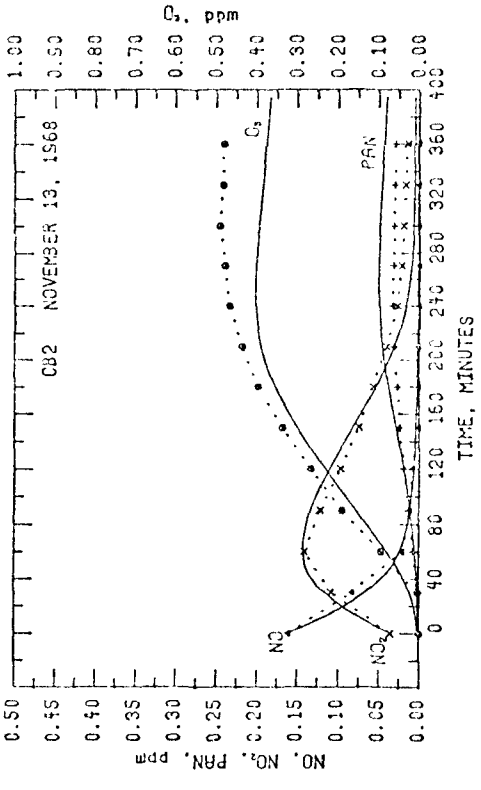
CB2 NOVEMBER 13, 1968
O_3, ppm
NO, NO_2, PAN, ppm
TIME, MINUTES
O_3
PAN
NO
NO_2

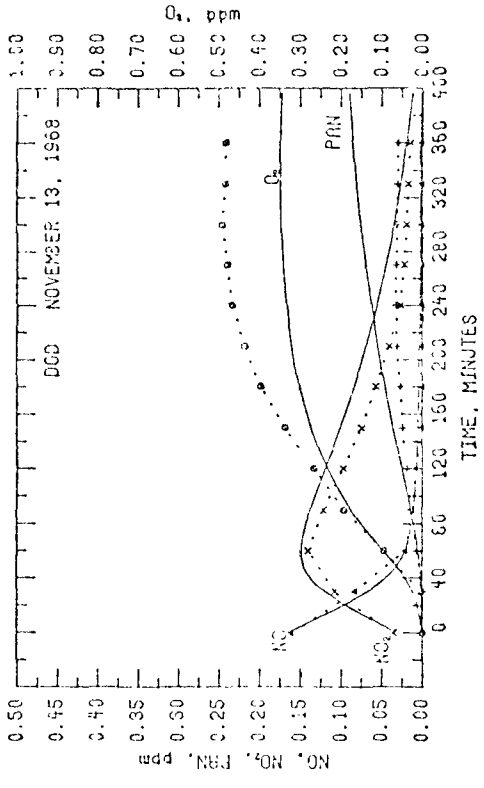
DCD NOVEMBER 13, 1968
O_3, ppm
NO, NO_2, PAN, ppm
TIME, MINUTES
O_3
PAN
NO
NO_2

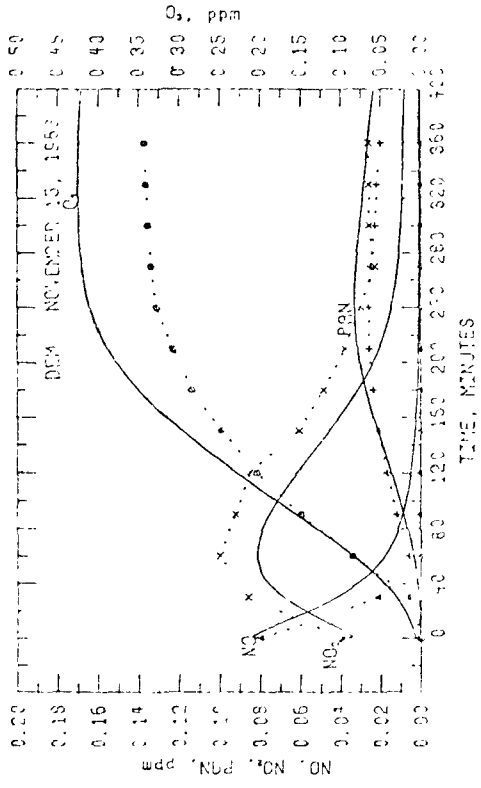
O₃, ppm
DOM NOVEMBER 15, 1968
PAN
NO
NO₂
TIME, MINUTES
NO, NO₂, PAN, ppm

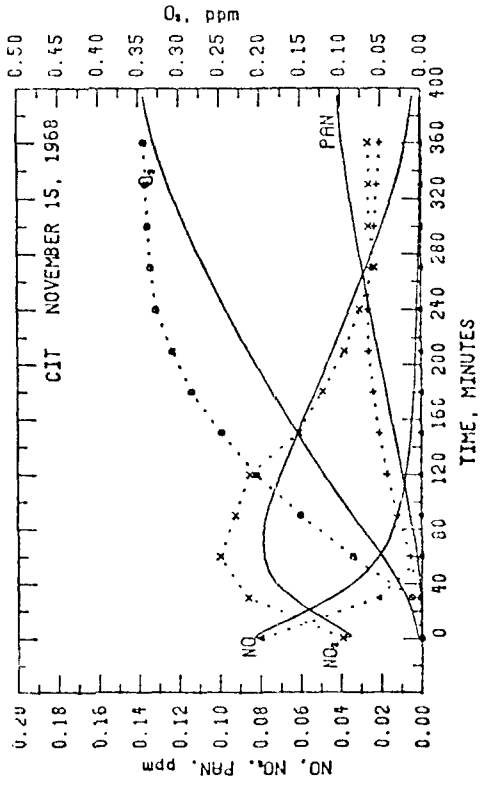
O₃, ppm
CIT NOVEMBER 15, 1968
PAN
NO
NO₂
TIME, MINUTES
NO, NO₂, PAN, ppm

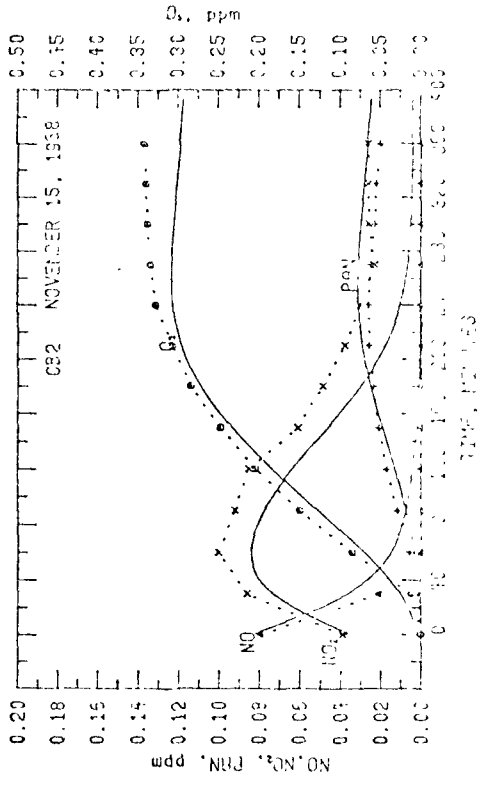
O₃, ppm
CB2 NOVEMBER 15, 1968
PAN
NO
NO₂
NO, NO₂, PAN, ppm

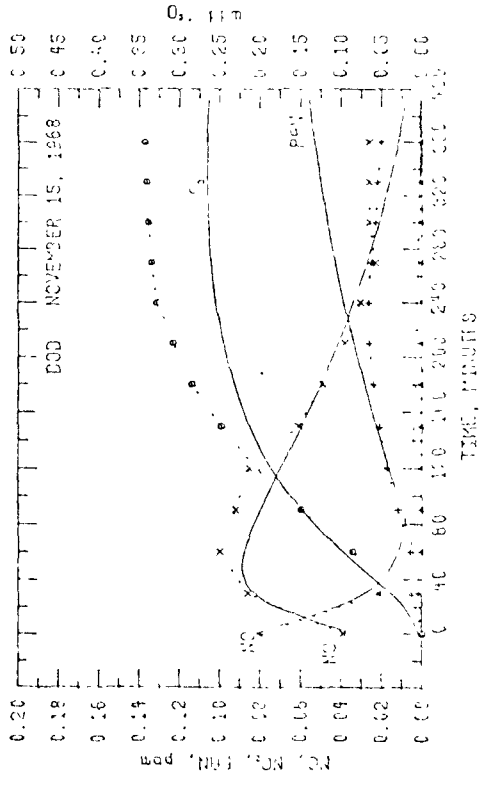
DOD NOVEMBER 15, 1968
PAN
NO
NO₂

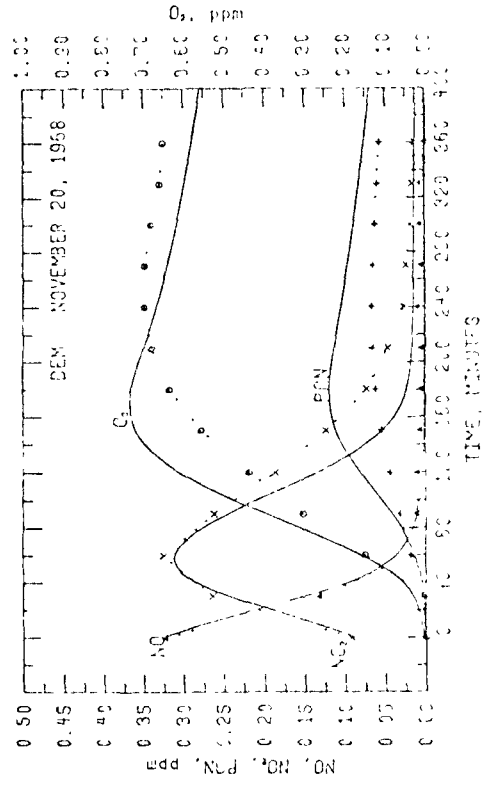
O₃, ppm
DEM NOVEMBER 20, 1968
O₃
PAN
NO
NO₂
TIME, MINUTES
NO, NO₂, PAN, ppm

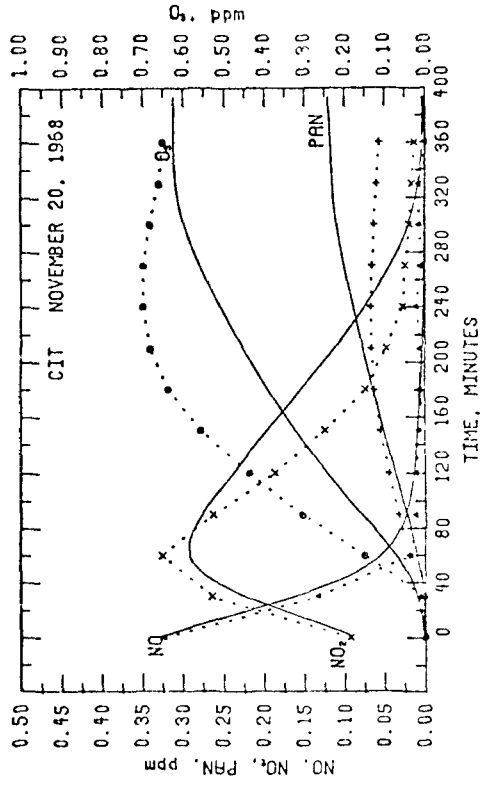
O₃, ppm
CIT NOVEMBER 20, 1968
O₃
PAN
NO
NO₂
TIME, MINUTES
NO, NO₂, PAN, ppm

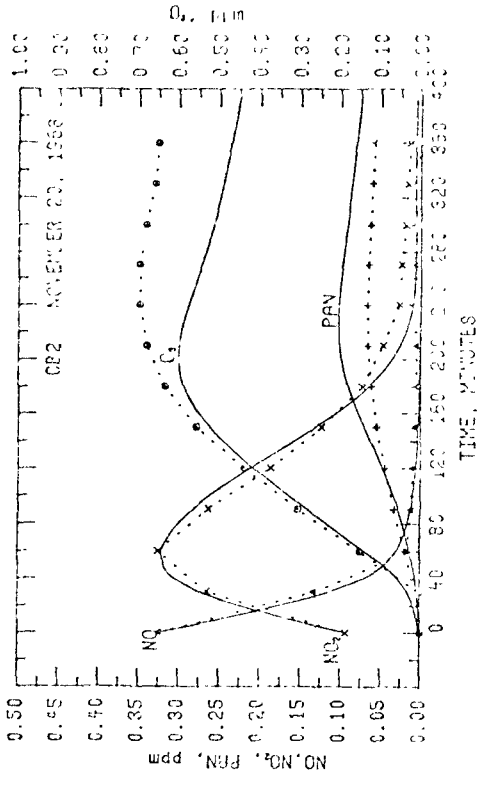
O₃, ppm
CB2 NOVEMBER 20, 1968
O₃
PAN
NO
NO₂
TIME, MINUTES
NO, NO₂, PAN, ppm

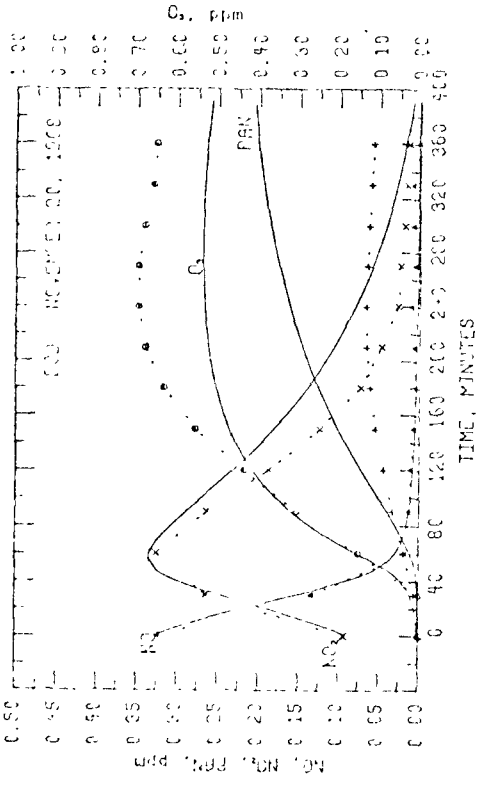
O₃, ppm
O₃
PAN
NO
NO₂
TIME, MINUTES
NO, NO₂, PAN, ppm

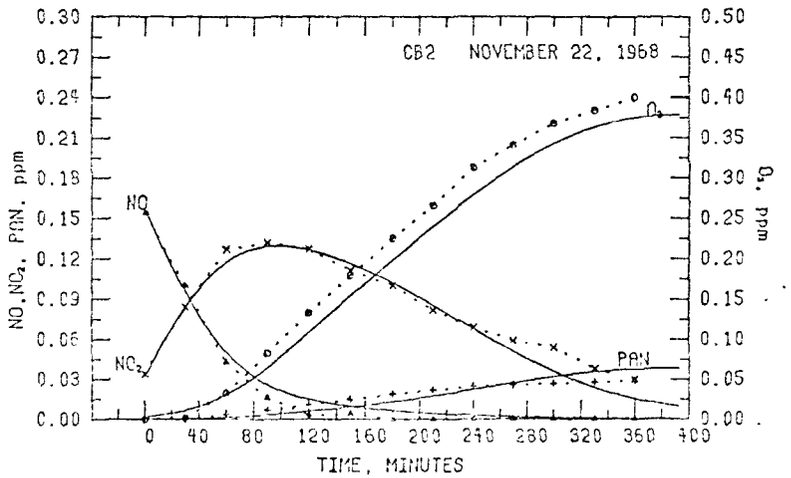
CB2 NOVEMBER 22, 1968
NO
NO2
O3
PAN
NO, NO2, PAN, ppm
O3, ppm
TIME, MINUTES

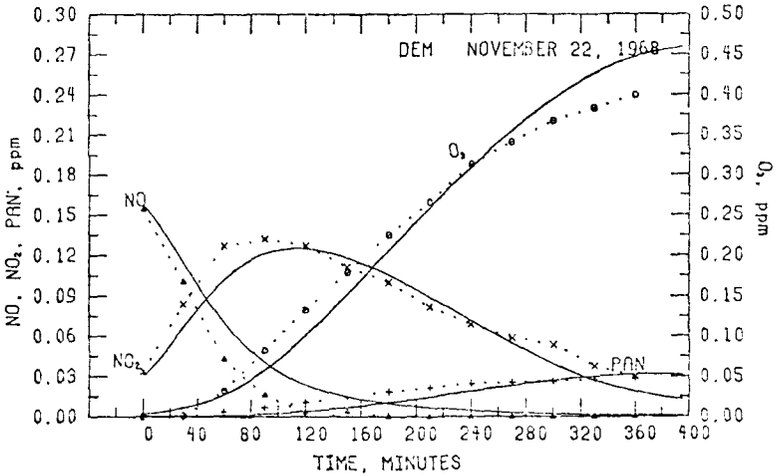
DEM NOVEMBER 22, 1968
NO
NO2
O3
PAN
NO, NO2, PAN, ppm
O3, ppm
TIME, MINUTES

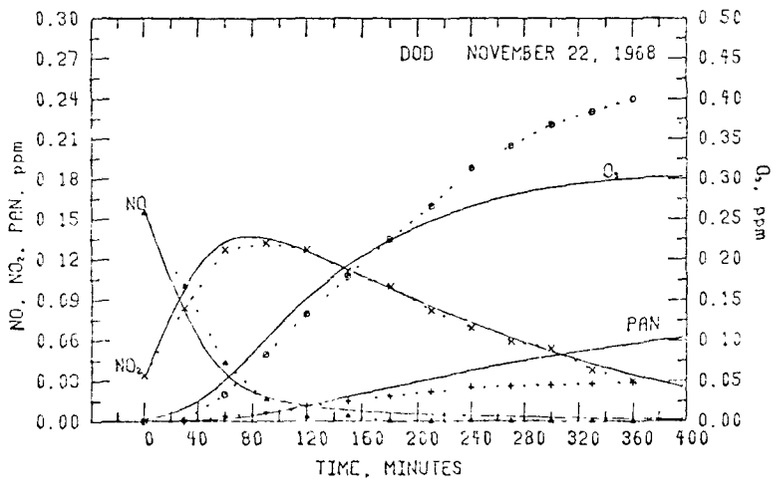
DOD NOVEMBER 22, 1968
NO
NO2
O3
PAN
NO, NO2, PAN, ppm
O3, ppm
TIME, MINUTES

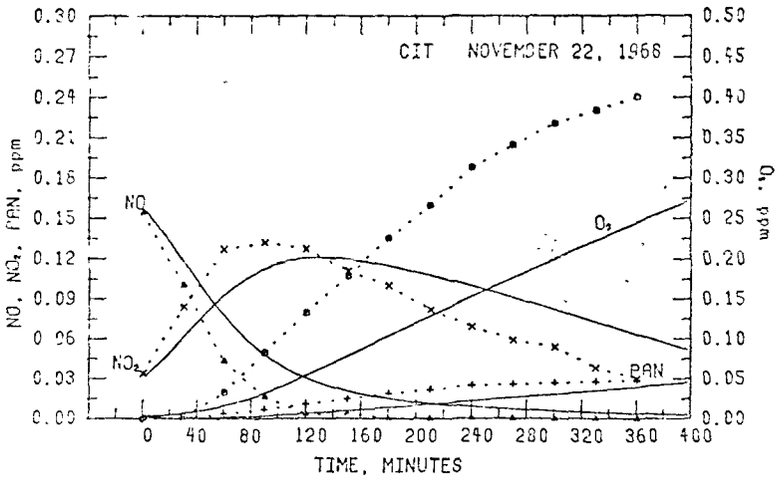
CIT NOVEMBER 22, 1968
NO
NO2
O3
PAN
NO, NO2, PAN, ppm
O3, ppm
TIME, MINUTES

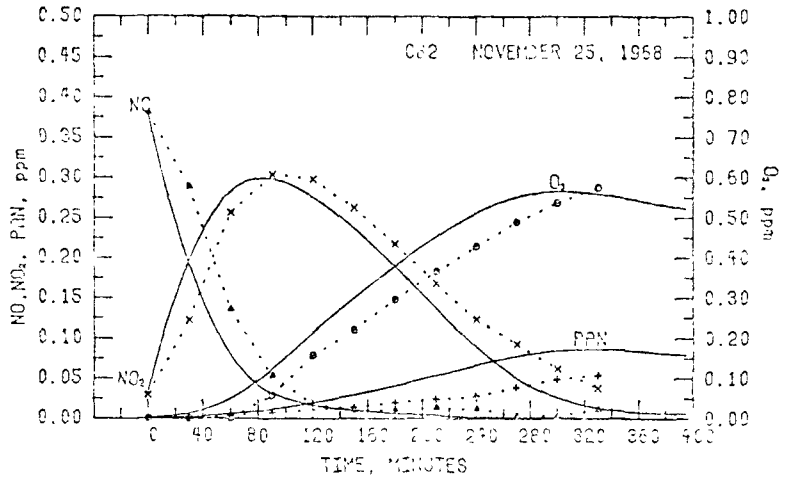
CAZ NOVEMBER 25, 1968
NO
NO2
O3
PAN
NO, NO2, PAN, ppm
O3, ppm
TIME, MINUTES

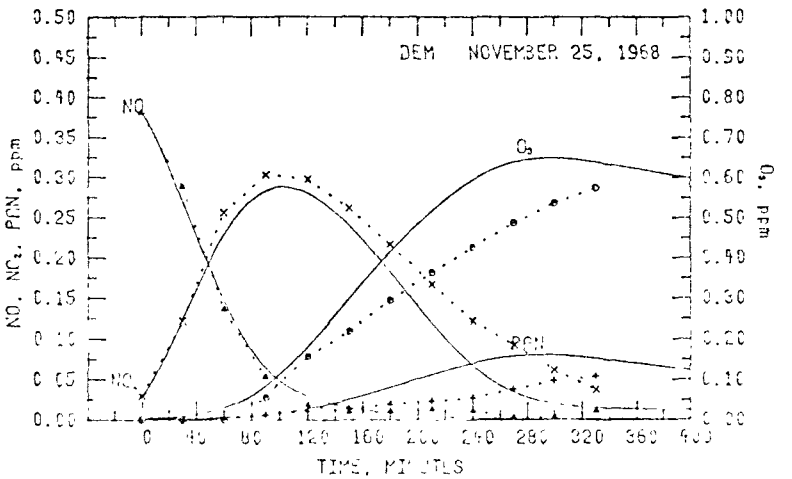
DEM NOVEMBER 25, 1968
NO
NO2
O3
PAN
NO, NO2, PAN, ppm
O3, ppm
TIME, MINUTES

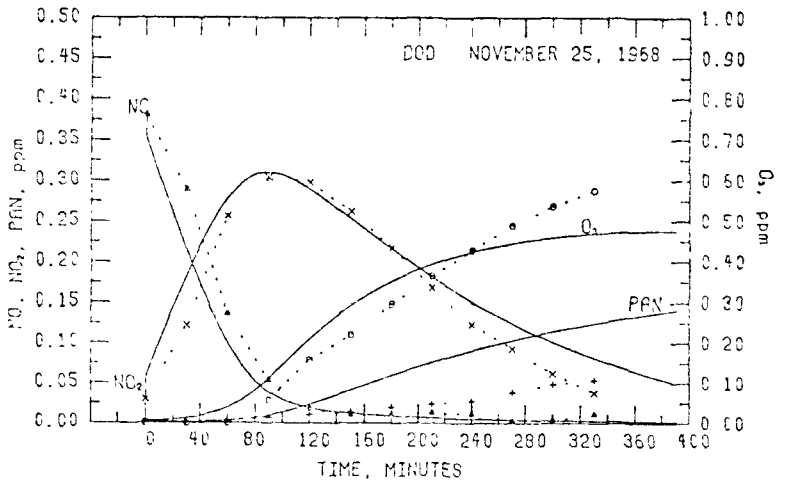
DOD NOVEMBER 25, 1968
NO
NO2
O3
PAN
NO, NO2, PAN, ppm
O3, ppm
TIME, MINUTES

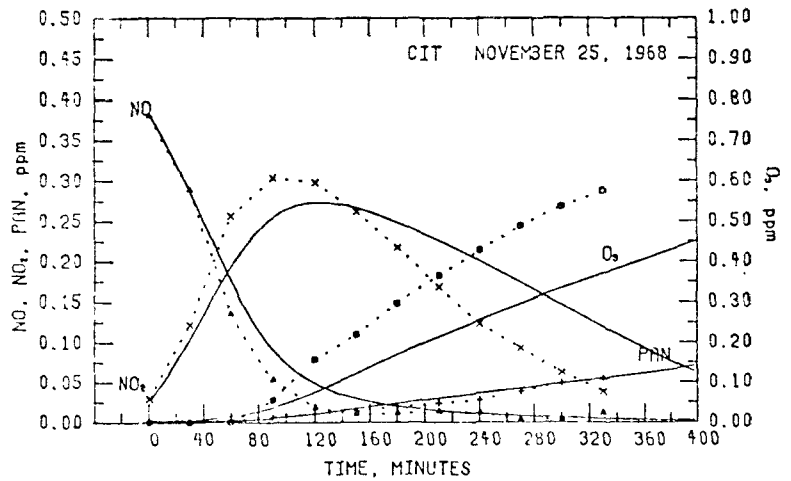
CIT NOVEMBER 25, 1968
NO
NO2
O3
PAN
NO, NO2, PAN, ppm
O3, ppm
TIME, MINUTES

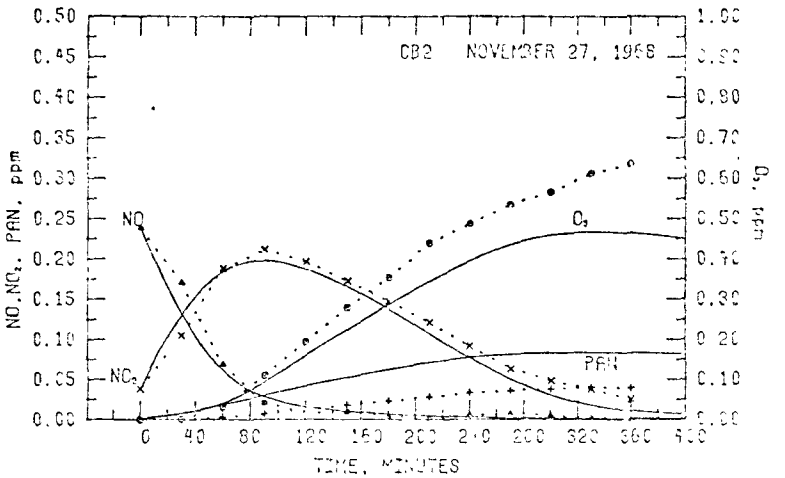
CB2 NOVEMBER 27, 1968
NO
NO2
O3
PAN
NO, NO2, PAN, ppm
O3, ppm
TIME, MINUTES

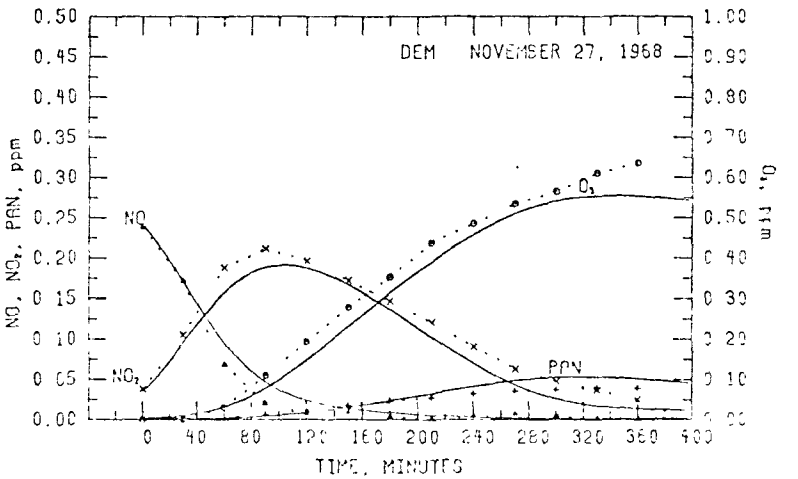
DEM NOVEMBER 27, 1968
NO
NO2
O3
PAN
NO, NO2, PAN, ppm
O3, ppm
TIME, MINUTES

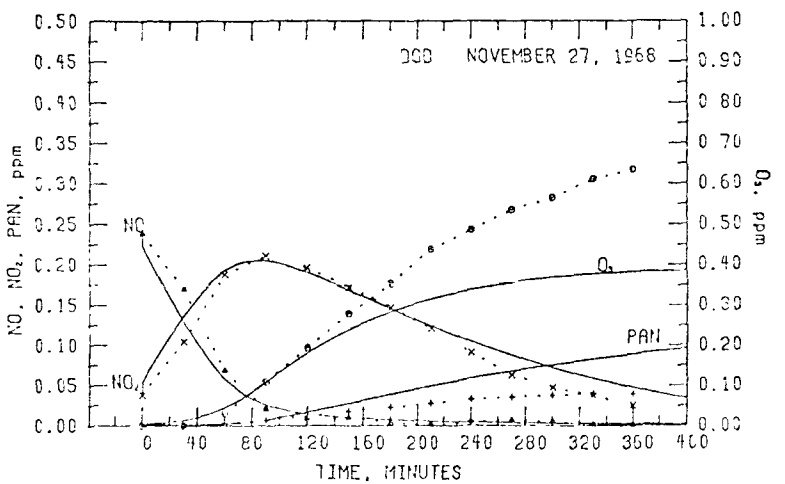
DOD NOVEMBER 27, 1968
NO
NO2
O3
PAN
NO, NO2, PAN, ppm
O3, ppm
TIME, MINUTES

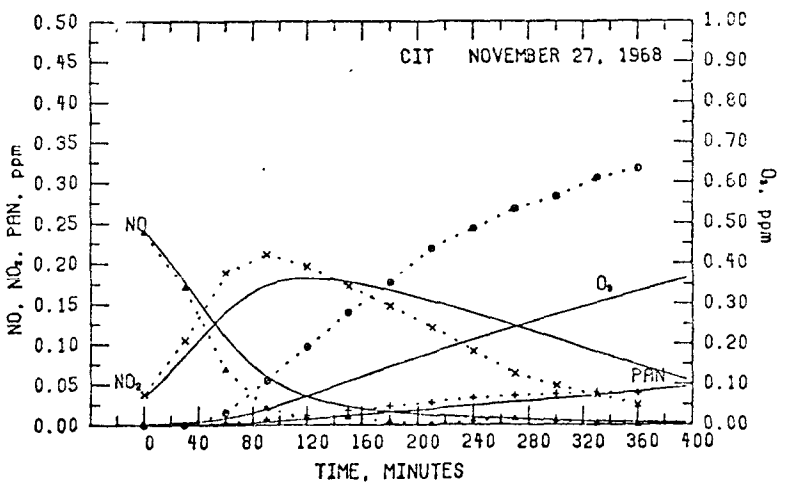
CIT NOVEMBER 27, 1968
NO
NO2
O3
PAN
NO, NO2, PAN, ppm
O3, ppm
TIME, MINUTES

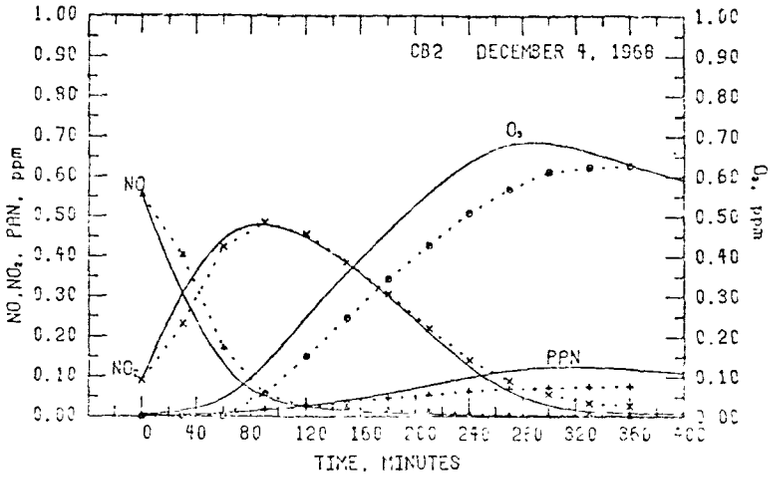
CB2 DECEMBER 4, 1968
NO, NO₂, PAN, ppm
O₃, ppm
NO
NO₂
O₃
PPN
TIME, MINUTES

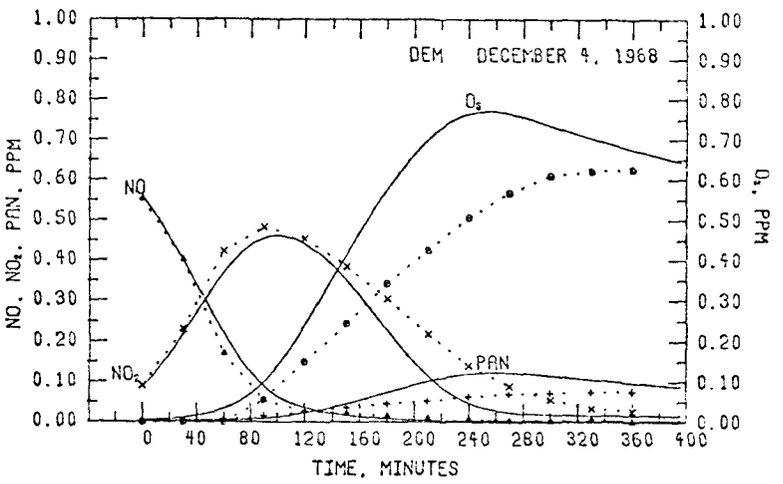
DEM DECEMBER 4, 1968
NO, NO₂, PAN, PPM
O₃, PPM
NO
NO₂
O₃
PAN
TIME, MINUTES

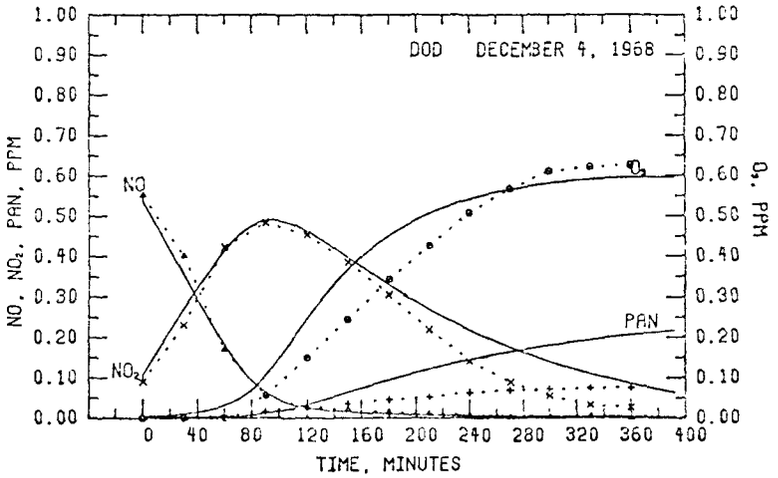
DOD DECEMBER 4, 1968
NO, NO₂, PAN, PPM
O₃, PPM
NO
NO₂
O₃
PAN
TIME, MINUTES

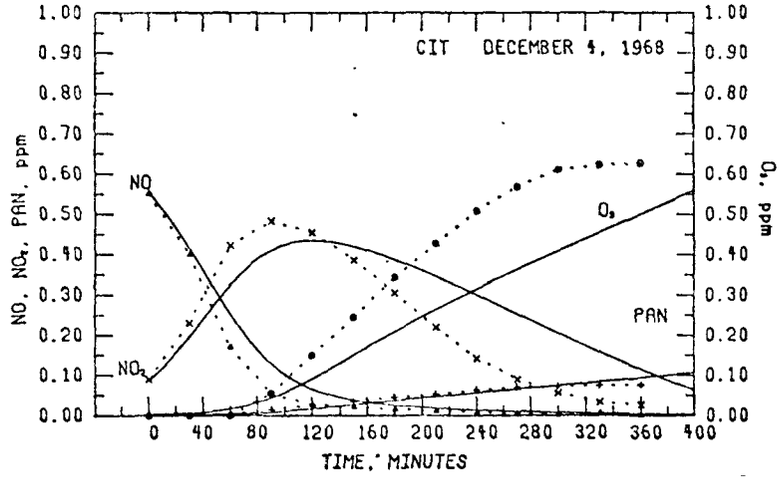
CIT DECEMBER 4, 1968
NO, NO₂, PAN, ppm
O₃, ppm
NO
NO₂
O₃
PAN
TIME, MINUTES

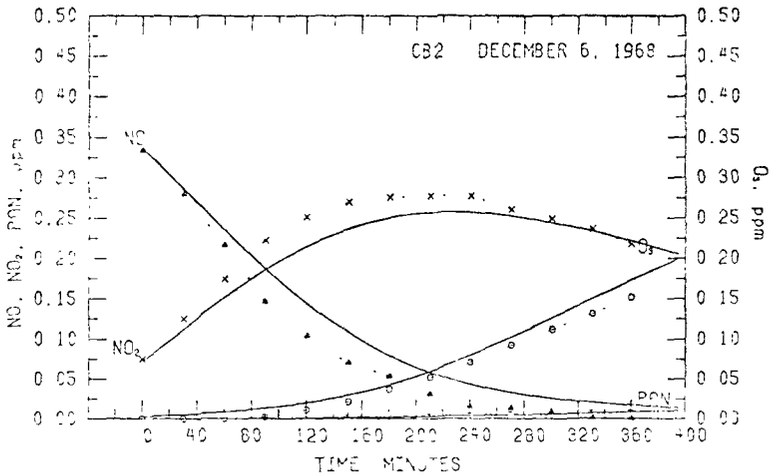
CB2 DECEMBER 6, 1968
NO
NO2
O3
PAN
NO, NO2, PAN, ppm
O3, ppm
TIME, MINUTES

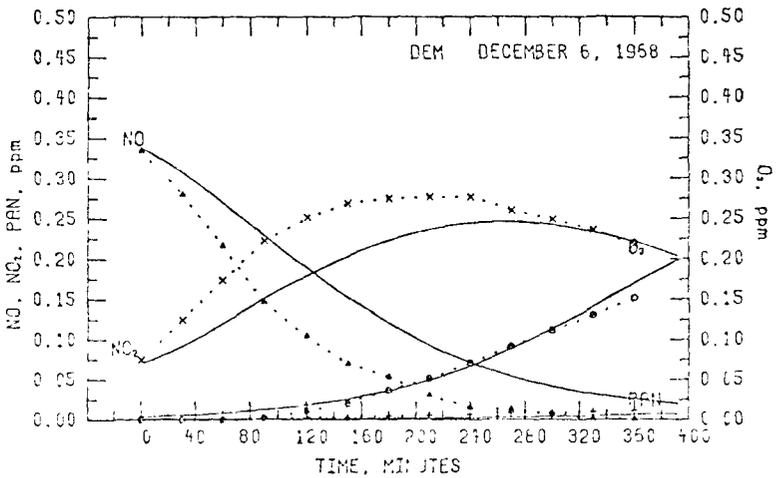
DEM DECEMBER 6, 1968
NO
NO2
O3
PAN
NO, NO2, PAN, ppm
O3, ppm
TIME, MINUTES

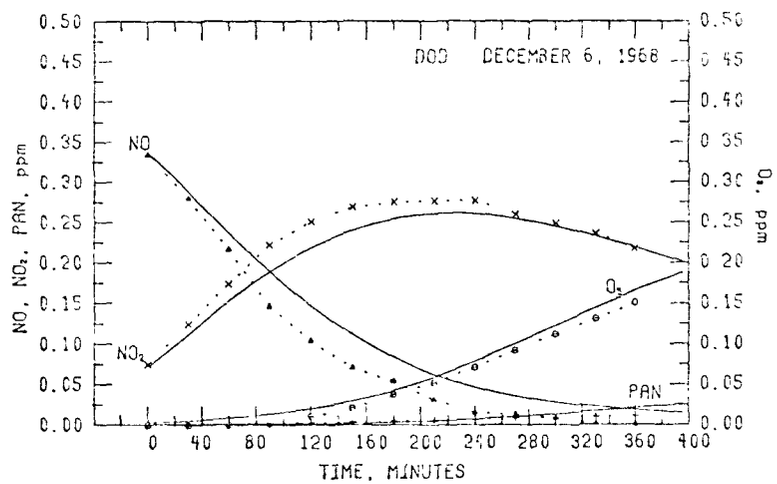
DOD DECEMBER 6, 1968
NO
NO2
O3
PAN
NO, NO2, PAN, ppm
O3, ppm
TIME, MINUTES

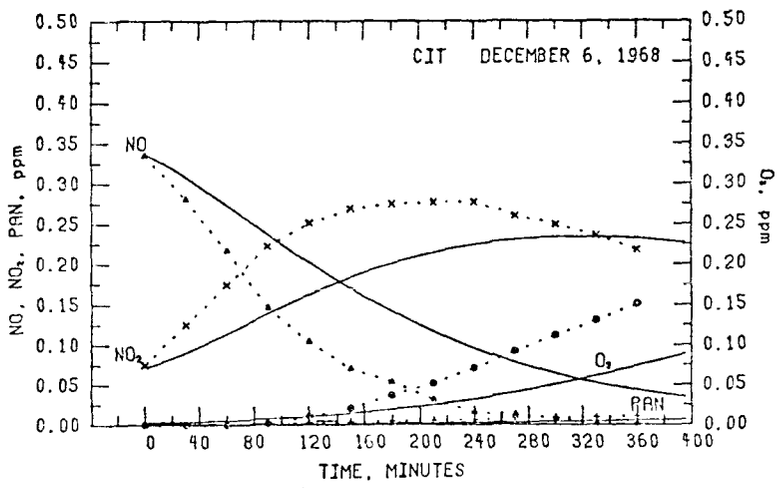
CIT DECEMBER 6, 1968
NO
NO2
O3
PAN
NO, NO2, PAN, ppm
O3, ppm
TIME, MINUTES

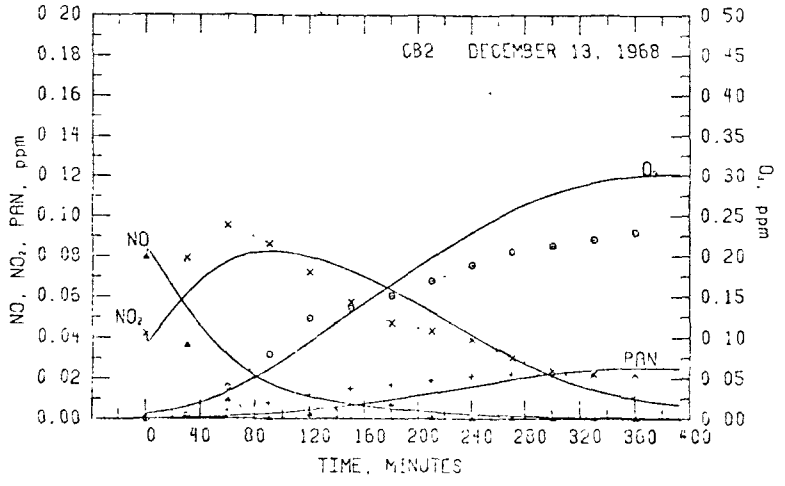
CB2 DECEMBER 13, 1968
NO, NO₂, PAN, ppm
O₃, ppm
TIME, MINUTES
NO
NO₂
O₃
PAN

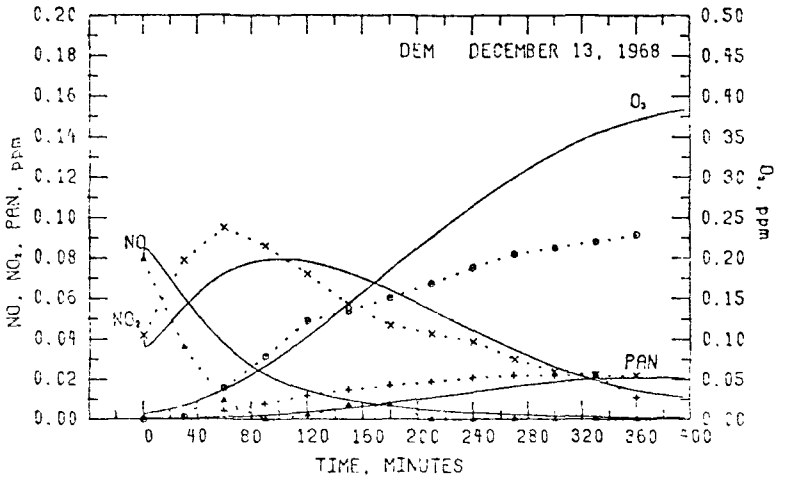
DEM DECEMBER 13, 1968
NO, NO₂, PAN, ppm
O₃, ppm
TIME, MINUTES
NO
NO₂
O₃
PAN

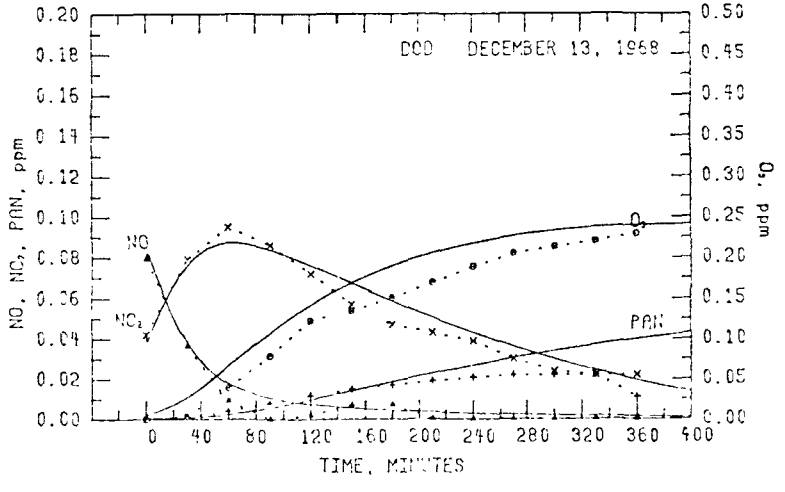
DCD DECEMBER 13, 1968
NO, NO₂, PAN, ppm
O₃, ppm
TIME, MINUTES
NO
NO₂
O₃
PAN

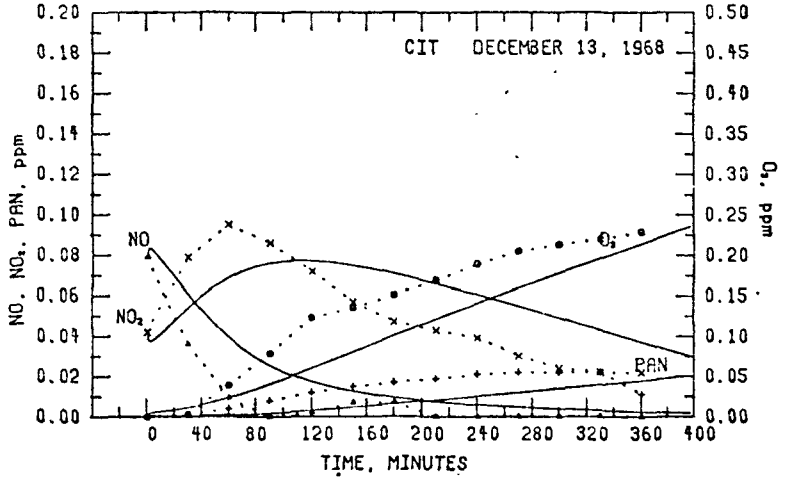
CIT DECEMBER 13, 1968
NO, NO₂, PAN, ppm
O₃, ppm
TIME, MINUTES
NO
NO₂
O₃
PAN

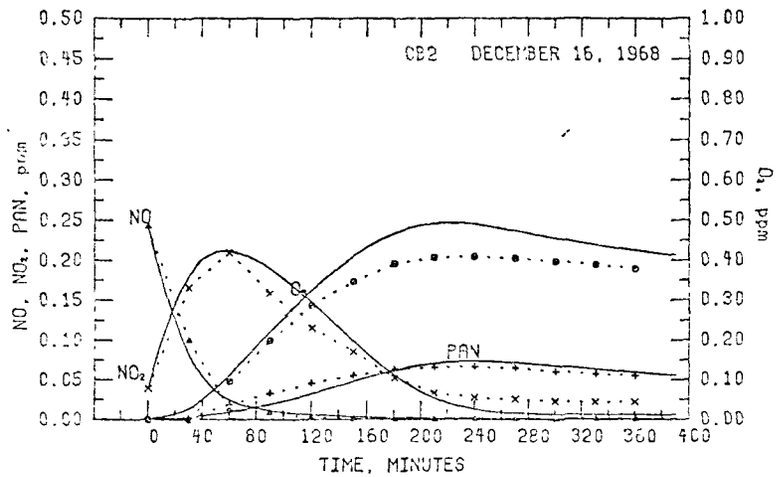
CB2 DECEMBER 16, 1968
NO
NO₂
O₃
PAN
NO, NO₂, PAN, ppm
O₃, ppm
TIME, MINUTES

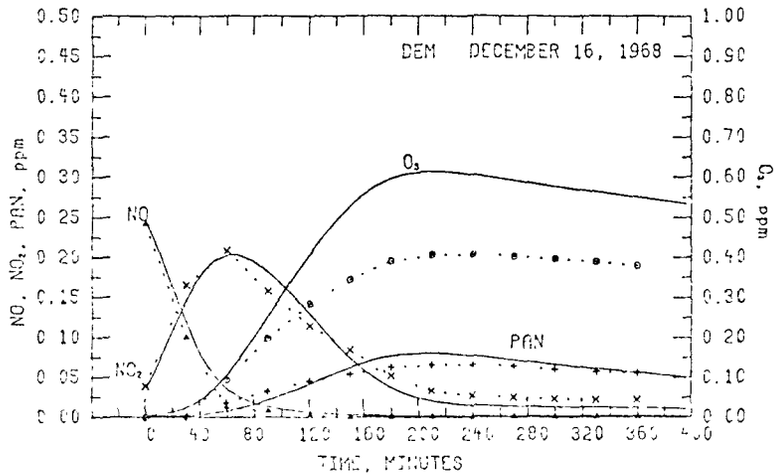
DEM DECEMBER 16, 1968
NO
NO₂
O₃
PAN
NO, NO₂, PAN, ppm
O₃, ppm
TIME, MINUTES

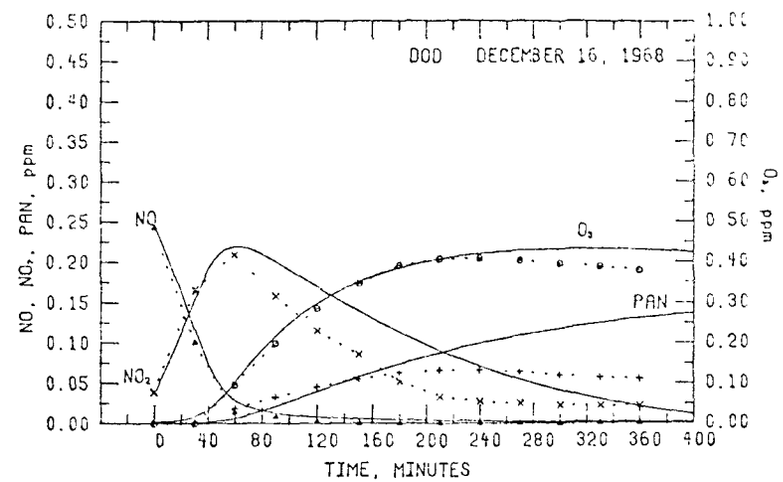
DOD DECEMBER 16, 1968
NO
NO₂
O₃
PAN
NO, NO₂, PAN, ppm
O₃, ppm
TIME, MINUTES

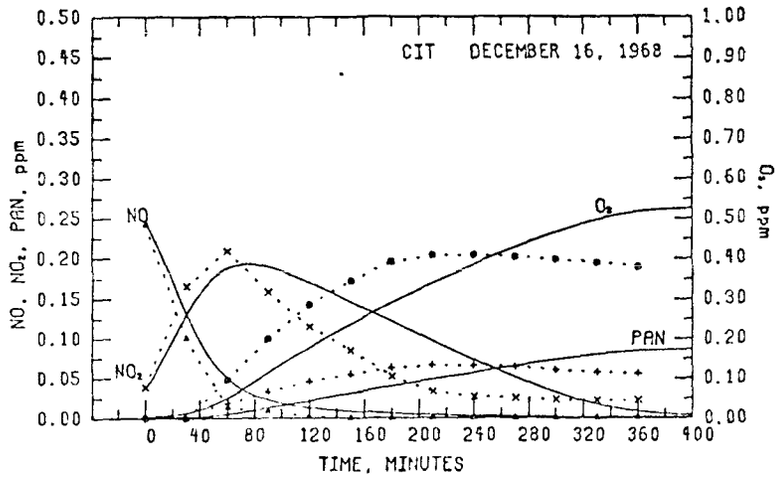
CIT DECEMBER 16, 1968
NO
NO₂
O₃
PAN
NO, NO₂, PAN, ppm
O₃, ppm
TIME, MINUTES

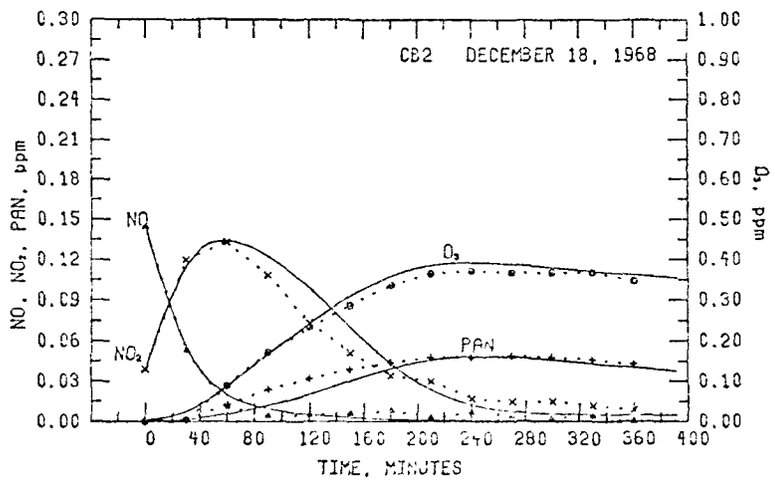
CB2 DECEMBER 18, 1968
NO
NO₂
O₃
PAN
NO, NO₂, PAN, ppm
O₃, ppm
TIME, MINUTES

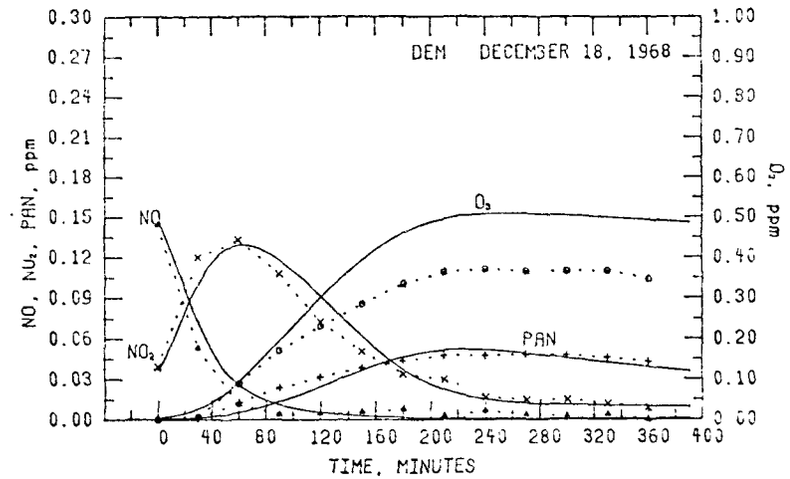
DEM DECEMBER 18, 1968
NO
NO₂
O₃
PAN
NO, NO₂, PAN, ppm
O₃, ppm
TIME, MINUTES

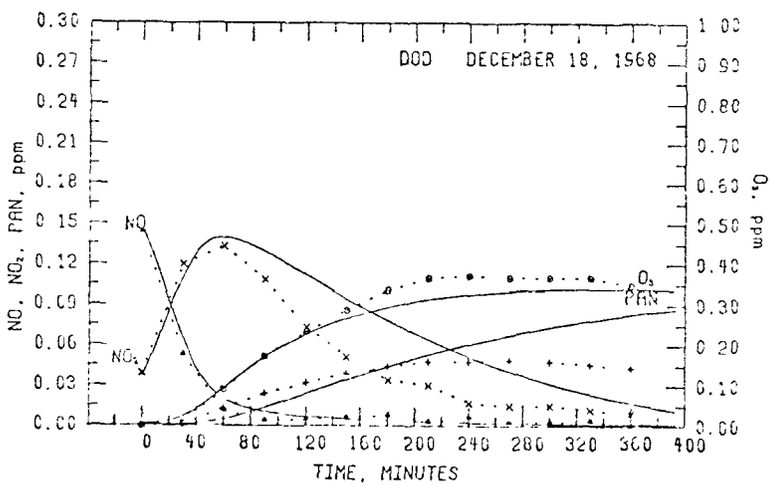
DOD DECEMBER 18, 1968
NO
NO₂
O₃
PAN
NO, NO₂, PAN, ppm
O₃, ppm
TIME, MINUTES

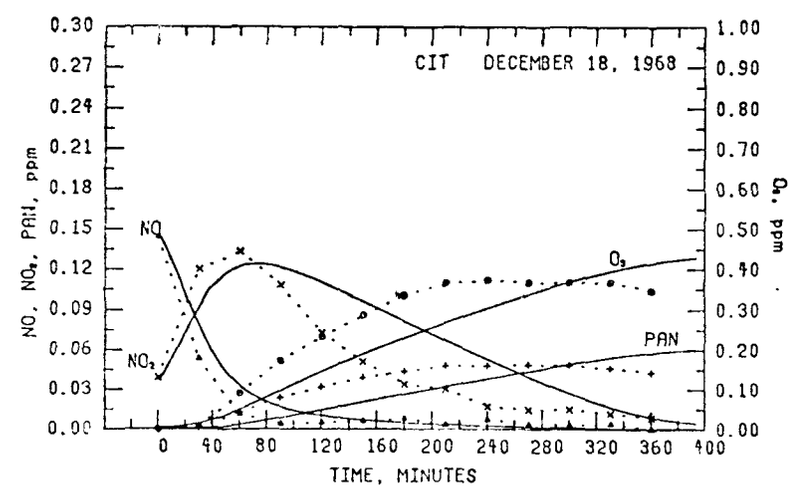
CIT DECEMBER 18, 1968
NO
NO₂
O₃
PAN
NO, NO₂, PAN, ppm
O₃, ppm
TIME, MINUTES

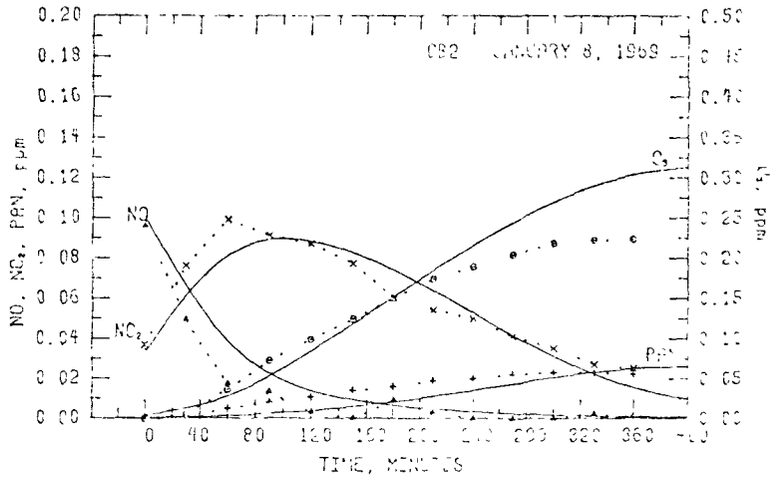
CBZ JANUARY 8, 1969
NO
NO2
O3
PAN
NO, NO2, PAN, ppm
O3, ppm
TIME, MINUTES

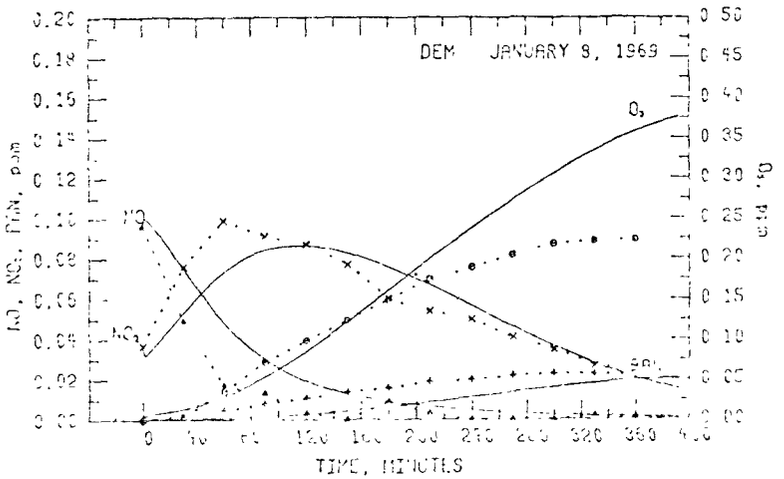
DEM JANUARY 8, 1969
NO
NO2
O3
PAN
NO, NO2, PAN, ppm
O3, ppm
TIME, MINUTES

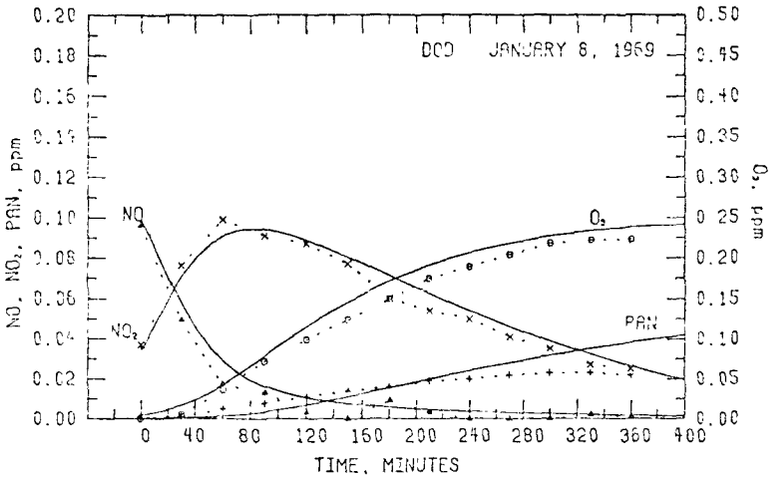
DCO JANUARY 8, 1969
NO
NO2
O3
PAN
NO, NO2, PAN, ppm
O3, ppm
TIME, MINUTES

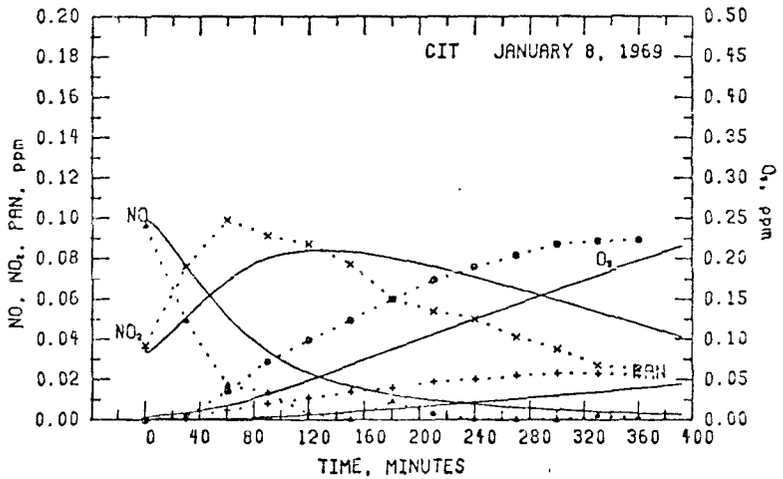
CIT JANUARY 8, 1969
NO
NO2
O3
PAN
NO, NO2, PAN, ppm
O3, ppm
TIME, MINUTES

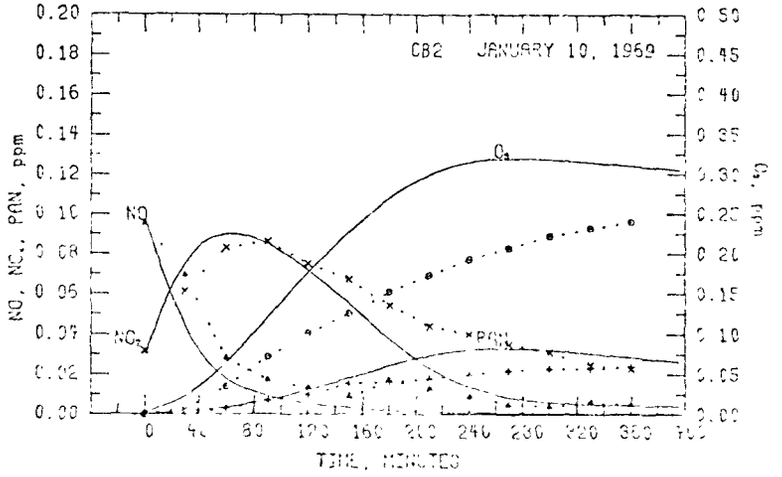
CB2 JANUARY 10, 1969
NO, NO2, PAN, ppm
O3, ppm
TIME, MINUTES
NO
NO2
O3
PAN

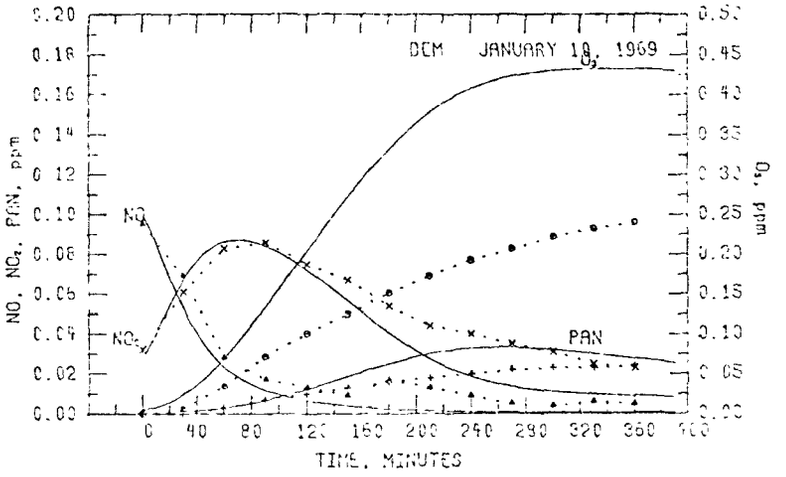
DEM JANUARY 10, 1969
NO, NO2, PAN, ppm
O3, ppm
TIME, MINUTES
NO
NO2
O3
PAN

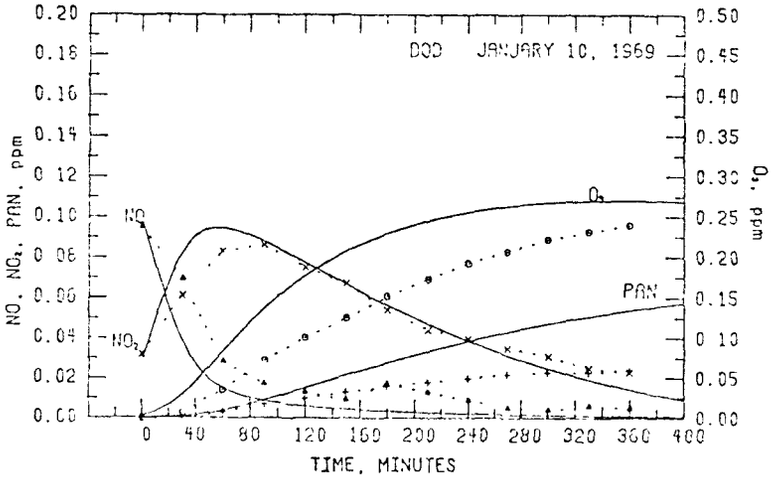
DOD JANUARY 10, 1969
NO, NO2, PAN, ppm
O3, ppm
TIME, MINUTES
NO
NO2
O3
PAN

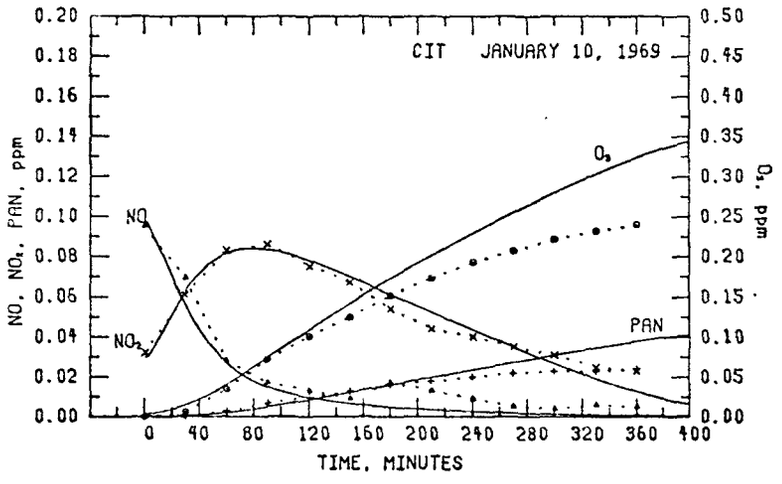
CIT JANUARY 10, 1969
NO, NO2, PAN, ppm
O3, ppm
TIME, MINUTES
NO
NO2
O3
PAN

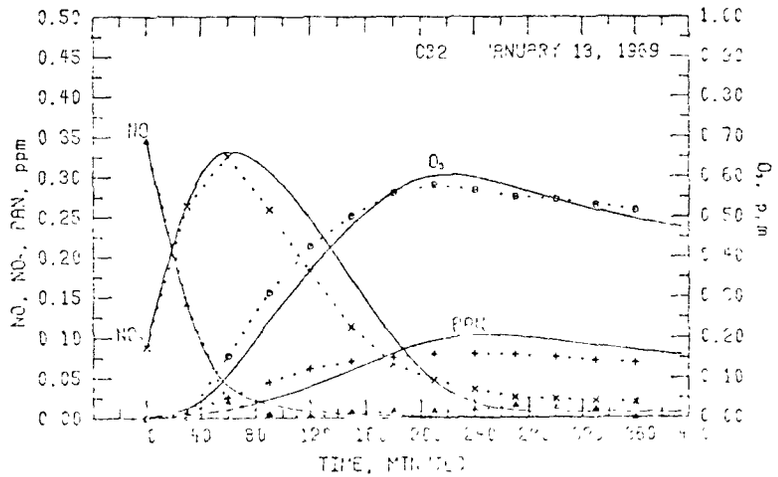
C32 JANUARY 13, 1969
NO
NO₂
O₃
PAN
NO, NO₂, PAN, ppm
O₃, ppm
TIME, MINUTES

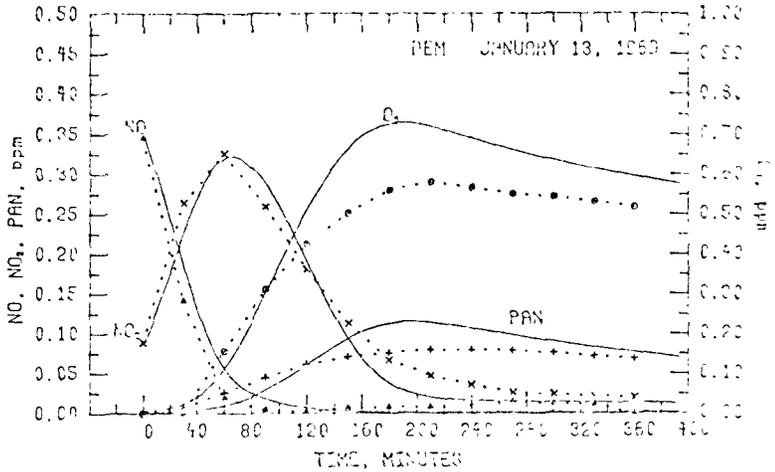
PEM JANUARY 13, 1969
NO
NO₂
O₃
PAN
NO, NO₂, PAN, ppm
TIME, MINUTES

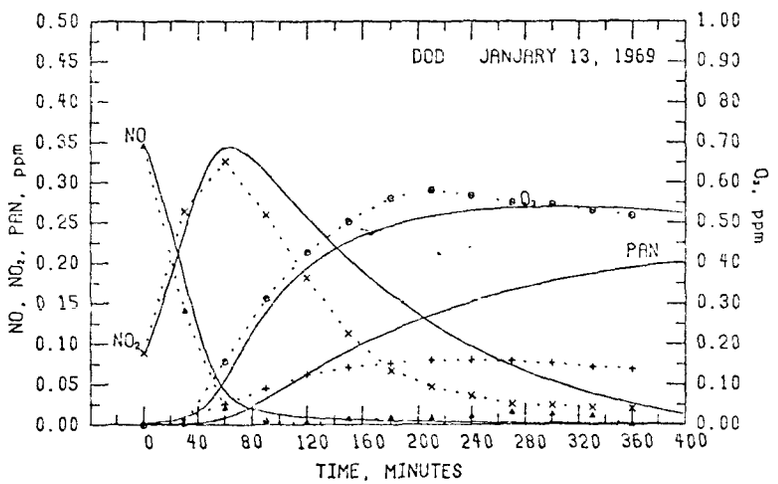
DOD JANUARY 13, 1969
NO
NO₂
O₃
PAN
NO, NO₂, PAN, ppm
O₃, ppm
TIME, MINUTES

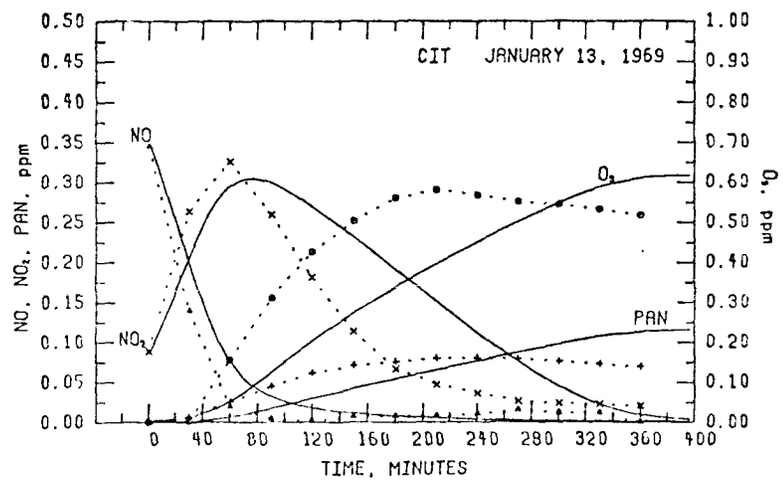
CIT JANUARY 13, 1969
NO
NO₂
O₃
PAN
NO, NO₂, PAN, ppm
O₃, ppm
TIME, MINUTES

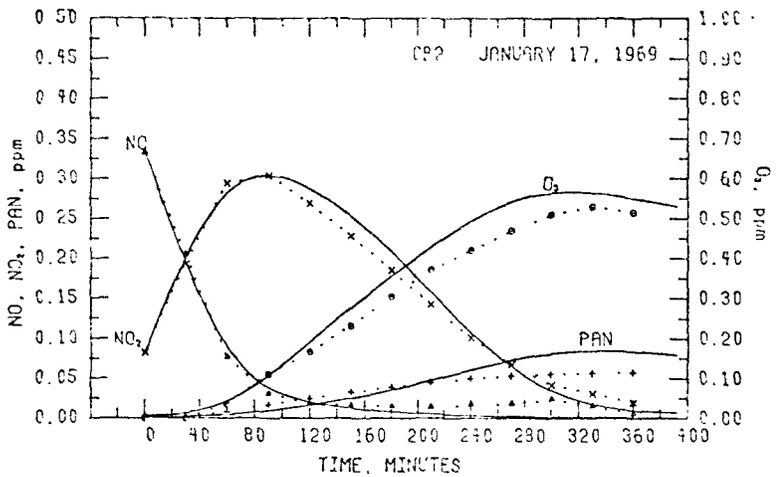
CPP JANUARY 17, 1969
NO
NO₂
O₃
PAN
NO, NO₂, PAN, ppm
O₃, ppm
TIME, MINUTES

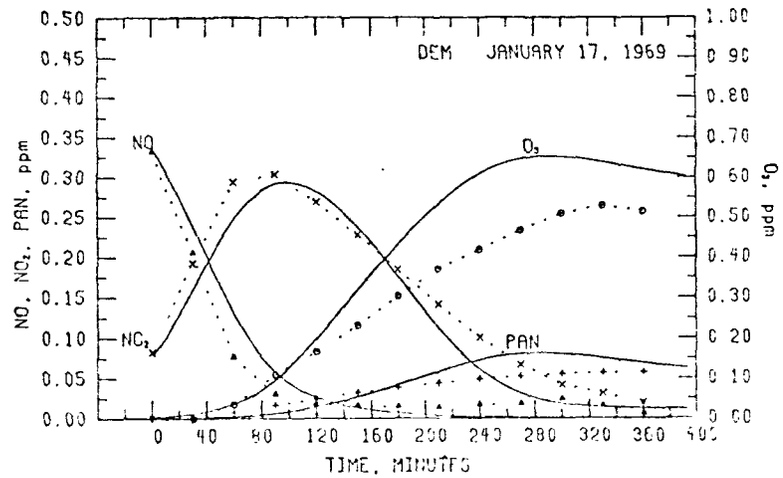
DEM JANUARY 17, 1969
NO
NO₂
O₃
PAN
NO, NO₂, PAN, ppm
O₃, ppm
TIME, MINUTES

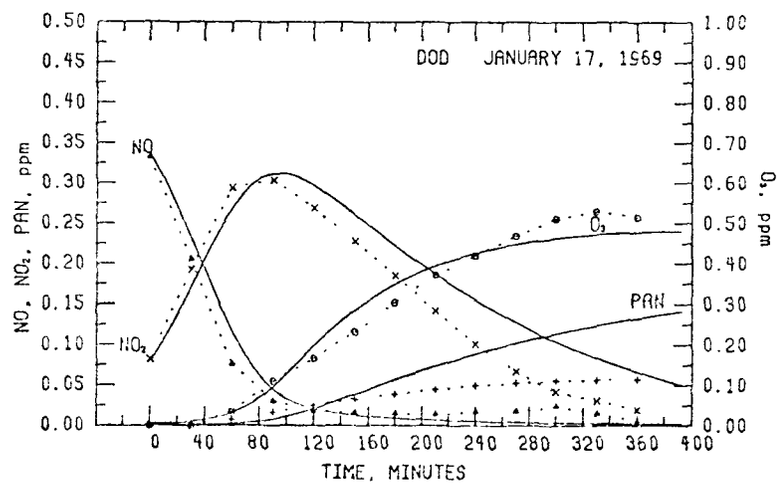
DOD JANUARY 17, 1969
NO
NO₂
O₃
PAN
NO, NO₂, PAN, ppm
O₃, ppm
TIME, MINUTES

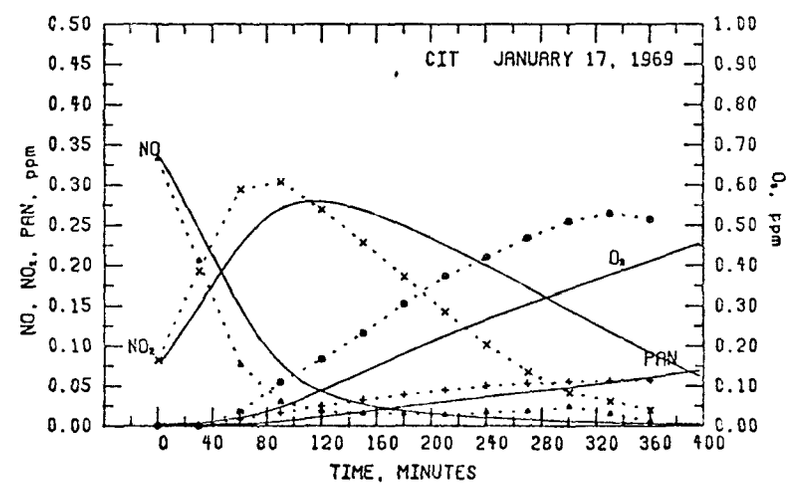
CIT JANUARY 17, 1969
NO
NO₂
O₃
PAN
NO, NO₂, PAN, ppm
O₃, ppm
TIME, MINUTES

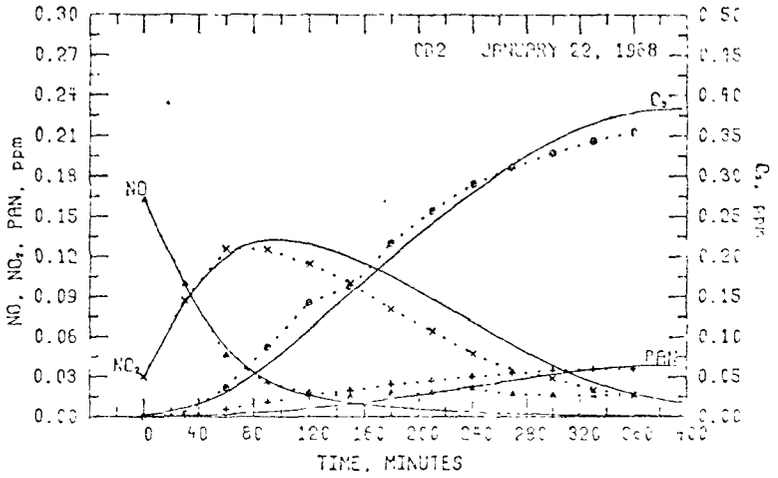
CB2 JANUARY 22, 1968
NO
NO2
O3
PAN
NO, NO2, PAN, ppm
O3, ppm
TIME, MINUTES

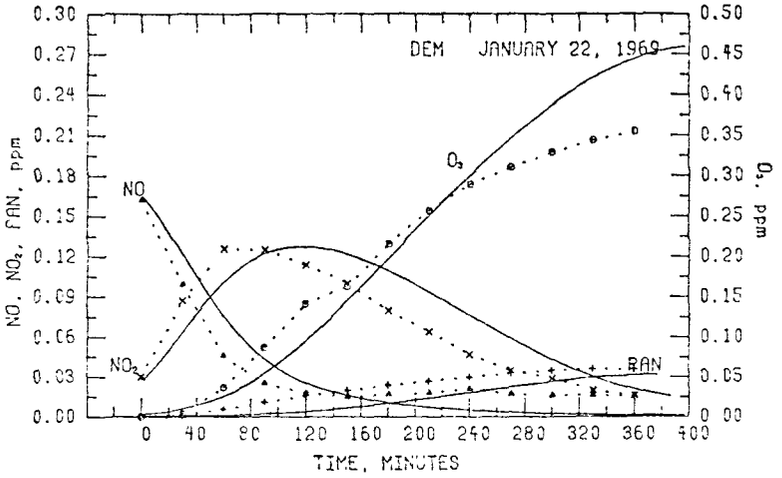
DEM JANUARY 22, 1969
NO
NO2
O3
PAN
NO, NO2, PAN, ppm
O3, ppm
TIME, MINUTES

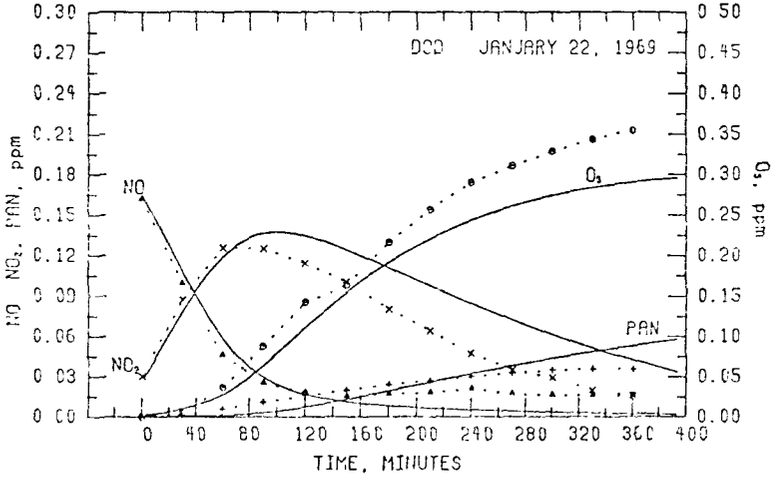
DCD JANUARY 22, 1969
NO
NO2
O3
PAN
NO, NO2, PAN, ppm
O3, ppm
TIME, MINUTES

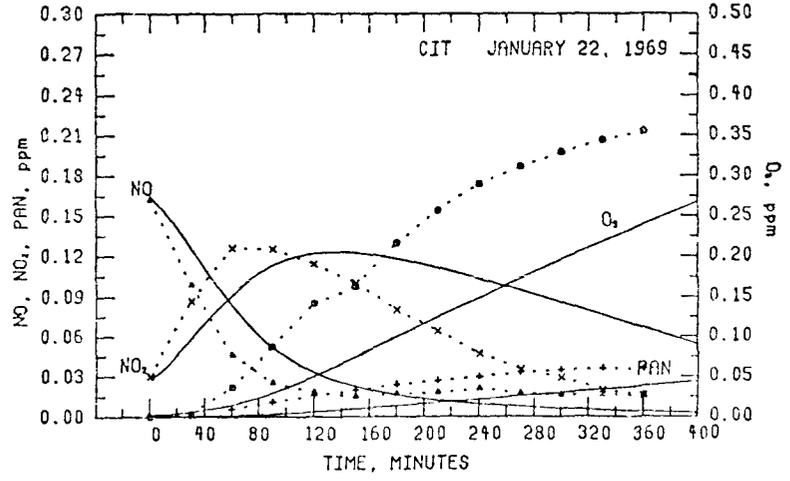
CIT JANUARY 22, 1969
NO
NO2
O3
PAN
NO, NO2, PAN, ppm
O3, ppm
TIME, MINUTES

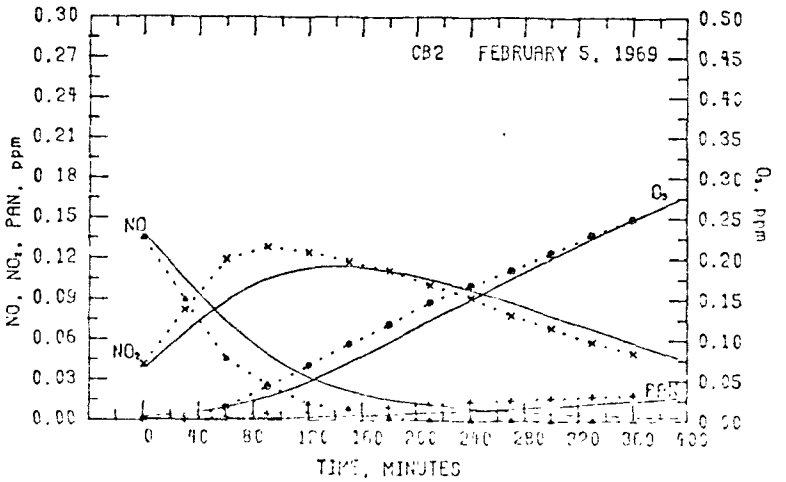
CB2 FEBRUARY 5, 1969
NO, NO₂, PAN, ppm
O₃, ppm
NO
NO₂
O₃
PAN
TIME, MINUTES

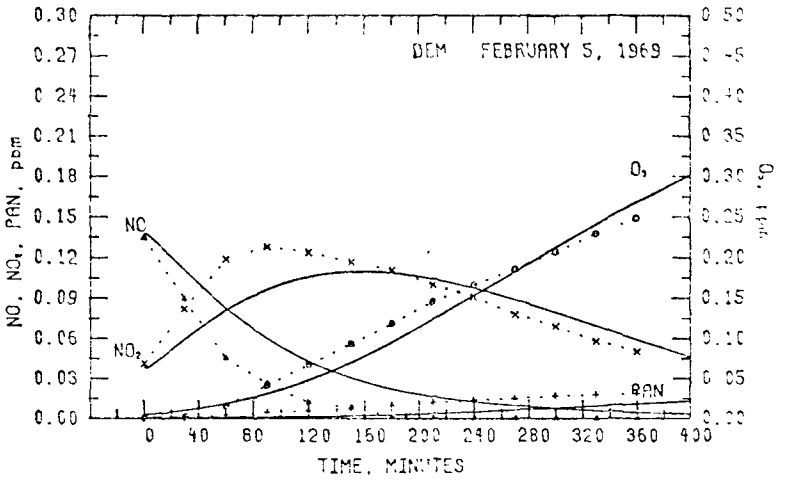
DEM FEBRUARY 5, 1969
NO, NO₂, PAN, ppm
O₃, ppm
NO
NO₂
O₃
PAN
TIME, MINUTES

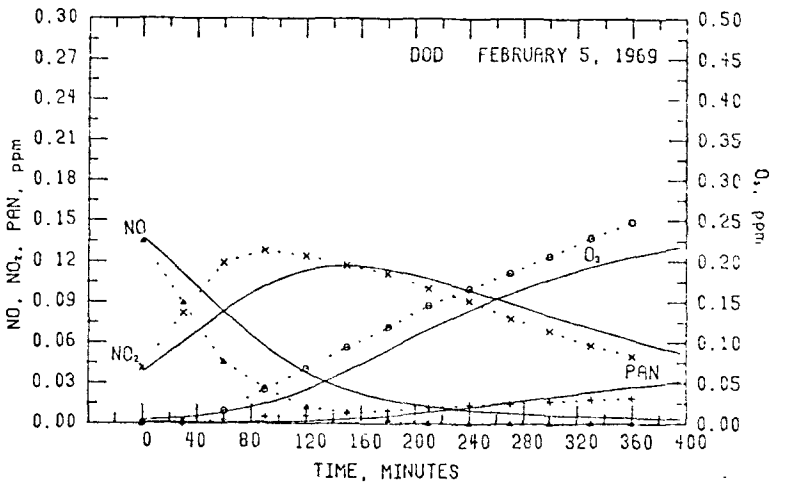
DOD FEBRUARY 5, 1969
NO, NO₂, PAN, ppm
O₃, ppm
NO
NO₂
O₃
PAN
TIME, MINUTES

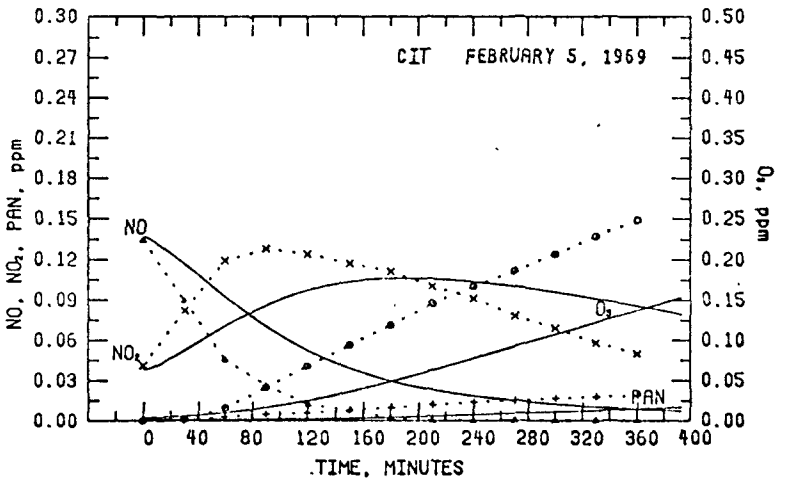
CIT FEBRUARY 5, 1969
NO, NO₂, PAN, ppm
O₃, ppm
NO
NO₂
O₃
PAN
TIME, MINUTES

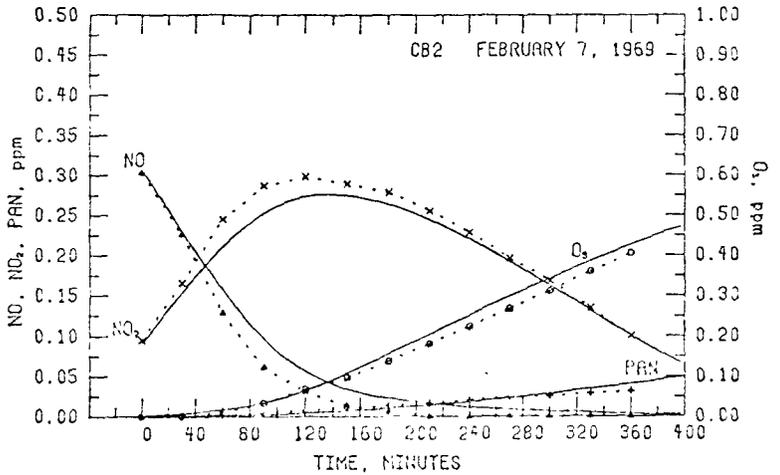
CB2 FEBRUARY 7, 1969
NO
NO2
O3
PAN
NO, NO2, PAN, ppm
O3, ppm
TIME, MINUTES

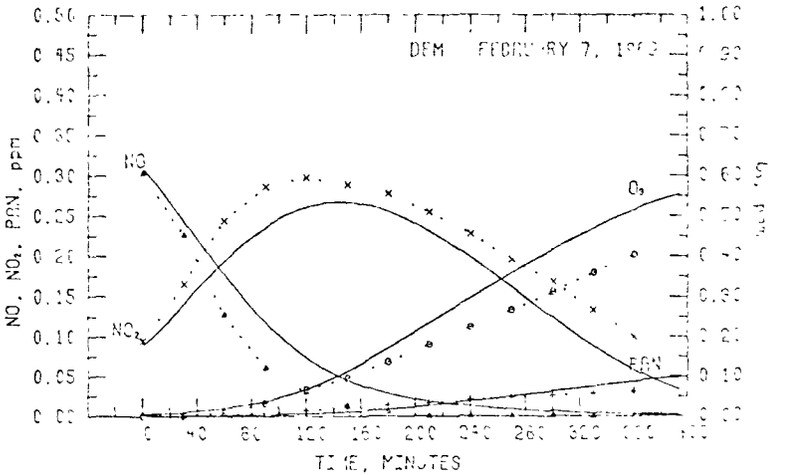
NO
NO2
O3
PAN
NO, NO2, PAN, ppm
TIME, MINUTES

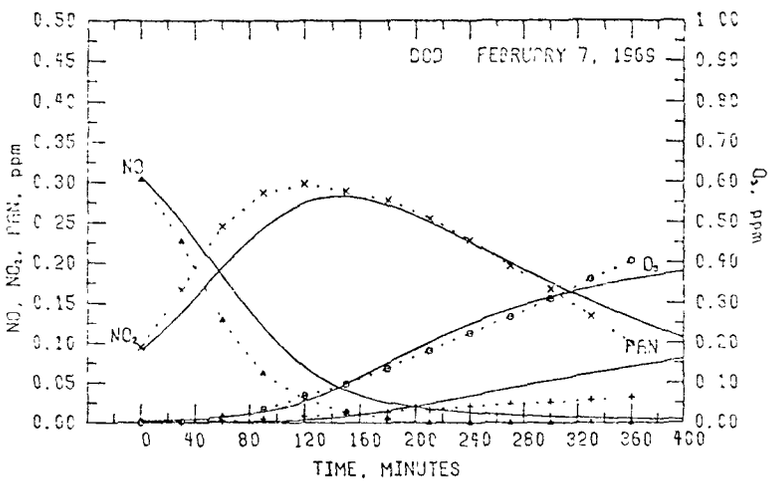
DCD FEBRUARY 7, 1969
NO
NO2
O3
PAN
NO, NO2, PAN, ppm
O3, ppm
TIME, MINUTES

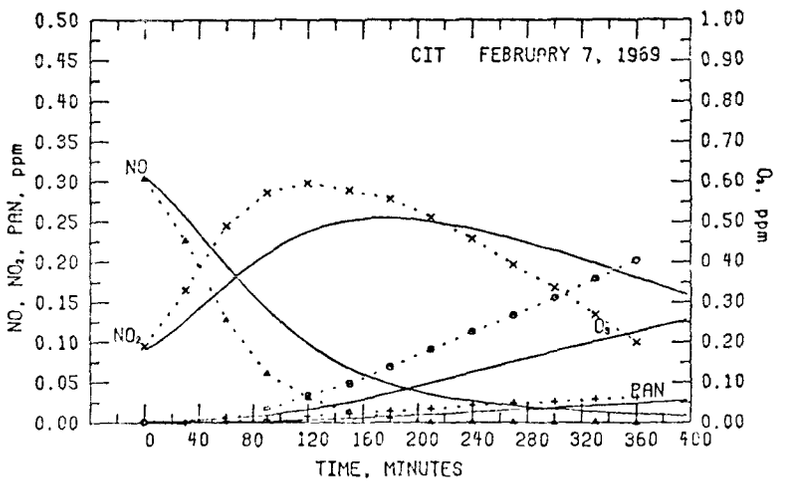
CIT FEBRUARY 7, 1969
NO
NO2
O3
PAN
NO, NO2, PAN, ppm
O3, ppm
TIME, MINUTES

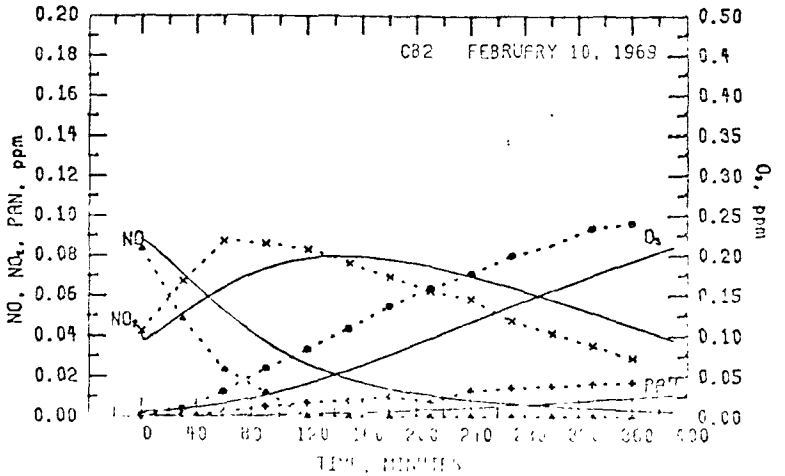
C82 FEBRUARY 10, 1969
NO, NO2, PAN, ppm
O3, ppm
NO
NO2
O3
PAN
TIME, MINUTES

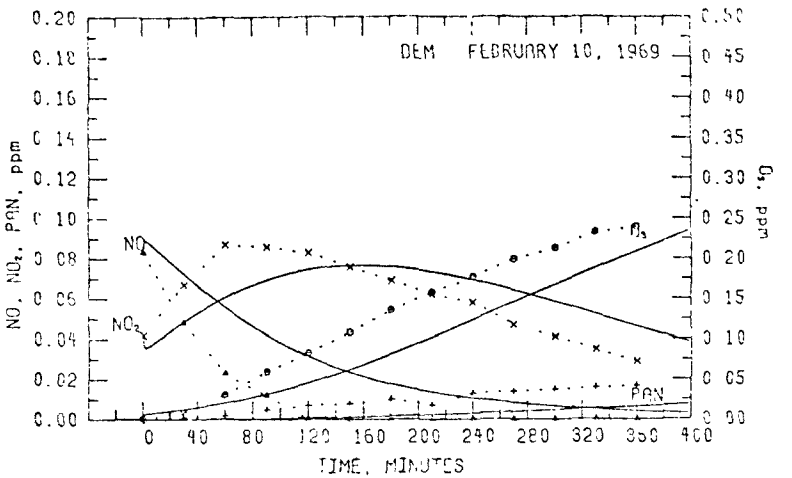
DEM FEBRUARY 10, 1969
NO, NO2, PAN, ppm
O3, ppm
NO
NO2
O3
PAN
TIME, MINUTES

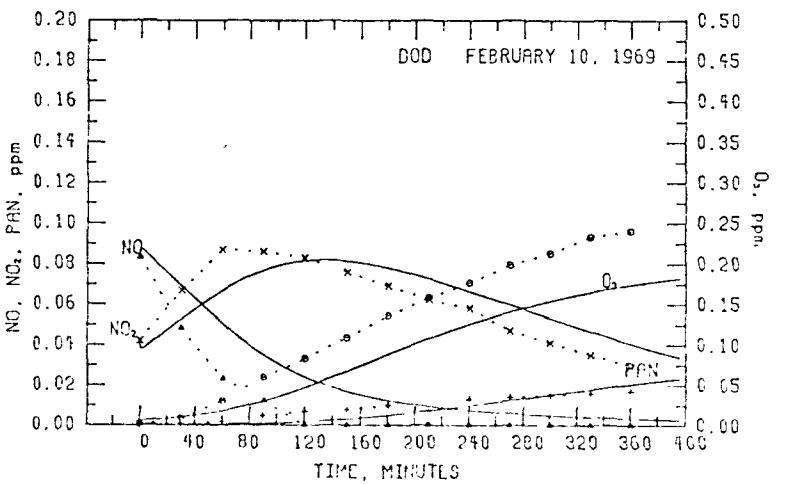
DOD FEBRUARY 10, 1969
NO, NO2, PAN, ppm
O3, ppm
NO
NO2
O3
PAN
TIME, MINUTES

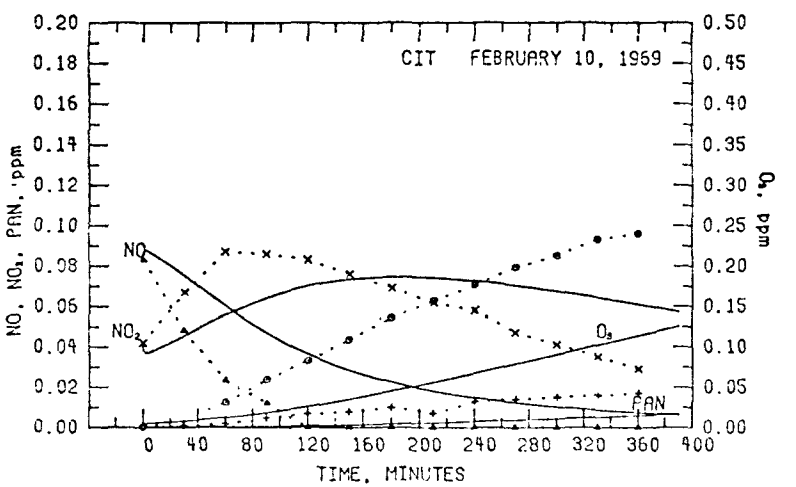
CIT FEBRUARY 10, 1969
NO, NO2, PAN, ppm
O3, ppm
NO
NO2
O3
PAN
TIME, MINUTES

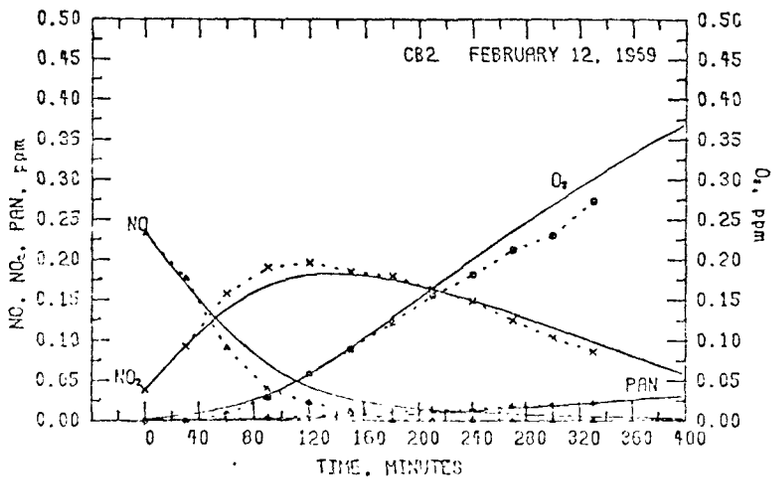
CB2 FEBRUARY 12, 1969
NO
NO2
O3
PAN
NO, NO2, PAN, ppm
O3, ppm
TIME, MINUTES

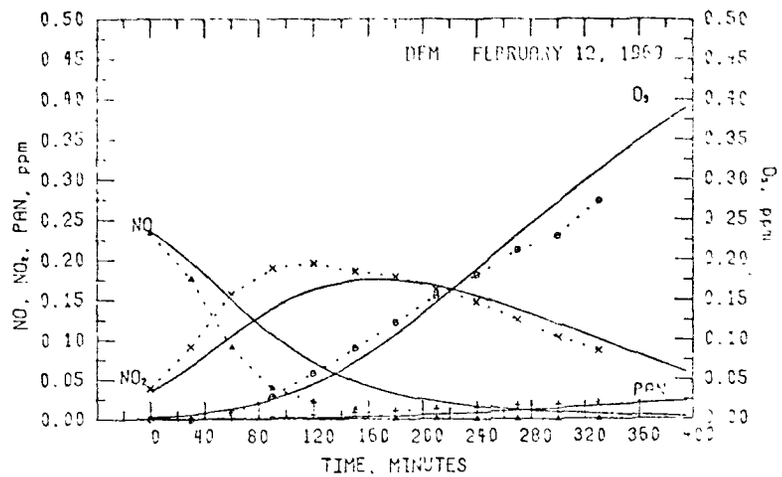
DFM FEBRUARY 12, 1969
NO
NO2
O3
PAN
NO, NO2, PAN, ppm
O3, ppm
TIME, MINUTES

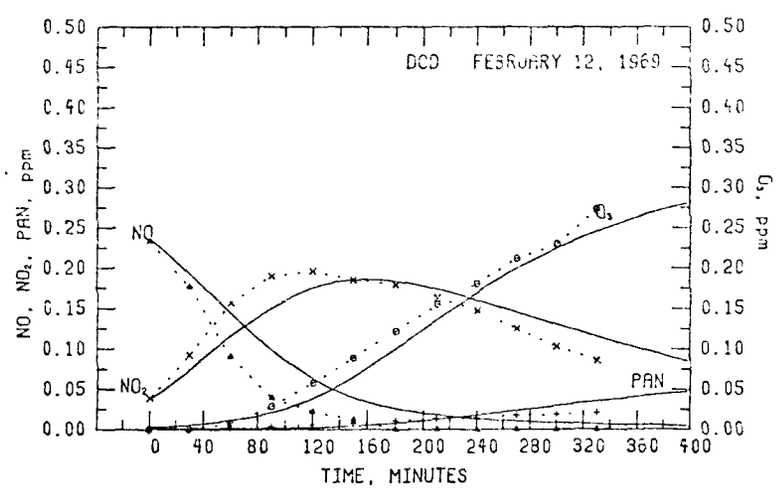
DCD FEBRUARY 12, 1969
NO
NO2
O3
PAN
NO, NO2, PAN, ppm
O3, ppm
TIME, MINUTES

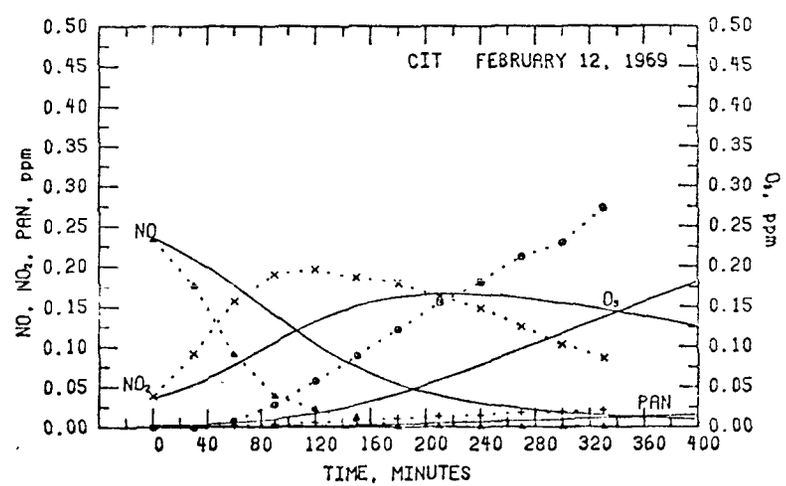
CIT FEBRUARY 12, 1969
NO
NO2
O3
PAN
NO, NO2, PAN, ppm
O3, ppm
TIME, MINUTES

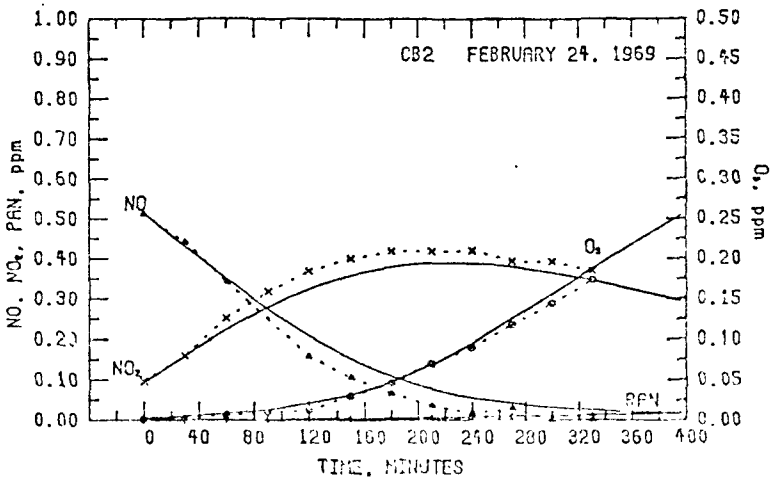
CB2 FEBRUARY 24, 1969
NO
NO₂
O₃
PAN
NO, NO₂, PAN, ppm
O₃, ppm
TIME, MINUTES

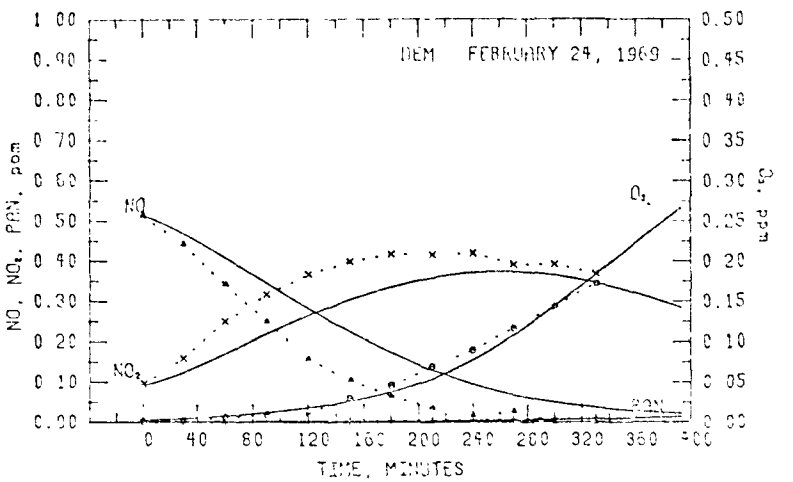
DEM FEBRUARY 24, 1969
NO
NO₂
O₃
PAN
NO, NO₂, PAN, ppm
O₃, ppm
TIME, MINUTES

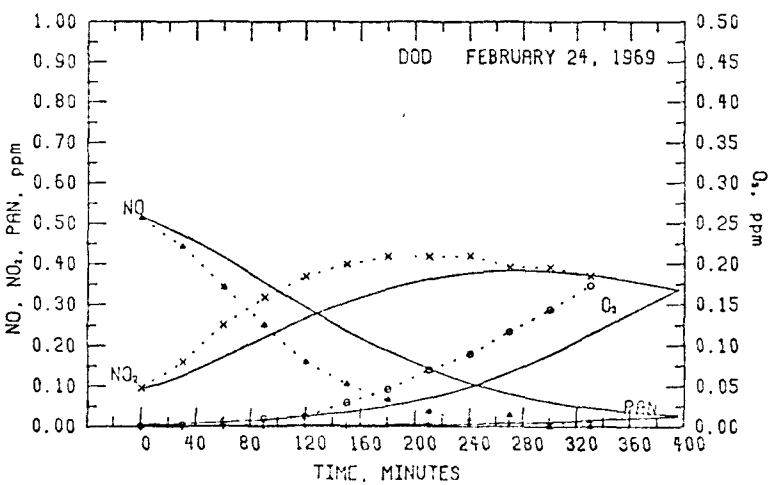
DOD FEBRUARY 24, 1969
NO
NO₂
O₃
PAN
NO, NO₂, PAN, ppm
O₃, ppm
TIME, MINUTES

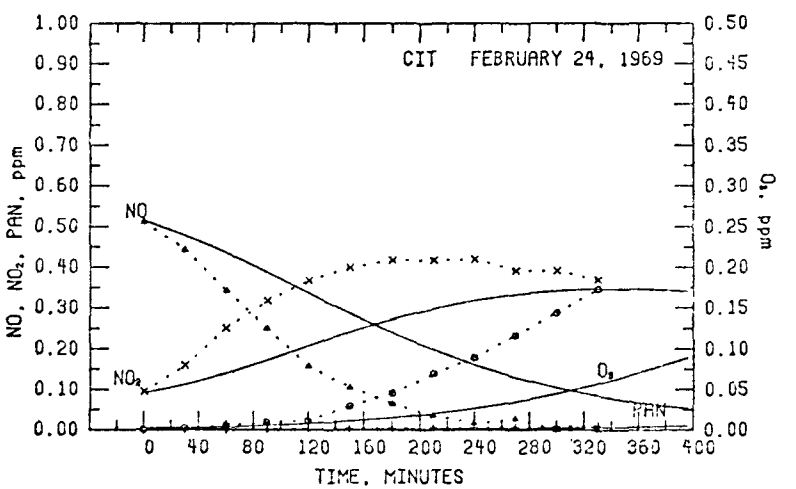
CIT FEBRUARY 24, 1969
NO
NO₂
O₃
PAN
NO, NO₂, PAN, ppm
O₃, ppm
TIME, MINUTES

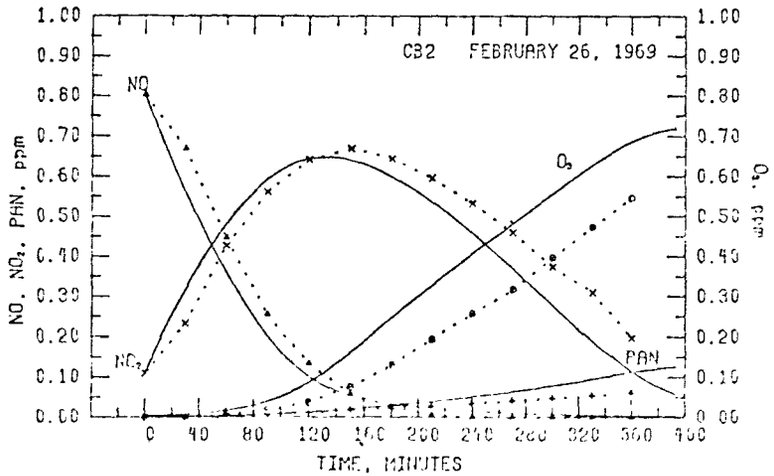
CB2 FEBRUARY 26, 1969
NO
NO₂
O₃
PAN
NO, NO₂, PAN, ppm
O₃, ppm
TIME, MINUTES

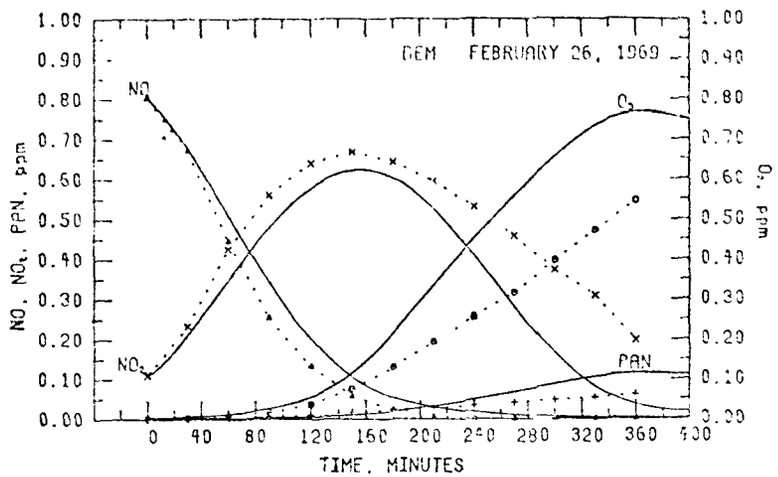
DEM FEBRUARY 26, 1969
NO
NO₂
O₃
PAN
NO, NO₂, PAN, ppm
O₃, ppm
TIME, MINUTES

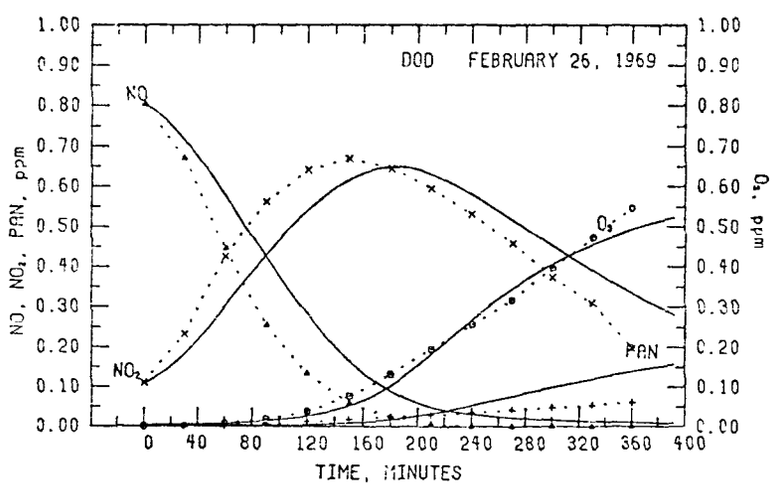
DOD FEBRUARY 26, 1969
NO
NO₂
O₃
PAN
NO, NO₂, PAN, ppm
O₃, ppm
TIME, MINUTES

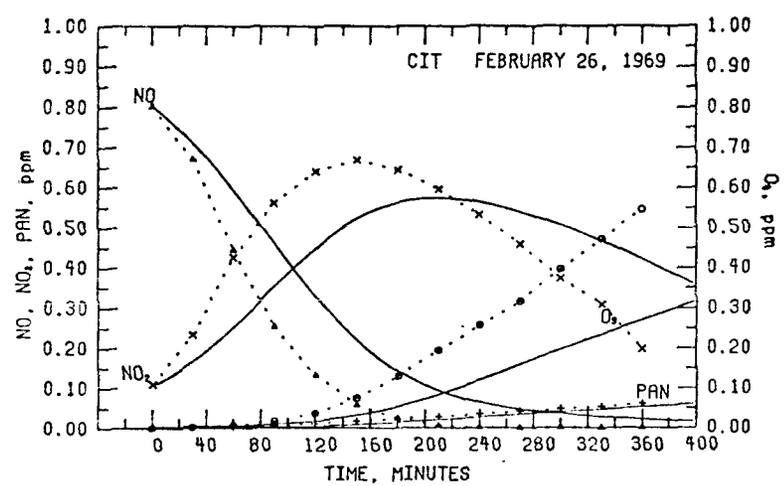
CIT FEBRUARY 26, 1969
NO
NO₂
O₃
PAN
NO, NO₂, PAN, ppm
O₃, ppm
TIME, MINUTES

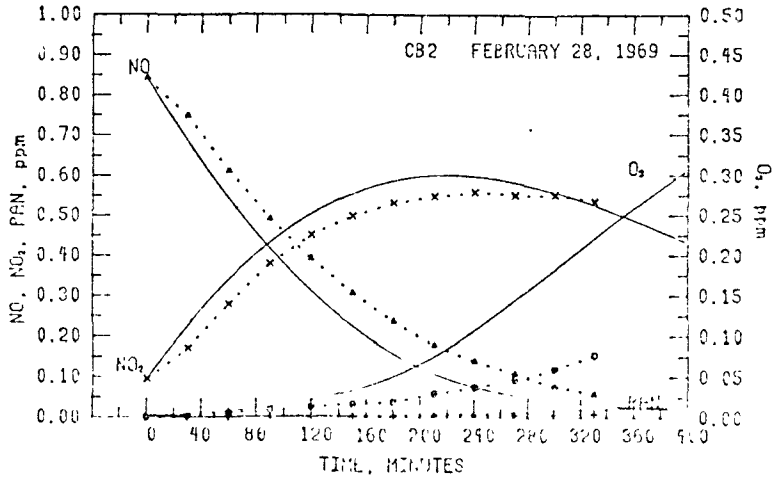
CB2 FEBRUARY 28, 1969
NO
NO₂
O₃
PAN
NO, NO₂, PAN, ppm
O₃, ppm
TIME, MINUTES

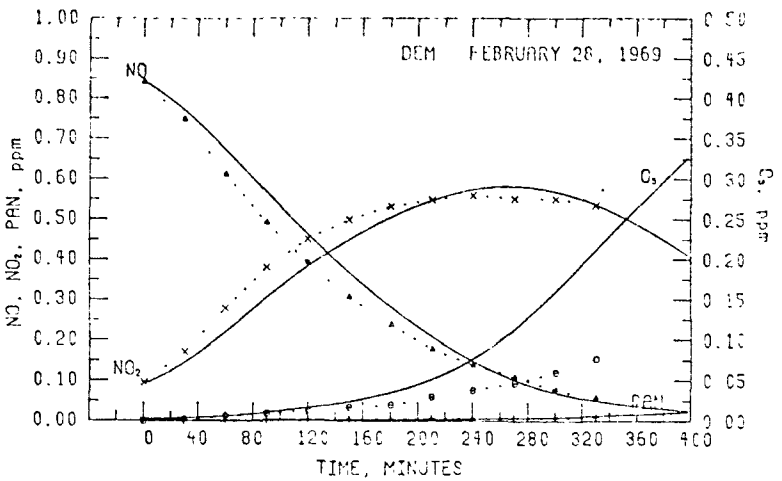
DEM FEBRUARY 28, 1969
NO
NO₂
O₃
PAN
NO, NO₂, PAN, ppm
O₃, ppm
TIME, MINUTES

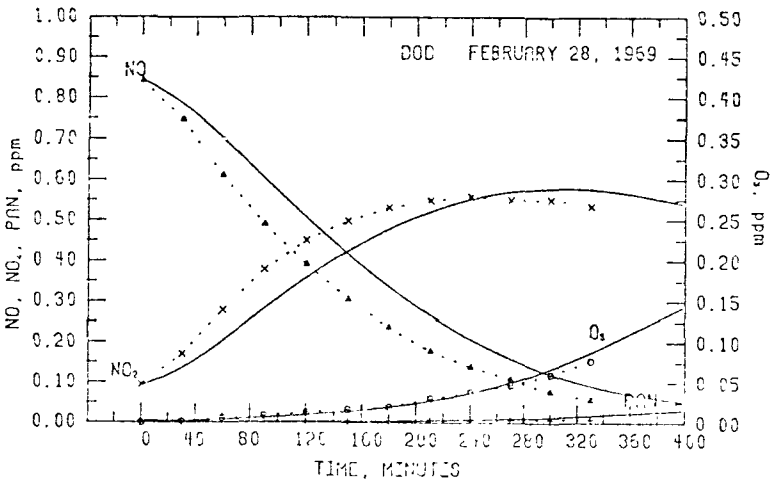
DOD FEBRUARY 28, 1969
NO
NO₂
O₃
PAN
NO, NO₂, PAN, ppm
O₃, ppm
TIME, MINUTES

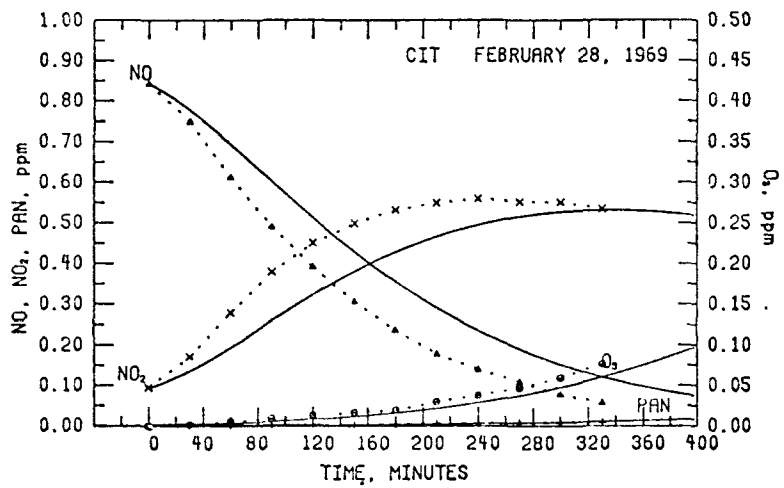
CIT FEBRUARY 28, 1969
NO
NO₂
O₃
PAN
NO, NO₂, PAN, ppm
O₃, ppm
TIME, MINUTES

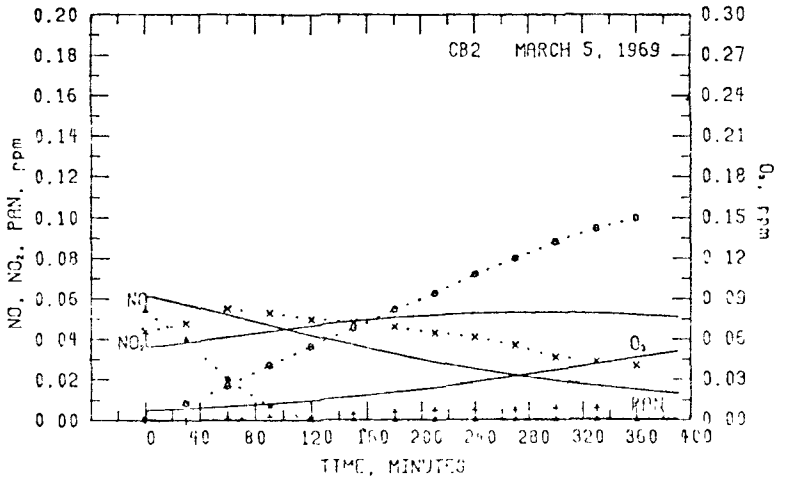
CB2 MARCH 5, 1969
NO, NO₂, PAN, ppm
O₃, ppm
NO
NO₂
O₃
PAN
TIME, MINUTES

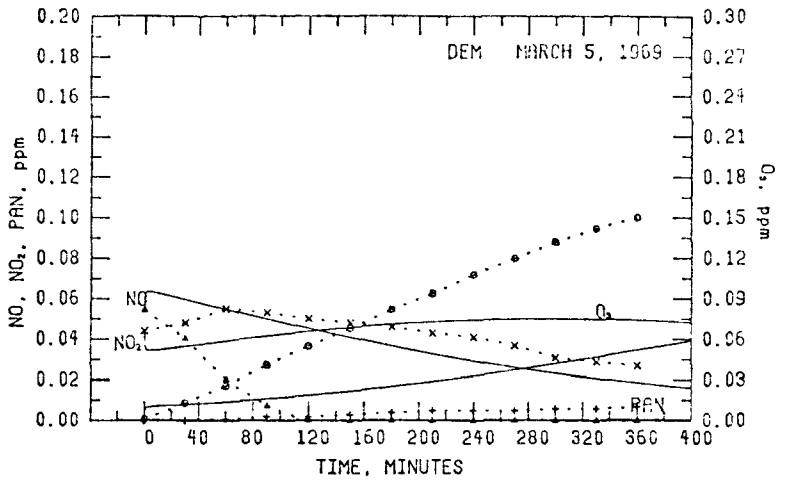
DEM MARCH 5, 1969
NO, NO₂, PAN, ppm
O₃, ppm
NO
NO₂
O₃
PAN
TIME, MINUTES

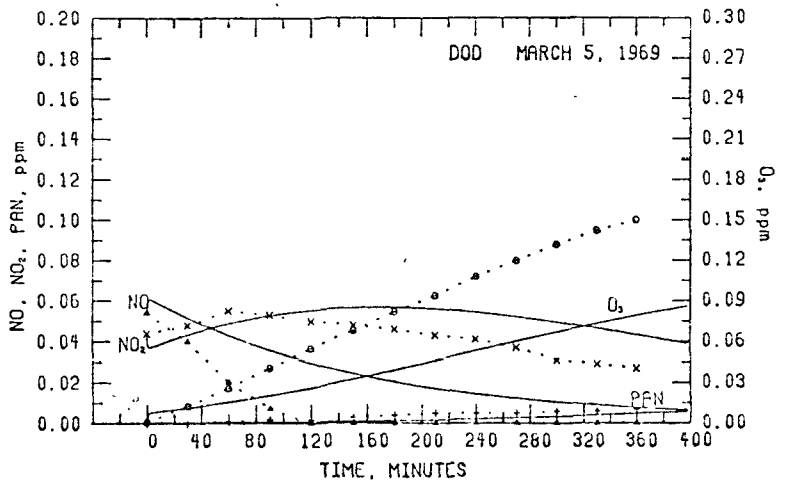
DOD MARCH 5, 1969
NO, NO₂, PAN, ppm
O₃, ppm
NO
NO₂
O₃
PAN
TIME, MINUTES

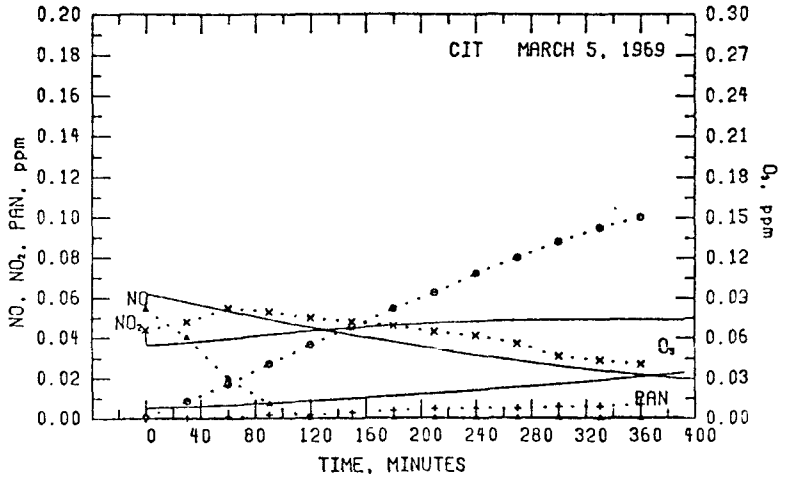
CIT MARCH 5, 1969
NO, NO₂, PAN, ppm
O₃, ppm
NO
NO₂
O₃
PAN
TIME, MINUTES

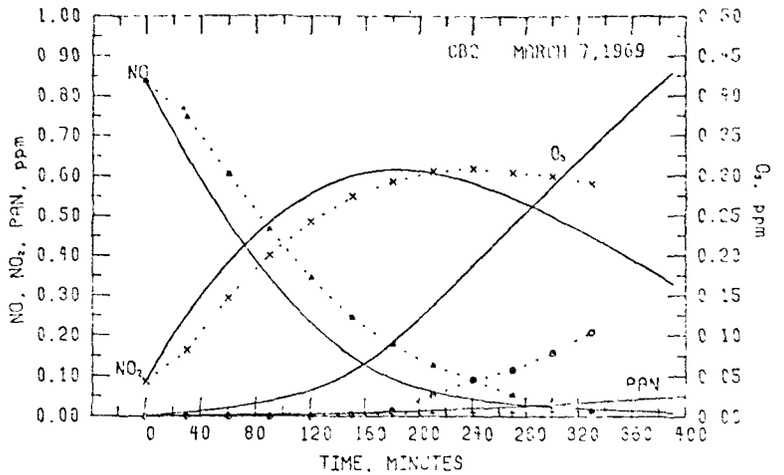
CBC MARCH 7, 1969
NO
NO₂
O₃
PAN
NO, NO₂, PAN, ppm
O₃, ppm
TIME, MINUTES

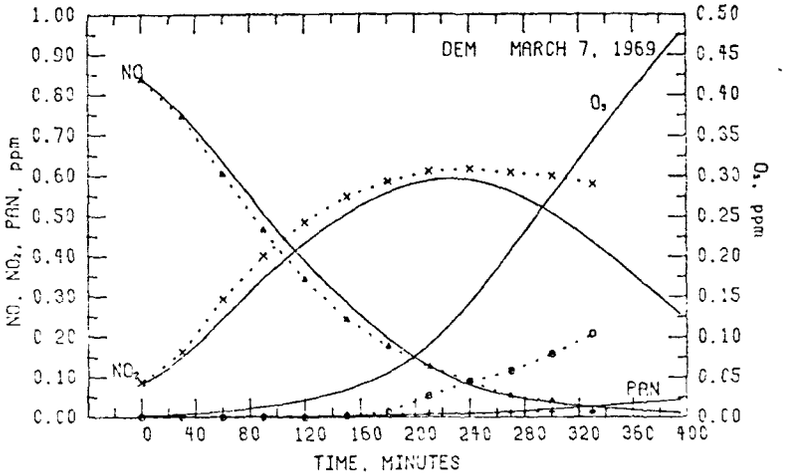
DEM MARCH 7, 1969
NO
NO₂
O₃
PAN
NO, NO₂, PAN, ppm
O₃, ppm
TIME, MINUTES

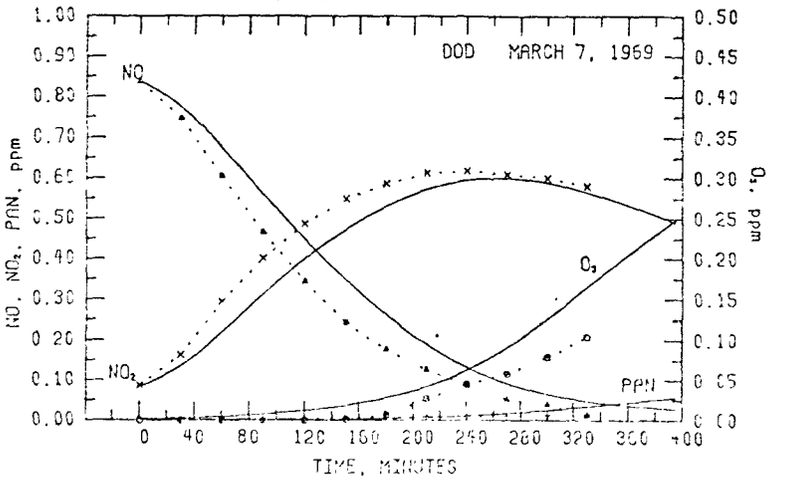
DOD MARCH 7, 1969
NO
NO₂
O₃
PAN
NO, NO₂, PAN, ppm
O₃, ppm
TIME, MINUTES

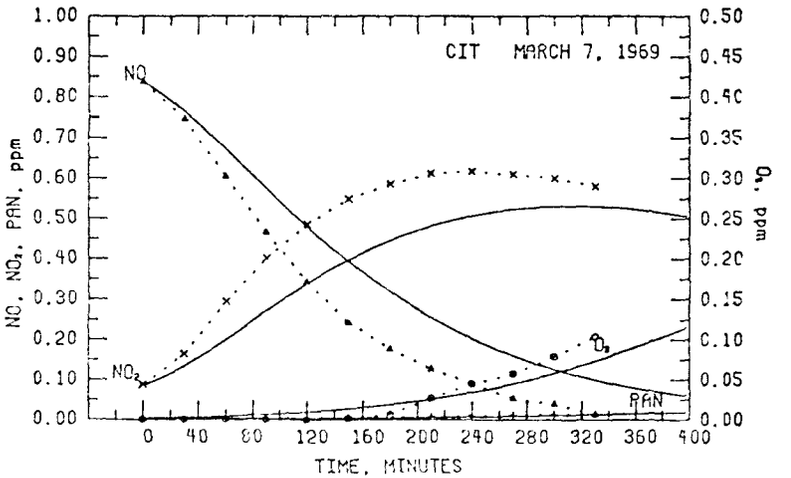
CIT MARCH 7, 1969
NO
NO₂
O₃
PAN
NO, NO₂, PAN, ppm
O₃, ppm
TIME, MINUTES

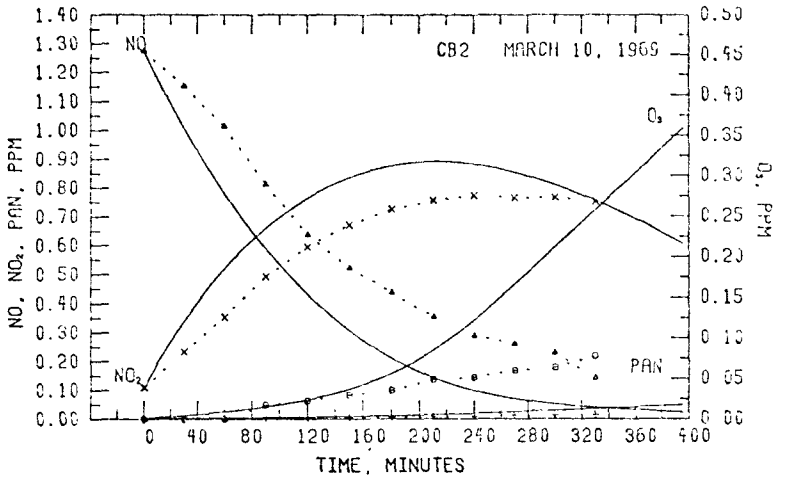
CB2 MARCH 10, 1969
NO
NO₂
O₃
PAN
NO, NO₂, PAN, PPM
O₃, PPM
TIME, MINUTES

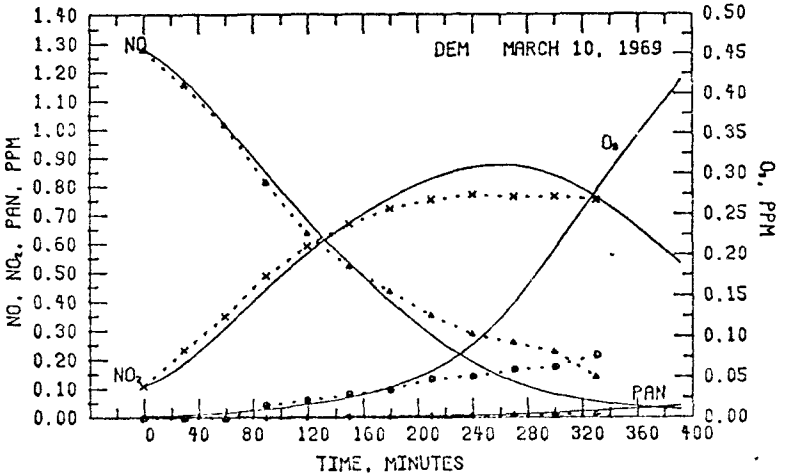
DEM MARCH 10, 1969
NO
NO₂
O₃
PAN
NO, NO₂, PAN, PPM
O₃, PPM
TIME, MINUTES

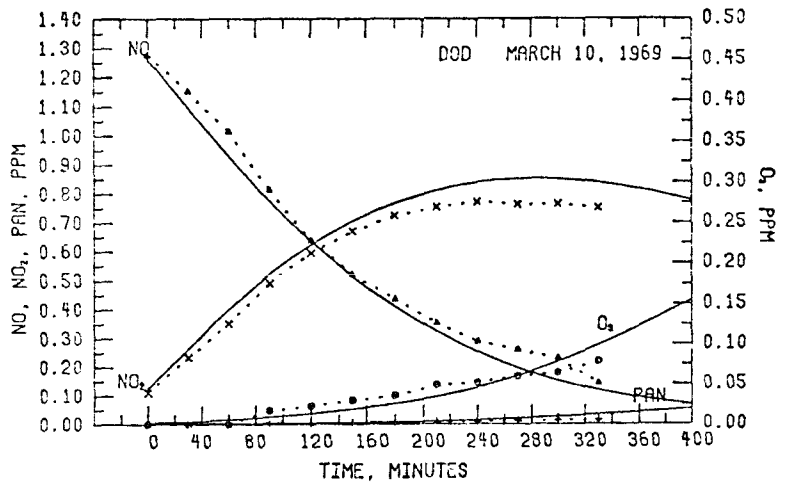
DOD MARCH 10, 1969
NO
NO₂
O₃
PAN
NO, NO₂, PAN, PPM
O₃, PPM
TIME, MINUTES

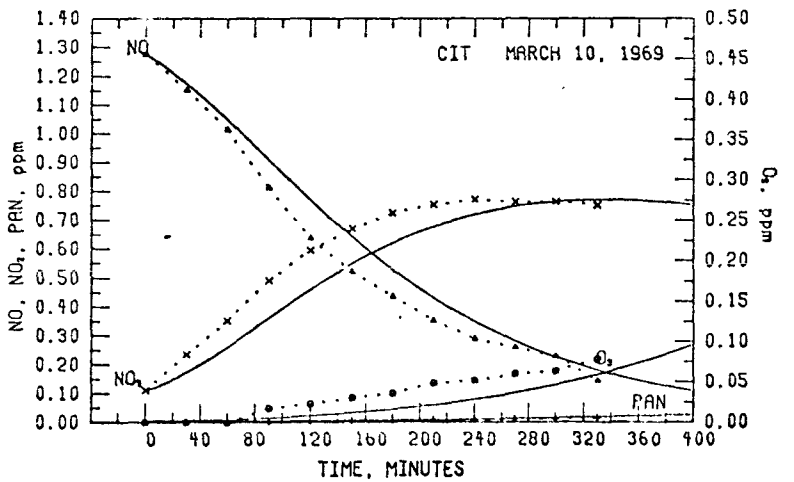
CIT MARCH 10, 1969
NO
NO₂
O₃
PAN
NO, NO₂, PAN, ppm
O₃, ppm
TIME, MINUTES

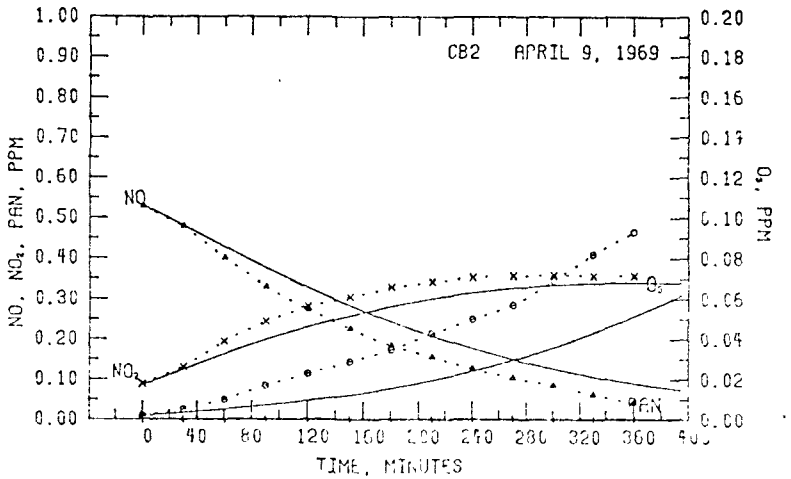
CB2 APRIL 9, 1969
NO, NO2, PAN, PPM
O3, PPM
TIME, MINUTES
NO
NO2
O3
PAN

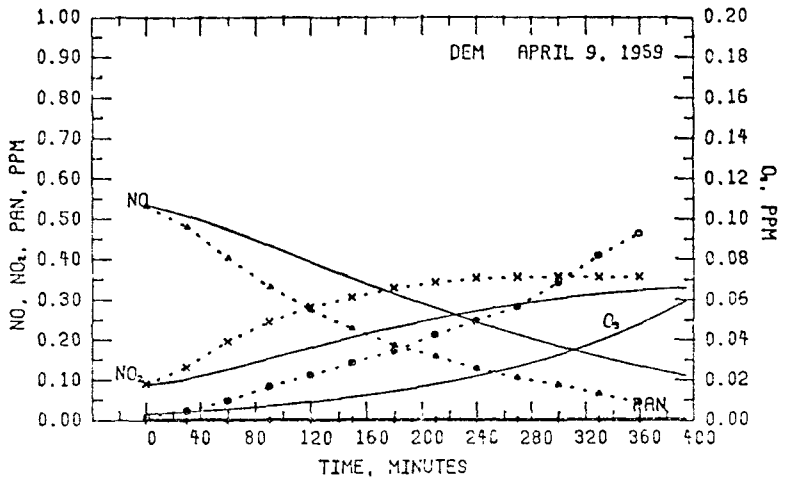
DEM APRIL 9, 1969
NO, NO2, PAN, PPM
O3, PPM
TIME, MINUTES
NO
NO2
O3
PAN

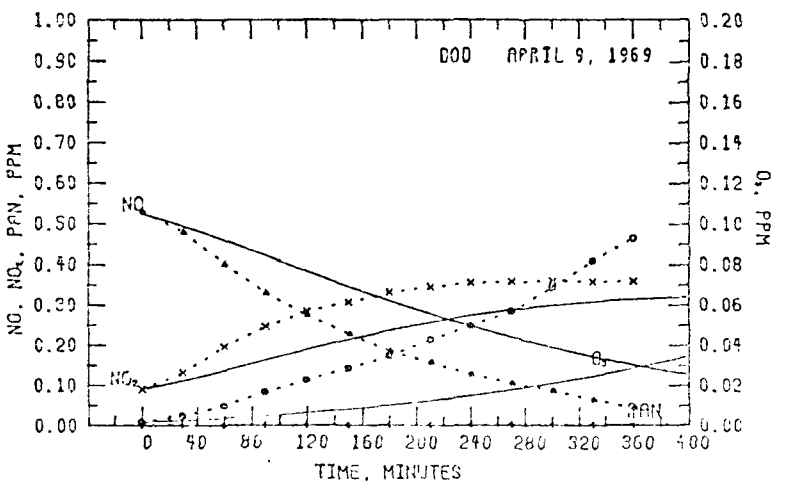
DOD APRIL 9, 1969
NO, NO2, PAN, PPM
O3, PPM
TIME, MINUTES
NO
NO2
O3
PAN

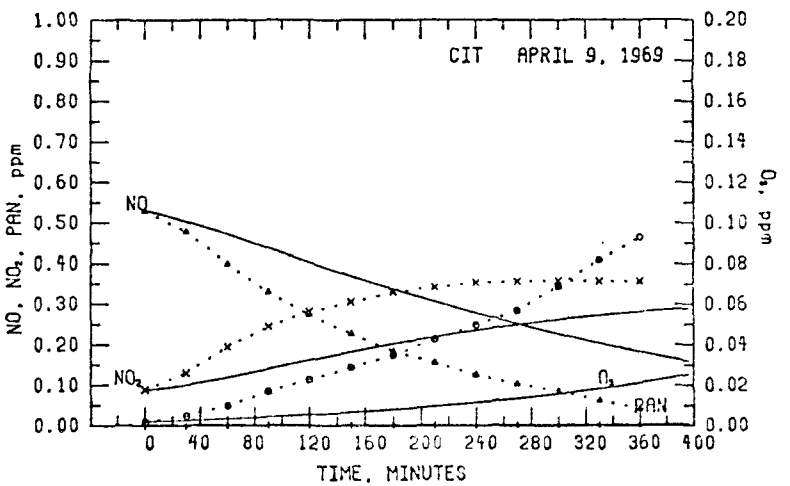
CIT APRIL 9, 1969
NO, NO2, PAN, ppm
O3, ppm
TIME, MINUTES
NO
NO2
O3
PAN

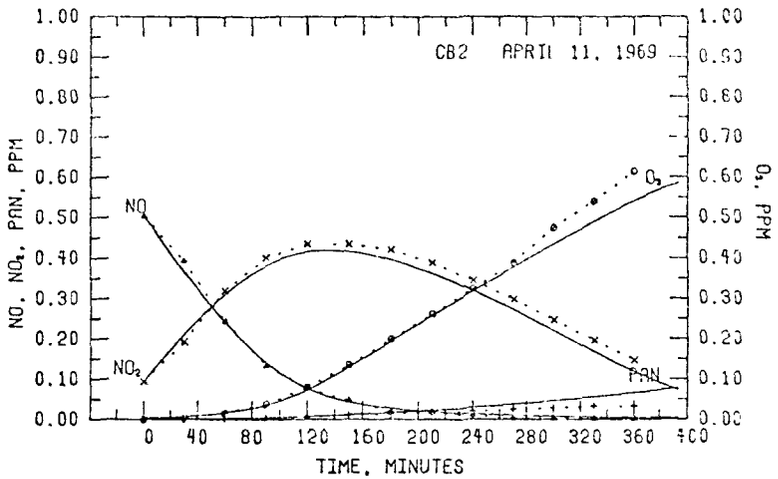
CB2 APRIL 11, 1969
NO, NO₂, PAN, PPM
O₃, PPM
TIME, MINUTES
NO
NO₂
PAN
O₃

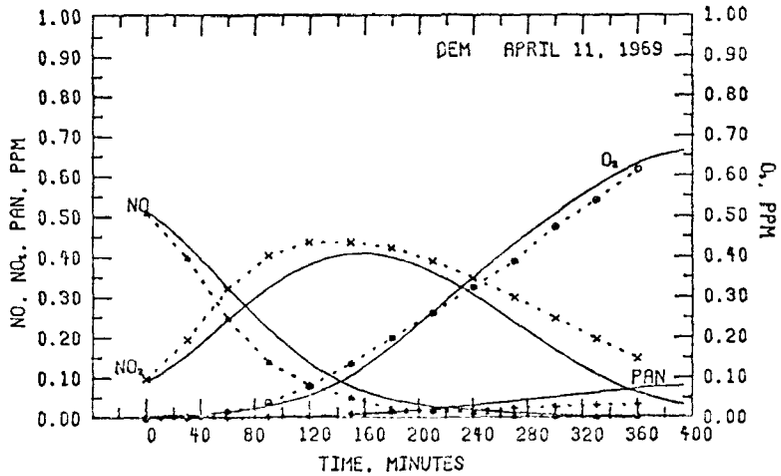
DEM APRIL 11, 1969
NO, NO₂, PAN, PPM
O₃, PPM
TIME, MINUTES
NO
NO₂
PAN
O₃

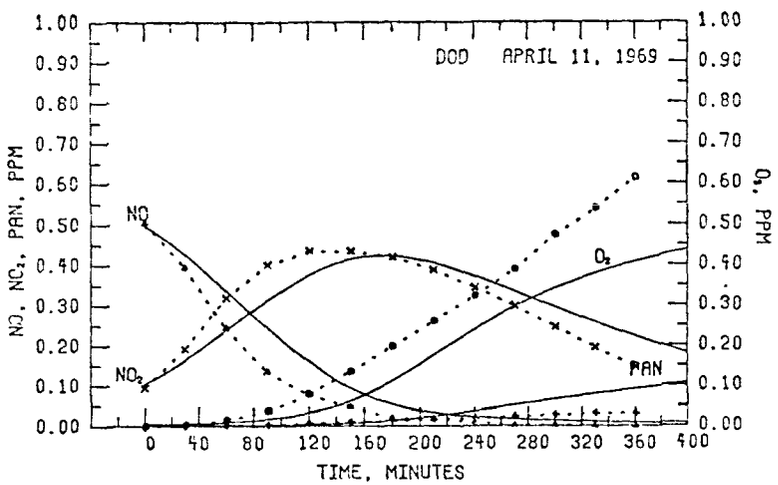
DOD APRIL 11, 1969
NO, NO₂, PAN, PPM
O₃, PPM
TIME, MINUTES
NO
NO₂
PAN
O₃

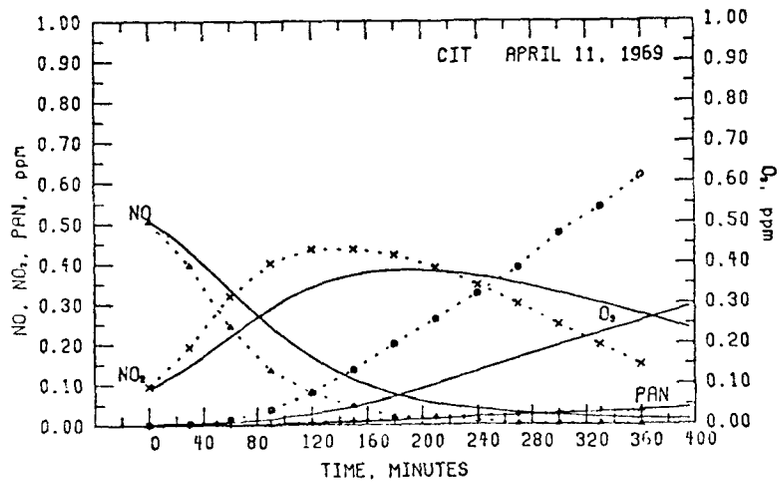
CIT APRIL 11, 1969
NO, NO₂, PAN, ppm
O₃, ppm
TIME, MINUTES
NO
NO₂
PAN
O₃

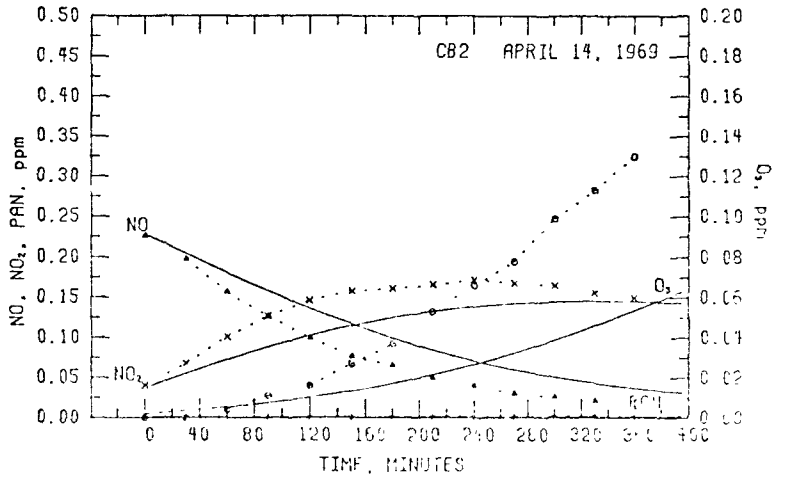
CB2 APRIL 14, 1969
NO
NO2
O3
PAN
NO, NO2, PAN, ppm
O3, ppm
TIME, MINUTES

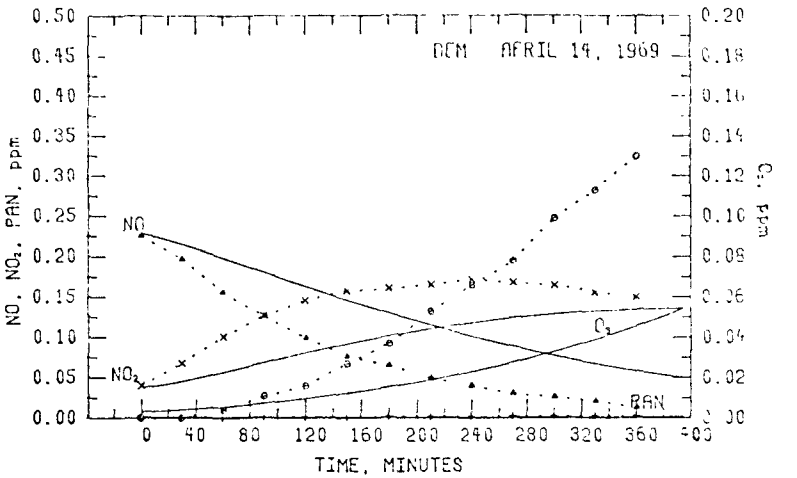
DEN APRIL 14, 1969
NO
NO2
O3
PAN
NO, NO2, PAN, ppm
O3, ppm
TIME, MINUTES

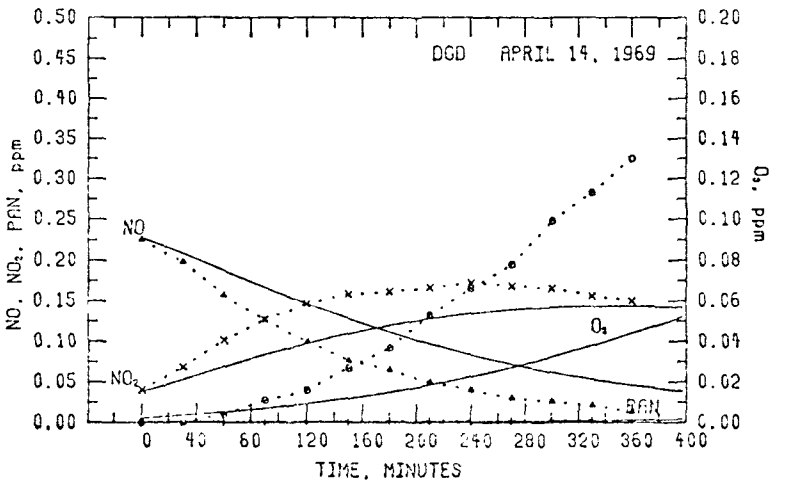
DGD APRIL 14, 1969
NO
NO2
O3
PAN
NO, NO2, PAN, ppm
O3, ppm
TIME, MINUTES

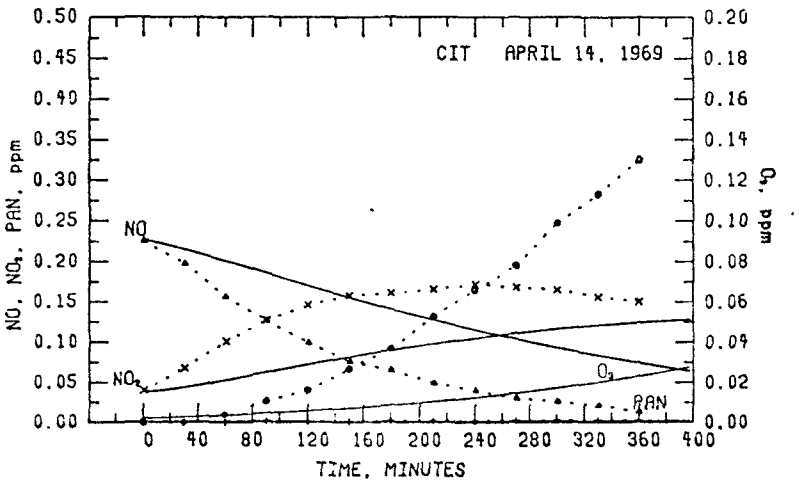
CIT APRIL 14, 1969
NO
NO2
O3
PAN
NO, NO2, PAN, ppm
O3, ppm
TIME, MINUTES

TECHNICAL REPORT DATA
(Please read Instructions on the reverse before completing)

1. REPORT NO. EPA-450/4-81-034	2.	3. RECIPIENT'S ACCESSION NO.
4. TITLE AND SUBTITLE Effects of Chemistry and Meteorology on Ozone Control Calculations Using Simple Trajectory Models and the EKMA Procedure		5. REPORT DATE November 1981
		6. PERFORMING ORGANIZATION CODE
7. AUTHOR(S) H. E. Jeffries, K. G. Sexton, C. N. Salmi		8. PERFORMING ORGANIZATION REPORT NO.
9. PERFORMING ORGANIZATION NAME AND ADDRESS University of North Carolina Department of Environmental Sciences and Engineering School of Public Health Chapel Hill, North Carolina 27514		10. PROGRAM ELEMENT NO
		11. CONTRACT/GRANT NO. 68-02-3523
12. SPONSORING AGENCY NAME AND ADDRESS U.S. Environmental Protection Agency Office of Air Quality Planning and Standards Research Triangle Park, North Carolina 27711		13. TYPE OF REPORT AND PERIOD COVERED
		14. SPONSORING AGENCY CODE

15. SUPPLEMENTARY NOTES

EPA Project Officer: Edwin L. Meyer

16. ABSTRACT

Three chemical kinetics mechanisms (Carbon Bond II, lumped species mechanism used in Demerjian and Schere's photochemical box model and the Cal Tech mechanism developed by McRae) were used in a modified version of the OZIPP model to replicate smog chamber data in which automotive exhaust was irradiated (Bureau of Mines data). Two of the mechanisms (CBII and Demerjian) agreed with the data, as well as the existing mechanism in OZIPP (Dodge propylene/butane). The OZIPP model was next used to simulate several days of observations made during the St. Louis RAPS. In several cases, it was found that the meteorological input and/or assumptions did not allow an adequate basis to compare the mechanisms. Three days in which the meteorological input appeard appropriate were simulated using OZIPP with the Dodge, Demerjian and CBII mechanisms. Differing peak ozone and control estimates were obtained, depending on the day simulated and choice of mechanism. Sensitivity tests were employed to explore observed differences among the mechanisms tested.

17. KEY WORDS AND DOCUMENT ANALYSIS

a. DESCRIPTORS	b. IDENTIFIERS/OPEN ENDED TERMS	c. COSATI Field/Group
Ozone Photochemical models Chemical kinetics mechanisms OZIPP EKMA Sensitivity studies		

18. DISTRIBUTION STATEMENT Unlimited	19. SECURITY CLASS (This Report)	21. NO. OF PAGES 393
	20. SECURITY CLASS (This page)	22. PRICE

EPA Form 2220-1 (Rev. 4-77) PREVIOUS EDITION IS OBSOLETE

U.S. Environmental Protection Agency
Region V, Library
230 South Dearborn Street
Chicago, Illinois 60604